The Institute of Paper Chemistry

Appleton, Wisconsin

Doctor's Dissertation

A Nuclear Magnetic Resonance Study of the Glycosidic
Linkage of the Xylo- and Cello-Oligosaccharides

John C. Gast

June, 1983

A NUCLEAR MAGNETIC RESONANCE STUDY OF THE GLYCOSIDIC
LINKAGE OF THE XYLO- AND CELLO-OLIGOSACCHARIDES

A thesis submitted by

John C. Gast

B.S. 1974, (Chemistry), Michigan Technological University

B.S. 1974, (Biology), Michigan Technological University

M.S. 1976, Lawrence University

in partial fulfillment of the requirements
of The Institute of Paper Chemistry
for the degree of Doctor of Philosophy
from Lawrence University,
Appleton, Wisconsin

June, 1983

TABLE OF CONTENTS

To Leslie with love in

appreciation for her unrelenting

patience, support, understanding,

and love.

ABSTRACT

Recently, the development of FT-NMR spectroscopy has resulted in easy access to several useful parameters for the study of carbohydrate conformations in solution. These include ^{13}C-^1H spin-spin coupling constants and both ^1H and ^{13}C spin-lattice relaxation times (T_1). Use of these parameters for a comparison of the cello- and xylo-oligosaccharide linkage conformations in solutions has been the central aim of this work.

^{13}C-NMR spectra were assigned for the xylo- and cello-oligosaccharides up to the pentamer and tetramer, respectively. Both model compounds and peak intensity variations were used to make assignments. ^{13}C-T_1 relaxation times were determined and assigned to the specific monomer units based on the developed assignments. This process revealed a clear pattern of relaxation times showing that the terminal units relax more slowly than the internal units. This was interpreted as evidence for a fast internal reorientation at the glycosidic linkage in both types of compounds.

Having established that the linkage conformation is a time average in solution, a comparison was made between the average conformations in both types of molecules. ^{13}C-^1H coupling constants were used to compare the dihedral angle χ between xylobiose, cellobiose, and related model compounds. By this method the average value for χ in xylobiose was determined to be farther removed from the 2-fold helix by 25-60°. Complimentary ^1H-T_1 relaxation measurements of the linkage anomeric protons show the H_1' to H_4 distance to be 0.1-0.2 Å greater in xylobiose. These data are interpreted in terms of a more staggered and open linkage for the xylo-oligosaccharides.

The comparison of average linkage conformations shows by inference that steric hindrance, from the glucose C_6 hydroxymethylene in the cello-oligomers, is the determining factor in the linkage conformation. A correlation between the C_4 chemical shift and the presence of the aglycone C_6 was established in support of this.

The existence of an intramolecular hydrogen bond from O_3H to O_5' has long been postulated for both types of systems. Hydroxyl proton chemical shift and coupling patterns show a weak and isolated bond in cellobiose in DMSO-d_6. In xylobiose the bond had some association with solvent.

COMPOUND DESIGNATIONS

The following is a list of compound designations and abbreviations used in this thesis. Because the different sections of the thesis were written non-sequentially, the designations were not made consistent from section to section. Designations for each section are listed below. In some sections the different anomers of the reducing disaccharides are distinguished by using a letter after the number, while in other sections only one anomer is designated. The specific meaning of the designation is given in each section at the first mention of the compound.

In numbering the atoms of the di- and oligo-saccharides the convention was used that places an additional prime on each successive ring removed from the reducing end. Thus, the ring at the reducing end is not primed, the next ring has one prime, and so forth, to the terminal ring that has n-1 primes, where n is the number of rings.

Compound Name[a]	Abbreviation	Compound Numbers by Section		
		2[b]	3[c]	4[d]
Arabinose				43
Arabinoside; Benzyl, β-				16
Arabinoside; Benzyl, 3,4-isopropylidene				17
Arabinoside; Benzyl, 3,4-isopropylidene,2-Tosyl				18
Arabinoside; Benzyl, 2-tosyl				19
Cellobiose	C2	2	1[a,b]	26
Cellobioside; Methyl β-	MBC2	3	2	21
Cellobioside; Methyl β-(d_8)	MBC2-d_8	7		44
Cellobiose Octaacetate				27
Cellobioside Heptaacetate; Methyl β-				23
Cellobiose; 1,5 Anhydro	1,5 ANC2			
Cellotriose			8	
Glucose		5	4[a,b]	42
Glucoside; Methyl β-	MBG	9	4[c]	30
Glucoside; Methyl β- (d_4)		10		45
Glucoside; Pentaacetate				34
Glucoside; Tetraacetate, Bromide				14
Lactose			10[a,b]	
Lactoside; Methyl β-	MBL			
Mannose; Glucosyl (epi-cellobiose)	GM		11[a,b]	
Riboside; Benzyl, 2,3-Anhydro				15
Riboside; Benzyl, 2,3-Anhydro, 4-Glucosyl	Ben 2,3 ANGR			11
Riboside; Benzyl, 2,3-Anhydro, 4-Methyl				36
Riboside; Benzyl, 2,3-Anhydro, 4-Xylosyl	Ben 2,3 ANXR			5
Riboside; Benzyl, 2,3-Anhydro, 4-Xylosyl Acetate				6
Riboside; Benzyl, 2,3-Anhydro, 4-Xylosyl TriMethyl				37
Securidebiose (Xylose, Glucosyl)	GX		6[a,b]	7
Securidebioside; Benzyl β-				9
Xylobiose	X2	1	5[a,b]	1
Xylobioside; Benzyl β-			7[b]	3
Xylobioside; Methyl β-		6	7[a]	20
Xylobiose; 2', 3', 4'-methyl				40
Xylobiose Hexaacetate				2
Xylobioside Pentaacetate; Benzyl β-				4
Xylobioside Pentaacetate; Methyl β-				22
Xylobiose Triacetate; 2', 3', 4'-Methyl				39

		Compound Numbers by Section		
Compound Name[a]	Abbreviation	2[b]	3[c]	4[d]
Xylose		4	3a,b	41
Xyloside; Methyl β–	MBX	8	3c	28
Xyloside; Methyl β– (d_2)				46
Xyloside; Methyl α–	MαX		3d	
Xylose Tetraacetate				33
Xylose Triacetate; Bromide				13
Xylose Trimethyl				35
Xylotriose			9	

[a]Compounds are alphabetized by the root name. All linkages are β-1,4-linked and all functional groups are attached to the carbon through the hydroxyl oxygen, except bromine.
[b]Also used in Appendices II, III, IV, and V.
[c]Also used in Appendices VI, VII, VIII, and IX.
[d]Also used in Appendices X, XI, XII, and XIII.

ABBREVIATIONS, DESIGNATIONS, AND SYMBOLS

Abbreviations

AT	Acquisition time
CP/MAS	Cross polarization/magic angle spinning
CSA	Chemical shift anisotropy
CW	Continuous wave
DD	Dipole-dipole
D_2O	Deuterium oxide
DMSO-d_6	Deuterated dimethyl sulfoxide
f.i.d.	Free induction decay
FT	Fourier transform
HZ	Hertz
IR	Inversion recovery
MHz	Megahertz
NMR	Nuclear magnetic resonance
^{1}H-NMR	Proton NMR
^{13}C-NMR	Carbon-13 NMR
NOE	Nuclear Overhauser effect (enhancement)
NRE	Nonreducing end
RE	Reducing end
SC	Scalar coupling
T_1	Spin lattice relaxation time
^{1}H-T_1	Proton spin lattice relaxation time
^{13}C-T_1	Carbon-13 spin lattice relaxation time
T_2	Spin-spin relaxation time
t.l.c.	Thin layer chromatography
whh	Width at half height
w/v	Weight to volume ratio

Designations

C_6 or C-6	Carbon atom number 6
^{13}C-^{1}H	Coupling between ^{13}C and ^{1}H atoms
^{2}H or ^{1}H	Isotope of hydrogen
$O_3H\ldots O_{5'}$	Intramolecular hydrogen bond
$H_{1'}$-H_4	Distance between $H_{1'}$ and H_4
Cl or 1C	Chair conformer
-d_n	Number (n) of substituted deuterium atoms

<u>Symbols</u>

A	Coefficient in Karplus equation
B	Coefficient in Karplus equation
C	Coefficient in Karplus equation
C	$\hbar^2 \gamma_H^2 \gamma_C^2$
E	Linear regression error
E_m	Energy of nucleus in magnetic field with magnetic quantum number m
ΔE	Change in energy E_m
f	Larmor frequency
f_o	Larmor frequency at H_o
f_r	Larmor frequency of reference
f_s	Larmor frequency of signal of interest
F	Instrumental line broadening
F(t)	Sinusoidal function in time domain
F(w)	Sinusoidal function in frequency domain
h	Planck's constant
$\hbar$	Planck's constant divided by 2π
$\vec{H}_o$	Strong magnetic field vector
H_o	Magnitude of H_o
$\vec{H}_1$	Detecting magnetic field vector
H_{eff}	Effective magnetic field
$\vec{H}_{loc}$	Local magnetic field vector
H_2	Magnitude of spin-decoupling field
I	Spin quantum number
I_i	Quantum mechanical operator for spin I
I_s	Spin quantum number for nucleus S
J_K	Spin-spin coupling constant over k bonds

$^iJ_{ij}$	Spin-spin coupling constant over i bonds between nuclei i and j
$^iJ(C_iH_i)$	Spin-spin coupling constant between C_i and H_i
$^3J_{COCH}$	Spin-spin coupling constant for COCH system
$J_i(w)$	Spectral density function
K	$\gamma_H{}^4$
$K_i(T)$	Correlation function
m	molol concentration
m	magnetic quantum number
$\vec{m}$	Total magnetization vector
M_o	Total magnetization at time 0
M_t	Total magnetization at time t
M_{z_i}	Z-magnetization at time 0
M_x, M_y, M_z	Components of total magnetization in lab coordinate system
$M_{x'}$, $M_{y'}$, $M_{z'}$	Components of total magnetization in rotating coordinate system
M_∞	Equilibrium magnetization
n	Number of nuclei in the magnetically equivalent set
N	Number of attached nuclei
NT_1	Normalized T_1 relaxation time
$\overline{NT_1}$	Average of normalized T_1 relaxation times
$\vec{p}$	Nuclear angular momentum
p	Magnitude of nuclear angular momentum
r_i	Distance from relaxing nucleus to other spins i
r_{ij}	Distance between nuclei i and j
r_{CH}	Distance between carbon and proton nuclei
$r_{1'-4}$	Distance from proton 1' to proton 4

r_{IS}	Distance from nuclei I and S
$\overline{r_o}^2$	Mean squared end to end distance
R	Relaxation rate
R_c	Carbon relaxation rate
R_1^T	Total spin-lattice relaxation rate
S	Second order contributions to line width
S^2	Variance
t	Time
t_g	Trans-gauche conformation at C_6
t_p	Duration of pulse (pulse width)
T_1	Spin-lattice relaxation time
$T_{1_{DD}}$	Dipole-dipole spin lattice relaxation time
T_1^T	Measured spin-lattice relaxation time
T_2	Spin-spin relaxation time
x	Coordinate in lab coordinate system
x'	Coordinate in rotating coordinate system
y	Coordinate in lab coordinate system
y'	Coordinate in rotating coordinate system
Y_i	Function related to spherical harmonics
Y_i^*	Complex conjugate of Y_i
z	Coordinate in lab coordinate system
z'	Coordinate in rotating coordinate system
Z	$(M_\infty - M_z)/2\, M_\infty$
Å	Angstroms
α	Anomer with axial hydroxyl in C1 conformation
α	Pulse angle
β	Anomer with equatorial hydroxyl in C1 conformation

β	Linear regression constant
χ	Dihedral angle for C-O bond of hydroxyl group
δ	Chemical shift
δ_{ij}	Chemical shift between nuclei i and j
$\Delta\delta$	Change in chemical shift
γ	Gyromagnetic ratio
γ_H	Proton gyromagnetic ratio
γ_C	Carbon-13 magnetic ratio
γ_I	Gyromagnetic ratio of nucleus I
$H^{(1)}$ or H'	Hamiltonian for spin-spin coupling
η	Nuclear Overhauser enhancement
$\emptyset$	Dihedral angle for system $H_4'C_1'OC_4$
Φ	Generalized dihedral angle
χ	Dihedral angle for system $C_1'OC_4H_4$
Σ	Sum
σ	Shielding factor
τ	Bridge angle at glycosidic linkage
τ_c	Correlation time
τC_i	Rotational correlation time for vector to nucleus i
τ_{eff}	Effective rotational correlation time for isotropic rotation
τIS	Motional correlation time for internuclear vector IS
τ_R	Motional correlation time for C-H vector.
θ	Angle between internuclear vector IS and the z-axis.
μ	Nuclear magnetic moment
μ_o	Nuclear Bohr magneton

ν_a	Frequency of resonance a
ν_o	Irradiating frequency
$\nu_{1/2}$	Width at half maximum intensity
$\Delta\nu_{1/2}$	Change in $\nu_{1/2}$
w	Linear regression weighting factor
ω	Angular frequency
ω_I	Angular frequency for nucleus I

Note: Refer to keys in the various appendices for definition of specific symbols used within that appendix.

FOREWARD

The continuing interest in studying the structure and properties of cellu-
lose and other structural polysaccharides attests to the importance of these
materials both biologically and commercially. Controversies pertaining to the
parallel or antiparallel packing of cellulose chains, chain folding in native
cellulose, the mechanism of cellulose deposition into the fiber, and the
inherent flexibility of the β-1,4-glycosidic linkage still persist. Some of the
mystery about the structural polysaccharides, and cellulose in particular, stems
from the ability to study these materials under only limited conditions.
Cellulose has been studied under the constraints of the crystalline state, in
strongly reacting solvents, or as a derivative. Generally, these studies pro-
vide only limited information and must be extrapolated to answer the specific
questions posed. Alternatively, the glycosidic linkage has been modeled in an
attempt to predict some overall property of the material. Inevitably the
results are restricted to the limitations of the model and the simplifying
assumptions made therein. While much has been learned from the many studies to
date, an incomplete picture of the structural polysaccharides still exists at
all levels.

A complete understanding of the structural polysaccharides will require a
thorough knowledge of these materials over at least four levels of structure:
monomer composition and sequence, intermonomer linkage conformation and dynamics,
overall molecular conformation, and molecular association. This thesis is con-
cerned with only one of these areas, the conformation and dynamics of the inter-
monomer linkage. Thus, a more complete description of the β-1,4-linkage
prevalent in cellulose and the hemicelluloses, is the goal of this work.
Specifically, this study focuses on the properties of the linkage in the xylo-
and cello-oligosaccharides.

Recent innovations in NMR and vibrational spectroscopy provide an opportunity to study the conformation and dynamics of the glycosidic linkage directly. In this thesis these techniques have been used to investigate some of the factors that affect the β-1,4-linkage of the cello- and xylo-oligosaccharides and related compounds, in solution. Specifically, differences in the conformation and linkage dynamics that exist between those structures that do and do not contain a C_6 hydroxymethyl were studied. The major factors that lead to these differences, C_6 steric hindrance and intermonomer hydrogen bonding, were explored.

The thesis is organized into 5 sections. The first section discusses the importance and properties of the β-1,4-linked carbohydrates and the methods of conformational analysis that have been applied, including recent NMR work concerning the β-1,4-glycosidic linkage. Following this are the objectives of the thesis and an outline of the experimental approach. Studies concerning what the dynamics and conformation of the linkage are, are presented in the second section. This is followed in the third section by an investigation of the important factors that determine the characteristics of the linkage. This section opens with a general discussion of the factors that might be important, followed by a description of the work on the effects of C_6 steric hindrance and intermonomer hydrogen bonding. The final part contains a discussion of some solid state NMR work relating to the effects of the crystalline lattice on the linkage. Section IV contains the experimental program used to acquire and characterize the compounds investigated. Included are the detailed ^{13}C-NMR assignments of both the derivatives and final compounds. Section V contains a summary of the conclusions reached and suggestions for possible future work.

SUMMARY

This thesis has been concerned with comparison of the glycosidic linkage conformations of the cello- and xylo-oligosaccharides in solution. These compounds are oligomeric constituents of cellulose and the xylans - important structural polysaccharides common to the higher plants. They differ structurally only by a pendant C_6 hydroxymethylene group which is present on each ring of the cello-oligosaccharides.

The comparison has a two-fold purpose. First, it provides information which relates to the different observable properties of these two classes of compounds. Second, it provides an opportunity to determine the influence of the hydroxymethylene carbon at C_6 in determining linkage conformation and to compare its relative importance to other structural features such as the $O_3H...O_5'$ intramolecular hydrogen-bond, possible for both systems. This comparison was primarily based on the various parameters of nuclear magnetic resonance (NMR) spectroscopy which are sensitive to structure and conformation.

The first question to be answered concerned the dynamics of the linkage. Is the linkage rigid so that individual molecules remain in a single conformation or is it dynamic with molecules changing from one conformation to another? If the second and more likely possibility is true then at what rate does the transition occur? The answers to these questions are important because they determine if the observed conformation is a time average or if it represents a discrete conformation.

The NMR parameter most useful in determining rates of motion in oligomeric systems is the ^{13}C spin-lattice relaxation time ($^{13}C-T_1$). In this study it was observed that the terminal units of the tri- and tetrasaccharides relaxed more slowly that the internal units for both types of oligomers. This was interpreted as

evidence for a dynamic linkage with rates of reorientation that are fast on the NMR time scale.

Having determined that the linkage is dynamic the next question was what is the average linkage conformation and how does the conformation differ between the two types of species? For the β-1,4-glycosidic linkage the relevant parameters are the dihedral angles ϕ and χ, the bridge angle T, and the internuclear distance between $H_1{}'$ and H_4. Knowledge of ϕ and χ and either of the latter two parameters would completely define the linkage conformation. All of the above parameters are obtainable by NMR in principle.

In this work the emphasis has been on comparing the linkage conformation of the xylo- and cello-oligosaccharides rather than obtaining absolute values. The NMR parameters used were the ^{13}C - ^1H across linkage coupling constants to give χ, and ^1H - T_1 values to give the linkage interproton distances. The value of χ was found to be 25-60°C greater in xylobiose. Likewise, the $H_1{}'$-H_4 distance was determined to be 0.1-0.2 Å greater in xylobiose. These values show that the average linkage conformation is more staggered in the xylo-oligosaccharides. By inference it is expected that this occurs because of a wider range of linkage conformations for the xylose containing oligomers which could be associated with a more open and accessible linkage.

The next question to be answered is what factors determine the average linkage conformation in the two classes of compounds? The effect of the obvious factor, the C_6 hydroxymethyl group, was surveyed by comparing the chemical shifts of the linkage carbons in a number of model disaccharides. A correlation was found for the relative chemical shift of C_4 and the presence or absence of the pendant C_6 on the aglycone. From this evidence, and the observed differences between average linkage

conformations, it was concluded that the pendant C_6 is the dominant factor in deter-mining the linkage conformation. Other factors, such as the potential $O_3H...O_5$, intramolecular hydrogen bond are at best of secondary importance.

The presence or absence of the intramolecular hydrogen bond, though not a pri-mary factor in determining the conformation, still is an indication of the accessi-bility of the area near the linkage in the two types of compounds. In all probability the bond only exists because sterically restricted rotation at the linkage prevents the solvent molecules from interacting with the atoms participating in the intramolecular hydrogen bond. ^1H chemical shift temperature coefficients and $^1H-^1H$ coupling constants for the hydroxyl protons were used to identify and characterize the intramolecular hydrogen bond in DMSO-d_6 solution. It was found that a weak, but isolated, intramolecular hydrogen bond exists in the cello-oligosaccharides. In the xylo-oligosaccharides the hydrogen bond was found to be very weak and partially associated with a solvent molecule. Again, this was interpreted as a more open linkage in the xylose containing oligomers. A similar conclusion was reached by comparing the chemical shifts of xylobiose and cellobiose in the solvents DMSO-d_6 and D_2O.

The final factor considered in this study, which might affect the linkage con-formation, was the effect of the crystal lattice. By comparing the chemical shifts of solid and dissolved cellobiose and methyl β-cellobioside, it was observed that the linkage conformation is different in the two states. It is speculated that the difference is related to a relaxation of the bridge angle T of about 3° in solution.

The above questions concerning the dynamics, structure, and important factors that affect linkage conformation form the main topics of discussion in the thesis. Preceding this discussion is a section containing background information. The

final topic in the thesis is the assignment of the ^{13}C-NMR spectra of the cello- and xylo-oligosaccharide compounds. This work was a necessary prerequisite for much of the work on linkage dynamics and structure. The major approach used was comparison of spectral intensities from different members of the oligomeric series. Some comparison to model compounds was also utilized. This work is discussed in Section IV.

SECTION I - PROGRESS AND DIRECTION IN THE

STUDY OF THE β-1,4-GLYCOSIDIC LINKAGE

BACKGROUND

INTRODUCTION

The set of polysaccharides distinguished by the presence of the β-1,4-linkage contains some of the most important natural products in existence. This class of compounds includes many of the structural plant and animal organic polymers. Up to 84% of some wood species consists of polysaccharides containing the β-1,4-linkage (1). Also included among this class are numerous articles of commerce. This group includes, gums, pectic substances, and the modified cellulosics, used as resins and rheology modifiers in many industries. Of major commercial importance is cellulose, a primary material of the housing, textile, and paper industries. Because of the ubiquity and the importance of the β-1,4-linked polysaccharides to industry, agriculture, and biology, many studies have been made relating the properties of these materials to their structure. Despite this concentrated effort, much remains to be learned about what factors control their properties. Particularly lacking is our knowledge of factors other than the composition and the properties of the constituent monosaccharides.

Of critical importance to the paper industry is the chemistry of cellulose and the hemicelluloses. Cellulose is the β-1,4-linked homopolymer of glucose. It makes up approximately 43% of the dry extractive free wood in both softwoods and hardwoods. Hemicelluloses make up between 28 and 35% of the wood in these two groups, respectively (1). Much of this is represented by the β-1,4-linked glucomannans and xylans. These are nearly always found modified with side groups: 4-O-methyl glucuronic acids, galactose and arabinose sugars, and acetate groups. For each of these types of materials the β-1,4-linkage is of primary importance in determining its structure and properties.

The polysaccharides containing the β-1,4-linkage can be classified in another manner; into hexosans and pentosans. Hexosans are distinguished as predominantly containing 6 carbon monosaccharides, each of which possesses a pendant hydroxymethyl group (C_6) attached at C_5 in the pyranose form. Pentosans are the 5 carbon equivalent without a pendant C_6. Cellulose and the glucomannans are both hexosans, while xylan is a pentosan.

Figure 1 illustrates the primary structure of cellulose and xylan. The glycosidic linkage, outlined in bold print, is identical within 2 bonds of the linkage oxygen[*]. The glucomannans also contain the identical linkage structure within 2 bonds, although in this case inversion of configuration at C_2 of mannose probably impacts the linkage conformation.[**]
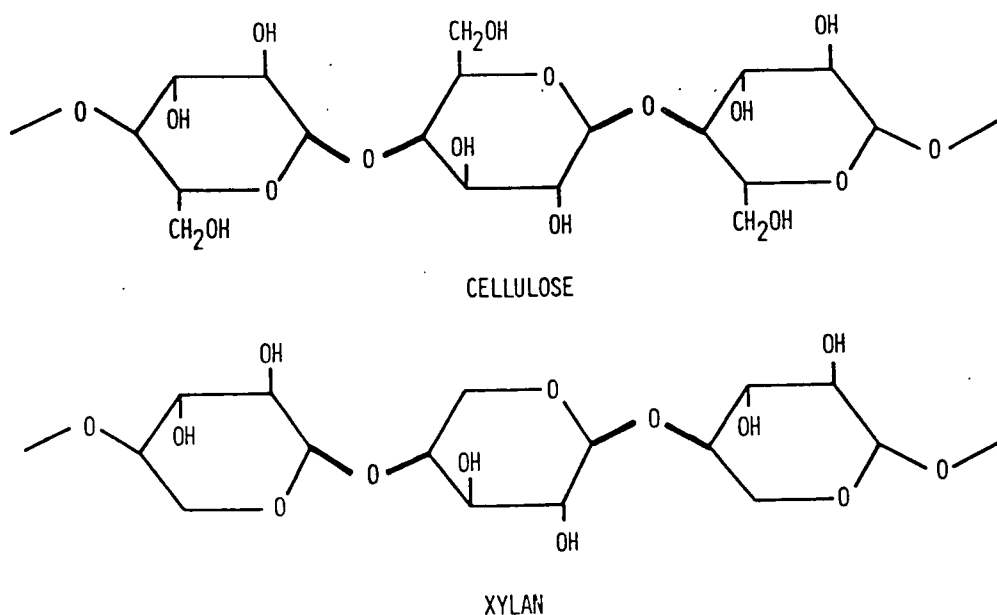
CELLULOSE

XYLAN

Figure 1. Cellulose and xylan primary structure. The β-1,4-linkages are highlighted.

---

[*] Referred to as isomorphic in later discussions.
[**]Galactouronogalactan, found in reaction wood, has a nonidentical β-1,4-linkage because of the inverted configuration at C_4 in galactose.

The properties of the β-1,4-linked hexosans and pentosans are to a large extent determined by the interactions at the linkage. Conformational analysis, using several techniques, has been performed on many of the β-1,4-linked polysaccharides or related models. Most of this work involves extrapolation, from polysaccharide dilute solution studies or theoretical model building, to characterize the allowed conformations and important interactions at the linkage. An exception are the x-ray diffraction studies which have determined the conformation of several β-1,4-linked disaccharides in the crystalline state (2,3,4,5). More recently, some work has appeared, using optical rotation (6) and $^{13}C-^{1}H$ coupling constants across the linkage (7,8,9), to determine the average conformation in solution of methyl β-cellobioside (MBC2).

This thesis describes application of several newly available NMR techniques to investigate the average conformation, and the factors which determine that conformation, for solutions of several β-1,4-linked oligosaccharides. In particular, the differences between the hexosans and pentosans are emphasized. It is hoped that an improved description of the factors that control the glycosidic linkage conformations will make it possible to better predict and control the properties of the parent polysaccharides.

Before continuing, a brief review of past conformational studies concerning the β-1,4-linked polysaccharides and related compounds will be given. This will be preceded by a brief discussion of the properties of the pertinent polysaccharides and the conformation of the constituent mono- and oligomeric species that make up these polysaccharides.

SURVEY OF PROPERTIES

Despite the common structure of the linkage, the properties of the different β-1,4-linked polysaccharides are considerably different. Cellulose is insoluble in water, dilute alkali, or dilute acid, at room temperature. It is commonly found as a semicrystalline solid of at least four distinct crystalline polymorphs. The cellooligosaccharides, the β-1,4-linked oligomer constituents of cellulose, rapidly become nearly insoluble beyond a chain length of 4 units (10). The properties of cellulose have been extensively studied, as evidenced by the large volume of literature concerning it (11).

In contrast to cellulose, xylan is well known for its ease of extraction in dilute alkali (12). While the acidic side groups are important in determining the solubility of xylan, the linkage also is certainly important. Evidence from intrinsic viscosity and light scattering measurements indicates that side groups, occurring at average intervals of 10 units in birch xylan, do not effect the overall conformation of the molecule in solution (13). Furthermore, the xylooligosaccharides are easily soluble up to at least a DP of 6 in water (14).

Most in-situ differences in reactivity, relative to cellulose, are related to increased accessibility, resulting from the substituted structure of native xylan. Removal of the acetate side groups will lead to an ordered structure for both xylan and glucomannan (1). Yundt prepared the first polymer single crystal from xylan in this manner (15). X-ray diffraction studies indicate that xylan crystallizes in a unit cell containing a three-fold helical axis along the chain direction, in contrast to the nearly two-fold symmetry in cellulose (16). This illustrates that both the side groups, and the characteristics of the linkage, are important in determining the properties of the xylans.

Intermediate in properties are the glucomannans. In situ they are closely associated with cellulose. They are soluble in moderate strength alkali when isolated as holocellulose ($\underline{1}$). Again, side groups contribute significantly to these properties. Isolated glucomannans are often crystalline. Intrinsic viscosity measurements show that the dissolved glucomannans are more similar in overall configuration to cellulose than to xylan. This is related to its isomorphic linkage* and the presence of a steric interaction between C_2 and C_6 which does not arise in xylan. Furthermore, the overall configuration was shown not to be dependent on the type or length of the side groups, within limits ($\underline{17}$).

A common property of the β-1,4-linked polysaccharides is a tendency for molecular association. This is a factor in many phenomena including the insolubility of cellulose in most solvents, the adsorption of glucomannan unto the cellulose fibers in kraft pulping ($\underline{1}$), formation of gel-like networks in the use of plant and bacterial gums ($\underline{18}$), and liquid crystal formation in certain cellulose derivatives ($\underline{19}$). This property also interferes with the study of many of these materials. For example, cellulose cannot be studied in theta solvents and determination of the molecular weight of xanthan gum ($\underline{20}$) and xylan ($\underline{13}$) is complicated by the inability to prevent interactions between molecules in solution. Molecular association results partly from the steric regularity imparted on the individual molecular chains by the properties of the β-1,4-linkage ($\underline{18}$).

CARBOHYDRATE CONFORMATIONAL ANALYSIS

Fundamental Considerations

The properties of cellulose and the hemicelluloses are closely related to their allowed conformations in the environment of interest. The concern of this thesis is

---

*Equivalent configuration.

an explanation of the factors that control conformation at the level of the individual β-1,4-linkage. Before proceeding, a brief review of carbohydrate conformational analysis will be given. No effort will be made to be exhaustive; the reader is referred to several recent publications for a more complete review (11,21-24).

Monosaccharides

Carbohydrate conformational analysis exists at several different levels extending from Fischer's elucidation of the stereochemistry of the simple sugars (25) to the configurational statistics of the polysaccharides in solution (26). Work at the monosaccharide level has been the starting point for most carbohydrate solution conformation work. The emphasis has been on which chair conformation is the most stable for a particular monosaccharide. Empirical rules for the determination of the most favored conformation have been established for the pyranose sugars (21). Further study has been concerned with how the chair form differs from ideality, the equilibria that exist between chair forms, and how the equilibria are affected by solvent, mutorotation, substitution, and temperature (23).

The chair conformation has long been accepted as the thermodynamically most stable form for the pyranose ring (23). Calculations estimating the relative free energies in water have been made by empirically considering nonbonded interaction energies and the anomeric effect. Aqueous solution conformations of the various aldopyranoses have been studied by NMR spectroscopy (23,27). The results agree favorably with the empirical calculations (28). Table I lists the favored conformations determined for each aldopyranose studied (23). The most stable conformation for the majority of the aldohexopyranoses is Cl. This is a result of relieving a syn-diaxial interaction, between the 5-(hydroxymethyl) group and the 1-hydroxy group, that would be present in the 1C conformer of the β-forms, and a favorable anomeric effect for the α-anomers (23).

TABLE I

FAVORED CONFORMATIONS OF D-ALDOPYRANOSES IN AQUEOUS SOLUTION[a]

| Aldopyranose | Conformation | | Estimated Free-Energies, kcal. mole^{-1} | |
	By Summation of Interaction Energies	By NMR Spectroscopy	C1	1C
α-D-Allose	C1	C1	3.9	5.35
β-D-Allose	C1	C1	2.95	6.05
α-D-Altrose	1C ⇄ C1	1C ⇄ C1	3.65	3.85
β-D-Altrose	C1	C1	3.35	5.35
α-D-Galactose	C1	C1	2.85	6.3
β-D-Galactose	C1	C1	2.5	7.75
α-D-Glucose	C1	C1	2.4	6.55
β-D-Glucose	C1	C1	2.05	8.0
α-D-Gulose	--	C1	4.0	4.75
β-D-Gulose	C1	C1	3.05	5.45
α-D-Idose	1C ⇄ C1	1C ⇄ C1	4.35	3.85
β-D-Idose	--	C1	4.05	5.35
α-D-Mannose	C1	C1	2.5	5.55
β-D-Mannose	C1	C1	2.95	7.65
α-D-Talose	C1	C1	3.55	5.9
β-D-Talose	--	C1	4.0	8.0
α-D-Arabinose	1C	1C	3.2	2.05
β-D-Arabinose	--	1C ⇄ C1	2.9	2.4
α-D-Lyxose	1C ⇄ C1	1C ⇄ C1	2.05	2.6
β-D-Lyxose	C1	C1	2.5	3.55
α-D-Ribose	1C ⇄ C1	1C ⇄ C1	3.45	3.55
β-D-Ribose	1C ⇄ C1	1C ⇄ C1	2.5	3.1
α-D-Xylose	C1	C1	1.95	3.6
β-D-Xylose	C1	C1	1.6	3.9

[a]From Reference (23).

The aldopentopyranoses and the ketopyranoses, which are not included in Table I, tend to favor either the C1 or 1C conformer; depending on the extent of diaxial interactions between the hydroxyl groups (23). Furanose forms have also been studied; they tend to rapidly interconvert between envelope and twist forms (21,23).[*]

Studies on the low temperatures NMR of β-D-ribopyranose tetraacetate in acetone-d$_6$ (29) have indicated that the aldo-pyranosides actually rapidly interconvert between the chair forms. At room temperature the time averaged

[*]The process is referred to as pseudorotation.

spectrum favors the major conformer. By comparing the coupling constants of the individual conformers at low temperature, with the time averaged coupling constants obtained at room temperature, an equilibrium constant for conformer interconversion can be obtained (23). In principle, chemical shift averaging could be used in an analogous way. In this case a similar study using chemical shifts was shown to give erratic results (29). Figure 2 shows the chair conformer equilibrium calculated for the eight aldopentopyranose tetraacetates (23). It can be noted that in every case, except α-D-xylopyranoside, there will be a significant amount of each chair form present.
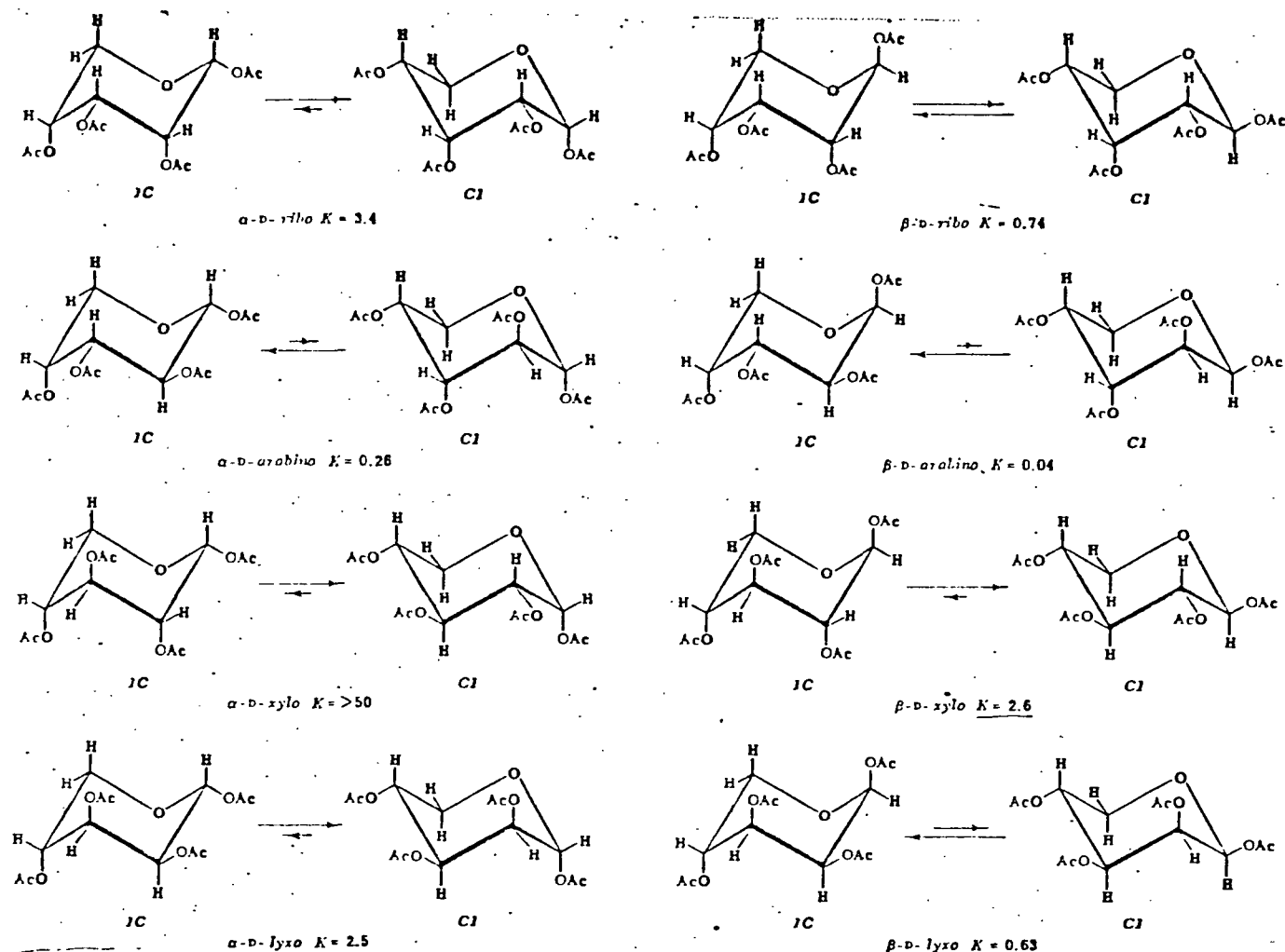

Figure 2. Chair conformer equilibria for the pentose acetates (23).

The equilibrium constant that describes the chair conformer equilibrium has been determined for various other substituted aldopyranosides and in different solvents. The equilibrium can be significantly altered by changing the substituents, particularly the aglycone (23). Solvent changes may also affect the equilibrium but usually to a smaller extent (23).

^{1}H-NMR studies indicate that the chair conformation is maintained in the glucose containing disaccharides; both α and β linked (1→1,1→2,1-3,1-4 and 1-6). This is based on the similarity, in both chemical shift and coupling constant, with the corresponding glucose (α or β) spectrum (24). This relationship is also found in the spectra of the common cellulose and amylose derivatives (24,30). Therefore, the Cl conformer is thought to exist as the predominant form for the glucopyranose ring in the oligo- and polysaccharides. This is also true in DMSO (31). Similar results would be expected for the xylo-series.

A related area, that has indirectly provided numerous observations concerning carbohydrate conformational effects, are the studies focusing on the complex formation between the sugars and electrolytes. Dorman and Roberts (32) have shown that the NMR spectra and the conformation of carbohydrates are affected by pH. Gaillard and Thompson (33) have shown that iodine complexes with the xylans in a manner similar to its effect on starch. Angyal and coworkers (34,35,36,37), in numerous publications, have used NMR to show that carbohydrates complex with some cations if their hydroxyl groups are arranged in an axial-equitorial-axial arrangement. They show that complex formation can cause a shift from one chair conformer to another. Atalla and Williams (38) have shown that ethylene glycol can also form a complex with divalent cations, illustrating that additional conformational factors, beyond those described by Angyal, may be involved in the carbohydrates.

Oligosaccharides

Monosaccharide conformational analysis predicts that C1 will be the dominant

ring structure for the β-1,4-linked oligomers of gluco-, xylo-, and mannopyranose.

Therefore, the most important undefined element in the conformation of these oligo-

mers, and the polysaccharides containing them, is the conformation of the glycosidic

linkage. Three parameters of fundamental importance are used to describe the

linkage conformation. Figure 3 depicts these: T is the $C_1'-O-C_4$ bridge angle, ϕ

is the torsional angle between $H_1-C_1'-O-C_4$, and χ is the torsional angle between

$H_4-C_4-O-C_1'$ (39). Along with the bond lengths and bond angles, these parameters

completely describe the linkage conformation.[*]
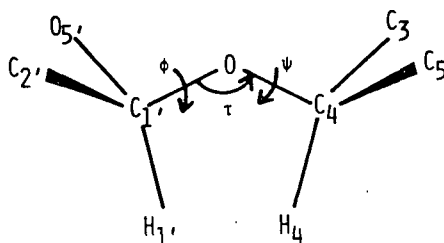
Figure 3.   The dihedral angles ϕ and χ, as well as the
bond angle T, of the β-1,4-glycosidic linkage.

Several factors combine to determine the allowed and preferred glycosidic

linkage conformations. These include nonbonded steric factors (Van der Waals

interactions), intramolecular (interresidue) hydrogen bonds, solvent modulated

dipole-dipole interactions, torsional strain, and the anomeric effect (39,40,41).[**]

Calculations considering steric interactions only indicate that cellobiose has

a highly restricted linkage (39). The rigidity associated with the β-1,4-linkage in

---

[*] An alternative approach, often used in polysaccharide configurational statistics,
  is to describe a virtual bond; the linear bond segment between successive linkage
  oxygens (40).
[**] While the mechanism is still under study, it is generally accepted that a σ-anti
  bonding orbital, intersects with the ring oxygen lone pair, to create the anomeric
  effect (41,42,42b). The specific influence on the rotamer states about the ano-
  meric bond (ϕ) to the aglycone, arising from the anomeric effect, is often
  referred to as the exo-anomeric effect (42).

cellulose and the related hexosans has been attributed to a steric interaction be-tween C_2 and the pendant C_6 on adjacent rings (17). An intramolecular hydrogen-bond ($O_3H\cdots O_5'$) is known to exist in crystalline cellobiose (2,3). Evidence also has been given for its existence in DMSO solution (43). Perez and Marchessault (41) have studied the x-ray derived structures for a number of 1,4-linked systems and have concluded that the exo-anomeric effect functions to restrict the allowed values of ϕ. Together, these factors combine to determine the allowed linkage confor-mations in the oligomer. In the polymer, long range effects must also be considered since their sum could act to modify the conformation at a specific linkage.

The most definitive work on oligosaccharide conformations has been done in the solid state where the technique of x-ray crystallography is applicable. The crystal structures of β-cellobiose (2,3), methyl β-cellobioside-methanol (4), α-lactose monohydrate (5), β-cellobiose octaacetate (44), β-xylobiose hexaacetate (45), β-cellotriose undecaacetate (46), and aldotriuronic acid trihydrate (47,48)[*] have all been determined. Unit cell dimensions have also been proposed for cellotetraose (49,50,51). The hexose containing sugars exhibit a limited range of linkage confor-mations (41). The angle ϕ varies only slightly, whereas χ adopts a wide range of values. Typical values are given in Table II.

The underivatized β-1,4-linked glucans all are observed to contain an intra-molecular hydrogen-bond from O_3H to O_5' ($O_3H\cdots O_5'$). Removal of this possibility in the acetylated derivatives only slightly affects ϕ but has a greater impact on χ.

Aldotriuronic acid, the 4-O-methyl glucuronic acid derivative of xylobiose substituted at 2', contains a lower value for the bridge valence angle (τ) than the

---

[*]O-(4-O-methyl-α-D-glucopyranosyluronic acid)-(1-2)-O-
  β-O-xylopyranosyl-(1-4)-D-xylopyranose trihydrate.

other oligomers in Table II. This was attributed to an absence of the backbone $O_3H\cdots O_5'$ intramolecular hydrogen-bond in its crystal structure. The authors (47,48) indicate that the linkage is more flexible in the xylobiose moiety because of the absence of the intramolecular hydrogen-bond.

TABLE II[a]

TYPICAL ϕ, χ, τ VALUES IN THE SOLID
β-1,4-LINKED SUGARS

Compound	ϕ[b]	χ[b]	τ	Reference
β-cellobiose	45	-14	116.1	(3)
Methyl β-cellobioside	31	-38	115.8	(4)
Cellobiose octaacetate	44	16	116.8	(44)
Cellotriose octaacetate (reducing-end)	46	12	115.5	(46)
Cellotriose octaacetate (non-reducing end)	24	-20	117.0	(46)
β-lactose monohydrate	27	-24	117.1	(5)[c]
β-xylobiose hexaacetate	20	-15	117.9	(45)
Aldotriuronic acid tri-hydrated [d]	30	35	113.8	(47)

[a]Part of table from Ref. (41).
[b](ϕ, χ)- 0 defined according to Ref. (41) and (45).
[c]Value calculated from crystal structure torsional angles assuming tetra-hedral symmetry.
[d]Referring to the β-1,4-linkage.

The first step in determining the solution conformation of the disaccharides has often been to assume that the solid state conformation is maintained. Jeffrey (52) points out that this is a reasonable assumption in polar solvents, in which intramolecular hydrogen-bonding to the solvent will replace that found in the crystal. Differences may arise if intermolecular hydrogen-bonds occur (or break) that are not in the crystal.

Many authors have employed computer modeling to predict the preferred conformation(s) in solution starting from the crystal structure atomic coordinates. Table III summarizes these results.

TABLE III

CALCULATED ϕ, χ VALUES INDICATING PREFERRED
CONFORMATIONS IN SOME β-1,4-LINKED DISACCHARIDES

Compound	ϕ	χ	%[a]	Reference
Cellobiose	+40	-8		(39)
	0	-33		
Cellobiose	51	0	60	(53)
	-10	-29	34	
Cellobiose	30	25	77	(54)
	30	180	20	
Xylobiose	63	25		(55)
	15	70		
	-18	-37		
Xylobiose	80	-8		(39)

[a]Percentage of molecules in this conformation based on
relative energies.

All of these calculations employ a force field that considers nonbonded interactions (39,55). Some utilize additional potential functions such as those associated with bond deformations, torsional deformations, valence angle deformations, and hydrogen bonding (53,54). In general, these results closely correspond to the crystal structure data.

Melberg and Rasmussen (53), in the most recent work, have used an energy minimization technique which uses no fixed internal coordinates. In cellobiose they find 6 local minima on the ϕ, χ map, of which 2 will be present in 94% of the molecules. They estimate that conversion between the 2 predominant conformations is fast on the NMR time scale. They further estimate that the glycosidic angle $C_1'-O_4-C_4$ (τ) is 113.4° for the conformation of lowest energy. This is much less than that obtained from the crystal structure. The saddle point conformation between the two lowest conformations is given as (ϕ, χ) = (26,-23). This should be

close to the average solution conformation which might be observed by NMR (21).
They calculate the average distance between H_1' and H_4 to be 2.28Å. The three least
populated conformations are near the antiparallel* conformation, $(\phi, \chi) = (\underline{30}, \underline{-180})$,
suggested by Rees and Smith, and are only of minor importance. All the major cello-
biose conformations have an $O_3 \ldots O_5'$ distance that would allow an intramolecular
hydrogen bond. If these results are extended to cellulose they predict that cellu-
lose should exist as an extended chain polymer in solution.

The calculations on xylobiose are generally not as complete as those for cello-
biose because of the need to use atomic coordinates from either xylose or cellobiose
as a starting point (39,55). The calculated energy minima suggest a more
staggered** conformation on average; a greater H_1' to H_4 distance is expected. The
lowest energy conformation predicted by Sandarajan and Rao, $(\phi, \chi) = (\underline{63,25})$,
corresponds to a 3-fold left-handed helical structure for xylan. The $O_3 \ldots O_5'$
distance is about 3.2Å so that any intramolecular hydrogen bond, if present at all,
is weak. These authors suggest that the helical structure in xylan is stabilized
mainly by Van der Waals forces. They suggest that the major difference between
xylobiose and cellobiose is that in the latter, the CH_2OH group restricts freedom of
rotation at the linkage.

Direct investigations of the solution properties of the cellooligosaccharides
have been made by Goring and coworkers (56,57). They measured intrinsic viscosities
and diffusion coefficients for the series up to cellohexaose. Using the
Einstein-Simha viscosity equation to calculate axial ratios they concluded that the

---

* The $C_1'-H_1'$ and C_4-H_4 vectors are nearly antiparallel as opposed to the more
  likely case, near $(\phi, \chi) = (0,0)$, where they are parallel. The $H_1' \ldots H_4$ distance
  is much greater for the antiparallel conformation.
** $C_1'-H_1'$ and C_4-H_4 vectors not near parallel.

cellooligosaccharides are fully extended in solution. They extended these measure-
ments from 25°-70°C and concluded that these molecules were extended over the entire
temperature range. They conclude that the unusually large decrease in intrinsic
viscosity with increasing temperature[*], observed both in the oligomers and in cellu-
lose and its derivatives, results from dehydration of the extended molecule.
However, others have suggested that the decrease in intrinsic viscosity is asso-
ciated with increased linkage flexibility, resulting in a reduction in overall
dimensions of the molecule toward a random coil (58,59).[**] In this regard, Swenson
(59) measured the intrinsic viscosity of low-DP cellulose fractions in cadoxene. He
found the cellulose chain to be inflexible up to DP 31.

Polysaccharide Conformational Analysis

Experimental studies, on both the macroscopic hydrodynamic properties of the
polysaccharides and direct x-ray diffraction measurements on the solid, when com-
bined with suitable theory, allow inferences to be made concerning the individual
linkage conformations. A related approach combines polymer configurational
statistics[***] with an estimate of the linkage conformation in an attempt to simu-
late the observed hydrodynamic parameters. After suitable refinements a good fit is
then used to justify the resulting estimate of the linkage conformation.

Each of these approaches requires an extrapolation over several orders of
magnitude, from polysaccharide to disaccharide to make definitive statements con-
cerning the linkage conformation in the smaller molecules. Goring (12) points out
that theories developed for random coiling high polymers are not readily applicable
to extrapolation into the low molecular weight region. Factors such as frictional

[*] Large negative temperature coefficients of the intrinsic viscosity are unusual
for polymers.
[**] The viscosity of xylan also has a large negative temperature dependence (59).
[***] In dealing with polymer conformations the terms configuration and conformation
are often used interchangeably in the literature.

effects with the solvent and higher energy local conformations can become important in the polymer. Brandt (60) proposed that high energy monosaccharide conformations, such as flexible boat and twist forms, are necessary to fully explain the negative coefficient of viscosity in cellulose. This illustrates the concept that the overall energetics of the polymer conformation can compensate for localized increases in energy. Therefore, measurements of overall polymer dimensions do not always relate directly to linkage flexibility.

A more specific problem occurs in the study of the hydrodynamics of cellulose. It is not possible to achieve a theta-solvent condition for cellulose in any of the common cellulose solvents. This severely limits the accuracy of any configurational analysis based on light scattering or intrinsic viscosity data. More accurate measurements are possible with cellulose derivatives soluble in organic solvents; but in this case, the factors affecting the linkage conformation are different by definition.

Despite the difficulties in relating the hydrodynamics of polysaccharides to local linkage conformations, much has been learned by studies of this type. Swenson and coworkers (17) have determined the Porod-Kratky persistence lengths[*] for cellulose, a number of cellulose derivatives and related polysaccharides, including; cellulose in cadoxene and alkaline ferric tartrate solvents, galactomannan triacetate from guar, glucomannan triacetate from orchid salep tubes, and xylans from spruce and birch. They used intrinsic viscosity data and molecular weight values from a number of different investigators. They conclude that the main chain configuration is similar for all of the hexosans and more rigid than for xylan. This is attributed to the nonbonded interaction between the C_2 and C_6 groups on adjacent

---

[*]The persistance length is defined as the mean length of projection of an infinitely long chain, along the direction of its first link (61).

rings of the hexosans. In a separate study (62), Swenson determined that cellulose

maintains an extended conformation in the DMSO/PF solvent system. In contrast,

earlier work by Lebel and Goring (13), using intrinsic viscosity data, suggested

that birch xylan is configurationally* similar to cellulose.

Extension of the conformational energy mapping approach to predict the observed

solution properties of a polysaccharide is possible using the techniques of sta-

tistical thermodynamics. Brandt and Goebel (63) give an excellent summary of the

techniques of the configurational statistics approach. As indicated previously,

Brandt and coworkers (60) have used this approach to reproduce the experimentally

determined $\overline{r}_o^2$ for cellulose chains using a small percentage of flexible monomer

units. A similar study by Yathindra and Rao (64) compares the calculated charac-

teristic ratios** (C_n) for xylan, mannan, and cellulose and shows that the C_n for

xylan is the least. This indicates that xylan is the more flexible polymer. They

calculate that cellulose does not become a random coil below a DP of 2000 (65).

The same authors (66) find that consideration of nonbonded interactions only, gives

good agreement between calculated C_n values and an experimentally derived value.

Morris and coworkers (67) modeled the behavior of β-1,4-linked polysaccharide

polyelectolytes at low ionic strength and came to similar conclusions. On the other

hand, Brandt and Goebel (63) warn against drawing conclusions concerning linkage

flexibility based on chain extensions or characteristic ratios. They calculate,

from the configurational entropy, that cellulose skeletal segments are slightly more

---

* Synonymous with conformation in this context.
**The characteristic ratio is often taken as a measure of relative linkage flexibi-

lity. It is given by $C_n = \dfrac{\langle r_o^2 \rangle}{nL^2}$ where $\langle r_o^2 \rangle$ is the mean squared end to end distance,

n is the number of monomer units (DP), and L is the length of the monomer. Theory

shows that C_n is a constant for random coils (61).

flexible than those of amylose, yet cellulose chains of equivalent length are 10 times more extended in solution because of the configurational differences of the two linkages.

X-ray measurements theoretically provide a direct means of investigating the linkage conformation as it exists in the polymer. In practice, the diffraction pattern does not contain sufficient information to compute a crystal structure without resorting to numerous assumptions. Enough information is available to compute the unit cell constants and symmetry. These values can be combined with model calculations to predict various parameters associated with the helical secondary structures commonly found in the β-1,4-linked polysaccharides. Marchessault and Settineri (16) used this approach to estimate the H_1´ to H_4 distance in xylan as 2.4Å. They predict that a weak intramolecular hydrogen bond exists between O_3 and O_5´. Recently, a set of detailed n, h* maps, relating dihedral angles to the x-ray derived helical parameters, have been published (68). Sarko and Woodcock (69) have extended the analysis one step further by calculating a minimum packing energy for a cellulose crystal consistent with the x-ray data. They conclude that cellulose I is a parallel chain structure with the O_6 atoms in the tg** conformation. Calculated ϕ, χ values of 25° and -26°, respectively, were given. These are similar to the values found in cellobiose (see Table II). They also predict that both O_3...O_5´ and O_2´... O_6 intramolecular hydrogen bonds exist in the crystal. The same type of analysis applied to the Cellulose II x-ray pattern leads to a prediction of antiparallel chain packing (70), a conclusion that is difficult to reconcile with the mechanisms of converting to the cellulose II structure.

The several approaches to polysaccharide conformational analysis mentioned, often have lead to conflicting results. Despite this, several conclusions have

---

*n is the number of residues per turn of the helix and h is the projection of the monomer length along the helical axis.
**This refers to the dihedral angles O-5,C-5,C-6,O-6, and C-4,C-5,C-6,O-6 tg refers to the trans-gauche conformation (41).

emerged. Persistence length determinations on cellulose derivatives and on cellulose in cadoxene have shown it to be a very rigid polymer. Measurements on other β-linked hexosans indicate that they have similar rigidities. Studies on xylan show that its persistence length is only about 1/2 that of cellulose indicating that it is a more flexible polymer (17). The flexibility of cellulose and amylose, on the other hand, are thought to be almost equal. The differences in their unperturbed dimensions are attributed to the geometrical differences of the linkage (63). The differences in flexibility between xylan and cellulose are thought by many to be a result of the absence of C_6 in the xylans.

One of the major inconsistencies remaining is the inability of most models to explain the large negative temperatue coefficient of intrinsic viscosity found for the β-1,4-linked polysaccharides in solution. This property is unique among high polymers. Three different explanations have been offered in the literature: Dehydration of the solvent (57), increased linkage flexibility (59), and increased flexibility combined with a small percentage of nonchair ring forms (63), as the temperature increases. Complete resolution of this problem will require an accurate appraisal of the factors that affect linkage flexibility. The importance of non-bonded interactions and the existence of intramolecular hydrogen bonds must be determined. Recent spectroscopic advances offer the possibility to directly answer some of these questions.

NEW TECHNIQUES FOR THE DIRECT OBSERVATION OF THE GLYCOSIDIC LINKAGE

Until recently no direct method has existed to explore the dynamic character of the glycosidic linkage in solution. Several relatively recent advances have occurred in both NMR and vibrational spectroscopy to reverse this situation. An improved theory relating optical rotation to linkage conformation also has been

developed (6,7). Of particular importance has been the development of Fourier transform NMR.

Because of recent instrumental and theoretical innovations, NMR spectroscopy is rapidly becoming the most powerful tool available for conformational and configurational analysis. A variety of parameters related to the phenomena of magnetic resonance exist to explore molecular structure. These include chemical shifts, coupling constants, relaxation times, nuclear Overhauser enhancements (NOE), and line shape. Each of these parameters is dependent on molecular structure as one of its contributing factors. All have been used for conformational and configurational analysis either in proton magnetic resonance (^{1}H-NMR) or carbon-13 magnetic resonance (^{13}C-NMR). A brief overview of the use of NMR for probing carbohydrate molecular structure will follow.

NMR has been used as a major tool in the study of oligosaccharide configurations as illustrated by these few examples. Kamerling and coworkers (72) have determined the configuration of the glycosidic linkage of several disaccharides by observing the chemical shift of the anomeric proton for their methylated derivatives. Minnikin (73) has done a similar study and has shown that the chemical shift of the anomeric proton, at the nonreducing end, is affected by the anomer present at the reducing end. More recently, Seymour and others (74,75,76) have extended this type of work toward polysaccharide sequence analysis.

Many other types of studies, beyond configurational studies, are approachable by means of NMR. Relaxation time measurements have been used to probe the interaction between cellulose and water in cellulose accessibility studies (77). Relaxation measurements have been used to study rotational barriers in hindered methyl groups in polycyclic compounds (78). This type of work should be directly

applicable to the study of the effect of 2-substitution on the linkage conformation in methyl glycosides. Recent work has appeared along these directions for methyl β-cellobioside.

Numerous conformational studies involving small molecules have been reported, usually with the employment of coupling constants in a Karplus type[*] relationship. Horton and coworkers (79) used vicinal and geminal ^{1}H-NMR coupling to study carbohydrate ring conformers. Several authors (80,81) have shown that ^{13}C-^{1}H coupling approximates a Karplus relationship and suggest that these measurements may be useful in studying torsional angles at a glycosidic linkage. Many other examples of the use of NMR in conformational analysis are available in the literature (82).

Several recent advancements in available NMR techniques have made these studies in conformational analysis more routine. Fourier-transform (FT) methods have replaced continuous wave (CW) methods as the most productive NMR technique. This allows a rapid pulsing of all the excitable frequencies at much higher power inputs. This replaces the much longer scanning of frequencies, at a very low power, employed in the CW method. After pulsing, a period of free-induction decay (f.i.d.) is monitored as a function of time. The final signal is a result of the exponential relaxation of each resonance back to its preexcitation distribution. The f.i.d. signal is then analyzed by Fourier analysis so that the typical NMR spectrum of absorbance vs. frequency is obtained. The time for pulsing and monitoring the signal is only a few seconds; thus allowing the process to be repeated many times in a signal averaging technique. This rapid acquisition of data at much higher powers drastically increases the sensitivity of the method (83,84,85). Additionally, it provides information concerning molecular dynamics that could not be obtained easily

---

[*]A relationship between the dihedral angle and the associated vicinal coupling constant. The relationship depends on the specific atomic system.

by older techniques (83). Most important, FT-NMR has made ^{13}C-NMR a routine labora-
tory procedure. This is most advantageous for the analysis of carbohydrates which
often have intractable ^{1}H-NMR spectra at low fields.

Improvements in magnetic field strength, brought on by the development of
superconducting magnets, have also lead to vast improvements in ^{1}H-NMR spectroscopy
of carbohydrates (86). The effect of higher field strength is to separate closely
spaced lines arising from different nuclei without altering the coupling constants.
This results in improved resolution and a more nearly first order spectrum which is
easier to analyze. DeBruyn and coworkers (87), using a 300 megahertz (MHz) spectro-
meter, have obtained and assigned the ^{1}H-NMR spectrum of the D-glucopyranosyl-(1-X)-
D-glucopyranoses (X=1,2,3,4, and 6). Hall (88), combining a high field instrument
with advanced pulse techniques, has correlated the ^{1}H-NMR and ^{13}C-NMR spectra of
cellobiose. This later technique, referred to as two-dimensional NMR (2D NMR)
offers exciting new possibilities for the complete analysis of complicated car-
bohydrate NMR spectra and the extraction of the wealth of conformational information
contained within (88b).

In recent years several specific examples have appeared of the use of ^{13}C-^{1}H
coupling to measure the glycosidic linkage angles of disaccharides. This work is an
extension of the early work by Lemieux (80,89). Lemieux used cyclonucleosides of
well defined geometry to develop a Karplus type relationship for a $^{3}J_{CNCH}$ system.[*]
He also found that $^{3}J_{COCH}$ systems fit closely on this curve. Recently a $^{3}J_{COCH}$
Karplus curve developed entirely from monosaccharide data was published (8,81).

^{13}C-^{1}H coupling constants across the glycosidic linkage have been published for

maltose, (7,90) cyclohexamylose (8,90) cellobiose (7), methyl β-cellobioside-d$_8$ (8),

---

[*]The notation $^{3}J_{CNCH}$ refers to a coupling over three bonds containing a carbon-
nitrogen-carbon-hydrogen system of atoms. The coupling is between the outer atoms
(C and H).

and for the corresponding peracetates (9,90,91). The $^3J_{COCH}$ for the peracetates of gentiobiose, nigerose, and laminarabiose have also been published (9,91). Values for maltose and the cellobiose related disaccharides are given in Table IV along with predicted ϕ, χ values. These can be compared to the solid state values given earlier (see Table II for references).

The values obtained have several sources of uncertainty but nevertheless fit reasonably well with data from the solid state. The value of χ is inherently easier to obtain because of the better resolution of the C_1' signal in the ^{13}C-NMR spectrum. From this data Perlin and colleagues (8,90) claim that methyl β-cellobioside does not change significantly from its solid state conformation but that maltose does. Furthermore, in comparing maltose to its acetate, they argue that the interresidue hydrogen bond is not a major factor in determining the maltose conformation in water. The use of ^{13}C-enriched material enables the sign of ϕ to be determined by employing ^{13}C-^{13}C vicinal coupling (9,91). This resulted in an excellent agreement with the χ value for cellobiose octaacetate in the solid state.

Rees (6,71,92) has developed a method to compare the solution conformation of a disaccharide with its crystal structure by comparing experimental optical rotations with those derived from the crystal structure data. He uses an additivity relationship to compute the calculated rotations. From this approach he concludes that maltose changes conformation upon dissolving in D_2O. Cellobiose appears to retain its crystal conformation in solution. Its conformation appears not to be greatly affected by temperature or solvent (6). This is in good agreement with conclusions drawn from the coupling constant data. From the same work methyl β-cellobioside is predicted to change conformation upon dissolving in D_2O. This is in contrast to the findings of Perlin.

TABLE IV

ϕ, ψ VALUES DERIVED FROM $^3J_{COCH}$ DATA[a]

	$^3J_{C_4OC_1'H_1'}$	ϕ	$^3J_{C_1'OC_4H_4}$	ψ	Reference
α,β-Cellobiose		± 60	1-2	± 60	(7)[b]
α-Cellobiose octaacetate			5.5	± 16	(9,91)
Methyl β-cellobioside-d8		± 25-30	4.3	± 25-30	(8)
Methyl β-cellobioside heptaacetate-d8		± 25-30	5.2	± 5-20	(8)
α,β-Maltose		< | 30 |	3-4	< | 30 |	(7)
Methyl β-maltoside		± 30-40	2.5	30-40	(90)
β-Maltose octaacetate		> | 40 |	2.5-4.0	< | 30 |	(90)
α-Maltose heptaacetate			3.8	- 20	(9,91)
		± 10-20	4.8	± 10-20	(8)
Cyclohexaamylose-d4		± 20	3.5[c]	± 20	(90)

[a]In Hertz.
[b]This was only an approximate value.
[c]The nondeuterated compound.

Another new approach that utilizes NMR to investigate glycosidic linkage conformations in solution involves the measurement of proton spin lattice relaxation times (^{1}H-T_1) of the linkage protons. The relaxation mechanism involves a $1/r_{ij}^6$ dependence where r_{ij} is the distances between the observed proton and all others in its vicinity. Hall and coworkers (93,94,95,96) have shown that the glycosidic linkage proton at C_1' of a disaccharide relaxes more rapidly than the equivalent anomeric proton on the reducing end. This results from an interring contribution from H_4 to its relaxation rate. Recently a value of 2.1 to 2.2 Å for the H_1' to H_4 distance in cellobiose was reported using this technique (53). The same authors report some ^{13}C-NMR T_1 measurements for methyl β-cellobioside that indicate that C_6 experiences a more hindered rotation than C_6'; suggesting that steric interactions with the linkage are important (97).

Recently a report has appeared that uses ^{13}C-NMR chemical shift data to estimate a χ value of 0-5° for chitobiose (β-1,4-linked disaccharide containing 2-amino 2-deoxy glucose) in D_2O (98). While this value is very speculative it illustrates the versatility of NMR in approaching problems concerning the conformation.

Yet another technique, useful for conformational analysis, is vibrational spectroscopy. Infrared spectroscopy of solid cellulose (99,100,101), xylan (102), and the corresponding oligosaccharides (99,100) have proven the existence of the $O_3\cdots O_5'$ intramolecular hydrogen bond in these molecules. The rapidly developing technique of laser Raman spectroscopy has significant advantages for this type of study.

The Raman effect is particularly sensitive to the carbohydrate skeletal vibrations. These vibrations are the most sensitive to conformational factors and least sensitive to intermolecular disturbances. Another advantage of both types of vibrational spectroscopy is the short time scale at which the scattering process occurs.

The time is short enough so that spectra averaged over all available conformations are not obtained. Rather, spectral contributions are observed from each conformer present. This theoretically allows the determination of preferred conformations in situations where one conformer is favored over another, as in a crystal. Finally, in Raman the solution spectra can easily be obtained in an aqueous environment since water has only a weak Raman signal.

A significant amount of effort has been spent on the assignment of the Raman bands to specific vibrational modes for the solid monosaccharides and inositols using normal coordinate analysis (NCA) (103,104,105,106,107). Extension of this work to cellulose has lead to the conclusion that cellulose I and II reside in different linkage conformations in the crystal and that this results in increased susceptability to hydrolysis for the latter (108,109).

The NCA method also has been applied in the analysis of the solid state Raman spectra of the cello- and xylo-oligosaccharides, maltose, and lactose (110,111). The region from 300-400 cm^{-1} is particularly sensitive to conformational affects. It was concluded that changes in the linkage conformation account for the spectral differences between methyl β-cellobioside and cellobiose and that these conformations are related to those present in cellulose I and II. Use of a structure derived from the cellobiose crystal gave a reasonable fit to the xylobiose spectrum suggesting that xylobiose has a similar crystal conformation.

Recently, studies have appeared giving the aqueous solution spectra of sucrose and glucose (112,113). Specific bands at 600 cm^{-1} and 374 cm^{-1} were assigned to the linkage O-C-O and C-O-C bending modes. Studies on the equivalent peaks for cellobiose, in different solvents, might be useful in detecting changes in linkage conformation. Changes in the frequency and intensity of the CH$_2$ bending vibration of glucose and sucrose, as a function of concentration, were interpreted in terms of

the interaction between sugar molecules and sugar and solute. This has utility in studying molecular association of carbohydrates in water and other solvents.

LITERATURE CITED

1. Rydholm, S. A., Pulping Processes. Interscience Publishers, New York, New York, 1965.

2. Brown, C. J., J. Chem. Soc. (A). 1966:927-932.

3. Chu, S. S. C. and Jeffrey, G. A., Acta Cryst. B24:830-8(1968).

4. Ham, J. T. and Williams, D. G., Acta Cryst. B26:1373-83(1970).

5. Fries, D. C., Rao, S. T., and Sundaralingham, M., Acta Cryst. B27:994-1005(1970).

6. Rees, D. A. and Thom, D., J. Chem. Soc.-Perkin II 1977:191-201.

7. Perlin, A. S., Cyr, N., Ritchie, R. G. S., and Parfondry, A., Carbohyd. Res. 37:C1-4(1974).

8. Hamer, G. K., Balza, F., Cyr, N., and Perlin, A. S., Can. J. Chem. 56:3109-16(1978).

9. Gagnaire, D. Y., Nardin, R., Taravel, F. R., and Vignon, M. R., Nouveau J. de Chimie 1:423-30(1977).

10. Ihnat, M. and Goring, D. A. I., Can. J. Chem. 45:2353-61(1967).

11. Bikales, N. M. and Segal, L., editors. Cellulose and cellulose derivatives, Parts IV and V, John Wiley & Sons, New York, New York, 1971.

12. LeBel, R. G., Goring, D. A. I., and Timell, T. E., J. Polymer Sci. Part C, 2:9-28(1963).

13. LeBel, R. G., and Goring, D. A. I., J. Polymer Sci. Part C, 2:29-48 (1963).

14. Whistler, R. L. and Tu, C. C., J. Am. Chem. Soc. 74:3609-12(1952).

15. Yundt, A. P., The preparation, characterization, and hydrolysis of crystalline and amorphous xylan. Doctoral Dissertation. The Institute of Paper Chemistry, Appleton, Wis, 1949.

16. Settineri, W. J. and Marchessault, R. H., J. Polymer Sci. Part C, 11:253-64(1965).

17. Swenson, H. A., Schmitt, C. A., and Thompson, N. S., J. Polymer Sci. Part C, 11:243-52(1965).

18. Dea, I. C. M., Morris, E. R., Rees, D. A., Welsh, E. J., Barnes, H. A., and Price, J., Carbohyd Res. 57:249-72(1977).

19. Werbowyj, R. S. and Gray, D. G., Mol. Cryst. Liq. Cryst. 34:97-103(1976).

20. Southwick, J. G., Lee, H., Jamieson, A. M., and Blackwell, J., Carbohyd. Res. 84:287-95(1980).

21. Stoddard, J. F., Stereochemistry of Carbohydrates, Wiley-Interscience, New York, New York, 1971.

22. Hall, L. D., Nuclear Magnetic Resonance. In Adv. in Carbohydrate Chem. 19:51-93(1964).

23. Durette, P. L. and Horton, D., Conformational analysis of sugars and their derivatives. In Adv. in Carbohydrate Chemistry and Biochemistry. 26:49-126(1971).

24. Rao, V. S. R., J. Indian Institute Science 56:253-89(1974).

25. Fischer, E., Ber Dtsch. Chem. Ges. 24:1836-45, 2683-7(1891).

26. Sundaralingham, M., Biopolymers 6:189-213(1968).

27. Lemieux, R. U. and Stevens, J. D., Can. J. Chem. 44:249-62(1966).

28. Angyal, S. J., Aust. J. Chem. 21:2737-46(1968).

29. Durette, P. L., Horton, D., and Bhaca, N. S., Carbohyd. Res. 10:565:77(1969).

30. Rao, V. S. R. and Foster, J. F., J. Phys. Chem. 69:636-40(1965).

31. Casu, B., Reggiani, M., Gallo, G. G. and Vigevani, A., Tetrahedron Letters 22:2253-9(1965).

32. Dorman, D. E. and Roberts, J. D., J. Am. Chem. Soc. 93:4463-72(1971).

33. Gaillard, B. D. E., and Thompson, N. S., Carbohyd. Res. 18:137-46(1971).

34. Angyal, S. J. and Evans, M. E., Carbohyd. Res. 25:1957-66(1972).

35. Angyal, S. J. and Evans, M. E., Carbohyd. Res. 25:43-8(1972).

36. Angyal, S. J. and Greeves, D., Aust. J. Chem. 29:1223-9(1976).

37. Angyal, S. J., Greeves, D., Littlemore, L., and Pickles, V. A., Aust. J. Chem. 29:1231-2137(1976).

38. Williams, R. M. and Atalla, R. H., J. Chem. Soc., Perkin II:1155-61(1975).

39. Rees, D. A. and Skerrett, R. J., Carbohyd. Res. 7:334-48(1968).

40. Whittington, S. G., Colstron. Pap. 307-22(1975).

41. Perez, S. and Marchessault, R. H., Carbohyd. Res. 65:114-20(1978).

42. Szarek, W. A. and Horton, D., Anomeric effect: origin and consequences, ACS Symposium Series 87, ACS, Washington, D. C., 1979.

42b. Lemieux, R. U. and Koto, S., Tetrahedron 30:1933-44(1974).

43. Casu, B., Reggiani, M., Gallo, G. G., and Vigevani, A., Tetrahedron 22:3061-83(1966).

44. Leung, F., Chanzy, H. D., Perez, S., and Marchessault, R. H., Can. J. Chem. 54:1365-71(1976).

45. Leung, F. and Marchessault, R. H., Can. J. Chem. 51:1215-22(1973).

46. Perez, S. and Brisse, F., Acta Cryst. B33:2578-84(1977).

47. Moran, R. A. and Richards, G. F., Acta Cryst. B29:2770-83(1973).

48. Moran, R. A. and Richards, G. F., Carbohyd. Res. 25:270-71(1972).

49. Poppleton, B. J. and Mathieson, A. McL., Nature 219:1046-8(1968).

50. Williams, D. G., J. of Polymer Sci. Part A-2, 8:637-42(1970).

51. Poppleton, B. J. and Gatehouse, B. M., J. Polym. Sci. Part A-2, 10:375-6(1972).

52. Jeffrey, G. A., In Carbohydrates in solution, ACS Symposium series 117:177-96(1973).

53. Melberg, S. and Rasmussen, K., Carbohyd. Res. 71:25-34(1979).

54. Rees, D. A. and Smith, P. J. C., J. Chem. Soc. Perkin II:836-40(1975).

55. Sundararajan, P. R. and Rao, V. S. R., Biopolymers 8:305-312(1969).

56. Ihnat, M. and Goring, D. A. I., Can. J. Chem. 45:2353-61(1967). (Repeat of Reference 10).

57. Ihnat, M. and Goring, D. A. I., Can. J. Chem. 45:2363-7(1967).

58. Flory, P. J., Spurr, O. K. and Carpenter, D. K., J. Polymer Sci. 27:231-40(1958).

59. Swenson, H. A., Tappi 56(2):106-10(1983).

60. Goebel, K. D., Harvie, C. E. and Brandt, D. A., Appl. Polymer Symp. 28:671-91(1976).

61. Brown, W. In Cellulose and cellulose derivatives, See Ref. 11.

62. Swenson, H. A., Appl. Polymer Symp. 28:945-52(1976).

63. Brandt, D. A. and Goebel, K. D., Marcromolecules 8:522-30(1975).

64. Yathindra, N. and Rao, V. S. R., Biopolymers 10:1891-1900(1971).

65. Yathindra, N. and Rao, V. S. R., Biopolymers 9:738-90(1970).

66. Yathindra, N. and Rao, V. S. R., Biopolymers 8:325-333(1969).

67. Morris, E. R., Rees, D. A., Welsh, E. J., Dunfield, L. G. and Whittington, S. G., J. Chem. Soc. Perkin II:793-800(1978).

68. Gagnaire, D., Perez, S. and Tran, V., Carbohyd. Res. 78:89-109(1980).

69. Woodcock, C. and Sarko, S., Macromolecules 13:1187-94(1980).

70. Stipanovic, A. J. and Sarko, A., Macromecules 9:851-63(1976).

71. Rees, D. A., J. Chem. Soc. (B) 877-84(1970).

72. Kamerling, J. P., De Bie, M. J. A. and Vliengenthart, J. F. G., Tetrahedron 28:3037-47(1972).

73. Minniken, D. E., Carbohyd. Res. 23:139-43(1972).

74. Seymour, F. R., Knapp, R. D., Chen, E. C. M., Jeanes, A. and Bishop, S. H., Carbohyd. Res. 75:275-94(1979).

75. Seymour, F. R., Polysaccharide branching and carbon-13 NMR. In ACS Symposium Series 103:27-61(1979).

76. Grasdalen, H. and Painter, T., Carbohyd. Res. 81:59-66(1980).

77. Froix, M. F. and Nelson, R., Macromolecules 8:726-30(1975).

78. Axelson, D. E. and Holloway, C. E., Can. J. Chem. 54:2820-6(1976).

79. Horton, D., Durette, P. L. and Wander, J. D., Ann. of the N.Y. Acad. of Sci. 222:884-914(1973).

80. Lemieux, R. U., Ann. of the N.Y. Acad. of Sci. 222:915-34(1973).

81. Schwarz, J. A., and Perlin, A. S., Can. J. Chem. 50:3667-76(1972).

82. Bovey, F. A., Polymer conformation and configuration, New York, New York, Academic Press, 1969.

83. Levy, G. C., Topics in carbon-13 NMR spectroscopy, Vol. 1, New York, New York, Wiley-Interscience, 1974.

84. Stothers, J. B., Carbon-13 NMR spectroscopy, New York, New York, Academic Press, 1972.

85. Hall, L. D., Preston, C. M. and Stevens, J. D., Carbohyd. Res. 41:41-52(1975).

86. Coxon, B., Proton magnetic resonance spectroscopy; Part I. In Adv. in Carbohydrate Chemistry and Biochemistry 27:112-25(1975).

87. De Bruyn, A., Anteunis, M. and Verhegge, G., Bull. Soc. Chim. Belg. 84:721-34(1975).

88. Hall, L. D., Morris, G. A., and Sukumar, S., J. Am. Chem. Soc. 102:1745-7(1980).

88b. Hall, L. D. and Morris, G. A., Carbohyd. Res. 82:175-84(1980).

89. Lemieux, R. U., Nagabhushen, T. L., and Paul, B., Can. J. Chem. 50:773-66(1972).

90. Parfondry, A., Cyr, N., and Perlin, A. S., Carbohyd. Res. 59:299-309(1977).

91. Excoffier, G., Gagnaire, D. Y., and Taravel, F. R., Carbohyd. Res. 56:229-38(1977).

92. Rees, D. A. and Skerrett, R. J., J. Chem. Soc. (B) 189-92(1970).

93. Berry, J. M., Hall, L. D., Welder, D. W., and Wong, K. F., Carbohyd. Res. 54:C22-24(1977).

94. Hall, L. D. and Preston, C. M., Carbohyd. Res. 29:522-4(1973).

95. Hall, L. D. and Hill, H. D. W., J. Am. Chem. Soc. 98:1269-70(1976).

96. Hall, L. D. and Preston, C. M., Carbohyd. Res. 49:3-11(1976).

97. Hall, L. D., Berry, J. M., and Wong, K. F., Carbohyd. Res. 56:C16-20(1977).

98. Tsukada, S. and Inoue, Y., Carbohyd. Res. 88:19-38(1981).

99. Michell, A. J., Aust. J. Chem. 23:833-8(1970).

100. Hatakeyama, H., Nagasaki, C. and Yurugi, T., Carbohyd. Res. 48:149-58(1976).

101. Blackwell, J. and Marchessault, R. H., Investigations of the structure of cellulose and its derivatives - infrared spectroscopy. In Bikales and Segals, Cellulose and Cellulose Derivatives, Part IV, p. 1-37, 1971.

102. Marchessault, R. H. and Liang, C. Y., J. Polymer Sci. 59:357-9(1962).

103. Pitzner, L. J., An investigation of the vibrational spectra of the 1,5 anhydropentitols. Doctoral Dissertation. The Institute of Paper Chemistry. Appleton, Wis., 1973.

104. Edwards, S. L., An investigation of the vibrational spectra of the pentose sugars. Doctoral Dissertation. The Institute of Paper Chemistry. Appleton, Wis., 1974.

105. Watson, G. M., Investigation of the vibrational spectra of the pentitols and erythritol. Doctoral Dissertation. The Institute of Paper Chemistry. Appleton, Wis., 1974.

106. Wells, H. A., An investigation of the vibrational spectra of glucose, galactose, and mannose. Doctoral dissertation. The Institute of Paper Chemistry. Appleton, Wis., 1976.

107. Williams, R. M., An investigation of the vibrational spectra of the inositols. Doctoral dissertation. The Institute of Paper Chemistry. Appleton, Wis., 1978.

108. Atalla, R. H. and Dimick, B. E., Carbohyd. Res. 39:C1-3(1975).

109. Atalla, R. H. Hydrolysis of cellulose: mechanisms of enzymatic and acid catalysis. In Adv. in Chemisry Series No. 181, R. D. Brown and L. J. Urasek, editors, ACS, 55-69(1979).

110. Carlson, K. P., An investigation of the vibrational spectra of the cellodextrins. Doctoral dissertation. The Institute of Paper Chemistry. Appleton, Wis., 1979.

111. Zhbankov, R. G. and Sivchik, V. V., Zh. Prikl. Spectra 27:853-9(1977). Translation T-1525 ABIPC.

112. Mathlouthi, M. and Luu, D. V., Carbohyd. Res. 81:203-12(1980).

113. Mathlouthi, M., Luu, C., Meffroy-Biget, A. M., and Luu, D. V., Carbohyd. Res. 81:213-23(1980).

APPROACH TO THE PROBLEM

OBJECTIVE

The objective of the thesis was to determine what differences exist in solution in the dynamics and conformation of the linkage in the β-1,4-linked oligosaccharides related to cellulose and xylan. The relative importance of factors, such as steric hindrance and intramolecular hydrogen-bonding ($O_3 \cdots O_5'$) on linkage flexibility, could then be assessed. In this way a more thorough understanding of the relationship between linkage structure and solution properties might be developed.

HYPOTHESIS

The structural difference between the aldopentoses and the aldohexoses – the hydroxymethyl group at C_6 – is of primary importance to the phenomenological differences observed for the β-1,4-linked oligo- and polysaccharides containing these monomers. Other backbone structural factors, such as intramolecular hydrogen bonding, are of secondary importance. The combination of these factors leads to measurable differences in linkage conformation which can be related to differences in solution characteristics and reactivity. Thus, the xylo-oligosaccharides are more soluble and exhibit faster rates of hydrolysis, relative to the cello-oligosaccharides, because of a more flexible and accessible glycosidic linkage, due to the absence of C_6.

APPROACH

While the hypothesis developed above could be inferred from the available evidence, these effects had not been measured directly. NMR spectroscopy can

theoretically be applied to the direct observation of these effects. The approach taken was to apply several recent developments in NMR to explore and compare the glycosidic linkage conformation and dynamics in the xylo- and cello-oligosaccharides in solution.

The glycosidic linkage angles ϕ and χ can be estimated for the disaccharides using $^{13}C-^1H$ vicinal coupling across the linkage. The relative H_1' to H_4 distance can be determined using proton spin lattice ($^1H-T_1$) relaxation measurements. Investigation of the dynamics of the linkage in the tri- and tetrasaccharides can be accomplished using carbon-13 spin lattice relaxation ($^{13}C-T_1$) measurements. This requires complete assignment of the ^{13}C-NMR spectra.

Interpretation of the results, in view of the known structures of the compounds investigated, can then be used to assess the importance of the available steric constraints on linkage conformation. This can be supplemented by correlating the relative chemical shifts for the linkage carbons for a series of disaccharides to the presence or absence of a reducing-end C_6. Determination of the existence of intramolecular hydrogen-bonds in DMSO-d_6 solutions of both oligomer series can be made using pertinent monosaccharide and disaccharide derivatives as models. Using the appropriate models the presence of these interresidue bonds can be determined by means of the effect of temperature on hydroxyl proton chemical shifts and by interpretation of vicinal coupling with the ring protons. Solid state NMR can be employed to study the effect of lattice forces on linkage conformation for cellulose, cellobiose, and methyl β-cellobioside. The relative importance of these factors on linkage conformation and flexibility may then be assessed.

SECTION II – DYNAMICS AND CONFORMATION OF THE

β-1,4-GLYCOSIDIC LINKAGE

EVIDENCE FROM CARBON-13 SPIN-LATTICE RELAXATION TIMES FOR
A DYNAMIC LINKAGE IN THE CELLO- AND XYLO-OLIGOSACCHARIDES

INTRODUCTION

Linear polysaccharides and their derivatives containing the β-1,4-linkage (e.g. cellulose, mannan) are found to exist in rigid "rod-like" conformations with persistence lengths extending up to 10-13 monomer units (1,2,3). Conformational energy calculations using disaccharide models, the so-called φ, χ map, predict that the number of allowed conformations are severely restricted in cellulose (4,5). The restriction is eased in the pentosans (xylan) because of the absence of the C_6 hydroxymethyl groups (6,7). The crystalline xylans are thought to form three-fold helices (8), in comparison to the near two-fold helices in crystalline cellulose (9). On this basis, the linkage in a β-1,4-linked xylan is said to be more flexible than that in cellulose, meaning that it can adopt a more staggered conformation[*].

X-ray diffraction studies on the crystalline polysaccharides, as well as hydrodynamic studies on dissolved polysaccharides, give indications of the types of linkage conformations possible along the chain but do not indicate if the geometry of a particular linkage is dynamic or static. In cellobiose, the solution conformation, determined by optical rotation (10), has been shown to be the same as in the solid state.[**] While it most certainly is true that a dynamic state exists in which the solution conformations oscillate in the neighborhood of the known solid state φ, χ values, no direct experimental verification of this exists. Rees and Thom (12)

---

[*] The linkage protons ($H_1{}'$ and H_4) are twisted further away from their minimum separation value which defines a two-fold helix.
[**]The solution conformation of methyl β-cellobioside determined by NMR (11) and optical rotation is similar to that of crystalline cellobiose.

have shown that the optical rotation is a function of both temperature and solvent for cellobiose solutions indicating that multiple linkage conformations are possible.

Melberg and Rasmussen (13) have recently used an empirical force-field calculation to evaluate the possible linkage conformations for cellobiose. They find that six local minima are present; two of these in 94% of the isolated molecules. A major advantage of their approach is that the most favorable path for conformational conversion can be investigated. An energy barrier of approximately 0.7 Kcal/mole is found between the two most populated minima. From this value they predict that the rate of conformational conversion is fast on the NMR time scale and similar to the overall rate of molecular tumbling.

For rapidly rotating molecules theory predicts that if internal reorientations are faster than overall molecular tumbling, then, in principle it is possible to detect the internal motions by relaxation studies (14). Woessner's (15) model of internal reorientation, superimposed on overall molecular tumbling, predicts an increase in the relaxation time of the reorienting group in the case of intramolecular dipole-dipole relaxation. This suggests that the measurement of ^{13}C spin-lattice (T_1) relaxation times might provide a method to prove the dynamics of the β-1,4 glycosidic linkage.

Allerhand and Doddrell (16) have used ^{13}C-T_1 measurements to separate and assign the terminal galactose signals from those of the adjacent internal galactose in stachyose. In this case the galactose units are joined by a flexible α-1,6-linkage. Neszmelyi, et al. (17) calculated the average NT_1,[*] (designated $\overline{NT_1}$)

---

[*]Average of the normalized spin-lattice relaxation times for each carbon within the pyranose ring system. Normalization refers to multiplying each carbon by the number of attached protons. In an isotropically rotating system all normalized relaxation times will be equal within experimental error for each monomer unit.

values for the carbons of each monosaccharide unit in the steroidal oligosaccharide k-strophanoside. They showed that the average value increases toward the terminal β-1,6-linked glucose unit. This allowed them to sequence the sugar units of the oligosaccharide side chain. Czarniecki and Thornton (18) investigated the β-1,4-linkage in the oligosaccharide, N-acetylneuraminyl lactose* as well as in lactose. They showed that the terminal glucose carbons in NeuNAc-Lac have a larger value of $\overline{NT_1}$ indicating that, in this case of a nonlinear oligosaccharide, the linkage is flexible. No difference was observed in the two rings of lactose.

In another type of study using relaxation times, Froix and Nelson (19) have measured the ^1H-T_1 and T_2 as a function of temperature for a dry cellulose. The data suggest that in amorphous cellulose there is a partially hindered rotation at the linkage.

The present paper uses ^{13}C-T_1 measurements to verify experimentally that the geometry of the β-1,4-linkage is dynamic in the aqueous cello- and xylo-oligosaccharides. Measurements were made up to the tetramer.

EXPERIMENTAL

Commercial samples of glucose, xylose, and cellobiose were used. The cellotriose, cellotetraose, xylotriose, and xylotetraose were obtained from other laboratories (see Appendix X). Their ^{13}C-NMR spectra have been previously assigned (20). Xylobiose was synthesized from a Koenigs-Knoer condensation of 2,3,4 tri-O-acetyl-α-D-xylopyranosyl bromide and benzyl 2,3 anhydro-β-D-ribopyranoside, as described elsewhere (21). Prior to use, an aqueous solution of the xylobiose was treated with IR-120 ion-exchange resin (acid form) to minimize the effects of

*NeuNAc-Lac [NeuNAc-(2-3)-β-galactose-(1-4)-glucose]

paramagnetic impurities. Samples were dissolved in NMR tubes (5 mm) using D_2O (99.8%) without prior exchange. The concentrations used were dictated by considerations of solubility and available spectrometer time. The different concentrations represent no difficulty since internal comparison of relaxation times was the goal.

^{13}C-NMR spectra were measured at 25.05 MHz on a Jeol FX-100 FT-NMR spectrometer equipped with a Jeol sample temperature controller ($\pm$ 1°C) and an internal deuterium lock. Spectra were obtained under conditions of complete proton noise decoupling. Relaxation measurements were by the inversion-recovery (IR) method ([22]) over a 2000 Hz band width with 8K data points collected in the time domain. The pulse repetition time (T) was 4-5 T_1 over 10 t values $(180°-t-90°-T)_x$.

T_1 values were determined using an exponentially weighted least squares fit to the semilogarithmic plot of ln $((M_0-M_t)/2 M_0)^*$ against t. Peak heights were used for M_0 and M_t. Individual T_1 values for specific carbons were rejected for use in the calculation of $\overline{NT_1}$ values for the following reasons:

a) large variance from the least squares fit;
b) nonideal behavior determined by a large residual magnetization of the least squares value for $(M_0-M_t)/2M_0$ at t = 0;
c) coincidence with a larger signal, except in the cases resulting from coincidence of both α- and β-anomer signals for carbons remote from the anomeric carbon, or coincidence of equivalent carbons on the internal rings of the tetrasaccharides.

All samples were run at least twice. Comparison of T_1 values between individual rings in a single oligosaccharide was consistent in all cases, though the results varied by 10-15% on an absolute basis (up to 40% for cellotetraose) for different runs.

NOE (nuclear Overhauser enhancement) values were obtained by the gated decoupling technique ([23]). The values were consistent with those in the literature,

---

$^*M_0$ is the equilibrium z-magnetization, M_t the z-magnetization after time interval t. Refer to Appendix I for a more detailed discussion.

(<u>24</u>) indicating that only the dipole-dipole mechanism for relaxation is operative. NOE determinations were not made on the trisaccharides and above because of low signal to noise.

Raman spectra were obtained at room temperature on a Jobin Yvon Ramonor HG2S spectrometer interfaced to a Tracor Northern TN-1500 computer. The spectrometer operated in the single monochromater mode; signal averaging was employed. The exciting source was the 4880 Å line of a Coherent Radiation Laboratories model 52 - Argon ion laser. The solid state NMR spectra were obtained on a modified Jeol FX-60Q spectrometer equipped with CP/MAS capabilities (see Acknowledgments).

RESULTS

T_1 Analysis

For molecules the size of small oligosaccharides the predominant relaxation mechanism is expected to result from ^{13}C-^1H dipole-dipole (DD) interactions. For protonated carbons of isotropically rotating molecules the spin-lattice relaxation time (DD) is given by (<u>14</u>)

$$1/T_1^{DD} = N \, \hbar^2 \, \gamma_H^2 \, \gamma_C^2 \, r_{CH}^{-6} \tau_R \tag{1}$$

where r_{CH} is the carbon-hydrogen internuclear distance, N the number of directly attached protons, and τ_R the motional correlation time of the C-H vector. For equal internuclear distances this reduces to

$$NT_1^{DD} \propto 1/\tau_R, \tag{2}$$

so that longer NT_1^{DD} values indicate shorter correlation times, i.e., more rapid motion (<u>18</u>). In the limit of isotropic rotation the NT_1^{DD} will be constant. For anisotropic rotation more than one correlation time is required, complicating the analysis (<u>15</u>).

Berry et al. (24) have shown that methyl β-cellobioside (MBC2), by virtue of nearly equivalent NT_1 values (except-OCH_3), appears to tumble isotropically because all of the C-H bonds are axially oriented. In contrast, α-lactose and methyl β-lactoside (MBL), each of which contains at least one equatorially disposed C-H bond, exhibit anisotropic tumbling. From these results they suggest that all oligomers of β-D-glucopyranose (or by inference, any monosaccharide with every C-H vector oriented in the same direction) will exhibit apparent isotropic tumbling despite an anisotropic rotation about the principal axis of the molecule. These authors further show that the α- and β-anomers of lactose tumble at similar rates.

In the case of apparent isotropic rotation, comparison of $\overline{NT}_1$ values should provide a sensitive indicator of the relative mobilities of the individual monosaccharide units of a linear oligosaccharide. As previously discussed, if the rate of internal reorientation is faster than the rate of overall tumbling, then, the $\overline{NT}_1$ values for the individual monosaccharides should reflect their difference in mobilities (14). Berry et al. (24) observed no difference in the $\overline{NT}_1$ values for the two rings of lactose, MBC2, or MBL implying that the rings tumble at the same effective rate in these disaccharides. They suggest that the linkage is rigid. However, the possibility exists that the internal reorientation is not observed because of the nearly equal size of the individual monomer units. If the internal reorientation is fast then in the trisaccharides the terminal units should appear to rotate relative to the rest of the molecule since the latter possess more inertia. Therefore, the $\overline{NT}_1$ values should differ between the terminal and central rings. The difference between $\overline{NT}_1$ values should increase in the tetrasaccharide since the difference in inertia should increase between the terminal unit and the remainder of the molecule.

Mono- and Disaccharides

Table I contains the results of the T_1 determinations for the mono- and β-1,4-linked disaccharides of glucose and xylose. Since the results were obtained

TABLE I

^{13}C SPIN-LATTICE RELAXATION TIMES (SEC) FOR GLUCO- AND
XYLO- MONO- AND β-1,4-LINKED DISACCHARIDES IN D_2O

Resonance[a]

Compound[b](%,W/V)	1'	2'	3'	4'	5'	6'	1	2	3	4	5	6	$\overline{NT_1}$[f]
Glucose (26.8)							0.80	0.74	0.71	0.71	0.71	0.41	0.75±0.05
							0.69	0.71	0.72	–	0.74	0.40	0.74±0.04
Xylose (25.8)							1.56	1.56	1.60	1.64	0.88[c]		1.59±0.04
							1.48	1.69	1.57	1.65	0.78		1.62±0.06
Cellobiose (10.1)	0.47	0.47	0.47	0.46	0.47	0.24	0.49	0.54	0.50	0.45	0.45	0.24	0.485±0.03
							0.39	0.48	0.49	0.46	0.49	0.24	0.48±0.01
													0.47±0.01(NR)
Xylobiose (13.5)	0.78	0.75	0.80	0.79	0.42		0.87	0.74[d]	0.70[d]	0.79	0.40		0.78±0.06
							0.61	0.78[e]	0.83[e]	0.80	0.34		0.79±0.03
													0.79±0.03(NR)

[a]β-anomer given on the top row. The assignments were based on the literature; gluclose (26), xylose (26), cellobiose (26), and xylobiose (20).

[b]Conditions: gluclose: 32°C. 350 pulses; xylose: 36°C, 300 pulses; cellobiose: 31.5°C, 1750 pulses; xylobiose: 36°C, 1750 pulses.

[c]Large variance from the semilogarithmic least squares plot, value not used in $\overline{NT_1}$ calculation.

[d]These values can be interchanged.

[e]These values can be interchanged.

[f]To get the $\overline{NT_1}$ value multiply by 2 for C_5 and C_6 xylose and glucose, respectively. The α-C_1 value is not used to calculate $\overline{NT_1}$. Values given are plus or minus 1 standard deviation. NR refers to the non-reducing end-group for both anomers combined.

under conditions of unequal microviscosities[*] no attempt at comparison of the abso-
lute values is made. In agreement with earlier work (24,25) the NT_1 values for
individual carbons are nearly equal within experimental error for each anomer, indi-
cating isotropic and equal rates of rotation. Slight deviations from this generali-
zation are found; for example, the NT_1 value for C_6 in glucose is high as a result
of either a very slight rotation about the C_5-C_6 bond or a slight error in the T_1
value.

The disaccharides also appear to rotate isotropically as evidenced by the close
agreement of the $\overline{NT}_1$ values for each ring. The T_1 value for α-C_1 is an exception;
in all cases it is significantly less than the average NT_1 value of the remaining
carbons. This has been related to the direction of the α-C_1 C-H bond which lies
nearly parallel to the long axis of the molecule (24).

Tri- and Tetrasaccharides

The resolution of individual signals for carbons on the terminal units of the
oligosaccharides is a necessary condition for the comparison of $\overline{NT}_1$ values. Heyraud
et al. (27) have reported 22 separate signals in the ^{13}C-NMR spectra of both
cellotriose and cellotetraose. Spectra of comparable resolution were obtained in
this study allowing the determination of individual T_1 values for most of the ter-
minal carbons. Figure 1 gives the spectrum of xylotetraose; 18 separate peaks are
observed illustrating the resolution of the terminal carbon resonances in the
xylooligosaccharides. Assignments for the cello- and xylooligosaccharide spectra
are based on variations in peak height and were given elsewhere (20).

Figures 2, 3, and 4 summarize the T_1 data for the β-1,4-linked tri- and tetra-
saccharides of glucose and xylose. Using the existing literature assignments

---

[*]Differences in molecular environment which will affect the overall rate of tumbling
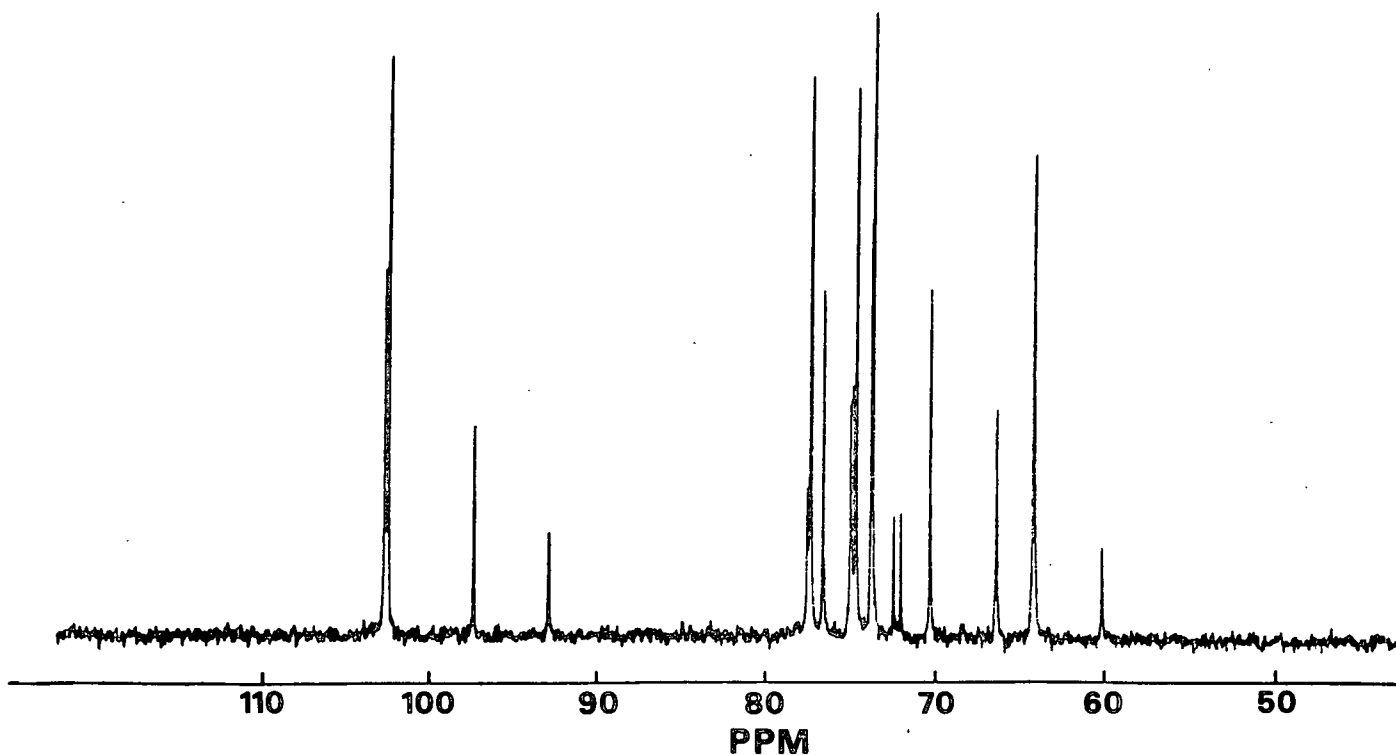and hence the absolute value of T_1.

XYLOTETRAOSE

Figure 1. ^{13}C-NMR spectrum of xylotetraose in D_2O (6.2%, w/v) at 35°C using a 2000 Hz spectrum width, 8192 K data points in the time domain, 5000 pulses, and 2.1 sec between pulses. Assignments(20): 102.7 ppm (1"), 102.5 (1",1'), 97.3 (β-1), 92.8 (α-1), 77.4 (α-4), 77.2 (4", 4', β-4), 76.4 3"'), 74.8 (β-2)*, 74.7 (β-3)*, 74.5 (3", 3'), 73.6 (2"'), 73.5 (2", 2'), 72.2 (α-2)*, 71.8 (α-3)*, 70.0 (4"'), 66.1 (5"'), 63.8 (5", β-5), and 59.7 (α-5) where * indicates the assignment is speculative.
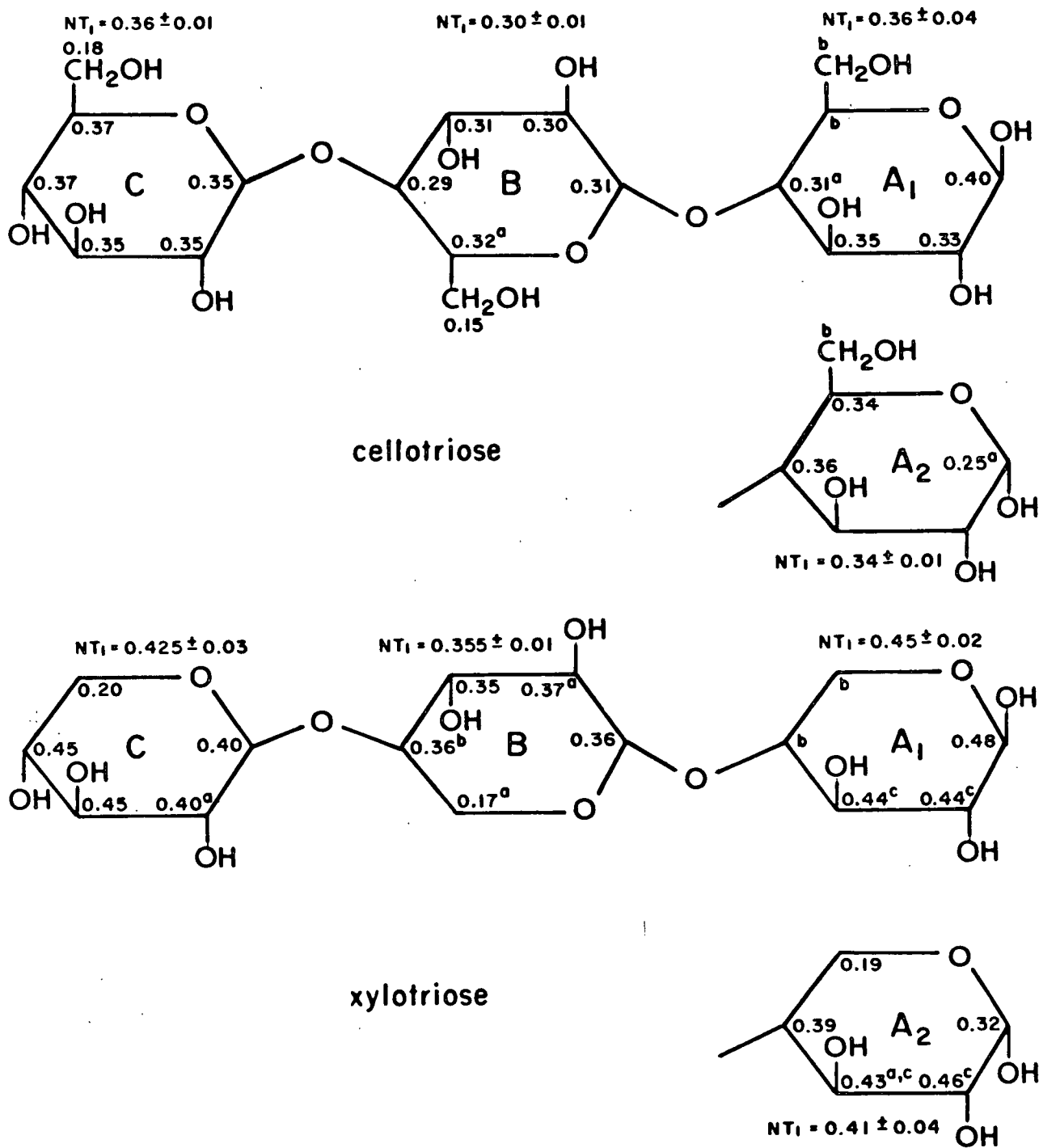
Figure 2. ^{13}C-T_1 (sec) for cellotriose (10.78% (w/v), 36°1 C) and xylotriose (11.71% (w/v), 34.5°C) in D_2O using 3500 pulses and a delay of 2.1 sec, for cellotriose, and 6750 pulses and a delay of 2.2 sec for xylotriose. Each data set represents 10 data points. Legend a: value not used in the calculation of $\overline{NT_1}$ because of a possible error in the T_1 value due to either poor S/N or close proximity to another peak (see text for explanation for α-C_1 signal). b: coincident with a larger signal. c: assignments can be reversed with nearby signal.

$NT_1 = 0.46 \pm 0.01$

$NT_1 = 0.39 \pm 0.02$

$NT_1 = 0.49 \pm 0.07$

OH

0.20
CH_2OH

OH

b
CH_2OH

OH
0.45 0.45

0.37

0.39 0.42

OH
0.39 0.42

OH
b

OH
0.45 0.45
OH
D
0.46
0.46
0.46

0.37^c
OH
C
0.41

OH
0.36^c
B
0.41

0.38^a
OH
A$_1$
0.47

0.47

0.39

0.37

0.44 0.57

CH_2OH
0.22

OH

CH_2OH
0.20

OH

b
CH_2OH

0.53^a

0.41
OH
A$_2$
0.32^a

OH

0.50 0.50

cellotetraose

$NT_1 = 0.47 \pm 0.05$ OH

Figure 3. $^{13}C-T_1$ (sec) for cellotetraose (7.75%, w/v) in D_2O at 59°C using 4500 pulses, a delay of 3.0 sec between pulse sequences, and 10 data points. Legend a: value not used in the calculation of $\overline{NT_1}$ because of larger error in the T_1 value due to poor S/N or close proximity to a larger peak (see text for explanation for $\alpha-C_1$ signal). b: coincident with a larger signal. c: assignments can be reversed, the average of the two values used to calculate $\overline{NT_1}$ for rings B and C.

NT₁ = 0.42 ± 0.01

NT₁ = 0.31 ± 0.01

NT₁ = 0.42 ± 0.02

xylotetraose

NT₁ = 0.41 ± 0.04
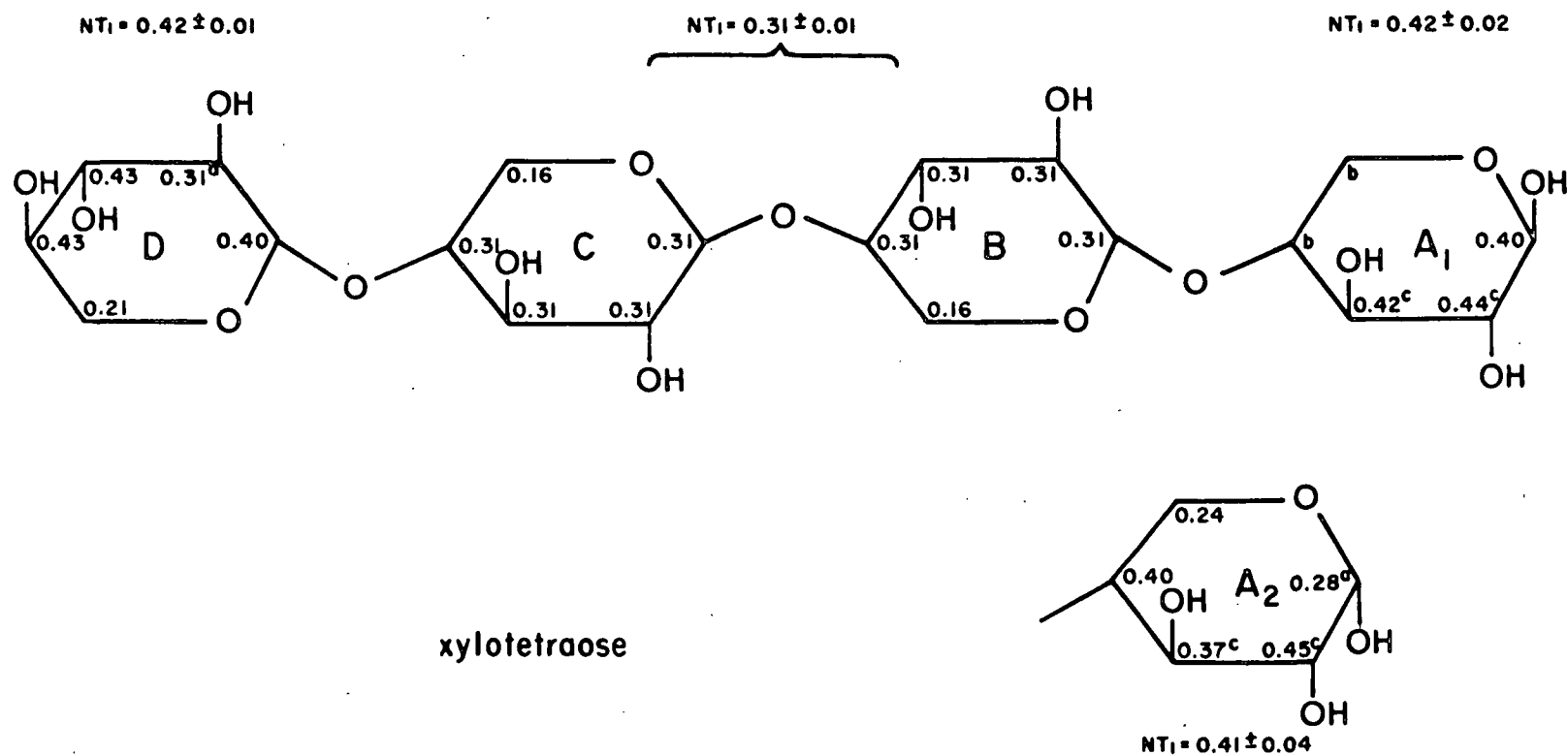
Figure 4. ^{13}C-T_1 (sec) for xylotetraose (6.20%, w/v) in D_2O at 35°C using 4000 pulses, a delay of 2.1 sec between pulse sequences, and 10 data points. Legend a: value not used in the calculation of $\overline{NT}_1$ because the close proximity to a larger peak (see text for explanation for α-C_1 signal), b: coincident with a larger signal, c: assignments can be reversed with nearby signal.

results in a separation of T_1 values so that the $\overline{NT}_1$ of the terminal units are significantly different. Clearly, in view of the previous discussion concerning internal reorientation, the β-1,4-linkage appears to possess a rapid internal motion at the linkage.

It should be emphasized that in the tetrasaccharides most of the internal carbons are coincident so that specific T_1 values for individual carbons are not available. Nevertheless, on the basis of the disaccharide results it is expected that the T_1 values are nearly identical for equivalent carbons on the internal rings, and therefore, the use of the values given here to calculate $\overline{NT}_1$ seems reasonable.

Corroborating Evidence

Comparison of the Raman spectra of crystalline and dissolved (10.1%, W/V; D_2O) cellobiose reveals a significant increase in the width at half height (whh) for the low frequency peaks common to each spectrum. For example, the peak at 570 cm^{-1} has a whh of 10-13 cm^{-1} in the solid in comparison to 52 cm^{-1} in D_2O. Comparable results are observed for xylobiose. This region of the spectrum is comprised of conformationally dependent heavy atom bending motions (29). In contrast to NMR, the time scale of the Raman effect is very short, so that, instead of a time average, all conformations are represented in the spectrum. Thus from the Raman data, it can be inferred that many conformations are present in cellobiose or xylobiose in solution, however, it cannot be concluded directly from this data alone that there is a shift between conformations for individual molecules.

Similar conclusions can be reached by inference from comparisons of the solid-state NMR spectra of amorphous cellulose and crystalline cellulose I (30) with the DMSO-d_6 solution spectrum of a low-DP cellulose (20). Comparisons show that in the

spectrum of amorphous cellulose the individual signals are significantly shifted and broadened[*] from those in the cellulose I spectrum. Additionally, the solution spectrum closely parallels that of amorphous cellulose. The peak broadening in the amorphous cellulose spectrum probably results from a large number of linkage conformations, whereas, the crystalline cellulose spectrum represents at most a few linkage conformations (30). The similarity of the solution and amorphous cellulose spectra suggests that the large number of linkage conformations persists in solution.

DISCUSSION

Most previous data, as well as the new evidence from solid-state NMR and Raman spectroscopy, point toward the existence of multiple linkage conformations in the dissolved cello- and xylooligosaccharides. The average of these conformations is expected to be similar to the solid-state conformation determined by diffraction methods (10,11). Nevertheless, experimental verification that the β-1,4-linkage exists in a dynamic state has not been previously obtained. The evidence given in the present paper rectifies this; it is clearly shown by the nonequivalence of $\overline{NT}_1$ values that the tri- and tetrasaccharides possess a dynamic linkage. Furthermore, it can be inferred that all β-1,4-linkages in solubilized oligomers are dynamic including that of the disaccharide in which the $\overline{NT}_1$ values are equivalent. Clearly, conformational studies based on NMR must be discussed in terms of time average conformations.

Comparisons of the data in Fig. 2-4 suggest several significant points. First, the difference in $\overline{NT}_1$ values between terminal and internal monomer units increases slightly with increasing chain length. This parallels the difference in size of the

[*]Particularly the C_4 signal.

two segments of the molecule, namely, the terminal unit and the remainder of the

molecule. Secondly, even though the xylooligosaccharides are expected to be more

flexible, the difference of $\overline{NT_1}$ values between the terminal and internal units is

similar to that of the cellooligosaccharides. Apparently the rate of reorientation

is similar in the two oligosaccharide series despite the probability that the xylo-

oligosaccharides possess more available linkage conformations (4,6). Finally, the

rate of reorientation must be as fast or faster than the rate of overall anisotropic

rotation. This is in agreement with the theoretical prediction of Melberg and

Rasmussen (13).

Other additional features of the data can also be discussed. First, there is

no difference between the $\overline{NT_1}$ values for the two terminal units, with respect to the

internal units, within experimental error. This is despite the expectation that the

linkages have different properties in the cellooligosaccharides (31,32). This is a

further indication that the rate of internal reorientation is similar at all

β-1,4-linkages. It is possible that slight differences are masked because of the

larger errors associated with the smaller signals of the reducing-end and the T_1

measurement in general (~10%).

Secondly, the anisotropic character of the overall rotation is observed in all

the compounds studied with two or more monomer units. In each case the NT_1 value of

$\alpha-C_1$ is significantly less than the value found for any other carbon in the mole-

cule. This is related to the nearly parallel orientation of the $\alpha-C_1$ C-H bond with

respect to the long axis of the molecule, the major rotational axis (24).

Finally, a note of caution should be made toward the over-extension of the use

of the present T_1 data in calculating correlation times. The applicability of the

Woessner[*] treatment (15) is questionable in the present case (33). Furthermore, molecules of this size that interact strongly with both the solvent and other like molecules possess correlation times near the extreme narrowing limit. Therefore, the simplifying assumptions often employed become tenuous (34). While the increase in $\overline{NT_1}$ values for the higher-oligosaccharide terminal units supports the contention that T_R is less than the Larmor frequency we were unable to confirm this with accurate NOE measurements. The relatively low concentrations used resulted in low signal to noise producing large errors in the measurement. Larger sample sizes could alleviate this problem.

In conclusion the following points can be made concerning the β-1,4-linkage in the linear oligosaccharides of glucose and xylose: a) the linkage is dynamic with an internal reorientation as fast as or faster than the overall rate of tumbling, b) the internal reorientation is superimposed on an anisotropic rotation about the long axis of the molecule, and c) discussions of the NMR-determined linkage conformation in solution should be in terms of a time average.

---

[*]Method of calculating correlation times from relaxation rates by assuming a specific model for molecular reorientation. Refer to Appendix I for details.

LITERATURE CITED

1. Swenson, H. A., Tappi 56:106-10(1973).

2. Ihnat, M. and Goring, D. A. I., Can. J. Chem. 45:2353-61(1967).

3. Foweraker, A. R. and Jennings, B. R., Polymer 17:508-10(1976).

4. Rees, D. A. and Skerrett, R. J., Carbohyd. Res. 7:334-48(1968).

5. Sathyanarayama, B. K. and Rao, V. S. R., Biopolymers 10:1605-15(1971).

6. Sundararajan, P. R. and Rao, V. S. R., Biopolymers 8:305-12(1969).

7. Swenson, H. A., Schmitt, C. A., and Thompson, N. S., J. Polymer Sci. Part C, 11:253-64(1965).

8. Settineri, W. J. and Marchessault, R. H., J. Polymer Sci. Part C, 11:253-64(1965).

9. Sarko, A. and Muggli, R., Macromolecules 7:486-94(1974).

10. Rees, D. A., J. Chem. Soc. (B):877-84(1970).

11. Hamer, G. K., Balza, F., Cyr, N., and Perlin, A. S., Can. J. Chem. 56:3109-16(1978).

12. Rees, D. A. and Thom, D., J. Chem. Soc. Perkin II:191-201(1977).

13. Melberg, S. and Rasmussen, K., Carbohyd. Res. 71:25-34(1979).

14. Allerhand, A., Doddrell, D., and Komoroski, R., J. Chem. Phys. 55:189-98(1971).

15. Woessner, D. E., J. Chem. Phys. 42:1855-9(1965).

16. Allerhand, A. and Doddrell, D. A., J. Am. Chem. Soc. 93:2777-9(1971).

17. Neszmelyi, A., Tori, K., and Lucas, G., J. Chem. Soc. Chem. Comm. 1977:613-4.

18. Czarniecki, M. F. and Thornton, E. R., J. Am. Chem. Soc. 99:8279-82(1977).

19. Froix, M. F. and Nelson, R., Macromolecules 9:726-30(1975).

20. Gast, J. C., Atalla, R. H., and McKelvey, R. D., Carbohyd. Res. 84:137-46(1980).

21. Kidd, J. R. and Schroeder, L. R., In preparation.

22. Vold, R. L., Waugh, J. S., Klein, M. P., and Phelps, D. E., J. Chem. Phys. 48:3831-2(1968).

23. Freeman, R., Hill, H. D. W., and Kaptien, R., J. Magn. Res. 7:327-9(1972).

24. Berry, J. M., Hall, L. D., and Wong, K. F., Carbohyd. Res. 56:C16-20(1977).

25. Bock, K. and Hall, L. D., Carbohyd. Res. 40:C3-5(1975).

26. Pfeffer, P. E., Valentine, K. M., and Parrish, F. W., J. Am. Chem. Soc. 101:1265-74(1979).

27. Heyraud, A., Rinaudo, M., Vignon, M., and Vincendon, M., Biopolymers 18:167-85(1979).

28. Carlson, K. P., An investigation of the vibrational spectra of the cellodextrins. Doctoral dissertation. The Institute of Paper Chemistry, Appleton, Wis, 1978.

29. Sivchik, V. V. and Zhharkov, R. G., Zh. Prikl. Spektr. 27:853-9(1977).

30. Atalla, R. H., Gast, J. C., Sindorf, D. W., Bartuska, V. J., and Maciel, G. E., J. Amer. Chem. Soc. 102:3249-51(1980).

31. Feather, M. S. and Harris, J. F., J. Am. Chem. Soc. 89:5661-4(1967).

32. Gast, J. C. and Atalla, R. H., In preparation.

33. Stilbs, P. and Moseley, M. E., J. Magn. Res. 33:209-10(1979).

34. Doddrell, D., Glushko, V., and Allerhand, A., J. Chem. Phys. 56:3683-9(1972).

A COMPARISON, USING NMR, OF THE LINKAGE CONFORMATIONS
OF XYLOBIOSE AND CELLOBIOSE IN SOLUTION

INTRODUCTION

The properties of the β-1,4-linked hemicelluloses, cellulosics, and related

oligomers, are significantly related to the conformation of the linkage.

Hydrodynamic studies on the dissolved polymer (1,2,3), x-ray diffraction analyses on

the solid (4,5), and model studies that account for various interactions at the

linkage (6,7), all have been utilized to investigate its conformation and inherent

flexibility. Cellulose[*] and xylan[**] are characterized as rodlike random coiling

polymers with an extremely limited set of available conformations (6,7). The xylose

containing structures are generally considered to have a linkage of greater confor-

mational freedom (flexibility), by virtue of the absence of the C_6 hydroxymethyl

group (2,8), though no direct evidence pertaining to this has been published.

Figure 1 depicts the structures and dihedral angle nomenclature for the model

disaccharides β-xylobiose (1) and β-cellobiose (2). The only primary structural

difference is the absence of C_6 in both rings of xylobiose. A complete confor-

mational description results from a knowledge of the linkage dihedral angles, $\emptyset$ and

χ, and the bridge oxygen bond angle T; assuming that the geometry of the monomer

units is invariant.[***]

---

[*] Defined here as the poly-(β-1,4-glucopyranose); an aldohexopyranose. Cellobiose
will be used as a model for the cellulose linkage throughout much of this report.
[**] Defined here as the linear poly-(β-1,4-xylopyranose); an aldopentopyranose. In
nature, xylan is always found with some type of side chain. Xylobiose
(β-1,4-xylopyranosyl-D-xylopyranose) is used as a representative model.
[***] This is a reasonable assumption on the "average" since the monomers are known to
be predominantly in the Cl conformation (9). Local ring "breathing" motions are
of course occurring all the time but they are minor so that the average can be
accepted as the Cl conformation.
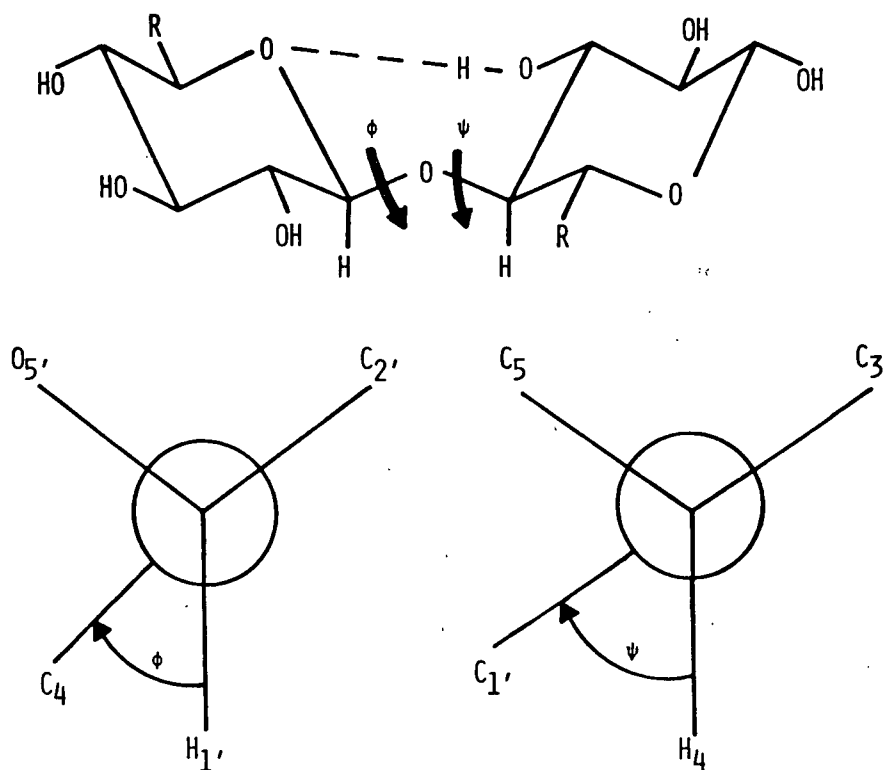
Figure 1. Depiction of β-xylobiose (R=H) and β-cellobiose
(R-CH$_2$OH) with the linkage angles φ, χ, and T
defined. The φ, χ value of 0° is assigned to the
conformation in which the $C_{1'}$-$H_{1'}$ bond is cis to
O_4-C_4 and C_4-H_4 is cis to $C_1{'}$-$O_1{'}$ for φ and χ,
respectively. The positive sense of φ and χ are
defined by the Newman projections shown in the
figure. This definition is the same as that used
by Leung and Marchessault (3,10). The angle T is
the $C_1{'}$-O_4-C_4 bond angle. The nonreducing end
is primed to facilitate discussions concerning
the higher oligomers.

Most previous efforts to determine the conformation of the β-1,4-linkage have

involved a large extrapolation from the physical property measured or have been

limited by the assumptions of the model. The exceptions are the x-ray diffraction

studies of several related disaccharides (11,12,13,14) and the corresponding aceta-

tes (10,15). The results for the angles φ χ, and T are summarized in Table I.

These studies, in terms of determining the preferred linkage conformation, are

limited by the constraints of lattice packing.

TABLE I

ϕ, χ DETERMINED BY X-RAY DIFFRACTION METHODS

	ϕ	χ	T	Reference
β-Cellobiose	45	-14	116.1	(11)
Methyl β-cellobioside	25	-38	115.8	(12)
β-Lactose monohydrate	27	-24	117.1	(13)
Aldotriuronic acid trihydrate[a]	30	35	113.8	(14)
Cellobiose octa-acetate	44	16	116.8	(15)
β-Xylobiose hexa-acetate	20	-15	117.9	(10)

[a] O-(4-O-methyl-α-D-glucopyranosyluronic acid)-(1-2)-O-β-D-xylopyranosyl-(1-4)-xylopyranose trihydrate. Values given are for the β-1,4-linkage.

Until recently, the relatively unconstrained conformation of the linkage in solution has not been amenable to study by direct methods[*]. A less constrained linkage is of more general utility in understanding the local factors that affect its conformation and flexibility. The properties of the dissolved sugars are also more directly related to their rheology and organic chemistry.

Recent developments in NMR have made it possible to investigate directly the linkage conformation of model oligosaccharides in solution. Perlin and coworkers (16,17,18,19) have measured interresidue $^{13}C-^{1}H$ coupling in maltose, cyclohexamylose, cellobiose (2), methyl β-cellobioside-d_8 (7), and their peracetates. Three-bond coupling constants across the linkage $^{3}J(C_1H_i)$ were determined by analysis of the fine structure of the proton coupled ^{13}C-NMR spectrum at natural abundance. Values of 4.2 Hz and 4.3 Hz were obtained for $^{3}J(C_4H_1')$ and $^{3}J(C_1'H_4)$ in compound 7,

[*] In a polar medium, such as water, the dissolved state is still far from ideal. In the concentrated solutions often required for spectroscopic studies association may play a role in determining the linkage conformation. In dilute solution the solvent can have a significant effect.

respectively. These values translate to (ϕ, χ) values of ±25-$30°$ each, using an empirical Karplus relationship for the ^3J C-O-C-H system. Other workers have measured both interresidue ^{13}C-^1H and ^{13}C-^{13}C coupling using ^{13}C selective enrichment for cellobiose octaacetate (20,21). A value of 5.5 Hz was obtained for $^3J(C_1\text{-}H_4)$. This was related to a χ value of about $+15°$. The ^{13}C-^{13}C coupling constant, $^3J(C_1\text{-}C_5)$, allowed a determination of the sign.

Hall and coworkers (21,22) have taken an alternate approach which measures the proton to proton $(H_1\text{-}H_4)$ interresidue distance. They measure the contribution of H_4 to the spin-lattice relaxation time (T_1) of H_1. Since the relaxation of H_1 is dominated by the dipole-dipole mechanism a $1/r_{ij}^6$ dependence exists. A value of 2.1-2.2Å for the H_1 to H_4 distance in cellobiose has been reported (7).*

In this work we use the NMR techniques discussed above to compare the β-1,4-linkage conformation in solution of the xylose- and glucose-containing disaccharides. Emphasis is given to the disaccharides 1 and 2 and their methyl-β-glycosides in D_2O. Some measurements were also obtained in DMSO-d_6. Raney nickel deuteration of the hydroxylated skeletal carbons was used in some instances to simplify the spectrum (18,24,25). This approach has the potential to allow a direct determination of the effect of the C_6 hydroxymethyl group on the linkage structure.

RESULTS AND DISCUSSION

Proton Spin Lattice Relaxation to Measure the H_1 to H_4 Distance

As a means of comparing the H_1 to H_4 distance in the disaccharides 1 and 2 their proton spin-lattice $(^1H$-$T_1)$ relaxation times were measured. ^1H-T_1 relaxation times were measured on degassed samples to ensure that relaxation due to oxygen, which is paramagnetic, did not occur (26). The temperature was controlled by means

---

*This value was reported as a personal communication in Ref. (7).

of a Jeol Model NM 5471 temperature controller. Samples were run consecutively to provide a check and to guard against fluctuations in temperature.

Table II gives the average ^{1}H-T_1 relaxation times for the anomeric protons of 1 and 2 at several temperatures. Values are averaged over all samples and include both resonances of the nonreducing end doublet (H_1') and in most cases the upfield resonance of the reducing end doublet (H_1). At the lower temperatures the downfield peak of the H_1 signal is partially obscured by the solvent (HOD) peak. The T_1 values for the individual lines are given in Appendix 3. Figures 2 and 3 show the 31°C ^{1}H-NMR spectra of 1 and 2, respectively. The anomeric protons are labeled.

TABLE II

AVERAGE ^{1}H-T_1 VALUES FOR CELLOBIOSE AND XYLOBIOSE

| Compound | Temp. (°C) | T_1(sec) | | R_1'/R_1[b] |
		H_1	H_1'	
Cellobiose (2)	31	0.83	0.38	2.2
	74.5	2.14	1.14	1.9
c	33	0.84	0.36	2.3
c	42	1.1	0.52	2.1
Xylobiose (1)[a]	31	1.12	0.61	1.8
	74.5	2.42	1.57	1.5

[a]Combines two determinations at 31°C and 31.5°C, respectively.
[b]R_1'/R_1 is the ratio of the relaxation rates (R). $R = 1/T_1$.
[c]Values from Hall (22).

In the disaccharides, the proton spin lattice relaxation should result entirely from the dipole-dipole (DD) mechanism (22,27). Equation 1 gives the relaxation time for dipole-dipole relaxation[*] (22).

___
[*]Refer to Appendix I for details.
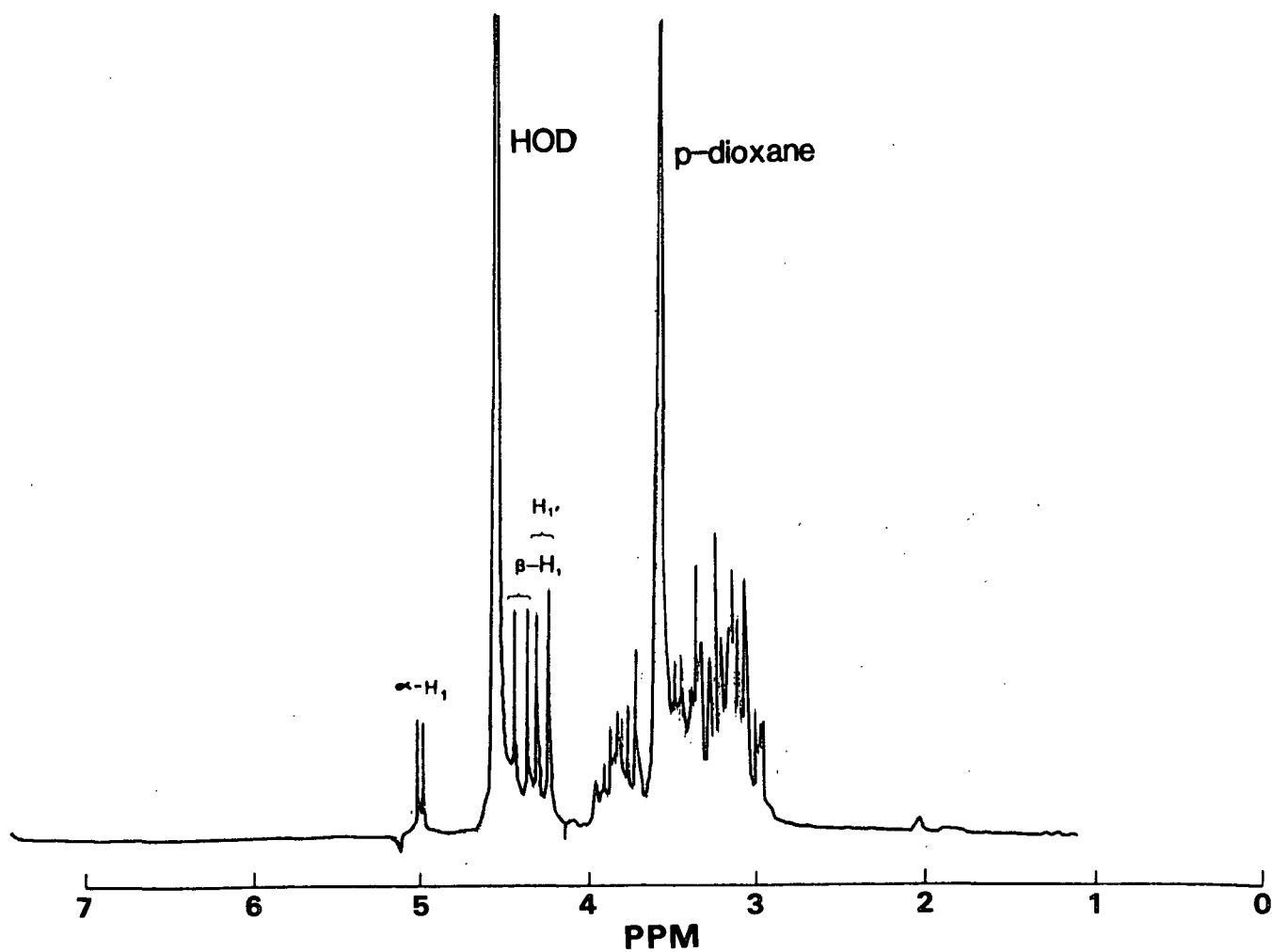
Figure 2. ^{1}H-NMR spectrum of xylobiose in D_2O at 31°C.
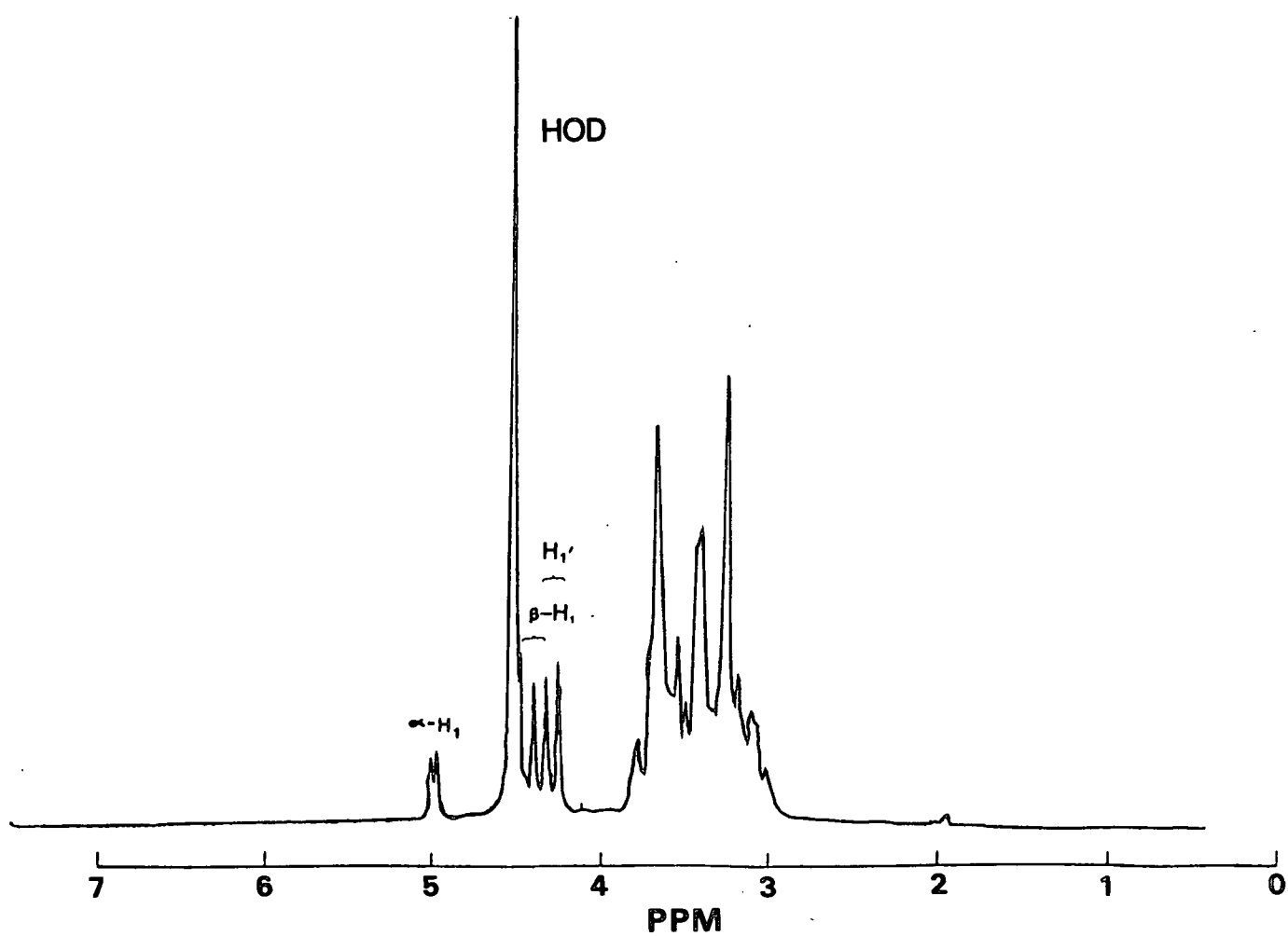
Figure 3. ^{1}H-NMR spectrum of cellobiose in D_2O at 31°C.

$$1/T_{1\,I} = \hbar^2 \, \gamma_I^2 \, \gamma_S^2 \Sigma(r_{IS}^{-6} \cdot T_{IS}) \tag{1}$$

where γ is the magnetogyric ratio, $\hbar$ is Planck's constant over 2π, r is the distance between nuclei I and S, and T_{IS} is the motional correlation time for the vector between nuclei I and S. S and I refer to the donor and relaxing nuclei, respectively. Equation 1 is strictly valid only in the motional narrowing region; a reasonable approximation for moderately sized organic molecules.

Contributions to the relaxation of nucleus I can be both intra- and intermolecular. At low concentrations and in the presence of a deuterated solvent (D_2O) only the intramolecular interactions are important. Equation 1 then simplifies to:

$$(R)_I = \hbar^2 \, \gamma_H^4 \, \underset{S}{\Sigma} \, (r_{IS}^{-6} \, T_{IS}) \tag{2}$$

where R is the relaxation rate of nucleus I and is the reciprocal of its relaxation time. In using this equation, it will be assumed that only intramolecular protons are significant contributors to the DD relaxation mechanism of nucleus I.

For isotropically rotating molecules,* exhibiting only intramolecular DD relaxation, the ratio of relaxation rates is simply related to the ratio of the interproton distances. This is given by the expression (22);

$$\frac{(R_1)_{I_1}}{(R_1)_{I_2}} = \frac{\underset{S}{\Sigma} \, (r_{I_1S})^{-6}}{\underset{S}{\Sigma} \, (r_{I_2S})^{-6}} \tag{3}$$

The summations on the right would include each proton distance for which an interacting proton S is close enough to contribute significantly to the relaxation

---

* T_{IS} is a constant for all I and S.

of nucleus I. For the anomeric protons the ratio R_1'/R_1 (Table III) is then a measure of the ratio of the relative distances from the nonreducing end (NRE) and reducing end (RE) anomeric protons to all intramolecular protons that contribute to their relaxation. Because of the position of the NRE anomeric proton, its relaxation will include contributions from RE protons, most notably H_4.

It is noteworthy that the R_1'/R_1 ratio of $\underset{\sim}{1}$ is less than 2.1. Hall (22) reported a number of these values. The only value less than 2.1 was for gentiobiose which is α-1,6 linked.* This linkage is expected to be considerably more flexible than the β-1,4-linkage of $\underset{\sim}{1}$ or $\underset{\sim}{2}$.

To apply this simplified picture to the analysis of the interring proton distance ($r_1'_{-4}$) for compounds $\underset{\sim}{1}$ and $\underset{\sim}{2}$ requires some estimation of the proton to anomeric proton distances in the two pyranose rings. Table III gives the distances reported for crystalline $\underset{\sim}{2}$, methyl β-cellobioside ($\underset{\sim}{3}$), glucose ($\underset{\sim}{5}$), and methyl β-xyloside ($\underset{\sim}{8}$)** (11,12,28,29). Values measured from a Drieding model, assuming a nonstrained C1 conformation, are also included. Only distances of less than 3.5 Å are given because of the rapidly diminishing importance of more distant protons due to the sixth power dependence.

Several significant points can be made from the data in Table III. First, except for interring contributions, the relaxation of the anomeric protons will be predominantly via the 1,3 diaxial interactions with H_3 and H_5. The only other significant intraring contribution would come from the vicinal proton H_2. The contribution of H_2 should be 10-15% of that of H_3 and H_5 combined and would be similar for both rings.***

---

* Gentiobiose has a value of 1.7 at 65°C.
** It was not possible to calculate reasonable values from the published fractional atomic coordinate data for aldotriuronic acid trihydrate (14).
***Refers to both rings in the disaccharide in this case.

TABLE III

PROTON TO ANOMERIC PROTON DISTANCES IN SELECTED SUGARS

Compound Reference: Interaction	β-Cellobiose 11	β-Cellobiose 28	MBC2 12	β-Glucose 11	MBX 29	Dreiding[a]	Type[b]
NRE							
$H_1{'}- H_4{'}$	2.21	2.23	2.08				AR
$H_1{'}- H_3{'}$	2.32	2.40	2.67			2.48	NR
$H_1{'}- H_5{'}$	2.39	2.46	2.24			2.30	NR
$H_1{'}- H_2{'}$	2.95	3.02	2.86			2.93	NR
$H_1{'}- H_{6a}$	2.83	2.81	–				AR
$H_1{'}- H_{6b}$	3.00	3.50	–				AR
$H_1{'}- OH_2{'}$	2.71	–	–				NR[c]
$H_1{'}- OH_3{'}$	3.16	–	–				AR[c]
RE							
$H_1{'}- H_{5ax}$	2.61	2.38	2.43	2.42	2.52	2.30	R
$H_1{'}- H_3$	2.77	2.56	2.82	2.73	2.24	2.48	R
$H_1{'}- H_2$	3.00	3.09	2.75	3.03	3.50[d]	2.93	R

[a] A C–C average distance of 1.525 Å was used as a reference. Assumes an ideal chair form. Only intraring distances are given because of uncertainty in the linkage conformation.

[b] NR = intraring interaction in NRE ring; R = intraring interaction in reducing ring; AR = interring interaction.

[c] Only important under conditions for which the hydroxyl protons have not been exchanged such as in DMSO.

[d] Published value may be in error.

Another point is the variation in intraring proton distances in the various crystal structures; including a significant difference between the two rings in compound 2. These variations result from strain applied to the individual 6-membered rings as they are forced to accommodate the crystalline lattice. In solution these strains would be largely absent. In addition, the chair structure in solution is a more dynamic structure so that the values calculated from the Drieding model are probably more realistic.

In the Drieding model the shorter distance for H_1-H_5; relative to H_1-H_3, results from the shorter C-O bond distances. In the nonreducing ring of crystalline 2 this distinction is lost because of a flattening of the ring. This represents a strain on the ring that probably is not present in solution.

Finally, in 2 the only significant interring contribution to the relaxation of $H_1{'}$ would come from H_4 and H_{6a}. The gauche proton at H_6 could contribute significantly to the relaxation of H_1, only if there are specific significant deviations from the 2-fold helix and if it remains in the tg conformation. In the crystalline 2 conformation the expected contribution would be approximately 20% of the total interring contribution. In solution the contribution would be less because of many contributions to the average conformation for which the $H_1{'}$ to H_6 distance exceeds 3 Å.

If it is assumed that the geometry of both disaccharide pyranose rings is the same in solution and that the molecules rotate isotropically, then the relationship $(1 - \frac{R_1}{R_1{'}})$ is directly related to the interring contribution to the relaxation of $H_1{'}$. These values are given in Table IV. Since the contribution from H_6 is small an estimate of $r_1{'}_{-4}$ can be made.

TABLE IV

INTERRING CONTRIBUTION TO THE RELAXATION
OF 1´ AND $r_{1´-4}$.

Compound	Temp., °C	Interring Contribution to the Relaxation of 1´ (%)	$r_{1´-4}$, Å
Cellobiose (2)	31	54	2.1
	74.5	47	2.2
Xylobiose (1)	31	44	2.2
	74.5	33	2.4

For the reasons stated above the values calculated from the Dreiding model will be used in the analysis below. Equation (4) shows the expansion of Eq. (3) for which only the 1,3 diaxal contributions and the $H_{1´}$ to H_4 contribution are included.

$$\frac{R_{1´}}{R_1} = \frac{1/r_{1´-3}^6 + 1/r_{1´-5´}^6 + 1/r_{1´-4}^6}{1/r_{1-3}^6 + 1/r_{1-5}^6} \tag{4}$$

$$\frac{R_{1´}}{R_1} = \frac{\frac{1}{(2.48)^6} + \frac{1}{(2.30)^6} + \frac{1}{r_{1-4}^6}}{\frac{1}{2.48^6} + \frac{1}{2.30^6}} \tag{5}$$

Using the $R_{1´}/R_1$ value of 2.2 determined for cellobiose at 31°C results in a calculated $r_{1´-4}$ distance of 2.1 Å. This is slightly less than that obtained for crystalline 2 and agrees with the average distance suggested by Hall.* Furthermore, it is close to the distance expected from the 2-fold helix. Since the β-1,4 linkage in 2 is dynamic and is predicted to have major conformations on both sides of the two fold helix line this value seems reasonable. Inclusion of the contributions

---

*This approach may indeed be how Hall came to his estimate.

from H_2, H_2', and H_{6_1}* changes the result by less than 1%. Table IV also gives the $r_1'_{-4}$ distance calculated from the R_1'/R_1 ratio for 1 and 2 for each of the conditions studied assuming the Dreiding model intraring distances remain the same.

The above analysis is based on a number of simplifications and assumptions which have been discussed above and in a previous thesis (30). Certainly, the values for $r_1'_{-4}$ can only be considered estimates. This is particularly true if the 1,3 diaxial distances are not equivalent in each ring. Surprisingly, despite the many reservations involved, including the inherent error [~10% (26)] of the relaxation measurement, entirely reasonable though probably low estimates are obtained for the interring proton distance. Furthermore, the results are consistent with the intuitive picture of more available conformations in 1 and 2, particularly at higher temperature. The fact that the values do not significantly deviate from the 2-fold helix distance (2.0-2.1 Å), with increasing temperature, can be explained by assuming that the two major conformations on both sides of the linkage became more equally populated. This counters an increase in the number of minor conformations tending to increase $r_1'_{-4}$. Conformations removed significantly from the 2-fold helix, such as those with $\chi \simeq 180$ (7), do not significantly become populated in view of the small H_1' to H_4 distance. Relaxation of the average bond angle T from 116° toward 109 Å would also contribute slightly (0.1 Å) to a shorter $r_1'_{-4}$ distance.

The estimates for $r_1'_{-4}$ in Table IV are probably lower than the actual values. Melberg and Rasmussen have calculated a weighted average distance of 2.28 Å for 2 in H_2O (7). The reasons for this discrepancy are the neglect of the contribution from H_{6_a} in compound 2 and more importantly the inaccuracy of the assumption of isotropic rotation. The later assumption is known to be slightly in error on the basis of

---

*Assuming an average value of 3.0 Å.

nonequivalent carbon relaxation times (27,31). As the molecule rotates in solution, the interior protons will exhibit a longer correlation time and hence a shorter T_1. This would increase the R_1'/R_1 ratio so that the apparent interring contribution to the relaxation of H_1' is greater than it actually is. On the other hand, molecular association, leading to intermolecular relaxation, would most affect the relaxation of H_1 which is on the exterior or the molecule. This would result in a small apparent interring contribution. Since molecular interactions* seem to be more prevalent in 2 than 1, on the basis of the smaller T_1 values for 2 at equivalent concentrations, it is probable that intermolecular relaxation is not as significant as the anisotropic rotation on the R_1'/R_1 ratio. The overall effect is to give a low $r_1'_{-4}$ distance.

More accurate methods of determining $r_1'_{-4}$ are available. Complete deuteration of the disaccharide, except in positions H_1' and H_4, would eliminate all contributions to the relaxation of H_1' except for H_4. Using this approach, an independent measure of $T_1'_{-4}$ could then be obtained from the carbon spectrum allowing a more accurate determination of $r_1'_{-4}$. Another method would be to directly use selective relaxation measurements (32). Finally, homonuclear NOE measurements at high field could also be used if the H_4 proton is sufficiently resolved (32). Each of these methods still would be in error due to the inherent error of the relaxation and NOE measurements, but would give more accurate absolute estimates.

Interresidue Carbon-Proton Coupling Constants (^3J) to Estimate ϕ and χ.

General Analysis

In an attempt to determine the relative ϕ and χ values of xylobiose (1) and cellobiose (2) in solution, a series of proton coupled carbon spectra were obtained

---

*This is a dynamic situation in which D_2O would predominantly interact with OD, so that the effective distance from H_1 to a proton on an adjacent molecule would be large.

using the technique of gated decoupling. This method retains the enhancement due to the nuclear Overhauser effect. This was essential for several of the samples available only in small amounts. The detailed results and a discussion of the technique used are given in Appendixes IV and V. Appendix V also contains representative examples of the spectra obtained.

Analysis of a 25.05 MHz coupled ^{13}C-NMR spectrum is not always straightforward because of second order effects. Much of the discussion below will be directed toward the limitations that must accordingly be applied to the data interpretation. Nevertheless, much still can be inferred from the data given below involving the relative linkage conformations of 1 and 2, though confirmatory work at higher fields is recommended.

Table V gives the width at half height ($v_{1/2}$) of the C_1' and C_1 peaks of compounds 1, 2, 3, xylose (4), glucose (5), methyl β-xylobioside (6), and methyl β-cellobioside-d_8 (7) in D_2O. Figures 4-10 show the spectral region containing C_1' and C_1 for compound 1-7.

TABLE V

WIDTH AT HALF HEIGHT FOR C_1 AND C_1' IN THE PROTON COUPLED
SPECTRA OF COMPOUNDS 1-7 AT 25.05 MHz IN D_2O

Compound	$v_{1/2}$	
	C_1	C_1'
β-Xylose (4)	19.8	--
Methyl β-Xylobioside (6)	I[b]	20.5
β-Xylobiose (1)	20.3	20.4
β-Glucose (5)	9.4	--
Methyl β-Cellobioside (3)	I	I
Methyl β-Cellobioside-d_8 (7)	13.9-15.2	7.9-9.2[a]
β-Cellobiose (2)	8.8-9.8	10.7-10.9

[a]A value of approximately 9.3 Hz is obtained from Fig. 2 Ref. (16).
[b]Indeterminant due to peak overlap or low signal to noise.
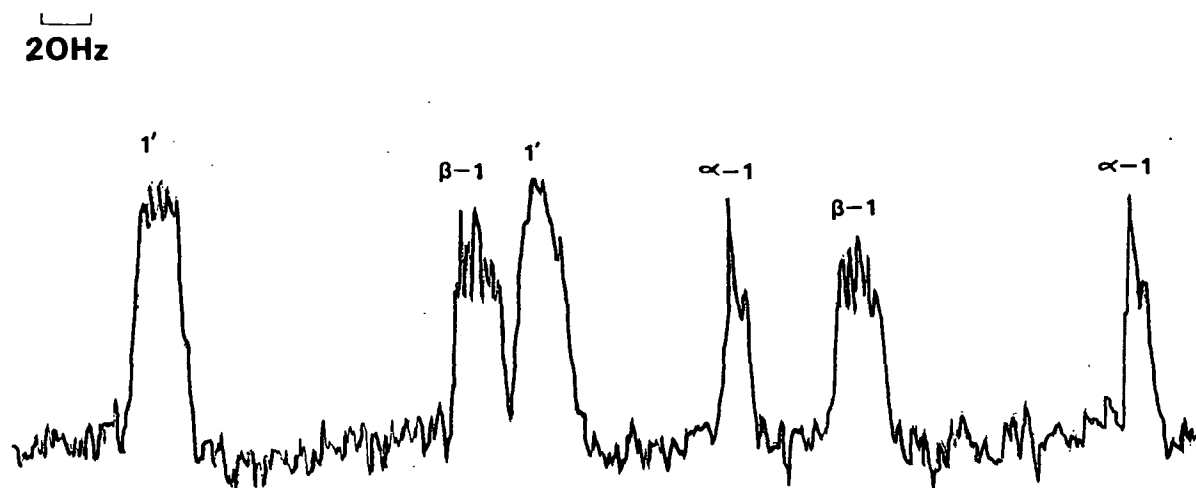
Figure 4. ¹H-coupled ¹³C-NMR spectrum of xylobiose in D_2O - downfield region.
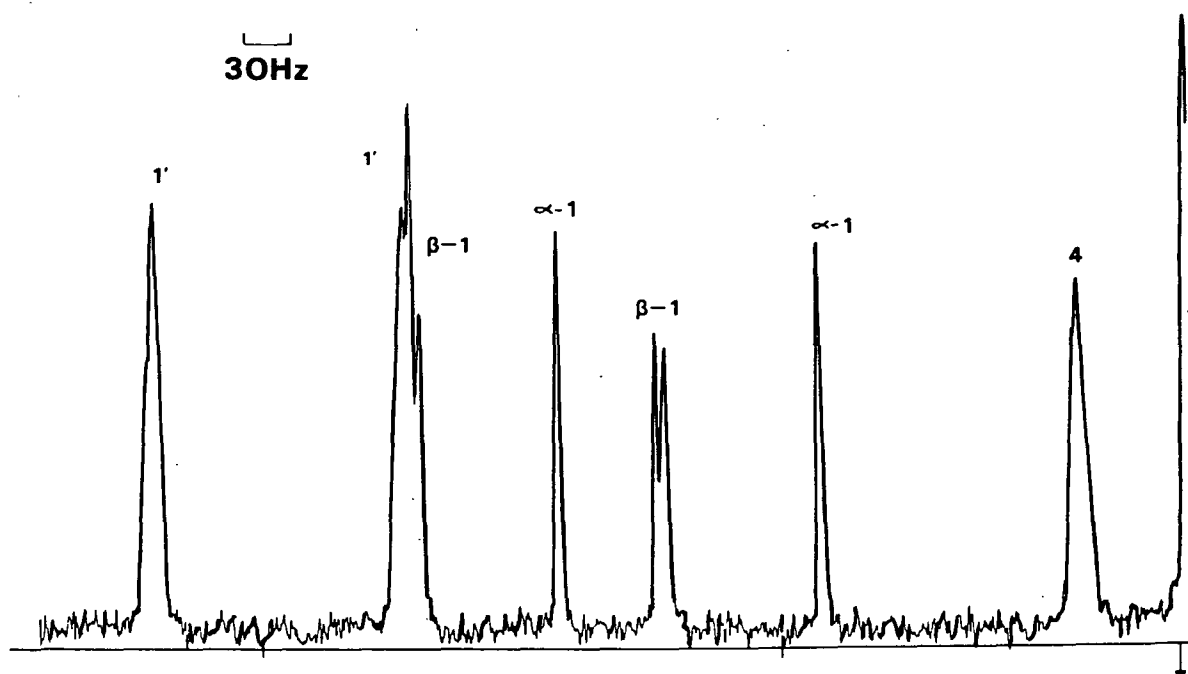
Figure 5. ¹H-coupled ¹³C-NMR spectrum of cellobiose in D_2O - downfield region.
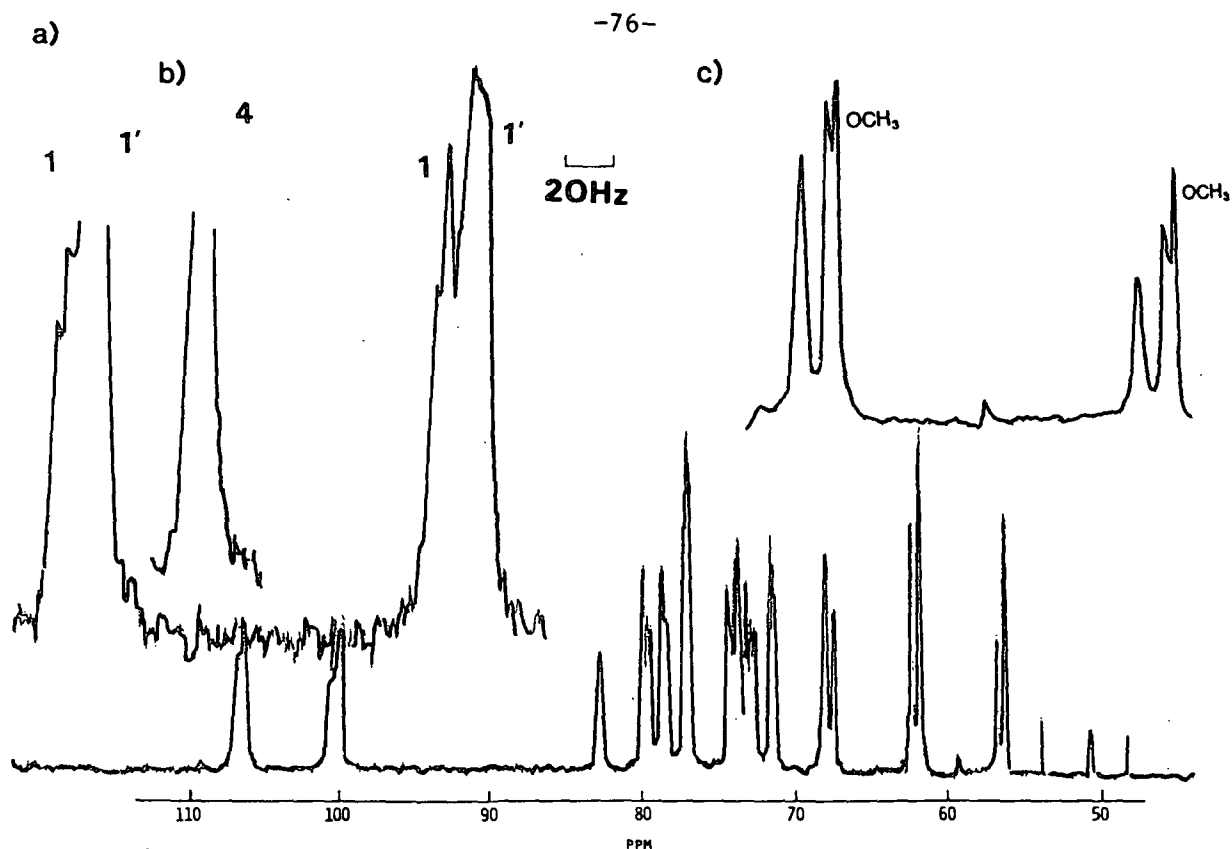
Figure 6. ^{1}H-coupled ^{13}C-NMR spectrum of methyl β-cellobioside in D_2O. Inserts are: a) downfield C_1', C_1, b) C_4, and c) upfield OCH_3, C_6, C_6' regions.
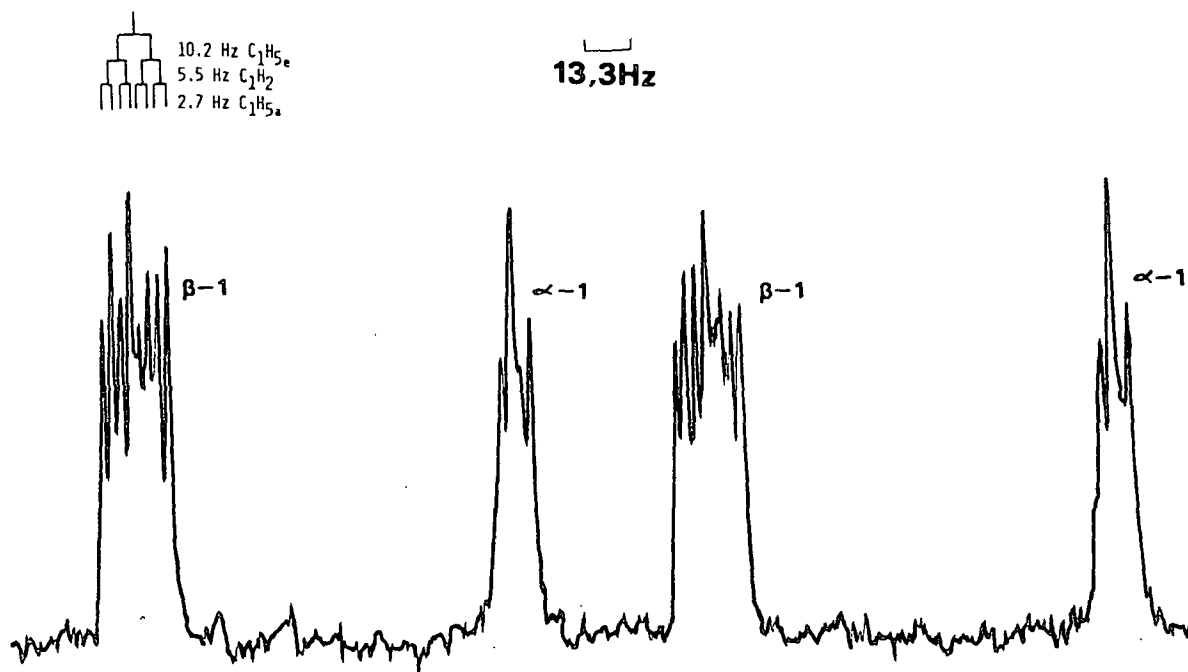
Figure 7. ^{1}H-coupled ^{13}C-NMR spectrum of xylose in D_2O - downfield region.

11,4Hz
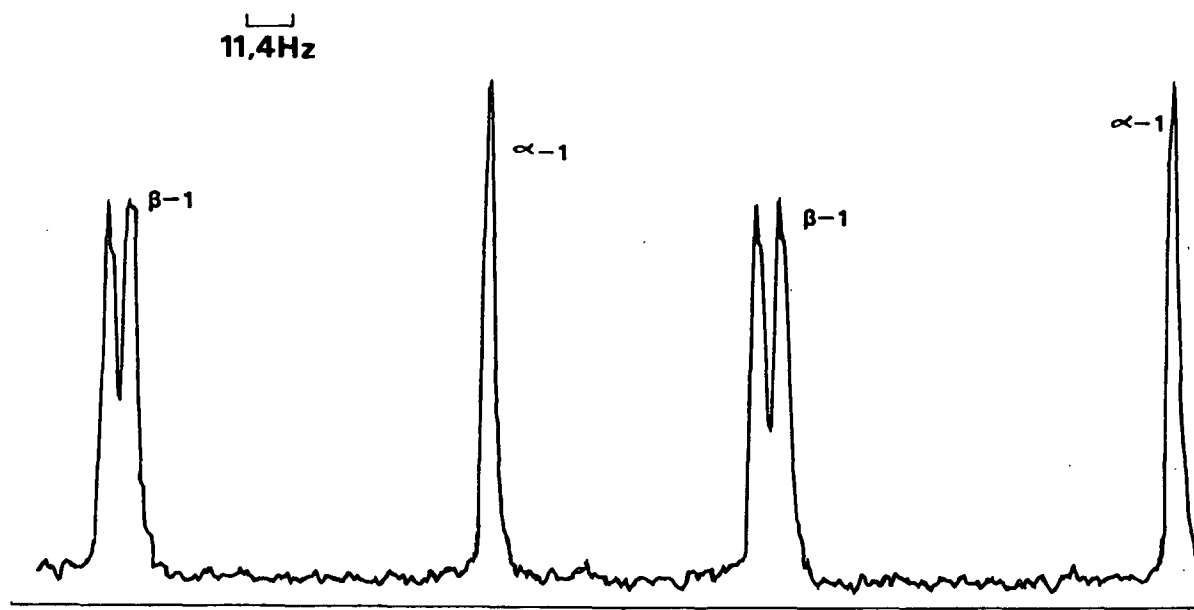
Figure 8. ^{1}H-coupled ^{13}C-NMR spectrum of glucose·in D_2O - downfield region.

METHYL β-XYLOBIOSIDE
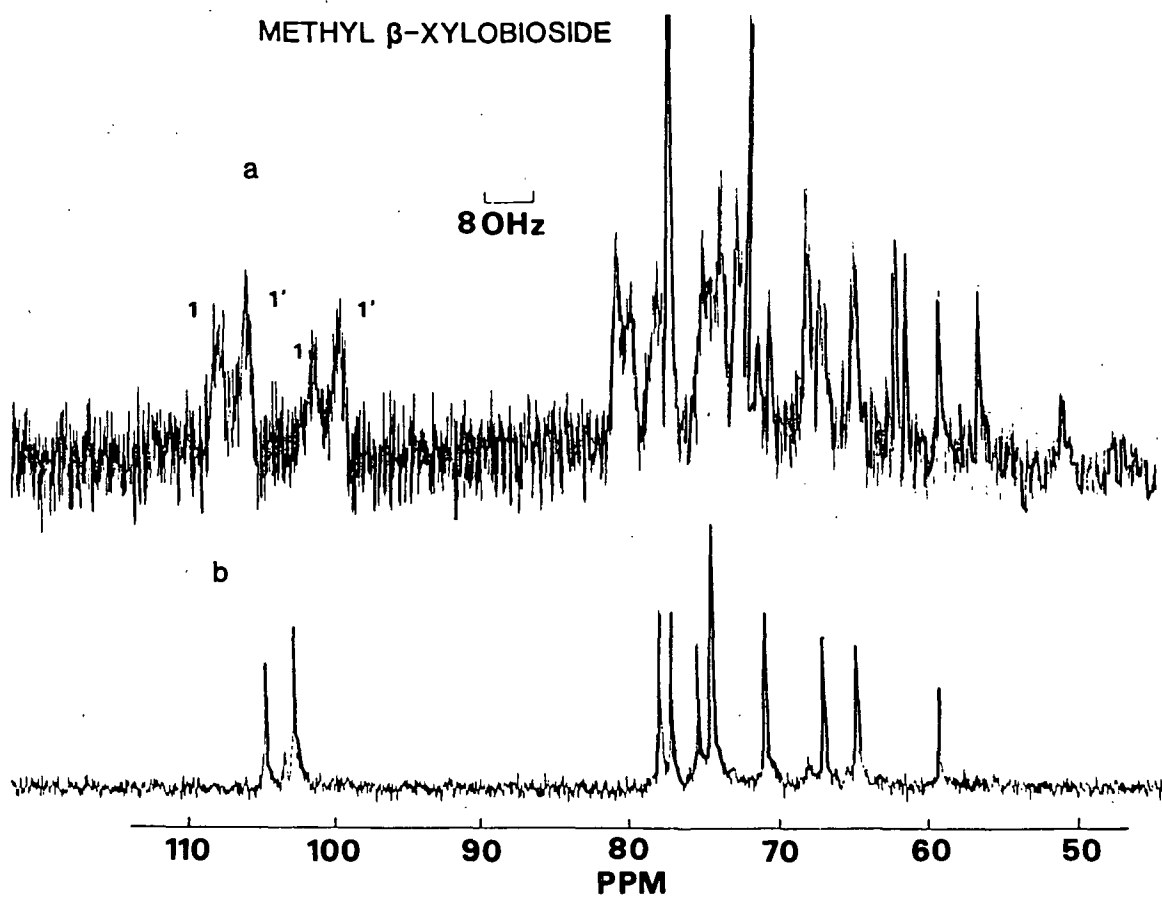
Figure 9. ^{1}H-coupled (a) and ^{1}H-decoupled (b) ^{13}C-NMR spectra of methyl β-xylobioside in D_2O.

10Hz
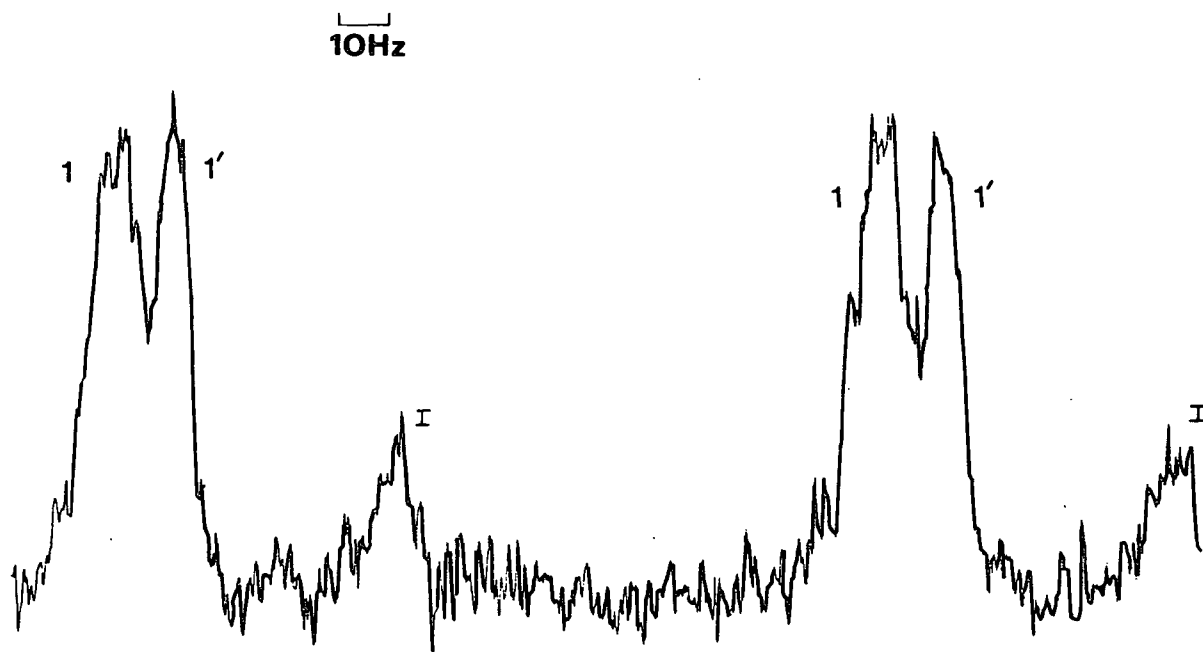
Figure 10. ¹H-coupled ¹³C-NMR spectrum of methyl β-cellobioside -d₈ in D₂O -
downfield region. I is due to an isomerization or decomposition
product.

Compound 3 was deuterated by heating it over Raney nickel in D₂O to form 7
(24). The ¹³C-NMR proton decoupled and coupled spectra of 7 are given in Fig. 11.
Both spectra essentially agree with those given by Perlin and coworkers (18) for the
same material. The structure listed was confirmed by them on the basis of enzymatic
hydrolysis and ¹³C-NMR (18).

Additional compounds studied included: lactose, 4-O-β-D-glucosyl-D-mannose,
4-O-β-D-glucosyl-D-xylose, maltose, methyl β-xyloside (8), and methyl β-glucoside
(9), as well as the Raney nickel deuterated versions of 8 and 9. The results for
these compounds are tabulated in Appendix V. They are essentially in agreement with
the discussion below and will not be specifically covered in the main discussion,
except as they aid the discussion for compounds 1-7.
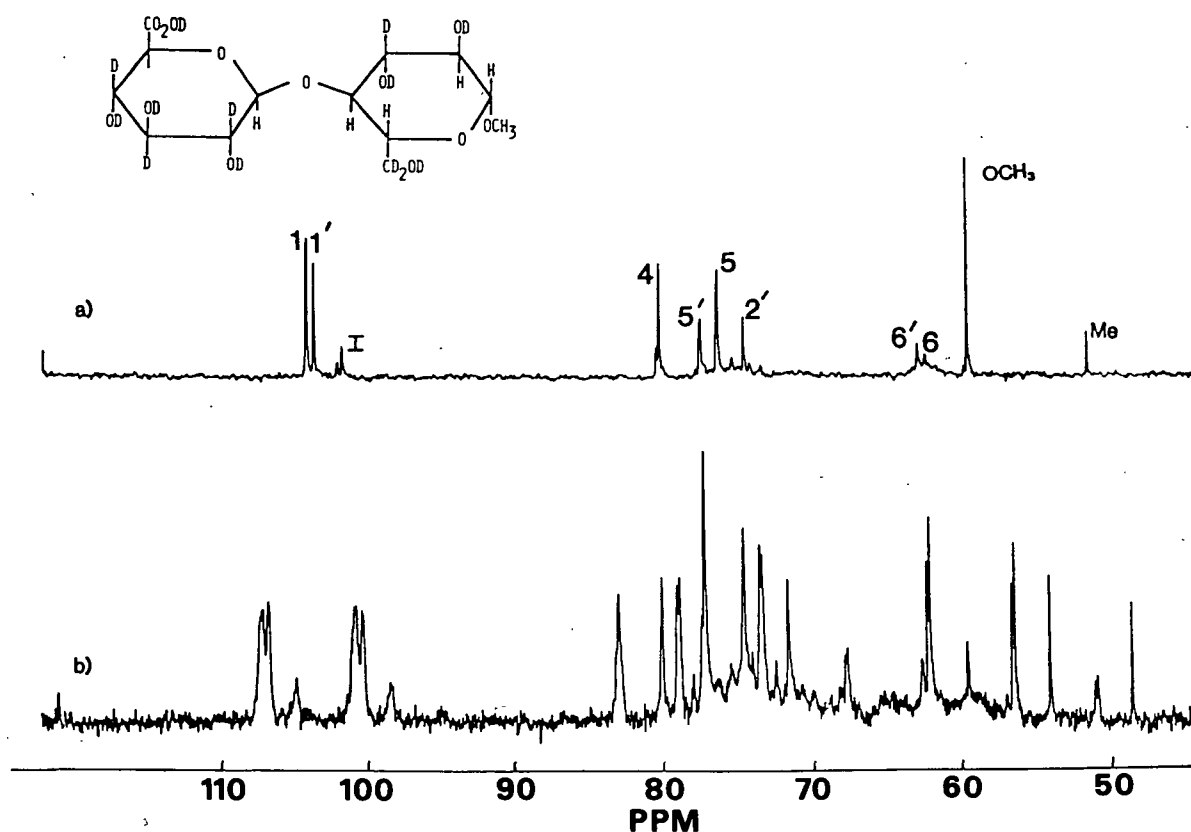
Figure 11. ^{1}H-decoupled (a) and ^{1}H-coupled (b) ^{13}C-NMR spectra of methyl β-cellobioside -d$_8$ in D$_2$O. Assignments are given on (a).

The values given in Table V represent the average $v_{1/2}$ values for both signals of the C$_1$H or C$_1$′H doublet, unless one half of the doublet is overlapped by another resonance. The spectrum of $\underset{\sim}{3}$ is given for reference only, since the C$_1$′ and C$_1$ signals overlap; making it impossible to obtain a value for $v_{1/2}$ for the anomeric carbons of this compound. This is one of the advantages of using its deuterated analog $\underset{\sim}{7}$. The deuterium at C$_2$′ in $\underset{\sim}{7}$ imparts a slight upfield shift to C$_1$′, separating the two peaks to the extent that $v_{1/2}$ can be measured. This subtle change can be seen by comparing Fig. 6 and 10. The coupled spectra in Fig. 5, 6, 8, and 10 are essentially the same as those in the literature (16,18,19). However, minor differences related to resolution, field strength (2nd order effects), and conditions under which the spectra were taken can be noted.

The coupling patterns associated with the anomeric carbons of compounds 1-7 have several common elements. All the anomeric protons are doublets, exclusive of fine structure, on the basis of $^1J_{CH}$ couplings of 155-170 Hz. The values measured for ^1J in the present study are given in Appendix V.

Figure 12 illustrates the important coupling constants contributing to the fine structure of C_1 in β-xylose and β-glucose. The contributions from H_3 and H_4 have been determined to be less than 1 Hz (16) for glucose. This is expected in view of the distance from C_1 (3 and 4 bonds, respectively) and on the basis of the geometry of the Cl conformation. The coupling to H_5 ($^3J(C_1H_5)$) has been measured from β-D-glucose-2,3,4,6,6′-d$_5$ as 2.0-2.2 Hz (18). Similarly, the coupling to H_2 ($^2J(C_1H_2)$) has been measured from β-glucose-5,6,6′-d$_3$ as -5.5 Hz (17,33). The value obtained for $^2J(C_1H_2)$ from Fig. 9 is $\pm$ 5.6 Hz;* in close agreement with the literature. An indication of the coupling to H_5 is also present as a shoulder on the major peaks.
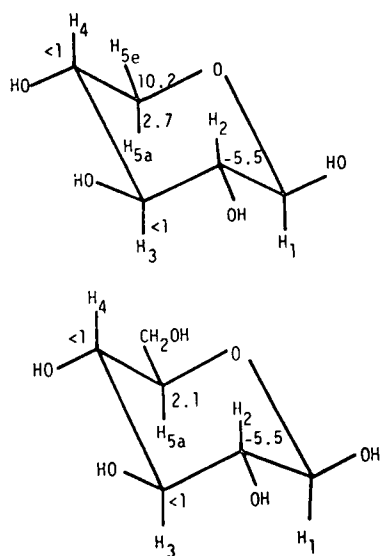
Figure 12. β-xylose (top) and β-glucose (bottom) with multiple bond C_1H coupling constants listed.

---

*The sign cannot be determined for ^2J by simple first order analysis. The + or − designation will be left out in the remainder of this discussion but should be understood to be implied.

Similar values to those in glucose would be expected for xylose; the values determined in the present study being 5.5 Hz for $^2J(C_1H_2)$ and 2.7 Hz for $^3J(C_1H_{5a})$. These values were measured directly from Fig. 7 and represent apparent coupling constants. An additional coupling of 10.2 Hz is evident. It can be attributed to the H_5 equatorial proton (H_{5_e}), which is present in xylo-related structures but absent in gluco-related structures. Again, this is an apparent coupling constant since some small second order effects would be expected for xylose (see below). A large value for $^3J(C_1H_{5_e})$ is expected on the basis of its 180° dihedral angle with C_1 in the C1 conformation of xylose. The Karplus relationship given by Perlin for the C-O-C-H system predicts a value of 6.5 Hz at 180°, which, on the basis of these results seems low. The second order effects expected do not suggest the existence of such a large difference between the two results. The first order analysis of the C_1' peak in β-Xylose is given in Fig. 7.

For the disaccharide 1 and 2 an additional contribution to the fine structure of the C_1' doublet is expected due to the 3 bond coupling with H_4 across the linkage ($^3J(C_1'H_4)$). Perlin (18) has given a value of 4.3 Hz for compound 7 for this coupling constant; obtained using a second order analysis. Table VI summarizes the directly measured coupling constant to C_1' and C_1 for the compounds studied in this work.

The value of $^3J(C_1'H_4)$ can be related to the dihedral angle χ depicted in Fig. 1. Perlin (18) has published a Karplus relationship based on empirical measurements of coupling constants found in systems containing the C-O-C-H structure. This is given as Fig. 13. The authors point out that this is not strictly valid for all C-O-C-H systems because the attached atoms to the nucleus of interest (C_1' or C_4) are not the same in all instances. Nevertheless, they have used this relationship to estimate values of (±) 25-30° for χ and φ in compound 7.

TABLE VI

APPARENT COUPLING CONSTANT MEASURED DIRECTLY IN D_2O

Compound	Apparent Coupling Constants (Hz)[a],[d]		Coupling
	C_1	$C_{1'}$	
β-Glucose (5)	161.3(162.)		^1J
	-5.6(-5.5)[b]		$^2J(C_1H_2)$
	(< 1)		$^3J(C_1H_3)$
	(2.0-2.2)(2.2)		$^3J(C_1H_5)$
β-Xylose (4)	161.9(160.5)		$^1J(C_1H)$
	-5.5[b]		$^2J(C_1H_2)$
	(< 1)		$^3J(C_1H_3)$
	2.7		$^3J(C_1H_{5_a})$
	10.2		$^3J(C_1H_{5_e})$
MBC2-d_8 (7)	162.0	162.8(162.1)	^1J
		(4.3)[c]	$^3J(C_{1'}H_4)$
β-Cellobiose (2)	161.6	162.0	^1J
	-5.4-5.9[b]		$^2J(C_1H_2)$
β-Xylobiose (1)	162.3	161.6	^1J
	-5.7[b]		$^2J(C_1H_2)$
	2.8		$^3J(C_1H_{5_a})$
	10.3		$^3J(C_1H_{5_e})$

[a]Values in brackets are literature values (17,18,34).
[b]Sign is assumed to be negative to correspond to earlier work (17,33).
[c]Derived by second order analysis. Not measured directly.
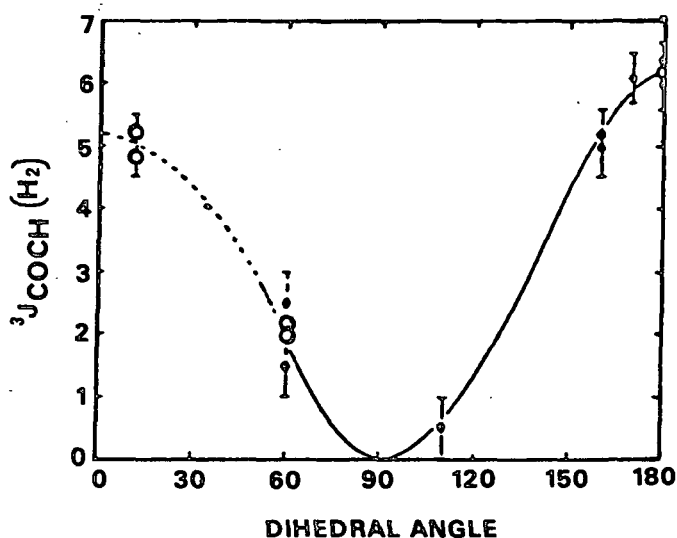[d]Based on distance between 2 resolved peaks.

Figure 13. Karplus type relationship for the $^3J_{C-O-C-H}$ system. Taken from Ref. (18).

In the methyl glycosides $\underset{\sim}{3}$, $\underset{\sim}{6}$, $\underset{\sim}{7}$, $\underset{\sim}{8}$ and $\underset{\sim}{9}$ a complex contribution to the fine structure of C_1 arises from the O-methyl protons. Because of this the C_1 peak in the methyl glycosides cannot be used in the present analysis.

A direct first order analysis to determine the contribution of $^3J(C_1\text{-}H_4)$ to the observed value for $\nu_{1/2}$ for $C_1\text{-}$ in $\underset{\sim}{1}$, $\underset{\sim}{2}$, $\underset{\sim}{3}$, $\underset{\sim}{6}$, or $\underset{\sim}{7}$ would merely involve taking the difference of $(\nu_{1/2})_{C_1\text{-}}$ and $(\nu_{1/2})_{C_1}$ of an appropriate model. For $\underset{\sim}{1}$ and $\underset{\sim}{2}$ an appropriate model would be C_1 of the reducing end of C_1 in the related mono-saccharide. For the methylated glycosides the C_1 of the related monosaccharide must be used. The basis for this analysis is that in the limit of first order coupling, the peak width at half height is simply related to the sum of all the coupling constants plus any natural or instrumental line broadening:

$$\nu_{1/2} = \underset{i}{\Sigma} \ J_i + F \tag{6}$$

In this equation F represents broadening due to several factors, including the natural line width (related to T_2; see Appendix I), slight dispersion of nearly degenerate signals arising from both α- and β-anomers, and to any instrumental broadening due to inhomogeneities or fluctuations in the magnetic field. It is always a positive quantity. For rapidly rotating molecules, broadening due to instrumental factors usually dominates.*

If it is assumed that the coupling from the protons within the pyranose ring is the same for both C_1 and $C_1\text{-}$, and that the instrumental broadening is equal, then

---

*This broadening can be estimated by measuring $\nu_{1/2}$ of the narrowest line in the spectrum and subtracting out the contribution from T_2 ($\nu_{1/2} = \frac{1}{\lambda T_2}$) and any known coupling constants. T_2 equals T_1 in the region of motional narrowing. In the glucopyranoses either half of the α-C_1 signal is appropriate since they appear without fine structure except for a small coupling of about 2.0 Hz to H_5. In the spectra reported here α-C_1 has a $\nu_{1/2}$ of 3.2-3.6 Hz suggesting an instrumental broadening of 1.0-1.6 Hz.

evaluation of the interring contribution to the coupling of C_1´ ($^3J(C_1$´$H_4)$) merely requires taking the difference of the $\nu_{1/2}$ values for C_1´ and C_1.

$$(\nu_{1/2})_{C_1´} - (\nu_{1/2})_{C_1} = {}^3J(C_1´H_4) \tag{7}$$

In a similar way the coupling at C_4 can theoretically be used to measure $^3J(C_4H_1´)$ which is related by the Karplus relationship (Fig. 13) to ϕ.

$$(\nu_{1/2})_{C_4} - (\nu_{1/2})_{C_4´} = {}^3J_{C_4 0 H_1´} \tag{8}$$

Again, C_4´ can be in the nonreducing ring, or in an appropriate model compound. Severe overlap of peaks for the appropriate C_4´ model is a problem at 25 MHz.

The assumption that within ring coupling constants are a constant appears to be a valid one for both disaccharide rings or the rings of an appropriate monosaccharide, as is evident from the data in Table VI. This is further evidence that the average C_1 conformation dominates in these systems and remains a constant.

Table VII contains the results of the simple first order analysis applied to C_1´ and C_1 in compounds 1, 2, 6, and 7. The model compound used for comparison is indicated in the table. The published results for MBC2-d$_8$ are also given (18). The corresponding average χ values based on the Karplus relationship in Fig. 13 are listed. Possible χ values greater than 90° are omitted as being physically improbable.

As expected, the results indicate that the disaccharides containing xylose are more staggered from the two fold helical structure than are the glucose-related disaccharides. This agrees with the expectation that 1 and 6 possess a more flexible linkage because of the absence of steric crowding imposed by the C_6 hydroxymethyl in 2, 3, and 7. Furthermore, it is in agreement with the ^1H-T_1 result

that the $r_1'_{-4}$ proton to proton distance is greater in 1 than 2 and with the fact that the intramolecular hydrogen bond ($O_3H\ldots O_5'$) is weaker in 1 than 2 (35). However, the discrepancy between the χ values for cellobiose and MBC2-d$_8$ suggests that the first order analysis is not entirely accurate and that complicating factors must temper the conclusions drawn. It is suggested here that a χ value of $\pm60°$ is unlikely for 2 and does not agree with the ^{1}H-T_1 data. On the basis of nearly equal ^{13}C chemical shifts for the linkage carbons of 2 and 3 it is expected that both compounds have the same average conformation in solution. Further remarks on the origins and the effect of second order factors on the $\Delta\nu_{1/2}$ value in 2 will be given later.

TABLE VII

FIRST ORDER ANALYSIS
ACROSS LINKAGE COUPLING CONSTANTS TO C_1' IN COMPOUNDS
1, 2, 6, AND 7 AND CORRESPONDING χ VALUES

Compound	$^3J_{C_1'OCH_4}$(Hz)	χ	Model
β-Xylobiose (1)	0.5		C_1 β-Xylose
	0.1	±75-$85°$	C_1 β-Xylobiose
Methyl β-xylobioside (6)	0.6	±70-$80°$	C_1 β-Xylose
β-Cellobiose (2)	1.4		C_1 β-Glucose
	1.0-2.0[c]	±60-$70°$	C_1 β-Cellobiose
MBC2-d$_8$ (7)	3.1-4.4	±25-$60°$	β-D-glucose-2,3,4,6', 6-d$_5$
	4.3[b]		2nd Order analysis
	4.5[b]	±25-$30°$	1st Order analysis

[a]Using a value of 4.8 Hz for $\nu_{1/2}$ from Fig. 2 Ref. 18.
[b]Literature values (18).
[c]A value of 1.0-2.0 Hz was also found by Perlin et al. (16).

Proton coupled ^{13}C-NMR spectra were also obtained from compounds 1-7 in DMSO-d$_6$. Deuterium exchanged materials were not used and, therefore, coupling to

the hydroxyl protons must be considered. Table VIII gives the $\nu_{1/2}$ values for $C_1{}'$ or C_1 in $\underset{\sim}{1}$, $\underset{\sim}{2}$, $\underset{\sim}{4}$, $\underset{\sim}{5}$, and lactose. A comparison to the D_2O results is also shown.

TABLE VIII

COMPARISON OF $\nu_{1/2}$ VALUES IN DMSO-d_6 AND D_2O

$$\nu_{1/2}(Hz)$$

	DMSO-d_6		D_2O		
	C_1	$C_1{}'$	C_1	$C_1{}'$	$\Delta\nu_{1/2}{}^a$
β-Xylose	18.8		19.8		-1.0
β-Xylobiose	19.4		20.3		-0.9
		19.6		20.4	-0.8
β-Glucose	11.0		9.4		+1.6
β-Cellobiose	10.7		9.4^b		+1.3
		12.1		10.8	
β-Lactose	10.6				
		11.1			

$^a\nu_{1/2}{}_{DMSO} - \nu_{1/2}{}_{D_2O}$.
^{b}Average value.

Additional contributions to the coupling to $C_1{}'$ should be small in the disaccharides in DMSO-d_6. Both $OH_2{}'$ and OH_3 (via intramolecular H-Bond) should be weak because of rapid proton exchange and because of the number of bonds that separates them from $C_1{}'$ (3+ and 2+, respectively). Instrumental and viscosity-related contributions to line broadening in DMSO-d_6 were also small (<1 Hz) since comparable line widths were obtained for peaks exhibiting equivalent coupling.* For C_1 the two-bond coupling with OH_1 is expected to be significant and probably contributes to line broadening (36).

In the glucose-containing molecules $\nu_{1/2}$ increases for both $C_1{}'$ and C_1. The increase in $\nu_{1/2}$ of $C_1{}'$ for $\underset{\sim}{2}$, when compared to $\nu_{1/2}$ for glucose in D_2O, corresponds

---

*The proton coupled O-CH_3 peak was compared in a series of methyl glycosides for D_2O and DMSO-$d6$ solutions. The additional broadening ranged from 0.1-1.2 Hz.

to a $\nu_{1/2}$ value of 2.7 Hz which is more nearly like that in MBC2-d_8. It is suggested that this represents a reduction in the second order factors that affect $\nu_{1/2}$ for C_1' in 2 in D_2O. In contrast, the xylose containing compounds show decrease in $\nu_{1/2}$ for both C_1 and C_1'. This may represent an increased contribution from second order factors in DMSO-d_6, particularly for C_1 for which the coupling to OH would be expected to increase $\nu_{1/2}$.

Of course other factors might also be operating to affect $\nu_{1/2}$ of C_1' and C_1 in DMSO-d_6. Changes in either the linkage conformation or the chain conformation are also possible so that comparisons between $\nu_{1/2}$ in the two solvents are complicated. In particular, $^3J(C_1, H_4)$ cannot be reliably determined using $\nu_{1/2}$ values obtained in the two different solvents. Similarly, in DMSO-d_6 the contribution of OH_1 to the $\nu_{1/2}$ of C_1 precludes the use of any possible model containing a reducing end to calculate $^3J(C_1OC_{me})$ in DMSO-d_6 itself. Synthesis of a methyl β-glycoside using CD_3OD or the use of deuterium exchanged materials should allow this determination to be made.

Information on the dihedral angle ϕ is theoretically obtained in analogous manner to that of χ by comparing $\nu_{1/2}$ of C_4 and C_4'. In practice, severe overlap of either component of the doublet[*] with either C_6, C_5, or C_2 makes it difficult to find a suitable model at the magnetic fields used in this study. Additionally, the nondegeneracy of the C_4 resonance for the α- and β-anomers of any reducing sugars negates the use of that peak. Use of the methyl glycosides could avoid this problem, but in most cases the accidental overlap would still prohibit their use.

Width at half height values ($\nu_{1/2}$) for the C_4 peak in 3, 6, and 7 in D_2O are given in Table IX. Also given are $\Delta\nu_{1/2}$ values calculated using $\nu_{1/2}$ equal to 7.7

---

[*]C_4 doublet for the monosaccharides.

Hz for methyl β-D-glucose-3,6,6'-d_3 (18) as a model. The $\Delta\nu_{1/2}$ value of 4.2 Hz, obtained by Perlin (18) using a second order analysis, is also listed for comparison. The low values (1.7-2.0 Hz) for $\Delta\nu_{1/2}$ in MBC2-d_8 suggest that severe second order broadening is present in the spectrum of the model compound and that the simple measurement of $\Delta\nu_{1/2}$ can be misleading. The value obtained by Perlin takes into consideration these second order effects and thus should be reliable. The only significant long range coupling constant to C_4 expected in methyl β-D-glucose-3,6,6'-d_3 is $^2J(C_4H_5)$ equal to (-)3.5-4.0 Hz. The much higher measured value of 7.7 Hz suggests a second order effect. As discussed below, such a broadening should be anticipated because of the close proximity of the H_4 and H_5 peaks in the glucose ^{1}H-NMR spectrum. Table X tabulates the known long-range coupling constants to C_4.

TABLE IX

WIDTH AT HALF HEIGHT FOR C_4 IN THE PROTON COUPLED SPECTRA
OF SEVERAL METHYL-β-DISACCHARIDES AT 25.05 MHz IN D_2O

	$\nu_{1/2}$	$\Delta\nu_{1/2}$
MBC2	11.6 12.7[a]	
MBC2-d_8	9.5 9.6[a]	1.7-1.9[b,c] 1.8-2.0[b,c]
MBX2	12.0-12.5	

[a]From Fig. 3 in Ref. (18).
[b]Relative to methyl-β-D-glucoside-3,6,6'-d_3 which has a $\nu_{1/2}$ value of 7.6-7.9 (18).
[c]Compare this to the value obtained for $^3J(C_4H_5)$ of 4.2 Hz by 2nd order analysis.

A more suitable reference might be the C_4 peak in compounds 8 and 9. However, the C_4 peak will be overlapped by the C_6 or C_5 peaks at the fields utilized in this work. At higher fields this should not be a problem. Measurements on C_4 in DMSO-d_6

are given in Appendix V. They cannot be used for determination of $\emptyset$ because of the absence of a suitable reference. Deuterium exchange of the hydroxyls, so that coupling to OH4' is not a factor, might render the nonreducing end C_4 as a suitable reference at higher fields where second order effects became less important.

TABLE X

INDIRECT COUPLING CONSTANTS (Hz) TO
C_4 IN GLUCOSE RELATED COMPOUNDS[b]

Compound	J	Compound
MBC2	147[b,c]	^1J
β-Glucose	4.5[b]	$^2J(C_4H_3)$
MBC2-d_8 and methyl β-glucose-3,6,6'-d_3	(-)3.0-3.5[b]	$^2J(C_4H_5)$
β-Glucose	<1[a,b]	$^3J(C_4H_2)$

[a]By stereochemical arguments, not actually measured.
[b]See Ref. (18) and (33).
[c]Measured directly in this work.

Second Order Effects

Complications to the simple first order analysis to determine $\Delta\nu_{1/2}$ are collectively known as second order effects. Second order effects can both broaden or narrow[*] the overall carbon peak for which $\nu_{1/2}$ is measured. To accommodate the potential for second order effects Eq. 6 must be modified:

$$\nu_{1/2} = \sum_i J_i + F \pm S. \tag{9}$$

S represents the contribution from second order factors.

At least three types of second order effects have been identified which might alter $\nu_{1/2}$ for a proton coupled carbon peak (exclusive of ^1J). They are tabulated

[*]Line narrowing, the more unusual manifestation of a second order process, is called deceptive simplicity.

below with a brief explanation. Each of these has relevance to the results presented above.

1) Jones and coworkers ($\underline{37}$) have shown that overlap between the ^{13}C satellite resonance associated with the directly bonded proton, and a signal arising from a proton coupled over more than one bond to the carbon, will lead to second order effects. Lines can be broadened or narrowed. This situation arises if the following condition is met in the ^{1}H spectrum:

$$\frac{2 \cdot \Delta\delta}{^{1}J_{C_1H_i}} = 1 \pm 0.38 \qquad (10)$$

with the effect being greatest for direct overlap. In this equation $\Delta\delta$ is the chemical shift in Hertz between the directly attached proton and another proton coupled to the carbon over more than one bond. The effect becomes less important at high field because of dispersion of the individual resonances. This will be termed the "Jones" effect in the discussion below.

2) When the signals from two strongly coupled protons are close in proximity to one another then second order effects arise in both the ^{1}H-spectrum and the ^{13}C spectrum. Two cases are possible. Both cases occur if the following is <u>not</u> true,

$$\frac{2|\nu_A - \nu_B|}{J_{AB}} >> 1 \qquad (11)$$

where ν_i is the location of protons A and B in frequency units and J_{AB} is the coupling constant between the two protons. Again, the problem is reduced at high field as $|\nu_A - \nu_B|$ increases. The two cases are:

a) Both protons A and B are coupled to the carbon in question. This is called the ordinary second order effect.

b) Only one proton is indirectly coupled to the carbon in question. The second proton has a 0Hz indirect coupling to the carbon, but exerts an effect on its apparent coupling constant through the coupled proton. This is referred to as virtual coupling.

It was previously mentioned that there was an inconsistency in the value for $^3J(C_1\prime H_4)$ obtained from cellobiose and possibly also MBC2-d_8. This can easily be seen by comparing the $C_1\prime$ $\nu_{1/2}$ value for 2 (Table V) to the theoretical value obtained by summing the coupling constants, including the small coupling to $^2H_2$ in MBC2-d_8.* Several such comparisons are given in Table XI. The measured value for $C_1\prime$ in Cellobiose (10.7-10.9 Hz) is considerably less than that predicted by Eq. (6) (13.0-13.6).**

Perlin and coworkers rejected the use of the measured $C_1\prime$ value of cellobiose (16,18) because the calculated value for $\Delta\nu_{1/2}$ was too low, suggesting that χ is on the order of $\pm60°$. Their explanation was that overlap of the $C_1\prime$ peak for the α- and β-anomers interfered with the measurement of $\nu_{1/2}$. However, the fact that the α-$C_1\prime$ and β-$C_1\prime$ peaks are not perfectly degenerate should give a line broadening. Since a significant line narrowing is observed, their reason for not using the $\nu_{1/2}$ value is invalid.

It is instructive to explore other possible reasons why the measured $\nu_{1/2}$ value for $C_1\prime$ in cellobiose is not useful. At both 90 and 100 MHz*** the ^{13}C-satellite

---

* Given by $\dfrac{^2J(^{13}C_1{}^1H_2)}{6.51}$

** If the predicted $C_1\prime$ value (ca. 13.3 Hz) is used, rather than the measured value, then $\Delta\nu_{1/2}$ is approximately 4.0 Hz when the measured C_1 value (ca. 9.3 Hz) is used. This is evidence that the C_1 $\nu_{1/2}$ value is not greatly affected by 2nd order effects [S in Equation (9)]. The same conclusion is reached by summing the coupling constants.

*** 90 MHz was used by Perlin while 100 MHz was used in this study.

peak for $H_1{'}$ will fall in the middle of the proton envelope of peaks between 3 and 4 ppm. Table XII gives the ^{1}H-NMR chemical shifts for the protons coupled to $C_1{'}$ and C_1 (38). Also included are the critical regions for which the Jones effect might be expected to operate as a function of magnetic field strength. For $C_1{'}$ the protons $H_5{'}$ and H_4 are well within this region at both 90 and 100 MHz. H_4 is particularly suspect because it is near the center of the critical region. This suggests that the measured $\nu_{1/2}$ values are deceptively simple; that is, there are several outer combination bands which are weak in intensity and that do not contribute to the observed signal.

Because the H_1 proton is farther downfield the critical region for the "Jones" effect for C_1 is also moved downfield. Only H_5 is within this region and then only on the fringe. Since H_5 is only weakly coupled, it is not expected that the effect would be very large for C_1; so that, the measured $\nu_{1/2}$ is close to what is expected based on Equation (6).

This analysis coincides precisely with what is observed in Table XI. The measured $C_1{'}$ signal is much narrower than expected, while the C_1 signal is about what is predicted when instrumental broadening is included.

Because of the uncertainty in the $C_1{'}$ $\nu_{1/2}$ measurement in cellobiose, the value for $^3J(C_1{'}H_4)$ obtained in this and the previous study was obtained from MBC2-d_8. The original reason for this was to simplify the $C_1{'}$ peak by removing the large coupling to H_2. A further factor was that the C_1 and $C_1{'}$ peaks would be further apart in the spectrum of MBC2-d_8 than in the MBC2 spectrum because of the β-deuterium isotope effect (18,39). In fact, the observed separation was slightly greater in this study (25 MHz) than in the previous one (18) (22.6 MHz) allowing a more accurate determination of $\nu_{1/2}$ for $C_1{'}$. Indeed, a slightly lower value was obtained for $\nu_{1/2}$ in this study.

TABLE XI

SUMMATION OF COUPLING CONSTANTS CONTRIBUTING TO C_1 OR $C_1\prime$
FINE STRUCTURE IN SEVERAL GLUCOSE CONTAINING COMPOUNDS

		Coupling[a] Constants	Coupling System
$C_1\prime$ Cellobiose		5.6	$C_1\prime\ H_2\prime$
		2.1	$C_1\prime\ H_5\prime$
		4.3	$C_1\prime\ H_4$
	Predicted[b]	12.0	
	Measured	10.7-10.9	
C_1 Cellobiose		5.6	$C_1\ H_2$
		2.1	$C_1\ H_5$
	Predicted[b]	7.7	
	Measured	8.8-9.8	
$C_1\prime$ MBC2-d_8		0.9[c]	$C_1\prime\ {}^2H_2$
		2.1	$C_1\prime\ H_5\prime$
		4.3	$C_1\ H_4$
	Predicted[b]	7.3	
	Measured	7.9-9.2	
C_1 β-D-glucose-2,3,4,6',6-d_5		0.9[c]	$C_1\ {}^2H_2$
		2.1	$C_1\ H_5$
	Predicted	3.0	
	Measured	4.8	

---

[a]Absolute values are used.

[b]Does not include additional broadening due to field inhomogeneity,
α,β peak overlap, or residual small couplings such as $C_1\prime H_3$ or
$C_1\prime{}^2H_2$. Peak broadening due to instrumental factors has been
estimated to be between 1.0-1.6 Hz for the data generated in this
work. Slightly higher values are observed in the literature data (18).

[c]The coupling to ${}^2H_2$ is given by $J({}^2H_1X) = \frac{1}{6.51} \cdot J(H_1X)$.

In the previous work it was recognized that virtual coupling could be a factor
in the analysis of the $C_1\prime$ coupling in the MBC2-d_8 spectrum. This could result from
the strong coupling between H_4 and H_5 (9.5 Hz) and their close proximity (3-6 Hz).
This is despite the fact that H_5 does not directly couple to $C_1\prime$. Perlin simulated

the spectrum using an ABMRX spin system and found that a value for $^3J(C_1\prime H_4)$ of 4.3 Hz closely reproduced the observed $C_1\prime$ peak shape. This compared to a $\Delta\nu_{1/2}$ value of 4.5 Hz measured directly from the spectra. In the present study the value obtained was 3.1-4.4 Hz by direct measurement.

TABLE XII

^{1}H CHEMICAL SHIFTS AND CRITICAL REGION FOR JONES EFFECT IN CELLOBIOSE

Proton	δ[a]
$H_1\prime$	4.51
$H_2\prime$	3.32
$H_5\prime$	3.50
H_4	3.65
H_1	4.67
H_2	3.29
H_5	3.58

CRITICAL REGION FOR JONES EFFECT AND AFFECTED PROTONS

MHz	$C_1\prime$	Protons	C_1	Protons
90	3.27-3.96	$H_2\prime$,$H_5\prime$,H_4	3.43-4.12	H_5
100	3.39-4.01	$H_5\prime$,H_4	3.55-4.17	H_5
360	4.20-4.37		4.36-4.53	

[a]From Ref. (39).

Compensation for the Jones effect was not explicitly considered in the earlier work. The chemical shifts for $H_1\prime$, $H_5\prime$, and H_4 should all be close to those in cellobiose suggesting that deceptive simplicity may again be a factor. Therefore, the actual value for $^3J_{C_1\prime OCH_4}$ could be larger than 4.3 Hz, representing a χ value closer to 0°. If 3.1 Hz is taken as a lower limit* for $^3J_{C_1\prime OCH_4}$ then χ could range from ($\pm$) 0-50° on the basis of this work.

*Much lower values for $\Delta\nu_{1/2}$ do not seem feasible on the basis of structure.

The wide spread in the χ value obtained from the present work should not be interpreted to mean that this approach is without merit. Table XII also shows the critical regions for the Jones effect at 360 MHz[*] for C_1' and C_1 in cellobiose. In this case none of the coupled protons would be close to the critical region and the Jones effect would not be a factor. Second order effects related to the strong couplings between protons would also be reduced or eliminated. In addition, the C_1 and C_1' peaks for MBC2-d_8 would be completely separated. Therefore, by simply operating at a higher field it should be possible to directly apply a first order analysis to $\underset{\sim}{2}$.

Since we are really interested in comparing the relative χ values in compounds $\underset{\sim}{1}$ and $\underset{\sim}{2}$, it is also necessary to consider the accuracy of $\Delta\nu_{1/2}$ for compound 1. The lack of specific assignments in the 3-4 ppm region of the ^{1}H-spectrum makes it difficult to predict the likelihood of second order effects operating in the spectrum. It has already been mentioned that the apparent value for $^3J(C_1H_{5_e})$ is larger than predicted on the basis of Fig. 13. This suggests an ordinary second order contribution to both C_1' and C_1, as well as a virtual coupling contribution to C_1' because of coupling between H_4 and the H_5 protons. It is likely that none of these contributions affect the results significantly. This follows from the large separation expected between H_{5_e}, H_{5_a}, and H_4 in $\underset{\sim}{1}$ based on the ^{1}H-spectra of β-xylose and methyl β-xyloside (see below) (40), and the small difference already noted for similar second order effects in compound $\underset{\sim}{7}$.

Of greater concern is the possibility of a Jones effect causing either deceptive simplicity in the C_1' signal or broadening of the C_1 signal, or both. It has already been mentioned that the C_1' peak of both $\underset{\sim}{1}$ and $\underset{\sim}{4}$ is narrowed in DMSO-d_6, relative to D_2O, in contrast to what is expected. Table XIII tabulates the expected

---

[*]Corresponding to the 90 MHz ^{13}C-spectrum.

proton chemical shifts for $\underset{\sim}{1}$ in D_2O. These estimates are based on the assigned

spectra of $\underset{\sim}{4}$ and $\underset{\sim}{8}$ (40), and on the known shifts caused by substitution of the glu-

copyranosyl unit for a proton in comparing $\underset{\sim}{2}$ and $\underset{\sim}{5}$ (38,41). Also given are the

estimated critical regions for the Jones effect. In β-xylose the strongly coupled

H_{5_e} proton is well within this region for C_1 but not $C_1{}^\prime$. In xylobiose it should be

only at the extreme downfield edge of this region. No strongly coupled signals are

expected to be in the middle of the critical region where the effect is greatest.

For $C_1{}^\prime$ both H_4 and H_{5_a} are on the periphery of the region of interest. Since both

are apparently weakly coupled to $C_1{}^\prime$ this should not affect $v_{1/2}$ for that signal.

This suggests that any error due to second order effects resides in the broadening

of the C_1 signal. Since the C_1 signals are nearly identical in compounds $\underset{\sim}{1}$ and $\underset{\sim}{4}$ it

is suggested that errors due to mixing of the ^{13}C-satellite signals with strongly

coupled proton signals are small. Therefore, a value of χ of ± 75-85° is probably

reasonable though probably slightly larger than the actual average value. Still, it

is reasonable to tentatively state on the basis of these coupling constant deter-

minations, that the χ value is greater in $\underset{\sim}{1}$ than in $\underset{\sim}{2}$. Further work at higher

fields should be able to clear up the tentative nature of this conclusion.

Before leaving the subject of the second order corrections to the observed

coupling constants it is necessary to consider the large apparent error in the

measured $\Delta v_{1/2}$ corresponds to $^3J(C_4H_1{}^\prime)$, which can be related to $\emptyset$ on the basis of

Fig. 13. Using a second order analysis Perlin and coworkers obtained 4.2 Hz for

$^3J(C_4H_1{}^\prime)$. If measured $v_{1/2}$ values are used than $\Delta v_{1/2}$ is only 1.7-2.0 Hz, (see

Table IX) considerably less than 4.2 H_z.

The reason for this large difference is related to the extremely strong

coupling between H_4 and H_5 in both compound $\underset{\sim}{7}$ and the reference compound methyl

β-D-glucoside-3,6,6${}^\prime$-d$_3$ ($\underset{\sim\sim}{10}$). The published chemical shifts for H_4 and H_5 in $\underset{\sim}{9}$ are

TABLE XIII

^{1}H CHEMICAL SHIFTS (ppm)[a]

	Reference	1	2	3	4	5_a	5_e	1′	2′	3′	4′	5_a′	5_c′
β-Glucose[b]	(41)	4.67	3.27	3.51	3.43	3.49							
β-Cellobiose	(38)	4.67	3.29	3.60	3.65	3.58		4.51	3.32	3.52	3.42	3.50	
Glycosidation Shift		0	0.02	0.09	0.22	0.99		-0.16	0.05	0.01	-0.01	0.01	
Methyl β-xyloside	(40)	4.32	3.25	3.44	3.62	3.33	3.99						
β-xylose	(40)	4.57	3.23	3.42	3.63	3.32	3.93						
β-xylobiose (estimate)[c]		4.57	3.25	3.51	3.85	3.41	4.02	4.41	3.28	3.43	3.62	3.33	3.94

Critical Regions at 100 MHz

	Coupled Protons[d]		Coupled Protons[d]	
β-Xylose	3.29-3.91	H4, H5′$_a$	3.45-4.07	H5$_e$
β-Xylobiose			3.45-4.07	H5$_e$

---

[a] Relative to TSP as internal standard.
[b] + 0.04 ppm to correspond to TSP reference.
[c] Applies same glycosidation shift for cellobiose using β-xylose as a model.
[d] Protons within the region strongly coupled to that carbon.

different by only 0.08 ppm (41). The coupling constant is 9.4 Hz (41). This system is strongly coupled and might be expected to show significant broadening. Indeed, $\nu_{1/2}$ for $\underset{\sim}{10}$ is 7.7 Hz whereas $^2J(C_4H_5)$ is only -3.0 to -3.5 Hz by second order analysis. The method of Perlin accounts for this so that the published value for $\emptyset$ should be accurate.

To briefly summarize, on the basis of first order analysis average χ values of ± 0-50° and ± 75-80° are estimated for methyl β-cellobioside-d_8 and xylobiose, respectively. Consideration of second order effects, which apparently are significant at the magnetic fields used for this and earlier studies, imparts some uncertainty to these values. However, the basic conclusion that the average χ value is greater in $\underset{\sim}{1}$ than $\underset{\sim}{7}$, and by inference $\underset{\sim}{2}$, remains unchanged. A value for ϕ of ± 25-30° in $\underset{\sim}{7}$ is judged to be accurate. No comparable value for $\underset{\sim}{1}$ was obtained.

SUMMARY

From ^1H-T_1 measurements on compounds $\underset{\sim}{1}$ and $\underset{\sim}{2}$ in D_2O we have concluded that the average distance between H_1' and H_4 (r_{1-4}) is 0.1-0.2 Å greater in $\underset{\sim}{1}$. Absolute values of 2.2 Å and 2.1 Å were obtained for $\underset{\sim}{1}$ and $\underset{\sim}{2}$, respectively. After consideration of the limitations of the technique it was concluded that these values are slightly less than the actual values. Melberg (7) has calculated an average value of 2.28 Å for $\underset{\sim}{2}$.

Measurements of the across linkage coupling constants, $^3J(C_1'H_4)$ and $^3J(C_4H_1')$, were made to compare the relative values of ϕ and χ in $\underset{\sim}{1}$ and $\underset{\sim}{2}$. On the basis of first order analysis, χ was estimated to be ± 75-85° in $\underset{\sim}{1}$ and ± 0-50° in $\underset{\sim}{7}$. The linkage conformation of $\underset{\sim}{7}$ is thought to be the same as that of $\underset{\sim}{2}$ from optical rotation studies (42) and from measurements of ^{13}C-NMR chemical shifts (43). Melberg (7) calculates the average χ value to be close to +25-30° for 2. Consideration of

possible second order effects on the fine structure of the C_1' and C_1 signals shows that the actual values are less certain but that χ is larger in compound $\underset{\sim}{1}$.

Perlin (18) gives a value of $\pm$ 25-30° for ϕ in $\underset{\sim}{7}$. No reliable experimental value was obtained from this work but the above value was judged to be reliable. On the basis of the exo-anomeric effect (44) it is expected that the value in $\underset{\sim}{1}$ is not greatly different. The ranges proposed for ϕ and χ in $\underset{\sim}{1}$ and $\underset{\sim}{2}$ are thus consistent with the $^1H-T_1$ data.

These studies represent an attempt at a direct experimental comparison of the solution conformations of $\underset{\sim}{1}$ and $\underset{\sim}{2}$. All previous work has involved either calculated structures, extrapolation from x-ray analysis of the solids, or inference from poly-saccharide solution studies. The conclusions drawn from this earlier work, that $\underset{\sim}{1}$ should have a more staggered and flexible conformation because of the absence of steric hindrance from C_6, have been experimentally substantiated.

Because of the uncertainty in the ϕ and χ values,* as well as the H_1' to H_4' distances, it is not possible to construct specific average structures from this work. Nevertheless, it is possible to mentally construct a comparison. The average conformation of $\underset{\sim}{1}$ consists of a greater degree of departure from the two-fold heli-cal structure** than is found in $\underset{\sim}{2}$. Both molecules possess conformational minima on either side of the two-fold helix line (7). The linkage conformation is dynamic with interconversion being rapid on the NMR time scale (7,31). The average distance between O_5' and O_3 will be greater in $\underset{\sim}{1}$ than in $\underset{\sim}{2}$ because of the greater amount of time spent in conformations far removed from the 2-fold helix in $\underset{\sim}{1}$. The average bridge angle T is calculated to be about 113.4° in $\underset{\sim}{2}$ which represents a considerable

---

*Uncertainty due to second order effects, uncertain accuracy of modified Kurplus relationship, and inability to distinguish between positive and negative values.
**$(\phi,\chi)=0,0$; H_1' and H_4 parallel and at a minimum separation.

relaxation from the value of 116° in the crystal (7). A similar relaxation of T is expected for 1.

EXPERIMENTAL

All NMR spectra were recorded on a Jeol FX-100 FT spectrometer (99.61 MHz ^{1}H, 25.05 MHz ^{13}C). Temperature control was obtained with a Jeol supplied NM 5471 model temperature controller stable to ± 0.5°C and calibrated to ± 2.0°C. The 5-mm dual probe (^{1}H/^{13}C) was used for all [1]H-T_1 and ^{13}C-gated decoupling work.

[1]H-T_1 measurements used the standard inversion-recovery pulse sequence. An interval of at least 5 times the longest carbohydrate T_1 was employed. T_1 values were obtained from signal intensities using a weighted least squares linear regression program provided by Jeol. Both the xylobiose and cellobiose samples were dissolved at 5% (w/v) in D_2O (99.8%) in constricted NMR tubes (527-PP Wilmad Glass Co.) and given 4 freeze-pump-thaw cycles prior to sealing. The xylobiose had been treated with a cationic ion-exchange resin (IR-120, acid form) to remove any residual paramagnetic impurities from its synthesis.

All coupled ^{13}C-NMR spectra were obtained using gated decoupling in which the decoupler is cycled on prior to acquisition to maintain the NOE enhancement and cycled off during acquisition to give a coupled spectrum. Most coupled ^{13}C-NMR spectra were obtained at ambient temperatures. All measurements of $\nu_{1/2}$ were by hand using expanded spectra.

Each compound was characterized by its ^{13}C-NMR spectrum. Literature assignments were used when available. Xylobiose (1), methyl β-xylobioside (6) and methyl β-cellobioside (3) were synthesized. Details are given elsewhere (44). Deuteration of 3, methyl β-glucoside, and methyl β-xyloside was done by refluxing in D_2O over

Raney nickel (<u>24</u>). Progress of the reaction was monitored by ^{13}C-NMR. All other compounds were purchased and used as is.

LITERATURE CITED

1. Brandt, D. A. and Goebel, K. D., Macromolecules 8:522-30(1975).

2. Yathindra, N. and Rao, V. S. R., Biopolymers 10:1891-1900(1971).

3. Sundararajan, P. R. and Rao, V. S. R., Biopolymers 8:305-12(1969).

4. Settineri, W. J. and Marchessault, R. H., J. Polymer Sci., Part C, 11:253-64(1965).

5. Woodcock, C. and Sarko, A., Macromolecules 13:1187-94(1980).

6. Rees, D. A. and Skerrett, R. J., Carbohyd. Res. 7:334-8(1968).

7. Melberg, S. and Rasmussen, K., Carbohyd. Res. 71:25-34(1979).

8. Swenson, H. A., Tappi 56:106-10(1973).

9. Stoddard, J. F., Stereochemistry of Carbohydrates, Wiley-Interscience, New York, New York, 1971.

10. Leung, F. and Marchessault, R. H., Can. J. Chem. 51:1215-22(1973).

11. Chu, S. S. C. and Jeffry, G. A., Acta Cryst. B24:830-8(1968).

12. Ham, J. T. and Williams, D. G., Acta Cryst. B26:1373-83(1970).

13. Fries, D. C., Rao, S. T., and Sundaralingham, M., Acta Cryst. B27:994-1005 (1971).

14. Moran, R. A. and Richards, G. N., Acta Cryst. B29:2770-83(1973).

15. Leung, F., Chanzy, H. D., Perez, S., and Marchessault, R. H., Can. J. Chem. 54: 1365-71(1976).

16. Perlin, A. S., Cyr, R., Ritchie, G. S., and Parfondry, A., Carbohyd. Res. 37: C1-4(1974).

17. Parfondry, A., Cyr, R., and Perlin, A. S., Carbohyd. Res. 59:299-308(1977).

18. Hamer, G. K., Balza, F., Cyr, N., and Perlin, A. S., Can. J. Chem. 56:3109-16(1978).

19. Perlin, A. S. and Hamer, G. K., In Amer. Chem. Soc. Symposium Series 103: 123-41(1979).

20. Gagnaire, D. Y., Nardin, R., Taravel, F. R., and Vignon, M. R., Nouveau J. de Chimie 1:423-30(1977).

21. Excoffier, G., Gagnaire, D. Y., and Taravel, F. R., Carbohyd. Res. 56:229-38 (1977).

22. Hall, L. D. and Preston, C. M., Carbohyd. Res. 49:3-11(1976).

23. Berry, J. M., Hall, L. D., Welder, D. W., and Wong, K. F., Carbohyd. Res. 54: C22-24(1977).

24. Koch, H. J. and Stuart, R. S., Carbohyd. Res. 59:C1-6(1977).

25. Balza, F., Cyr, N., Hammer, G., Perlin, A. S., Koch, H. J., and Stuart, R. S., Carbohyd. Res. 59:C7-11(1977).

26. Levy, G. C. and Peat, I. R., J. of Magn. Reson. 18:500-21(1975).

27. Berry, J. M., Hall, L. D., and Wong, K. F., Carbohyd. Res. 56:C16-20(1977).

28. Brown, C. J., J. Chem. Soc. (A),927-32(1966).

29. Takai, S. and Jeffrey, G. A., Acta. Cryst. B33:3033-40(1977).

30. Preston, C. M. C., Applications of fourier transform NMR spectroscopy: proton spin lattice relaxation in organic molecules. Doctoral Dissertation, The University of British Columbia, October, 1975.

31. Part 1 of this section.

32. Freeman, R., Hill, H. D. W., Tomlinson, B. L., and Hall, L. D., J. Chem. Phys. 61:4466-4473(1974).

33. Cyr, N., Hamer, G. K., and Perlin, A. S., Can. J. Chem. 56:297-301(1978).

34. Bock, K. and Pedersen, C., Acta Chem. Scand. B29:284-64(1975).

35. Part 3, Section III, this work.

36. Sundholm, E. G., Acta Chem. Scand. B32:177-81(1978).

37. Jones, A. J., Jenkins, G. A., and Heffernam, M. L., Aust. J. Chem. 83: 1275-9283(1980).

38. De Bruyn, A., Anteunis, M., and Verhegge, G., Bull. Soc. Chim. Belg. 84: 721-34(1975)

39. Pfeffer, P. E., Valentine, K. M., and Parrish, F. W., Jr., J. Am. Chem. Soc. 101:1265-79(1979).

40. De Bruyn, A., Hosten, N., and Anteunis, M. J. O., Bull. Soc. Chim. Belg. 88: 43-51(1979).

41. Perkins, S. J., Johnson, L. N., Phillips, D. C., and Divek, R. A., Carbohyd. Res. 59:19-34(1977).

42. Rees, D. A. J., Chem. Soc. (B)877-84(1970).

43. Part 2, Section III, this work.

44. Perez, S. and Marchessault, R. H., Carbohyd. Res. 65:114-20(1978).

45. Section IV.

SECTION III - IMPORTANT INTERACTIONS AFFECTING

THE GLYCOSIDIC LINKAGE CONFORMATION

IN β-1-4-LINKED CARBOHYDRATES

INTRODUCTION: FACTORS THAT DETERMINE THE GLYCOSIDIC LINKAGE CONFORMATION

The most favorable conformations of the glycosidic linkage are determined by a number of intra- and intermolecular interactions. In this section, several of these important factors will be investigated experimentally. Prior to discussing the results of this work, a brief general discussion of these interactions will be given.

In the classical semiempirical approach often used to calculate the preferred linkage conformations, it is customary to identify the important molecular interactions and model them using an appropriate potential function. In practice, one or more interactions is neglected, either to simplify the computational effort or because it is difficult to adequately describe the interaction mathematically. The neglected factors are usually estimated to be of less importance than the other factors (1,2,3).

The interactions that have been identified as being a factor in determining the linkage conformation are: Van der Waals attraction and repulsion,[*] intrinsic torsional barriers, bond and torsional strain, dipole-dipole interactions, intramolecular hydrogen bonding, and intermolecular effects of various types. The relative importance of each depends on the molecular configuration and the surrounding environment.

Intramolecular Van der Waals interactions have generally been considered to be the dominant factor in determining the linkage conformation of the isolated molecule for β-1-4-linked carbohydrates. Thus, it has been shown by considering hard sphere[**] interactions only that severe steric constraints are present in cellobiose that restrict the possible number of conformations to a small percentage of the

---

[*]The Van der Waals interaction is one of several nonbonded interactions to be considered. In it, the attractive force arises from the polarizability of the individual atoms which results in an induced dipole. This force, which is also termed the London dispersion force, is always present between two atoms. The repulsive force, which operates only at very short range, is due to steric overlap of the electron clouds of closely approaching atoms. Though the Van der Waals interaction is often modeled as an interaction between hard spheres, it is instructive to consider what actually happens using a simple classical argument. As two atoms approach, their electron clouds change shape in accordance with their polarizability. As they further approach, the repulsive force becomes dominant and the electron clouds of both atoms become compressed. This compression results in an increased electron density near the nucleus.

In terms of NMR, this compression increases the shielding constant which results in an upfield shift of the NMR signal for either a ^{13}C or ^{1}H nuclei. This is termed the steric compression shift. This differs from the change in the shielding constant which might result from conformational factors that affect hybridization of the atom. For instance, if the valence angle of an atom is altered by a conformational change, then this will change the hybridization of the electron cloud which in turn also alters the shielding constant. As the s-character increases ($sp^3 \rightarrow sp^2$), corresponding to an increase in the valence angle above 109°, the nucleus becomes more shielded with a resulting upfield shift. At an adjacent atom, the effect would be reversed because electrons will be withdrawn from the nucleus to compensate for the decrease in electron density in the bond between the atoms. Thus, the neighboring nuclei would become less shielded with a resulting downfield shift of its NMR signal. Examples of both of these phenomena will be given below.

[**]Each atom is assigned its Van der Waal radii and is considered incompressible.

total conformational map.[*] The dominant steric interactions involve overlap of the linkage protons and overlap of C_6 with either the C_2' hydroxyl or H_1'. By utilizing a potential function to model the Van der Waals interaction, it was further shown that energy minima should exist on both sides of the 2-fold helix line (1). In this work, comparisons of linkage conformations and various spectral parameters, in compounds with and without C_6, have been made to assess the effect of C_6 steric hindrance on linkage structure.

The primary intrinsic torsional barrier present arises from the anomeric effect (see Section I). It has been shown using quantum-mechanical calculations (4), correlation of known crystal structures (5), and spectroscopic methods (6,7) that the dihedral angle ϕ has a conformational preference largely determined by the anomeric effect. This is often termed the exo-anomeric effect. This recently has been estimated to be between 2-3 Kcal/mole (4,6).

The dihedral angle χ is not restricted by this interaction. It has been shown in a number of compounds that χ possesses a wider range of possible values than ϕ (4,5,6,7). Lemieux (6) proposes that this effect is most important in solution when crystal forces are not operating to force the linkage into a specific conformation. In this study, no specific work was done concerning the contribution of the anomeric effect to the linkage conformation.

The effects of bond and torsional angle strain are generally not considered in most model calculations because of their complexity, though in a recent report, Melberg and Rasmussen have included them (3). The magnitude of these effects is generally considered to be small (1). In this work, these strains are considered to

---

[*]The common method of plotting "allowed" linkage conformations (ϕ, χ) on the so-called ϕ, χ map. See Ref. (1) for an example.

result from, rather than to control it, conformational change. As such, conclusions concerning the effect of a change in the bridge angle τ in going from the crystal to solution, on the chemical shift of the linkage carbons, have been made.

Intramolecular dipole-dipole interactions are generally neglected in attempts to model the linkage because they are generally weak in these systems. The overall effect is modulated by the solvent (2). It is not considered in the study.

The possibility of an intramolecular hydrogen bond between O_3 and $O_{5'}$ has been postulated by many authors (1,3) to be a factor in determining the linkage conformation. This bond is known to exist in the crystals of both cellobiose and xylobiose from x-ray diffraction and vibrational spectroscopic studies (8,9,10). The bond has also been postulated to exist in the DMSO solution of cellobiose (11). Rees and Scott (12) have suggested that this hydrogen bond is only a secondary factor in determining the conformation in solution, if it exists at all (12). The presence of the intramolecular hydrogen bond in the DMSO-d_6 solutions of cellobiose, methyl β-cellobioside, and xylobiose has been confirmed in this work. From analysis of the ^{1}H-NMR spectra of these systems, a description of the bond geometry is given, and inferences are made relative to its importance in determining the conformation.

In the crystal, the effect of intermolecular interactions is certainly an important factor in determining the overall conformation of the molecule. The large decrease in free energy accompanying lattice formation could dominate and override many of the other factors discussed above. In solution, interaction with the solvent should be much less dominant (1). These factors are briefly considered below by considering the effects of solvation and phase on the linkage carbon chemical shifts.

LITERATURE CITED

1. Rees, D. A. and Skerrett, R. J., Carbohyd. Res. 7:334-48(1968).

2. Whittington, S. G., Colston. Pap. 1975:307-22.

3. Melberg, S. and Rasmussen, K., Carbohyd. Res. 71:25-34(1979).

4. Tvaroska, I. and Kozar, T., Carbohyd. Res. 90:173-85(1981).

5. Perez, S. and Marchessault, R. H. Carbohyd. Res. 65:114-20(1978).

6. Lemieux, R. U. and Koto, S., Tetrahedron 30:1933-44(1974).

7. Tsukada, S. and Inoue, Y., Carbohyd. Res. 88:19-38(1981).

8. Chu, S. S. C. and Jeffrey, G. A., Acta Cryst. 1968:B24-30.

9. Hatakeyama, H., Nagasaki, C., and Yurugi, T., Carbohyd. Res. 48:149-58(1976).

10. Marchessault, R. H. and Liang, C. Y., J. Polymer Sci. 59:357-78(1962).

11. Casu, B., Reggiani, M., Gallo, G. G., and Vigevani, A., Tetrahedron 22:3061-83(1966).

12. Rees, D. A. and Scott, W. E., J. Chem. Soc. B, 1971:469-79.

THE EFFECT OF C_6 ON THE LINKAGE CONFORMATION

It has been postulated that the steric hindrance, created by the introduction of the C_6 hydroxymethyl group on the reducing-end anhydropyranose ring, is the single most important factor in determining the average conformation of the β-1,4-linked oligomers based on glucose (1,2,3). In the oligomers based on xylose, the absence of this group allows a greater conformational freedom resulting in a different average conformation. In this case, other interactions such as the anomeric effect, combined with the remaining steric factors, function to limit the allowed set of conformations (1).

The steric crowding associated with C_6 can readily be seen using space filling models. Refer to Fig. 1 in which a model of cellobiose is compared to a model of xylobiose. C_6 is identified by the arrow. As the reducing end group rotates, relative to the nonreducing group, C_6 interacts sterically with both the $C_{2'}$ hydroxyl and $H_{1'}$. In the absence of C_6, a much greater breadth of conformations are available at the linkage.

In the present work, the effect of C_6 steric hindrance on the linkage conformation has been explored in several ways. First, by determining the relative conformations of xylobiose and cellobiose, the effect of C_6 on linkage conformation is obtained by inference. For instance, in Section II, it was shown that both cellobiose and xylobiose possess a dynamic linkage. Using ^{13}C long range proton coupling constants and ^1H-T_1 data, it was concluded that xylobiose possesses a more staggered* linkage conformation. Therefore, since the major difference between the

---

*Further removed from the 2-fold helix line.
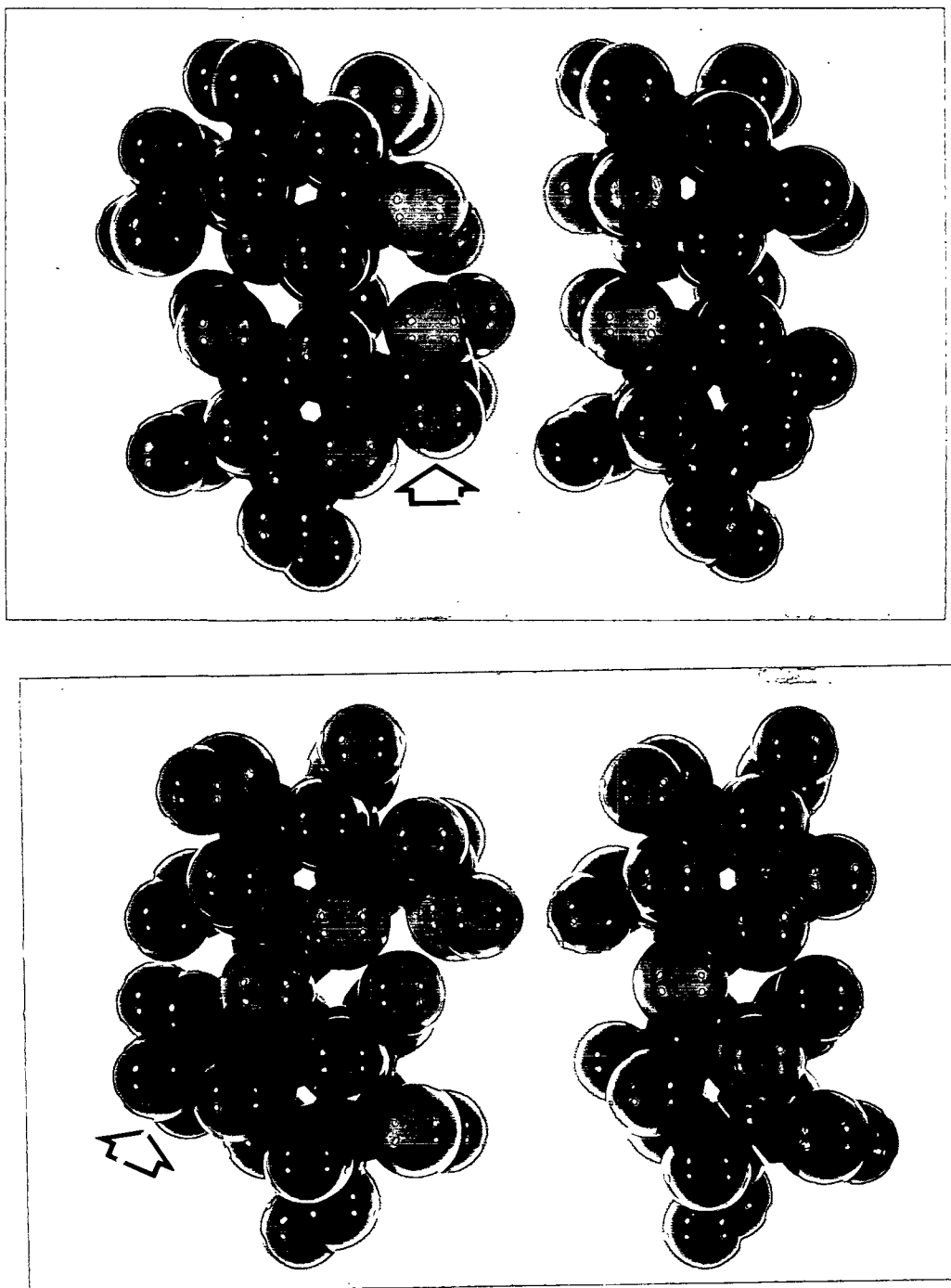
Figure 1. Comparison of the structures of cellobiose (left) and xylobiose (right) using space filling models. Both front and back views are shown. The reducing end is down in each case. The impact of C_6 (arrows) on steric crowding is readily apparent.

two is the absence of the C_6 groups, it is readily inferred that C_6 is of primary importance in determining the linkage conformation in cellobiose.[*]

In a similar way, the absence of a strong intramolecular hydrogen bond in xylose or securidebiose (see Part III this section), in comparison to cellobiose, can be inferred to mean that C_6 is a primary factor in determining the characteristics of the intramolecular hydrogen bond. To carry this further, it also can be inferred that the hydrogen bond is at best of secondary importance, since only a weak bond is present in xylobiose even though the conformations are available for a bond of greater strength (4).

A second approach in assessing the effect of C_6 on linkage conformation was to measure a characteristic spectroscopic property of the linkage in model compounds that do and do not contain the C_6 group. It turns out that the differences of the linkage C_4 chemical shift with an appropriate monosaccharide model correlates with the presence or absence of this group.

The approach utilized was to compare this shift differential in several xylo- and cello-oligosaccharides and in some related disaccharide models. The contrasts between the spectra[**] of the xylo- and cello-oligosaccharides suggest significant differences between the two series in the constraints on the linkage. While the chemical shift of C_4 differs only slightly between glucose and xylose (5), indicating that presence of a hydroxymethyl group (C_6) at C_5 in glucose has a relatively small effect, the difference between the linkage C_4 chemical shifts of the xylo- and cello-oligosaccharides is ~1.8 ppm in D_2O.[***] Such a large difference would not be

---

[*]A model shows that C_6' is too distant from the linkage to be a significant steric factor in the cellobiose linkage.

[**]Refer to Section IV.

[***]In dimethyl sulfoxide-d_6 the differences becomes 5.2 ppm.

expected on the basis of the effect of more replacement of a xylosyl by a glucosyl residue, as those two substituents, which differ only by the absence of C_6 for xylosyl, would be perceived (6) as nearly equivalent by the C_4 atom. It appears most likely that this difference is a manifestation of significant differences in the average conformation, or in the solvation environment, of the β-(1→4) linkages in the two, homologous, oligosaccharide series. Differences in average linkage-conformation or in accessibility to the linkage may explain differences in reactivity and solubility of the two types of oligosaccharides.

Colson et al. (7), in comparing the chemical shifts of the linkage C_1 and C_4 atoms in maltotriose with those of the cycloamyloses, found downfield shifts of 1.8 and 4.0 ppm, respectively, for these atoms in the (more constrained) cycloamyloses. The comparable shifts for the cello-oligosaccharides relative to the xylo-oligosaccharides are downfield by 0.7 and 1.8 ppm.

The greater constraints at the linkage for the cello-oligosaccharides appear to result from the presence of C_6. The role of C_6 is further suggested by the pattern of chemical shifts of the disaccharides, recorded in Table I. The chemical shifts of the linkage C_4 atom of xylobiose and cellobiose, relative to those of the appropriate monosaccharides, are compared with data for several other β-(1→4)-linked disaccharides. Both mannobiose and 4-O-β-D-glucosyl-D-mannose, which possess reducing-end C_6 groups similarly constituted to that of cellobiose, have chemical shifts, relative to the respective monosaccharides, comparable with that of cellobiose. In contrast, the chemical shifts of C_4 for 4-O-β-D-galactosyl-D-xylose and 4-O-β-D-glycosyl-D-xylose, which do not have a C_6 atom in the reducing ring, are nearly identical to that for xylobiose. This pattern is also found in the methyl disaccharides and the acetates.

TABLE I

CHEMICAL SHIFTS OF THE LINKAGE C$_4$ ATOM FOR
SEVERAL β(1→4)-LINKED DISACCHARIDES

	Chemical Shift of C4	Chemical-Shift Change Relative to Monosaccharide
β-Xylobiose	77.3	7.1
4-O-β-D-Galactosyl-D-xylose	77.7[a]	7.5
4-O-β-D-Glucosyl-D-xylose	77.4	7.2
β-Cellobiose	79.5	8.9
β-Mannobiose	77.5	9.9
4-O-β-D-Glucosyl-β-D-mannose	77.3	9.7
β-Xylose	70.2[b]	
β-Glucose	70.6[b]	
β-Mannose	67.6[b]	

[a]Relative to external Me$_4$Si (8).
[b]See Ref. (5).

Since a substituent effect is not operating and in view of the large magnitude of this shift in DMSO-d$_6$, it is virtually certain that a linkage conformational change is the cause of this shift differential.[*] The actual relationship of linkage conformation to C$_4$ chemical shift is not well understood.

The final approach used to investigate the steric effect of C$_6$ was to measure a property of the hydroxymethyl group itself. To do this, a comparison was made between the ^{13}C-T$_1$ values for C$_6$ and C$_{6'}$ in cellobiose. In the present work, the values were identical and very low indicating that neither 6-carbon undergoes rapid internal rotation. A slightly lower value was observed for the reducing end C$_6$ for methyl β-cellobioside and methyl β-lactosides by Hall et al. (10). This is indicative of a longer correlation time and hence a slightly greater barrier to internal rotation for C$_6$ based on the overall low T$_1$ values for both groups.

[*]It is not related to steric compression since this would reverse the order, i.e., cellobiose would have a C$_4$ shifted farther upfield than xylobiose. A recent study comparing chitobiose to cellobiose does claim that steric compression is a factor in the C$_{1'}$ shift (9).

SUMMARY

Evidence has been found to show that the reducing end C_6 hydroxymethyl group is a primary factor in determining the β-1,4-linkage conformation of glucose-containing polymers. Thus, the major difference between the conformations of cellobiose and xylobiose are related to the steric restrictions imparted by this group.

LITERATURE CITED

1. Sundararajan, P. R. and Rao, V. S. R., Biopolymers 8:305-12(1969).

2. Swenson, H. A., Schmitt, C. A., and Thompson, N. S., J. Polymer Sci., Part C, 11:243-52(1965).

3. Rees, D. A. and Skerrett, R. J., Carbohyd. Res. 7:334-48(1968).

4. Rees, D. A. and Scott, W. E., J. Chem. Soc. B 1971:469-79.

5. Gorin, P. A. and Mazurek, M., Can. J. Chem. 53:1212-23(1975).

6. Colson, P. and King, R. R., Carbohyd. Res. 47:1-13(1976).

7. Colson, P., Jennings, H. J., and Smith, I. C. P., J. Am. Chem. Soc. 46:8081-6 (1974).

8. Erbing, B., Lindberg, B., and Norberg, T., Acta Chem. Scand. Ser. B 32:308-10 (1978).

9. Tsukada, S. and Inoue, Y., Carbohyd. Res. 88:19-38(1981).

10. Berry, J. M., Hall, L. D., and Wong, K. F., Carbohyd. Res. 56:C16-20(1977).

^{1}H-NMR SPECTRA OF SEVERAL β-1,4-LINKED DISACCHARIDES UNDER CONDITIONS OF SLOW EXCHANGE: NEW EVIDENCE FOR AN INTRAMOLECULAR HYDROGEN-BOND

INTRODUCTION

Studies to determine the most likely conformations of the glycosidic linkage in the β-1-4-linked di- and oligosaccharides have often considered the presence of an intramolecular hydrogen-bond between the adjacent rings (1,2,3). The most likely intramolecular H-bond would occur between the hydroxyl at C_3 and the ring oxygen in a contiguous unit ($O_3H....O_5$') as illustrated in Fig. 1. X-ray diffraction studies clearly show that this bond exists in crystalline β-cellobiose (1a) (4,5). Crystalline methyl β-cellobioside (2) similarly contains this bond with the added participation of the hydroxyl at C_6', in a bifurcated arrangement (6). The vibrational spectra of the solid cello-oligosaccharides (7) and of xylan (8) also exhibit evidence of an intramolecular H-bond.
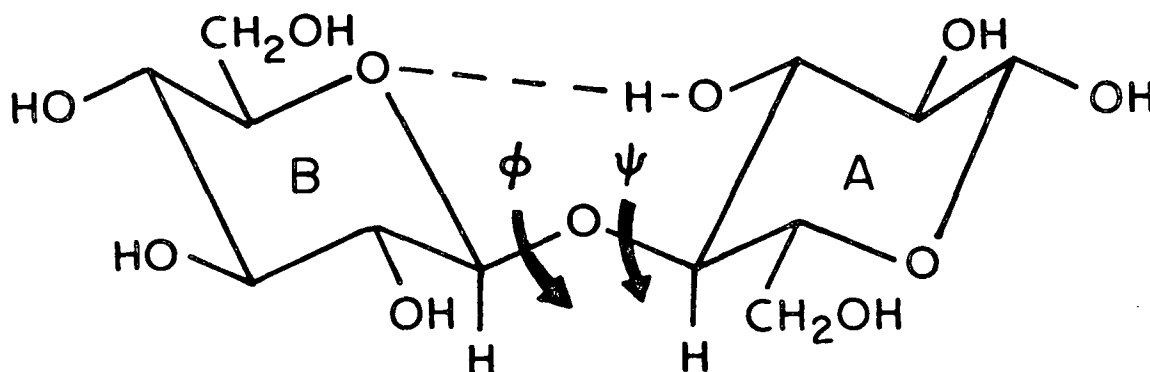
Figure 1. Structure of β-cellobiose illustrating the $O_3H...O_5$' intramolecular hydrogen-bond and the linkage dihedral angles φ and χ. In the number system used in this paper, the B ring is primed.

In solution, the $O_3H\ldots O_{5'}$ intramolecular H-bond has been proposed by Casu et al. for cellobiose in DMSO (9). They cite the downfield (>5 ppm)[*] location of the $O_{2'}H$ and O_3H resonances in the ^{1}H-NMR spectrum of maltose as being indicative of an intramolecular H-bond.[**] By analogy, the appearance of a nonanomeric hydroxyl at 5.18 ppm (38°C)[***] in cellobiose was taken as evidence for an intramolecular H-bond. On the basis of chemical shift (9) and hydrogen-deuterium exchange equilibria (11) it was proposed that this H-bond is weak.

The ^{1}H-NMR of 2 in DMSO-d_6 contains two nonanomeric hydroxyls downfield of 5 ppm. From spin-decoupling experiments and a comparison with the spectrum of methyl β-glucoside (4c), one of these resonances can be assigned to O_2H. Based on this observation, Michell (12) questioned the validity of using the downfield location of a nonanomeric hydroxyl as the criterion for an intramolecular H-bond in cellobiose.

An $O_3H\ldots O_{5'}$ intramolecular H-bond has also been proposed, on the basis of computer studies, as a stabilizing factor in xylan (1,2). The proposed bond is calculated to be longer and weaker than that proposed for cellulose. No evidence for this bond exists for a dissolved xylan or xylobiose (5). Raman and IR evidence for the bond in solid xylobiose has been found (22).

Because of the uncertainty in the evidence for interring intramolecular H-bonds in solutions of the β-1,4-linked disaccharides, a reinvestigation of their existence was pursued as part of broader study concerning the dynamics and structure of the linkage. The present work re-evaluates the hydroxyl proton NMR assignments using

---

[*]All chemical shifts are given relative to internal TMS using the δ scale.
[**]The exchange of the hydroxyl protons in acid-free DMSO-d_6 is slowed so that individual resonances can be observed (10).
[***]Hydroxyl proton resonances in DMSO are temperature sensitive requiring the chemical shift value to be referenced to a temperature.

comparisons to model compounds and spin-decoupling of the spectra at higher temperatures. Evaluation of the chemical shift temperature behavior and coupling constants of the hydroxyl proton resonances is used as an indication of intramolecular H-bonding (13). In particular, the existence of intramolecular hydrogen-bonds in xylobiose, cellobiose, and related compounds was investigated. This was a part of a more extensive study to better describe the structure of the β-1,4-linkage in these types of compounds.

The remainder of the discussion is organized into two parts. The results section contains the assignment methods and results leading to a complete description of the hydroxyl region in the ^{1}H-NMR spectra of methyl β-cellobioside, cellobiose, xylobiose, and related compounds in DMSO-d_6. Included is a discussion involving the response to temperature of the hydroxyl proton signals. Emphasis is given to the assignment of the OH_3 hydroxyl which is thought to participate in the intramolecular H-bond.

In the first part a brief introduction into the existing literature assignments of the pertinent monosaccharides is given for clarification. Supplemental material can be found in the appendices. Representative spectra are given in Appendix VI, while the detailed assignments for the hydroxyl regions are compiled in Appendix VII. Appendix VII contains a complete description of the spin decoupling work applied to the spectrum of methyl β-cellobioside.

This is followed by a discussion section in which the unique characteristics of the OH_3 signal are discussed and related to that hydroxyls participation in the intramolecular H-bond. In this part the differences between the O_3H signal in the cellobiose and xylobiose type structures are emphasized.

RESULTS

Assignments

Monosaccharides

Assignment of the ^{1}H-NMR hydroxyl regions in the disaccharides 1 and 2 is aided by comparisons to monosaccharide model compounds. In particular, xylose (3a,b), glucose (4a,b), methyl β-xyloside (3c), methyl α-xyloside (3d), and methyl β-glucoside (4c), which are depicted in Fig. 2, served as useful models for the disaccharides studied. Assignments based on the literature (9,14) or spin-decoupling are given in Table I for 56°C. Figures 3 and 4 show the spectra of 4a,b and 4c; each at three different temperatures. A major feature of these spectra is the upfield shift of the hydroxyl proton peaks with increasing temperature.
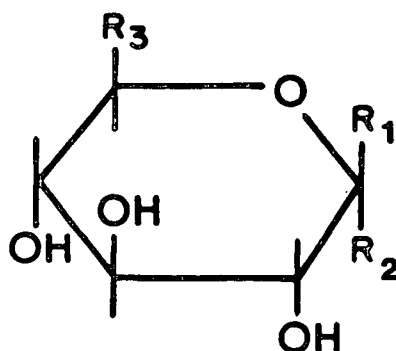
For: $R_3 = H$

IIIa : $R_1 = OH$

IIIb : $R_2 = OH$

IIIc : $R_1 = OCH_3$

IIId : $R_2 = OCH_3$

For: $R_3 = CH_2OH$

IVa : $R_1 = OH$

IVb : $R_2 = OH$

IVc : $R_1 = OCH_3$

IVd : $R_2 = OCH_3$
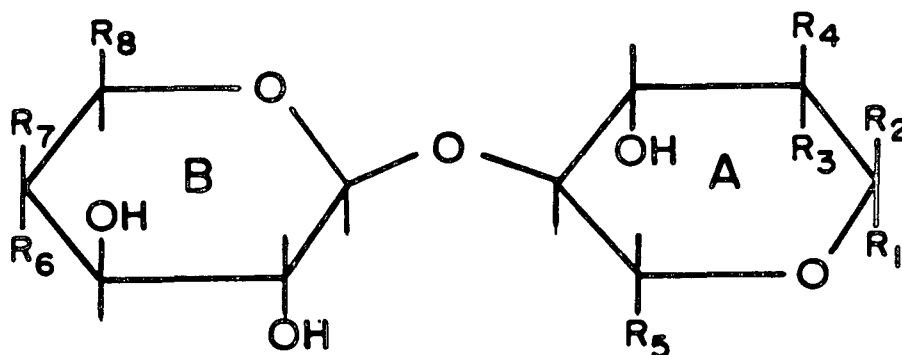
For: $R_4, R_6 = OH$

$R_5, R_8 = CH_2OH$

Ia : $R_1 = OH$

Ib : $R_2 = OH$

II : $R_1 = OCH_3$

For: $R_4, R_6 = OH$

Va : $R_1 = OH$

Vb : $R_2 = OH$

VIa : $R_1 = OH, R_8 = CH_2OH$

VIb : $R_2 = OH, R_8 = CH_2OH$

VIIa: $R_1 = OCH_3$

VIIb: $R_1 = OBn$

For: $R_5, R_8 = CH_2OH$

Xa : $R_1, R_4, R_7 = OH$

Xb : $R_2, R_4, R_7 = OH$

XIa : $R_1, R_3, R_6 = OH$

XIb : $R_2, R_3, R_6 = OH$

Figure 2. Compounds used in this study. If no group is given for R_i it is a proton. The compounds are: 1a,b cellobiose, 2 methyl β-cellobioside, 3a,b xylose, 3c methyl β-xyloside, 3d methyl α-xyloside, 4a,b glucose, 4c methyl β-glucoside, 4d methyl β-glucoside, 5a,b xylobiose, 6a,b securidebiose, 7a methyl β-xylobioside, 6b benzyl β-xylobioside, 10a,b lactose, and 11a,b 4 O-(β-D-glucopyranosyl)-O-mannopyranose.

TABLE I

HYDROXYL AND ANOMERIC PROTON CHEMICAL SHIFTS $(^3J_{HCOH})^a$
FOR SEVERAL MONOSACCHARIDES AT 56°C[b]

	3				4̰			
	a	b	c	d	a	b	c	d[c]
O_1H	6.33(6.5)	5.95(4.5)			6.36(6.5)	6.01(4.1)		
O_2H	4.64[d]	4.24	4.80(4.7)	4.44(5.9)	4.61[d]	4.26[b]	4.80(4.4)	
O_3H	4.64[d]	4.50(4.1)	4.70[e]	4.55	4.61[d]	4.41(4.4)	4.69[d]	
O_4H	4.64[d]	4.64[d]	4.74[e]	4.70	4.61[d]	4.60[d]	4.69[d]	
O_6H					4.26	4.26	4.30(5.9)	
C_1H	4.23	4.86	4.00	4.49	4.27	4.91	4.04	4.55
OM_e			3.35	3.26			3.38	

[a]Chemical shift on δ scale; $^3J_{HCOH}$ in Hz. The coupling values may be from spectra not recorded at 56°C.
[b]For 4a,b, and 3a,b,c the shifts are obtained from a regression analysis of the chemical shift temperature behavior over at least three temperatures. All shifts are relative to internal TMS using the central DMSO-d_5 (2.50 ppm) as a secondary reference.
[c]4d is methyl α-glucopyranoside. The value given is for 38°C from a reference by Casu (9).
[d]Part of a complex of peaks throughout temperature studied; value only approximate.
[e]Assignments speculative.
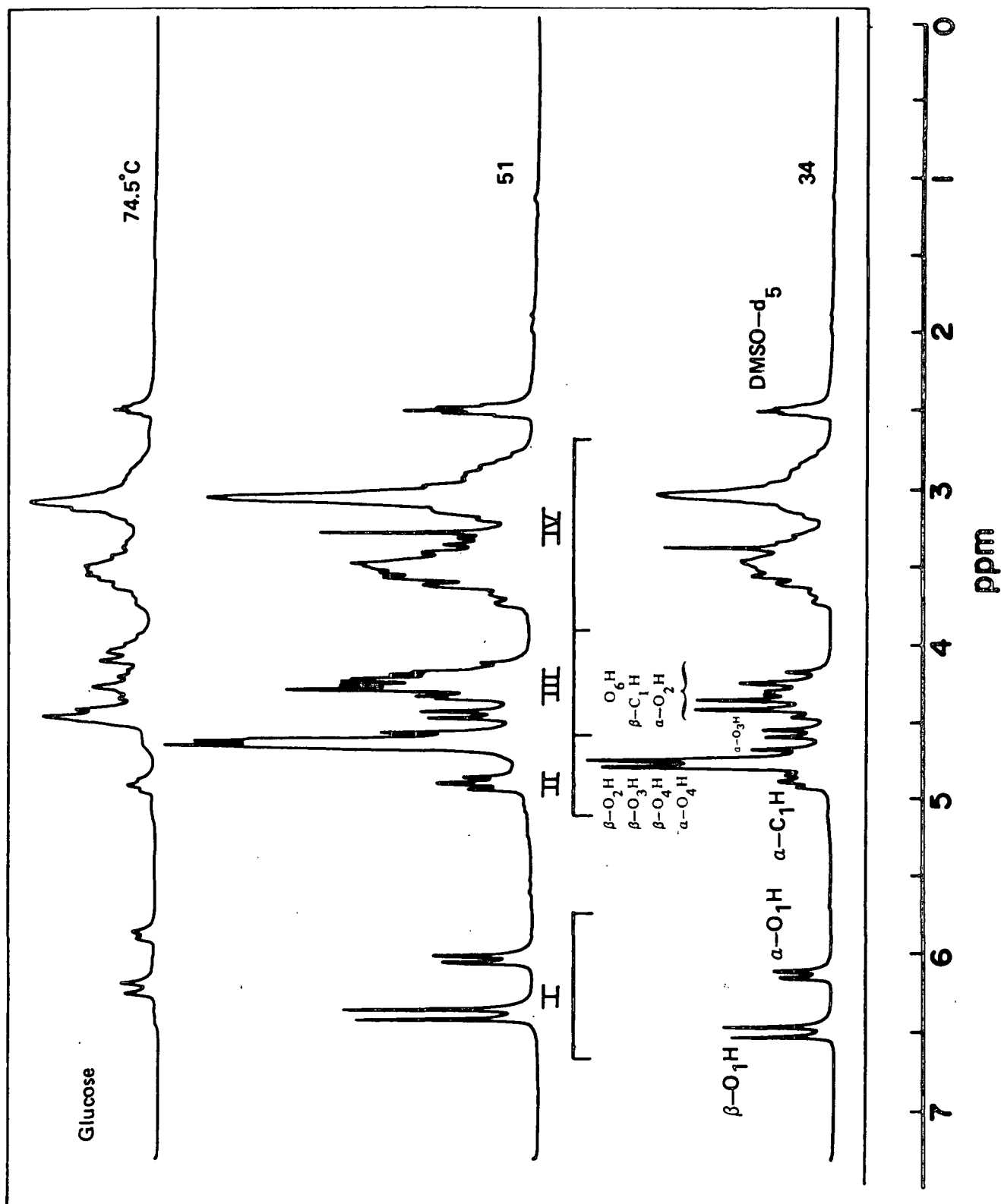
Figure 3. 100 MHz H-NMR spectra of glucose (4a,b) in DMSO-d_6 at 34, 51, and 74.5°C. Regions I-IV are defined (see p. 125).
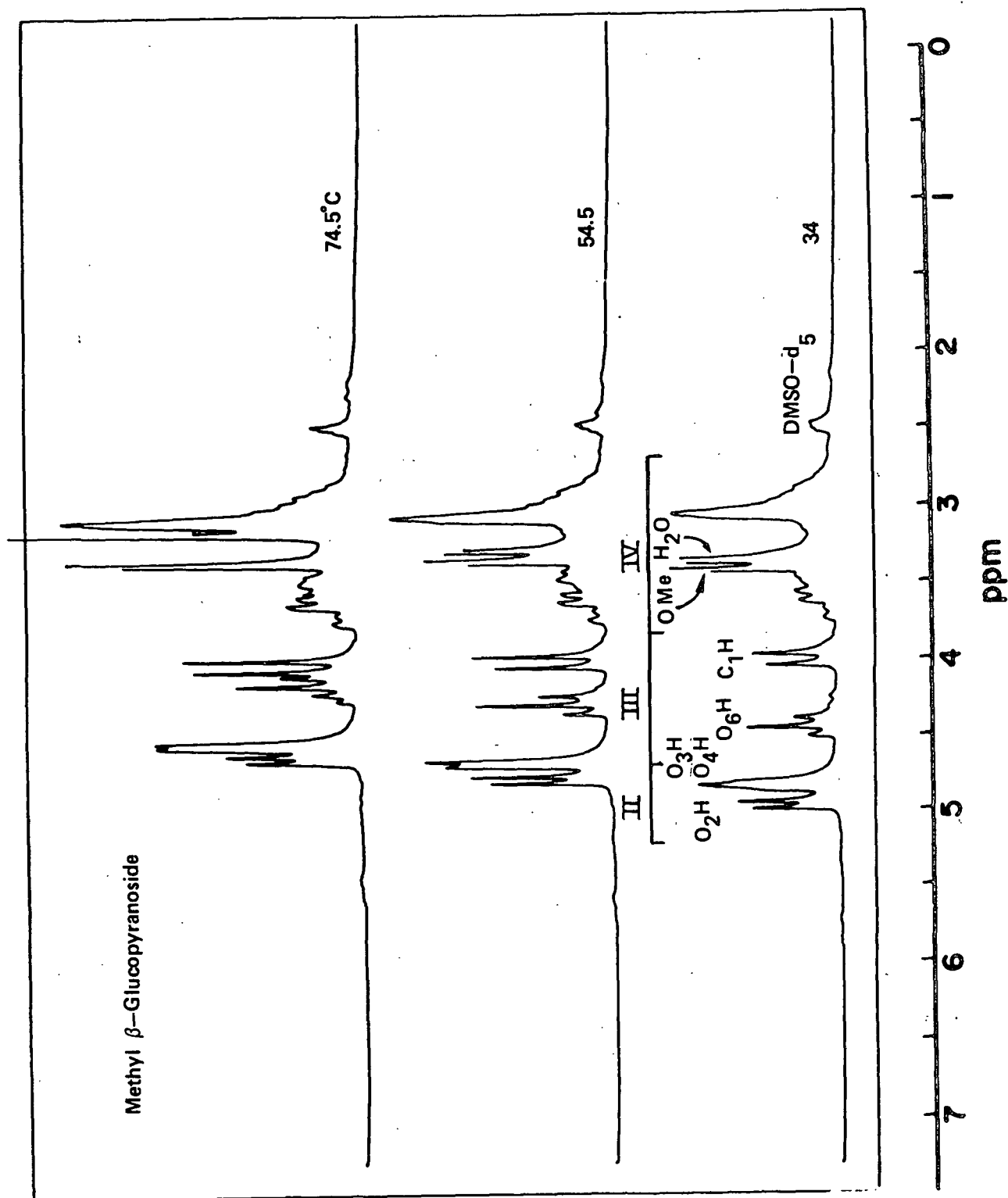
Figure 4. 100 MHz H-NMR spectra of methyl β-glucoside (4c) in DMSO-d$_6$ at 34, 54.5, and 74.5°C. The O-Me and residual H$_2$O peaks are off scale.

A discussion of the hydroxyl proton signals common to the β-1,4-linked gluco- and xylobioses studied is facilitated by reference to Fig. 3 and 4. To assist the discussion, the spectra have been divided into four regions.[*]

Region I: The furthest downfield signals result from the anomeric hydroxyls of a reducing sugar. Equatorial hydroxyls are found from δ=6.10 - 6.70 ppm (J=6.5Hz) while axial hydroxyls are located at δ=5.90 -6.30 ppm (J=4.0 - 4.5) over the temperature range studied.

Region II: This group of signals is located on the downfield side of the major hydroxyl and anomeric-proton complex (Fig. 3 and 4). The largest signal in the hydroxyl region of the spectrum is located in this region between 4.60 - 4.80 ppm at 56°C. This peak consists of the coincident O_4H, O_3H, and O_2H doublets of the β-anomer as well as the O_4H doublet of the α-anomers of glucose and xylose. For the β-glycosides (Fig. 4) the O_2H signal is shifted downfield by approximately 0.10 ppm. Spin-decoupling has been used to confirm this assignment (12). Another signal in this region results from C_1H of 3b and 4b. This resonance, which appears as an apparent triplet, is easily distinguished by its temperature insensitivity and resistance to D_2O addition.

Region III: This region contains the remaining signals from the hydroxyl protons and the anomeric protons of the glycosides. For 4c (Fig. 4) this region simply contains the O_6H triplet and the C_1H doublet. This latter peak is shifted upfield by 0.23 ppm from its position in 4a. For a reducing sugar (Fig. 3), this region is further complicated by the presence of O_2H and O_3H signals for the α-anomer and the location of the $β-C_1H$ signal closer to the O_6H signal. Perlin (14) has used spin-decoupling to assign the peaks in this region for α-glucose.

Region IV: The remainder of the carbohydrate protons are found from 2.9-4.0 ppm. These comprise all the methine and methylene protons (skeletal) and, in general, are not considered here except for the purpose of spin-decoupling. Several attempts have been made at assignments in this region for the D_2O solutions of 3b and 4b (16,17,18,19). In general, the skeletal proton signals are shifted downfield in D_2O relative to DMSO-d_6 but remain in the same relative positions with respect to each other.

Methyl β-Cellobioside (2)

Figure 5 shows the ^{1}H-NMR spectrum of methyl β-cellobioside in DMSO-d_6 at room temperature (a) and at 56°C (b). Spectrum (a) is identical to that given by Michell (12) and illustrates the location of the two hydroxyl protons in region II, downfield of 5 ppm (as overlapping doublets). Spectrum (b) shows the effect of temperature in improving resolution by eliminating the overlap of several peaks.

---

[*]Some of the following discussion is given in the literature (9,14,15). It is repeated here to clarify the logic presented later in assigning the disaccharides.
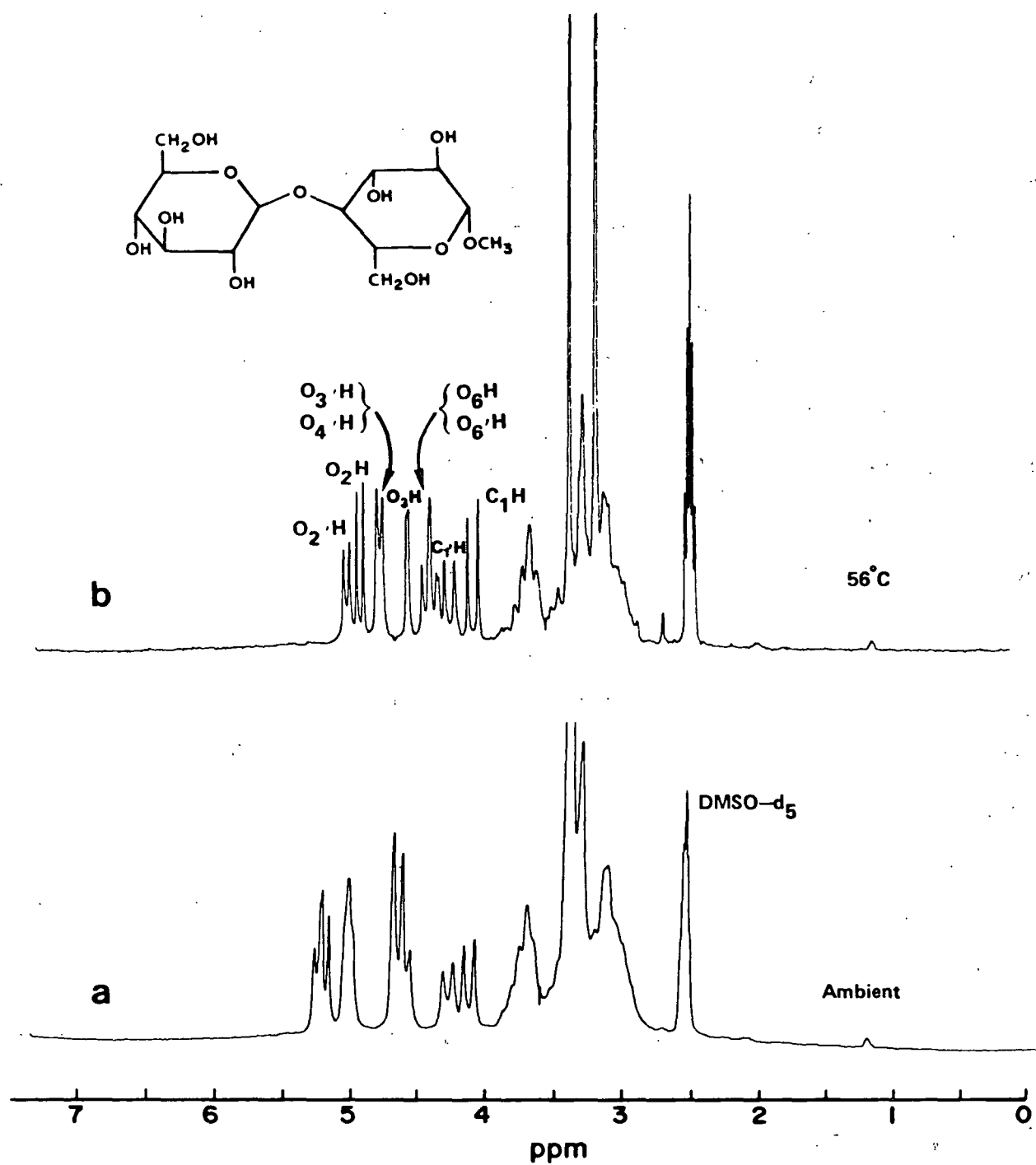
Figure 5. 100 MHz ^{1}H-NMR spectra of methyl β-cellobioside (2) in DMSO-d_6 at room temperature (a) and 56°C (b).

The overall spectrum can best be discussed in terms of the four regions mentioned above. As expected, region I is empty verifying the absence of a reducing-end. The nonanomeric methine, methylene, methoxyl, and residual H_2O protons are contained in region IV from 2.9 to 3.9 ppm. Regions II and III, downfield of 4.0 ppm, contain all the hydroxyl protons and the two anomeric methine-protons. These two regions will be the concern of this section.

Table II lists the center of the coupled peaks in regions II and III for methyl β-cellobioside at 31 and 56°C. Integration shows that there are nine separate proton signals here; based on the structure, seven hydroxyl and two anomeric-proton signals are expected. Assignment of the protons, $O_{3'}H$, $O_{4'}H$, $O_{6'}H$, O_6H, $C_{1'}H$, and C_1H is straightforward; it is based on comparisons with the spectra of 4c (Fig. 6) and cellobiose, addition of D_2O, and spin-decoupling (12,20). These assignments are given in the table.

Only three peaks remain to be accounted for in the 56°C spectrum; the downfield doublets at 5.04 and 4.94 ppm and the singlet at 4.58 ppm. The hydroxyls corresponding to these peaks must be $O_{2'}H$, O_2H, and O_3H. Assignment of these remaining signals will determine if the location of a nonanomeric hydroxyl downfield of 5 ppm, at room temperature, is a result of the participation in an intramolecular H-bond (9).

Previous spin-decoupling experiments, verified in this study, show that at least one of the downfield doublets is attached at a 2-carbon (12). This is illustrated in Fig. 7a with the decoupler set at 3.00 ppm. In this case, the anomeric-proton doublets, as well as the two downfield doublets, are simultaneously decoupled. This shows that at least one of the downfield doublets is coupled to the same protons as are the anomeric protons. At this point, the possibility of the C_3H proton being near the location of the decoupler cannot be excluded.

TABLE II

DOWNFIELD SIGNALS IN THE ^{1}H-NMR OF
METHYL β-CELLOBIOSIDE IN DMSO-d_6

Assignment	Integration[a]	Chemical Shift[b] ($^3J_{HCOH}$)[c]	
		31°C	56°C
$O_2{}'H$	1	5.20	5.04(4.5)
O_2H	1	5.12(4.8)	4.94(4.8)
$O_3{}'H$, $O_4{}'H$	2	4.98	4.78(4.2)
O_3H	1	4.65	4.58(2.8)
O_6H, $O_6{}'H$	2	4.57(5.6)	4.42(5.4)
$C_1{}'H$	1	4.24(7.3)	4.28(7.5)
C_1H	1	4.09(7.7)	4.10(7.5)
OMe		3.36	3.40

[a]See Ref. (12).
[b]Downfield of internal TMS using DMSO-d_5 as the intermediate
reference (2.50 ppm). The center of the complex (doublets
except for O_6H, $O_6{}'H$, and O_3H) is given.
[c]Coupling in Hz; for O_3H this is the width at half height
(whh). For $C_1{}'H$ and C_1H the value for $^3J_{H_1CCH_2}$ is given.

Figure 7b illustrates the case with the decoupler set at 3.40 ppm.[*] In this
case, no peaks are decoupled in the downfield region except that the singlet at 4.58
ppm (56°C) is sharpened. Clearly, this hydroxyl[**] is not coupled to the same proton
as the anomeric protons. By the process of elimination, this peak must be assigned
to O_3H which is contrary to the previous assignment based on maltose (9). The two
downfield doublets at 5.04 and 4.94 ppm (56°C) now must be assigned to $O_2{}'H$ and O_2H.
The differentiation of these two peaks is made on the basis of comparisons with 4c
and the reassigned spectrum of 1 (see later). Table II tabulates the assignments
for methyl β-cellobioside.

[*]Highfield NMR studies indicate that C_3H is downfield (3.65 ppm) in cellobiose in
D_2O (17,21).
[**]Addition of D_2O diminishes this peak showing it is due to an exchangeable proton.
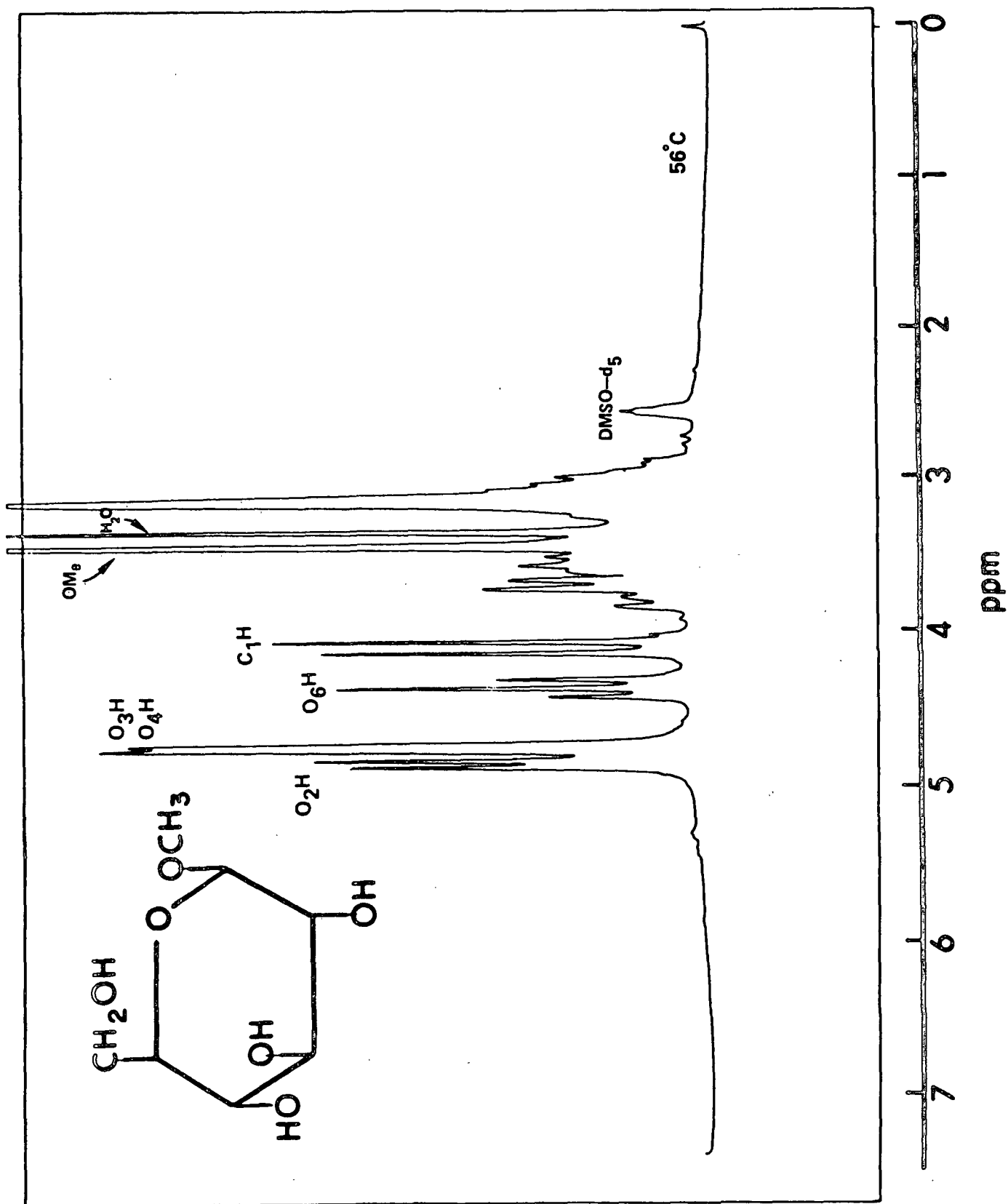
Figure 6. The 100 MHz ^{1}H-NMR spectrum of methyl β-glucoside ($\underline{4}\underline{C}$) at 56°C.
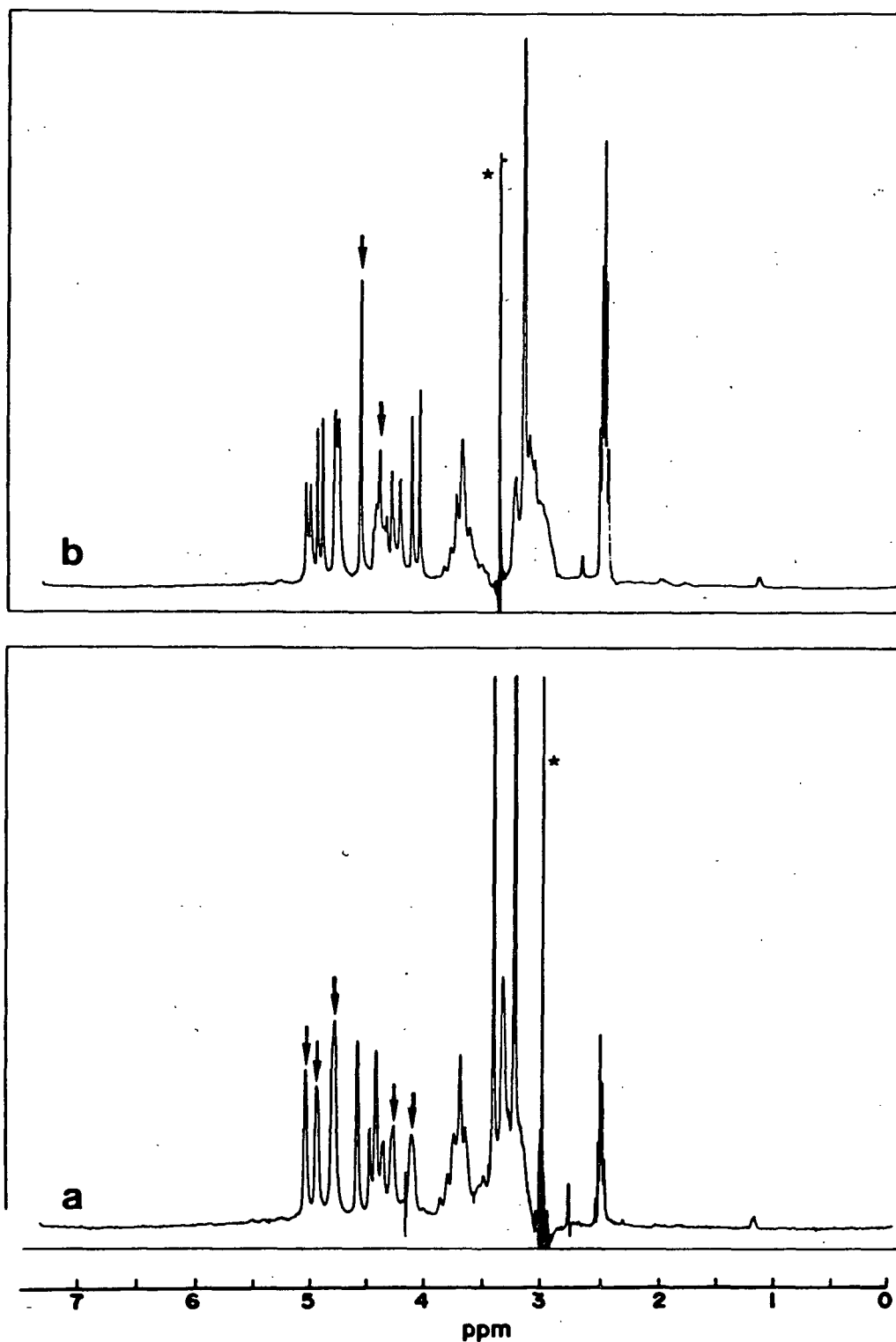
Figure 7. 100 MHz spin-decoupled spectra of methyl β-cellobioside with the
decoupler set at 3.00 ppm (a) and 3.40 ppm (b). The arrows illustrate
the downfield signals affected by the decoupler. (*)

Cellobiose (1)

Except for the effects of the methyl group, it can be anticipated that the spectra of $\underset{\sim}{1a}$ and $\underset{\sim}{2}$ will be similar. The similarities should include a broadened singlet near 4.58 ppm (56°C) corresponding to O_3H. The significant differences expected involve the O_2H and C_1H signals in regions II and III; these signals being nearer the position predicted from the spectrum of $\underset{\sim}{4a}$ rather than $\underset{\sim}{4c}$.* In region I, the anomeric hydroxyls should be observed, while in region IV, the methoxyl peak should be absent.

A further difference will be the spectrum of the α-anomer ($\underset{\sim}{1b}$) which will be superimposed on the spectrum of $\underset{\sim}{1a}$. Contributions from $\underset{\sim}{1b}$ should reinforce those from $\underset{\sim}{1a}$ for the nonreducing end and should approximate those of $\underset{\sim}{4b}$ for protons from the reducing end. One exception to this is the O_3H signal for $\underset{\sim}{1b}$, which, on the basis of the shift observed in methyl β-cellobioside, is expected to move upfield from its location in $\underset{\sim}{4b}$. This would place this signal in the complex of peaks made up of the O_6H, $O_{6'}H$, $C_{1'}H$, β-C_1H, and α-O_2H signals.**

The close correspondence expected on the basis of the above discussion can be observed in Fig. 8 which gives the spectrum of $\underset{\sim}{1}$ at 55°C. As expected, the most obvious difference is the disappearance of the doublet at 4.94 ppm corresponding to O_2H and the presence of the anomeric hydroxyls in region I. A singlet is observed at 4.54 ppm which compares favorably with the one found in $\underset{\sim}{2}$ (Fig. 5b). The size of the singlet indicates that this peak only results from the β-anomer. Spin-decoupling confirms that the singlet is not coupled to C_2H or $C_{2'}H$ and by deduction must represent O_3H of $\underset{\sim}{1a}$.

---

*In general, the disaccharide hydroxyl signals remote from the linkage are all shifted downfield relative to the monosaccharide. The shift is nearly the same for each hydroxyl.

**The prefix α or β refers to the peak found only in the α-anomer or β-anomer. If no prefix is given and both anomers are present, the signals results from both.

Cellobiose

55°C

ppm
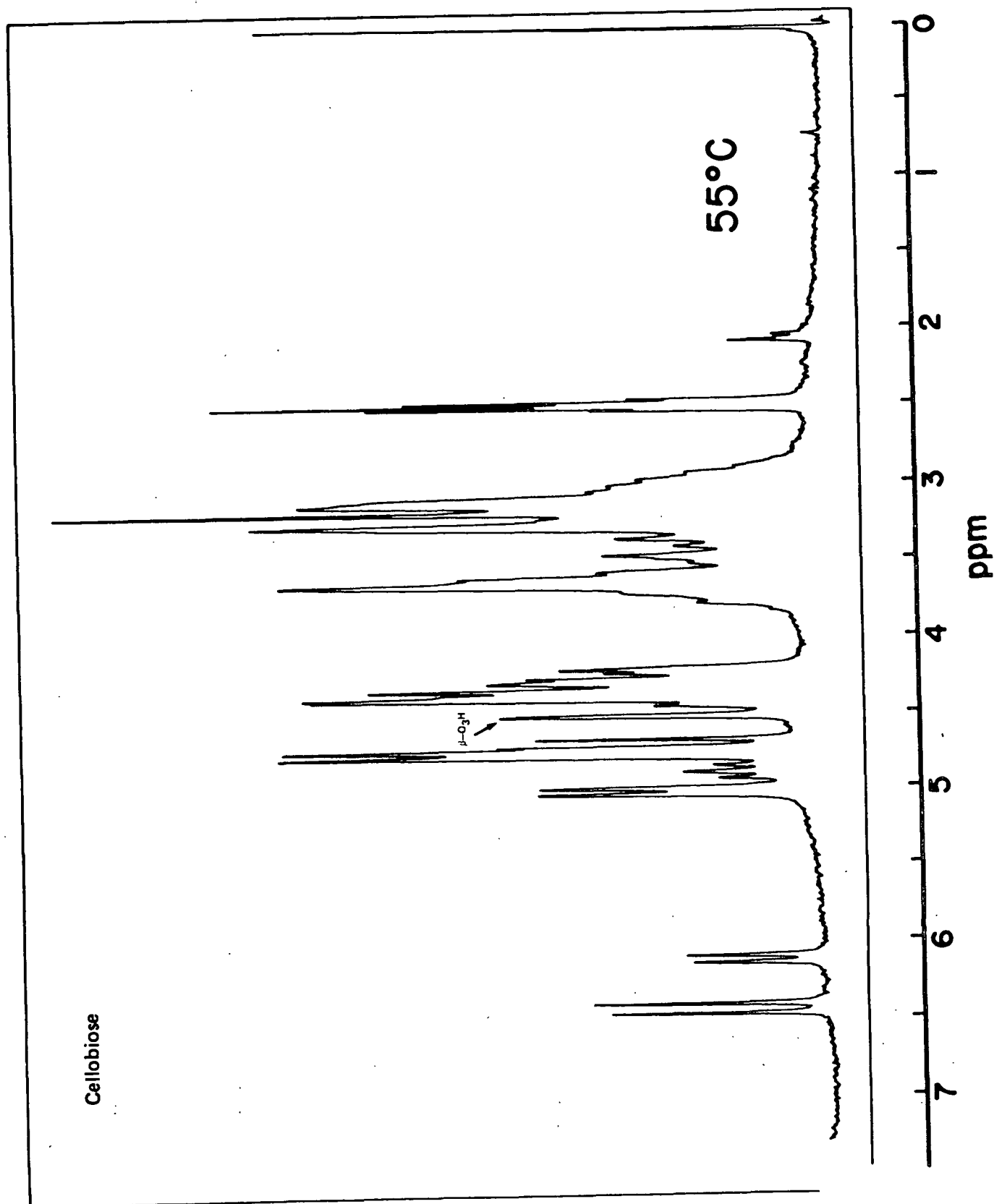
Figure 8. The 100 MHz ^{1}H-NMR spectrum of cellobiose (1a,b) in DMSO-d_6 at 55°C. The isolated singlet assigned to β-O$_3$H is illustrated.

Table III tabulates the assignments for the cellobiose spectrum at 32 and 56°C. At the lower temperature the β-O_3H singlet is hidden under the 6-hydroxyl proton signals which may explain why it was not previously mentioned (9). Figure 9 illustrates this with the 32°C spectrum. An important point to emphasize is that the O_3H signal, unlike the signals of the other hydroxyls, appears as a singlet in the spectra of both 1 and 2.

TABLE III

CHEMICAL SHIFTS[a] $(^3J_{HCOH})$[b] AND ASSIGNMENTS FOR HYDROXYL REGION SIGNALS IN DMSO-d_6 SOLUTIONS OF CELLOBIOSE[c]

Assignment	32°C		56°C[d]	
	α	β	α	β
O_1H	6.28(4.5)	6.62(6.5)	6.13(4.5)	6.45(6.6)
O_2H	4.50[f]	4.94[e]	4.33[f]	4.72(4.7)
O_3H	4.40[f]	4.60	4.33[f]	4.54(3.0)
O_6H	4.54[e]		4.37[d]	
$O_2{}'H$	5.18(4.2)		5.03(4.1)	
$O_3{}'H$, $O_4{}'H$	4.94[e]		4.78	
$O_6{}'H$	4.54[e]		4.37[d]	
C_1H	4.91[e]	4.28	4.91	4.30[d]
$C_1{}'H$	4.24	4.24	4.30[d]	4.30[d]

[a]Relative to internal TMS using DMSO-d_5 (2.50 ppm) as a secondary reference.
[b]In Hz, for β-O_3H the number given is the whh. value.
[c]Concentration of 4.1% (W/V).
[d]Determined from a linear regression analysis using at least four data points. All regressions have a correlation coefficient of -0.998 or better.
[e]Part of a complex of peaks in this region, value only approximate.
[f]Presumed to be part of the complex of signals in this region on the basis of integration and comparison to monosaccharides. For the α-O_3H signal the 32°C value is estimated using the chemical shift temperature coefficient of the β-O_3H signal with the assumption that the 56°C value is correct.
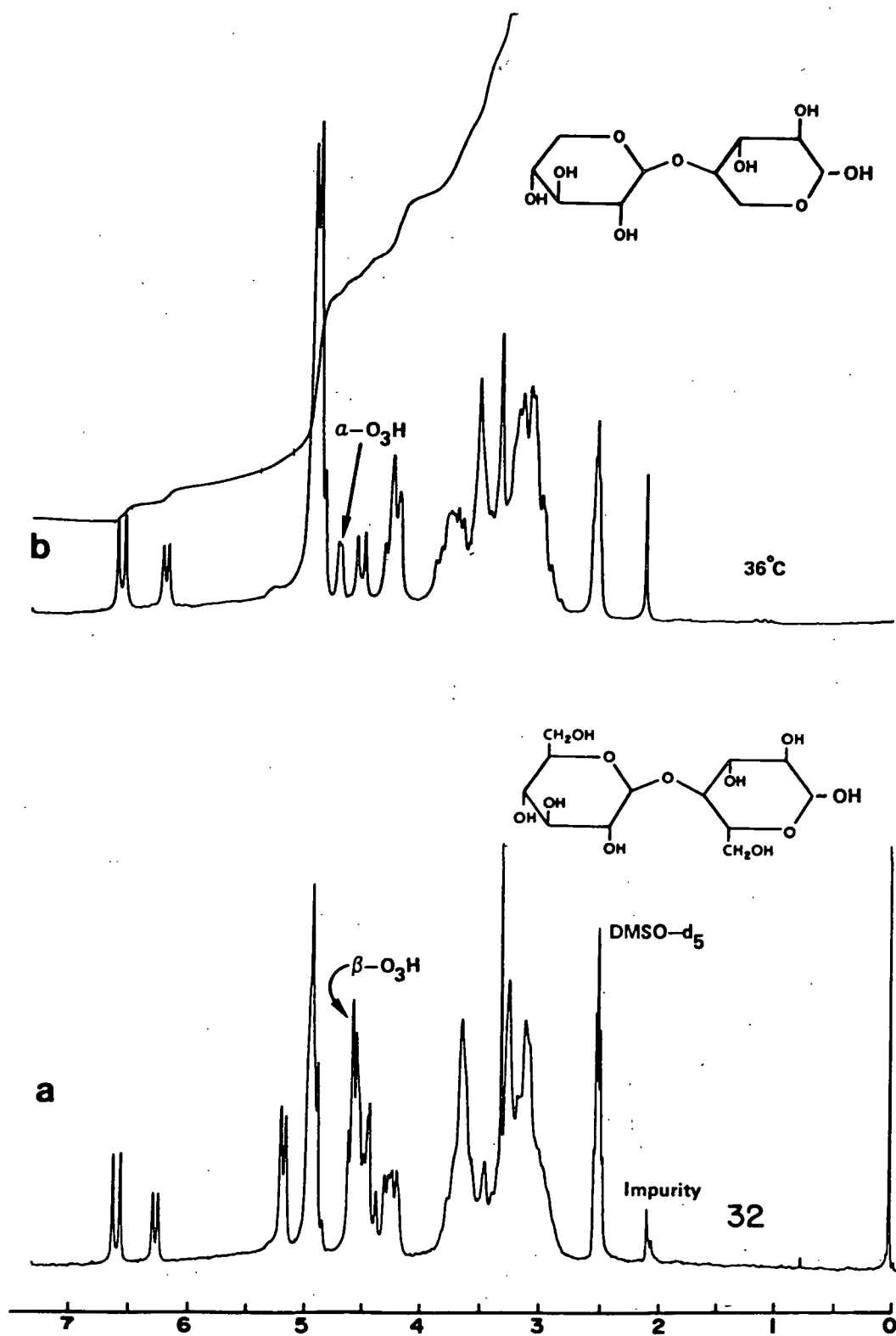
Figure 9. A comparison of the 100 MHz ^{1}H-NMR spectra of cellobiose (a) and
xylobiose (b).

Xylobiose and Related Disaccharides

Figure 2 gives the structures for the disaccharides used in this study which contain a xylopyranose moiety as ring A (see Fig. 2). In some of these disaccharides, the absence of a hydroxy-methyl group (C_6) results in a simplification of region III in the ^{1}H-NMR spectrum. This is illustrated in the spectrum of 5 presented in Fig. 9b where it is observed that the absence of the O_6H and O_6,H signals simplifies the spectrum. Further differences from the low temperature spectrum of 1 (Fig. 9a) are the absence of the downfield doublet in region II and the appearance of an isolated singlet at 4.69 ppm (36°C).

Table IV lists the assignments for xylobiose and securidebiose (6)* at 56°C. The assignments given are based on integration, comparison to models (see Table I), and spin-decoupling. Except for the O_3H and O_2,H signals, the assignments are straightforward. In general, the peaks not perturbed by the linkage are shifted about 0.12 ppm downfield relative to xylose. This is analogous to the difference between cellobiose and glucose.**

The temperature sensitive broadened-singlet at 4.56 ppm (56°C) can be spin-decoupled by irradiating at 3.50 ppm. It is the only downfield peak affected, indicating that it is not O_2,H or $\beta-O_2H$. Signals resulting from these peaks are expected to be decoupled simultaneously with the C_1,H and $\beta-C_1H$ proton signals. The O_3,H, O_4,H, and $\alpha-O_2H$ signals all can be assigned by comparison to xylose because of their distance from the linkage. By elimination, this requires the near-singlet to be assigned to $\beta-O_3H$ or $\alpha-O_3H$. Direct comparison to cellobiose would suggest that this is the O_3H signal from the β-anomer.

---

*4 O-(β-D-glucopyranosyl)-D-xylopyranose.
**For 1, the value is 0.11 ± 0.04 ppm calculated by averaging the shift, relative to glucose, for each hydroxyl signal more than two carbons from the linkage.

TABLE IV

CHEMICAL SHIFT[a] ($^3J_{HCOH}$)[b] OF THE HYDROXYL AND ANOMERIC PROTONS
AT 56°C FOR SEVERAL DISACCHARIDES RELATED TO XYLOBIOSE

Assignment	5[c]		6[d]		7a[e]
	α	β	α	β	
O_1H	6.06(4.8)	6.43(6.6)	6.10(4.6)	6.44(6.6)	
O_2H	4.35	4.76-4.78[f]	4.38[f]	4.76[f]	4.92(5.1)
O_3H	4.56(2.4)	4.76-4.87[f]	4.61	4.76[f]	4.76[f]
$O_{2'}H$, $O_{3'}H$, $O_{4'}H$	4.76-4.78[f]		4.76[f]		4.76[f]
$O_{6'}H$			4.38[f]		
C_1H	4.88	4.23[f]	4.88	4.32[f]	4.06
$C_{1'}H$	4.23[f]		4.25		4.26
OMe					3.36

[a]Relative to internal TMS using DMSO-d$_5$ (2.50) ppm) as a secondary reference.
Values obtained from a regression analysis over at least three points.
[b]In Hz.
[c]6.0% (W/V).
[d]7.7% (W/V).
[e]At 57°C; 7.8% using microprobe.
[f]Values only approximate, part of a complex of peaks.

However, several factors disagree with this conclusion. Assuming the singlet results from β-O_3H, then at lower temperatures a second signal, for α-O_3H, would be expected in the vicinity of α-O_2H (4.44 ppm, 36°C). This assumes that each of the 3-hydroxyl signals shifts upfield, relative to xylose, in a similar way as occurs for cellobiose, relative to glucose. Thus a normalized shift of 0.18 ppm is observed for the O_3H signal in 1a.* No signal fitting these criteria is observed in the spectrum of 5. Secondly, no signal corresponding to the near-singlet found in 5

*This includes the usual downfield shift of 0.11 ppm observed for hydroxyl protons remote from the linkage, which is added to the observed upfield shift of 0.07 ppm for the β-O_3H signal, to get 0.18 ppm. (Tables I and III).
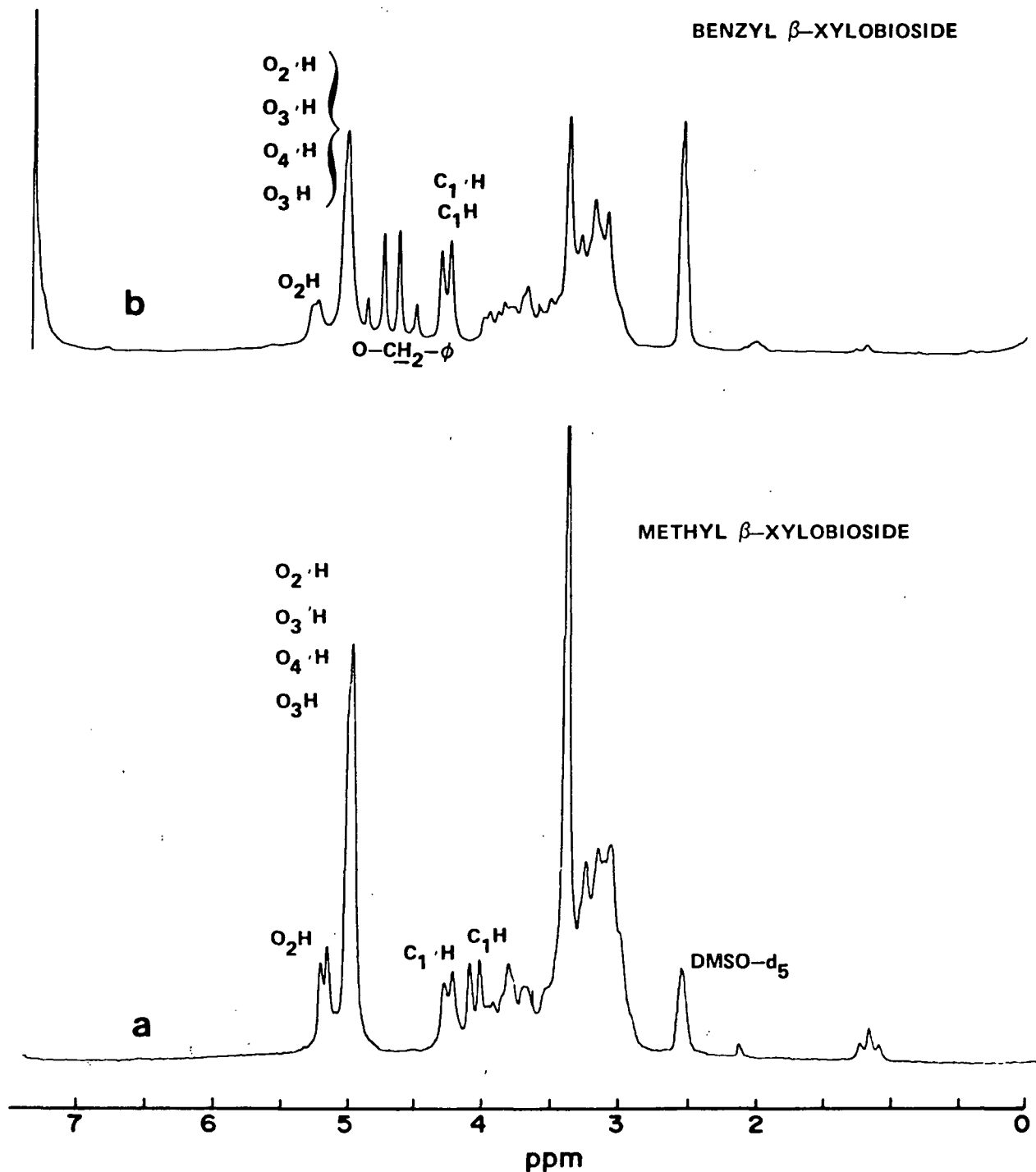
is observed in region III of methyl β-xylobioside (7a) or benzyl β-xylobioside (7b) as shown in Fig. 10. From these observations, it is necessary to assign the broadened-singlet to O_3H of α-xylobiose.

As noted above, the overall shift of the hydroxyl signals of xylobiose, relative to those of xylose, is 0.12 ± 0.01 ppm.[*] Considering this a normalized upfield shift of only 0.06 ppm is calculated for α-O_3H in 5 at 56°C.[**] This is in comparison to a shift of 0.18 ppm for the β-O_3H signal of 1.[***] Using the normalized upfield shift observed for α-O_3H in 5, it is predicted that the signal for β-O_3H rests in the large complex of peaks centered at 4.75 ppm (56°C) in region II. This assignment is in accord with the integral. Again, it should be emphasized that the O_3H signal is observed as a singlet in contrast to the other hydroxyl signals. In this case, a slight coupling of 2.3 Hz (36°C) is observed.

In 1, the downfield doublet (5.03 ppm, 56°C), originally thought to be an intramolecularly H-bonded O_3H (9), has been reassigned to $O_{2'}H$ in the present paper. This represents a shift of 0.42 ppm downfield relative to the same peak in glucose. This is approximately 0.31 ppm more than the average shift experienced by the hydroxyls remote from the linkage, and results from the presence of the nonprimed glucose ring. In 2, a second downfield hydroxyl, O_2H (4.94 ppm, 56°C), is observed which is shifted 0.34 ppm relative to glucose (0.23 ppm if the average shift relative to glucose is excluded). An analogous signal is also found in both methyl β-glucoside and methyl β-xyloside.

---

[*]Averaged over all hydroxyls not within 2-carbons of the linkage.

[**]The actual shift, relative to the xylose spectrum, is downfield by 0.06 ppm. This is 0.06 ppm less than the average observed for the other hydroxyl protons. It is significant that the OH_3 shift is only slightly different from the other hydroxyl protons in 5 but significantly different in 1.

[***]This includes the usual downfield shift of 0.11 ppm observed for hydroxyl protons remote from the linkage, which is added to the observed upfield shift of 0.07 ppm for the β-O_3H signal, to get 0.18 ppm (Tables I and III).

Figure 10. 100 MHz ^{1}H-NMR spectra of methyl β-xylobioside (7c) (a) and benzyl β-xylobioside (7b) (b) at room temperature. Note the absence of a singlet near 4.70 ppm.

For $\underset{\sim}{5}$, no downfield doublet is present (Fig. 9b) but for $\underset{\sim}{7}$a and $\underset{\sim}{7}$b[*], one is observed (Fig. 10). For $\underset{\sim}{7}$a, this is easily assigned to O_2H by comparison to methyl β-xyloside. Integration of the large complex at 4.77 ppm (56°C) in $\underset{\sim}{5}$ indicates that the $O_{2'}H$ signal must be included. This represents no unusual shift from xylose and is evidence that the presence of the aglycon has no significant effect on the $O_{2'}H$ signal in the case of xylobiose.

Spectra of $\underset{\sim}{6}$ at 36, 51, and 67.5°C are shown in Fig. 11. The downfield portion of the 36°C spectrum is identical to that of $\underset{\sim}{5}$ except that the α-O_2H signal is overlapped by the triplet from O_6H of the glucopyranosyl ring. As in $\underset{\sim}{5}$, the $O_{2'}H$ signal is found in the large hydroxyl complex at 4.76 ppm (56°C) indicating that the presence of the xylopyranose unit is not a factor in its chemical shift. Also, a broadened singlet is present, which, by analogy to $\underset{\sim}{5}$, can be assigned to O_3H of the α-anomer. It is shifted upfield by 0.02 ppm, relative to xylose, after correcting the overall shift of the disaccharide.[**] This value is much less than the shift observed for $\underset{\sim}{1}$ and slightly less than that observed for $\underset{\sim}{5}$.

Trisaccharides

^{1}H-NMR spectra of the cello-oligosaccharides up to cellopentaose have been previously published (12). At that time, it was noted that two nonanomeric hydroxyls appear downfield of 5 ppm in the higher oligomers. Assignments were not made.

Figure 12 shows spectra of cellotriose ($\underset{\sim}{8}$) (a) and xylotriose ($\underset{\sim}{9}$) (b) in DMSO-d_6. Table V lists and partially assigns the downfield resonances observed.

---

[*]The spectra of benzyl 2,3-anhydro-4-$\underline{O}$-(β-D-xylopyranosyl)-D-ribopyranoside and benzyl 2,3-anhydro-4-$\underline{O}$-(β-D-glucopyranosyl)-D-ribopyranoside also contain a downfield doublet. In this case, it probably is $O_{2'}H$ and definitely is not O_2H. This indicates that the benzyl group may affect the shift of $O_{2'}H$ even though it is an entire ring away. From this evidence, the downfield signal in $\underset{\sim}{7}$b cannot readily be assigned to O_2H.

[**]The average shift for hydroxyls attached more than 2-carbons from the linkage is 0.13 ± 0.02 in $\underset{\sim}{6}$.
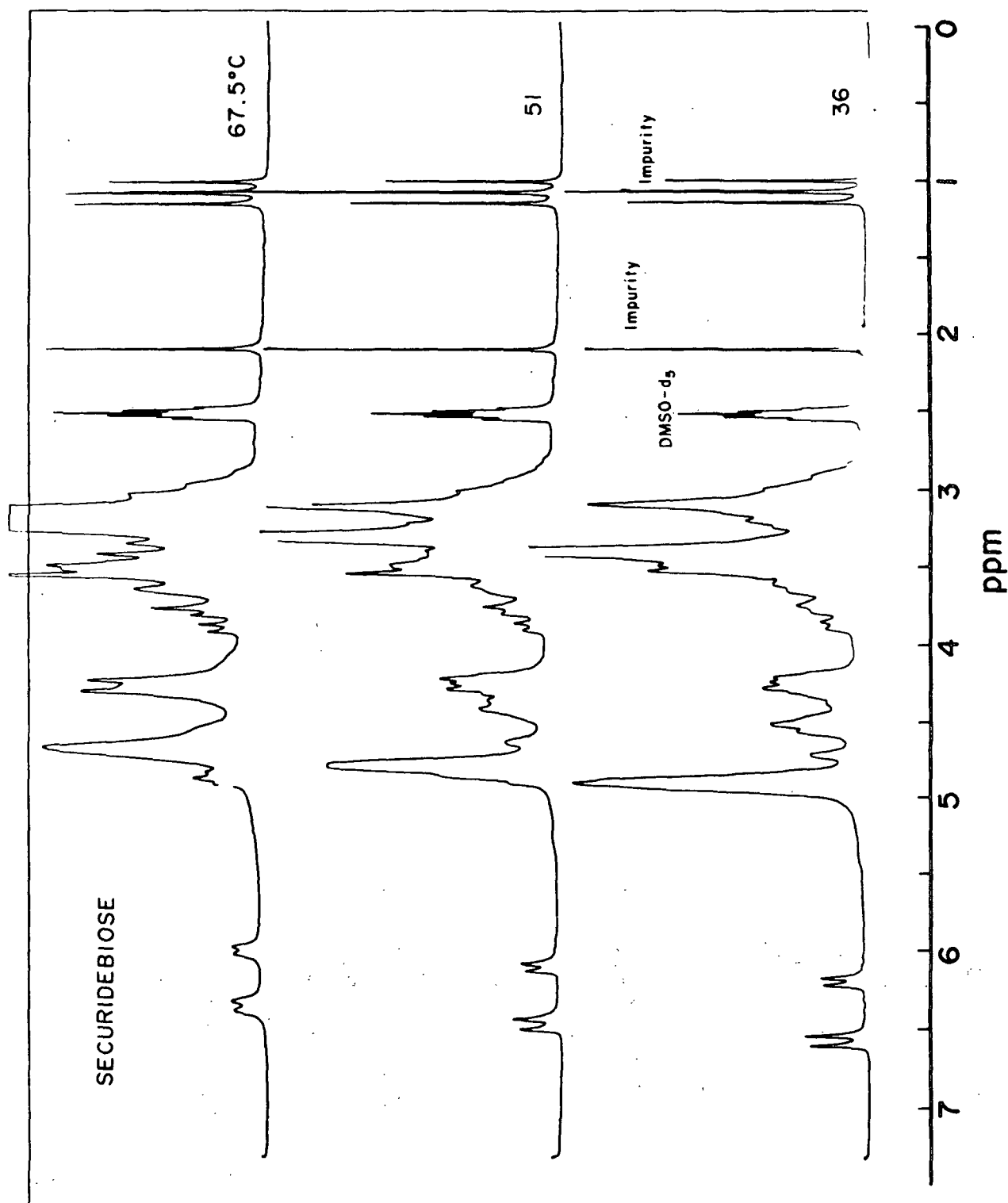
Figure 11. A series of ^{1}H-NMR spectra of 4-O-β-O-glucosyl-D-xylose (5a,b) at 36, 51, and 67.5°C in DMSO-d$_6$.
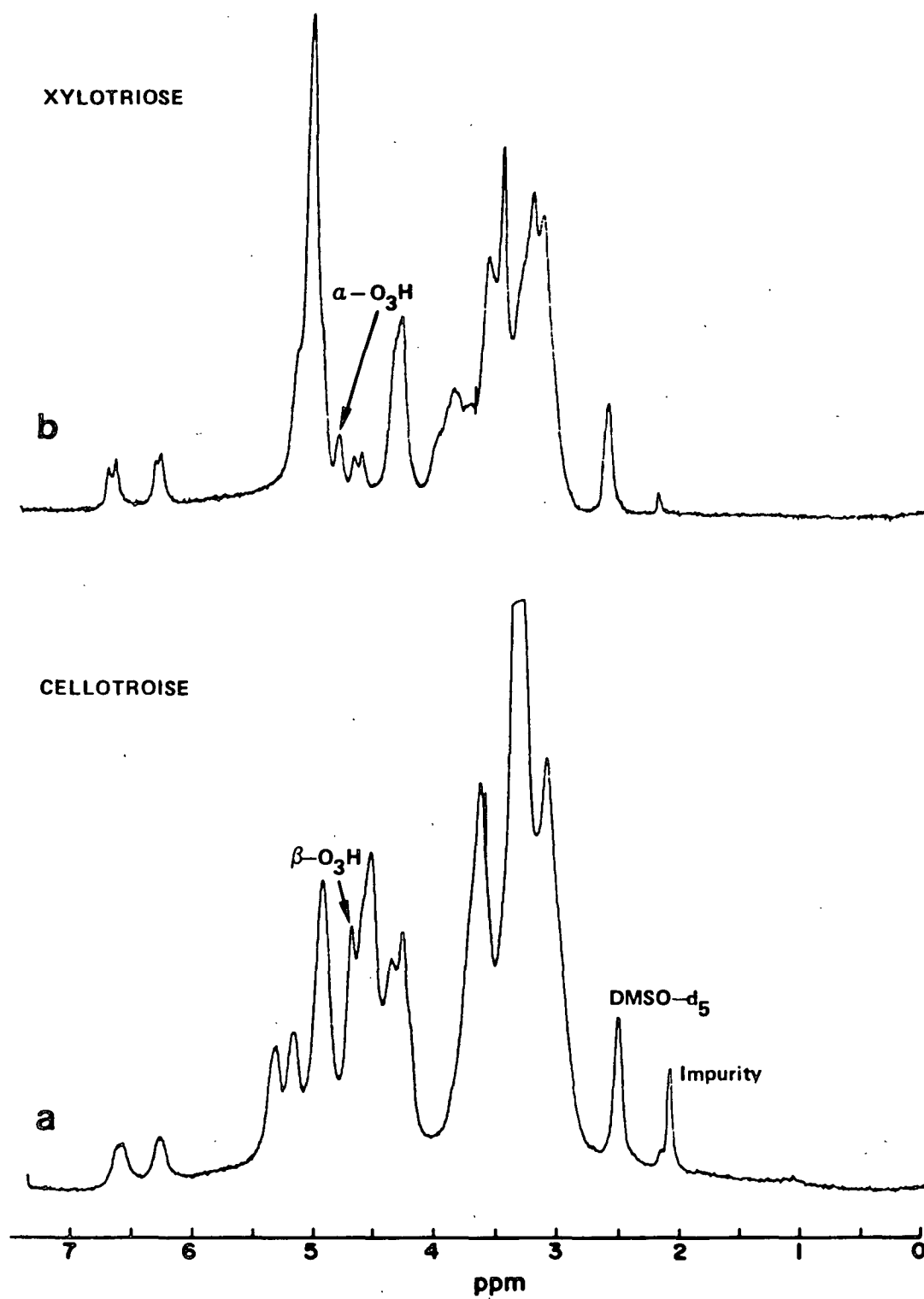
Figure 12. 100 MHz ^{1}H-NMR spectra of cellotriose (a) (8) and xylotriose (b) (9) in DMSO-d_6.

Comparison with earlier results reveals a close correspondence to the disaccharide spectra.

TABLE V

HYDROXYL AND ANOMERIC PROTON SIGNALS IN CELLOTRIOSE AND XYLOTRIOSE[a]

Assignment	Cellotriose[b]	Xylotriose[c]
β-O_1H	6.57	6.60
α-O_1H	6.26	6.23
$O_2'H$	5.32	
$O_2''H$	5.16	
Large Complex[d]	4.94	4.95
Singlet[e]	4.69	4.72
α-O_2H		4.53
O_6H, $O_6'H$, $O_6''H$[f]	4.54	
$C_1'H$, $C_1''H$, β-C_1H	4.32	4.21

[a]Relative to internal TMS using DMSO-d_6 as secondary reference.
[b]At 36°C in microprobe.
[c]At room temperature in microprobe.
[d]$O_3''H$, $O_4''H$, β-O_2H in cellotriose, in the higher cello-oligosaccharides this peak gets smaller with increasing chain length (12). For xylotriose: $O_3''H$, $O_4''H$, $O_3'H$, β-O_3H, β-O_2H, $O_2'H$.
[e]β-O_3H and $O_3'H$ in cellotriose; α-O_3H in xylotriose.
[f]Probably contributions from α-O_3H and α-O_2H also.

In agreement with the literature, an additional downfield resonance at 5.32 ppm (36°C) is observed for 8. It can be speculated that this results from $O_2'H^*$ on the central ring. The resonance at 5.16 ppm (36°C), which corresponds to $O_2'H$ in

*In the higher oligomers, each additional ring is designated with an additional prime. Therefore, $O_2'H$ indicates the hydroxyl in the center ring of the trisaccharide.

cellobiose, can be assigned to $O_{2''}H$. This assignment is further substantiated in the literature where it is observed that the 5.32 ppm signal steadily increases in intensity as the number of monomer units increases (12). Since the linkage appears to affect the 2-hydroxyl chemical shift differently in each ring, it can be inferred that the linkages are nonequivalent in some respect. Linkage nonequivalence in cellotriose has been previously demonstrated concerning their unequal rates of hydrolysis (23).

The singlets previously observed and assigned to O_3H in 1 and 5 also appear in the trisaccharides. In 9, a small broadened-singlet at 4.72 ppm (room temperature) is present. Its intensity is further verification of its assignment to α-O_3H in 5. If the signal resulted from the β-anomer, a contribution from the internal $O_{3'}H$ should also be observed in the spectrum of 9. In the spectrum of 8 (Fig. 12a), a sharp peak partially obscured by the 6-hydroxyls is found; it appears in a manner similar to that observed in the 32°C spectrum of 1 (Fig. 9a). It is shifted slightly downfield in the trisaccharide.

Temperature Dependence

The temperature dependence of the hydroxyl or amino-proton chemical shift has previously been used to differentiate between inter- and intramolecular H-bonded systems (13). In the study by St. Jacques and co-workers, involving maltose, amylose, and the cyclodextrins, it was demonstrated that as the temperature increases the O_3H signal shifts upfield at a lower rate than the other hydroxyl signals. This hydroxyl is thought to be involved in an intramolecular H-bond with $O_2'H$ ($O_3H\cdots O_2'$) (13). Classically, a reduced temperature dependence has been interpreted in terms of a H-bonded system in which the hydroxyl proton is shielded from the solvent (24).

Cellobiose and Related Disaccharides

The chemical shift dependence on temperature for the hydroxyl region protons in DMSO-d_6 solutions of 4, 4c, 1, and 2 are given in Table VI. The literature data for maltose is also given for comparison (13). From the table, it can be noted that all the hydroxyl proton signals are shifting rapidly upfield with increasing temperature. The anomeric protons, as well as the remainder of the skeletal protons, are shifted slightly downfield relative to the solvent resonance.

TABLE VI

CHEMICAL SHIFT TEMPERATURE COEFFICIENTS[a] FOR THE HYDROXYL
AND ANOMERIC PROTONS IN SOME GLUCOSE CONTAINING SUGARS

	Monosaccharides			
	β	4	α	4c
O_1H	-0.67		-0.59	
O_2H	-0.74[b]			-0.80
O_3H	-0.74[b]		-0.80	-0.67[b]
O_4H	-0.74[b]			-0.67[b]
O_6H		-0.74		-0.70
C_1H	0.07		0.05	0.10

	Disaccharides				
	β	1c	α	2	Maltose[d]
O_1H	-0.65		-0.58		
O_2H	-0.82			-0.78	-0.74
O_3H	-0.24			-0.28	-0.44
$O_{2'}H$		-0.62		-0.67	-0.65
$O_{3'}H, O_{4'}H$		-0.68		-0.81	-0.74
$O_{6'}H, O_6H$		-0.64		-0.64	-0.74
C_1H			0.08	0.06	
$C_{1'}H$				0.12	

[a]Obtained from a linear regression analysis over a range of 29°-91°C; minimum correlation coefficient - 0.996. In Hz/°C.
[b]Peaks coincident.
[c]For cellobiose this is an average over six different concentrations. Largest standard deviation (σ) is ± 0.03 Hz/°C except for the O_6H signal with a σ = ± 0.06 Hz/°C.
[d]From Ref. (13). Data given at 200 MHz and converted to 100 MHz (99.61). Signals resulting from different anomers were not differentiated.

With one exception, the rate of change for all hydroxyl signals is -0.58 to -0.82 Hz/°C. The exception is the disaccharide O_3H signal which moves upfield at -0.24 to -0.28 Hz/°C for the β-1,4-linked disaccharides and -0.44 Hz/°C for α-1,4-linked maltose. Clearly, O_3H in 1 and 2 is not H-bonded in a manner similar to the other hydroxyls. Apparently, a temperature dependent equilibrium involving H-bonding to the solvent is not a major factor. Therefore, the H-bond in which O_3H participates must be intramolecular and most certainly is the one previously proposed (O_3H....O_5.). In comparison to maltose, this H-bond is more isolated from disruption by the solvent.

In addition to being a singlet and its different chemical shift relative to the equivalent monosaccharide signal, its reduced temperature dependence provides yet another feature which distinguishes this signal from the other hydroxyl signals. These properties must be a direct result of its participation in an intramolecular H-bond with the ring oxygen on the adjacent ring. It is reasonable to expect that other molecules capable of possessing a similar intramolecular H-bond will also exhibit a resonance with similar qualities.

The disaccharides lactose (10)[*] and 4 O-(β-D-glucosyl)-D-mannopyranose (11) are isomorphic with 1 within 2 bonds of the linkage and would be expected to have the O_3H....O_5. bond in solution. This bond has been found in crystalline α-lactose (25). Figures 13 and 14 contain the ^{1}H-NMR spectra of 10 and 11 at three different temperatures. Each spectrum contains a singlet with a temperature dependence comparable to 1. In the case of lactose, the singlet is located at 4.54 ppm (56°C) just as in cellobiose.[**] By analogy, it can be assigned to β-O_3H. For 11 the

---

[*]4 O-(β-D-galactosyl)-D-glucopyranose.
[**]A similar signal has also been observed in 1,5 anhydrocellobiotol.
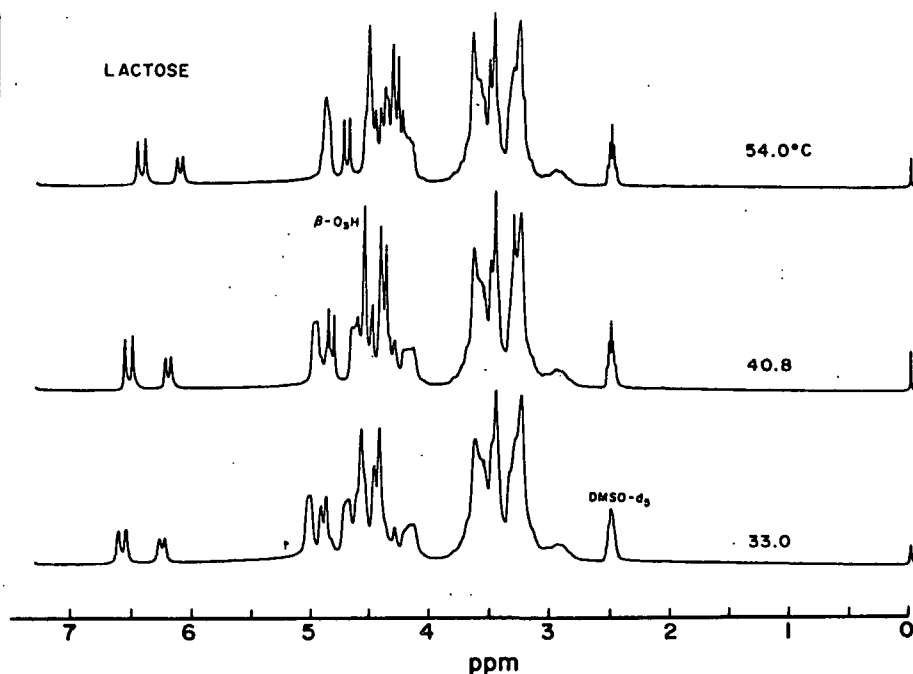
Figure 13. 100 MHz ^{1}H-NMR spectra of lactose (10a,b) in DMSO-d$_6$ at 33.0, 40.8, and 54.0°C. At 56°C the β-O$_3$H signal is located at 4.54 ppm with a temperature coefficient of -0.22 Hz/°C by linear regression analysis.
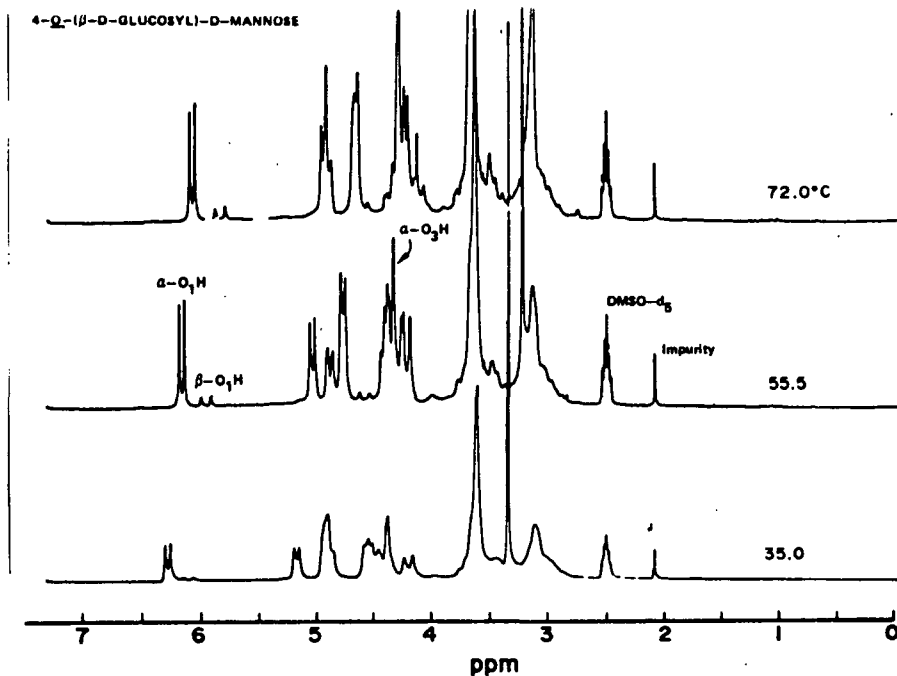

Figure 14. 100 MHz ^{1}H-NMR spectra of 4-O-(β-D-glucopyranosyl)-D-mannopyranose (11a,b) in DMSO-d$_6$ at 35.0, 55.5, and 72.0°C. At 56°C the α-O$_3$H signal is located at 4.34 ppm with a temperature coefficient of -0.27 Hz/°C by linear regression analysis.

singlet is found at 4.34 ppm and can be assigned to α-O_3H since the α-anomer dominates the spectra presented.[*]

Disaccharides Related to Xylobiose

Previously, it was shown that the spectra of 5 and 6 contain isolated near-singlets assignable to O_3H. The temperature dependence of the singlet is similar to the other hydroxyls since it remains isolated over a wide temperature range (Fig. 11). The temperature dependence of the identifiable hydroxyl resonances for 5 and 6 are given in Table VII. The temperature coefficient of the O_3H signal for the α-anomer is -0.60 Hz/°C; only slightly less than that of the other hydroxyls, except α-O_1H. As in cellobiose, O_2H is observed to have a large temperature coefficient. The other hydroxyls exhibit the same general trend as observed in the disaccharides related to cellobiose. The results observed with 5 and 6 are consistent with considerable H-bonding of O_3H with the solvent.

TABLE VII

CHEMICAL SHIFT TEMPERATURE COEFFICIENTS[a] FOR THE HYDROXYL
AND ANOMERIC PROTONS IN XYLOBIOSE AND SECURIDEBIOSE

	β	5[b]	α	β	6	α
O_1H	-0.64		-0.59	-0.66		-0.63
O_2H	c		-0.78	c		
O_3H	c		-0.60	c		-0.60
$O_{2'}H$, $O_{3'}H$, $O_{4'}H$		-0.65			-0.70	
$O_{6'}H$					-0.70	
$C_{1'}H$, C_1H					0.13	

[a]In Hz/°C; see Footnote (a) Table VI.
[b]Averaged over three concentrations with a maximum $\sigma = \pm 0.05$ Hz/°C.
[c]Included in the largest peak ($O_{2'}H$, $O_{3'}H$, $O_{4'}H$) and presumed to have a similar temperature coefficient.

[*]These solutions are not necessarily at equilibrium. In general, the ratio of anomers changes significantly with time.

DISCUSSION

Criteria for the $O_3H\cdots O_5'$ Intramolecular Hydrogen-Bond

Previous literature reports have indicated that the normal chemical shift range for nonanomeric hydroxyl protons H-bonded to DMSO is 4-5 ppm. It was proposed, based on comparisons to maltose, that signals of this type found downfield of 5 ppm resulted from intramolecularly H-bonded hydroxyls (9). Several examples can be found of this criterion having been used in the literature to identify intramolecular H-bonded protons (1,3,9,26). The present paper has demonstrated, using comparison to model compounds and spin-decoupling, that the intramolecularly H-bonded O_3H is not downfield of 5 ppm in several disaccharides. On the contrary, the resonance found in cellobiose at 5.18 ppm (32°C) has been assigned to $O_2'H$. The O_3H resonance is found at 4.60 ppm (32°C) in β-cellobiose. Clearly, the criteria previously utilized for signals exhibiting the properties of intramolecular H-bonded protons in carbohydrates are invalid. Nevertheless, the conclusion that 1 contains an intramolecular H-bond in DMSO-d_6 remains firm, as discussed below.

Temperature Behavior

The data given above for cellobiose-related disaccharides demonstrates that the resonance assigned to O_3H has several characteristics distinct from the other hydroxyl signals. First, the signal exists as a broadened singlet. At higher temperatures, this becomes more obvious since the signal is no longer overlapped by other signals (Fig. 6 and 8). All of the other nonoverlapped hydroxyls observed have couplings of at least 4.0 Hz.[*] Secondly, the chemical shift temperature coefficient of the O_3H signal is considerably less than that observed for the other hydroxyls.

---

[*]If paramagnetic or acidic impurities are present, the signals no longer exhibit this coupling but rather appear as very broad peaks.

The behavior of a H-bonded system as a function of temperature is complex (24). For a hydroxyl H-bonded to the solvent, the shift of the hydroxyl signal upfield with increasing temperature is primarily related to the shift to the right of the following equilibrium.

$$RO..H....O=S\overset{CH_3}{\underset{CH_3}{<}} \qquad ROH + O=S\overset{CH_3}{\underset{CH_3}{<}}$$

This results from the increase in thermal energy. The proton in the free hydroxyl has a greater electron density and would be expected to be more shielded. In contrast, for a H-bonded proton protected from the solvent, the shift upfield is related to a weakening of the H-bond (24).

$$O_5......H...O_3 \longrightarrow O_5......H..O_3$$
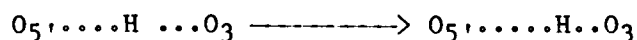
Obviously, this is also a factor for the solvated proton but in the latter case, it must be the only factor. For protons prevented from forming any type of H-bond, a slight downfield shift is expected because of the thermal weakening of the OH bond.

On this basis, the resonance of the solvent-protected proton is expected to have a much lower temperature coefficient, similar to that previously observed in maltose (13). For 1, 2, 10, and 11, this is observed in the present study. Each of these molecules has a β-1,4-linkage and contains an aglycon with a hydroxymethyl group attached to C_5. The temperature dependence of the O_3H signal is only 29-42% of the other hydroxyls which exhibit a nearly uniform and large dependence on temperature. This compares to α-1,4-linked maltose where the ratio is 59-68%. This is a clear indication that the O_3H signal results from a hydroxyl that is shielded from interacting with the solvent, i.e., intramolecularly hydrogen-bonded.

The data for the disaccharides 5 and 6 are tabulated in Tables IV and VII. For the α-anomer, the dependence on temperature of the O_3H signal is only slightly less

than that of the other hydroxyls. Apparently, the solvent participates in the H-bond to O_3H for these compounds.

Vicinal Coupling-Singlets

The measureable spin-spin coupling value ($^3J_{HCOH}$) for the isolated hydroxyls were given in Tables I-IV. Over the temperature range studied, these values are nearly constant.* This was previously shown to be true for cyclohexamylose and was interpreted in terms of a dominant local conformation for the hydroxyl (13). For the $O_3H\ldots O_2'H$ intramolecular H-bond in cyclohexamylose a value of 2.5 Hz was observed for $^3J(O_3H,C_3H)$. The same authors used a Karplus type relationship (27) to estimate a value of +110° for the dihedral angle

$$^3J_{HCOH} = 10.4 \cos^2\chi - 1.5 \cos\chi + 0.2 \tag{1}$$

(χ) in amylose.** The proposed conformation for O_3H in amylose is illustrated in Fig. 15 (13). For linkage dihedral angles (ϕ, χ) near those of crystalline methyl β-maltopyranoside, it was shown that this value of χ gives nearly a linear H-bond.

For the disaccharides containing a hexose as an aglycon, a slightly broadened singlet was observed for O_3H. In Fig. 7b, the sharpening of the O_3H singlet, relative to that observed in Fig. 5, clearly indicates a nonzero coupling constant. Measurement of width at half height gives a value of 3.0 (± 0.1) Hz, about twice that of the decoupled peak in Fig. 7b. Though an accurate measurement can't be made, a coupling of between 1-2 Hz can be estimated. Whatever the value, it certainly is less than that observed in maltose.

---

*At very high temperatures or if impurities that catalyze proton exchange are present, this will not be true. In the case of $O_2'H$ in cellobiose, this is particularly the case, even when no decrease in J is observed for the other hydroxyl signals.
**J = 2.0 Hz.
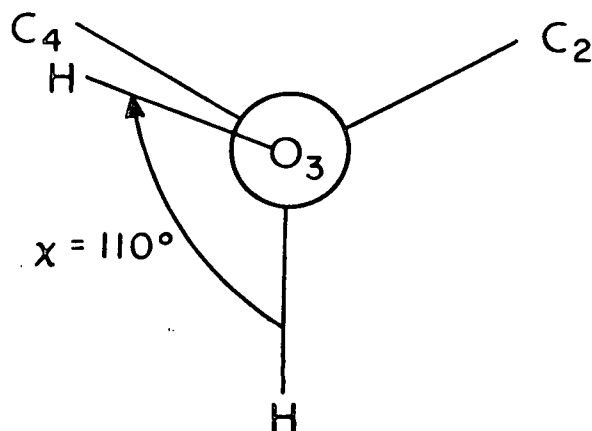
Figure 15. The proposed conformation of O_3H in amylose as depicted in Ref. (13). In this paper the dihedral angle, χ, is defined as the clockwise rotation of the hydroxyl proton relative to the vicinal ring carbon. This is the negative of the definition of χ in Ref. (13).

Values of $^3J_{HCOH}$ in this range correspond to a value of approximately 90° for χ. In this range of dihedral angles, the modified Karplus equation is somewhat insensitive so that only an approximate value for χ can be expected (28,29). Nevertheless, for the known crystalline conformations of 1 and 2 (4,5,6), any χ value in the vicinity of 90° gives nearly a linear intramolecular H-bond, as expected. Therefore, the reduced coupling of O_3H to C_3H is a further manifestation of the presence of the $O_3H\cdots O_5$, intramolecular H-bond in DMSO-d_6 solutions of 1, 2, and related disaccharides.

Figures 9b and 11 illustrate the appearance of the O_3H signal in 5 and 6, respectively. In this case, a broadened singlet to a very weak doublet (2.4 Hz) is observed. Again, this contrasts sharply with the much larger couplings of the anomeric hydroxyls. As in cellobiose, the O_3H signal represents a different conformation from that exhibited by the other hydroxyls. For a coupling contrast of 2.4 Hz values for χ of ± 113° and ± 57° are obtained using the modified Karplus equation

(1). This assumes only one dominant conformation.[*] The positive values are required to orient the proton toward $O_{5'}$. For either of these values to be involved in a near linear intramolecular H-bond, the linkage conformation must be somewhat more removed from the 2-fold helix conformation ($\phi=0, \gamma=0$) than in the cellobiose-related disaccharides.[**]

The fact that the O_3H conformation is dissimilar indicates that a weak interaction with $O_{5'}$ is involved. A bifurcated H-bond might be proposed in which the solvent participates. Such a bond would exhibit both a strong temperature dependence and an orientation toward the adjacent ring oxygen. Figure 16 depicts a possible arrangement. Because of the flexible nature of the linkage, this is only one of a number of probable arrangements. The one depicted in Fig. 16 agrees with the prediction that the O_3H....$O_{5'}$ bond in the xylans in less significant than that of cellobiose (3,8).
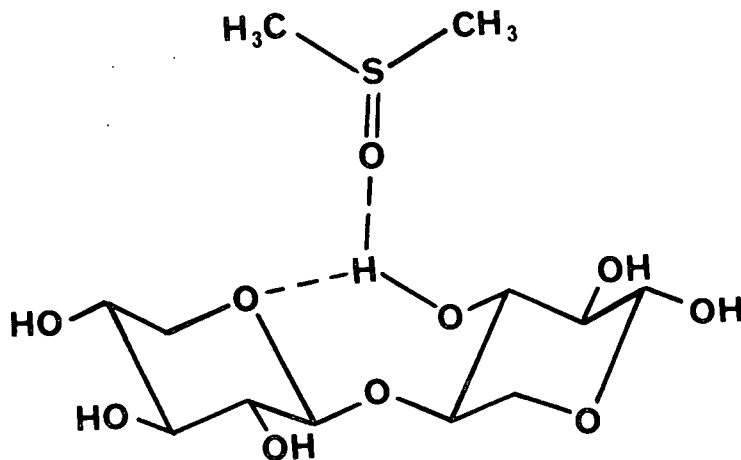
Figure 16. A depiction of a possible bifurcated hydrogen-bond in β-xylobiose (5a).

---

[*]Recent evidence indicates that the linkage is flexible (3,30) so that no dominant conformation is expected if a linear H-bond is maintained. Therefore, a range of χ values between these limits is probable.

[**]Work in this lab concerning $^{13}C-^{1}H$ coupling constants across the linkage and $^{1}H-T_1$ relaxation times agree with this. It can be shown that the average absolute value for χ is greater in 5 than in 1. This results from greater freedom for movement of the aglycon past $H_{1'}$ because of the absence of the hydroxymethyl group attached to C_5 (4,31). To maintain a linear intramolecular H-bond, values of χ nearer to +113° are required for this linkage conformation.

Relative Chemical Shifts

In comparing the relative chemical shifts of the disaccharides to the corresponding monosaccharides, it was observed that there is a general downfield shift of the hydroxyl protons in the disaccharides (0.11-0.13 ppm). This is probably related to interaction with the solvent and suggests that solvent is more tightly bound to the disaccharide, resulting in a stronger hydrogen bond with the hydroxyls. This is expected because of the lower mobility of the larger molecules.

Exceptions to the above generalization are the hydroxyl protons in close proximity to the linkage (O_3H and $O_{2'}H$ in $\underset{\sim}{1}$ and $\underset{\sim}{2}$). In cellobiose and MBC2 the O_3H signal is actually shifted upfield (0.07 ppm) relative to the same signal in glucose.[*] This suggests that the 3-hydroxyl proton is more closely associated with solvent in glucose then in the disaccharides. This is analogous to the effect of temperature noted above and agrees with the description of an intramolecular hydrogen-bond without any significant participation of the solvent.

The signal from $O_{2'}H$ is shifted even further downfield than the remaining hydroxyls. This may suggest that its interaction with the solvent is increased, however, the impact of steric crowding from the linkage and a possible intramolecular H-bond with OH_6 must also be considered. Further discussion on this point is given in Appendix IX.

In the case of xylobiose and related compounds the only exceptions to the above generalization are the O_3H signals. They are shifted downfield slightly less than the other hydroxyls. This is consistent with an intramolecular hydrogen bond that has a significant participation from the solvent, as described above.

---

[*]Giving a normalized upfield shift of 0.18 ppm.

Weak vs. Strong Intramolecular Bonds: Impact of C_6

The IR spectra of the solid cellooligosaccharides contain several temperature sensitive bands in the OH stretch region; 3100-3560 cm^{-1}. On the basis of their relative insensitivity to temperature, the bands on the high frequency side of this region are attributed to intramolecularly H-bonded hydroxyls [7,32,33]. As the temperature increases, the peaks representing H-bonded hydroxyls shift to larger wave numbers. Since a OH-stretch band at higher frequencies represents a weaker H-bond,[*] it can be inferred, with caution, that the intramolecular H-bond in the solid cellodextrins is a weak H-bond [34].

In general, the participation in a H-bond leads to deshielding of a proton signal in the NMR spectrum; the amount of deshielding being related to the strength of the H-bond. This is supported by the simultaneous H-bond weakening and upfield movement of the hydroxyl signal with increasing temperature. In the original study involving intramolecular H-bonds in dissolved cellobiose, the ^{1}H-NMR signal assigned to O_3H was downfield of its location in glucose [9]. In the present study, the O_3H signals for 1a and 2 are shown to shift upfield relative to the monosaccharide signal (Tables I, II, and III). The more recent result is in agreement with the expectations from IR and is in general indicative of a weak H-bond.

In 5 and 6, the upfield shift of the O_3H signal, relative to xylose, is small. Therefore, the criteria outlined above indicate that the O_3H H-bond in 5 is stronger[**] than that in 1. The H-bond involves the solvent in 5, while in 1, it is only intramolecular. Apparently, the solvent can participate in a stronger H-bond.

The characteristics of the intramolecular H-bond in cellobiose result from linkage geometrical constraints which act to restrict the allowed $O_3 - O_{5'}$ distance

---

[*]The hydrogen-bonded proton is more closely associated with the hydroxyl oxygen.
[**]The hydrogen-bonded proton is less closely associated with the hydroxyl oxygen.

to values near 2.8 Å (1). Such constraints are not as severe for compounds such as xylobiose, with the result that the solvent can penetrate close to the 3-hydroxyl proton. Continuing with this logic, it can be assumed that the intramolecular H-bond in 1 is weaker than a potential H-bond with the solvent. In 5, the O₃H....O₅' bond is just as capable of forming as in 1 but does so only marginally. Therefore, in 1 it appears that the intramolecular H-bond forms as a consequence of the allowed linkage conformations and does not act to promote the linkage conformations except in a minor way.* Rather, it is the presence of the hydroxymethyl group that restricts the available linkage conformations relative to 5 (1,35). For 1, the allowed set of linkage conformations prevents access by the DMSO-d₆ molecules to O₃H.**

SUMMARY

The ¹H-NMR spectra of a series of β-1,4-linked disaccharides have been studied over a range of temperatures and under conditions of slow proton-exchange (DMSO-d₆). The disaccharides which contain a 6-hydroxymethyl group, such as cellobiose and methyl β-cellobioside, were found to contain a hydroxyl-proton with a chemical shift that is relatively insensitive to temperature. Furthermore, the resonance of this proton appears as a singlet while all other hydroxyl-protons exhibit large couplings with the adjacent skeletal protons. The temperature-insensitive singlet has been assigned to the 3-hydroxyl proton (O₃H) of the reducing-end in cellobiose on the basis of homonuclear decoupling experiments. This assignment represents a departure from earlier studies. The unusual characteristics of this proton have been

---

*The conformation is restricted to only a small percentage of all the possible φ, χ values (1). Within this small domain, the establishment of a stable intramolecular H-bond is a factor in promoting conformational stability but it is not a factor in restricting the linkage to the few conformations available.
**In H₂O, this restriction may not be as severe. It has not been determined if the O₃H....O₅' bond survives in H₂O for 1 or 5. In the latter case, it is unlikely.

interpreted in terms of an intramolecular hydrogen-bond (O_3H....O_5) that results from the constraint on the rotational freedom of the linkage arising from the reducing-end 6-hydroxymethyl group.

For the disaccharides which do not contain a 6-hydroxymethyl group at the reducing-end, xylobiose and securidebiose, a temperature-sensitive signal is assigned to O_3H. The signal appears as a broadened singlet. This is interpreted in terms of strong hydrogen-bonding to the solvent in conjunction with a weak intramolecular interaction with the ring oxygen on the adjacent ring.

EXPERIMENTAL

Spectrum Acquisition

The ^1H-NMR spectra were recorded on a Jeol FX-100 FT spectrometer (99.61 MHz) supplied with homonuclear decoupling capabilities. Either the 5 mm or 1 mm dual probes were used. Spectra were accumulated for 10-50 pulses using 8K of data points. Temperature control was obtained with a Jeol supplied NM 5471 model temperature controller stable to ± 0.5°C and calibrated to ± 2.0°C. All chemical shifts are referenced to TMS using the DMSO-d_5 central line as a secondary reference [2.50 ppm, (13)]. In the variable temperature studies, the shift of the DMSO-d_5 signal relative to TMS changes by no more than ± 0.01 ppm relative to internal TMS.

Solutions were prepared using 99.5% DMSO-d_6 that had been stored over A-4 molecular sieves to reduce residual water. Sample concentrations ranged from 3.6 - 7.9% (w/v). Over this concentration range, no significant changes in hydroxyl proton chemical shifts were observed for spectra of the same compound. Previous authors also report a concentration independence at these values (9). Water was added up to 6% without a complete loss of the hydroxyl resonances in an 8.8% solution of 1 in DMSO-d_6. Under these conditions, the β-O_3H singlet could still be observed.

Several samples required pretreatment with IR-120 cation exchange resin (acid-form) before individual hydroxyl signals could be observed. A similar dependence of the hydroxyl signal resolution on sample purity has been observed by others (14).

Both the chemical shift temperature coefficients and their extrapolation to 56°C were calculated using a linear regression analysis program over at least three temperatures. In all cases, a correlation coefficient greater than 0.99 was obtained. Coupling constants were measured directly from the computer output of signal location. All coupling constants reported are apparent coupling constants.

Compound Acquisition

All compounds were characterized via their ^{13}C-NMR spectra which are being reported separately (36). Corrected melting points were obtained if enough crystalline sample was available; except for methyl β-xylobioside, they agree with the literature.

The following compounds were purchased and used without further purification: cellobiose (1a,b), xylose (3a,b), methyl β-xylopyranoside (3c), methyl α-xylopyranoside (3d), glucose (4a,b), and lactose (10). Cellotriose (8), xylotriose (9), and 4-O-(β-D-glucopyranosyl)-D-mannopyranose (11) were obtained as gifts as discussed in Appendix X. Xylobiose (5a,b) and securidebiose (6a,b)* were synthesized via a Koenigs-Knorr condensation using benzyl 1,3-anhydro-β-D-ribopyranoside and the appropriate acetyl bromide. A slight modification was used of the procedure given by Aspinall (37,38). Methyl β-cellobioside (2) was prepared using known procedures from cellobiose octaacetate via a Koenigs-Knorr condensation of the bromide with methanol (39); mp. 175-178°C. Literature mp. 170.5-174°C (39), mp. 193°C (40). Methyl β-xylobioside (7a) was prepared starting from xylobiose hexaacetate using the

---

*4-O-(β-D-glucopyranosyl)-D-xylopyranose.

same procedures: mp. 174-177.5°C. Literature mp. 103-104°C (41), mp. 148.5-149°C

(42). The different melting points probably represent different polymorphs (42);

the ^{13}C-NMR spectrum is consistent with the proposed structure (36). Benzyl β-

xylobioside (7b) was isolated as a syrup in one of the intermediate steps to 5.

LITERATURE CITED

1. Rees, D. A. and Skerrett, R. J., Carbohyd. Res. 7:334-48(1968).

2. Settineri, W. J. and Marchessault, R. H., J. Polymer Sci., Part C, 11:253-64(1965).

3. Melberg, S. and Rasmussen, K., Carbohyd. Res. 71:25-34(1979).

4. Brown, C. J., J. Chem. Soc. (A) 1966:927-32.

5. Chu, S. S. C. and Jeffrey, G. A., Acta Crystallogr. B24:830-8(1968).

6. Ham, J. T. and Williams, D. G., Acta Crystallogr. B26:1373-83(1983).

7. Hatakeyama, H., Nagasaki, C., and Yurugi, T., Carbohyd. Res. 48:149-58(1976).

8. Marchessault, R. H. and Liang, C. Y., J. Polymer Sci. 59:357-8(1962).

9. Casu, B., Reggiani, M., Gallo, G. G., and Vigevani, A., Tetrahedron 22:3061-83 (1966).

10. Chapman, O. L. and King R. W., J. of Amer. Chem. Soc. 86:1256-8(1964).

11. Casu, B., Reggiani, M., Gallo, G. G., and Vigevani, A., Chemical Society (London), Special Publication 23:217-26(1968).

12. Michell, A. J., Carbohyd. Res. 12:453-8(1970).

13. St.-Jacques, M., Sundararajan, P. R., Taylor, K. J., and Marchessault, R. H., JACS 98:4386-91(1976).

14. Perlin, A. S., Can. J. Chem. 44:539-50(1966).

15. Perlin, A. S. and Mackie, W., Can. J. Chem. 44:2037-49(1966).

16. Lemieux, R. U. and Stevens, J. D., Can. J. Chem. 44:249-62(1966).

17. Dzizenko, A. K., Ovedov, Y. S., Isakov, V. V., and Trofimov, V. I., Izv. Akad. Nauk. SSSR, Ser. Khim. 8:1854-6(1969).

18. Koch, H. J. and Perlin, A. S., Carbohyd. Res. 15:403-10(1970).

19. Perkins, S. J., Johnson, L. N., Phillips, D. C., and Dwek, R. A., Carbohyd. Res. 59:19-34(1977).

20. Usui, T., Yokoyama, M., Yamaoka, N., Matsuda, K., Tuzimara, K., Sugiyama, H., and Seto, S., Carbohyd. Res. 33:105-16(1974).

21. De Bruyn, A., Anteunis, M., and Verhegge, G., Bull. Soc. Chim. Belg. 84:721-34(1975).

22. Carlson, K. P., Doctoral Dissertation, The Institute of Paper Chemistry, 1979.

23. Feather, M. S. and Harris, J. F., J. of Amer. Chem. Soc. 89:5661-4(1967).

24. Muller, N. and Reiter, R. C., J. Chem. Phys. 42:3265-9(1965).

25. Fries, D. C., Rao, S. T., and Sundaralingham, M., Acta Crystallogr. B127: 994-1005(994).

26. Perlin, A. S., Du Penhout, P. H., Isbell, H. S., In Carbohydrates in Solution, ACS Symp. Series 117:39-50(1973).

27. Fraser, R. R., Kaufman, M., Morand, P., and Govil, G., Can. J. Chem. 47:408-9(1969).

28. Karplus, M., J. of Amer. Chem. Soc. 85:2870-1(1963).

29. Kotowycz, G., and Lemieux, R. U., Chem. Rev. 73:669-98(1973).

30. Gast, J. C., and Atalla, R. H., in preparation.

31. Gast, J. C., and Atalla, R. H., in preparation.

32. Zhabankov, R. H., J. Polymer Sci., Part C 16:4629-43(1969).

33. Michell, A. J., Aust. J. Chem. 23:833-8(1970).

34. Pimentel, G. C. and McClellan, A. L., The hydrogen bond. W. H. Freeman and Co., 1960.

35. Sundararajan, P. R. and Rao, V. S. R., Biopolymers 8:305-12(1969).

36. See Section IV.

37. Aspinall, G. O. and Ross, K. M., J. Chem. Soc. 1961:3674-7.

38. Kidd, J. R. and Schroeder, L. R., in preparation.

39. Best, E. V. and Green, J. W., Tappi 52:1321-5(1969).

40. Pacsu, E. J., J ACS 52:2571-5(1930).

41. Whistler, R. L., Bachrach, J., and Tu, C. C., J. of Amer. Chem. Soc. 74:3059-60 (1952).

42. Kovac, P., Hirch, J., and Kovacik, V., Chem. Zvesti 32:514-18(1978).

INTERMOLECULAR EFFECTS ON THE LINKAGE CONFORMATION IN
CELLOBIOSE, METHYL β-CELLOBIOSIDE, AND XYLOBIOSE

The solid state NMR spectra of cellobiose and methyl β-cellobioside were obtained using the CP/MAS technique.[*] The spectra were recorded on a modified Jeol FX-60Q system ([1]). The cellobiose was purchased and the methyl β-cellobioside was synthesized (see Section IV). X-ray diffraction showed each sample to be crystalline.

The spectra are shown in Fig. 1 and 2. Table I tabulates the chemical shifts for the solids and compares them to the shifts in D_2O. Assignments are given for the C_1, $C_{1'}$, C_4, C_6, and $C_{6'}$ signals.

From the table, a consistent downfield shift can be noted for all the assigned carbons. Most of the shifts are about the same order of magnitude as a solvent shift (1-3 ppm). This shift is primarily related to the hydrogen bonding pattern of the crystal, though small changes in the conformation of the anhydroglucose rings is probably also a factor.

Of greater significance is the large downfield shift for C_4. The magnitude of this shift is 5.2-5.4 ppm for the two compounds. This is significantly greater than for any other carbon. Furthermore, the location of the C_4 signal in D_2O is about the same as it is for amorphous cellulose, but still upfield from where it is in crystalline cellulose I or II[**] ([1],[2],[3]).

The conclusion that arises by comparing the solid and solution C_4 shifts is that the glycosidic linkage conformation is probably significantly different in the

---

[*]Spectra recorded at Colorado State University by the group of Dr. G. E. Maciel ([1]). CP/MAS refers to cross polarization/magic angle spinning.
[**]87-90 ppm.

CELLOBIOSE
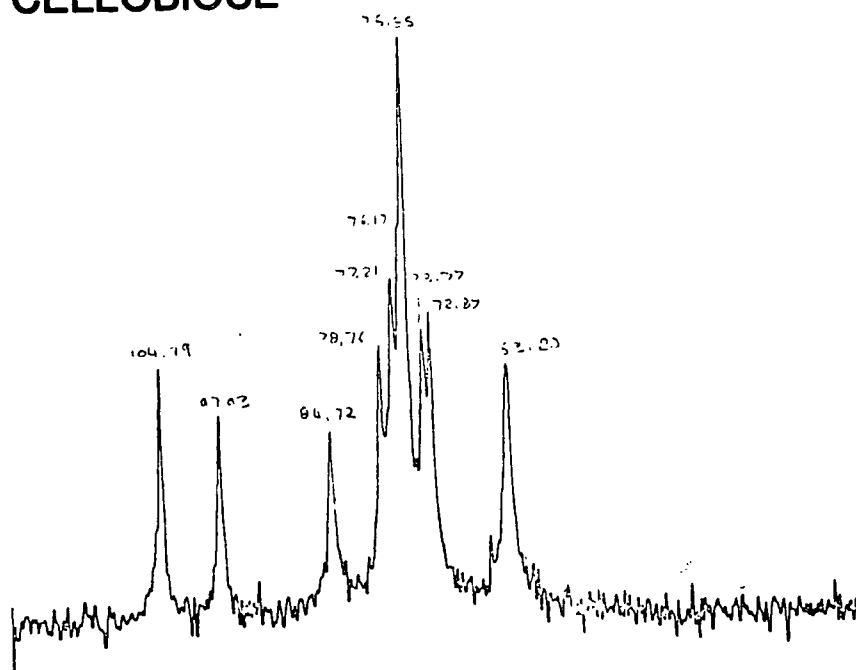
Figure 1. Solid state ^{13}C-NMR spectrum of cellobiose. Chemical shifts are given adjacent to each resonance.

Methyl β Cellobioside
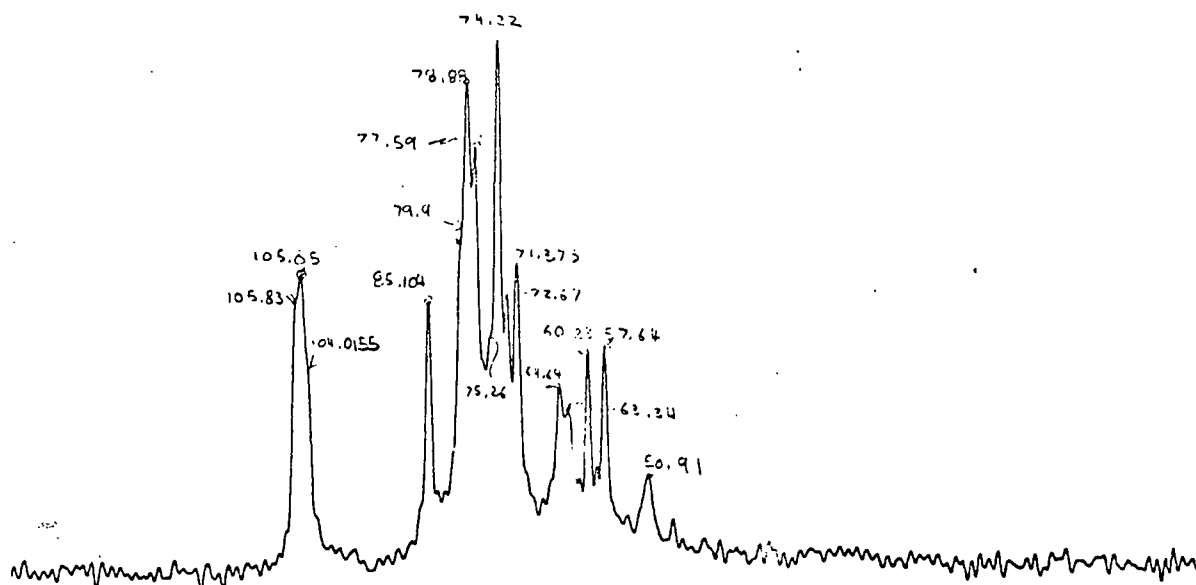
Figure 2. Solid state ^{13}C-NMR spectrum of methyl β-cellobioside. Chemical shifts are given adjacent to each resonance.

TABLE I

CHEMICAL SHIFTS FOR CRYSTALLINE β-CELLOBIOSE AND METHYL β-CELLOBIOSIDE

Compound	Phase	$C_{1'}$	C_1	C_4	Other	$C_6, C_{6'}$	OMe
β-Cellobiose	Crystal	104.8	97.9	84.7	72.9-78.8	63.8	
β-Cellobiose	D_2O	103.4	96.9	79.5	70.3-76.8	61.0-61.5	
Methyl β-cellobioside	Crystal	(104.0 - 105.8		85.1	71.4-79.9	63.3-64.6[b]	60.2
Methyl β-cellobioside	D_2O	103.4	103.9	79.7	70.3-76.8	61.0-61.5	58.1

[a]Referenced to $(CH_3)_4Si$.
[b]An additional signal is observed at 57.6 which is unassigned. It could result from either O-methyl or methanol. It suggests that at least two types of environments are present for one of these components in the crystal. The signal at 50.9 is also assigned to methanol.

two states. Furthermore, the conformation is also probably significantly different from that of either polymorph of cellulose. The differences are too great to be related to instrumental effects (4).

It can be speculated that two important factors are involved. First, in comparing crystalline cellulose to crystalline disaccharide to dissolved disaccharide, the chemical shift change is much greater for C_4 than for $C_{1'}$. From the exoanomeric effect, it would be expected that χ would change more than ϕ over this transition. Since the C_4 carbon is part of the C_4 to O_4 (linkage oxygen) bond, which is the bond central to χ, it is reasonable that a greater change should result for C_4 (5,6).

Secondly, the large upfield shift in C_4 probably reflects a change in hybridization at the bridge oxygen. From x-ray diffraction work τ has been determined to be 116.1 in crystalline β-cellobiose and 115.8 in crystalline methyl β-cellobioside, respectively (7,8). However, the bridge angle for β-cellobioside has been calculated to be 113.4 in the isolated molecule using an empirical force field (9). This should be more typical of the solution value. Thus, in going from the crystal to solution, the bridge angle τ relaxes about 3°. This is equivalent to developing more sp^3 character at the linkage oxygen, meaning that the electrons will be less closely associated with the oxygen nucleus and will act to increase the electron density at the linkage carbons. Therefore, the C_4 carbon would be expected to shift upfield going from the solid to the dissolved states of the disaccharide.

It should be emphasized that the downfield shift in the crystalline disaccharides is not related to steric compression of linkage protons. Steric shifts are always upfield. Besides, the $H_{1'}$ to H_4 distance is known to be 2.2 Å in crystalline β-cellobiose. This is greater than the maximum distance possible, 2.0 Å, for

overlap of these protons if they are considered as hard spheres (10). Therefore, steric compression is not expected to be a significant factor in determining the chemical shifts of the linkage carbons.

To summarize, the effect of the crystal lattice is to significantly change the linkage conformation for both methyl β-cellobioside and β-cellobiose, relative to the average solution conformation. This change is related to either a change in the dihedral angle χ, a change in the bridge angle τ, or both. Since the angle χ has been determined to be similar[*] in the crystalline and dissolved states (Section 2, Part 2) (11), it is probable that this shift is primarily caused by an increase in τ upon crystallization.

The effect of solvent on the ^{13}C-NMR chemical shifts of cellobiose and xylobiose was also studied to try to determine if there is a conformational difference in the two solvents. Table II compares the spectra in DMSO-d_6 and D_2O for both disaccharides.

In going from D_2O to DMSO-D_6, nearly every signal is shifted upfield from -0.3 to -1.8 ppm in xylobiose.[**] The C_4 signal is included in this group with an upfield shift of -1.8 ppm. For cellobiose, it is also observed that nearly every signal is either stationary or moves upfield (+ 0.1 to -0.9 ppm), with one exception. C_4 shifts downfield by 1.2 ppm in going from D_2O to DMSO. Heyraud and coworkers (12) have suggested that this is related primarily to the degree of solvation, but also at least partly to a conformational change. It is suggested here that the major difference is that DMSO-d_6 can penetrate close to the linkage in xylobiose where it

_____

[*] The magnitude of the effect of small changes on the chemical shift of C_4 is not known.

[**]The reducing end anomeric carbon is an exception. It shows no significant change. Because of the higher acidity of this signal, the DMSO-d_6 is still able to interact with it strongly.

may interact either with the weak intramolecular hydrogen bond (Part III) or with the bridge oxygen itself. In cellobiose, there is no penetration to the vicinity of the linkage by the DMSO-d_6. And, since the solvent can't interact with the C_3 hydroxyl, because of the protected intramolecular hydrogen bond, it can only remotely affect the chemical shift at C_4.[*] The fact that the C_4 shift is as large as it is may further reflect a change in the linkage conformation.

[*]C_1' is still shifted upfield because of the interaction of the solvent at $O_2'H$.

TABLE II

COMPARISON OF THE D_2O AND DMSO-d_6 CHEMICAL SHIFTS[a]
OF β-CELLOBIOSE AND β-XYLOBIOSE

		1	2	3	4	5	6	1'	2'	3'	4'	5'	6'
β-Cellobiose	D_2O	96.6	74.8	75.1	79.5	75.6	61.1	103.4	74.0	76.4	70.3	76.8	61.5
	DMSO-d_6	96.6	74.5	75.0	80.7	74.7	60.6	103.1	73.3	76.5	70.1	76.8	61.0
β-Xylobiose	D_2O	97.3	74.9	74.9	77.3	63.9		102.7	73.7	76.5	70.1	66.1	
	DMSO-d_6	97.4	74.4	74.9	75.5	63.1		101.9	72.4	76.2	69.4	65.7	

[a]Relative to $(CH_3)_4Si$ internally or using p-dioxane (67.4 ppm) as a secondary reference.

LITERATURE CITED

1. Atalla, R. H., Gast, J. C., Sindorf, D. W., Bartuska, V. J., and Maciel, G. E., J. Amer. Chem. Soc. 102:3249-51(1980).

2. Earl, W. L. and VanderHart, D. L., J. Am. Chem. Soc. 102:3251-2(1980).

3. Earl, W. L. and VanderHart, D. L., Macromolecules 14:570-4(1981).

4. VanderHart, D. L., Earl, W. L., and Garroway, A. N., J. Magn. Res. 44:361-401 (1981).

5. Tsukada, S. and Inoue, Y., Carbohyd. Res. 88:19-38(1981).

6. Lemieux, R. U. and Koto, S., Tetrahedron 30:1933-44(1974).

7. Chu, S. S. C. and Jeffry, G. A., Acta Cryst B24:830-8(1968).

8. Ham, J. T. and Williams, D. G., Acta Cryst B26:1373-83(1970).

9. Melberg, S. and Rasmussen, K., Carbohyd. Res. 71: 25-34(1979).

10. Rees, D. A. and Skerrett, R. J., Carbohyd. Res. 7:334-8(1968).

11. Hamer, G. K., Balza, F., Cyr, N., and Perlin, A. S., Can. J. Chem. 56:3109-16 (1978).

12. Heyraud, A., Rinaudo, M., Vignon, M., and Vincendon, M., Biopolymers 18:157-85 (1979).

SECTION IV - PREPARATION AND CHARACTERIZATION

OF MATERIALS

PREPARATION OF MATERIALS

INTRODUCTION

The objective of this work has been to compare the solution conformations of the xylo-oligosaccharides and the cello-oligosaccharides. Special emphasis has been given to the respective disaccharides and in some cases the β-methyl anomers of those disaccharides. In the latter case this was primarily to avoid complications arising from mutarotation of the reducing end group. Specific disaccharide models containing the β-1,4- linkage have also been used for comparison purposes.

Fortunately, the major technique utilized in this work, NMR spectroscopy, did not require large quantities of material. Use of the Jeol ^{13}C/^{1}H dual nuclei microprobe further reduced the sample requirements. Therefore, despite having only limited available quantities of the cello- and xylo-oligosaccharides, it was possible to do much of the spectroscopic work without further synthesis or isolation. Exceptions to this were xylobiose (1) and 4-O-(β-D-glucosyl)-D-xylopyranose (7)* which were obtained via a multistep synthesis featuring a silver oxide promoted Koenigs-Knorr condensation reaction. Early attempts to isolate 1 from birchwood failed to provide a sufficient quantity of material. In addition, methyl β-xylobioside (20) and methyl β-cellobioside (21) were synthesized via a Koenigs-Knorr condensation with methanol using mercury salts as the acid acceptor. The deuterated analog, methyl-β-cellobioside-3, $6_a,6_b,2',3',4',6_a',6_b',-d_8$, was prepared using a recently developed catalytic C-deuteration reaction using Raney nickel (1).

---

*Securidebiose.

Characterization of the final compounds, as well as their synthetic intermediates, was primarily by ^{13}C-NMR spectroscopy. Melting points (m.p.), thin layer chromatography (t.l.c.), and conversion to an acetate of known physical properties were also used. Comparison of these results to literature values, or to data from identical compounds concurrently prepared and extensively characterized elsewhere in this laboratory (2), sufficed to prove the authenticity of the synthesized compounds.

Details of the synthetic procedures and the physical constants obtained are given in Appendix X. The general synthetic schemes are outlined below. ^{13}C-NMR spectra of the intermediates and the acetates are reproduced in Appendix XI and XII while the spectra of the final underivatized products are shown in Appendix XIII. Detailed spectral assignments are given below in parts 2 and 3 of this section. Included are the ^{13}C-NMR assignments of 2´,3´,4´-tri-O-methyl xylobiose (40) and intermediates leading up to it. These were kindly made available as an aid in assigning the derivative spectra (2).

SYNTHESIS OF XYLOBIOSE (1) AND SECURIDEBIOSE (7)

Disaccharide Formation

Figure 1 depicts the reaction scheme leading to xylobiose from two monosaccharide intermediates: Benzyl 2,3-anhydro-β-D-ribopyranoside (15) and 2,3,4-tri-O-acetyl-α-D-xylopyranosyl bromide (13). The key steps of this reaction scheme are the modified Koenigs-Knorr condensation to give 6 and the selective opening of the 2,3-epoxide bond to provide the xylo-configuration in the intermediate 3. This reaction scheme was first proposed by Aspinall and Ross (3). Slight modifications recently have been utilized by others to prepare the methylated xylo-oligosaccharides (4), xylobiose hexa-acetate (5) and to study the ^{1}H-NMR of the

$R_1 = H : 1, 2, 3, 5, 6, 13$

$R_1 = CH_2OH : 7, 9, 11$

$R_1 = CH_2OAc : 8, 12, 14$
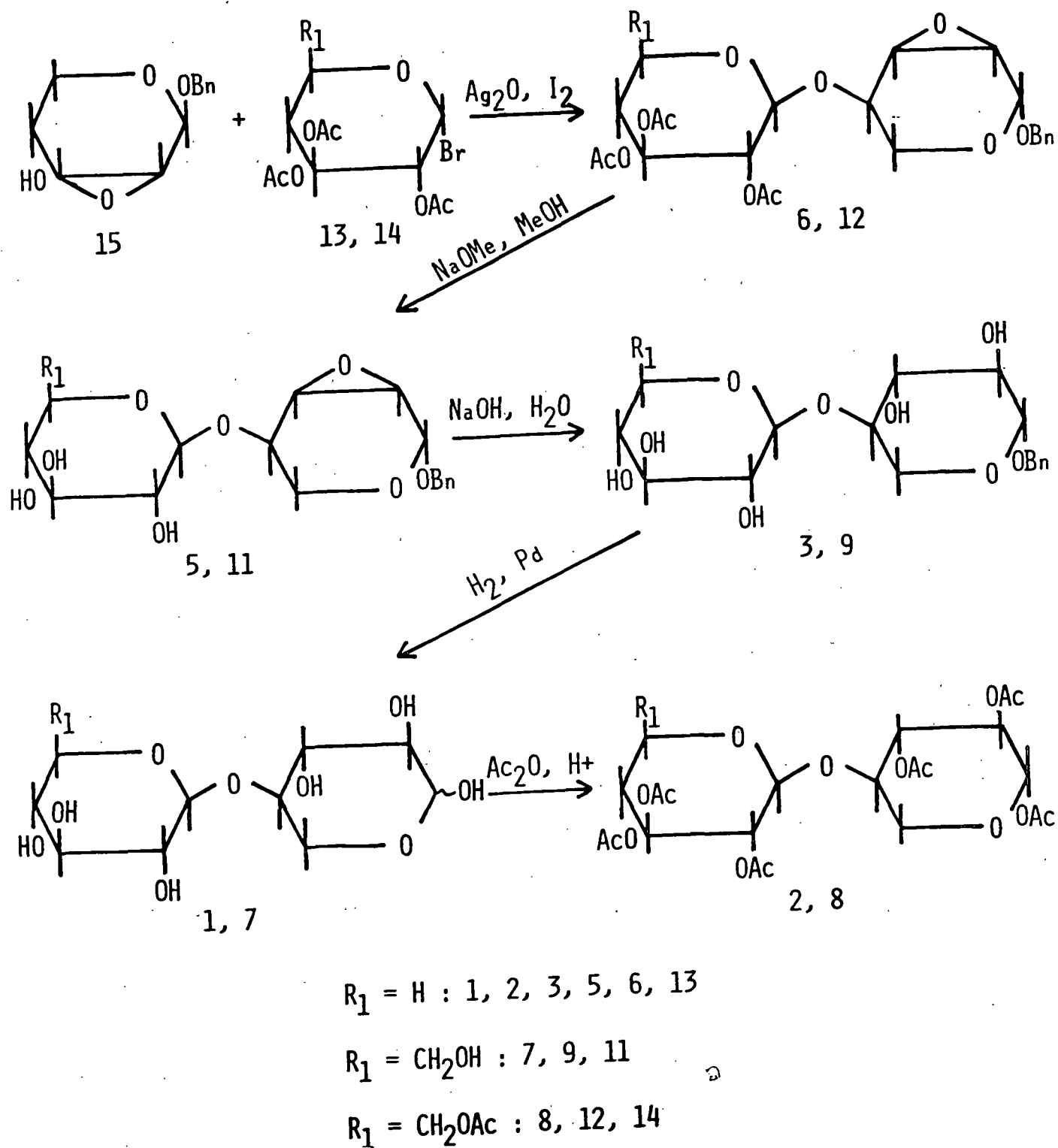
Figure 1. Synthetic scheme for the preparation of xylobiose (1), securidebiose (7), and their acetates.

epoxide intermediates (6). For the synthesis of 7, 2,3,4,6-tetra-O-acetyl-α-D-glucopyranosyl bromide (14) was substituted for 13.

The modified Koenigs-Knorr condensation was effected using silver oxide as the acid acceptor. The resulting acetate syrup was deacetylated directly with methanolic sodium methoxide to compound 5. Yields up to 31% were achieved.

The opening of the epoxide ring to form 3 was accomplished by reacting 5 in aqueous sodium hydroxide (2N) at a temperature close to boiling. This produced a hard yellow syrup that would not crystallize. It has been reported, using gas-liquid chromatography (g.l.c.), that the ring opening is not entirely selective for the xylo configuration. Up to 10% of the arabino configuration was detected by g.l.c. (2). ^{13}C-NMR of the syrup did not reveal significant amounts of this contaminant so no further purification was required.

Subsequent reaction to form 1 was by hydrogenation over palladium on carbon (Pd/C) catalyst. The resulting syrup was isolated as the acetone powder. ^{13}C-NMR of 1 and its peracetate (2) confirmed the structure. Presence of the arabino-impurity prevented crystallization of 1 or its acetate.

Preparation of Monosaccharide Intermediates

The epoxide intermediate (15) was prepared from arabinose using a 5-step synthetic sequence as shown in Fig. 2. Established literature procedures were used throughout (7,8).

The α-bromides 13 and 14 were prepared from the acetates using established literature techniques (9). This also is depicted in Fig. 2.
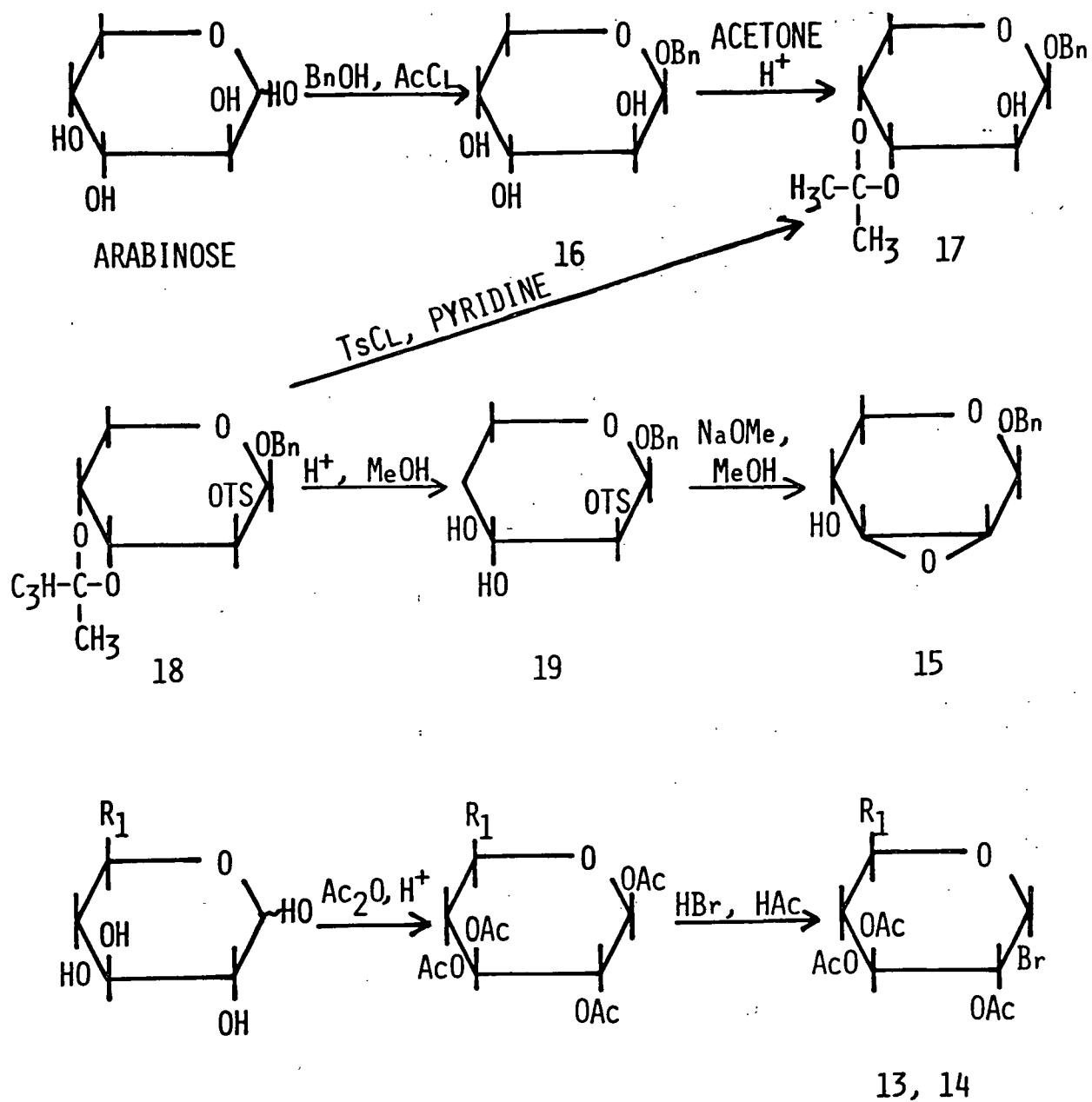
Figure 2. Synthetic schemes for the monosaccharide intermediates 13-15.

PREPARATION OF METHYL β-XYLOBIOSIDE (20) AND METHYL β-CELLOBIOSIDE (21)

Figure 3 depicts the synthetic scheme for preparing 20 and 21. The procedure is patterned after standard literature methods (10,11). The reaction proceeds from the disaccharide to the α-acetate. The α-acetate is then brominated and used in a Koenigs-Knorr condensation, employing mercury salts (yellow HgO, $HgBr_2$) as the acid acceptor. The crystalline product was then deacetylated with sodium methoxide.

C-DEUTERATION OF METHYL GLYCOSIDES

Exchange of the backbone protons with deuterium occurs over deuterated Raney nickel for all carbons possessing a free hydroxyl (1). To avoid excessive side reactions a nonreducing sugar must be used. The idealized reaction is illustrated in Fig. 4.

In actual practice some inversion of configuration occurs at all carbons possessing a free hydroxyl as a side reaction. The isomerization is a minimum for the glucopyranose configuration because it provides the lowest energy form of the Cl conformer. By careful monitoring of the reaction by ^{13}C-NMR[*] the isomerization can be minimized. For the methyl β-glycosides substitution at C_2 is sterically hindered by the methyl group so that complete exchange of H_2 cannot be achieved without isomerization. Methyl β-cellobioside, methyl β-glucoside, and methyl β-xyloside were deuterated using this approach.

---

[*]Deuteration of a carbon essentially destroys its ^{13}C-NMR signal due to slow relaxation and indirect coupling to ^{2}H.

Figure 3. Synthetic scheme for the methyl β-disaccharides.
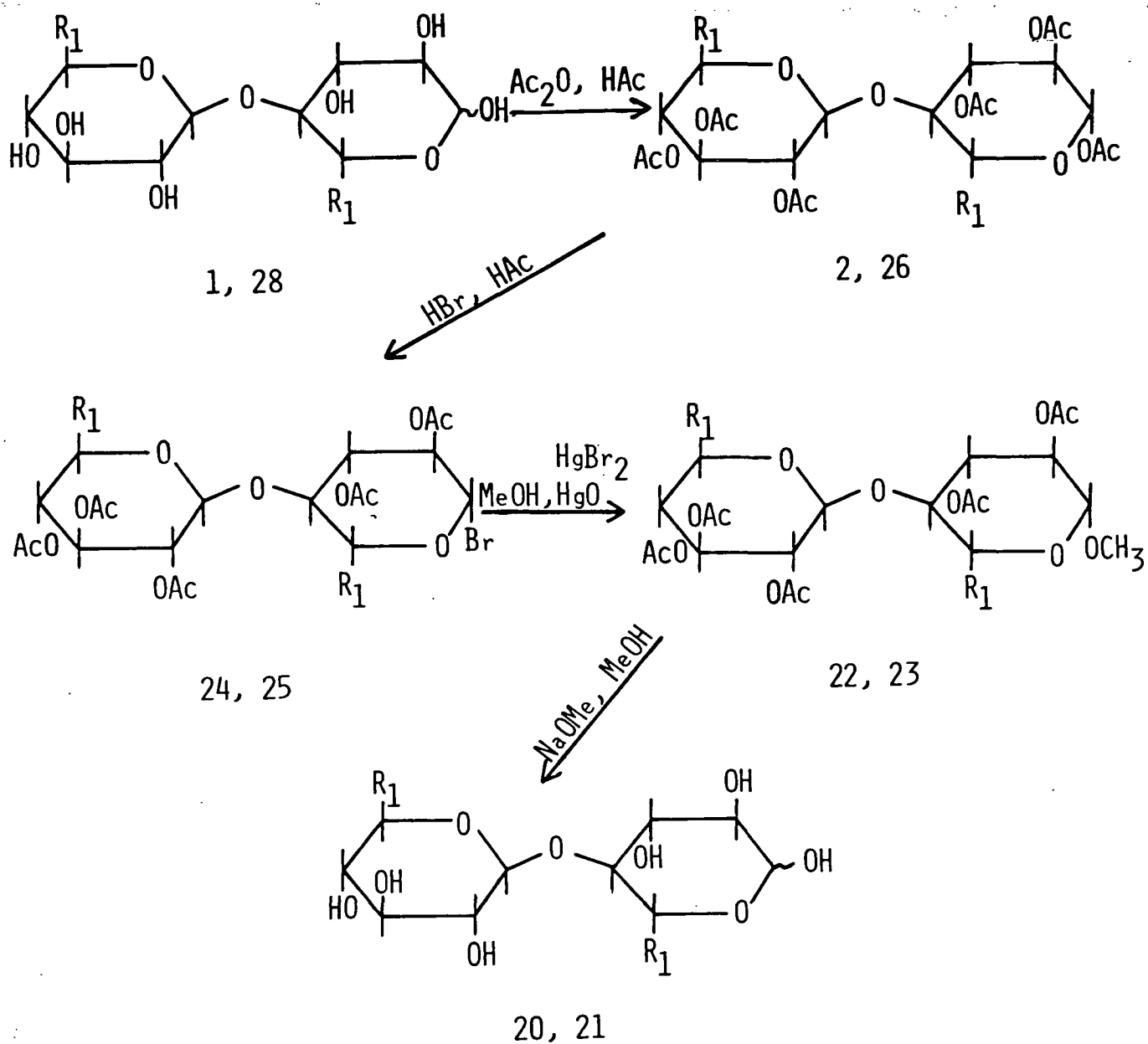
R_1 = H : 1, 2, 20, 22, 24

R_1 = CH_2OH : 21, 28

R_1 = CH_2OAc : 23, 25, 26

Raney Nickel Deuteration
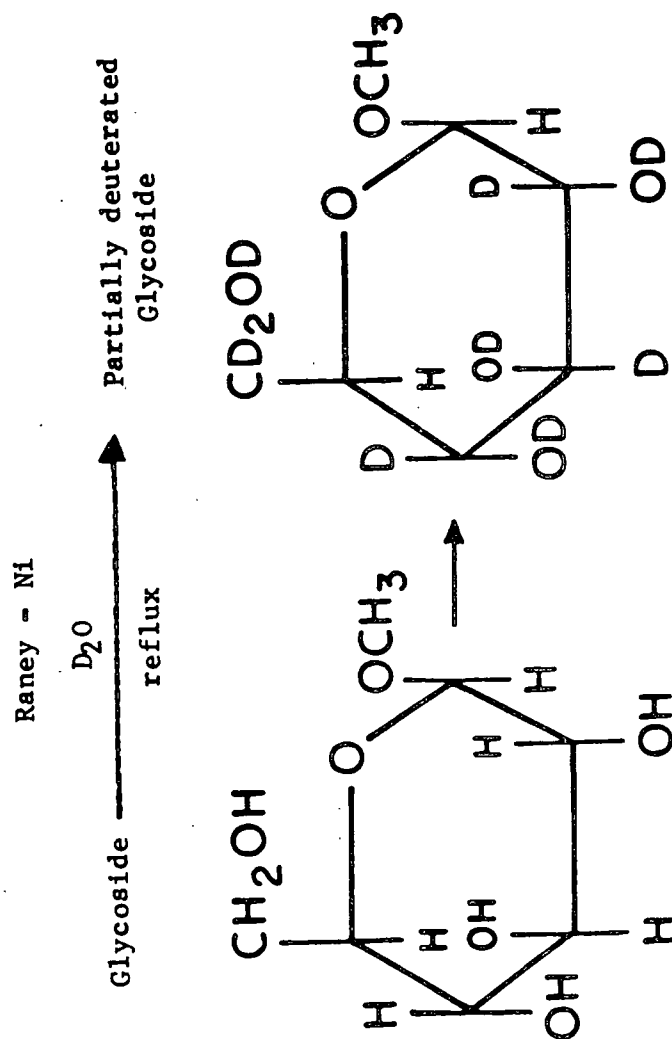
Figure 4. Exchange at C_2 is generally only partially complete.

LITERATURE CITED

1. Koch, H. J. and Stuart, R. S., Carbohyd. Res. 59:C1-6(1977).

2. Kidd, J. R. Synthesis and alkaline degradation of xylobiose and 2´,3´,4´, tri-O-methyl xylobiose. Doctoral Dissertation, The Institute of Paper Chemistry, Appleton, WI, 1980.

3. Aspinall, G. O. and Ross, K. M., J. Chem. Soc. 1961:3674-7.

4. Kovac, P., Hirsch, J., and Kovacik, V., Chem. Zvesti 32:514-8(1978).

5. Utille, J. P. and Vottero, P. J. A., Carbohyd. Res. 53:259-62(1977).

6. DeBruyn, A., Rijsberger, R. V., Anteunis, M. J. O., Claeyssens, M., and Deleyn, F., Bull Soc. Chem. Belg. 87:783-90(1978).

7. Buchanen, J. G., Clode, D. M., and Uethaviyasar, N., J. Chem. Soc. Perkin I: 1976:1449-53.

8. Ballou, C. E., J. Am. Chem. Soc. 79:165-6(1957).

9. Schroeder, L. R., Counts, K. M., and Haigh, F. C., Carbohyd. Res. 37:368-72 (1974).

10. Schroeder, L. R. and Green, J. W., J. Chem. Soc. (C) 1966:530-1.

11. Best, E. V. and Green, J. W., Tappi 52:1321-5(1969).

^{13}C-NMR ASSIGNMENTS OF SYNTHETIC INTERMEDIATES AND RELATED ACETATES

INTRODUCTION

^{13}C-NMR is rapidly becoming the preferred technique for characterization of carbohydrates and their derivatives. The simple 1 to 1 correspondence, between the number of carbons in the expected product and the number of peaks in the spectrum, often make it possible to merely count the signals to verify the structure. Further assessment on the basis of chemical shift, peak intensity, and correlation to model compounds then can substantiate the initial assignment. It is particularly useful for following the progress of a reaction scheme.

This technique was used extensively throughout this work to monitor progress toward the synthesis of compounds 1, 7, 20, and 21. In so doing, a considerable amount of information was obtained concerning the effect of various functional groups on the chemical shift of the backbone carbons in the β-1,4-linked disaccharides.* The correlations developed were helpful in verifying the ^{13}C-NMR spectral assignments of 1, 7, 20, and 21, which had not yet appeared in the literature.** In the development of these correlations use was made of the ^{13}C-NMR spectra of a number of model compounds synthesized concurrently within these laboratories (see Acknowledgments) (2).

ADVANTAGE OF ^{13}C-NMR

The benefits of ^{13}C-NMR for carbohydrates are basically derived from three factors. First, the large chemical shift range (200 ppm) of the carbon spectrum

---

*Refer to Ref.1 for a recent review on this subject.
**The primary method of assignment for 1 was by peak intensities of the oligosaccharides as well as comparison to xylose and cellobiose as models (See Part III).

assures that little overlap of peaks will occur. Even if peaks do overlap the peak heights generally indicate this, providing no unusual relaxation mechanisms are involved. Secondly, the decoupled spectrum commonly obtained is not complicated by difficult-to-analyze coupling patterns. This is the reason for the 1 to 1 correspondence usually observed. If coupling information is required it can be easily obtained using gated decoupling or off-resonance techniques. Finally, the observed chemical shifts in a series of similar compounds remain approximately constant for those carbons that are several bonds removed from the point of dissimilarity (3). Therefore, provided a sufficient data base exists, the assignment of a spectrum often merely involves a comparison with the spectra of several similar compounds.

^{13}C-NMR SPECTRAL ASSIGNMENTS OF THE DERIVATIVES RELATED TO XYLOBIOSE (1) AND SECURIDEBIOSE (7).

The work reported below includes the analysis of the ^{13}C-NMR spectra of most of the derivatives obtained during the synthesis of 1 and 7, as well as a number of model compounds. Figure 1 gives the structure and designation for each compound studied. Nearly complete spectral assignments have been obtained by internal comparison as well as comparison to similar acetylated and underivatized sugars. Where assignments were not complete a 1:1 correspondence was observed for the backbone carbon signals (55-110 ppm) and the number of signals expected on the basis of the structure. From these assignments observations concerning the effect of acetylation, benzylation, and O-methylation, on the chemical shift of β-1,4-linked carbohydrate ring carbons have been made. The location and identification of the functional group ^{13}C resonances are also discussed.

Functional Groups

In Tables I and II are tabulated the chemical shifts for all functional group signals in the spectra of the compounds studied. Pertinent model compounds are also

15 : R_1 = OH
36 : R_1 = OMe

17 : R_1 = OH
18 : R_1 = OTs

16 : R_2 = OBn
19 : R_2 = OBn, R_3 = OTs
43b : R_2 = OH

21 : R_2 = OMe, R_3 = R_4 = OH, R_5 = R_6 = CH_2OH
22 : R_2 = OMe, R_3 = R_4 = OAc
23 : R_2 = OMe, R_3 = R_4 = OAc, R_5 = R_6 = CH_2OAc
26a : R_1 = R_3 = R_4 = OH, R_5 = R_6 = CH_2OH
26b : R_2 = R_3 = R_4 = OH, R_5 = R_6 = CH_2OH
27a : R_1 = R_3 = R_4 = OAc, R_5 = R_6 = CH_2OAc
27b : R_2 = R_3 = R_4 = OAc, R_5 = R_6 = CH_2OAc
39b : R_2 = R_3 = OAc, R_4 = OMe
40a : R_1 = R_3 = OH, R_4 = OMe
40b : R_2 = R_3 = OH, R_4 = OMe

1a : R_1 = R_3 = R_4 = OH
1b : R_2 = R_3 = R_4 = OH
2a : R_1 = R_3 = R_4 = OAc
2b : R_2 = R_3 = R_4 = OAc
4 : R_2 = OBn, R_3 = R_4 = OH
4 : R_2 = OBn, R_3 = R_4 = OAc
7a : R_1 = R_3 = R_4 = OH, R_5 = CH_2OH
7b : R_2 = R_3 = R_4 = OH, R_5 = CH_2OH
9 : R_2 = OBn, R_3 = R_4 = OH, R_5 = CH_2OH
20 : R_2 = OMe, R_3 = R_4 = OH

28 : R_2 = OMe, R_3 = OH
30 : R_2 = OMe, R_3 = OH, R_4 = CH_2OH
33a : R_1 = R_3 = OAc
33b : R_2 = R_3 = OAc
34a : R_1 = R_3 = OAc, R_4 = CH_2OAc
34b : R_2 = R_3 = OAc, R_4 = CH_2OAc
35a : R_2 = OH, R_3 = OMe
41a : R_1 = R_3 = OH
41b : R_2 = R_3 = OH
42a : R_1 = R_3 = OH, R_4 = CH_2OH
42b : R_2 = R_3 = OH, R_4 = CH_2OH

5 : R_1 = OH
6 : R_1 = OAc
11 : R_1 = OH, R_2 = CH_2OH
37 : R_1 = OMe

Figure 1. Chemical structures for the compounds listed in Tables I-VII. The following abbreviations are used: Acetyl (Ac), benzyl (Bn), methoxyl (Me), and tosyl (Ts). If no designation is given for R_1 it is considered to be a proton.

presented for comparison. Reference to literature assignments of these or similar compounds are given in the tables. Table III summarizes the chemical shift ranges found for the functional groups.

Because of differing solubilities it was necessary to obtain the data in a number of different solvents. The effects of solvent dielectric constant and/or direct interaction with the sample make it difficult to make specific comparisons of chemical shifts (11). Nevertheless, all the functional group signals still fall within relatively narrow regions. These regions are diagnostic for the derivative and provide a simple method for determining the progress or success of derivatization. A number of derivatives common to carbohydrate synthesis are represented. They are discussed below.

Acetyl Groups

The carbonyl carbon peaks fall within the narrow range of 168.6-171.0 ppm. This is in the middle of the range for ester carbonyls reported in the literature (12,13). Signals above 170 ppm were only observed in the peracetates of the cello-oligosaccharides (see Table II and Appendix XII) in acetone-d_6. In β-glucose penta-acetate this was not observed, nor was it observed in 2b. This suggests that the downfield shift is related to the linkage of the cello-oligosaccharide peracetates.[*]

In general, the number of carbonyl carbons does not equal the number of acetate groups in the molecule. Several factors are responsible for this. Because of the small chemical shift range involved it is probable that several peaks are degenerate. For most substituents this would be manifest in peaks that are approximate

---

[*]This is not a steric compression shift which would cause upfield movement of the signals (3).

TABLE I

MONOSACCHARIDE DERIVATIVES FUNCTIONAL
GROUP CHEMICAL SHIFTS[a]

Compound	Solvent	CH₃O	$\underline{C}H_3$-C-	$\underline{C}H_3$-φ-S-	-$\underline{C}H_2$-φ	O CH₃-$\underline{φ}$-S- or O -CH₂-$\underline{φ}$	C - C	CH₃-$\underline{C}$-	$\underline{C}H_3$	$\underline{C}H_3$	$\underline{C}H_3$	$\underline{C}H_3$	Ref.
16	DMSO-d₆				68.3[b]	127.1-138.0 (4)							
17	CDCl₃				69.8[b]	127.9-137.1 (4)			25.9 27.8		109.2		
18	Acetone-d₆				70.2	128.1-145.5 (11-12)			26.2 27.8		109.3		
19	CDCl₃			21.6	69.4[b]	127.8-145.2(8)							
15	CDCl₃				70.0	127.9-137.0 (4)	51.9(2)						(4,5) (4,6)
28	D₂O	58.2											
30	D₂O	58.1											
33b	Acetone-d₆		20.6(1)					168.9-169.8 (4)					(7)
34b	Acetone-d₆		20.5(1)					168.9-169.8 (4)					(8,9)
35ₐ[c]	Acetone-d₆	58.1,58.8 60.6											
36[c]	CDCl₃	56.5			70.2	127.6-137.0 (5)	49.5 51.3						

[a] All relative to (CH₃)₄Si at 0 ppm except for those in D₂O which are externally referenced to (CH₃)₄Si using p-dioxane at 67.4 ppm as a secondary reference.
[b] Tentative assignment; could be exchanged with nearby signal within 2 ppm.
[c] See Ref. 2 for spectrum.

TABLE II

DISACCHARIDE DERIVATIVES FUNCTIONAL GROUP CHEMICAL SHIFTS[a]

Compound	Solvent	CH_3O	$\overset{O}{\overset{\|}{CH_3\text{-}\underline{C}}}$	$-\underline{C}H_2\text{-}\phi$	$\underline{C}H_2\text{-}\phi$	$\overset{O}{\overset{\|}{\underline{C}\text{-}C}}$	$\overset{O}{\overset{\|}{CH_3\text{-}\underline{C}\text{-}}}$	Reference
2b	Acetone-d$_6$	58.1	20.6(3), 20.8(1)		127.4-137.8(3)		169.2-169.8(3)	(7)
3	DMSO-d$_6$			69.6[b]	129.1-137.7(4)			
	D$_2$O			72.2				
4	Acetone-d$_6$		20.5(2), 20.8(1)	71.0[b]	128.0-138.3(4)		169.2-169.7(4)	
5	DMSO-d$_6$			69.3	127.5-137.4(4)	51.1, 52.0		
6	Acetone-d$_6$		20.6	70.6[b]	128.2-138.4(4)	51.9, 53.4	169.2-169.8(3)	
9	D$_2$O			72.3	129.3-137.4(3)	52.0, 52.2		
11	D$_2$O				129.3-137.4(3)	51.5, 52.5		
	DMSO-d$_6$			69.5[b]	127.5-137.4(4)			
20	D$_2$O	58.1	20.1(2), 20.2(2), 20.3(1)					(5)
21	D$_2$O	58.1						(10)
22	CDCl$_3$	56.2					168.6-169.4(4)	(5,7)
23	CDCl$_3$	56.9	20.5(35), 20.8(1)				168.9-170.4(7); 168.9-170.4(7)	
27a	Acetone-d$_6$		20.8(2), 20.5(3), 20.7(3)			52.3, 53.5	169.2-170.7(6)	(8,9)
37[c]	Acetone-d$_6$	58.5, 60.1, 60.2		70.6[b]	128.4-138.5(4)			
39b[c]	Acetone-d$_6$	58.4, 60.4(2)	20.4(1), 20.6(1), 20.7(1)				169.0-169.5(3)	
40a,b[c]	DMSO-d$_6$	57.8[b], 59.7(2)[b]						

[a] Referenced to $(CH_3)_4Si$. Samples in D_2O were arbitrarily referenced with C_6' = 61.5 or C_4' to 70.1 if no C_6' is present.

[b] Tentative assignment; could be exchanged with nearby signal within 2 ppm.

[c] Consult reference 2 for spectrum.

multiples in intensity. Because of the long relaxation time of the carbonyl carbons this approximate relationship in peak heights is not maintained. Another consequence of this is that the carbonyl carbons give very small peaks. Indeed, if care is not taken these peaks can easily be lost.

TABLE III

FUNCTIONAL GROUP CHARACTERISTIC CHEMICAL SHIFT RANGES

Group	Chemical Shift Range (PPM)	
Acetyl	20.1-20.8 (CH_3)	168.6-171.0 (C=O)
Methoxyl	56.1-60.6	
Benzyl	68-72.3 (CH_2)	127-138.5 ($\emptyset$)
Tosyl	21-22 (CH_3)	127-146 ($\emptyset$)
2,3-anhydro	49.5-53.5	
3,4-O-isopropylidene	25.9-27.8 (CH_3)	109-110(C)

The acetate methyl groups also resonate within a narrow range from 20.1 to 20.8 ppm. This is well within the values reported in the literature (12). Again, it is not possible to directly determine the number of acetate substituents by counting the acetyl methyl peaks. This is a result of the methyl carbon not being strongly affected by the ring position to which it is attached.

The acetyl methyl carbon chemical shifts are affected by steric crowding. This can be seen in Tables I and II by comparing the acetylated monosaccharides, which only have one acetyl methyl peak, to the disaccharides which have at least two types of such peaks. The ratio of peak heights represent the approximate ratio of sterically hindered to nonhindered acetate groups. The more hindered acetyl groups are shifted slightly downfield. This is also true for the cello-oligosaccharides (see Appendix XII).

Methoxyl Groups

Methoxyl carbons are found in the region from 56.1 to 60.6 ppm in the derivatives listed in Tables I and II; well within the reported range (13). In general, interpretation of this region may be complicated by the presence of methylene carbons from the carbohydrate backbone; particularly from 58-61 ppm. These two types of peaks can usually be distinguished by off-resonance decoupling or T_1 measurements. In the latter case, the methoxyl carbons generally have T_1's longer than the ring carbons because they freely rotate. The methylene carbons, with two attached protons, have T_1's approximately 1/2 those of the ring methine carbons.

Aromatic Carbons

Two types of aromatic groups were utilized in the derivatives prepared: benzyl and p-toluene sulfonate. Each gives a characteristic pattern in the ^{13}C-NMR spectrum.

The presence of a benzyl group is easily confirmed by ^{13}C-NMR. Tables I and II show that all the benzylated compounds show a characteristic aromatic pattern from 127 to 138.5 ppm. From correlations concerning the substitution of aromatic rings it can be calculated that the directly substituted carbon would have a resonance at approximately 137 ppm. Because this carbon has no directly attached proton it has a low intensity. The remaining aromatic carbons should show little change from benzene (3). For each benzylated derivative studied 3 or 4 peaks were observed that closely follow this pattern.

For the two derivatives containing the 2-O-tosyl group, 18 and 19, the aromatic region was observed to contain additional signals. One of these signals is observed as a weak line at about 145.5 ppm. This is characteristic of the carbon directly bonded to a sulfonate group (14). This easily allows the two types of aromatic groups to be distinguished.

Assignment of the benzylic carbon is complicated by the presence of the carbohydrate ring-carbons. Compounds 15 and 16 have well resolved peaks at 70.0 and 70.2 ppm, respectively, that can be identified as a methylene carbon on the basis of their off-resonance spectra. The ring methylene (C_5) can be assigned to the peak at 62.1 ppm in 15 by comparison with 3, and literature values for the aldo-pentoses (4). Therefore, the peaks near 70 ppm are assigned to the benzylic carbon. In each of the other benzylated compounds there is at least one peak in the region from 68 to 72.3 ppm that can be assigned to the benzylic carbon. The location is somewhat affected by the solvent with the signal being at lower field in D_2O. In some cases the assignment can be confirmed by off-resonance techniques.

The methyl group from the 2-O-tosyl group is observed at about 21.5 ppm in both 18 and 19. This is at slightly lower field than for the acetyl methyl group. It agrees well with the methyl group in toluene (15). It also is diagnostic for the tosyl group.

Epoxides

Formation of an epoxide ring results in a characteristic shift of the directly bonded carbons to the region of 49.5 to 53.5 ppm. This falls in the middle of the region given for epoxides in the literature (13). This region is devoid of any carbohydrate peaks or other functional groups and thus is quite characteristic. The methanol carbon appears in this region which may complicate the interpretation if this solvent is present as an impurity.

Assignment of the C_2 and C_3 signals for the derivatives containing the 2,3 anhydro-ribopyranoside configuration are given in Tables IV and V. It is based on the effect of substitution at C_4. Comparison of compounds 15 and 36 shows that one of the signals shifts upfield. This is consistent with the anticipated affect of

methylation at C_4; an upfield β-substituent effect (13). In compounds 6 and 37 the addition of an acetyl group on the adjacent ring has the opposite effect of shifting one of the signals downfield. Again, because of its closer proximity to the adjacent ring this signal has been assigned to C_3.

TABLE IV

MONOSACCHARIDES

SKELETAL − CARBON CHEMICAL SHIFTS[a]

Compound	Solvent	1	2	3	4	5	6	Ref.
36	D_2O	93.4	69.5	69.5	69.5	63.4		(6)[d]
16	DMSO-d_6	98.8	68.1[b]	69.0[b]	68.5[b]	63.2		
17	$CDCl_3$	96.9	69.9[b]	75.9[b]	72.9[b]	60.0		
18	Acetone-d_6	96.4	80.1	74.5[b]	73.1[b]	59.1		
19	$CDCl_3$	95.8	78.2	67.2	69.5[b]	62.0		
15	$CDCl_3$	93.6	51.9	51.9	61.7[b]	62.1[b]		
33a	$CDCl_3$	89.4	69.4	69.4	68.8	60.7		(7)[d]
33b	Acetone-d_6	92.2	69.6[b]	71.1	68.5	62.9		(7)[d]
34a	$CDCl_3$	89.2	69.4[b]	70.0	68.1	70.0[b]	61.6	(8)[d]
34b	Acetone-d_6	91.8	70.5	72.8[b]	68.0	72.8[b]	61.7	(8,9)
35a[c]	Acetone-d_6	91.0	83.2[b]	83.0[b]	80.7	59.6		
36[c]	$CDCl_3$	94.1	51.3	49.5	71.0	59.0		

[a]Chemical shift relative to $(CH_3)_4Si$. β-arabinose (43b) was relative to external $(CH_3)_4Si$ with p-dioxane at 67.4 ppm used as a secondary reference.
[b]Tentative assignment; can be interchanged with signal within 2 ppm.
[c]Refer to reference 2 for spectrum.
[d]Values from the literature.

Isopropylidene Group

Compounds 17 and 18 contain the isopropylidene group. This group has two sets of signals diagnostic to the group. The methyl carbons appear between 25.9 and 27.8 ppm in agreement with the literature (13). The quaternary carbon appears at 109.2 ppm which is different than the literature value reported (13). It is a relatively weak signal as a result of a long relaxation time related to the absence of attached protons. The location of both of these groups is far removed from the skeletal carbons and thus is very diagnostic for this functional group.

TABLE V

DISACCHARIDE DERIVATIVES
SKELETAL CARBON CHEMICAL SHIFTS[a]

Compound	Solvent	1	2	3	4	5	6	1'	2'	3'	4'	5'	6'	Reference
1a	D₂O	92.8	72.3[b]	71.9[b]	77.5	59.8		102.7	73.7	76.5	70.1	66.1		(7)
1b	D₂O	97.3	74.9	74.9	77.3	63.9	—	102.7	73.7	76.5	70.1	66.1		
2b	Acetone-d₆	92.7	70.6[b]	72.6[b]	75.4[b]	63.9		100.6	71.6[b]	71.6[b]	69.4[b]	62.5		
3	DMSO-d₆	102.7	72.4[b]	74.4[b]	75.3[b]	63.9		101.8	73.1[b]	76.1[b]	69.4[b]	65.7		
4	D₂O	103.0	73.6	74.7	77.3	63.9		102.7	73.9	76.6	70.1	66.2		
5	Acetone-d₆	100.8[b]	73.2[b]	72.1[b]	76.1	63.5		100.6[b]	71.7[b]	71.3[b]	69.3[b]	62.4		
7a	DMSO-d₆	94.2	52.0[b]	51.1[b]	69.8[b]	58.8		103.5	72.9	76.6	69.3[b]	65.6	61.5	
7b	D₂O	92.7	74.7	71.8[b]	77.4	59.5		101.9	73.6	76.3	70.3	76.7	61.5	
6	Acetone-d₆	97.2	51.9[b]	53.4	77.3	63.7		101.9	73.6	76.3	70.3	76.7		
9	D₂O	95.5	73.6	74.7	71.5[b]	59.6		101.2	71.8[b]	72.2[b]	69.6[b]	62.7	61.5	
11	DMSO-d₆	102.8[b]	52.1[b]	51.9[b]	77.3	63.7		101.9[b]	73.6	76.4	70.3	76.7		
	D₂O	94.4	52.5[b]	51.5[b]	70.3[b]	59.8		102.5	73.7	76.3	70.3	76.7	71.5	
	DMSO-d₆	94.4			70.2[b]	58.7		102.7	73.2	76.8	69.9[b]	76.9	61.2	
37[c]	Acetone-d₆	95.7	52.3[b]	53.5[b]	71.6	59.7		104.4	84.2	86.1	80.3	63.7		
39[bc]	Acetone-d₆	92.7	70.7[b]	72.7[b]	75.3	64.1		103.7	84.0	85.8	80.1	63.7		
40a[c]	DMSO-d₆	92.2	72.2[b]	71.4[b]	77.2	58.4		101.5	82.8	84.4	78.8	62.4[b]		
40b[c]	DMSO-d₆	97.5	74.7[b]	74.4[b]	76.8	62.4[b]		101.5	82.8	84.4	78.8	62.4[b]		

[a]Relative to internal (CH₃)₄Si. Samples in D₂O were arbitrarily set to C₆' = 61.5 or to C₄' to 70.1 in the absence of C₆'.
[b]Tentative assignment; can be interchanged with nearby signal within 2 ppm.
[c]Refer to reference 2 for spectrum.

Skeletal Carbons

In the previous discussion it was pointed out that each of the derivatives pre-
pared had the correct number of skeletal carbons within the region from 55-110 ppm.[*]
To determine the site of substitution it is also necessary to consider the ring-
carbon assignments. By comparing a series of similar compounds it is possible to
develop the detailed assignments necessary to assign the majority of the ring-
carbons. The rationale involved in using closely similar models has been applied in
numerous instances (3,12,16).

A number of the skeletal carbon assignments are tentative because of their
close proximity within a narrow region (68.0-74.0 ppm). This is particularly true
for the derivatives containing the arabino-configuration and the peracetates. In
the case of β-arabinose carbons C_2, C_3, and C_5 all resonate at 69.5 ppm. In the
acetates the effect of acetyl substitution is to give a variable and complex upfield
shift to most of the backbone carbons. This compresses the signals into a narrow
region. Recent work has appeared in the literature that attempts to correlate the
effect of the acetyl group on the skeletal carbon shifts for the xylo- (7) and
gluco-configurations (8,9). Appendix XII contains the spectra and chemical shifts
of the α-cello-oligosaccharides thru cellohexaose peracetate. The variation in
peak intensities should be useful in assigning the spectra of the disaccharide
acetates.

Fortunately, there are a number of skeletal carbons that are easily assigned in
both the xylopyranose (C_1, C_4, C_5) and the glucopyranose (C_1, C_4, C_6) configurations
(3). Observation of the effect of functional groups on these signals make it
possible to determine accurately the substituent effect of a number of functional

---

[*]With C_2 and C_3 of the 2,3 anhydro-ribopyranoside being considered as functional
group carbons.

groups on skeletal protons.* This is a result of the additive nature of most substituent affects on ^{13}C-NMR spectra.

Tables IV and V give the skeletal carbon assignments for each of the derivatives prepared as well as several model compounds (2). Appendix XI contains the spectra. The assignments for the end-products, 1 and 7, are based on several factors including comparisons with the other derivatives, and with xylose, glucose, cellobiose, and their oligosaccharides. In making these comparisons the assumption is used that substitution at one carbon has little effect on the chemical shift of carbons several bonds away.

Methylation

In the methylated compounds 35, 37, 39, and 40 a consistent 8-11 ppm deshielding is expected, based on earlier work with methylated glucoses (13). These compounds are all methylated on the xylosyl ring at carbons 2', 3', and 4'. If assignments are made such that C_3' is the furthest downfield and C_4' the furthest upfield then a consistent 8-11.3 ppm deshielding is observed. Any other assignment order for the three methylated carbons would not be consistent with the known effects of methyl groups on carbohydrate chemical shifts. The consistency of these data helps verify the assignments of carbons 2' and 3' for 1.

Compound 36, which is methylated only at the 4 position, is indicative of the effect of methylation on carbons adjacent to the site of substitution. Comparing compounds 15 and 36 shows that the carbons adjacent to C_4 are shifted upfield by -2.4 and -3.1 ppm. C_2, which is two bonds removed from the site of methylation is only slightly shifted. Comparison of the methylated disaccharides (37, 39, 40) to the appropriate nonmethylated compound (5, 1, 1).

---

*This is not true for acetylation for which the effect of substitution is complex.

substantiates the upfield shift of a β-carbon. However, in this case the effect of different solvents complicates the analysis. These observations are consistent with the literature (13).

Acetylation

It was previously mentioned that the substituent effects of acetylation are complex (7,8,9,12,17). A detailed analysis is not given here. It can be stated that the spectra reported in Tables IV and V are reflective of the general upfield shift commonly observed for total acetylation. The assignments given are generally in agreement with the literature. However, the literature assignments are in some cases not well substantiated. Refer to Appendix XII for a more detailed analysis on the effects of acetylation.

Effect of Benzyl, Tosyl, Epoxy, and Isopropylidene Groups

Substitution of a benzyl group at C_1 produces a pronounced downfield shift from + 5.4 to 5.7 ppm. In Tables IV and V this can be seen by comparing compounds 1, 7, and 16 to compounds 3, 9, and 43b, respectively. Slight upfield shifts from -1.2 to -1.4 ppm are observed for C_2.

The effect of epoxide formation on carbons adjacent to the epoxide group can also be determined for Tables IV and V. Comparison of derivatives 5, 11 and 16 to derivatives 3, 9, 16, respectively, shows that the adjacent carbons (1 and 4) are shifted upfield by -5.2 to -8.5 ppm by the presence of an epoxide functionally at C_2 and C_3. C_5 which is two bonds removed from the epoxide is also shifted upfield from -1 to -4.3 ppm. This long range effect of the epoxide group probably reflects the shift out of the chair conformation.

The effect of tosylation at C_2 is determined by comparing compounds 16 and 17 to compounds 19 and 18, respectively. The C_2 carbon is shifted about 10 ppm

downfield while the adjacent carbons are shifted slightly upfield by -0.2 to -3.0 ppm. Change of solvents and uncertainty in some of the assignments makes the comparison less certain.

The 3,4,-O-isopropylidene group shifts C_3 downfield from 6.9 to 7.3 ppm and C_4 downfield from 3.6 to 4.4 ppm. This comes from comparing compounds 16 and 18 to compounds 17 and 19, respectively. All of the other carbons within the ring are also shifted, though the results are variable. This is due to the change in conformation brought about by the derivatization and by the uncertain effect of the tosyl group on the conformation.

Table VI summarizes the substituent effects discussed above. A general trend of downfield α-substituent effects and upfield β-substituent effects is noted.

TABLE VI

SUBSTITUENT EFFECTS[a,b] OF VARIOUS FUNCTIONAL GROUPS

	α	β
Acetyl	Variable	0 to -4.0 ppm
Methoxyl	7.3 to 11.3	-0.5 to -3.3
Benzyl	5.4 to 5.7	-1.2 to -1.4
Tosyl	10 to 11	0 to -3.0
2,3-Anhydro	-	-5.2 to -8.5
3,4-O-isopropylidene	3.6 to 7.3	Variable

[a] α-refers to directly bonded carbon, β to the adjacent carbon.
[b] Negative shifts are upfield.

ASSIGNMENT OF METHYL β-XYLOBIOSIDE PENTAACETATE (22)
METHYL β-CELLOBIOSIDE HEPTAACETATE (23)

The ^{13}C-NMR spectra of 22 and 23 are given in Appendix XI. The assignments are

given in Table VII. Also included for comparison are the assignments for the

disaccharides (see Part III) and the disaccharide peracetates.

For both 22 and 23 the spectra are consistent with the proposed structure. In

both cases a methoxyl group is observed near 57 ppm and the acetyl functional groups

are present (Table II). The general upfield shift of all the ring carbons is also

noted. Assignment of C_2, C_3, C_2', and C_3' is difficult because of their close

proximity and the variable acetyl substituent effect. The assignments given are

consistent with the literature assignments for 2b and 27b.

ASSIGNMENT OF C-DEUTERATED DERIVATIVES

Raney nickel deuteration with D_2O was used to prepare the C-deuterated

derivatives; methyl β-cellobioside-3,6_a,6_b,2',3',4',$6'_a$,$6'_b$-d$_8$ (44), methyl

β-glucoside-3,4,6_a,6_b-d$_4$ (45) and methyl β-xyloside-3,4-d$_2$ (46). In this reaction

exchange occurs at each carbon with a free hydroxyl (18). These compounds are

illustrated in Fig. 2.

Since deuteration does not occur at the same rate for all carbons the actual

product is a mixture of deuterated isomers. Furthermore, some inversion of con-

figuration occurs to give various epimers.

To limit the extent of epimerization but ensure sufficient deuterium exchange,

it is convenient to follow the progress of reaction by ^{13}C-NMR. This takes advan-

tage of the relaxation mechanism for the ^{13}C-nuclei. After exchange of the attached

proton for deuterium, the signal is essentially lost because it is easily saturated

and cannot relax back to the ground state.

β TABLE VII

CHEMICAL SHIFTS[a] OF METHYL β-XYLOBIOSIDE PENTAACETATE (22), METHYL

β-CELLOBIOSIDE HEPTAACETATE (23), AND RELATED COMPOUNDS

Compound	Solvent	1	2	3	4	5	6	1´	2´	3´	4´	5´	6´	OMe	Ref.
20	D_2O	104.7	73.7	74.7	77.3	63.8		102.7	73.7	76.5	70.1	66.1		58.1	(5)
22	$CDCl_3$	101.5	70.1[b]	72.3	74.7	62.5		99.3	70.3[b]	70.9[b]	68.0	61.2		56.2	
2b	$CDCl_3$	92.4	70.2[b]	72.2[b]	74.3	63.5		99.7	70.6[b]	70.9[b]	68.6	61.8			(7)[c]
21	D_2O	103.9	73.7	75.2	79.7	75.7	61.0	103.4	74.0	76.4	70.3	76.8	61.5	58.1	(10)
23	$CDCl_3$	101.4	71.7[b]	72.6[b]	76.4	73.0[b]	61.9	100.7	71.6[b]	72.7[b]	67.9	72.0[b]		56.9	(10)
27b	$CDCl_3$	91.6	70.4[b,d]	72.4[b,d]	75.9	73.6	61.7	100.6	71.6[b]	72.9[b]	67.9	72.0	61.7		(8)[c]
27a	$CDCl_3$	89.0	69.4	69.4	76.0	70.8	61.5	100.9	71.7	73.0	67.9	72.0	61.7		(8)[c](9)

[a]Chemical shifts relative to internal $(CH_3)_4Si$ or in D_2O to C_6' = 61.5 ppm for 21 and C_4 = 70.1 for 20 as arbitrary settings.
[b]Tentative assignment; could be exchanged with nearby signal within 2 ppm.
[c]Assignment taken from the literature.
[d]Reversed from literature.
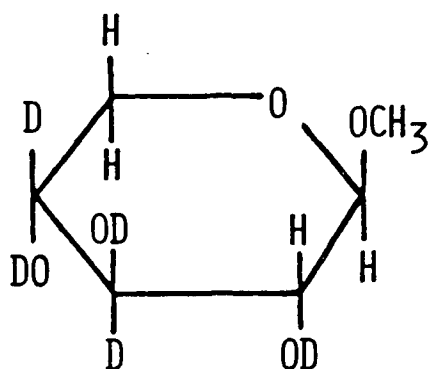
46: METHYL β-XYLOSIDE-3, 4-d_2
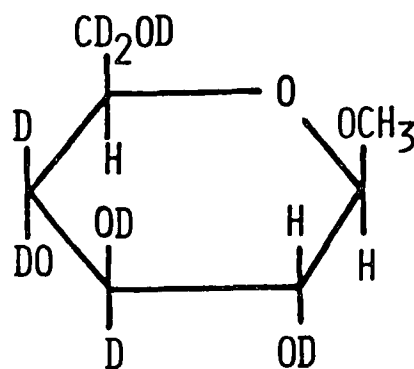
45: METHYL β-GLUCOSIDE- 3, 4, 6_a, 6_b-d_4
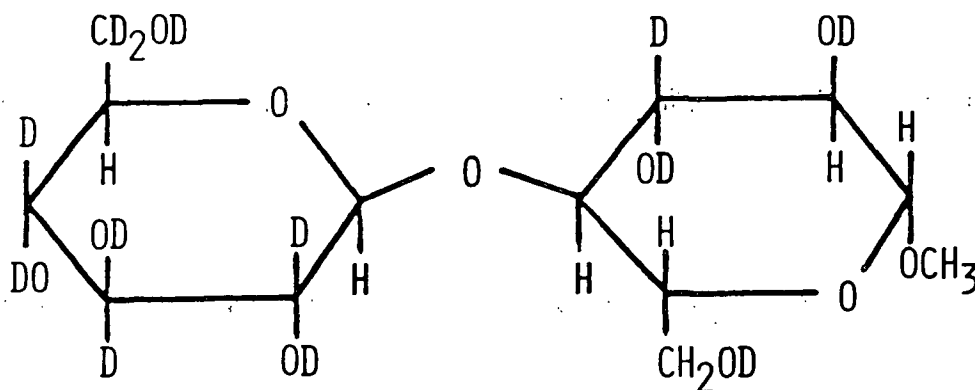
44: METHYL β-CELLOBIOSIDE-3, 6_a, 6_b, 2', 3', 4', $6'_a$, 6_b-d_8

Figure 2. Deuterated carbohydrates.

Figure 3 illustrates the progress of the reaction to form 44. The bottom spectrum (a) is the starting product while spectra (b-d) follow the progress of the reaction over time. It is expected that those carbons without free hydroxyls will maintain their signals while those with a free hydroxyl will be lost. This is what
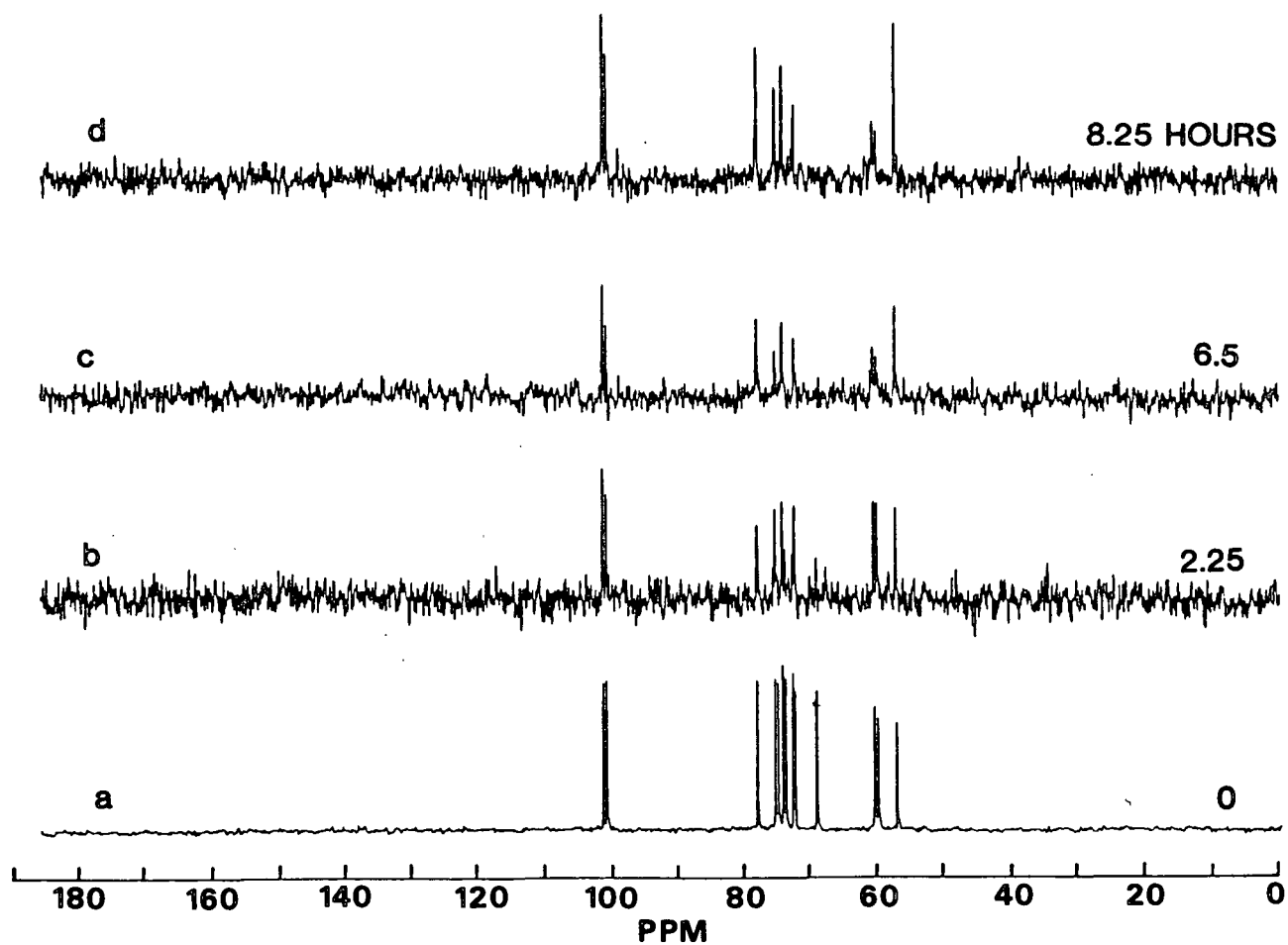
Figure 3. Formation of 44 followed by ^{13}C-NMR; a) starting material 21 b) 2.25 hours, c) 6.5 hours, and d) 8.25 hours. Refer to Fig. 31 in Appendix V for assignments.

occurs in (a-d) as the signals for C_1, C_1', C_4 C_5', and C_5 remain.[*] They are shifted slightly (<0.2 ppm) upfield due to the β-substituent effect for deuterium (6). Also present in spectrum (d) are a broad residual C_6 signal, several small signals due to epimers, and either C_2' or C_2.

The critical question is which 2-carbon (C_2' at 74.0 and C_2 at 73.7 ppm) has been exchanged, since this determines the $^{13}C-^1H$ coupling pattern near the linkage (see Section II, Part II). Comparison with the spectrum of the starting material tentatively suggests that C_2' has been exchanged and the C_2 signal remains. This is also what is expected from the reaction to form 45 and 46 which showed that exchange at C_2 is sterically hindered by the methyl group (10,18).

Hamer and coworkers (10) provided further proof of the assignment of the signal at 73.6 ppm in Fig. 3d to C_2 by enzymatically hydrolyzing 44. A major product was methyl β-glucoside-3, 6_a, 6_b-d_3. The spectrum given in Fig. 3d is essentially the same as that given in the literature. On this basis 44 has been assigned the structure in Fig. 2

_____

[*]This is one method by which the nearby signals C_5', C_3' and C_5, C_3 have been assigned (10). The earlier assignments had been incorrect (19,20).

LITERATURE CITED

1. <u>In</u> Advances in Carbohydrate Chemistry and Biochemistry Vol. 38: New York, N.Y., Academic Press, Inc., 1981.

2. Kidd, J. R., Synthesis and alkaline degradation of xylobiose and 2',3',4' tri-<u>O</u>-methyl xylobiose. Doctoral Dissertation, The Institute of Paper Chemistry, Appleton, Wis., 1980.

3. Levy, G. C. and Nelson, G. L., Carbon-13 nuclear magnetic resonance for organic chemists, New York, N.Y., Wiley-Interscience, 1972.

4. Gorin, P. A. J. and Mazurek, M., Can. J. Chem. 53:1212-23(1975).

5. Kovac, P., Hirsch, J., Shashkov, A. S., Usov, A. I., and Yarotsky, S. V., Carbohyd. Res. 85:177-85(1980).

6. Pfeffer, P. E., Valentine, K. M., and Parrish, F. W., J. Am. Chem. Soc. 101:1265-74(1979).

7. Utille, J. P. and Vottero, P. J. A., Carbohyd. Res. 85:289-97(1980).

8. Gagnaire, D. Y., Taravel, F. R., and Vignon, M. R., Carbohyd. Res. 51:157-68(1976).

9. Capon, B., Rycroft, D. S., and Thomson, J. W., Carbohyd. Res. 70:145-9(1979).

10. Hamer, G. K., Balza, F., Cyr, N., and Perlin, A. S., Can. J. Chem. 56:3109-16(1978).

11. Royayne, J. and Williams, D. H., Ann. Rev. of NMR Spect. 2:82-124(1969).

12. Wehrli, F. W. and Wirthlin, T., Interpretation of Carbon-13 NMR Spectra, London, Heydron, 1976.

13. Perlin, A. S., <u>In</u> Int. Rev. Sci.: Org. Chem. Ser. Two., Edited by Hey, D. H., 7:1-34(1976).

14. Voelter, W., Fuchs, S., Seuffer, R. H., Zech, K., Monatash. Chem. 105:1110-35(1974).

15. Buchanan, G. W., Montaudo, G., and Finocchiaro, P., Can. J. Chem. 52:3196-200(1974).

16. Roberts, J. D. and Dorman, D. E., J. Amer. Chem. Soc. 92:1355-61(1971).

17. Christl, M., Reich, H. J., and Roberts, J. D., J. Am. Chem. Soc. 91:3463-8(1971).

18. Koch, H. J. and Stuart, R. S., Carbohyd. Res. 59:C1-6(1977).

19. Dorman, D. E. and Roberts, J. D., J. Am. Chem. Soc. 93:4463-71(1971).

20. Usui, T., Yamaoka, N., Matsuda, K., Tuzimura, K., Sugiyama, H., and Seto, S., J. Chem. Soc. Perkin I:2435-32(1973).

13C-NMR ASSIGNMENTS OF THE β-1,4-
LINKED CARBOHYDRATES

Analysis of the $^{13}C-T_1$ data required the complete assignment of the xylo- and cello-oligosaccharides. Small amounts of each of these compounds were available in the lab or were obtained with the cooperation of others. Spectral assignments, as explained below, were made by reference to model compounds and with regard to variations in signal intensity. The spectra are shown in Appendix XIII.

Assignment of the ^{13}C-NMR spectra of all of the other di- and trisaccharides, obtained or synthesized in the course of this work, follow in Tables VI and V. The spectra are also found in Appendix XIII.

13C-NMR SPECTRA OF THE XYLO- AND CELLO-OLIGOSACCHARIDES*

Introduction

Assignment of the ^{13}C-NMR spectra of various oligosaccharides has proven useful for evaluating the composition, configuration, and sequence of soluble polysaccharides (1-3). The usual method of assignment involves comparison of the spectrum of the oligosaccharide with those of the constituent monosaccharides (4-5) or closely related disaccharides (2,6).

For homologous oligosaccharides, it is also possible to use the variation of peak intensities with chain length to aid in assignment (1). The similarity of chemical shifts for equivalent carbon atoms of the internal residues may be used to distinguish peaks associated with them from those assigned to terminal groups.

---

*This section has appeared in the literature in Carbohydrate Research 84:137-46(1980).

Signals from carbon atoms several bonds removed from the linkage in a disaccharide should become relatively less intense in the spectrum of the corresponding oligo-saccharide whereas carbon atoms close to the linkage should appear more intense. In this way, lines of similar chemical shift may be differentiated on the basis of peak intensities, as this feature can be related to proximity to the glycosidic linkage.

In a study of factors that affect the β-(1$\rightarrow$4) linkage-conformation of the xylo- and cello-oligosaccharides, it was necessary to obtain and assign their ^{13}C-NMR spectra. The xylo-oligosaccharides were studied up to xylopentaose, and the cello-oligosaccharides up to cellotetraose. The spectra of these compounds have been considered on the basis of the corresponding mono- and disaccharides, as well as on the basis of variations in peak intensity. Intensity variations have been used to verify some of the previous assignments of cellobiose (5) in the case of the cello-oligosaccharides, and to assist in developing assignments for the previously unassigned xylobiose.* Manifestations of differences in linkage-conformation or solvation between the xylo- and cello-oligosaccharides have also been explored from these ^{13}C-NMR assignments.

Results and Discussion

The spectral assignments for the cello-oligosaccharides in D_2O and a low-d.p. cellulose in dimethyl sulfoxide-d_6 are given in Table I. In order to avoid contaminating our meager supply of the cello-oligomers with a reference material, we chose to set C-1 of the nonreducing end-group to the value of the equivalent carbon atom of cellobiose. A close correspondence of peak locations is observed throughout the series from biose to tetraose, permitting ready assignment of the triose and

*Refer to Section IV for correlation to the spectra of several related derivatives. Also see Ref. (7).

tetraose spectra. The assignments agree in general with those made by Inoue and Chujo[6] on cello-oligosaccharide fractions having d.p. 3.7 and 5.3, the exceptions being C-3 and C-5. Several different groups (8-10) have recently presented evidence to support reversal of the earlier assignments of C-3 and C-5. The new assignments have been adopted in the present study.

Examination of the assignments listed in Table I, as well as the line spectra displayed in Fig. 1, reveals that differences from the chemical shifts of cellobiose are 0.2 ppm or less for the equivalent carbon atoms of the cello-oligosaccharides. The largest variations are at C-1, C-2, and C-4 of the internal residues. These small changes may be a result of the influence of an additional substituent many bonds away (the next glucosyl ring) or may result from the effects of slight differences in linkage-conformation or solvation between the exterior and interior linkages. The influence of linkage conformation was suggested by Colson et al. (11) to explain the relatively large changes noted when the C-1 and C-4 chemical shifts of the malto-oligosaccharides were compared with those of the cycloamyloses.

The spectra shown in Fig. 1 also illustrate the differences in peak intensities that appear within the cello-oligomer series. The variations in intensity are related to the location of a carbon atom on the reducing end-group, on the internal residues, or on the nonreducing end-group. This relation follows from the equivalence or near equivalence of chemical shifts for carbon atoms that occupy the same positions relative to the glycosidic linkage. The variation in environment is illustrated in Fig. 2, where the carbon atoms at position 2 are taken as representative. In the disaccharide there are two types (a and b), whereas four types (a,b,b', and b") exist in the tetra-saccharide. However, those marked b,b', and b" are essentially equivalent with respect to their position relative to a glycosidic linkage. The C-2 atom of the reducing group, in contrast, has an environment that

‑

TABLE I*

13C-NMR CHEMICAL SHIFTS[a] OF THE CELLO-OLIGOSACCHARIDES IN D_2O SOLUTION

Compound	Residue or group		C-1	C-2	C-3	C-4	C-5	C-6
Cellobiose	Reducing end-group	α	92.6	72.2b	72.3b	79.7	70.9	61.0
		β	96.6	75.1b,c	74.8b,c	79.5	75.6b	61.1
	Nonreducing end-group		103.4	74.0	76.4b	70.3	76.8b	61.5
Cellotriose	Reducing end-group	α	92.7	72.1	72.1	79.5d	70.9	60.8
		β	96.6	75.1b,c	74.8b,c	79.5b	75.7b	60.8
	Internal residues		103.2	73.8	74.9b,c	79.3d	75.7b	60.8
	Nonreducing end-group		103.4	74.0d	76.4b	70.4b	76.8b	61.5
Cellotetraose	Reducing end-group	α	92.7	72.2	72.2	79.4d,f	71.0	60.9
		β	96.6	75.2b,c	75.0b,c,e	79.4d,f	75.7b	60.9
	Internal residues		103.2	73.8d	75.0b,c,e	79.3d,g	75.7b	60.9
	Nonreducing end-group		103.4	74.1d	76.5b	70.4	76.9b	61.6
In Me2SO-d6								
Cellulose	Reducing end-group	α	92.0	sh	s	80.7f	s	60.6
		β	96.8	s	74.9b	80.7f	75.1b	60.6
	Internal residues		102.7	73.2	74.9b	80.1	75.1b	60.6
	Nonreducing end-group		s		76.7b	70.3	76.9b	61.2

*While the present report was in the editorial process, L. D. Hall, G. A. Morris, and S. Sukumar, [J. Am. Chem. Soc., 102 (1980) 1745-1747], have demonstrated utilizing the techniques of homo- and hetero-nuclear two-dimensional NMR spectroscopy, that the C-2 atom resonates at 74.8 ppm while the C-3 atom resonates at 75.1 ppm, in β-cellobiose. Since it is the 74.8 ppm peak that increases in intensity in the higher oligomers it must be the signal for the C-3 atoms in the internal residues that is shifted upfield relative to C-3 in β-cellobiose. This upfield shift may result from variations in the energies of the 3-OH···O-5' intramolecular hydrogen-bonds at the internal linkages.

a Chemical shifts in ppm relative to Me4Si by setting the shift of the terminal, nonreducing endgroup C-1 atom equal to the value observed in cellobiose. The shifts for cellobiose are relative to dilute 1,4-dioxane at σ 67.4. The cellulose is referenced to Me2SO-d6 at 39.5 ppm from Me4Si.

b Some authors have reversed these assignments (4-6) with the most recent assignments appearing here (see footnote e (8-10,19,20).

c The assignments for C-2 and C-3 are different from those found in the literature during revision of the article (19,20). The reasons for the assignments here are explained in the text. The alternative assign-ments (19,20) are based on homonuclear decoupling (19) and (20) a "differential isotope effect". The decoupling experiment replies on the assignment of H-2 in β-cellobiose in the skeletal-proton region, which is difficult to interpret. The assignment resulting from the "differential isotope effect" does not con-sider the possible existence of the 3-OH···O-5' intramolecular hydrogen-bond†.

d Assignments confirmed by the spectrum of low-d.p. cellulose.

e Resolved in cellotriose only.

f Observed as shoulders on the peak of internal C-4.

g Actually two distinct peaks are resolved.

h Peaks observed as a weak shoulder on a larger peak or as a very weak peak are marked s.

differs considerably. The intensities would approximate a 1:2:1 or 3:1 pattern, depending on whether or not b" can be resolved from b and b', which are expected to be coincident. Assignments of peaks that are slightly shifted in the internal residues are based on these variations in intensity.
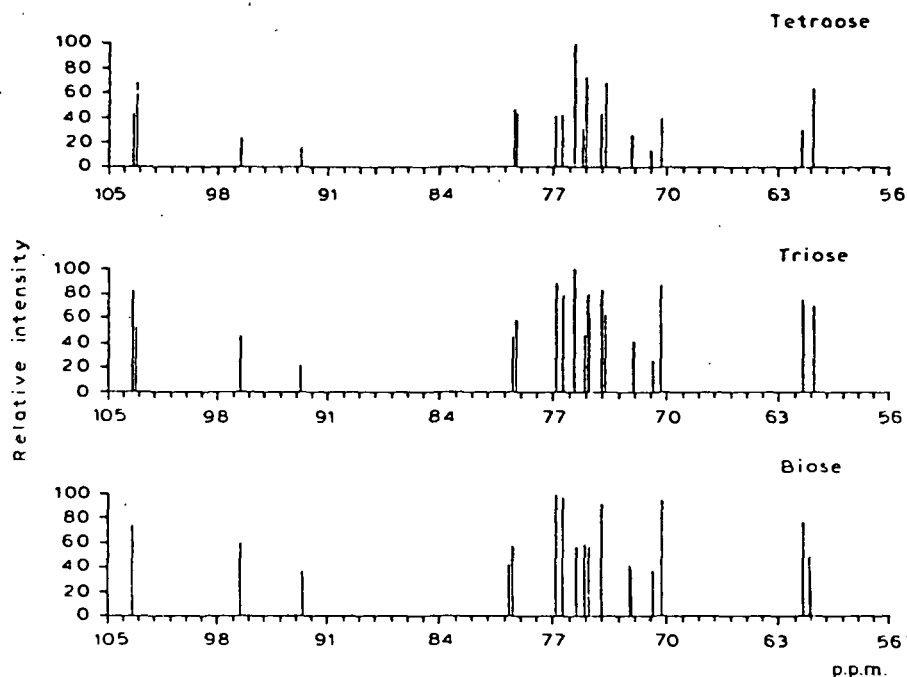
Figure 1. Comparison of ^{13}C-NMR spectra of cellobiose, -triose, and -tetraose.
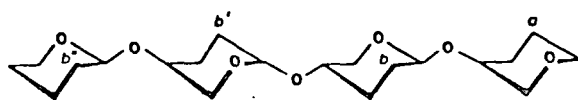
Figure 2. An illustration of the nearly equivalent carbon atoms of a homologous oligosaccharide.

The lowest-field peak of cellobiose, the C-1' resonance at 103.4 ppm, is representative of the difference expected between b" and b' in Fig. 2. In the spectra of the higher oligomers, two peaks are observed in this region, at 103.2 and 103.4 ppm. Because the peak at 103.2 ppm increases in intensity, relative to the 103.4-ppm peak, as the number of pyranose residues increases, it may be assigned to the

internal-linkage carbon atoms (C-1), and the 103.4 ppm peak may be assigned to the nonreducing, terminal group. The spectrum of a low-d.p. cellulose (Fig. 3) shows a small, downfield shoulder corresponding to C-1 of the nonreducing end-group. Following a similar analysis, the less-intense of the pairs of lines centered at 73.9 and 79.4 ppm may be assigned to C-2 and C-4 of the oligomer terminal-groups, respectively.
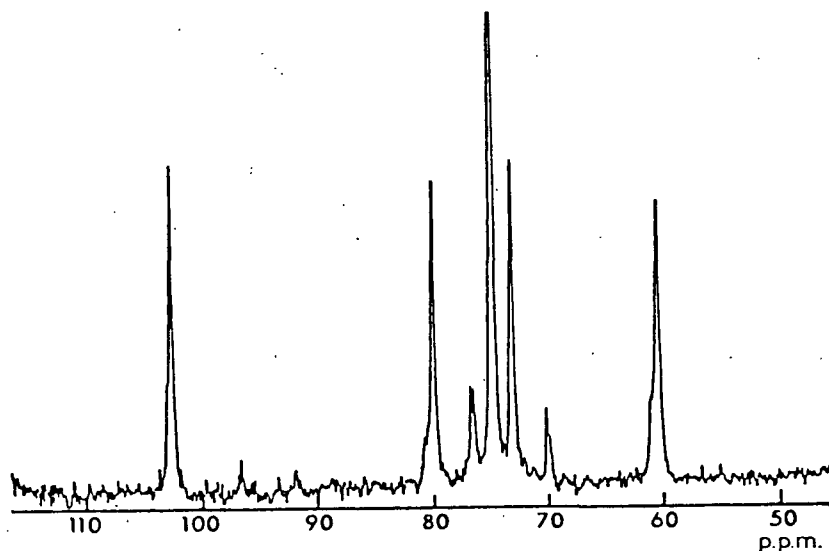
Figure 3. The ^{13}C-n.m.r. spectrum of a low-d.p. cellulose.

In a reciprocal manner, the spectra of the higher cello-oligosaccharides (Fig. 1) may be used to confirm some of the assignments for cellobiose. An obvious example corresponding to the difference between a and b in Fig. 2 is the assignment of the 61.5 ppm resonance to C-6 of the nonreducing end-group; this peak declines steadily in the spectra of the higher oligomers. The 61.0 ppm peak, which corresponds to C-6 of the internal residues and reducing-end groups, increases, as expected, in the higher cello-oligosaccharides. Thus, the differences in position of the C-6 atoms, relative to the glycosidic linkage, appear to result in the changes observed in chemical shift.

A pattern of variation similar to the one reported here suggests the assignment of the peak at 75.1 ppm to C-2 in β-cellobiose.[*] While previous authors (4-6) have reported two peaks in this region and have viewed the 75.1 ppm peak a coincidence of signals for C-2 and either C-3 or C-5, three distinct peaks are resolved in the present report, the others appearing at 74.8 and 75.6 ppm. As the 75.1 ppm peak declines steadily, relative to the other two peaks, with increasing chain-length, the latter must contain contributions from carbon atoms on internal residues; differentiation of C-3 and C-5 is not possible on the basis of these spectra.

The spectrum of a low d.p. cellulose fraction in dimethyl sulfoxide-d_6 is shown in Fig. 3. The appearance of the spectrum is similar to that reported by Gagnaire, Mancier, and Vincendon (10,12) for a degraded cellulose of d.p. 10. In the present work, several reducing-end-group peaks were also observed. The assignments for the low d.p. cellulose are consistent with those of the cello-oligosaccharides.

Previous reports (6) have suggested that the intensities of the C-1 peaks may be used to estimate the number-average d.p. for oligosaccharides of low molecular weight. Comparison of these intensities for cellotriose, cellotetraose, and the low d.p. cellulose suggests that this correlation is not generally true under all conditions. The spectrum of cellotriose, in particular, shows a significant difference in the intensity for C-1 in the nonreducing group and the internal residue, suggesting that the two carbon atoms possibly have different nuclear Overhauser enhancements or that, with the present degree of resolution of these signals, the peak heights are not a true indication of peak intensity.

---

[*]See note added in Proof, p. 204

The ^{13}C-NMR spectra of the xylo-oligosaccharides are graphically depicted in Fig. 4 with the corresponding assignments in Table II. Assignments for xylobiose have been developed from comparisons with assignments for xylose ($\underline{8}$,$\underline{13}$,$\underline{14}$) and cellobiose. Again, as in the cello-oligosaccharides, intensity variations confirm these assignments. For example, changes in the intensities of the lines at 66.1, 63.9, and 59.8 ppm support assignment of the 63.9 ppm line to C-5 of β-xylobiose and the internal C-5 resonances of the higher oligomers.
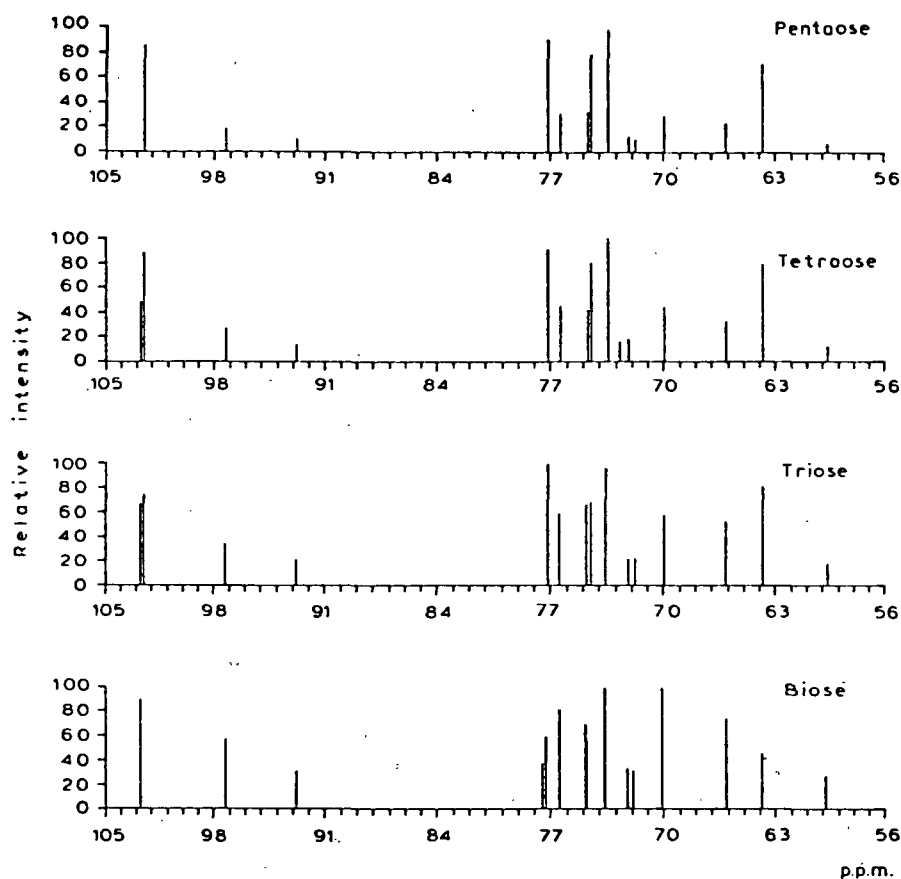
Figure 4. Comparison of the ^{13}C-NMR spectra of xylobiose, -triose, -tetraose, and -pentaose.

For the xylo-oligosaccharides, the chemical shifts are reported relative to C-1' of the nonreducing group of xylobiose. In comparing the series xylobiose-xylopentaose, the shifts of C-2 and C-5 do not vary by more than 0.2 ppm from the

values anticipated from the spectrum of xylobiose. C-1 and C-4, next to the glyco-sidic linkage, vary to a slightly greater extent, suggesting that slightly different conformations might exist at the interior linkages (2,11). Internal C-3 atoms undergo upfield shifts of the same order of magnitude, indicating the sensitivity to conformational change at the linkage. As for the cello-oligosaccharides, the small shifts may also arise from the substitution in the internal residues of a mono-saccharide group for a proton.

TABLE II

^{13}C-NMR CHEMICAL SHIFTS[a] OF THE XYLO-OLIGOSACCHARIDES IN D_2O SOLUTION

Compound	Residue or Group		C-1	C-2	C-3	C-4	C-5
Xylobiose	Reducing end-group	α	92.8	72.3[b]	71.9[b]	77.5	59.8
		β	97.3	74.9[c]	74.9[c]	77.3	63.9
	Nonreducing end-group		102.7	73.7	76.5	70.1	66.1
Xylotriose	Reducing end-group	α	92.8	72.2[b]	71.8[b]	77.2	59.7
		β	97.3	74.8	74.8	77.2	63.8
	Internal residues		102.5	73.6	74.5	77.2	63.8
	Nonreducing end-group		102.7	73.6	76.5	70.0	66.1
Xylotetraose	Reducing end-group	α	92.8	72.2[b]	71.8[b]	77.2	59.7
		β	97.3	74.7	74.7	77.2	63.8
	Internal residues		102.5	73.5	74.5	77.2	63.8
	Nonreducing end-group		102.7	73.5	76.4	70.0	66.1
Xylopentaose	Reducing end-group	α	92.8	72.2[b]	71.8[b]	77.2	59.7
		β	97.3	74.7	74.7	77.2	63.8
	Internal residues		102.7	73.5	74.5	77.2	63.8
	Nonreducing end-group		s[d]	73.5	76.4	70.0	66.1

[a]Chemical shifts in ppm relative to Me_4Si by setting the shift of the terminal, non-reducing C-1 atom equal to the value observed in xylobiose. The spectrum of xylo-biose is referenced to dilute 1,4-dioxane given a value of 67.4 ppm
[b]These resonances may be exchanged.
[c]These resonances are slightly resolved in xylobiose.
[d]A shoulder on the 102.5-ppm peak.

The contrasts between the spectra of the xylo- and cello-oligosaccharides suggest significant differences between the two series in the constraints on the linkage. While the chemical shift of C-4 differs only slightly between glucose and

xylose (18), indicating that presence of a hydroxymethyl group (C-6) at C-5 in glucose has a relatively small effect, the difference between the linkage C-4 chemical shifts of the xylo- and cello-oligosaccharides is ~ 1.8 ppm in D_2O.[*] Such a large difference would not be expected on the basis of the effect of mere replacement of a xylosyl by a glucosyl residue, as those two substituents, which differ only by the absence of C-6 for xylose, would be perceived (3) as nearly equivalent by the C-4 atom. It appears most likely that this difference is a manifestation of significant differences in the average conformation, or in the solvation environment, of the β-(1$\rightarrow$4) linkages in the two, homologous, oligosaccharide series. Such an interpretation is consistent with model studies of the linkage conformation of the disaccharide (15). Differences in average linkage-conformation or in accessibility to the linkage may explain differences in reactivity and solubility of the two types of oligosaccharide.

Colson et al. (11), in comparing the chemical shifts of the linkage C-1 and C-4 atoms in maltotriose with those of the cycloamyloses, found downfield shifts of 1.8 and 4.0 ppm, respectively, for these atoms in the (more constrained) cycloamyloses. The comparable shifts for the cello-oligosaccharides relative to the xylo-oligosaccharides are downfield by 0.7 and 1.8 ppm.

The greater constraints at the linkage for the cello-oligosaccharides appear to result from the presence of C-6. The role of C-6 is suggested by the pattern of the chemical shifts of the disaccharides, recorded in Table III. The chemical shifts of the linkage C-4 atom of xylobiose and cellobiose, relative to those of the appropriate monosaccharides, are compared with data for several other β-(1$\rightarrow$4)-linked disaccharides. Both mannobiose and 4-O-β-D-glucosyl-D-mannose, which possess

---

[*]In dimethyl sulfoxide-d_6, the difference becomes 5.2 ppm.

reducing-end C-6 groups constituted similarly to that of cellobiose, have chemical shifts, relative to the respective monosaccharides, comparable with that of cellobiose. In contrast, the chemical shifts of C-4 for 4-O-β-D-galactosyl-D-xylose (17) and 4-O-β-D-glucosyl-D-xylose, which do not have a C-6 atom in the reducing ring, are nearly identical to that for xylobiose.

TABLE III

CHEMICAL SHIFTS OF THE LINKAGE C-4 ATOM FOR SEVERAL β-(1→4)-LINKED DISACCHARIDES

Compound	Chemical Shift of C-4	Chemical Shift Change Relative to Monosaccharide
β-Xylobiose	77.3	7.1
4-O-β-D-Galactosyl-D-xylose	77.7[a]	7.5
4-O-β-D-Glucosyl-D-xylose	77.4[c]	7.2
β-Cellobiose	79.5	8.9
β-Mannobiose	77.5[c]	9.9
4-O-β-D-Glucosyl-β-D-mannose	77.3[c]	9.7
β-Xylose	70.2[b]	
β-Glucose	70.6[b]	
β-Mannose	67.6[b]	

[a]Relative (17) to external Me_4Si.
[b]See Ref. (18).
[c]See following discussion.

Summary

Internally consistent assignments have been developed for the ^{13}C-NMR spectra of the xylo- and cello-oligosaccharides. Variations of peak intensity with chain length made it possible to distinguish between the resonances of terminal groups and internal monosaccharide residues. These intensity variations also permitted verifications of previously published assignments for cellobiose.

While differences between the chemical shifts of equivalent carbon atoms on internal residues and terminal groups are slight, larger changes are observed for the linkage carbon atoms (C-1 and C-4). This difference may result from variations in linkage conformation along the chain. A more significant observation is the difference between the chemical shifts of C-4 for xylobiose and cellobiose. Comparison with several disaccharide-models suggests that the absence of C-6 at the reducing end makes the linkage more accessible to the solvent and probably allows a much wider range of conformations for the glycosidic linkage. Thus the β-(1→4) linkage appears to be more flexible in the xylo-oligosaccharides than in the cello-oligosaccharides.

Experimental

Spectra – ^{13}C-NMR spectra were recorded with a Jeol FX-100 NMR spectrometer operating at 25.05 MHz in the noise-decoupled mode. Spectra were accumulated for 50,000–100,000 pulses for the trioses, tetraoses, mannose disaccharides, and xylopentaose by using a 5000-Hz spectral width and a 1-sec pulse-interval, and 8192 data-points. All spectra were recorded at room temperature, except for cellotetraose (44°) and low d.p. cellulose (75°). A Jeol microprobe was used to obtain the spectra of the trioses, tetraoses, xylopentaose, mannobiose, and of 4-O-β-D-glucosyl-D-mannose, because of the limited amount of sample available. Concentrations of 2–8 mg in 75 μL of D_2O were used. The spectra of cellobiose, xylobiose, and 4-O-β-D-glucosyl-D-xylose were recorded with a 5-mm probe at equivalent concentrations with internal 1,4-dioxane at 67.4 ppm as a reference. All other chemical shifts were referenced to the value of the internal C_1' of the relevant disaccharide or C_1 of mannose. This calibration procedure was used to avoid potential contamination of the small amounts of available sample with any internal reference. The spectrum of

low d.p. cellulose was recorded by using a 10-mm probe with dimethyl sulfoxide-d_6 as the solvent.

Samples – The xylo-oligosaccharides were obtained from the collection of carbohydrates available at The Institute of Paper Chemistry, as were the mannose-containing disaccharides. The cello-oligosaccharides were prepared by acid hydrolysis of cellulose, followed by column chromatography on carbon-celite (16). The low d.p. cellulose was obtained from the methanol-treated filtrate of phosphoric acid-hydrolyzed, Whatman CF-1 cellulose powder. Xylobiose and 4-O-β-D-glucosyl-D-xylose were synthesized (Section 4, Part I). Cellobiose was purchased (Matheson, Colemen, and Bell).

[13]-C-NMR ASSIGNMENTS OF SEVERAL DI- AND TRISACCHARIDES IN D_2O AND DMSO-d_6.

Tables IV and V tabulate the ^{13}C-NMR chemical shift data for all the disaccharides encountered in this work. Table IV reports assignments in D_2O while Table V gives the assignments in DMSO-d_6. The spectrum of aldotriuronic acid is also given as are those of several model compounds. The assignments given are based on the model compounds, internal comparisons, and spectral intensity variations. The assignments are consistent with the literature assignments of the same or similar compounds, unless indicated.

It is useful to compare chemical shift values in the two solvents, D_2O and DMSO-d_6, for several reasons. First, the shifts, particularly at the linkage, are indicative of interaction with the solvent. Different carbons are affected to different extents by a change in solvent. (See Section 3, Part 2). Secondly, the relative order of shifts is not always the same in the two solvents. This can be seen by comparing the C_3' and C_4 signals for xylobiose (1) in the two tables. In D_2O the C_4 signal is furthest downfield while in DMSO-d_6, C_3' is further downfield.

Other examples are also evident by comparing the two tables. This information is essential for analysis of the coupled ^{13}C-NMR spectra and for any selective decoupling work that might be used to assign the ^{1}H-NMR spectra.

TABLE IV

^{13}C-NMR CHEMICAL SHIFTS[a] OF MONO- AND DISACCHARIDES IN D_2O

Compound[f]		1	2	3	4	5	6	1'	2'	3'	4'	5'	6'	OM$_e$	Ref.
41a		92.9	72.2	73.6	70.1	61.7									(8)
41b		97.3	74.8	76.5	70.0	65.9									(8)
28		104.8	73.9	76.7	70.1	66.0								58.2	(8,21)
1a		92.8	72.3[b]	71.9[b]	77.5	59.8		102.7	73.7	76.5	70.1	66.1			
1b		97.3	74.9	74.9	77.3	63.9		102.7	73.7	76.5	70.1	66.1			(8)
7a		92.7	72.1[b]	71.8[b]	77.4	59.5		101.9	73.6	70.3	76.7	61.5			
7b		97.2	74.7	74.7	77.3	63.7		101.9	73.6	76.3	70.3	76.6	61.5		
20		104.7	73.7	74.7	77.3	63.8		102.7	73.7	76.5	70.1	66.1		58.1	(21)
42a		92.8	72.2[b]	73.5	70.4	72.1[b]	61.4								(8)
42b		96.6	74.9	76.5	70.3	76.6	61.5								(8)
30		104.0	74.1	76.8	70.6	76.8	61.8							58.1	(8,19)c
26a		92.6	72.2[b]	72.3[b]	79.7	70.9	61.0	103.4	74.0	76.4	70.3	76.8	61.5		(5,19)
26b		96.6	74.8	75.1	79.5	75.6	61.1	103.4	74.0	76.4	70.3	76.8			(5,19)
21		103.9	73.7	75.2	79.7	75.7	61.0	103.4	74.0	76.4	70.3	76.8	61.5	58.1	(22)
GM[d]	α	94.5	71.0[b]	69.7[b]	77.7	71.8[b]	61.1[b]	103.4	74.0	76.3	70.3	76.7	61.5[b]		(8,23)
	β	94.4	71.5[b]	72.5[b]	77.3	75.7[b]	61.1[b]	103.4	76.3	70.3	76.7	61.5[b]			(8,23)
Mannobiose	α	94.7	71.2[b]	69.9[b]	77.8	71.8[b]	61.5[b]	101.1	71.5	73.8[b]	67.7	77.3	62.0[b]		(8,23)
	β	94.6	71.5[b]	72.7[b]	77.5	75.7[b]	61.5[b]	101.1	71.5	73.8[b]	67.7	77.3	62.0[b]		(8,23)
AX3[e]	α	92.8	72.5[b]	71.8[b]	77.0[b]	59.6		102.4	82.3g	75.2[b]	70.3	65.8			(24)
	β	97.3	74.8[b]	74.8[b]	77.0[b]	63.8		102.4	92.3g	75.2[b]	70.3	65.8			(24)
(4MG)[e]								98.6	71.8	73.1	77.8[6]	70.3	174.5	60.9	

[a]Referenced to external $(CH_3)_4Si$ using p-dioxane (67.4 ppm) as a secondary reference, except GM which had C_4, arbitrarily set at 70.3 ppm and mannobiose which had C_6 arbitrarily set at 61.5 ppm.

[b]Tentative assignment. Can be changed with another signal within 2 ppm.

[c]Taken directly from the reference indicated.

[d]4-O-(β-D-glucosyl)-D-mannopyranose.

[e]Aldotriuronic acid = 4-O-(2'-O-(4-O-methyl-α-D-glucuronysl)-β-D-xylopyranosyl)-D-xylopyranose. 4 MG refers to the 4-O-methyl-glucuronic acid group.

[f]Refers to Fig. 1 Part II of this section.

[g]Given as 78.5 ppm in reference 21.

TABLE V

13C-NMR CHEMICAL SHIFTS[a] OF MONO- AND DISACCHARIDES IN DMSO-d6

Compound	1	2	3	4	5	6	1'	2'	3'	4'	5'	6'	OMe	Ref.
41a	92.5	72.3	73.2	70.1	61.6									
41b	97.7	74.7	97.7	69.8	65.6									
28	104.7	73.3	76.6	69.7	65.7								56.0	
1a	92.3	71.0	72.2[b]	75.8	58.9		101.9	72.4	76.2	69.4	65.7			
1b	97.4	74.4[b]	74.6[b]	75.5	63.1		101.9	72.4	76.2	69.4	65.7			
20	104.5	73.2[b]	74.3	75.5[b]	63.3		102.0	72.6[b]	76.3[b]	69.5	65.8		56.0	
42a	92.2	72.4[b]	73.2	70.7	72.0[b]	61.3								
42b	96.6	74.9	76.8[b]	70.4	76.7	61.3								
30	103.9	73.5	76.8[b]	70.2	76.6[b]	61.2							56.1	
26a	92.0	71.4[b,c]	72.1[b,c]	80.9	69.8	60.6	103.1	73.3	76.5	70.1	76.8	61.0		(20)
26b	96.6	74.5[b]	75.0	80.7	74.7[b]	60.6	103.1	73.3	76.5	70.1	76.8	61.0		(20)
1,5 ANC2	69.1	79.5	76.4[b]	80.6	71.5	61.0	103.1	73.3	76.6[b]	70.0	76.5[b]	60.6		
Lactose α	92.0	71.3[b]	72.1[b]	81.3	69.8	60.4[b]	103.7	70.6	73.2[b]	68.1	75.5	60.4[b]		(19)
β	96.6	74.5[b]	74.7[b]	80.9	75.0[b]	60.7[b]	103.7	70.6	73.2	68.1	75.5	60.4[b]		(19)

[a]Referenced from internal TMS at 0 ppm. In some cases DMSO-d6 (35.5 ppm) alone was used as a secondary reference.
[b]Tentative assignment; can be exchanged with nearby signal.
[c]Assignments reversed from the literature. The assignments given here are more consistent with the solvent shifts observed for the β-anomer.

LITERATURE CITED

1. Gorin, P. A. J., Can. J. Chem. 51:2375-83(1973).

2. Friebolin, H., Frank, N., Keilich, G., and Siefert, E., Makromol. Chem. 177: 845-8(1976).

3. Colson, P. and King, R. R., Carbohyd. Res. 47:1-13(1976).

4. Dorman, D. E. and Roberts, J. D., J. Am. Chem. Soc. 83:4463-72(1971).

5. Usui, T., Yamakova, N., Matsuda, J., Sugiyama, H., Seto, S., and Tuzimura, K., J. Chem. Soc., Perkin Trans. 1:2425-32(1973).

6. Inoue, Y. and Chūjō, R., Carbohyd. Res. 60:367-70(1978).

7. Kidd, J. R., Synthesis and Alkaline Degradation of Xylobiose and 2',3',4' tri-O-Methyl Xylobiose. Doctoral Dissertation, The Institute of Paper Chemistry, Appleton, Wis. 1980.

8. Gorin, P. A. J. and Mazurek, M., Can. J. Chem. 53:1212-23(1975).

9. Balza, F., Cyr, N., Hamer, G. K., Perlin, A. S., Koch, H. J., and Stuart, R. S., Carbohyd. Res. 59: C7-C11 (1977).

10. Gagnaire, D., Mancier, D. and Vincendon, M., Abstr. Pap. Am. Chem. Soc. Meet. 74:CELL-003(1977).

11. Colson, P., Jennings, H. J., and Smith, I. C. P., J. Am. Chem. Soc. 46:8081-6 (1974).

12. Gagnaire, D. and Vincendon, M., Bull. Soc. Chim. Fr., 1977, p. 478-82.

13. Dorman, D. E. and Roberts, J. D., J. Am. Chem. Soc. 92:1355-61(1970).

14. Walker, T. E., London, R. E., Whaley, T. W., Barker, R., and Matwiyoff, N. A., J. Am. Chem. Soc. 98:5807-13(1976).

15. Rees, D. A. and Skerrett, R. J., Carbohyd. Res. 7:334-8(1968).

16. Whistler, R. L. and Durso, D. F., J. Am. Chem. Soc. 72:677-9(1950).

17. Erbing, B., Lindberg, B., and Norberg, T., Acta Chem. Scand., Ser. B 32:308-10 (1978).

18. Stothers, J. B., Carbon-13 NMR for Org. Chem., Academic Press, New York, 1972.

19. Pfeffer, P. E., Valentine, K. M., and Parrish, F. W., J. Am. Chem. Soc. 101: 1265-79(1979).

20. Heyraud, A., Rinaudo, M., Vignon, M. and Vincendon, M., Biopolymers 18:167-85 (1979).

21. Kovac, P., Hirsch, J., Shaskov, A. S., Usov, A. I., and Yarotsky, S. V.; Carbohyd. Res. 85:177-85(1980).

22. Hamer, G. K., Balza, F., Cyr, N., and Perlin, A. S., Carbohyd. Res. 56:3109-16 (1978).

23. Gorin, P. A. J., Carbohyd. Res. 39:3-10(1975).

24. Hirsch, J., Kovac, P., Alföldi, J., and Mihalov, V., Carbohyd. Res. 88:146-52 (1981).

SECTION V

CONCLUDING REMARKS

CONCLUSIONS

The primary goal of this thesis work has been a direct experimental comparison of the glycosidic linkages of the cello- and xylo-oligosaccharides. Secondary to this has been an attempt to demonstrate the general usefulness of NMR spectroscopy in studying carbohydrates and polysaccharides; and in particular in exploring the conformational aspects of their chemistry. In a sense, both goals have been achieved - if only partly - since significant steps have been made in both cases along a complex and lengthy path.

The usefulness of NMR has been amply demonstrated in this work and during the time of this work in the general literature. At the time this thesis work began the application of NMR, and particularly ^{13}C-NMR, to carbohydrate conformational problems was just beginning. In the ensuing years the number of examples of this type of work has grown rapidly - as indicated by reference to any recent issue of Carbohydrate Research. Almost every recent study of carbohydrate structure and conformation, particularly of polysaccharides, has utilized ^{13}C-NMR. In this work NMR has been successfully employed to explore linkage conformation, linkage dynamics, the existence of intramolecular hydrogen bonds, the differences in structure resulting from different physical states, the effect of steric hindrance of the linkage, and to identify intermediate synthetic species. Thus, the usefulness of NMR for carbohydrate and polysaccharide research appears to have been amply demonstrated.

The primary goal of directly comparing linkage conformations of the compounds of interest also has been achieved and is best illustrated by mentally constructing a description of what aspects of the linkage conformation have been verified. It should be emphasized that the results obtained are in agreement with the prevailing

view found in the literature, which largely has resulted from extrapolation from polysaccharide studies or computer modeling of the linkage.

The β-1,4-linked xylo- and cello-oligosaccharides are essentially rigid molecules with highly restricted and protected linkages between the adjacent monomer units. Nevertheless, motion at the linkage is fast on the NMR time scale, even if it is only between a relatively small set of available conformations. This dynamic linkage state has been demonstrated experimentally by showing that the terminal monomer units have longer $^{13}C-T_1$ relaxation times. This is in agreement with model calculations on cellobiose where it is predicted that motion of the linkage will be rapid even though restricted to a small percentage of the possible dihedral angles (1).

A comparison of the average linkage conformation of the xylo- and cello-oligosaccharides shows the xylo-oligomers to be more staggered.* This is in agreement with a number of previous investigators who have conducted modeling and polysaccharide studies (2,3,4). In this work it was shown that the dihedral angle χ is 25-60° greater in xylobiose while the H_1' to H_4 distance is 0.1-0.2 Å greater, also. These values were obtained by $^{13}C-^{1}H$ across linkage coupling and anomeric proton $^{1}H-T_1$ relaxation measurements, respectively. Therefore, even though both types of molecules have conformations on either side of the 2-fold helix line, the xylo-oligosaccharides appear to spend a far greater amount of time in conformations significantly removed from the linkage. The result of this is a more open and accessible linkage for the xylo-oligomers.

The dominant factor in determining the average linkage conformation appears to be steric (4,5,6). Specifically, the presence of the C_6 hydroxymethylene group acts

---

*Removed from the 2-fold helical structure.

to severely inhibit the number of populated linkage conformations in the cello-oligosaccharides. This has been demonstrated in this work by comparing the C_4 chemical shifts of compounds with and without a C_6 hydroxymethylene group on the aglycone. The presence of C_6 results in a consistent downfield shift of the C_4 signal which can only be related to conformational differences.

The existence of the intramolecular hydrogen bond located between O_3H and O_5· on adjacent rings has been verified in DMSO-d_6 solutions of both cellobiose and xylobiose. This bond, which is known to exist in the solid state (7), is expected to be less pronounced in xylobiose. Measurements of ^1H chemical shift temperature coefficients and ^1H-^1H coupling constants, from the ring proton to the O_3H proton, confirm this. The intramolecular hydrogen bond is more isolated in cellobiose. In xylobiose some participation of a solvent molecule in the bond is probable. This difference correlates well with the observed differences in linkage conformation. It probably results from, rather than is a cause of, the greater steric hindrance associated with the C_6 group. However, it may be an additional factor in the reduced reactivity of the C_3 hydroxyl in the cello-oligosaccharides.

Finally, a comparison can be drawn between the linkage conformation of the above compounds in the solid dissolved states. Comparison of the ^{13}C-NMR spectra of cellobiose and methyl β-cellobioside as a solid and in solution show significant chemical shift differences. These have been related to a relaxation in the bridge angle T to about 113°C. This agrees with the average calculation of Melberg (1) and shows that crystallization results in a significant conformational change, at least for the cello-oligosaccharides.

This picture of the xylo- and cello-oligosaccharide solution conformations, while being somewhat short of a quantitative description, appears to fit all the

available data. It is hoped that this verification of previous predictions can be incorporated into ever more accurate models or experimental elucidations of the structure of these important compounds. Furthermore, it is hoped that this example of the use of NMR techniques further stimulates the application of this rapidly improving discipline to the elucidation of carbohydrate and natural product structure.

SUGGESTIONS FOR FUTURE WORK

Continuation of this work could evolve along three possible directions. First, the incorporation of the improved description of the glycosidic linkage into a configurational statistics approach to describe cellulose and hemicellulose structures is feasible. The experimental support for previous concepts of linkage conformation, developed in this work, should result in a higher degree of confidence in this type of study. Second, a continuation of the NMR techniques applied in this thesis to new systems, or by using the more powerful high field instruments, would be appropriate. Finally, the use of the newer NMR instrumentation combined with the many new pulse sequences developed since the inception of this work opens up numerous new experimental approaches not formerly envisioned. Below I have provided a few specific examples related to each of these areas.

1. Use the improved glycosidic linkage description provided by Melberg and Rasmussen (1) to model cellulose in a configurational statistics approach. Incorporate a function to account for the linkage dynamics to give a more realistic simulation.

2. Use the $^{13}C-T_1$ values to calculate effective correlation times. Accurate work would require obtaining T_1 values at different field strengths.

3. Extend the T_1 and $^{13}C-^1H$ coupling studies to determine the effects of concentration, temperature, and derivatization on linkage dynamics and average conformation. Possibly determine the effect of molecular association by this technique (8,9).

4. Use specific ^{13}C and ^2H derivatives to get more accurate across-linkage coupling constants. Specifically, try to use $^{13}C-^{13}C$ coupling to determine T (10).

5. Use higher fields to remove second order effects and peak overlap to determine ϕ and χ more accurately in cellobiose and xylobiose. Apply second order analysis.

6. Using an external lock search for evidence for a cellobiose intramolecular hydrogen bond in H_2O at low temperature (11).

7. Use a model system such as the inositols to study hydroxyl group orientation in DMSO-d_6 (12).

8. Apply higher fields and special pulse techniques for 2-dimensional NMR of the higher oligosaccharides (13). Use high field ^1H-NMR to make an NOE distance map of the ring protons of the disaccharides (14).

LITERATURE CITED

1. Melberg, S. and Rasmussen, K., Carbohyd. Res. 71:25-34(1979).

2. Rees, D. A. and Skerrett, R. J., Carbohyd. Res. 7:334-48(1968).

3. Settineri, W. J., and Marchessault, R. H., J. Polymer Sci., Part C 11:253-64 (1965).

4. Sundararajan, P. B. and Rao, V. S. R., Biopolymers 8:305-12(1969).

5. Parfondry, A., Cyr, R., and Perlin, A. S., Carbohyd. Res. 59:299-309(1977).

6. Rees, D. A. and Scott, W. E., J. Chem. Soc. (B), 469-79(1971).

7. Carlson, K. P., An Investigation of the Vibrational Spectra of the Cellodextrins. Doctoral Dissertation. The Institute of Paper Chemistry, Appleton, Wis., 1979.

8. Mathlouthi, M., Carbohyd. Res. 91:113-23(1981).

9. Tsukada, S., and Inoue, Y., Carbohyd. Res. 88:19-38(1981).

10. Gagnaire, D. Y., Nardin, R., Taravel, F. R., and Vignon, M. R., Nouveau J. de Chimie 1:423-30(1977).

11. Symons, M. C. R., Benbow, J. A., and Harvey, J. M., Carbohyd. Res. 83:9-20 (1980).

12. Gillet, B., Nocole, D., Delpaech, J. J., and Gross, B., Org. Magn. Reson. 17:28-36(1981).

13. Hall, L. D., Morris, G. A., and Sukumar, S., J. Am. Chem. Soc. 102:1745-7 (1980).

14. Taravel, F. R., and Vignon, M. R., Polymer Bulletin 7:153-7(1982).

ACKNOWLEDGMENTS

I would like to thank The Institute of Paper Chemistry and its member companies for partial fellowship support during the preparation of this thesis. In particular, I am thankful to the Institute faculty and staff who have always been willing to serve when needed. The advice and counsel of Dr. Rajai Atalla, who served as major thesis advisor, is deeply appreciated. His pioneering work on cellulose structure has served as an inspiration throughtout. A special debt is owed to Dr. Ronald McKelvey who suggested and guided my early use of the NMR spectrometer. The advice and encouragement of Dr. Donald Dimmel and Dr. Norman Thompson, who sat on my thesis advisory committee, is also appreciated.

One of the most important contributions to the success of any thesis comes from the other students engaged in similar endeavors. This work has been no different. Dr. James (M.D.) Kidd developed or initially implemented most of the synthetic work leading to xylobiose. Frequent discussions with my lab partner, Dr. Thomas Arnson helped me focus on the significant points of the work and made the hours pass more quickly. Samples were provided by Dr. Thomas Wylie, Dr. Ken Carlson, and Mr. Jerry Ellis. Comaraderie and good times were provided by all. To each of them I am deeply thankful.

A special thanks goes to Hercules Inc., which through its management's patience, allowed me to finish writing the manuscript. Ms. Denise Spencer carefully typed and corrected the majority of the work for which I am thankful.

My deepest appreciation and thanks goes to my family. My parents, Charles and Barbara, who always encouraged me to continue and my children, Adriene, Laura, and Aaron, who make life so enjoyable, have been tremendous throughout. The deepest debt of all goes to my wife Leslie. Her love and patience throughout the long years

of this work were beautiful. The long hours spent alone or caring for a crying child, the willingness to put up with the old clothes and car, and all the long nights and days of caring for children and then continuing on to work, always without complaint, were truly the real substance of this work. I only hope she always knows how much I appreciate her support and how very much I love her. Any accomplishment or accolade earned by this work goes to her and her alone.

APPENDIX I

NMR THEORY AND TECHNIQUES

INTRODUCTION

The following discussion is meant to briefly introduce and summarize the various NMR theories and techniques necessary to the understanding of the thesis. For a complete discussion the reader is referred to the references discussed below.

The field of NMR spectroscopy has been the subject of numerous texts and reviews. Introductions to the subject are found in most physical chemistry or spectroscopy texts (1). More complete discussions are available concerning the following: applications of ^{1}H-NMR* to organic chemistry (2,3); applications of ^{13}C-NMR to organic chemistry (4,5,6,); intermediate level texts and monographs introducing advanced topics (7,8,9,10,11); pulsed and Fourier transform techniques (12,13); NMR of other nuclei (14); specialized topics including relaxation theory (15,16,17), the nuclear Overhauser effect (NOE) (18), solid-state NMR (19), and spin-spin coupling theory (20), and advanced treatises on general theory and techniques (21,22). In addition to the texts mentioned, numerous reviews are available which focus on specialized topics. The reviews by Netzel and Miknis (23) on relaxation theory and Breitmaier, Spohn, and Berger (24) concerning applications of ^{13}C spin-lattice relaxation times to studies on the mobility of organic molecules in solution are especially pertinent to the following discussion.

NUCLEAR PRECESSION

Nuclear magnetic resonance (NMR) spectroscopy is basically a form of absorption spectrometry in which electromagnetic radiation in the radio-frequency region is

*Also designated PMR.

absorbed at a characteristic frequency by a nucleus in a magnetic field. Nuclei possessing an angular momentum $\vec{p}$ (i.e. ^1H, ^{13}C, ^{14}N, ^{15}N, ^{23}Na, ^{27}Al, ^{31}P, others)* have a magnetic moment $\vec{\mu}$ given by

$$\vec{\mu} = \gamma\vec{p} \qquad \qquad (1)$$

where γ is the gyromagnetic ratio. Such a nucleus experiences m** orientations (energy levels) with respect to a static magnetic field depicted by the vector $\vec{H_o}$. The number of orientations is given by the relationship

$$m = 2I+1 \qquad \qquad (2)$$

For a nucleus with $I = 1/2$ (i.e. ^1H, ^{13}C)*** only two orientations are possible in the magnetic field. A quantum mechanical treatment shows that these orientations are represented by energies E_m where

$$E_m = \gamma \hbar m H_o \qquad \qquad (3)$$

Substitution of the two possible values for m gives the energy ΔE associated with a transition between the two orientations;

$$\Delta E = \nu \hbar H_o \qquad \qquad (4)$$

Combining Eq. 4 with Planck's equation, relating the change in energy between quantum states to the irradiation frequency ($\Delta E = hf$), results in the Larmor equation

$$f = (\gamma/2\pi) \, H_o. \qquad \qquad (5)$$

---

*All nuclei possessing a spin quantum number $I \neq 0$; $p = \hbar I$.
**m is also termed the magnetic quantum number; $m = I, I-1, I-2....-I$.
***The remainder of the discussion focuses on spin 1/2 nuclei.

This equation states that the frequency of irradiation necessary to induce a transition between energy levels is proportional to the magnetic field.*

Physically the spin 1/2 nucleus precesses about the magnetic field vector $\vec{H}_o$ with two possible orientations. The frequency of the precession is the Larmor frequency f. Transitions between the two orientations can be induced by a small magnetic field $\vec{H}_1$ that is frequency f about $\vec{H}_o$.** The latter requirement ensures that $\vec{H}_1$ is in phase with the precessing nucleus. Figure 1 depicts the nuclear precession and the directions of $\vec{H}_o$ and $\vec{H}_1$. By convention H_o is taken in the z-direction of a cartesian coordinate system.
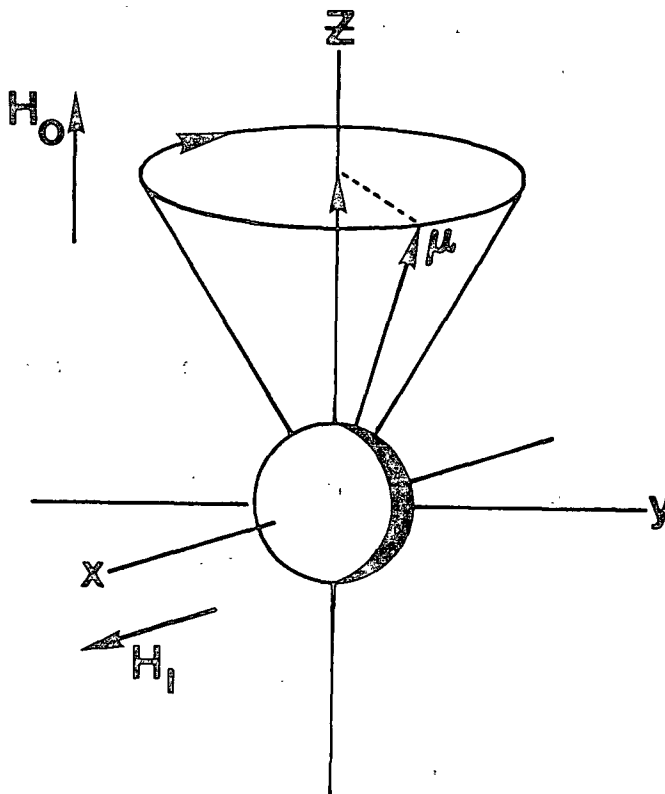
Figure 1. Nuclear precession.

*For ^{1}H-NMR a field (H$_o$) of 23,490 gauss requires a frequency (f$_o$) of 100 MHz since γ = 26, 753 rad./sec gauss. For ^{13}C γ = 6,728 rad./sec gauss and f$_o$ is 25.15 MHz at this H$_o$.

**The field $\vec{H}_1$ lies in the x direction but can be resolved into two counter rotating components one of which rotates in phase with the precessing nucleus.

Figure 2 depicts the situation for an assembly of nuclei with the same Larmor frequency. The total magnetization of this system is given by $\vec{M}_o$ and lies entirely in the z-direction because the spins are not in phase.
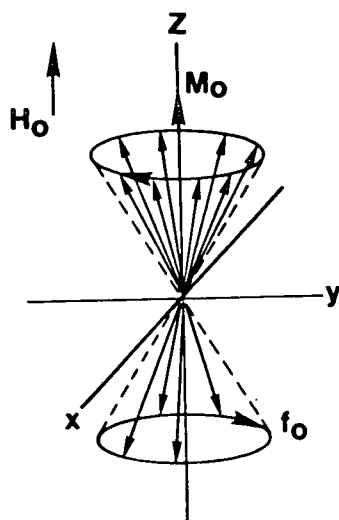
Figure 2. Equilibrium magnetization.

Nuclear Induction

A simplified description of the NMR process will result by allowing the x,y,z Cartesian coordinate system to rotate about the z-axis at the Larmor frequency f; the 'so-called' rotating coordinate described by the coordinates x´, y´, z´.* In this system the perturbing field $\vec{H}_1$ lies in the x´-direction. The action of $\vec{H}_1$ is to rotate $\vec{M}_o$ in the y´z´ plane as depicted in Fig. 3. As a result of $\vec{H}_1$ the nuclei initially precess in phase so that immediately after the perturbation the magnetization $\vec{M}$ has components in the y´ and z´ directions but not in the x´ direction.

If $\vec{H}_1$ is of sufficient power and duration (pulsed NMR) the angle of rotation α about the x´-axis can be adjusted to 90° so that all the magnetization is in the y´-direction (Fig. 3c). In pulsed NMR α is dependent on both $\vec{H}_1$ and the duration of the pulse t_p; and is given by the relation

---

*z and z' are coincident in the two systems.

$$\alpha = \gamma H_1 t_p \text{ (radians)} \qquad (6)$$

The pulse duration, also termed the pulse width, is typically in microseconds (μs).
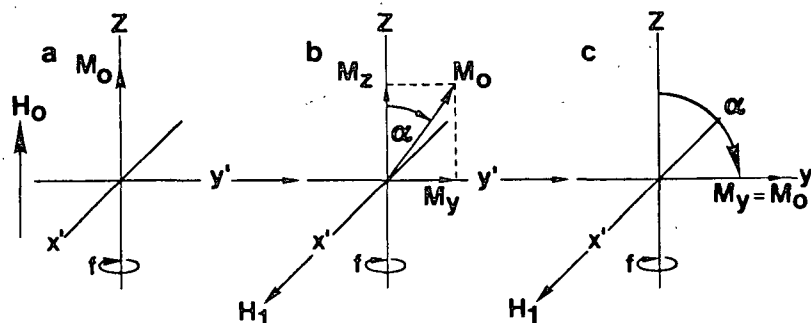
Figure 3. Motion of the magnetization vector M_0 in a rotating coordinate system under the influence of the field H_1: a) equilibrium, b) deflection through angle α, c) deflection by 90°.

The component of transverse magnetization M_y' induces an alternating potential in a receiver coil placed in either the x or y direction; this potential constitutes the detected signal. It should be emphasized that it's a magnetization in the xy (or the equivalent $x'y'$) plane and not M_z that induces the detectable signal.

INSTRUMENTATION

The phenomenon of NMR can be investigated in many ways. The method familiar to most chemists is the continuous wave (CW) technique in which either the magnetic field $\vec{H}_0$ or the radio frequency field $\vec{H}_1$ is varied while the other remains fixed. The most common method is to fix $\vec{H}_0$ and to vary the r.f. field. For most experiments the r.f. field is swept slowly across the region of interest. Most continuous wave methods utilize a weak perturbing field (ca. 10^{-4} gauss).

An alternate method utilizes short bursts of relatively high r.f. power (10-400 gauss) at a discrete frequency ν_0. It can be shown by Fourier analysis that a short intense pulse, with a rapid rise and fall (square wave), contains frequencies over

the approximate range

$$\nu_o \pm 1/t_p. \qquad\qquad (7)$$

Equation 7 shows that the shorter the pulse the greater the range of excited frequencies. Essentially all the nuclei of interest can be excited simultaneously. This is the basis of the class of techniques referred to collectively as pulsed methods. Various types of pulses can be employed in concert, which results in an increased versatility of the NMR technique, particularly in regard to dynamic measurements.

In the pulse method the observation of the nuclear spin-system occurs while the r.f. is turned off. For this reason pulsed methods are sometimes called free-precession techniques since the decay of the magnetization M_y' is studied in the absence of the perturbing field. Figure 4a illustrates the establishment and decay of M_y' in response to a 90° pulse; the resulting induced signal which would be recorded is given in 4b. The envelope of the trace is proportional to M_y' as a function of time and is termed the free induction decay (f.i.d.). M_y' is observed to decrease exponentially. The spacing of the peaks is related to the Larmor frequency f of the effected nucleus.

If several nuclei with different Larmor frequencies and/or relaxation-times are present in the sample then the resulting f.i.d. is too complicated to analyze by inspection. Figure 5a is the actual f.i.d. for the ^{13}C-NMR spectrum of ethyl benzene. The technique of Fourier analysis has recently been applied to the analysis of pulsed NMR data; the resulting discipline is called Fourier transform NMR (FT-NMR) (25). It is well known that for many continuous functions a relationship exists between the time and frequency domains as expressed by the Fourier transform F(w) of f(t);

$$F(w) = \int_{\infty}^{\infty} f(t)e^{-iwt}dt \tag{8}$$

In the case of FT-NMR $F(w)$ is equivalent to $M_y{'}(w)$; the frequency spectrum of the magnetization. This is equivalent to the conventional NMR spectrum obtained by CW methods as shown in Fig. 5b.

a

b
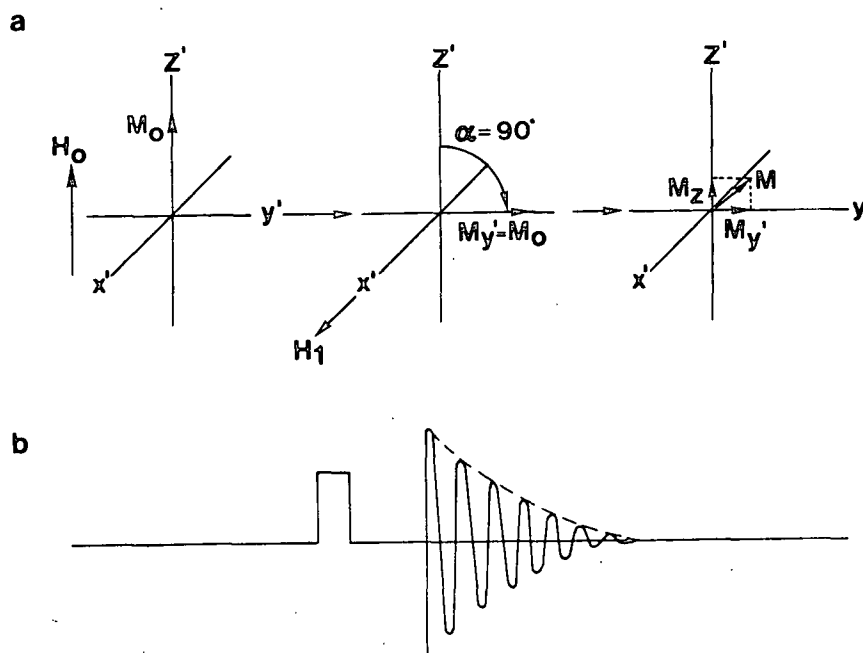
Figure 4. Depection of the establishment and decay of $M_y{'}$ for a slightly off resonance 90° pulse: a) Orientation of $M_y{'}$ immediately before the pulse, immediately after the pulse, and at a time t after the pulse; b) time behavior of events in the $x{'}y{'}$ plane depicting the pulse and subsequent f.i.d.

Most new spectrometers utilize pulse methods combined with a computerized variation of Eq. 8 to obtain the conventional NMR spectrum. Two major advantages are realized from the use of FT-NMR over continuous wave methods: a) Measurements in the time domain allow the study of time dependent phenomena such as relaxation times on a routine basis; b) in contrast to CW. - methods, a single spectrum can be obtained in a few seconds[*] so that signal averaging is much more efficient.[**] The

_____

[*]This depends on the observed frequency domain (window), the number of data points sampled in the f.i.d., and possibly the relaxation time T_1.

[**]The S/N increases in proportion to $(n)^{1/2}$ where n is the number of pulses.

latter advantage is particularly useful in the measurement of NMR spectra for less sensitive and/or rare nuclei such as carbon-13.
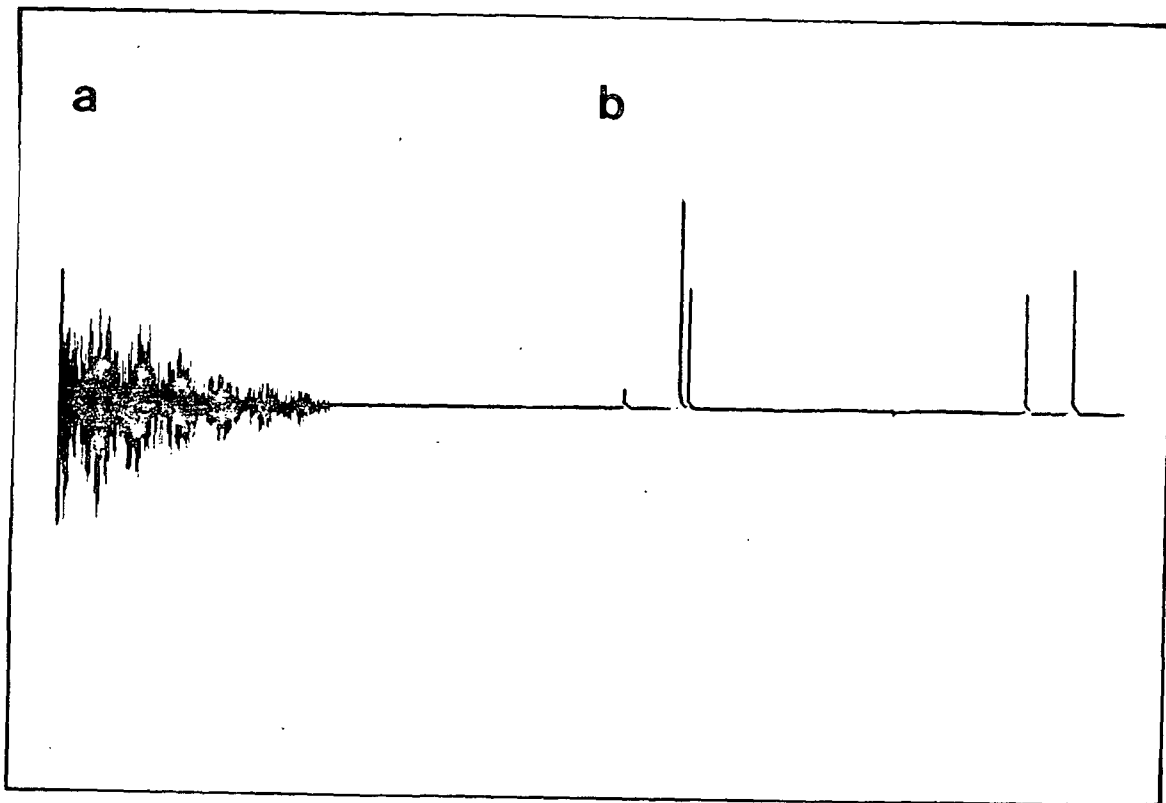
Figure 5. The ^{13}C-NMR spectrum of 90% ethyl benzene in acetone – d_6: a) free induction decay; b) frequency domain spectrum resulting from Fourier transformation of the data.

NMR PARAMETERS*

Figure 6 gives as an example the ^{1}H-NMR spectrum of ethanol under conditions of slow exchange. The spectrum illustrates the NMR parameters familiar to most chemists: chemical shift, spin-spin coupling, and peak intensity.

The chemical shift results from a reduction of the magnetic field at each nucleus due to the surrounding electrons. The motion of the electrons results in a

*The discussion in this section focuses on small molecules in solution for which magnetic dipole interactions and chemical shift anisotropy effects, both present in solids or many dissolved polymers, are averaged to zero.

weak magnetic field that opposes $\vec{H}_o$. The resultant effective field H_{eff} is given by

$$H_{eff} = H_o(1-\sigma)$$ (9)

where σ is the shielding factor and has a value of approximately 10^{-5} for protons.[*] Because of the shielding by the electrons each type of nucleus experiences a slightly different H_{eff} and therefore resonates at a characteristic frequency. This is observed in the ethanol spectrum where the three types of nuclei are at different frequencies.
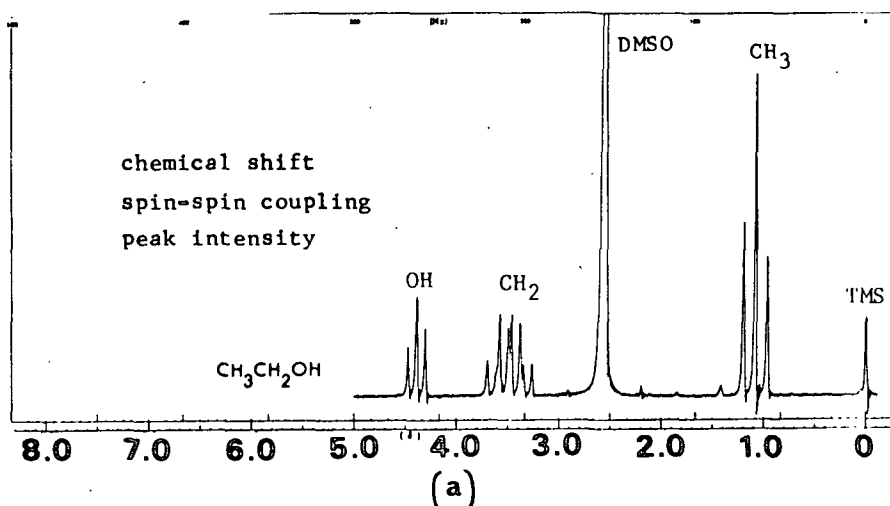
Figure 6. ^{1}H-NMR spectrum of ethanol in DMSO.

The chemical shift is commonly measured in the dimensionless unit δ (given in parts per million; ppm) so that spectra taken at different magnetic fields are comparable. δ is defined by the equation

$$\delta = \frac{f_s - f_r}{f_r} \times 10^6$$ (10)

where f is the Larmor frequency of the reference (r) or sample (s) proton, respectively. For ^{1}H-NMR the chemical shift of the methyl protons in tetramethylsilane (TMS) is taken as 0 ppm by convention. From a combination of Eq. 5 and 9 it can be

*For all other nuclei σ > 10^{-5} so that the frequency range of chemical shifts is greater. [13]C, for example extends approximately over a range of 200 ppm.

shown that a large shielding factor results in a lower resonant frequency at a $\vec{H}_o$. The protons in TMS are highly shielded and therefore resonate at a relatively low frequency. Most organic compounds have protons resonating at higher frequencies than TMS corresponding to δ values between 0-100 ppm. In general the greater the electron density around a nucleus the smaller will be its chemical shift.[*]

In Fig. 6 the three types of ethanol protons are observed to have a fine structure rather than being single lines. The methyl group, for example, is observed as a triplet. The splitting of the signal results from spin-spin coupling; an interaction between nuclear spins mediated by the intervening bonding electrons. Figure 7 illustrates the action of electrons in orienting the nuclear spins. Because of the electron mediated spin-spin coupling the energy of transition between orientations is dependent on the orientation of nearby nuclei.
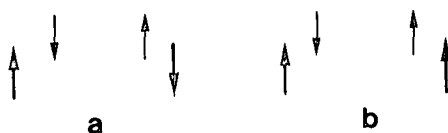
Figure 7. Electron mediated spin-spin coupling a) antiparallel (lower energy) orientation of nuclear spins; b) parallel orientation of nuclear spins. The nuclear spins are denoted by boldface arrows.

Spin-spin coupling is generally treated quantum-mechanically. This approach involves the addition of the term H' to the Hamiltonian describing the spin system. The form of H' is

---

[*]The nucleus is said to be shielded or deshielded depending on the relative value of δ.

$$\frac{1}{H} = \Sigma_{i<j}{}^{\Sigma} J_{ij} I_i I_j \tag{11}$$

where I is the quantum mechanical operator for the angular momentum of the spins i

and j and J_{ij} is the coupling constant in Hertz (hz). The equation emphasizes that

spin-spin coupling is dependent only on the relative orientations of the nuclear

spins and not on their orientations relative to $\vec{H}_o$.

Spin-spin coupling can occur between any nuclei possessing a magnetic moment.

Both ^1H-^1H and ^{13}C-^1H couplings are widely used in organic chemistry. Equation 12

illustrates a commonly used notation which denotes which nuclei are coupled and the

number of intervening bonds.

$$^3J_{HCOH} = 5.07 \text{ Hz} \tag{12}$$

The value given is for the coupling between the hydroxyl proton and the methylene

protons in ethanol dissolved in DMSO. A simple first order treatment[*] allows this

value to be read directly from the spectrum (Fig. 6); it is equal to the peak

spacing in Hertz. The first order treatment also makes it possible to apply the n+1

rule which applies for spin 1/2 nuclei. This rule states that a set of nuclei

coupled to a second set of n nuclei will be split into n+1 lines as a result of the

coupling.

The theory of spin-spin coupling is complex and incomplete. The important

parameters include hybridization, electron density at the nucleus, electronegativity

of substituents, and dihedral bond-angle geometry. Because of the theoretical

complexity an empirical approach is generally used to estimate coupling constants.

---

[*]A first order analysis is applicable if two conditions exist: a) $f_A - f_B \gg J_{AB}$ where A and B are the two sets of coupled nuclei; b) all nuclei in sets A or B must be magnetically equivalent. Nuclei are magnetically equivalent when each nucleus in the set has the same chemical shift and is coupled equally to all other nuclei in the molecule.

Karplus ($\underline{26}$) has proposed on both theoretical and empirical grounds that a relationship exists between vicinal coupling constants and the dihedral angle. For an $H_a-C_a-C_b-H_b$ system the relationship has the form

$$^3J_{H_aC_aC_bH_b} = A + B \cos \Phi + C \cos 2 \Phi \qquad (13)$$

where A, B, and C are empirically determined constants and Φ is the dihedral angle between the H_a-C_a and H_b-C_b bonds. Coupling in other vicinal systems exhibits a similar dependence on geometry which can be empirically determined if a set of compounds with well defined and different geometries are available. In general, the use of "Karplus" type equations should be undertaken with care since many factors can affect the observed dependence of ^3J on Φ.

The final parameter illustrated in Fig. 6 is the signal intensity. In general an integration of the area under the individual multiplets will be proportional to the number of magnetically equivalent nuclei associated with that particular signal. In the ethanol spectrum the methyl signal is approximately three times the intensity of the hydroxyl signal and 3/2 times the methylene signal. It should be noted that exchange[*] or saturation effects can result in exceptions to the above generalization. Saturation effects are particularly critical in FT-NMR of ^{13}C-nuclei if the spin-systems are not allowed to fully relax between pulses.

In addition to the three commonly used parameters discussed above, three additional parameters have become increasingly important and accessible since the availability of the newer generation of NMR spectrometers, based on pulse techniques, has increased. These parameters are, the spin-lattice relaxation time (T_1); the spin-spin relaxation time (T_2); and the nuclear Overhauser enhancement (NOE).

---

[*]The rapid interchange of two or more nuclei.

The time dependence present in the data resulting from pulsed techniques provides a more direct approach to the measurement of T_1 and T_2, in most cases. Measurements of the NOE are generally approached by double resonance techniques which also are most easily pursued using the pulse techniques. A discussion of these parameters will follow after a brief digression to discuss the advantages of ^{13}C-NMR.

ADVANTAGES OF ^{13}C-NMR

The carbon-13 nucleus occurs in nature with a natural abundance of 1.11% and has a sensitivity of 1.59×10^{-2} relative to the proton. Because of this the observation of ^{13}C-NMR was limited to enriched samples until the arrival of FT-NMR. With the signal averaging techniques now available the acquisition of ^{13}C-NMR spectra has become routine in most instances.

The use of ^{13}C-NMR spectra for the study of organic molecules has several advantages over ^1H-NMR. These are listed below:

1) Since carbon-13 is a rare nucleus the probability of spin-spin coupling between ^{13}C-^{13}C nuclei is minimal and can be ignored in nonenriched samples.

2) ^{13}C spectra are generally observed under ^1H-decoupled conditions so that each carbon in the molecule is generally represented by a single line.

3) The large range for the chemical shift results in improved resolution at lower fields, relative to ^1H-NMR.

4) In general, the relative chemical shifts are controlled by the same factors important in ^1H-NMR so that relative peak positions generally correlate well for the two techniques.

5) Carbon atoms are usually not located at the periphery of the molecule so that interpretation of chemical shifts, coupling constants, and relaxation times are less complicated by intermolecular effects.

6) ^{13}C-^{1}H coupling constants can be readily obtained in the ^{13}C-spectrum using gated decoupling techniques; formerly these data were obtained from hard to measure ^{13}C-satellite signals in the ^{1}H-spectrum.

Figure 8 illustrates several of these points by comparing the ^{1}H- and ^{13}C-NMR spectra of cellobiose in DMSO-d_6. It is readily seen that the decoupled ^{13}C-spectrum is more easily interpreted than the ^{1}H-spectrum; each carbon is represented by a single line.* In the spectrum shown there are 15 separate lines, each of which can be assigned to a specific carbon. This is in contrast to the ^{1}H-spectrum which requires much higher fields and specialized techniques (27) for a complete and unambiguous assignment.

RELAXATION TIMES AND THE NOE

Bulk Magnetization - Bloch's equations**

Early in the development of NMR theory Bloch (28) developed a series of equations which describe the time dependent behavior of the bulk magnetization $\vec{M}$. In the absence of saturation effects $\vec{M}$ obeys the equation

$$d\vec{M}/dt = \gamma\ \vec{M}\text{x}\vec{H} \qquad (14)$$

This equation describes the torque exerted on the $\vec{M}$ by the effective magnetic field $\vec{H_1}$. In the rotating coordinate system Bloch equations in component form are

---

*The nonreducing end carbon signals are coincident in the α- and β-anomer as are the C_6 carbons on the reducing end. Eighteen separate signals have been obtained using a smaller observation window.
**The relaxation equations can also be developed in terms of the probabilities for transition between energy levels.
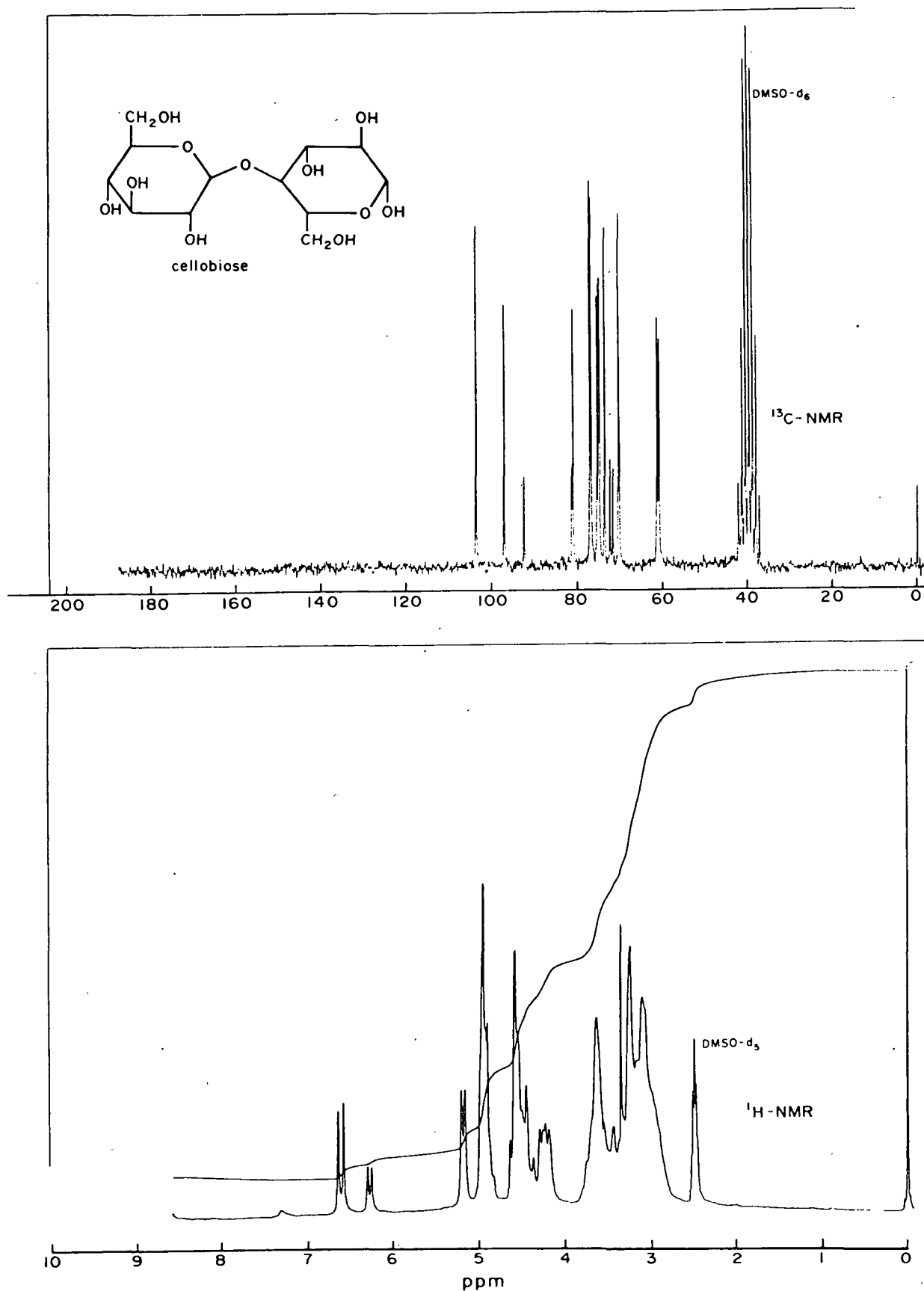
Figure 8. Comparison of the ^{13}C-NMR and ^{1}H-NMR spectra for cellobiose in DMSO-d$_6$.

$$dM_x{'}/dt = \gamma \left[M_y{'} H_o - (w/\gamma)M_y{'} \right] \qquad (15)$$

$$dM_y{'}/dt = \gamma \left[M_z{'} H_1 - M_x{'}H_o + (w/\gamma)M_x{'} \right] \qquad (16)$$

$$dM_z{'}/dt = -\gamma M_y{'} H_1 \qquad (17)$$

where $\vec{H_1}$ is in the $x{'}$ direction.

For completeness an additional term must be added to each equation to describe relaxation effects. These additional terms describe the first order processes that result in the return of $\vec{M}$ to its equilibrium value in the absence of any perturbing field.*

The resulting equations take the form

$$dM_x{'}/dt = \gamma \left[M_y{'}H_o-(w/\gamma) M_y{'} \right] - M_x{'}/T_2 \qquad (18)$$

$$dM_y{'}/dt = \gamma \left[M_z{'}H_1-M_x H_o + (w/\gamma)M_x{'} \right] - M_y{'}/T_2 \qquad (19)$$

$$dM_z{'}/dt = -\gamma M_y{'}H_1-(M_z -M_o)/T_1 \qquad (20)$$

where T_1 and T_2 are the time constants for spin-lattice and spin-spin relaxation, respectively. T_1 and T_2 are also termed the longitudinal and transverse relaxation times since they describe the relaxation of $\vec{M}$ parallel and perpendicular to the field $\vec{H_o}$.** The mechanisms of relaxation will be described later.

Equations 18-20 can be solved to give the time dependent behavior of $\vec{M}$*** under a variety of conditions. Of particular interest is the case of free precession for

---

*The probability of a spontaneous transition between energy levels is 10^{-25} $\sec^{-1}$ while the probability for induced transitions is 10^{-10} sec.$^{-1}$ (22). On this basis coupling with a radiation field is negligible and relaxation (return to equilibrium) must occur by a coupling of the spin system to the lattice or another spin.

**T_2 describes the decay of $M_x{'}$ and $M_y{'}$ to 0 which occurs from a loss of phase coherence in the spin system. T_1 describes the increase of $M_z{'}$ back to the equilibrium value M_o.

***The decay of $M_y{'}$ is proportional to the f.i.d.

which $H_1=0$; Eq. 20 then becomes

$$dM_z'/dt = -(M_z'-M_0)/T_1 \tag{21}$$

Integration of Eq. 21 gives M_z' as a function of time;

$$M_z' = M_0 + (M_{z_i} - M_0)e^{-t/T_1} \tag{22}$$

where $M_{z'_i}$ is the value of M_z' at time 0. The physical picture described by Eq. 22 is that immediately after a pulse the nuclear spin system returns exponentially to its equilibrium value $\vec{M}_0$ by interacting with the lattice. The process is quantitatively described by the time constant T_1. At equilibrium $\vec{M}_0$ lies entirely in the z'-direction. (See Fig. 4).

Transverse relaxation is described by T_2 in a similar manner. This time constant describes the processes that allow the nuclear spins to come into equilibrium with each other rather than the lattice. In the absence of other line broadening factors the uncertainty principle indicates that the line width of the NMR signal is related to the relaxation time. T_2 is often defined as

$$T_2 = 1/\pi\nu_{1/2} \tag{23}$$

where $\nu_{1/2}$ is the width at half maximum intensity (whh) of the signal. For solids and viscous polymer solutions T_2 often can be measured directly from the NMR spectrum. For rapidly tumbling molecules inhomogeneities in the magnetic field contribute to line broadening so that T_2 must be measured by pulse techniques.

RELAXATION MECHANISMS

General

As a molecule moves about in space the motion of the individual nuclei creates a fluctuating local magnetic field. Individual spin systems can interact with this

fluctuating field, resulting in the relaxation of the spin system so that it comes into equilibrium with the lattice. It can be shown that processes with a Fourier component at the Larmor frequencey are most efficient in promoting the relaxation. Important processes which might lead to a fluctuating local magnetic field with components at the Larmor frequency include: molecular reorientation (tumbling), translational diffusion, reorientation of molecular magnetic moments, chemical exchange, and relaxation of a distant spin. Equally important for the relaxation process is the interaction energy which couples the spin system to the fluctuating field. The molecular motions and their coupling to the spin system can be classified into distinct mechanisms of relaxation: dipole-dipole (DD), spin-rotation (SR), chemical shift anisotropy (CSA), scalar coupling (SC), and quadrupolar. Each of these will be discussed with emphasis on the dipole-dipole mechanism. For most moderate sized organic molecules the DD mechanism is the only significant contributor to nuclear relaxation.

Before proceeding to a discussion of the relaxation mechanisms it is important to illustrate how a combination of relaxation processes is treated. For spin-lattice relaxation the rate of relaxation R_1 is defined as the reciprocal of the relaxation time;

$$R_1 = 1/T_1 \tag{24}$$

The relaxation rates are additive so that

$$R_1^T = R_1^{DD} + R_1^{SR} + R_1^{CSA} + R_1^{SC} \tag{25}$$

where R_1^T is the total relaxation rate while the other relaxation rates are for the specific mechanisms. R_1^T is obtained directly from the measured relaxation time. Individual contributions to the relaxation rate are determined by measurements of T_1 as a function of temperature and magnetic field strength and by determining the NOE.

Molecular Reorientation

For molecules moving in solution a broad spectrum of molecular motions exists. To calculate the effect of the motion on the relaxation rate it is necessary to know the distribution of molecular motions as a function of frequency. To assist in the calculation it is helpful to define a parameter T_c, the rotational correlation time, which is roughly defined as the average time between collisions for a molecule in some state of motion.[*] The molecular motions can be expressed on a quantitative basis using the correlation function $K_i(T)$[**] where

$$K_i(T) = K_i(o) \exp(-|T|/T_c) \tag{26}$$

and

$$K_o(0) = 12/15 \ r^{-6} \tag{27}$$

$$K_1(0) = 2/15 \ r^{-6} \tag{28}$$

$$K_2(0) = 8/15 \ r^{-6} \tag{29}$$

The motional frequencies and intensities can be obtained from $K_i(T)$ by a Fourier transformation to yield $J_i(\omega)$, the spectral density function. The transformation has the form

$$J_i(\omega) = \int_{-\infty}^{+\infty} K_i(T) \exp(i\omega T)dT \tag{30}$$

which is analogous to the calculation of an NMR frequency spectrum from a f.i.d. If Eq. 27-29 are substituted into Eq. 30 the subsequent integration yields the equations

$$J_0(\omega) = 24/(15 \ r^6) \cdot [T_c/(1 + \omega^2 \ T_c^2] \tag{31}$$

---

[*]For molecular reorientation it also can be interpreted as the time constant for the loss of phase coherence of a system of rotating particles.

[**]$K_i(T) \equiv Y_i(t) Y_i^*(t+T)$ where Y_i (i=0,1,2) are functions related to the spherical harmonics and Y_i^* is its complex conjugate.

$$J_1(\omega) = 4/(15 \ r^6) \cdot [T_c/(1 + \omega^2 \ T_c^2)] \qquad (32)$$

$$J_2(\omega) = 16/(15 \ r^6) \cdot [T_c/(1 + \omega^2 \ T_c^2)] \qquad (33)$$

These are the spectral density functions commonly used to relate molecular reorientational motions to T_1 and T_2.

Figure 9 is a plot of $J_i(\omega)$ vs. ω for different values of T_c. The graph shows how the correlation time effects the distribution of molecular motions. Values of T_c fitting the relationship $\omega_0 \ T_c \sim 1$ produce the most efficient relaxation since the spectral density[*] at the Larmor frequency is greatest for this value. At modest magnetic fields most organic molecules have correlation times for which

$$\omega_0 \ T_c \ll 1 \qquad (34)$$

This condition is referred to as the extreme narrowing condition;[**] it often leads to a simplification of the relaxation equations.
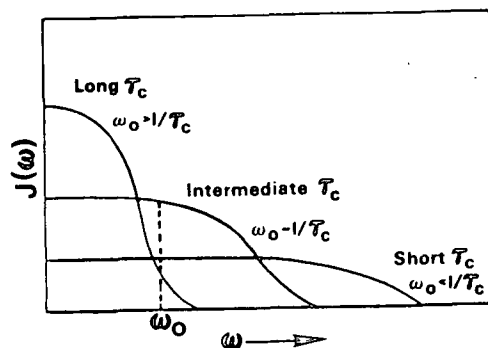
Figure 9. Spectral density J(w) as a function of the frequency for different values of the correlation time in the case of rotational correlation.

---

[*]Distribution of molecular motions.
[**]Correlation times that are less than the reciprocal of the Larmor angular frequency are said to exceed the motional narrowing limit. It is this realm of correlation times for which $T_1 = T_2$. Short correlation times correspond to rapid molecular reorientation.

Dipole-Dipole (DD) Relaxation

Let us assume a molecule has two nuclei labeled I and S each of which possess a magnetic moment. During the NMR experiment the magnetic field at nucleus I will contain a contribution $\vec{H}_{LOC}$ resulting from the magnetic moment of nucleus S.[*] The magnitude of H_{LOC} is given by

$$H_{LOC} = \pm \left((\gamma_S \, I_S \, \hbar)/r^3_{IS} \right) (3 \cos^2 \theta_{IS} - 1) \qquad (35)$$

where r_{IS} is the distance between nuclei, θ_{IS} is the angle between the internuclear vector and the z-axis and I_S is the spin quantum number for spin S. As the molecule tumbles θ_{IS} varies resulting in a fluctuating field at nucleus I. For rapid tumbling the average value of H_{LOC} is 0.[**] As $\vec{H}_{LOC}$ fluctuates at nucleus I any component at the Larmor frequency of I can cause a change in its spin-state. As this process continues the ensemble of I nuclei in the sample eventually returns to its equilibrium distribution of spin states established by $\vec{H}_o$. The rate of spin-lattice relaxation depends on the intensity of $\vec{H}_{LOC}$ and its rate of fluctuation. Theoretically the relaxation rate is given by (13)

$$R_1^{DD} = 1/T_1^{DD} = \gamma^2_I \, \gamma^2_S \, \hbar^2 \, I_S \, (I_S + 1) \left\{ (1/12) \, J_0 \, (\omega_I - \omega_S) + (3/2) J_1 \, (\omega_I) \right.$$
$$\left. + (3/4) \, J_2 \, (\omega_I + \omega_S) \right\} \qquad (36)$$

where ω_I and ω_S are the angular Larmor frequencies of spins I and S, respectively. An equation of identical form describes the dipole-dipole relaxation of spin S. The spin-spin relaxation rate is described by a similar equation with the addition of a spectral density component at low frequency. Substitution of the spectral density Eq. (31)-(33) into Eq. (36) yields the result

---

[*]This is in addition to the fields $\vec{H}_o$ and $\vec{H}_1$.
[**]In solids or viscous dissolved polymers $\vec{H}_{LOC}$ does not average to 0 resulting in very strong direct dipole-dipole coupling which produces line broadening.

$$R_1^{DD} = (2\gamma_I^2 \gamma_S^2 I_S (I_S + 1)\hbar^2/15 \ r_{IS}^6) \cdot [T_c/(1 + \omega_I - \omega_S)^2 T_c^2 +$$
$$3 T_c/(1 + \omega_S^2 T_c^2) + 6 T_c/(1 + (\omega_I + \omega_S)^2 T_c^2)] \tag{37}$$

which is valid for rotational motion and intramolecular relaxation.

Figure 10 is a plot of Eq. (37) which shows T_1^{DD} as a function of T_c and magnetic field strength.[*] A plot of T_2^{DD} vs. T_c is also included. Figure 10 illustrates that T_1 and T_2 are equal and linearly related to $1/T_c$ at short correlation times.[**] Under the extreme narrowing condition (Eq. 34), Eq. (37) simplifies to

$$R_1^{DD} = 1/T_1^{DD} = (4/3) \ \gamma_I^2 \ \gamma_S^2 \ h^2 I_S (I_S + 1) \ r^{-6}_{IS} \ T_c \tag{38}$$

which for spin 1/2 nuclei further reduces to

$$R_1^{DD} = 1/T_1^{DD} = \gamma_I^2 \ \gamma_S^2 \ \hbar^2 \ r^{-6}_{IS} \ T_c \tag{39}$$

Equation (39) indicates that if either T_c or r_{IS} is known from another measurement the unknown parameter can be calculated from measurements of T_1^{DD}. This suggests that relaxation time determinations should be useful in conformational or dynamic measurements. The equation also shows that in the motional narrowing limit an increase in temperature or decrease in concentration, will result in a longer T_1^{DD} since these changes should produce more rapid molecular rotations.

Figure 10 illustrates that the shortest T_1^{DD} values occur for correlation times near the reciprocal of the Larmor frequency.[***] Since ω_0 is different for different magnetic field strengths the minimum T_1^{DD} value is a function of $\vec{H}_0$. At even longer correlation times T_1^{DD} increases since the relaxation process is less efficient

---

[*]Recall that the Larmor frequency depends on $\vec{H}_0$.
[**]Rapid rotation.
[***]At 23 KG f_0 is 10^8 HZ for [1]H-nuclei so that T_c is approximately 10^{-8} sec: this corresponds to the condition $\omega_0 T_0 \sim 1$.

because of a smaller spectral density at the Larmor frequency. This latter case is common in solids or viscous polymers for which molecular reorientation is slow. These materials generally have long T_1^{DD} values. As the temperature or concentration is changed these materials will exhibit changes in T_1^{DD} opposite to the change expected for small molecules.
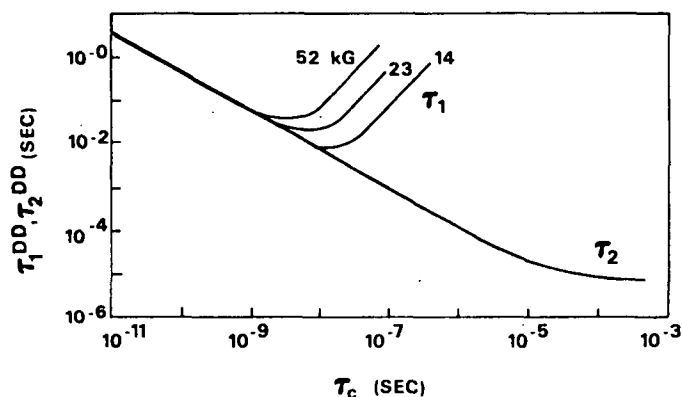
Figure 10. Dipolar spin-lattice and spin-spin relaxation times as a function of the molecular rotational correlation times at various magnetic fields.

Figure 10 shows that T_2^{DD} steadily decreases with increasing correlation times which is consistent with the importance of low-frequency motions for the T_2 process. Both viscous polymers and solids have very short T_2 values which contribute to line-broadening in the NMR signal of these materials [see Eq. (23)].

For a ^{13}C-nucleus Eq. (39) can be modified to include the interactions between all spins so that

$$R_1^{DD} = 1/T_1^{DD} = \gamma^2_C \, \gamma^2_H \, \hbar^2 \sum_i r_i^{-6} \, \tau_{c_i} \qquad (40)$$

where r_i is the distance from the relaxing nucleus to every other spin 1/2 nucleus and τ_{c_i} is the rotational correlation time for the vector connecting each of the i nuclei to the relaxing nucleus. The assumptions implicit in Eq. (40) can be restated;

the spins are within the same molecule, the correlation time is for molecular reorientation, all pertinent nuclei are of 1/2 spin, and the extreme narrowing condition applies. Under the further constraint of isotropic rotation Eq. 40 simplifies to

$$R_1^{DD} = 1/T_1^{DD} = \gamma^2_C \gamma^2_H \hbar^2 \tau_{c_{eff}} \sum_i r_i^{-6} \qquad (41)$$

where $\tau_{c_{eff}}^*$ is the effective correlation time for all spin interactions. For most ^{13}C-nuclei[**] this further reduces to

$$R_1^{DD} = 1/T_1^{DD} = N \gamma^2_C \gamma^2_H \hbar^2 r^{-6} \tau_{eff} \qquad (42)$$

since in nonenriched molecules the r^{-6} dependence usually causes only directly bonded protons to be important in DD relaxation. In Eq. 42 N refers to the number of directly bonded protons.

For the proton, Eq. 39 reduces to

$$R_1^{DD} = 1/T_1^{DD} = \gamma^4_H \hbar^2 \tau_{eff} \sum_i r_i^{-6} \qquad (43)$$

for the case of isotropic rotation. For anisotropic rotation the above equations must be modified by the inclusion of additional correlation times.

In concentrated solutions T_1^{DD} calculations can be complicated by intermolecular relaxation effects. This case is difficult to treat theoretically since translational motions must also be considered. A particular type of intermolecular

---

[*]To simplify the notation τ_{eff} is used in the remainder of this appendix.
[**]^{13}C-T_1 studies are simplified relative to ^1H-T_1 studies because of; 1) interactions with other ^{13}C-nuclei are negligible; 2) ^{13}C-signals in ^1H-decoupled spectra usually appear as one line so that only one time constant describes the relaxation; and 3) ^{13}C is usually internal to the molecule so that intermolecular relaxation is less likely.

dipole-dipole relaxation occurs when paramagnetic materials are present. In this case spin S in Eq. 36 is an unpaired electron. Since the magnetic moment of the electron is approximately three orders of magnitude greater than that of the proton a very efficient relaxation pathway is provided. Because of this, paramagnetic impurities, such as oxygen or some transition metal ions, must be removed whenever intermolecular relaxation interactions are likely or when long intramolecular relaxation times are being studied.

The dipole-dipole coupling interaction between a proton and a ^{13}C-nucleus also produces a nuclear Overhauser enhancement (NOE) for the ^{13}C-nucleus. The enhancement (η) is manifested by an increase in the ^{13}C-signal intensity under ^{1}H-decoupled conditions. The theoretical maximum enhancement, given by

$$\eta + 1 = 1.988, \tag{44}$$

is expected when nuclear-nuclear dipole-dipole interactions contribute exclusively to the relaxation of the ^{13}C-nucleus. Because of the dependence of the NOE on DD interactions measurements of η will indicate the percentage of the relaxation time that results from this mechanism according to the equation

$$T_1^{DD} = \frac{1.988}{\eta} T_1^T \tag{45}$$

T_1^T is the measured relaxation time. Equation 45 is only valid for the extreme narrowing condition.

Spin-Rotation (SR) Relaxation

A molecule may have an induced magnetic moment because of the modulation of the magnitude and direction of the molecular angular momentum by rotation of the molecule. As the molecule or molecular segment rotates faster significant fluctuating local magnetic fields can result leading to relaxation of the nearby nuclei. This

mechanism is applicable to small rapidly tumbling molecules or molecular segments such as attached methyl groups. The mechanism is particularly prevalent in nonprotonated carbons within small molecules. The mechanism is most important at elevated temperatures and is differentiated from the DD mechanism by an increase in the relaxation rate with increasing temperature. The pertinent correlation time T_C measures the persistance of the molecular angular momentum.

Chemical Shift Anisotropy (CSA) - Relaxation

The chemical shift of a nucleus is in general an anisotropic quantity described by the tensor σ. In liquids the Brownian motion averages the shift over all orientations so that a scalar chemical shift is observed. Nevertheless, a fluctuating local magnetic field is produced at the nucleus which can have components at the Larmor frequency. Relaxation via the CSA mechanism is known to be field dependent and thus can be detected by measurements at two magnetic field strengths under the extreme narrowing condition. At 23 KG no molecule has been found which is predominantly relaxed by the CSA mechanism. The mechanism is most likely to occur in molecules such as benzene which exhibit directional shielding. The pertinent correlation time is the same as for the dipole-dipole mechanism.

Scalar Coupling (SC) Relaxation

When two nuclei are spin-spin coupled a rapid relaxation of one nucleus can create a fluctuating local magnetic field at the other nucleus. This is only important for ^{13}C-nuclei coupled to quadrupolar nuclei such as ^{35}C and ^{79}Br which relax rapidly via quadrupolar relaxation.[*] The relevant correlation time is equal to the relaxation time of the quadrupolar nucleus. This mechanism is particularly important in reducing T_2 with a resultant broadening of the signal.[**]

---

[*]A similar effect is achieved by the modulation of spin-spin coupling created by rapid chemical exchange.

[**]^2H reduces the intensity of an attached ^{13}C-nucleus NMR signal by coupling with it and indirectly by eliminating the efficient $^{13}C-^1H$ DD mechanism. SC relaxation is not a factor.

Quadrupolar Relaxation

Nuclei with spin quantum numbers greater than 1/2 have an electric quadrupole moment Q resulting from a nonspherical charge distribution. Molecular reorientation of a quadrupolar nucleus produces a fluctuating field at the nucleus. Nuclei such as ^2H relax rapidly by the quadrupolar mechanism with the relaxation time being a function of Q and T_C.

Summary-Relaxation Theory

The relaxation times, T_1 and T_2 can be related to molecular geometry and dynamics through their dependence on interatomic distances and molecular motion. The resulting equations make the measurement of T_1 and T_2 a powerful tool for probing the conformation and dynamics of dissolved organic molecules. The major mechanism of relaxation for intermediate sized organic molecules is the nuclear-nuclear dipole-dipole interaction; the other mechanisms only become important in special cases. In the motional narrowing limit the molecular motion can be simply described for DD relaxation; for isotropic rotation only one correlation time is required.

LITERATURE CITED

1. Silverstein, Robert M., Bassler, G. Clayton, and Morrill, Terence, C.,
    Spectrometric Identification of Organic Compounds, 3rd Ed. New York, N.Y., John
    Wiley & Sons, Inc., 1974. p. 340.

2. Jackman, L. M. and Sternhell, S., Applications of Nuclear Magnetic Resonance
    Spectroscopy in Organic Chemistry, 2nd Ed. New York, N.W., Pergamon Press,
    1969. p. 456.

3. Bible, Roy H., Jr., Interpretation of NMR Spectra: An Empirical Approach, New
    York, N.Y., Plenum Press, 1965. p. 150.

4. Levy, G. C. and Nelson, G. L., Carbon-13 Nuclear Magnetic Resonance for
    Organic Chemists, New York, N.Y., Wiley-Interscience, 1972. p. 222.

5. Wehrli, F. W. and Wirthlin, T., Interpretation of Carbon-13 NMR Spectra, New
    York, N.Y., Heyden, 1976. p. 310.

6. Stothers, J. B., Carbon-13 NMR Spectroscopy, New York, N.Y., Academic Press,
    1972. p. 559.

7. Bovey, F. A., Nuclear Magnetic Resonance Spectroscopy, New York, N.Y., Academic
    Press, 1969. p. 396.

8. Becker, E. D., High Resolution NMR: Theory and Applications, New York, N.Y.,
    Academic Press, 1969. p. 310.

9. Levy, G. C., editor, Topics in Carbon-13 NMR Spectroscopy, Vol. 1, New York,
    N.Y., Wiley-Interscience, 1974. p. 292.

10. Levy, G. C., editor, Topics in Carbon-13 NMR Spectroscopy, Vol. 2, New York,
    N.Y., Wiley-Interscience, 1976. p. 485.

11. Jackman, L. M. and Cotton, F. A., editors, Dynamic Nuclear Magnetic Resonance
    Spectroscopy, New York, N.Y., Academic Press, 1975. p. 660.

12. Shaw, D., Fourier Transform NMR Spectroscopy, New York, N.Y., Elsevier
    Scientific Publishing Company, 1976. p. 357.

13. Farrer, Thomas C. and Becker, Edwin D., Pulse and Fourier Transfer NMR:
    Introduction to Theory and Methods, New York, N.Y., Academic Press, 1971.
    p. 115.

14. Axenrod, T. and Webb, G. A., editors, Nuclear Magnetic Resonance Spectroscopy
    of Nuclei Other Than Protons, New York, N.Y., Wiley-Interscience, 1974. p. 407.

15. Carrington, A. and McLachlin, A. D., Introduction to Magnetic Resonance:
    With Applications to Chemistry and Chemical Physics, New York, N.Y., Harper &
    Row, 1967. p. 266.

16. Slichter, C. P., Principles of Magnetic Resonance, 2nd Ed., New York, N.Y., Springer-Verlag, 1978. p. 397.

17. Poole, C. P., Jr. and Farach, H. A. Relaxation in Magnetic Resonance. New York, N.Y., Academic Press, 1971. p. 392.

18. Noggle, J. H. and Schirmer, R. E. The Nuclear Overhauser Effect: Chemical Applications, New York, N.Y., Academic Press, 1971. p. 259.

19. Mehring, M. High Resolution NMR Spectroscopy in Solids. New York, N.Y., Springer-Verlag, 1976. p. 246.

20. Corio, P. L. Structure of High-Resolution NMR Spectra. New York, N.Y., Academic Press, 1966. p. 548.

21. Pople, J. A., Schneider, W. G., and Bernstein, H. J. High-Resolution Nuclear Magnetic Resonance. New York, N.Y., McGraw-Hill Book Co., Inc., 1959. p. 501.

22. Abragam, A. The Principles of Nuclear Magnetism. Oxford, England, Oxford University Press, 1961. p. 599.

23. Netzel, D. A. and Miknis, F. P., Applied Spectroscopy 31:365-86(1977).

24. Breitmaier, E., Spohn, K. H., and Berger, S., Angew. Chem. Internat. Edit., 14:144-59(1975).

25. Ernst, R. R., and Anderson, W. A., Rev. Sci. Instr. 37:93-xx(1966).

26. Karplus, M., J. Amer. Chem. Soc. 85:2870-1(1963).

27. Hall, L. D., Morris, G. A., and Sukumar, S., J. Am. Chem. Soc. 102:1745-7 (1980).

28. Bloch, F., Physical Rev. 70:460-74(1946).

APPENDIX II

CARBON-13 SPIN LATTICE RELAXATION DATA

INTRODUCTION

This appendix presents the tabulated ^{13}C-T_1 data collected for the cello- and xylo-oligosaccharides and related compounds. In addition, the rationale behind the technique is briefly presented along with an explanation of the methods of measurement. Several preliminary runs are discussed to highlight potential sources of error.

DIPOLE-DIPOLE RELAXATION: RELEVANCE

Of the several mechanisms for relaxation of an NMR spin-system the dipole-dipole mechanism is the only significant contributor to relaxation in molecules the size of small oligosaccharides. For this type of mechanism the spin-lattic relaxation time (T_1) is given by (1):

$$1/T_1^{DD} = \hbar^2 \gamma^2_C \gamma^2_H \sum_i r^{-6}_{CH_i} T_{CH_i} \qquad (6)$$

provided that the motional narrowing limit is not exceeded.* In this equation γ_C and γ_H are the magnetogyric ratios for the appropriate nuclei, r_{CH} is the distance from the relaxing carbon nuclei to each contributing proton nuclei, and T_{CH} is the rotational-correlation time for each carbon-hydrogen interaction. For an isotropically rotating molecule in which no nonbonded C-H interactions are important this expression reduces to

---

*The region of motional narrowing represents rotational correlation times of about 5 x 10^{-9} sec. and smaller and is distinguished by frequency independent relaxation times. See Appendix I for further explanation.

$$1/T_1{}^{DD} = N\hbar^2\gamma^2_C\gamma^2_H r^{-6}_{CH}\tau_{eff} \tag{2}$$

where N is the number of directly attached protons, $T_1{}^{DD}$ is the dipolar spin-lattice relaxation time, and τ_{eff} is the effective rotational correlation time. τ_{eff} is the same for all carbons and protons in the molecule.

The nuclear Overhauser effect (NOE), η, defined as the change in total ^{13}C intensity upon irradiation of the proton-resonances, is a measure of the extent of the dipole-dipole relaxation mechanism. A theoretical enhancement of 1.988 is expected if only the nuclear-nuclear dipole-dipole mechanism is involved.

Most intermediate size molecules (MW>50,<1000) in solution have rotational correlation times less than the motional narrowing limit. For this rate of rotation the effect on T_1 of various changes in molecular environment can be estimated from Eq. (1). For instance, increasing the temperature or decreasing the concentration, either of which is expected to increase molecular mobility, will result in greater T_1 values. Likewise, free internal rotation will lead to longer T_1 values as is found with freely rotating methyl groups. A freely jointed chain, such as the side chain on cholesterol or the carbon backbone of an extended alkane, exhibits gradually increasing T_1 values toward the end of the chain. On the other hand, factors that contribute to increased τ_{CH} values, such as greater molecular size (inertia) or hydrogen bonding functional groups which act to increase intermolecular interactions (microviscosity), will result in lower T_1 values.

Carbohydrates with an extensive ability to interact with the solvent have T_1 values significantly lower than those of molecules of equivalent size but with fewer intermolecular interactions. Hall et al. (2) report relaxation times on the order of 1 sec for monosaccharides and 0.2 sec for disaccharides at concentrations of 1 molar in D_2O at 35°C. This is compared to relaxation times of several seconds in molecules of similar size but without the hydrogen-bonding functional groups (3).

From the above considerations it should be apparent that ^{13}C T_1's should be ideally suited to study the dynamics of motion of moderate size molecules, at least on a qualitative basis. For example, the study of segmental motion of freely jointed chains can be extended to the study of segmental motion in oligosaccharides. In this respect the group of atoms comprising the monosaccharide sub-units are analogous to the single methylene and methine units in a freely jointed chain of an extended alkane. At the trisaccharide level, or higher, the terminal units would be expected to have longer relaxation times than the internal units if the glycosidic linkage allows some degree of motional freedom. Allerhand and Doddrell (4) used this criteria to assign lines to the terminal galactose residue in the tetra-saccharide stachyose. The present study has employed the variation of relaxation times among adjacent monosaccharides in the xylo- and cello-oligosaccharides to compare the flexibility of the glycosidic linkages in and between these types of molecules. In addition, indications of the degree of anisotropic rotation at the mono-, di-, tri-, and tetrasaccharide level have been studied.

MEASUREMENT: INVERSION RECOVERY

The most common method for relaxation time measurement is the inversion-recovery (IR) technique. This method is characterized by the following pulse sequence:

$$(180° -t-90° -T)_n \qquad (3)$$

Here t is the delay between the inverting 180° pulse and a 90° observation pulse. The waiting time T, between the n pulses, is critical and should be 3-5 T_1 so that all spins are fully relaxed after each pulse. Commonly, the experiment is performed by measuring the individual peak heights for a series of delay times. Figure 1 depicts the process diagramatically, while Fig. 2 illustrates a typical IR data set.
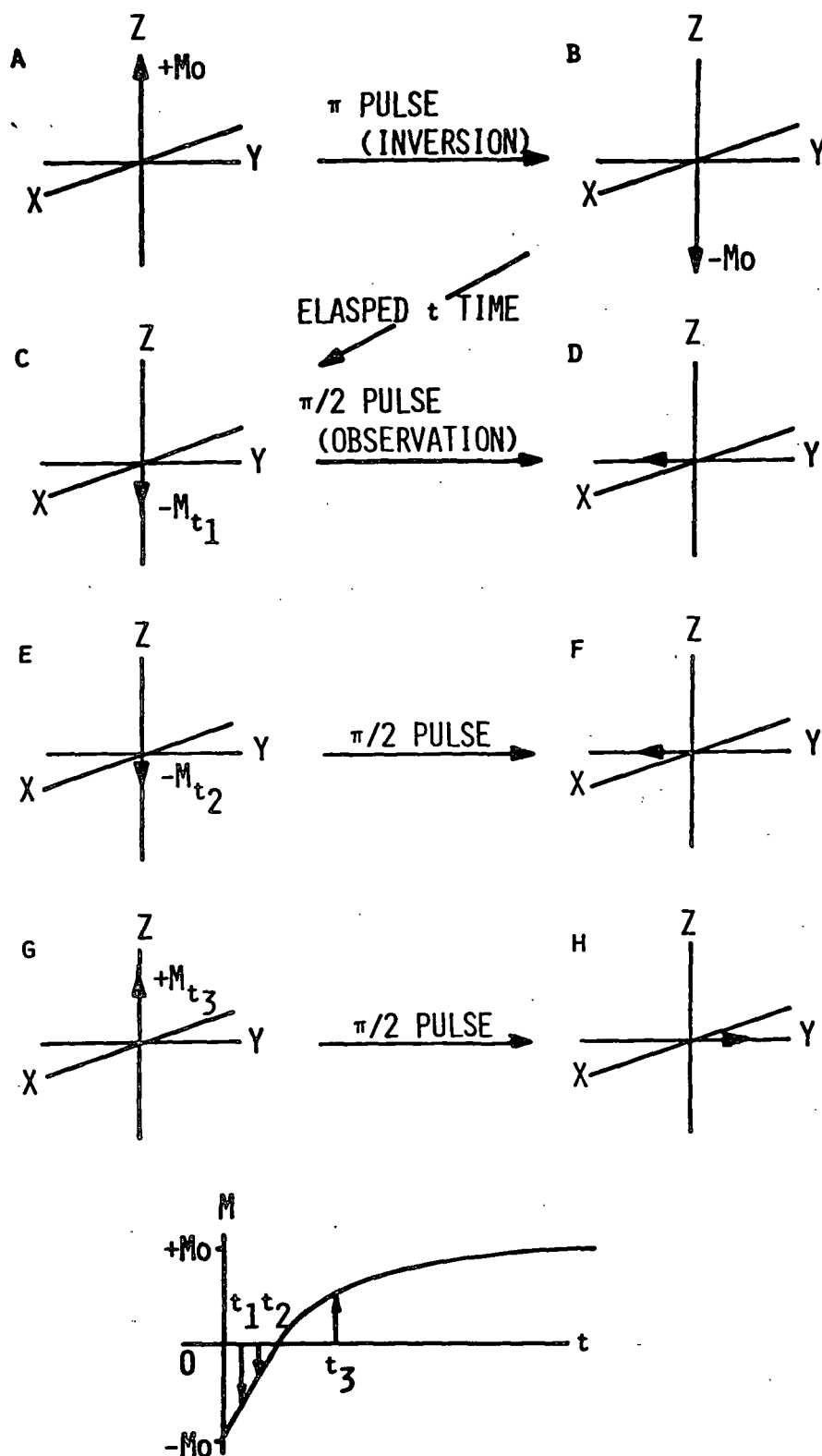
Figure 1. Depicted of the macroscopic magnetization vector ($\vec{m}$) during the inversion recovery experiment: a) prior to the pulse, b) immediately after the 180° pulse, c) after delay t, d) after the 90° observation pulse, e-h) repeat of a-d with longer delay times, i) plot of $\vec{m}$ vs. t.
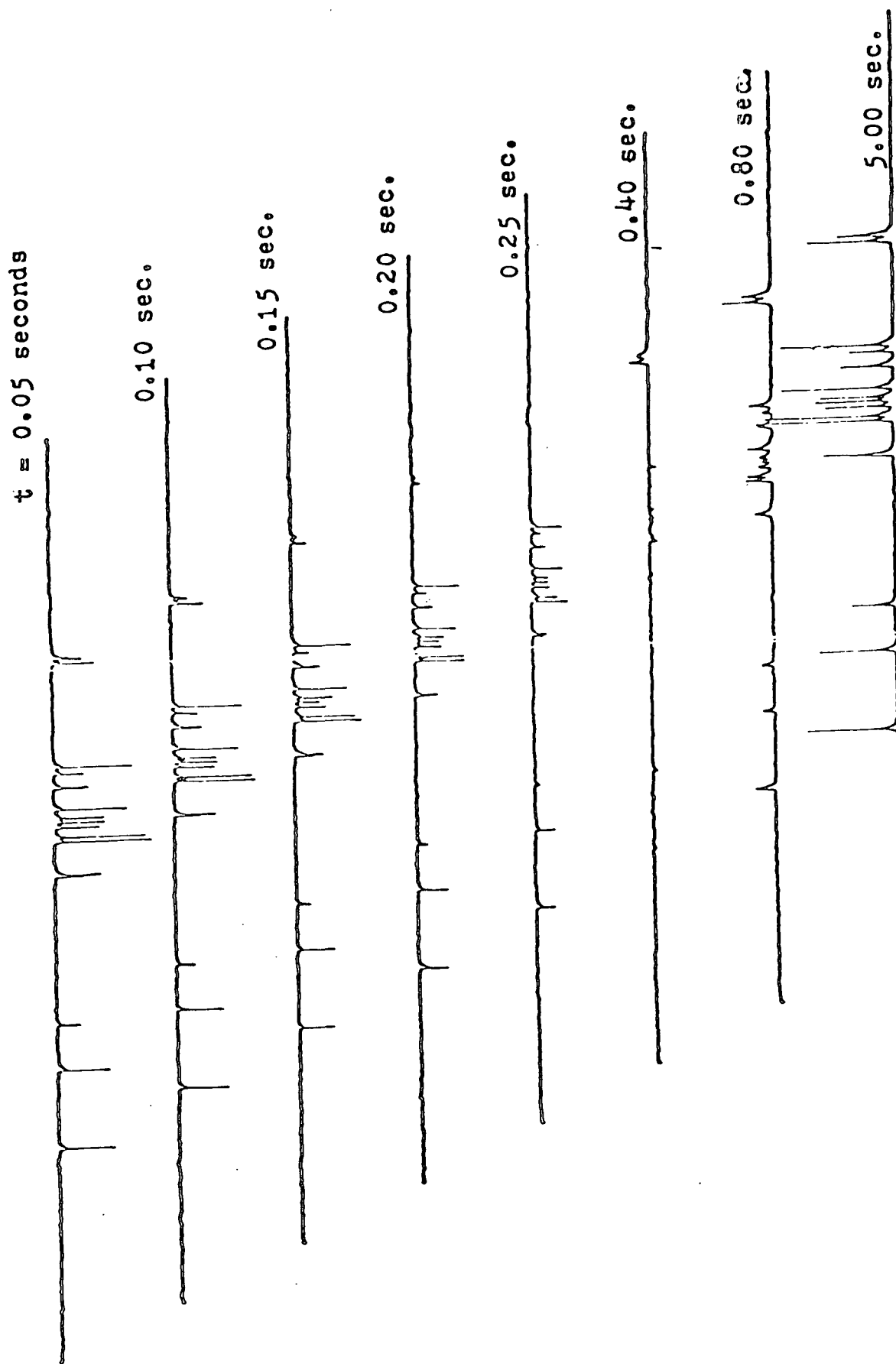
Figure 2. Spectra obtained by the inversion-recovery technique in measuring the ^{13}C T_1's of a 0.33 molal cellobiose solution in D_2O at 46°C.

The relaxation of the z-magnetization component for each spin can be described by a first-order differential equation:

$$dM_z/dt = - (M_z - M_\infty)/ T_1 \qquad (4)$$

where M_∞ and M_z are the equilibrium z-magnetization and z-magnetization measured after t, respectively. This is equivalent to Eq. (21) in Appendix I. The relaxation time for each individual spin is given by T_1. M_∞ is measured by applying a long delay time (bottom spectrum in Fig. 2). Integrating Eq. (4) produces

$$M_\infty - M_z = 2M_\infty e^{-t/T_1} \qquad (5)$$

where the initial condition that $M_z = - M_\infty$ after the inverting pulse has been applied. Rearrangement of Eq. (5) results in a linear equation which can be plotted to yield T_1:

$$\ln Z = \ln [(M_\infty - M_z)/ 2M_\infty) = -t/T_1 \qquad (6)$$

where $Z = (M_\infty - M_z)/ 2M_\infty$.

CALCULATION OF T_1

The Jeol FX-100 system contains a weighted linear regression program that uses peak intensity and delay time data to calculate T_1 in a modification of Eq. (6). This involves minimizing the error in the linearized equation resulting from Eq. (6):

$$\{[\ln Z - (t/T_1) - \beta] \omega\}^2 \equiv E \qquad (7)$$

where β is a constant and ω a weighting factor related to Z. The method of least squares is used to determine the values of T_1 and β resulting in a minimum value of E. Equation (6) can be rewritten in the form,

$$\ln Z = -(t/T_1) + \beta \qquad (8)$$

from which it is seen that $\beta = \ln Z$ at $t=o$.

β is thus a measure of the validity of the first order relaxation model described by Eq. (4); ideally $\beta = 0$ in this model. A second indicator of error involves the variance (S^2) in the data given by:

$$S^2 = \frac{\Sigma[\ln Z)_{obs} - \ln Z]^2}{N} \qquad (9)$$

where $(\ln Z)_{obs}$ is obtained from the actual data while in $\ln Z$ is calculated from Eq. (8) for the N data points. Only $\ln Z$ values less than 80% of $\ln Z_o$ are used in the calculation of T_1.

The relaxation data tables contained later in this appendix record the value of $\beta = \ln Z_o$ as well as an indication of relative variance for each T_1 value obtained. These tables indicate which T_1 values were not used to calculate average ring T_1 values $(\overline{NT_1})$ in Section 2 of the thesis. The criteria for rejection are listed below for quick reference.

1. Unusually large values of β or S^2 relative to other values in the data set.

2. Uncertainty in the assignment.

3. Peak is degenerate with a larger peak that is not in an equivalent environment relative to the glycosidic linkage.

4. The $\alpha-C_1$ value is not used because its value is dependent on its orientation relative to the major axis of the molecule.

SOURCES OF ERROR

Relaxation time measurements contain several potential sources of systematic error if care is not taken (5). Of particular concern is the time between pulses,

which should be 3-5 T_1 to avoid signal deterioration, and the need for a uniform and strong pulse throughout the observation window. The pulse interval requirement is easily met if the longest relaxation time can be estimated. The uniformity of the pulse is a function of the instrument design and should not be a problem with the FX-100.

Several other sources of error resulting from the sample or experimental set-up are possible. Included in this category are the use of peak heights rather than peak area, inaccuracies resulting from low signal to noise ratios at low concentration, variability in resolution resulting in inaccuracies for closely spaced peaks, and systematic errors that can result if a non-180° pulse is used. Except for the inaccuracies observed for closely spaced peaks these problems are relatively unimportant, leading to only a slight variability in the data.

Two additional sources of error, which are potentially more detrimental, are long-term temperature variations and paramagnetic impurities. Over the time period of the experiment any temperature change could lead to large errors since relaxation times are a strong function of temperature (6). To minimize this problem the Jeol Fx-100 is equipped with a temperature controller stable to ± 1°C.

Paramagnetic impurities provide a highly efficient relaxation mechanism which can mask dipole-dipole relaxation times. Some of the transition metal ions and oxygen have this property. Bock and Hall (6) have shown that removal of oxygen by nitrogen purging does not significantly affect carbohydrate ^{13}C-relaxation times. Proton T_1's may be expected to be more significantly affected by virtue of being on the exterior of the molecule. For ^{13}C-T_1 studies freeze-pump-thaw degassing has been used when comparisons between samples are made, as suggested in the literature (7). Preferential binding of Gd^{+3} at the reducing-end does lead to systematic

reductions in relaxation times near the site of binding (8), illustrating the need to remove any paramagnetic impurity that binds at a specific site.

Table I compares the ^{13}C-T_1 values obtained under a variety of conditions for the linkage carbon (C-1´) in cellobiose and methyl β-cellobioside. Comparison of examples 1-5 with example 6 illustrate the effect of concentration. Higher concentrations give lower relaxation times. Comparison of examples 6 and 7 show the effect of temperature. An 11°C increase in temperature produced a 61% increase in T_1. The effects of purging with N_2 or using a non-180° pulse are small.

TABLE I

^{13}C-T_1 RELAXATION TIMES FOR THE C-1´ OF CELLOBIOSE
IN D_2O UNDER DIFFERENT CONDITIONS

Example	Concentration, %	Temp., °C	Comment	T_1, sec
1	25.48	35		0.32
2	25.48	35	Repeat of 1	0.31
3	25.48	35	N_2 purge	0.33
4	25.48	35	Non 90° pulse	0.33
5	25.48	35	Fewer data points	0.35
6	10.07	35		0.54
7	10.07	46		0.87

NUCLEAR OVERHAUSER ENHANCEMENT (NOE)

In Appendix I it was shown that the percentage of relaxation occurring by the dipole-dipole (DD) mechanism could be determined by NOE measurements. If the DD mechanism is the only one operative then an enhancement of 1.988 is expected for a decoupled carbon spectrum relative to the proton-coupled spectrum.

NOE measurements were made by comparing peak heights between successively obtained proton gated-decoupled and proton decoupled carbon spectra. The gated-decoupled spectra were obtained by applying the decoupler only during signal

acquisition; in this manner the spectrum contains no proton-carbon coupling as in the decoupled spectrum while the NOE is destroyed by the absence of decoupling between pulses.

NOE measurement suffers from several error sources. The FX-100 data system is only equipped to give standardized peak height measurements. Electronic integration of two separate standardized spectra cannot be performed. The error involved can be estimated by manually integrating and comparing the decoupled and gated decoupled spectra. A more serious concern is the effect of long term temperature instability which tends to give fluctuations in the data when sequential decoupled and gated decoupled spectra are recorded. Freeman (9) has designed a pulse sequence which simultaneously collects the decoupled and gated decoupled spectra. Unfortunately, this is not available on our instrument.

Table II summarizes the results of several NOE determinations. It also includes some of the available literature data. Hall and coworkers (2) have measured the NOE for several mono- and disaccharides. In all cases they observed 100% of the theoretical enhancement for proton decoupling, indicating that the nuclear-nuclear dipole-dipole mechanism is the only one operating. They used a pulse sequence which allows a simultaneous accumulation of the gated decoupled and decoupled spectra. This effectively minimizes errors from long term temperature drifts.

The data collected in the present study for the cellodextrins support the conclusion that the only relaxation mechanism present is nuclear-nuclear dipole-dipole relaxation. The larger deviation in these data, compared to the literature data, reflects the use of peak heights rather than peak areas and the effects of long term temperature drifts.

The results for xylobiose and xylotriose show only 84 and 87% of theoretical enhancement. The reasons for these low values may be several. It is possible that these values result from the same systematic errors mentioned above or that an inert paramagnetic material is present in low concentration. This would function to suppress the NOE. The latter possibility can result from an electron-nuclear dipole-dipole relaxation mechanism that acts to decrease the observed relaxation times by a nonspecific intermolecular interaction. Equation (10) gives the amount of reduction in the observed relaxation for this situation:

$$\eta' \, / \, \eta \; = T_1 / \; T_1^{DD} \tag{10}$$

In this equation η' and T_1 are the observed NOE and relaxation time, respectively, and η is the maximum enhancement possible. T_1^{DD} is the nuclear-nuclear dipole-dipole relaxation time.

TABLE II

NUCLEAR OVERHAUSER ENHANCEMENTS

Run	Sample[a]	% NOE[b]	σ[c]	High	Low	Peaks
1	C2	110	8	118	83	18
2	C2	96	5	104	88	17
3	C3	97	7	109	87	21
4	X3	87	6	99	80	18
5	X2	84	6	96	76	14
d	MBC2	100	1	103	97	13
d	Lactose	99	2	102	97	18

[a]All samples were run at 35°C using a comparison of a completely decoupled spectrum and a gated decoupled spectrum. Normalized peak heights were measured. C2 = 1 m cellobiose, C3 = 0.23 m cellotriose, X3 = 0.32 m xylotriose, and X2 = 0.55 m xylobiose.
[b]Percent of the theoretical enhancement, 1.988 averaged over all peaks.
[c]Standard deviation.
[d]From Ref. (2).

While either of the above error sources may be present in this case, the contribution from other intramolecular relaxation mechanisms is almost certainly nonexistent. If the error is due to an inert paramagnetic material, which does not bind specifically at one site, then comparisons of relative T_1 data among carbons of the same molecule will not be affected.*

At low signal to noise values NOE determinations become more difficult because of the long accumulations required. Because of this difficulty in obtaining accurate NOE values no further work was done on the higher oligosaccharides investigated in this thesis.

TABLES

The remainder of this appendix contains the ^{13}C-T_1 relaxation data for the carbohydrates studied. Tables IV-XV give the assignments, relaxation times, and errors for each peak. Tables XVI-XXV contain the average T_1 values for the individual rings for each molecule studied. The number of carbons used to determine the average is also given. Table XXVI compares the T_1 ring averages for the tri- and tetrasaccharides using the student t-test to compare means. In almost every case the average T_1 for the terminal rings differs from that for the internal rings at a confidence level of 90%. In most cases confidence intervals were 99.0% or above.

Table III contains a key to the abbreviations used in Tables IV-XXV.

---

*Preparation of the xylobiose sample included a final treatment with IR-120 to remove paramagnetic cations.

TABLE III

KEY TO TERMINOLOGY USED IN TABLES IV–XXV

Term	Explanation
A_1	Reducing-end ring of the β-anomer.
A_2	Reducing-end ring of the α-anomer.
B,C,D	Remaining rings in the oligosaccharide lettered sequentially. The terminal ring is given the letter furthest from A.
data	The number of spectra accumulated to determine the relaxation time.
ln Z_0	The same as β in Eq. (7). The value of ln Z [see Eq. (6)] at time = 0.
N	The number of relaxation times included in the ring average.
$\overline{NT_1}$	The average of the relaxation times for that ring. Each relaxation time is multiplied by n, the number of attached protons.
PR	Time between pulses.
S^2	The variance between (ln Z)$_{observed}$ and (ln Z)$_{calculated}$. See Eq. (9).
T_1	The longitudinal relaxation time in seconds.
α	The α-anomer. In the carbon number system used an α refers specifically to the α-anomer. If no anomer designation is given then the peaks for each anomer are coincident.
β	β-anomer.
σ	Standard deviation.

TABLE IV

Cellotetraose - 7.75% (W/V)

Run[a]

Assignment	Shift[b]	31		32		33	
		T_1	$\ln Z'_o$	T_1	$\ln Z'_o$	T_1	$\ln Z'_o$
1"'	103.3	0.60	10g	0.54	6	0.46	-2
1",1'	103.1	0.51	8g	0.44	4	0.41	1
β-1	96.6	0.61	3g	0.71	10	0.47	-2
α-1[c]	92.7	0.37	2g*	0.43	16g*	0.32	-4g
α-4	79.8	0.55	10g	0.61	6	0.41	-8
β-4	79.6[h]	0.52	5g*	0.62	11	0.38[f]	-8g*
4'[d]	79.5	0.45	5g	0.45	6	0.36	-6
4"[d]	79.4	0.50	11g*	0.39	5	0.37	-0.1
5"'	76.8	0.62	9g	0.60	7	0.47	-3
3"'	76.5	0.58	6g	0.60	7	0.45	-7g
5",5',β-5[e]	75.7	0.54	12g*	0.44	5	0.37	-5
β-3	75.2	0.52	6g	0.65	11	0.44	-5
3",3'	75.0	0.51	7g	0.45	6	0.39	-3
β-2	74.9	0.49[f]	5g*	0.58	10	0.57	9
2"'	74.0	0.62	10g	0.57	6	0.45	-5g
2",2'	73.8	0.50	8g	0.44	6	0.42	1
α-3,α-2	72.2	0.59	4g	0.66	9	0.50	-2g
α-5	71.0	0.64[f]	11g*	0.70	9	0.53[f]	2g*
4"'	70.4	0.62	6g*	0.64	5	0.46	-8g
6"'	61.6	0.35	11g*	0.28	6	0.22	-9
6	61.1	0.24	7g	0.22	1	i	
6",6'	61.0	0.22	5	0.22	5	0.20[e]	2

| $\ln Z'_d \pm \sigma$ | | 7.3±2.9 | | 7.1±3.1 | | 4.4±2.9 | |

[a]Conditions: 59°C; Run 31: 5000 pulses, PR = 2.3 sec., 10 data; Run 32: 4500 pulses PR = 3.0 sec, 7 data; Run 33: 4500 pulses, PR = 3.0 sec, 10 data, poor S/N.

[b]Referenced to earlier cellotetraose spectrum by setting C_4"' to the equivalent value.

[c]$\alpha-C_1$ value is not used in the calculation of average NT_1 because of its unusually low value resulting from the orientation of the CH vector parallel to the major axis of rotation (2).

[d]Assignments can be interchanged; the average of these values was used in calculating the NT_1 average.

[e]Not used in calculating the NT_1 average because of coincidence with another signal.

[f]Not used in calculation of average NT_1 values because of an unusually large error as determined by $\ln Z_o$, or S^2.

[g]S^2 values greater than 0.0020;* indicates a S^2 value much larger than the others in the data set for that sample.

[h]79.7 ppm in run 31.

[i]Shoulder on another peak.

TABLE V

Xylotetraose - 6.20% (W/V)

Run[a]

Assignment	Shift[b]	27		28	
		T_1	ln Z'_o	T_1	ln Z'_o
1"'	102.7	0.40	3	0.36	-3
1",1'	102.5	0.31	1	0.31	1
β-1	97.3	0.40	-4	0.42	-4
α-1[c]	92.8	0.28	-3[g]	0.27	-5[g]*
α-4	77.4	0.40	6[g]	0.40	5
4"4',β-4[e]	77.2	0.31	1	0.32	2
3"'	76.4[h]	0.43	4	0.39	0.2
β-2[d]	74.8	0.44	4	0.40	1
β-3[d]	74.7	0.42	3	0.39	3
3",3'	74.5	0.31	1	0.31	1
2"'	73.6	0.31[e]	-5	0.32[e]	-2
2",2'	73.5	0.31	1	0.31	3
α-2[e]	72.2	0.45	3	0.41	-3[g]*
α-3[d]	71.8	0.37	-3	0.41	1[g]*
4"'	70.0	0.43	3	0.40	0.7
5"'	66.1	0.21	2	0.23	7
5",5',β-5[e]	63.8	0.16	2	0.16	2
α-5	59.7	0.24[f]	11[g]*	0.18	-4[g]
$\overline{\lvert \text{ln } Z'_o \rvert}$ ± σ			3.3±2.4		2.7±1.8

---

[a]Conditions: Runs 27 and 28: 35°C, 4000 pulses, PR = 2.1 sec, 10 data points.
[b-g]See Table IV b-g.
[h]76.5 ppm in Run 28.

TABLE VI

Cellotriose - 10.78% (W/V)

Run[a]

Assignment	16			17	
	Shift[b]	T_1	ln Z'_o	T_1	ln Z'_o
1"	103.4	0.35	7	0.36	8
1'	103.2	0.31	5	0.31	6
β-1	96.6	0.40	6	0.39	4
α-1[c]	92.7	0.25	5[e]	0.24	6[e]
α-4	79.6	0.36	11	0.34	3
β-4	79.5	0.31[d]	4	0.33[d]	6
4'	79.4	0.29	5	0.31	8
5"	76.9	0.37	9	0.38	9
3"	76.4	0.35	4	0.38	7
5'[d], β-5[d]	75.7	0.32	5	0.33	6
β-3	75.2	0.35	4	0.41	10
3'	75.0	0.31	5	0.32	6
β-2	74.8	0.33	6[e]	0.35	5[e]
2"	74.0	0.35	7	0.35	7
2'	73.0	0.30	5	0.32	9
α-3, α-2	72.1[f]	0.33	1	0.32	1
α-5	71.0	0.34	5[e]	0.34	6
4"	70.4	0.37	7	0.37	7
6"	61.5	0.18	7	0.16	3
6	61.0	g		g	
6'	60.9	0.15	4	0.15	5
$\overline{\ln Z'_o} \pm \sigma$			5.6±2.1		5.8±2.5

[a]Conditions: 36°C, 3500 pulses; Run 16: 10 data points; Run 17: 8 data points.
[b]Referenced to earlier cellotriose spectrum by setting C_4" to the equivalent value.
[c]See Table IV c.
[d]See Table IV e.
[e]S^2 values greater than 0.0020.
[f]72.2 ppm in run 17.
[g]Shoulder on another peak.

TABLE VII

Xylotriose - 11.71% (W/V)

Run[a]

Assignment	Shift[b]	18		26	
		T_1	$\ln Z'_0$	T_1	$\ln Z'_0$
1"	102.7	0.40	-4	0.40	-3[g]
1'	102.5	0.36	-1	0.36	-1[g]
β-1	97.3	0.50	4	0.48	-1[g]
α-1[c]	92.8	0.31	-5	0.32	-2[g]
α-4	77.4	0.37	-4	0.29	-3[g]
4'e, β-4e	77.3	0.36	-3	0.36	-2
3"	76.5	0.41	-5	0.45	-1[g]
β-3[d]	74.9	0.46	2	0.44	-2
β-2[d]	74.8	0.43	0	0.44	1
3'	74.6[h]	0.37	-3	0.35	-2
2"	73.6	0.39e	-2	0.40e	-3[g]*
2'	73.5	0.39e	5	0.37e	1[g]
α-2²	72.2	0.47	4	0.46	1
α-3[d]	71.8	0.45	-1[g]	0.43[f]	-1[g]
4"	70.0	0.43	3	0.45	-1[g]
5"	66.1	0.23	3	0.20	-2[g]
5'e, β-5e	63.9[h]	0.21	7	0.17	-3[g]
α-5	59.7	0.23	4[g]	0.19	-1[g]

| $\boxed{\ln Z'_0}$ ± σ | | | 3.3±1.7 | | 1.7±0.8 |

---

[a]Conditions: 6750 pulses, 10 data points; Run 18: 35°C, PR = 2.1 sec; Run 28: 34.5°C, PR = 2.2 sec.
[b-g]See Table IV, b-g.
[h]74.5 ppm and 63.8 ppm, respectively, in Run 26.

TABLE VIII

Methyl β-Cellobioside – 16.65%

Run

Assignment	Shift	5	
		T_1	ln Z'_o
1	103.9	0.64	14[c]
1´	103.4	0.62	16[c]
4	79.6	0.54	11[c]
5´	76.8	0.61	15[c]
3´	76.4	0.59	13[c]
5	75.6	0.64	17[c]
3	75.2	0.58	12[c]
2´	74.0	0.61	16[c]
2	73.7	0.62	15[c]
4´	70.3	0.58	13[c]
6´	61.5	0.34	19[c]*
6	61.0	0.33	18[c]*
OCH₃	58.0	1.34	14[c]

ln Z'_o			14.8±2.3

[a]Conditions: Run 5: 35°C, 1000 pulses, PR = 5 sec, 8 data points.
[b]Referenced to $C_{4'}$ of cellobiose. Assignments based on the literature (10).
[c]See g in Table IV.

TABLE IX

Cellobiose - 10.07% (W/V)

Run[a]

Assignment	Shift[b]	7		25	
		T_1	ln Z'_o	T_1	ln Z'_o
1´	103.4	0.54	8	0.47	0.4
β-1	96.6	0.61	9	0.49	-4
α-1[c]	92.6	0.43	6	0.39	0
α-4	79.7	0.56	9[e]	0.46	-1
β-4	79.5[f]	0.58	11[e]*	0.45	-0.5
5´	76.8	0.60	12	0.47	-1
3´	76.4	0.56	7[e]	0.47	-2
β-5	75.6	0.61	12[e]	0.45	-2
β-3	75.1	0.63	11	0.50	1
β-2	74.7	0.61	10[e]*	0.54	4
2´	74.0	0.54	8[e]	0.47	-1
α-3[d]	72.2	0.60	8	0.49	-1
α-2[e]	72.1	0.53	7[e]	0.48	-0.4
α-5	70.9	0.59	9[e]	0.49	2
4´	70.3	0.58	9[e]	0.46	-3
6´	61.5	0.30	9	0.24	1
β-6	61.0	0.27	8	0.24	1
α-6	60.9	0.31	14	0.24	5

| | ln Z'_o | ± σ | | 9.3±2.1 | | 1.7±1.4 |

[a]Conditions: Run 7: 35°C, 1000 pulses, PR = 5 sec, 8 data points;
Run 25: 31.5°C, 1750 pulses, PR = 2.3 sec, 10 data points.
[b]See Table VIII 8 b.
[c-d]See Table IV c and d.
[e]See Table IV g.
[f]79.6 ppm in Run 7.

TABLE X

Cellobiose

Run[a]

Assignment	Shift[b]	11		35	
		T_1	ln Z'_o	T_1	ln Z'_o
1'	103.4	0.32	4	0.67	17
β-1	96.6	0.35	2	0.73	17g*
α-1[c]	92.6	0.26	1	0.48	10g*
α-4	79.7	0.32	3	0.69	16g*
β-4	79.6[h]	0.34	7	0.72	20
5'	76.8	0.33	2	0.74	21
3'	76.4	0.34	5	0.74	21
β-5	75.6	0.34	4	0.71	19
β-3	75.1	0.34	3	0.74	18g
β-2	74.7	0.35	5	0.61	10g
2'	74.0	0.32	2	0.70	18
α-3[d]	72.2	0.35	4	0.74[e]	14g*
α-2[e]	72.1	0.33	4	0.69[e]	13g*
α-5	70.9	0.34	4	0.82[f]	19g*
4'	70.3	0.34	5	0.69	17
6'	61.5[h]	0.18	7	0.31	11
β-6	61.0	0.17	4	0.32	12
α-6	60.9[h]	0.16	4	0.31	10g
$\lceil$ ln $Z'_o \rceil$ ± σ			3.9±1.6		15.7±3.9

[a]Conditions: Run 11: 25.48% (W/V) in D_2O, 35°C, 800 pulses, PR = 2.3 sec, 10 data points (saturated solution); Run 35: 5.00% (W/V) in D_2O, 31°C, 1000 pulses, PR = 7.0 sec, 10 data points. Low S/N gives a large error.
[b-d]See Table IX b-d.
[e-g]See Table IV e-g.
[h]79.5, 71.0, 61.4 and 60.8 ppm in Run 35.

TABLE XI

Xylobiose - 13.52% (W/V)

Run[a]

Assignment	Shift[b]	19		20		21	
		T_1	$\ln Z'_o$	T_1	$\ln Z'_o$	T_1	$\ln Z'_o$
1´	102.7	0.66	0	0.70	4	0.78	9
β-1	97.3	0.74	1	0.78	6	0.87	12
α-1[c]	92.8[h]	0.80[f]	12[i]	0.54[f]	5[g]*	0.61	10
α-4	77.5	0.65	1	0.71	7	0.80	12
β-4	77.3	0.62	1	0.72	9	0.79	13
3´	76.5	0.62	-2	0.75	7	0.80	11
β-2[d]	74.86[h]	-	-	0.70	3	0.74	6
β-3[d]	74.77	0.62[e,j]	-2	0.72	5	0.70	4
2´	73.6	0.59	-4	0.74	6	0.75	9
α-2[d]	72.2	0.66	1	0.78	8	0.78	9
α-3[d]	71.8	0.64	-0.4	0.80	9	0.83	15
4´	70.0	0.62	-4	0.76	8[g]	0.79	10
5´	66.1	0.35	2	0.42[f]	10[g]*	0.42	10
β-5	63.9	0.33	2	0.41[f]	12[g]*	0.40	11
α-5	59.8	0.31[f]	-4[g]*	0.37	7	0.38	9

| $\overline{\mid \ln Z'_o \mid} \pm \sigma$ | | | 1.9[i]±1.4 | | 7.1±2.4 | | 10.0±2 |

[a]Conditions: Run 19: 35.5°C, 1500 pulses, PR = 2.1 sec (too short), 10 data points; Run 20: 35.5°C, 2000 pulses, PR = 4.0 sec, 10 data points, noise decoupler off; Run 21: 36°C, 1750 pulses, PR = 4.2 sec, 10 data points.
[b-g]See Table X b-g.
[h]92.9 ppm in Run 19; 74.84 in Run 20.
[i]Not included in average for $\mid \ln Z_{o'} \mid$.

TABLE XII

Xylobiose - 7.25%

Run[a]

Assignment	Shift[b]	24	
		T_1	ln Z'_o
1'	102.7	0.93	12
β-1	97.3	0.98	11[f]
α-1[c]	92.8	0.78	14[f]
α-4	77.5	0.97	15[f]
β-4	77.3	0.85	9[f]
3'	76.5	0.86	9
β-2[d]	74.84	0.81	5
β-3[d]	74.77	0.88	9[f]
2'	73.6	0.92	12[f]
α-2[d]	72.2	0.97	15[f]
α-3[d]	71.8	0.98	13
4'	70.0	0.99	14[f]
5'	66.1	0.52[e]	13[f]*
β-5	63.9	0.46[e]	13[f]*
α-5	59.8	0.51[e]	15[f]*

| $\overline{\ln Z'_o} \pm \sigma$ | | | 11.8±3.1 |

---

[a]Conditions: Run 24: 31.5°C, 1750 pulses, PR = 7.0 sec, 10 data points, sample purged with nitrogen.
[b-d]See Table IV b-d.
[e]See f Table IV.
[f]See g Table IV.

TABLE XIII

Xylobiose - 5.00%

Run[a]

Assignment	Shift	34 T_1	34 $\ln Z'_o$	36 T_1	36 $\ln Z'_o$	37 T_1	37 $\ln Z'_o$
1′	102.7	1.01	18g	0.88	12	0.84	9
β-1	97.3	1.05	17g*	0.99	14	1.07	14
α-1[c]	92.8	0.72	12g	0.62	4g	0.74	12g
α-4	77.5[h]	0.78e	12g	0.70e,f	1g*	0.93	16g
β-4	77.3	0.93	16g	0.79	10g	0.90	14
3′	76.5	1.00	18g	0.84	9	0.90	13
β-2[d]	78.84	0.88e	8g	0.91	12	0.98	17
β-3[d]	74.77[h]	1.02	14	0.89	12	0.98	16
2′	73.6	0.96	17g	0.96	13	0.95	15
α-2[d]	72.2	1.09f	15g*	0.93	12g	0.96	13g*
α-3³	71.8	1.01	17g*	0.91	11g	1.06	15
4′	70.0	1.06	20g	0.77	3	0.92	12
5′	66.1[h]	0.43	10g	0.42	8	0.48	15
β-5	63.9[h]	0.40	5g	0.39	5	0.45	10g
α-5	59.7	0.45f	12g*	0.37f	5g*	0.49	18
$\overline{|\ln Z'|} \pm \sigma$		14.1±4.2		8.7±4.1		13.9±2	

[a]Conditions: Run 34: 31°C, 1500 pulses, PR = 8.0 sec, 10 data points; Run 36: room temperature, 1500 pulses, PR = 10.0 sec, 8 data points; Run 37: 31.5°C, 1500 pulses, PR = 7.5 sec, 10 data points. Each has a low S/N.
[b]Referenced to β-C_1 in the earlier xylobiose spectra.
[c-g]See Table IV c-g.
[h]77.4, 74.60, 66.0, and 63.8 ppm, respectively, for Runs 36 and 37.

TABLE XIV

Glucose

Run[a]

Assignment	Shift[b]	15 T_1	15 $\ln Z'_o$	29 T_1	29 $\ln Z'_o$	30 T_1	30 $\ln Z'_o$
β-1	96.7	1.08	1	0.84	10	0.80	5
α-1[c]	92.9	1.04	3	0.78	8	0.69	-2
β-5	76.6	1.04	2	0.81	9	0.71	-1
β-3	76.6	1.06	1	0.60[f]	-11[h]	0.71	-1
β-2	75.0	1.04	1	0.81	11	0.74	4
α-3	73.6	0.95	3	0.78	7	0.72	-2
α-2[d]	72.3	0.91	7	0.78[e,i]	8	0.71	1
α-5[d]	72.2	1.00	0.4	-		0.74	4
α-4[d]	70.5	0.65[e,f]	31[h]	-		0.54[e,f]	-20[g*,h]
β-4[d]	70.4	0.98	1	0.77[e,j]	8	0.71	2
β-6	61.6	0.55	1	0.43	9	0.41	4
α-6	61.5	0.58	2	0.29[e]	-19[h]	0.40	0
$|\ln Z'_d| \pm \sigma$		2.0[h]±1.9		8.7[h]±1.2		2.4[h]±1.6	

[a] Conditions: Run 15: 18.10% (W/V) in D_2O, 36°C, 2000 pulses, PR = 5.0 sec, 10 data points; Run 29: 26.81% (W/V) in D_2O, 31.5°C, 350 pulses, PR = 8.0 sec, 10 data points, 5000 Hz observation window; Run 30: 26.81% (W/V) in D_2O, 32°C, 350 pulses, PR = 6.0 sec, 10 data points, 2000 Hz observation window.

[b] Referenced to β-C_1 as given by Perkins et al. (11). Their reference is relative to internal TMS using p-dioxane (67.4 ppm) as a secondary reference. The assignments agree with those in the literature (12,13).

[c-g] See Table IV c-g.

[h] Unusually large value, not included in $|\ln Z_o|$.

[i] Two signals not resolved.

TABLE XV

Xylose - 25.83% (W/V)

Run[a]

Assignment	Shift[b]	22		23	
		T_1	ln Z'_o	T_1	ln Z'_o
β-1	97.3	1.58	9	1.56	5
α-1[c]	92.9	1.40	9	1.48	8
β-3	76.5	1.55	9	1.60	7
β-2	74.7	1.53	10	1.56	6
α-3	73.6	1.60	10	1.57	5
α-2	72.2	1.54	9	1.69	11
α-4	70.1	1.54	9	1.65	12
β-4	70.0	1.49	9	1.64	12
β-5	65.9	0.86	9	1.64	11[e]
α-5	61.7	0.86	11	0.78	7[e]

| $\overline{\ln Z'_o}$ ± σ | | | 9.6±0.8 | | 8.4±2.8 |

---

[a]Conditions: Run 22: 35°C, 400 pulses, PR = 6.0 sec., (too short) 10 data points; Run 23: 36°C, 300 pulses, PR = 8.5 sec., 10 data points.

[b]Reference to the β-C_1 signal of xylobiose which was set with respect to internal TMS using p-dioxane at 67.4 ppm. The assignments are given in the literature (12,13).

[c]See Table IV c.

[d]See Table IV f.

[e]See Table IV g.

TABLE XVI

Cellotetraose- Run 31

Ring	$\overline{NT}_1$	σ	N
A_1	0.53	0.06	4
A_2	0.55	0.05	4
B,C	0.50	0.03	6
D	0.62	0.05	6

Cellotetraose - Run 32

A_1	0.60	0.10	5
A_2	0.61	0.10	5
B,C	0.44	0.01	6
D	0.58	0.04	6

Cellotetraose - Run 33[a]

A_1	0.49	0.07	3
A_2	0.47	0.05	3
B,C	0.39	0.02	6
D	0.46	0.01	6

[a]Used in text.

TABLE XVII

Xylotetraose - Run 27[a]

Ring	$\overline{NT}_1$	σ	N
A_1	0.42	0.02	3
A_2	0.41	0.04	3
B,C	0.31	0.004	5
D	0.42	0.01	4

Xylotetraose- Run 28

A_1	0.40	0.02	3
A_2	0.40	0.02	4
B,C	0.31	0.01	5
D	0.40	0.04	4

[a]Used in text.

TABLE XVIII

Cellotetriose- Run 16[a]

Ring	$\overline{NT}_1$	σ	N
A_1	0.36	0.04	3
A_2	0.34	0.01	4
B	0.30	0.01	5
C	0.36	0.01	6

Cellotetriose - Run 17

Ring	$\overline{NT}_1$	σ	N
A_1	0.38	0.03	3
A_2	0.33	0.01	4
B	0.31	0.01	5
C	0.36	0.02	6

[a]Used in text.

TABLE XIX

Xylotetriose - Run 18

Ring	$\overline{NT}_1$	σ	N
A_1	0.46	0.04	3
A_2	0.44	0.05	4
B	0.365	0.01	2
C	0.425	0.03	4

Xylotetriose- Run 26[a]

Ring	$\overline{NT}_1$	σ	N
A_1	0.45	0.02	3
A_2	0.41	0.04	3
B	0.355	0.01	2
C	0.425	0.03	4

[a]Used in text.

TABLE XX

Methyl β-cellobioside

Ring	$\overline{NT_1}$	σ	N
A	0.61	0.05	6
B	0.615	0.04	6

Hall[12] (1 molar, 35°C)

A	0.23	0.01	6
B	0.23	0.01	6

TABLE XXI

Cellobiose - Run 7

Ring	$\overline{NT_1}$	σ	N
A_1	0.60	0.03	6
A_2	0.58	0.04	5
B	0.57	0.03	6

Cellobiose - Run 25[a]

A_1	0.485	0.03	6
A_2	0.48	0.01	5
B	0.47	0.01	6

Cellobiose - Run 11

A_1	0.34	0.01	6
A_2	0.33	0.01	5
B	0.335	0.02	6

Cellobiose - Run 35

A_1	0.69	0.05	6
A_2	0.655	0.05	2
B	0.69	0.05	6

[a]Used in text.

TABLE XXII

Xylobiose - Run 19

Ring	$\overline{NT}_1$	σ	N
A_1	0.67	0.06	3
A_2	0.64	0.02	4
B	0.64	0.04	5

Xylobiose - Run 20

A_1	0.73	0.03	4
A_2	0.76	0.04	4
B	0.74	0.03	4

Xylobiose - Run 21[a]

A_1	0.78	0.06	5
A_2	0.79	0.03	4
B	0.79	0.03	5

Xylobiose - Run 24

A_1	0.87	0.08	4
A_2	0.97	0.01	3
B	0.925	0.05	4

[a]Used in text.

TABLE XXIII

Xylobiose - Run 34

Ring	$\overline{NT}_1$	σ	N
A_1	0.95	0.11	4
A_2	0.955	0.08	2
B	0.98	0.07	5

Xylobiose - Run 36

A_1	0.87	0.09	5
A_2	0.92	0.01	2
B	0.85	0.07	5

Xylobiose - Run 37

A_1	0.97	0.07	5
A_2	0.98	0.06	4
B	0.91	0.05	5

TABLE XXIV

Glucose – Run 15

Ring	$\overline{NT}_1$	σ	N
A_1	1.05	0.04	6
A_2	1.005	0.11	4

Glucose – Run 29

A_1	0.83	0.02	4
A_2	0.78	–	1

Glucose – Run 30[a]

A_1	0.75	0.05	6
A_2	0.74	0.04	4

[a]Used in text.

TABLE XXV

Xylose – Run 22

Ring	$\overline{NT}_1$	σ	N
A_1	1.57	0.09	5
A_2	1.60	0.08	4

Xylose – Run 23[a]

A_1	1.59	0.04	4
A_2	1.62	0.06	4

[a]Used in text.

TABLE XXVI

COMPARISON OF $\overline{NT_1}$ RESULTS BY STUDY T TEST

Rings	Run	Cellotetraose			Xylotetraose		Cellotriose		Xylotriose	
		31	32	33	27	28	16	17	18	28
T-I	m	10	10	10	7	7	9	9	4	4
	t_c	5.04	8.32	7.67	22.73	4.92	9.91	5.06	2.62	3.06
	p	99.5	99.5	99.5	99.5	99.5	99.5	99.5	95.0	97.5
I-R_β	m	8	9	7	6	6	6	6	3	3
	t_c	1.06	3.94	3.44	12.55	8.81	3.35	5.01	3.14	6.01
	p	75.0	99.5	99.5	99.5	99.5	99.0	99.5	97.5	99.5
I-R_α	m	8	9	7	6	7	7	7	4	3
	t_c	2.00	4.18	3.58	5.87	8.87	5.96	2.98	1.99	1.82
	p	95.0	99.5	99.5	99.5	99.5	99.5	99.0	90.0	90.0
T-R_β	m	8	9	7	5	6	7	7	5	5
	t_c	2.58	0.45	1.11	0	0	0	1.21	1.33	1.24
	p	95.0	<75.0	75.0	-	-	-	75.0	75.0	75.0

Legend: T = Terminal ring.
  I = Internal ring.
  R_β = Reducing ring of β-anomer.
  R_α = Reducing ring of α-anomer.
  t_c = Calculated student -t value.
  m = $n_1 + n_2 - 2$
  P = Probability that the mean of the two data sets are significantly different. Refer to handbook of standard math tables.
  n_i = Number of data points.

LITERATURE CITED

1. Wehrli, F. W. and Wirthlin, T. Interpretation of Carbon-13 NMR Spectra. Heydron & Sons, New York, 1976.

2. Hall, L. D., Berry, J. M., and Wong, K. F., Carbohyd. Res., 56:C16-20(1977).

3. Levy, G. C., editor. Topics in Carbon-13 NMR Spectroscpy. Wiley-Interscience, New York, 1974.

4. Allerhand, A. and Doddrell, D., Am. Chem. Soc. 93:2777-9(1971).

5. Levy, G. C. and Peat, I. R., J. Magn. Reson. 17:500-21(1975).

6. Bock, K. and Hall, L. D., Carbohyd. Res. 40:C3-5(1975).

7. Preston, C. M. and Hall, L. D., Carbohyd. Res. 37:267-82(1974).

8. Hall, L. D. and Preston, C. M., Carbohyd. Res. 41:53-61(1975).

9. Freeman, R., Hill, H. D. W., and Kaptien, R., J. Magn. Reson. 7:327-9(1972).

10. Hamer, G. K., Balza, F., Cyr, N., and Perlin, A. S., Can. J. Chem. 56:3109-16 (1978).

11. Perkins, S. J., Johnson, L. N., Phillips, D. C., and Dwek, R. A., Carbohyd. Res. 59:19-34(1977).

12. Gorin, P. A. J. and Mazurak, M., Can. J. Chem. 53:1212-23(1975).

13. Pfeffer, P. E., Valentine, K. M., and Parrish, F. W., J. Am. Chem. Soc. 101: 1265-74(1979).

APPENDIX III

PROTON SPIN LATTICE RELAXATION (^{1}H-T_1):
SUMMARY OF DATA

SUMMARY

In the text an equation (1) was developed relating the ratio of relaxation

rates for the anomeric protons to the distance between H_1' and H_4 ($r_1'_{-4}$) in

xylobiose (1) and cellobiose (2).

$$\frac{R_1'}{R_1} = \frac{\sum_s r_1'_s^{-6}}{\sum_s r_{1s}^{-6}}$$

(1)

This equation contains within it several assumptions; including, exclusively dipole-

dipole (DD) relaxation, correlation times in the region of motional narrowing, and

isotropic rotation. In general, it has been shown that these assumptions are valid

for compounds 1 and 2 (1,2). Also implied is the absence of cross relaxation.[*]

Evidence for this is given in Tables I and II which contain the relaxation times for

the individual peaks of the anomeric proton doublets for all the T_1 measurements

made on 1 and 2. Except for the effect of the overlapping solvent peak (HOD) on the

downfield resonance of H_1 at 31°C all values are within 10% for signals arising from

the same proton. This indicates that cross relaxation is not a factor.

A second class of assumptions inherent to the use of Eq. (1) involves the use

of specific and unmeasured values for the distance r_{IS}. Values obtained from a

Dreiding model were compared to those derived from crystallography for the solid,

_____

[*]Nonequivalent relaxation times for different peaks arising from the same proton.

TABLE I

^{1}H-T_1 (SEC) FOR XYLOBIOSE (5% W/V)

Run	Date	Pulse Interval (sec)	Temp. (°C)	Av. α-H-1	H-1 Left	H-1 Right	α-H-1 β-1-1	H-1 Left	H-1 Right
20	9-21	12	31	2.23	1.35	1.24	1.8	0.66	0.70
21	9-24	12	31	2.08	1.45	1.205	1.7	0.69	0.72
33	11-25	10	31.5	1.83	1.87	1.07	1.7	0.52	0.63
34	11-25	10	31.5	1.85	1.18	1.03	1.8	0.51	0.53
22	9-24	12	69.5	4.18	3.49	2.73	1.4	1.94	1.98
35	11-26	22	74.5	3.60	2.40	2.44	1.5	1.52	1.61
36	11-26	22	74.5	3.70	3.41	3.38	1.1	1.58	1.67
31	11-20	10	AMB	1.90	1.24	1.02	1.9	0.54	0.55
32	11-20	10	AMB	1.81	1.01	0.99	1.8	0.52	0.56

Comments

Run 20 – Error in data set 3.
Run 33 – Poor baseline.
Run 22 – Poor resolution.
Run 36 – Pulse may be non-90°.
Run 32 – Only 5 data points.

^{13}C-T (sec) for Xylobiose (5% W/V)

Run	Date	Pulse Interval	Temp. (°C)	C-1'	C-1	Av. ^{13}C-T_1
34	9-23		31	1.01	1.05	0.95 ± 0.09
36	11-20		AMB	0.88	0.99	0.85 ± 0.09
37	11-23		31.5	1.07	0.845	0.95 ± 0.06

TABLE II

^1H-T_1 (SEC) FOR CELLOBIOSE (5% W/V)

Run	Date	Pulse Interval (sec)	Temp. (°C)	Av. α-H-1	H-1 Left	H-1 Right	α-H-1/β-1-1	H-1 Left	H-1 Right
24	10-1	12	31	1.02	3.24	0.87	1.2	0.58	0.61
25	?	12	31	1.49	1.98	1.01	2.0	0.45	0.47
26	10-12	10	31	1.55	1.34	0.845	1.8	0.39	0.39
27	10-13	10	31	1.64	1.21	0.89	1.8	0.38	0.39
29	10-27	10	31	1.51	1.57	0.81	1.9	0.37	0.39
30	10-27	10	31	1.52	1.62	0.79	1.9	0.35	0.37
Hall			33	1.6		0.84	0.36		
28	10-14	24	68.5	3.48	1.90-2.25	2.10-2.36	1.6	1.26	1.32
37	12-1	22	74.5	3.97	2.04	2.08	1.9	1.08	1.14
38	12-1	22	74.5	4.09	2.19	2.23	1.9	1.12	1.19

Comments

Run 24 - Only 7 data points.
Run 28 - Poor resolution.

^{13}C-T (sec) for Celloboise (5% W/V)

Run	Date	Pulse Interval	Temp. (°C)	C-1'	β C-1	Av.
35	10-27		31	0.67	0.73	0.70 ± 0.06

and when used, produced entirely reasonable estimates for $r_{1'-4}$. Despite this close correspondence, it would be useful to investigate the accuracy of the data independent of the specific proton-to-proton distances measured above. This is particularly necessary in view of the r^{-6} dependence on distance. An alternate approach is to compare the $^1H-T_1$ and $^{13}C-T_1$ values and to show that an approximate estimate of $r_{1'-4}$ can be obtained independently of any specific value for the several proton to proton distances involved. In so doing, confidence is gained in the values obtained both for the $^{13}C-T_1$ and $^1H-T_1$ measurements.

The relationship for the DD spin lattice relaxation rate for both ^{13}C and ^1H is the same except that the magnetogyric ratio of the ^{13}C-nucleus is involved in the former. Assuming isotropic rotation, the relaxation rates for $H_{1'}$, H_1 and all singly protonated carbons are given by Eq. (2)-(4).

$$R_1 = K \, T_{eff} \sum_{intra} r_{1S}^{-6} \qquad (2)$$

$$R_{1'} = K \, T_{eff} \left(\sum_{intra} r_{1'S}^{-6} + \sum_{inter} r_{1S}^{-6} \right) \qquad (3)$$

$$R_C = C \, T_{eff} \, r_{CH}^{-6} \qquad (4)$$

In these equations K is given by,

$$K = \hbar^2 \, \gamma_H^4 \qquad (5)$$

while C is given by,

$$C = \hbar^2 \, \gamma_H^2 \, \gamma_C^2 \qquad (6)$$

In Eq. (2) only intraring contributions to R_1 are considered while in Eq. (3) additional contributions from inter-ring ($r_{1'-4}$ predominantly) protons are present.

Because of the close proximity of the directly bonded proton it is the only significant factor in the relaxation of a singly protonated ^{13}C nucleus. The assumption that the rotation is isotropic infers that all singly bonded carbon nuclei relax at the same rate. This is approximately true for $\underset{\sim}{1}$ and $\underset{\sim}{2}$ so that an average $^{13}C\text{-}T_1$ value can be used.

Subtraction of Eq. (2) from Eq. (3) gives

$$R_1{}' - R_1 = K\ T_{eff}\cdot r_1{}'_{-4}{}^{-6} \tag{7}$$

if the intraring contributions are assumed to be equal. Dividing Eq. (7) into Eq. (4) eliminates the correlation time.

$$\frac{R_C}{R_1{}' - R_4} = \frac{\gamma_C^2}{\gamma_H^2}\ \frac{r_1{}'_{-4}{}^6}{r_{CH}^6} \tag{8}$$

Rearrangement of Eq. (8) gives the ratio of $r_1{}'_{-4}$ to r_{CH} in terms of the carbon and proton relaxation times and independent of any specific proton to proton distance

$$\left(\frac{\gamma_H^2}{\gamma_H^2}\right)^{1/6}\left(\frac{R_C}{R_1{}'(1-R_1/R_1{}')}\right)^{1/6} = \left(\frac{r_1{}'_{-4}}{r_{CH}}\right) \tag{9}$$

$$1.58\ (R_f)^{1/6}\ r_{CH} = r_1{}'_{-4} \tag{10}$$

The average value for r_{CH} from the carbohydrate crystallographic studies is 1.05 Å. This value should not change in solution. Table III gives average values for R_1, $R_1{}'$, R_C, and R_f. The R_C values (See Appendix II) came from Tables I and II. Substitution of these values into Eq. (8) gives an estimate of 1.7 Å for $r_1{}'_{-4}$ for both compounds. This is independent of any unmeasured proton to proton distance.

Given the many assumptions made in the derivation of Eq. (8) it is not a bad esti-mate and indicates the reasonableness of the measured ^{13}C and ^1H relaxation times. On the other hand, Eq. (10) is not very sensitive to the ratio of R_C/R_1' because of the 1/6 dependence and can't be used to compare $r_1'_{-4}$ for $\underset{\sim}{1}$ and $\underset{\sim}{2}$.

TABLE III

AVERAGE VALUES FOR R_1, R_1', R_c AND R_f FOR XYLOBIOSE AND CELLOBIOSE

	Temp.(°C)	R_1/R_1'	$1 - \dfrac{R_1}{R_1'}$	R_1'	R_c	$\dfrac{R_c}{R_1'}$	R_f	$R_f^{1/6}$
Cellobiose	31	0.45	0.55	2.64	1.42	0.54	0.98	1.00
Xylobiose	31	0.54	0.46	1.64	0.95	0.58	1.26	1.04

SOURCES OF ERROR

Tables I and II contain the results for all the $^1H-T_1$ measurements made on degassed samples of $\underset{\sim}{1}$ and $\underset{\sim}{2}$. Sources of potential error in the measurement of relaxation times were covered in Appendix II. In the case of ^1H relaxation the location of most of the hydrogen nuclei are on the periphery of the molecule which makes it imperative that paramagnetic species be removed. This is necessary to eliminate any contribution from electron-proton DD relaxation. To avoid paramagne-tic contributions in the present work the samples were subject to 4 freeze-pump-thaw cycles to remove dissolved oxygen. The tubes were then immediately sealed. Paramagnetic ions which might be present in compound $\underset{\sim}{1}$ from the Koenigs-Knorr or catalytic hydrogenation steps were removed by treatment with an ion-exchange resin. Purchased cellobiose was used without further purification.

Errors related to instrumental operation also occasionally occurred; primarily due to poor resolution from improper set-up, field-frequency instabilities, or loss of lock. Runs containing these types of errors are indicated in Tables I and II and

were not included in the final values used to get average R_1 and R_1' values. The final values are given in Table IV along with those from the literature for comparison (3). Data were rejected for use if the signal-to-noise-ratio was low, if a poor baseline was observed, or if poor peak resolution was obtained. In each case rejected data had a ratio of $R_{\alpha-1}/R_{\beta-1}$* of less than 1.8. Hall (3) reports that this ratio is constant and between 1.8 and 2.0 for all β-1,4-linked disaccharides and glucose. All the data used to calculate the average R_1'/R_1 values at 31°C had values of 1.8-2.0. The α-H_1 peak is particularly sensitive to problems with signal to noise or resolution because of its low intensity which makes it a good indicator of low quality data.

TABLE IV

RATIO OF ^1H-T_1 FOR REDUCING END
AND LINKAGE ANOMERIC PROTONS

Compound	Run	Temp.	H_1	H_1'	$\dfrac{H_1}{H_1'}$	Av.
Cellobiose	25	31	1.01	0.46	2.2	
	26	31	0.845	0.39	2.2	
	27	31	0.89	0.385	2.3	
	28	31	0.81	0.38	2.1	
	29	31	0.79	0.36	2.2	
						2.2±0.1
	Hall	33	0.84	0.36	2.3	
	Hall	42	1.1	0.52	2.1	
	37	74.5	2.06	1.11	1.9	
	39	74.5	2.21	1.16	1.9	
						1.9
Xylobiose	31	AMB	1.02	0.545	1.9	
	21	31	1.205	0.705	1.7	
	34	31.5	1.03	0.51	2.0	
						1.85±0.2
	35	74.5	2.42	1.565	1.5	
						1.5

At 31°C only 1 peak of the H_1' doublet is usable due to overlap by the Hob peak. All other values are averages for both peaks of the doublet.

Figure 1 shows a typical stack plot obtained in the ^1H-T_1 measurement of cellobiose.

*$R_{\alpha-1}$ refers to the relaxation rate for H_1 of the α-anomer; $R_{\beta-1}$ refers to the β-anomer.
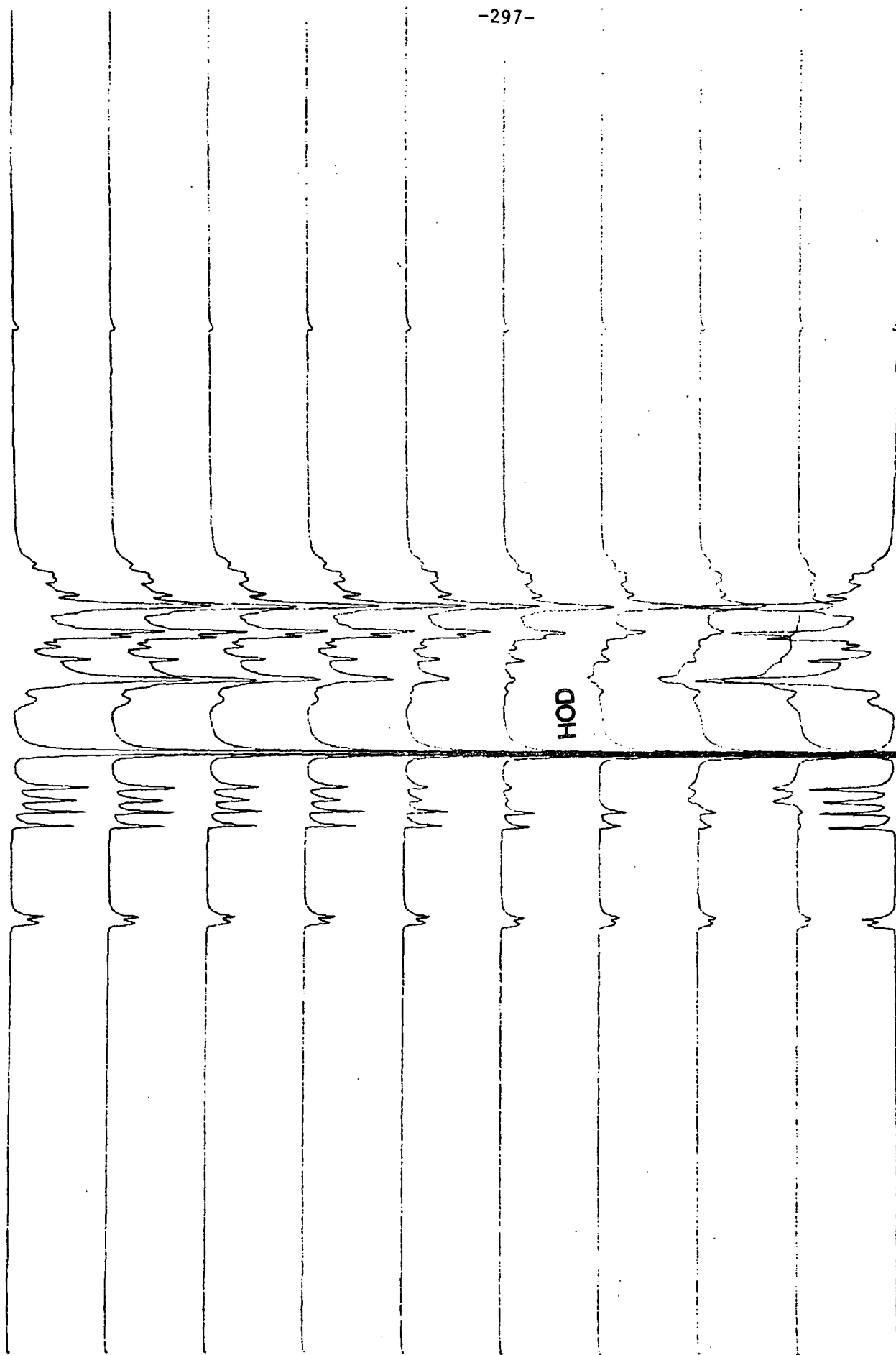
Figure 1. ^1H-T_1 relaxation data for cellobiose in D_2O at 74.5°C. The anomeric protons are downfield of the HOD signal.

HOD

LITERATURE CITED

1. Part 2, Section 2.

2. Preston, C. M. C., Applications of fourier transform NMR spectroscopy: proton spin lattice relaxation in organic molecules. Doctoral Dissertation, The University of British Columbia. October, 1975.

3. Hall, L. D. and Preston, C. M., Carbohyd. Res. 49:3-11(1976).

APPENDIX IV

GATED DECOUPLING TO OBTAIN PROTON
COUPLED ^{13}C-NMR SPECTRA WITH NOE

Measurements of natural-abundance proton coupled ^{13}C-NMR spectra can simply be made using a modern FT-NMR spectrometer. If the measurement must be made at low concentrations or with limited sample this can often involve very long (several days) acquisition times to obtain a reasonable signal to noise ratio. For this reason it is customary to use a gated decoupling technique which maintains the NOE advantage of regular decoupled ^{13}C-NMR but provides a fully coupled spectrum. The NOE represents a potential 3-fold increase in the carbon signal as a result of proton decoupling (see Appendix II).

The pulse sequence used is shown in Fig. 1. The top portion (a) of the figure shows the duty cycle of the ^{13}C detecting pulse. It is turned on and off in the same manner as the regular decoupled experiment except that a slightly longer interval between pulses is maintained to allow the NOE to build up. The receiver is turned on shortly after the pulse to acquire the signal (AT).
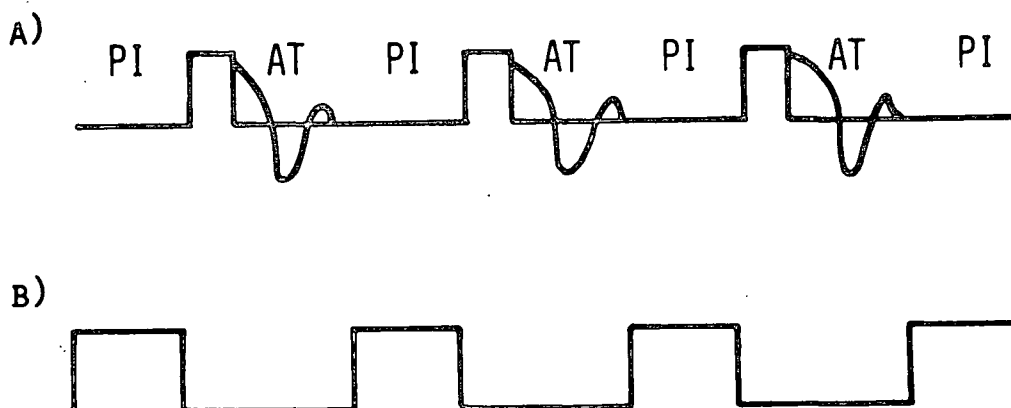
Figure 1. a) Duty cycle of the detecting pulse. AT is the acquisition time and PI the pulse interval. b) Duty cycle of the decoupler.

The middle diagram (b) depicts the duty cycle of the decoupler. In a standard decoupled ^{13}C-NMR experiment the decoupler is left on continuously. For gated decoupling it is only on from the completion of acquisition to just prior to the detecting pulse (PI). In this way the NOE builds up in the usual way. During the actual acquisition the decoupler is off so that coupling is observed between the ^{13}C and ^{1}H nuclei (1).

The theory of the gated decoupling technique is given elsewhere (2).

LITERATURE CITED

1. Gray, G. A., Anal. Chem. 47:546A-75A(1975).

2. Shaw, D. Fourier transform NMR spectroscopy. New York, N.Y., Elsevier Scientific Publishing Company, 1976. p. 357.

APPENDIX V

$^{13}C-^{1}H$ COUPLING CONSTANT DATA

This appendix tabulates the data concerning $^{13}C-^{1}H$ coupling constants for the β-1,4-linked carbohydrates and related monosaccharide models. Part A contains the data in tabulated form. Part B gives representative spectra with partial assignments.

TABULATED DATA

Key: Refer to footnotes for additional information.

$\nu_{1/2}$ = width at half height.
J = coupling constant.
I = indeterminant in present spectra.

TABLE I

COMPARISON OF $\nu1/2$ FOR C_1' AND C_1 IN D_2O

	C_1'			C_1			$\Delta\nu1/2$	
	1_J	Multiplicity[c]	$\nu1/2$[b]	1_J	Multiplicity[c]	$\nu1/2$[b]	Internal	External
Glucose Containing								
methyl β-cellobioside	161[a]	C	I	161.7	T	I	-	-
methyl β-cellobioside-d₈	162.8	C	7.9-9.2	162.0	C	13.9-15.2	-	3.1-4.4[d]
β-cellobiose	162.0	S	10.7-10.9	161.6	D	8.8-9.8	1.4[a]	1.4[a,e]
methyl β-glucoside-d₄				160[a]	6	11.9		
β-glucose				161.3	D/D	9.4		
Xylose Containing								
methyl β-xylobioside	163[a]	C	20.5[a]	160[a]	8	20.3	-	0.6[e]
β-xylobiose	161.6	5-8	20.4	162.3	5-6	19.1	0.1	0.5[e]
methyl β-xyloside-d₂				161[a]	8	19.8		
β-xylose				161.9				

[a] Approximate value only; generally ± 1 Hz.

[b] Indeterminant (I) due to overlap or poor spectral quality. Values from single peak or average of both. A range refers to more than one spectrum.

[c] C = complex, S = singlet, D = doublet, T = triplet, Q = quadret, D/D = doublet of doublets. Refers to coupling of more than one bond.

[d] Using 4.8 Hz for $\nu1/2$ of β-D-glucose-2,3,4,5,6,6´-d₅ formed from the enzymatic hydrolysis of MBC2-d₈. Value measured directly from Fig. 2 in Ref. (1). Measurement of $\nu1/2$ for MBC2-d₈ from the same figure gives a value of 9.3 Hz. Taking the difference gives a value of 4.5 Hz which is similar to the calculated value of 4.3 Hz obtained by computer simulation.

[e] Relative to xylose or glucose.

TABLE II

COMPARISON OF $\nu_{1/2}$ FOR C_1' AND C_1 IN DMSO-d_6

	C_1'			C_1			$\Delta\nu_{1/2}$	
Glucose Containing	Multiplicity	^1J	$\nu_{1/2}$[b]	Multiplicity	^1J	$\nu_{1/2}$[b]	Internal	External
methyl β-cellobioside	s	159.9	I	s	156.2	I	1.4	1.1[e]
β-cellobiose	Q	160[a]	12.1	Q	I	10.7	0.5	0.1[e]
β-lactose	s	159.7	11.1	D	158[a]	10.6		0.8[e]
4-O-β-D-glucosyl-D-mannose	s	158.3	11.8	s	167.1[f]	10.2[f]		
4-O-β-D-glucosyl-D-xylose	s	159.7	11.4	I	159[a]	I		
methyl β-glucoside				s	156.7	13.7		2.7
β-glucose				s	156.7	11.0		
α-maltose[d]	s	167.5	10.2	s	165.0	7.2	3.0	2.5
β-maltose[d]		167.5	-	s	156.7	11.8		
Xylose Containing								
methyl β-xylobioside	I	162	21.8[a]	I	I	20[a]		3.0[a,e]
β-xylobiose	Q	160.5	19.6	Q	160.5	19.4	0.2	0.8[e]
methyl β-xyloside				Q	158.2	20.4		
β-xylose				Q	157.2	18.8		1.6[e]

a-c Same as Table I. Value of 3.5 for $\Delta\nu_{1/2}$ in D_2O (2).

d α-1,4-linked.

e Relative to xylose or glucose. The coupling $^2J_{COH}$ is not factored out.

f Value for α-C_1.

TABLE III

COMPARISON OF νl/2 FOR LINKAGE AND NONLINKAGE C_4 IN D_2O

Glucose Containing	Linkage C_4			Nonlinkage C_4			Δνl/2	
	^1J	Multiplicity[c]	νl/2[b]	^1J	Multiplicity	νl/2[b]	Internal	External
methyl β-cellobioside	147[a]	s	11.6	148.5[a]	s	I		1.6-3.1[d]
methyl β-cellobioside-d8	147.2[a]	s	9.5	-	-	-		1.7-1.9[f]
β-cellobiose	148[a]	s	<10.9-12.2[e]	150[a]	s	I		0.9-3.7[d]
Xylose Containing								
β-xylobiose	144.8	s	I[e]	I	-	I		
methyl β-xylobioside	I	s	12.0-12.5[e]	148[a]	D	I		

a-c Same as Table I.

d Methyl β-maltoside is reported as 8.5 Hz while phenyl β-maltoside is 10.0 Hz for C-4 (2)

e Broadened by nondegenerate α- and β-anomers. Therefore, value is an upper limit.

f Compared to methyl β-D-glucoside-3,6,6'-d3 value for νl/2 of 7.6-7.8 in Ref (1).

TABLE IV

COMPARISON OF $\nu 1/2$ FOR LINKAGE AND NONLINKAGE C_4 in DMSO-d_6

	Linkage C_4			Nonlinkage C_4		
Glucose Containing	1_J	Multiplicity[c]	$\nu 1/2$[b]	1_J	Multiplicity	$\nu 1/2$[b]
methyl β-cellobioside	143[a]	S	12.1	142.8	S	11.4
β-cellobiose	I	S	<14.8[d]	143.6	S	13.7[a]
4-0-β-D-glucosyl-D-mannose	145.8[a]	S	<14.1[d]	I	S	11.0
methyl β-glucoside				143.1	S	11.4
β-glucose				143.6	S	<12.4[d]
Xylose Containing						
β-xylobiose	I	I	I	I	S	11.6
methyl β-xyloside				144.0	S	11.3
β-xylose				143.6	I	I

a-c Same as Table I.
d Measured value but since α-C_4 and β-C_4 are slightly resolved this is a maximum value.

TABLE V

COMPARISON OF ν1/2 IN DMSO-d6 AND D2O

	DMSO-d6				D2O				
	1_J	Multiplicity[c]	m_J	$ν1/2^b$	1_J	Multiplicity[c]	m_J	$ν1/2^b$	$Δν1/2$
α-C1									
Cellobiose	164.9[a]	s	-	8.0	170.0	s	-	3.3-3.6	
Lactose	170[a]	s	-	7.2	-	-	-	-	
4-O-β-D-glucosyl-D-xylose	170[a]	c	-	I	-	-	-	-	
Glucose	164.1	s	-	7.7	169.7	s	-	3.2	
Xylobiose	166	C	-	12.6	169.7	C	-	9.0	
Xylose	164.6	D/D	I	11.5	169.8	D/D	2.4/5.9	9.6	
Maltose	165.0	s	-	7.2	-	-	-	-	
OCH3									
methyl β-cellobioside	142.2	D	4.7	7.5	143[a]		4.4	6.3	1.2
methyl β-cellobioside-d8					144.3		4.6	6.4	1.1
methyl β-glucoside	142.1	D	4.3	6.6					
methyl β-glucoside-d4					144.3		4.6	6.0	0.6
methyl β-xyloside	142.2	D	4.5	6.4					
methyl β-xyloside-d2					144.5		4.5	6.3	0.1

a-cSee Table I.

TABLE VI

ONE BOND (^1J) COUPLING CONSTANTS IN D_2O

	Carbon												
	1'	2'	3'	4'	5'	6'	1	2	3	4	5	6	OCH$_3$
MBC2	161[a]	143[a]	146[a]	148.5[a]	141[a]	145	161.7	143[a]	146[a]	147[a]	145[a]	145[a]	143[a]
MBC2-d$_8$	162.8				141.8		162.0	145[a]		147.2	143.8[a]		144.3
β-Cellobiose	162.0	147[b]	148[b]	150[a]	143.6	143.6	161.6	145.1[a]	142.9	148[b]	144.0	144.0	
α-Cellobiose	-	-	-	-	-	-	170.0	145[a]	145[a]	-	-	-	
MBX2	163[a]			148[a]									144.0
β-Xylobiose	161.6	145.9					162.3			144.8			
α-Xylobiose							169.7						
MBX-d$_2$							161[a]						144.5
β-Glucose							161.3	144.0	143.5[a]	-	143[a]	144[a]	
α-Glucose							169.7	145[a]	146.5	-	145[a]	144	
β-Xylose							161.9	145.2	144.0	147.5	142.0[a] 143.6[a]		
α-Xylose							169.8	144.8	144.4	147[a]			

a ± 1 Hz.
b ± 3 Hz.

TABLE VII

ONE BOND (^1J) COUPLING CONSTANTS IN DMSO-d_6

	1'	2'	3'	4'	5'	6'	Carbon 1	2	3	4	5	6	OCH$_3$
MBC2	169.9	143[a]	142[a]	142.8	142[a]	140.4[a]	156.2	143[a]	140[a]	143[a]	140[a]	140[b]	142.2
β-Cellobiose	150[a]	144[a]	-	143.6	-	139.2	-	-	-	-	-	140.5	
α-Cellobiose	-	-	-	-	-	-	164.9	-	-	-	-	-	
β-Lactose	159.7						158[a]						
α-Lactose							170[a]						
α-GM	158.3						167.1			145.8			
β-GX	159.7						159[a]						
α-GX							170[a]						
MBX2	162.5	144[a]											
β-Xylobiose	160.5						160.5						
α-Xylobiose							166						
β-Maltose	167.5					140[a]	156.7						140[a]
α-Maltose	167.5						165.0						
MBG							156.7	141.1	140[a]	143.1	140[a]	139.5[b]	142.5
MBX							158.2	142.6	138.7	144.0	149.4 / 140.1	-	142.2
β-Glucose							156.7	141.6	140[a]	143.6	140[a]	140[a]	
α-Glucose							157.2	141.6	142.6	143.6[a]	139.4 / 148.2	-	
β-Xylose							164.6	141.1	147[a]	143.6	-	-	

a ± 1 Hz.
b ± 3 Hz.

TABLE VIII

Apparent Long Range Coupling Constants

Compound	Solvent	^2J	^3J	System
β-Glucose	D_2O	5.6		C_1H_2
			<2	C_1H_5
		4.6		C_2H_3
α-Glucose	D_2O	5.6[a]/5.4		$C_3H_4{}^b, C_3H_2{}^b$
β-Xylose	D_2O	5.5		C_1H_2
			2.7	C_1H_5
			10.2	$C_1H_5{}^a$
		5.1		C_2H_3
		3.4-4.4		$C_5H_4{}^b$
α-Xylose	D_2O		2.8	$C_1H_{5_a}$
			5.8	$C_1H_{5_e}$
		3.9		$C_2H_3{}^b$
		2.7		$C_5H_4{}^b$
β-Xylobiose	D_2O	5.7		C_1H_2
			2.8	$C_1H_5{}^a$
			10.3	$C_1H_5{}^e$
		4.8		$C_2{}^-H_3{}^b$
β-Cellobiose	D_2O	5.4-5.9		C_1H_2
			<2	C_1H_5
β-Cellobiose	D_2O	5.9[a]		C_3H^a
		3[a]		C_2H_3
methyl β-cellobioside	D_2O	6.5		$C_3{}^-H^b$
		6.3		C_3H^b

[a] Possibly part of a complex pattern.
[b] Assumed coupling system.

Xylose

a

b

110   100   90   80   70   60   50

PPM
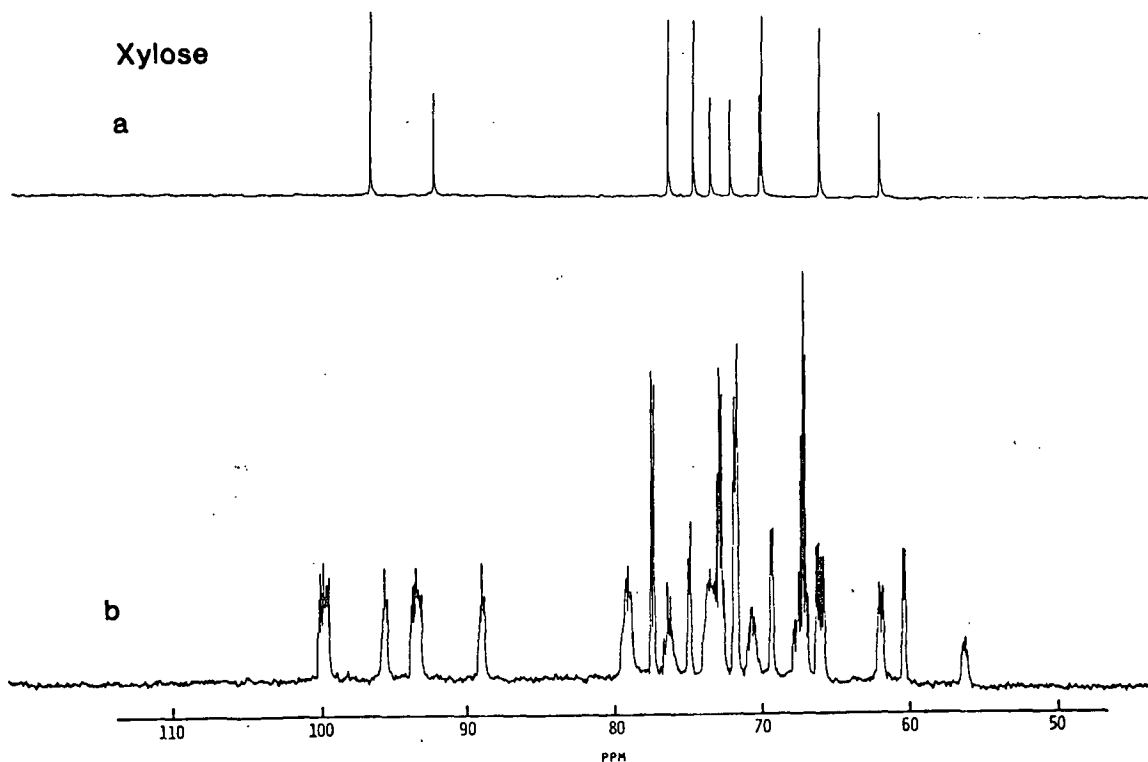
Figure 1. Proton decoupled (a) and proton coupled (b) ^{13}C-NMR spectra of xylose in D$_2$O. Assignment of the decoupled spectrum is as follows: 97.3 (β-C$_1$), 92.9 (α-C$_1$), 76.5 (α-C$_3$), 74.8 (β-C$_2$), 73.6 (α-C$_3$), 72.2 (α-C$_2$), 70.1 (α-C$_4$), 70.0 (β-C$_4$), 65.9 (β-C$_5$), and 61.7 (α-C$_5$). Full scale is 2000 Hz.

10.2 Hz C$_1$H$_{5e}$
5.5 Hz C$_1$H$_2$
2.7 Hz C$_1$H$_{5a}$

13.3Hz

β-1 α-1 β-1 α-1
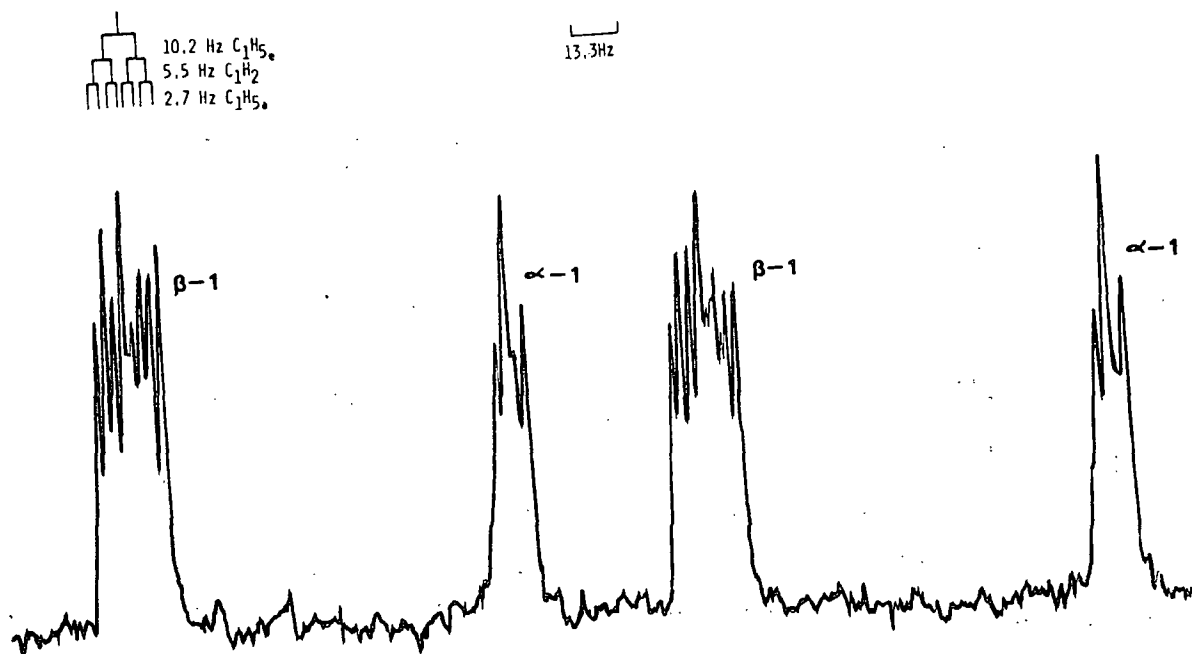
Figure 2. Expansion of C$_1$ region of Fig. 1. Detailed first order analysis of the downfield β-C$_1$ signal is given on the figure. Full scale is 333.3 Hz.
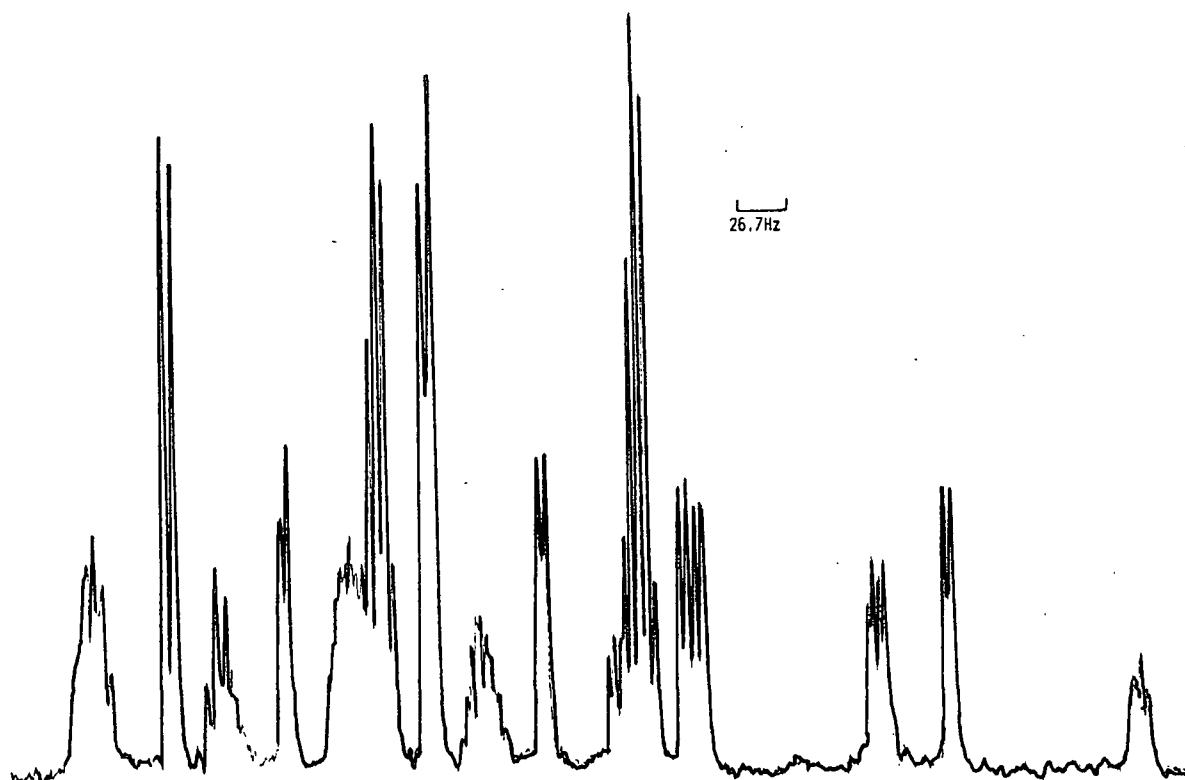
Figure 3. Expansion of the region from 55-80 ppm in Fig. 1. Full scale is 666.5 Hz.
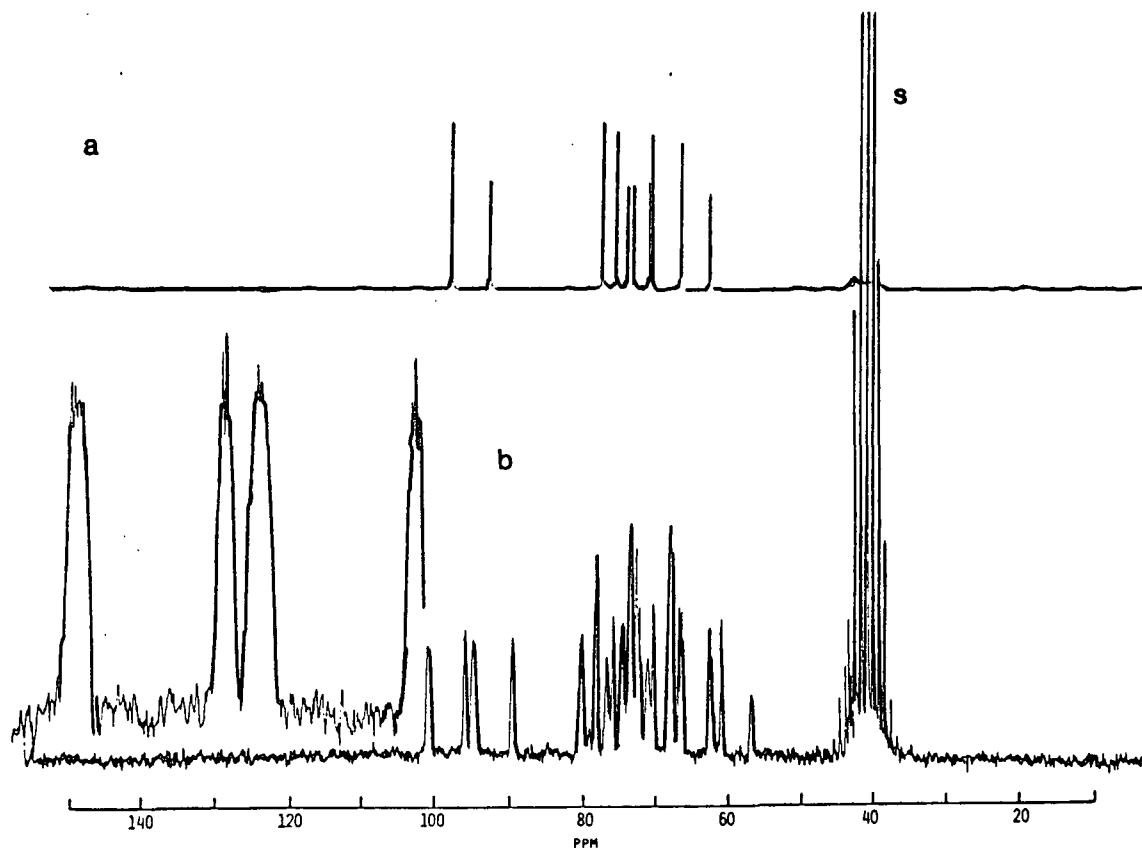
Figure 4. Proton decoupled (a) and proton coupled (b) ^{13}C-NMR spectra of xylose in DMSO-d$_6$. Full scale is 4000 Hz. Inset is the C1 region expanded 2X.

a Methyl β-Xyloside

b

140   120   100   80   60   40   20
PPM
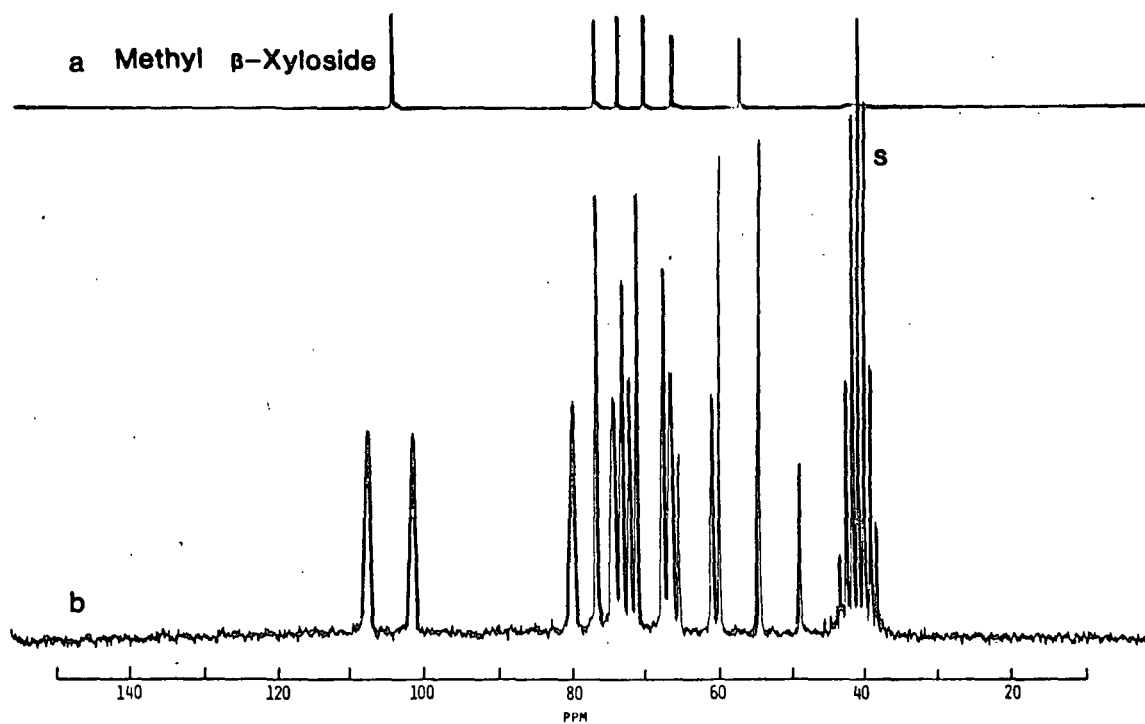
Figure 5. Proton decoupled (a) and proton coupled (b) ^{13}C-NMR spectra of methyl
β-xyloside in DMSO-d$_6$. Assignment of (a) is as follows: 104.7 (C$_1$),
76.6 (C$_3$), 73.3 (C$_2$), 69.7 (C$_4$), 65.7 (C$_5$) and 56.0 (OCH$_3$). Full scale
is 4000 Hz.

40Hz
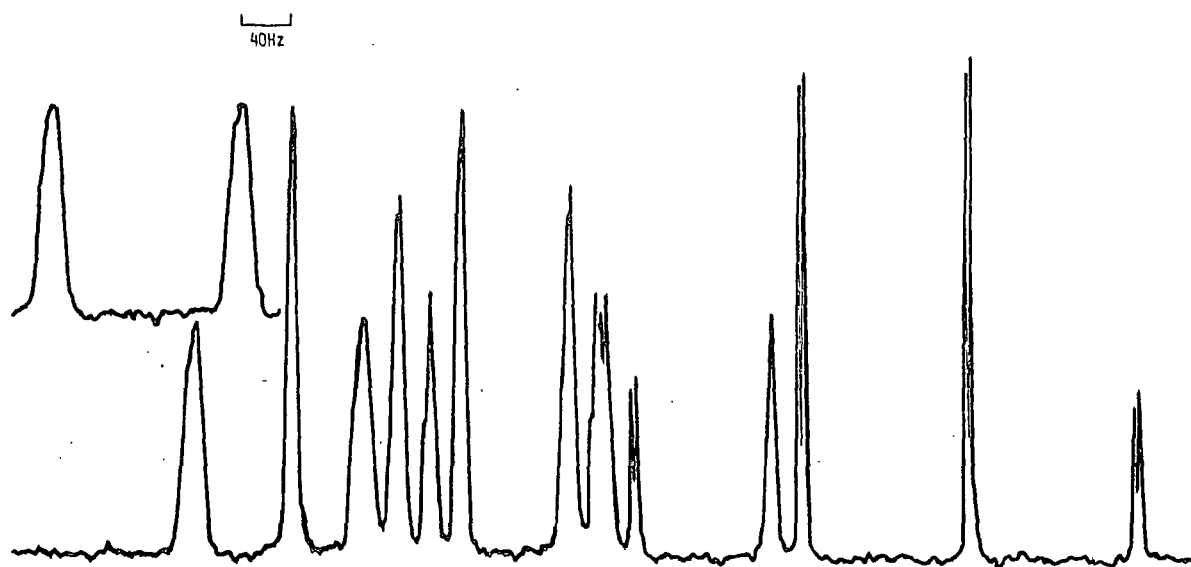
Figure 6. Expansion of Fig. 5. Inset is the C$_1$ region. Full scale is 1000 Hz.
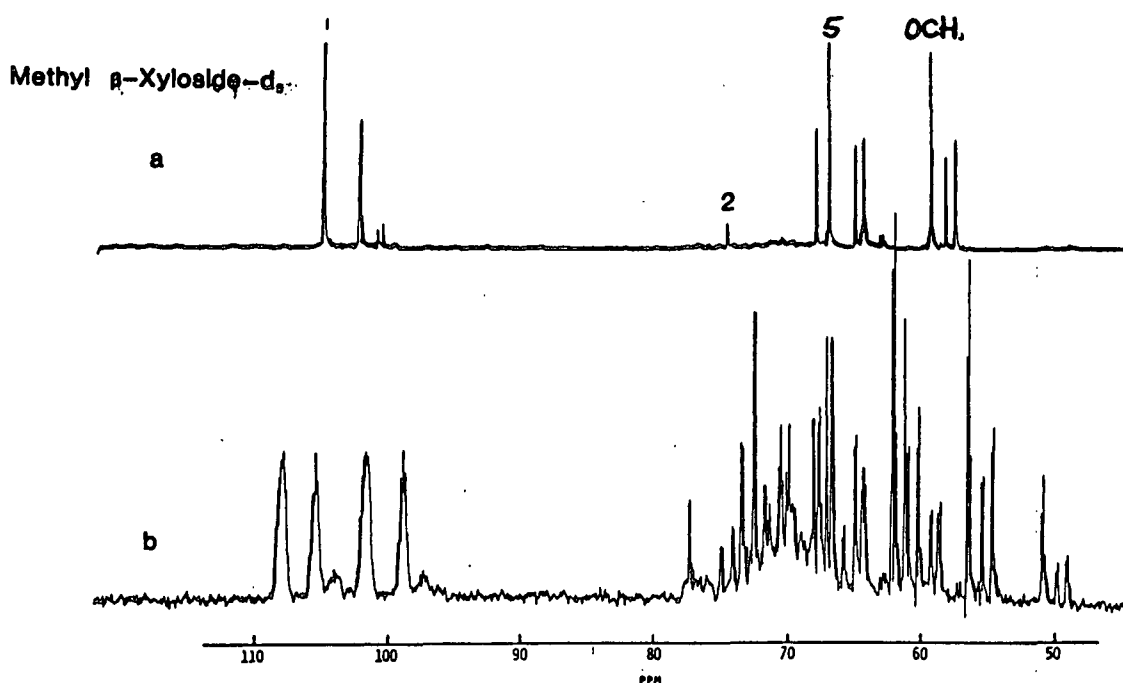
Figure 7. Proton decoupled (a) and proton coupled (b) ^{13}C-NMR spectra of methyl β-xyloside-3,4-d$_2$ in D$_2$O. Assignments are shown. Significant isomerization is apparent with at least 4 isomers indicated in the C$_5$ and OCH$_3$ regions. A small residual C$_2$ signal also is present illustrating the difficulty in exchanging this carbon. Full scale is 2000 Hz.
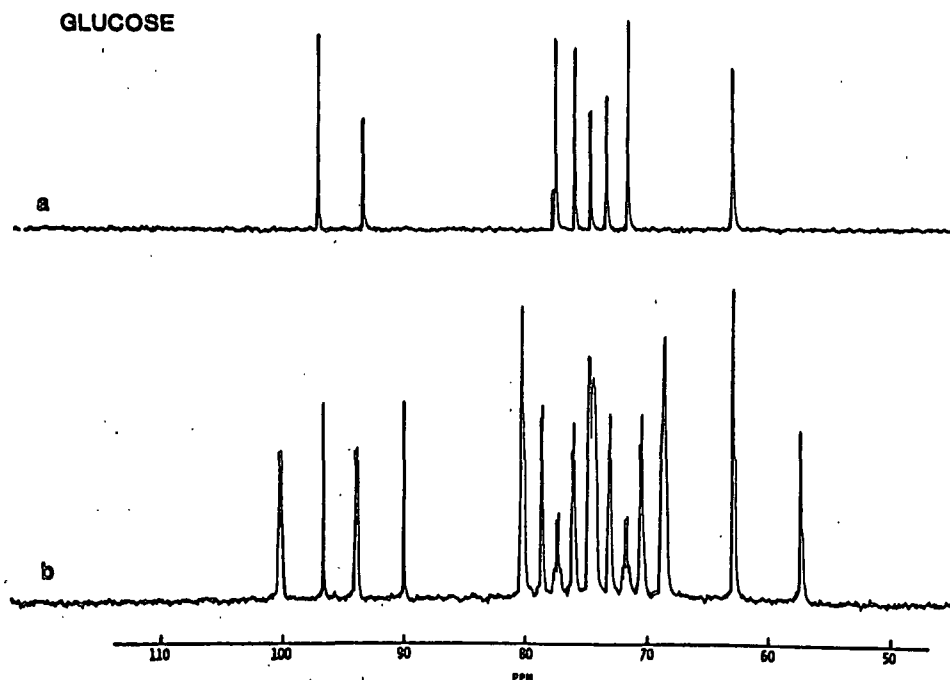
Figure 8. Proton decoupled (a) and proton coupled (b) ^{13}C-NMR spectra of glucose in D$_2$O. Assignment of (a) is as follows 96.6 (β-C$_1$), 92.8 (α-C$_1$), 76.6 (β-C$_5$), 76.5 (β-C$_3$), 74.9 (β-C$_2$), 73.5 (α-C$_3$), 72.2 (α-C$_2$ or α-C$_5$), 72.1 (α-C$_2$ or α-C$_3$), 70.4 (α-C$_4$), 70.3 (β-C$_4$), 61.5 (β-C$_6$), 61.4 (α-C$_6$). Full scale is 2000 Hz.
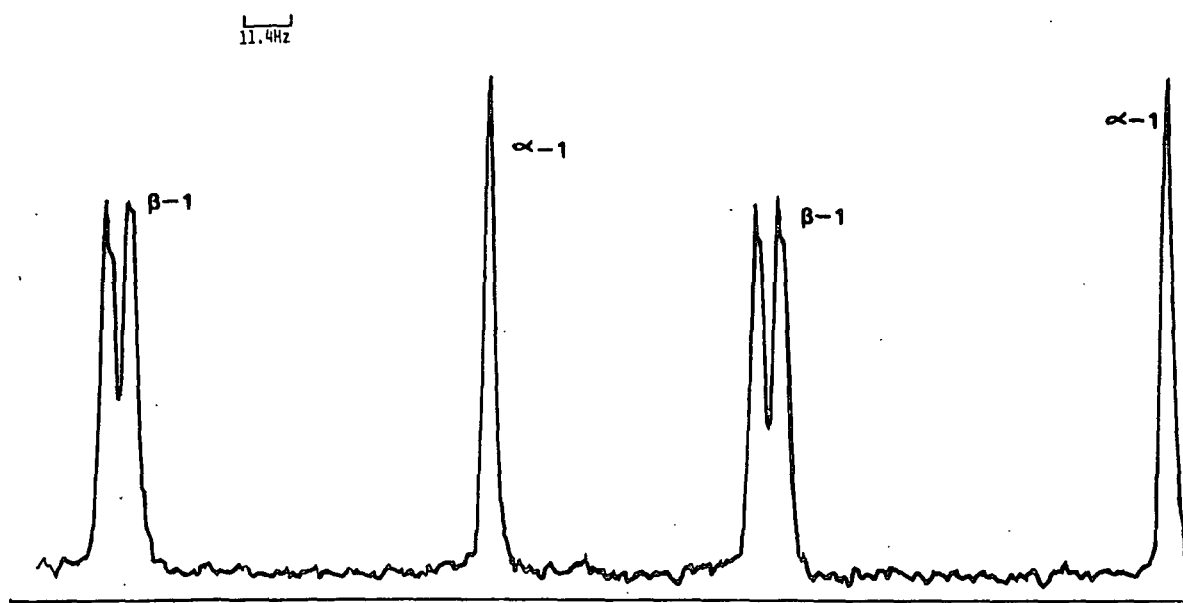
Figure 9. Expansion of the C_1 region of Fig. 8. Full scale is 285.6 Hz.
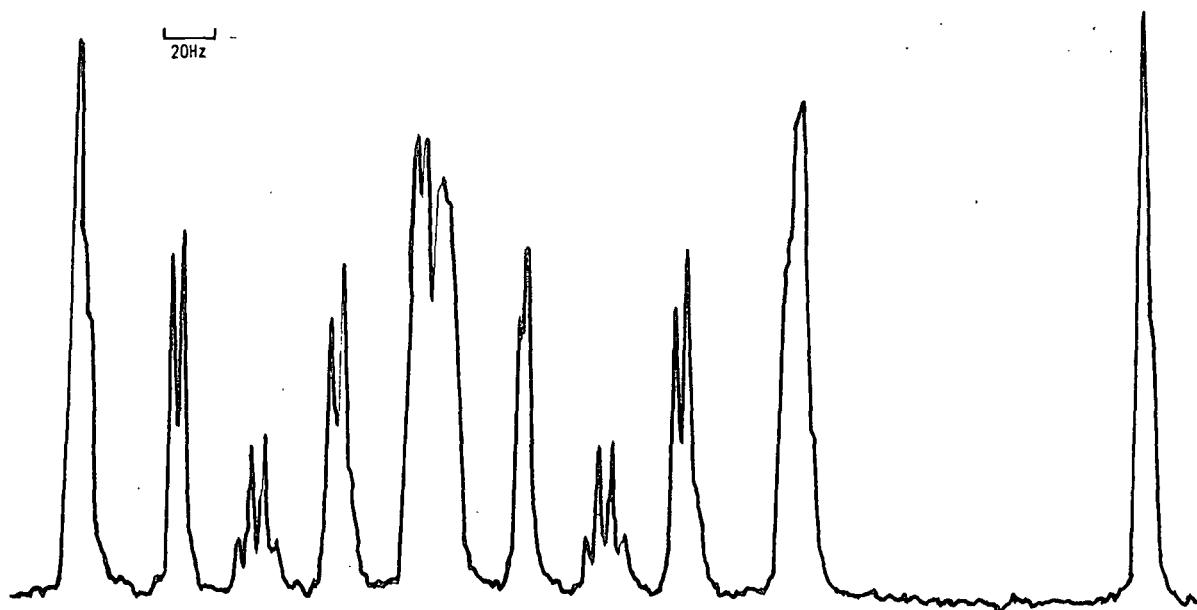
Figure 10. Expansion of upfield proton of Fig. 8. Full scale is 500 Hz.
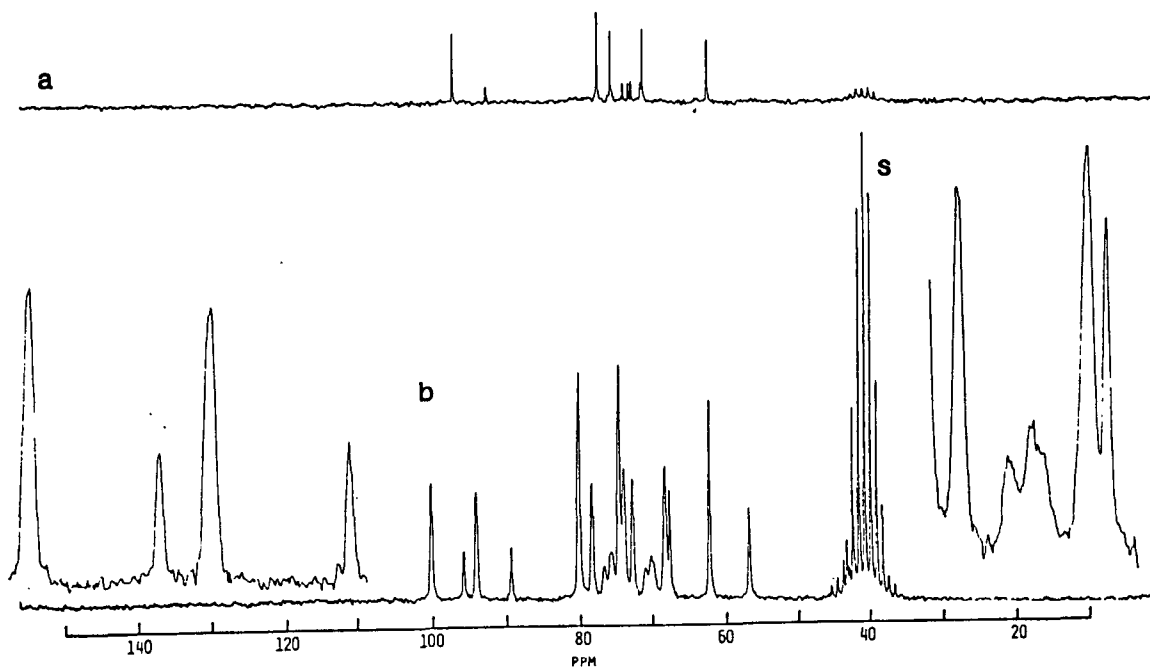
Figure 11. Proton decoupled (a) and proton coupled (b) ^{13}C-NMR spectra of glucose in DMSO-d_6. Full scale is 4000 Hz. Insets are the C_1 and C_4 regions at 1000 Hz full scale.

Methyl β-Glucoside
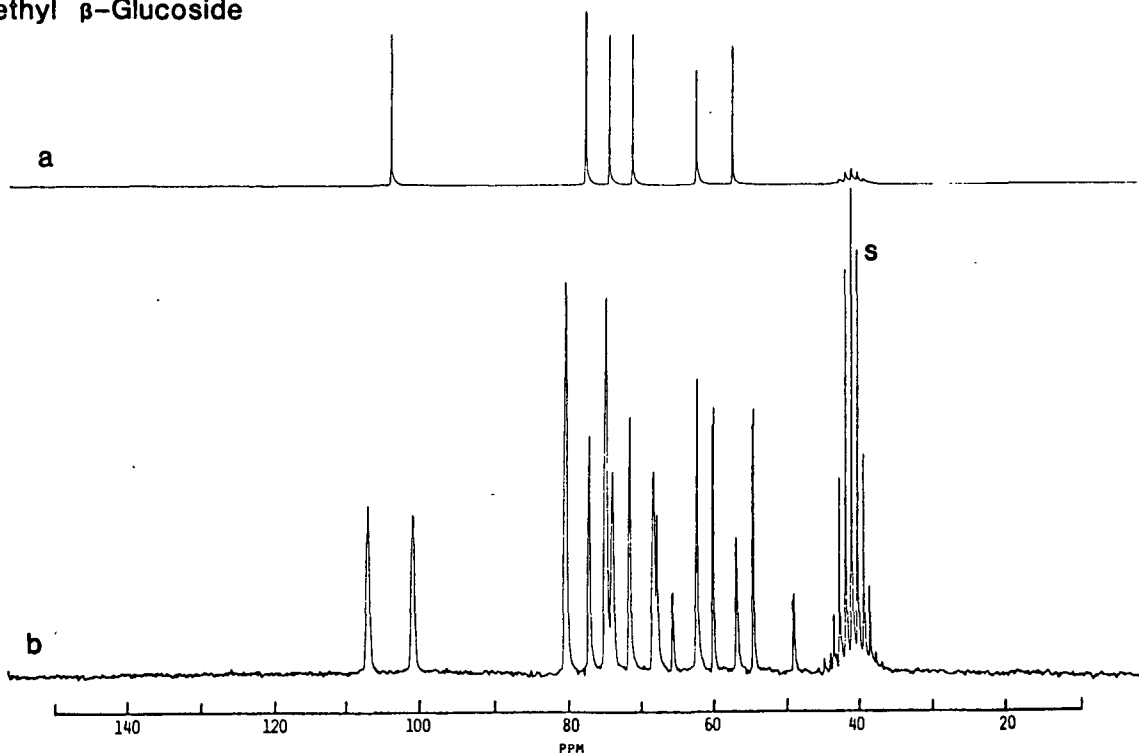
Figure 12. Proton decoupled (a) and proton coupled (b) ^{13}C-NMR spectra of methyl β-glucoside in DMSO-d_6. Assignments are as follows 103.9 (C_1), 76.8 (C_5 or C_3) 76.7 (C_5 or C_3), 73.5 (C_2), 70.2 (C_4), 61.2 (C_6), and 56.1 (OCH$_3$). Full scale is 4000 Hz.

METHYL β-GLUCOSIDE-d₄

OCH₃

1

5 2

6

a

b

110   100   90   80   70   60   50

PPM
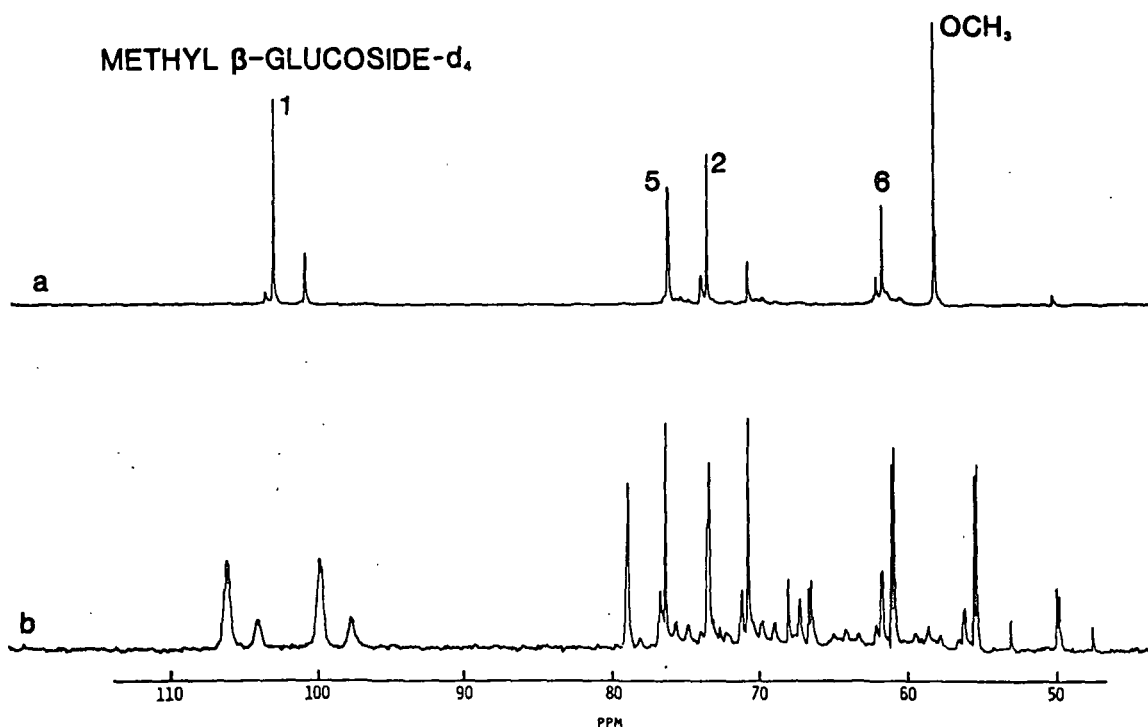
Figure 13.   Proton decoupled (a) and proton coupled (b) ^{13}C-NMR spectra of methyl β-glucoside-3,4-6,6´-d₄ in D₂O. Assignments are shown. Only partial exchange was achieved. Full scale is 2000 Hz.

Xylobiose   p-dioxane

a

b

130   120   110   100   90   80   70   60   50   40   30

PPM
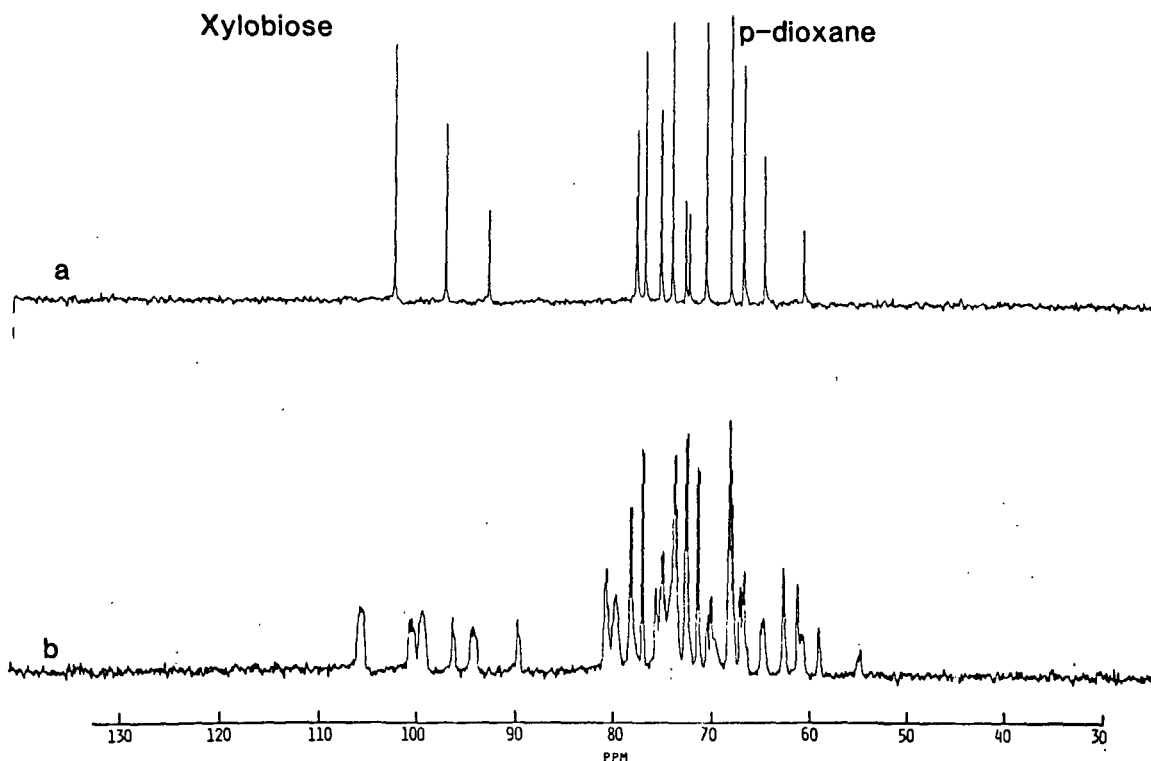
Figure 14.   Proton decoupled (a) and proton coupled (b) ^{13}C-NMR spectra of xylobiose in D₂O. Assignments are given in the experimental section. Full scale is 3002 Hz. p-Dioxane is present as a reference at 67.4 ppm.
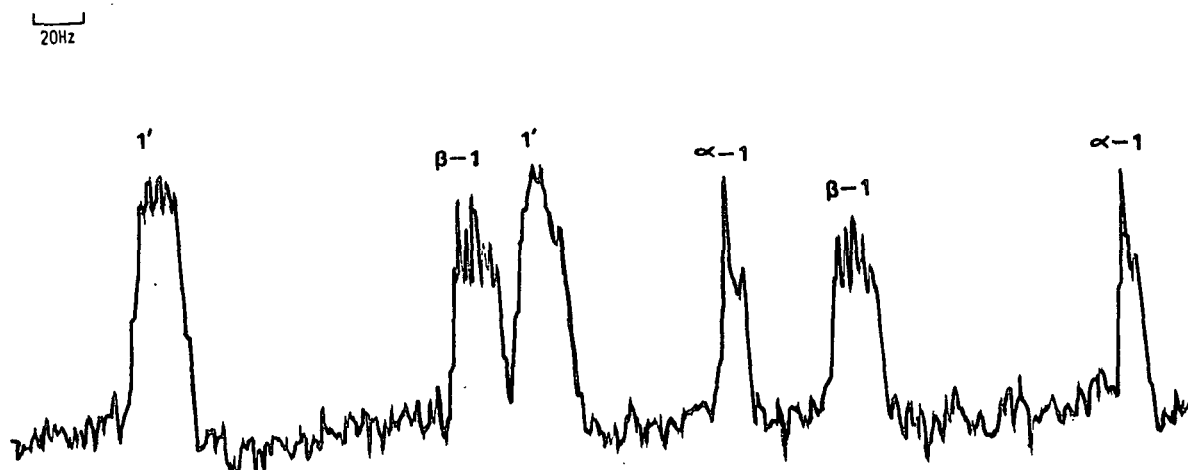
Figure 15. Expansion of C_1´, C_1 region of Fig. 14. Full scale is 500 Hz.
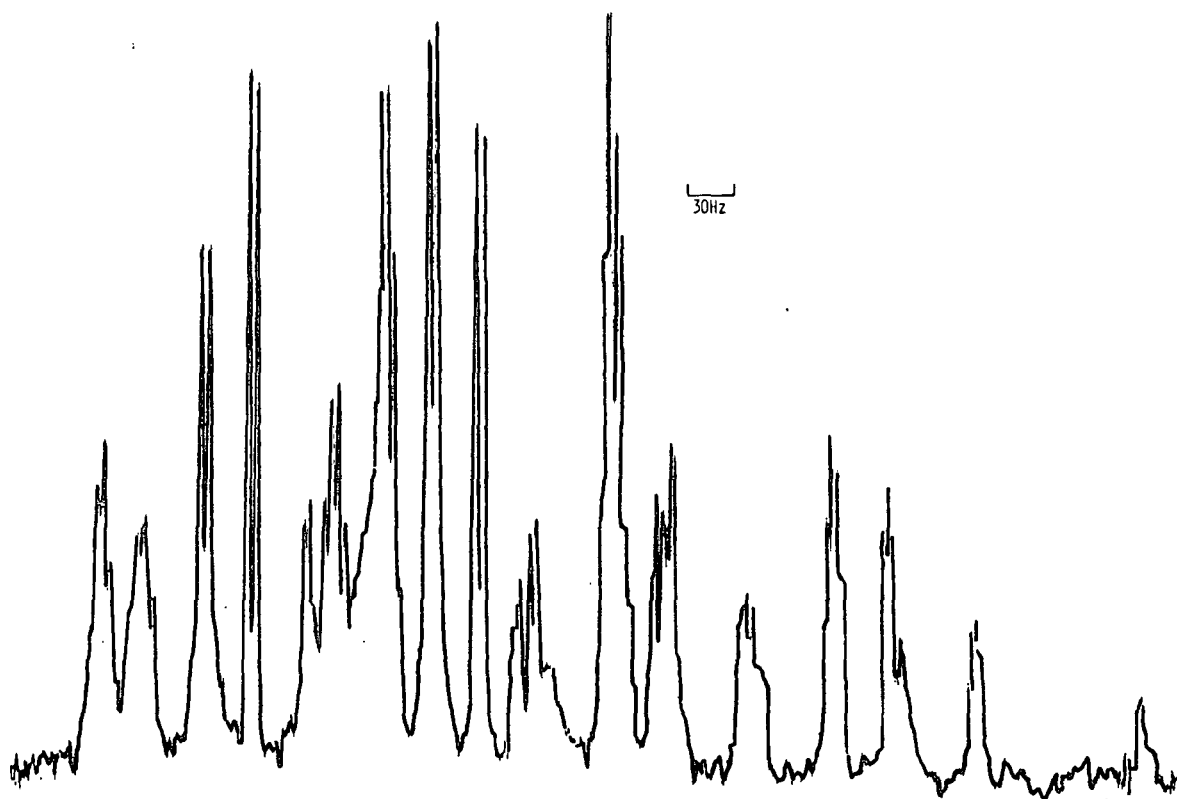
Figure 16. Expansion of upfield region of Fig. 14. Full scale is 750 Hz.
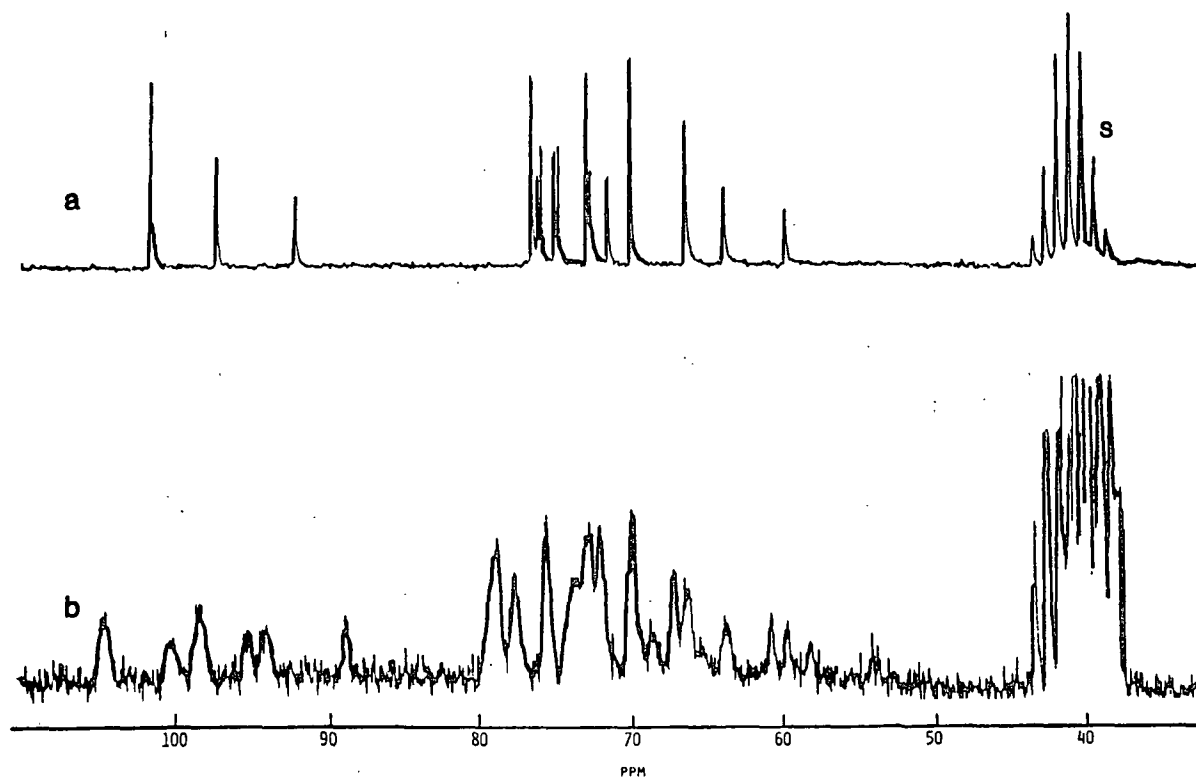
Figure 17. Proton decoupled (a) and proton coupled (b) ^{13}C-NMR spectra of xylobiose in DMSO-d_6. Note the relative change in position of the C_4 signal from Fig. 14. Full scale is 2000 Hz.
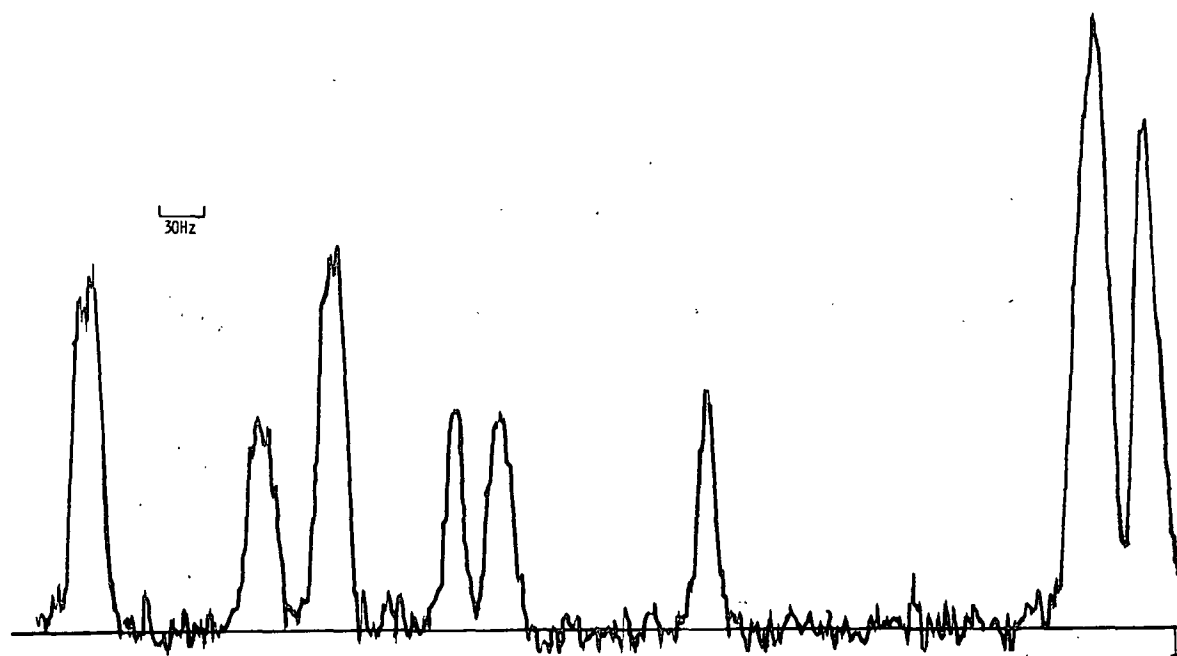
Figure 18. Expansion of the C_1', C_1 region of a coupled ^{13}C-NMR spectrum of xylobiose in DMSO-d_6. Full scale is 750 Hz.

METHYL β-XYLOBIOSIDE

a

R0Hz

1   1'   1'

1   1'

b

110   100   90   80   70   60   50

PPM
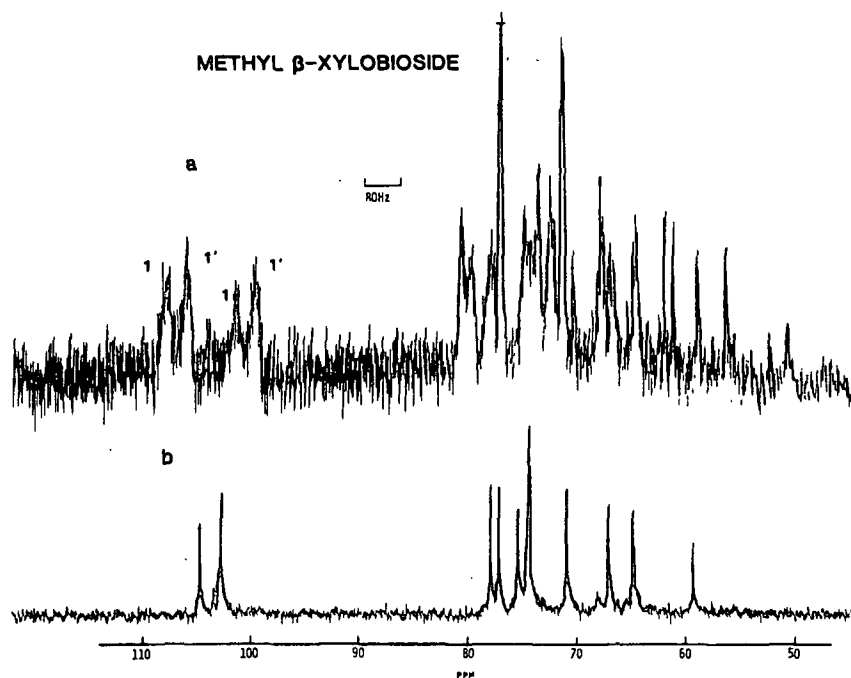
Figure 20.   Proton coupled (a) and proton decoupled (b) spectra of methyl β-xylo-
bioside in DMSO-d_5. Full scale is 5000 Hz. The top spectrum is 51,600
pulses while the bottom spectrum is 40,000 pulses. The inset is an
expansion of the C_1, C_1' region with full scale of 625 Hz.

S

a

b   S

180   160   140   120   100   80   60   40   20   0

PPM
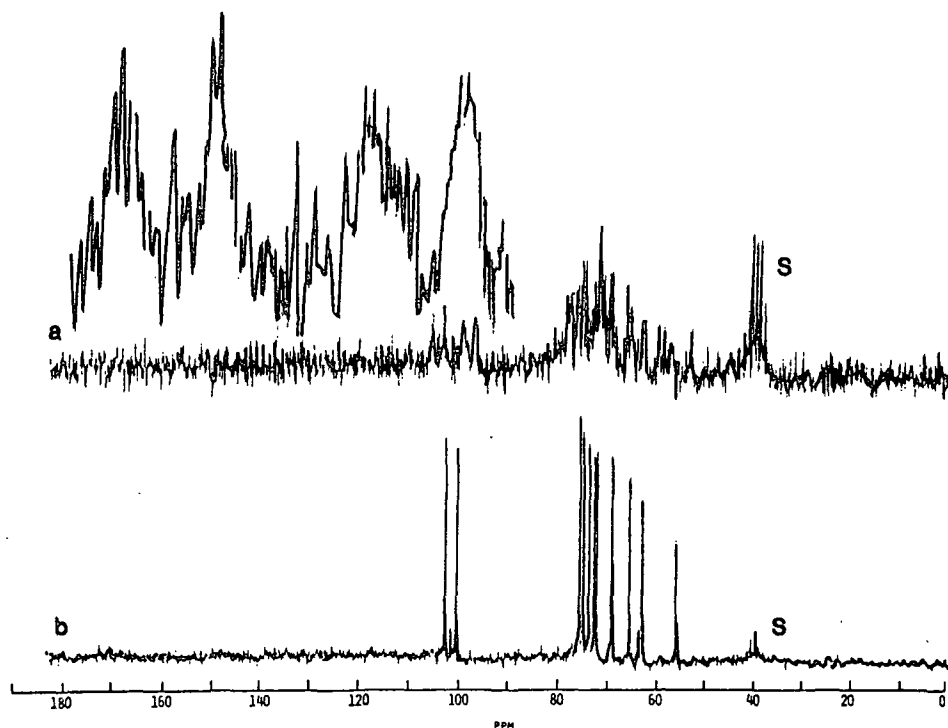
Figure 19.   Proton coupled (a) and proton decoupled (b) ^{13}C-NMR spectrum of methyl
β-xylobioside in D_2O. Assignments are as follows 104.7 (C_1), 102.7
(C_1'), 77.3 (C_4), 76.5 (C_3'), 74.7 (C_3), 73.7 (C_2 and C_2'), 70.1 (C_4'),
66.1 (C_5'), 63.8 (C_5), and 58.1 (OCH_3). These assignments agree with
the recent literature assignments for this compound (3). Full scale is
2000 Hz.

Securidebioside
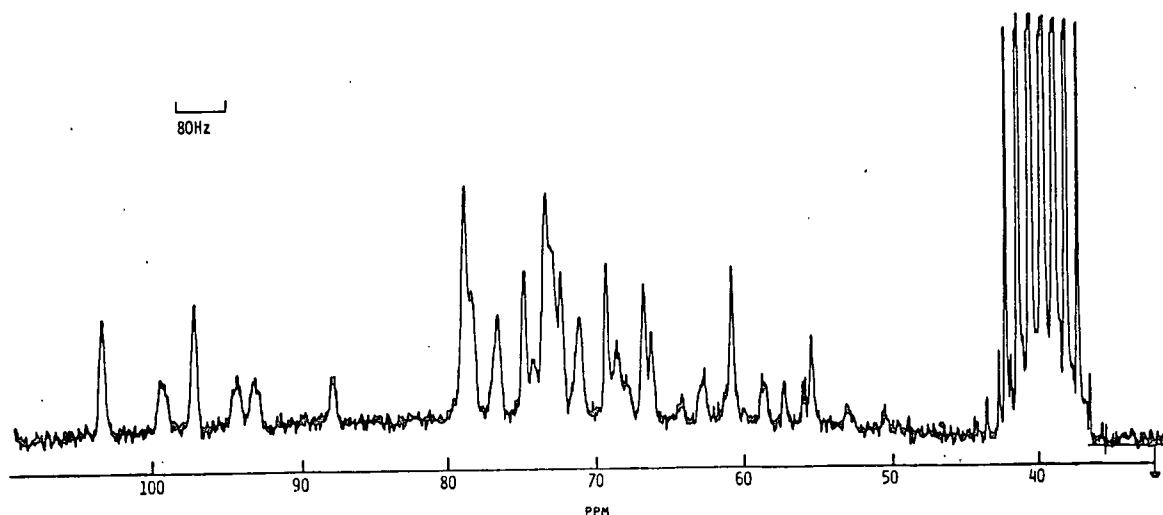
Figure 21. Proton coupled spectrum of 4-O-(β-D-glucopyranosyl)-D-xylopyranose in DMSO-d₆. Full scale is 2000 Hz.

Cellobiose
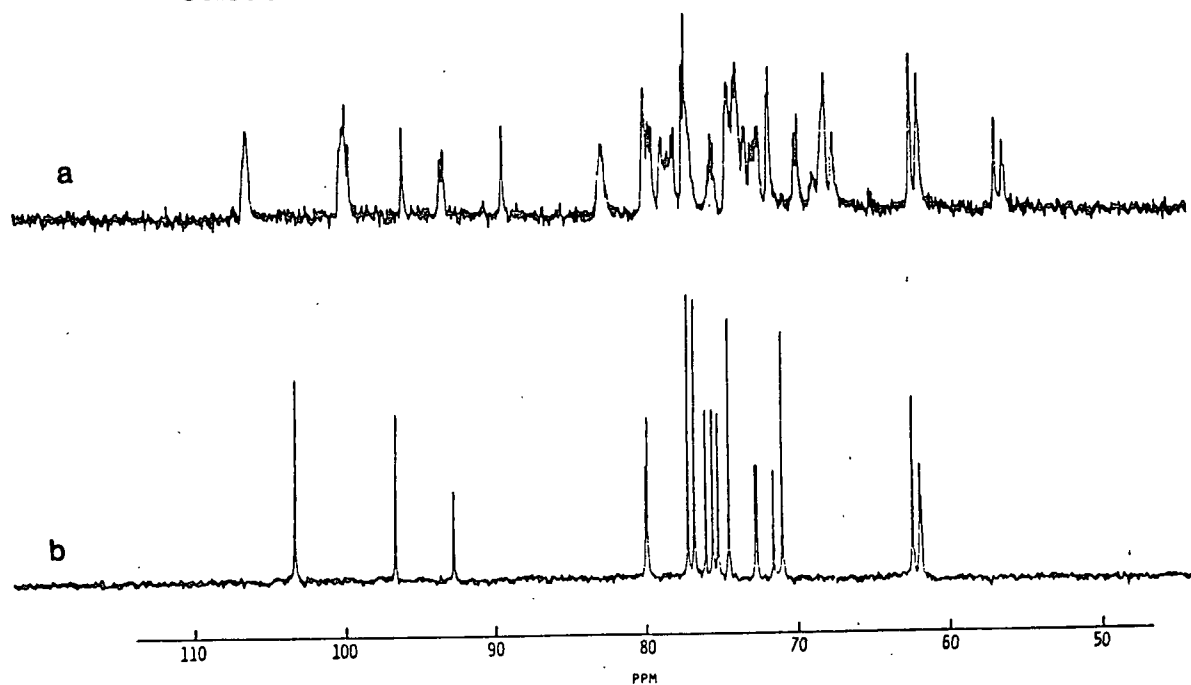
Figure 22. Proton coupled (a) and decoupled (b) ^{13}C-NMR spectra of cellobiose in D$_2$O. Assignments are given in the experimental section. Full scale is 2000 Hz.
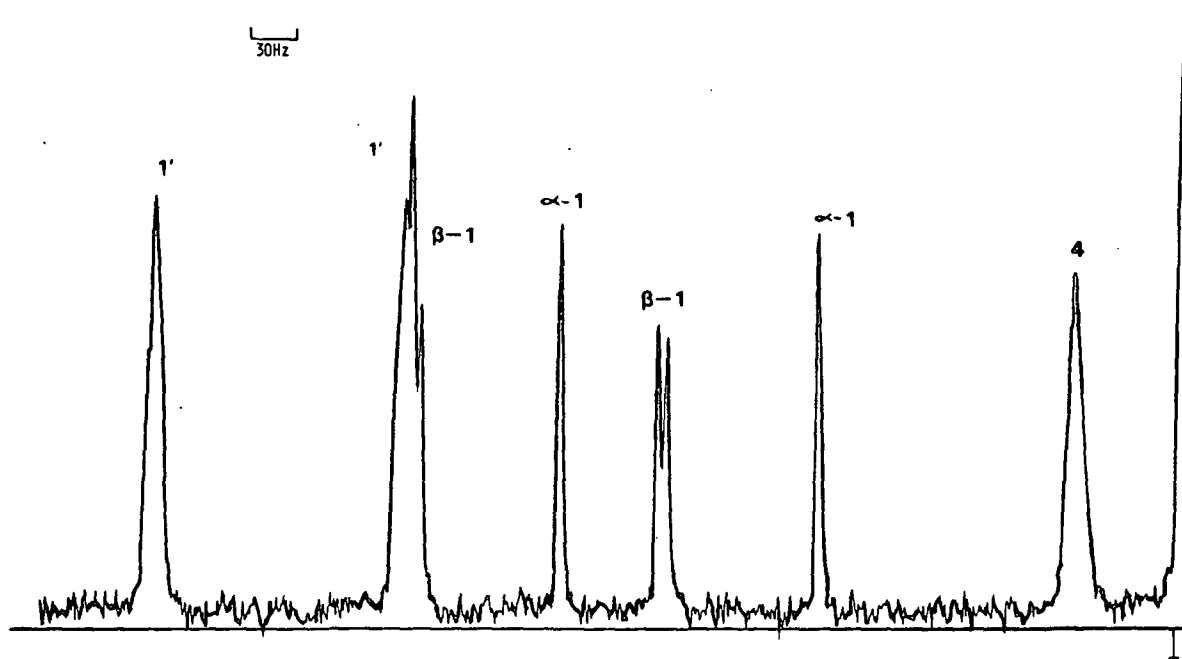
Figure 23. Expansion of the downfield (C_1', C_1, C_4) region of a coupled ^{13}C-NMR spectrum of cellobiose in D_2O. Full scale is 750 Hz.
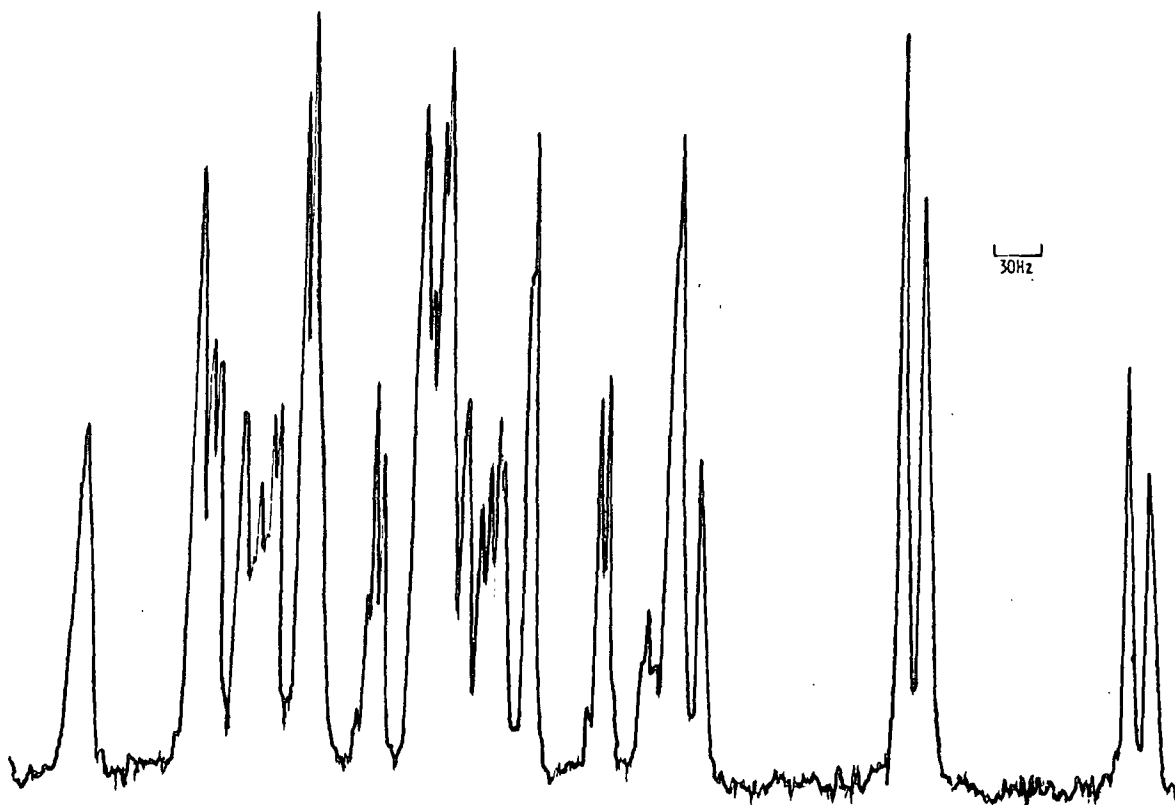
Figure 24. Expansion of the upfield region of the proton coupled ^{13}C-NMR spectrum of cellobiose in D_2O. Full scale is 750 Hz.
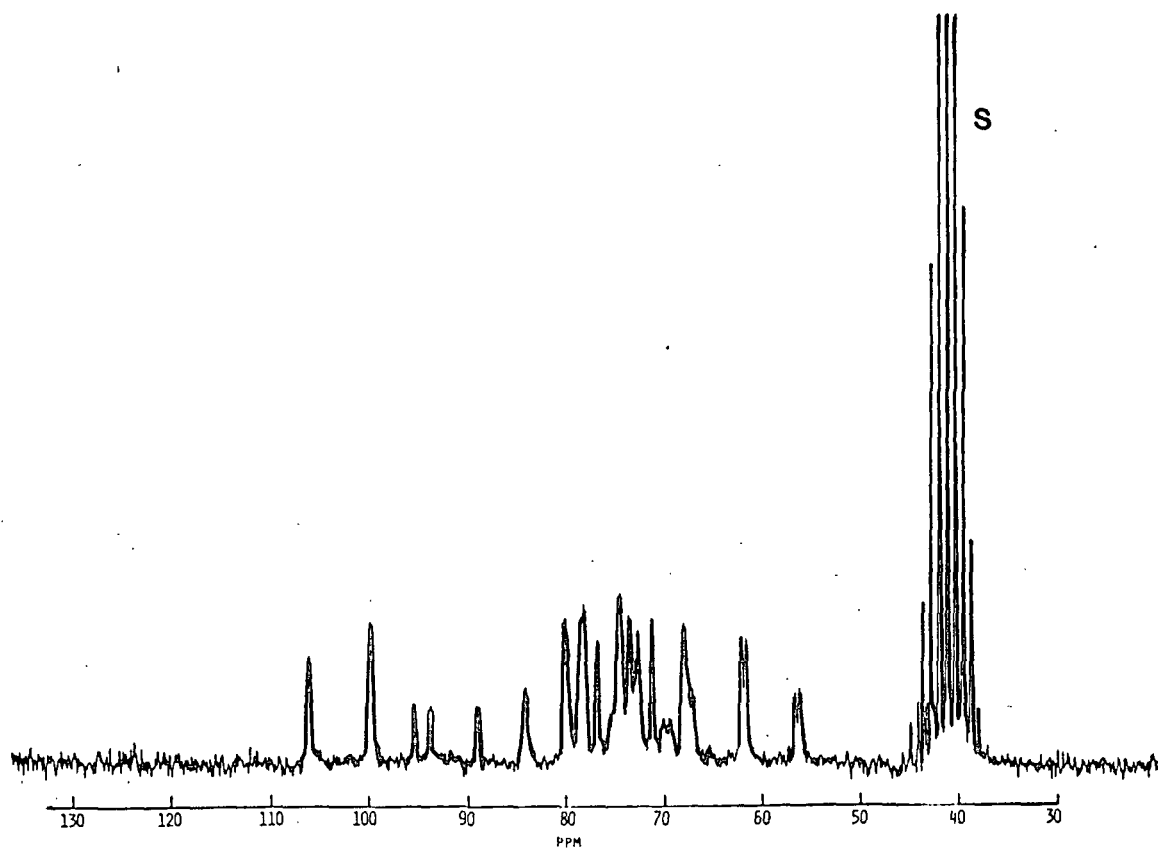
Figure 25. Proton coupled spectrum of cellobiose in DMSO-d_6. Full scale is 3000 Hz.
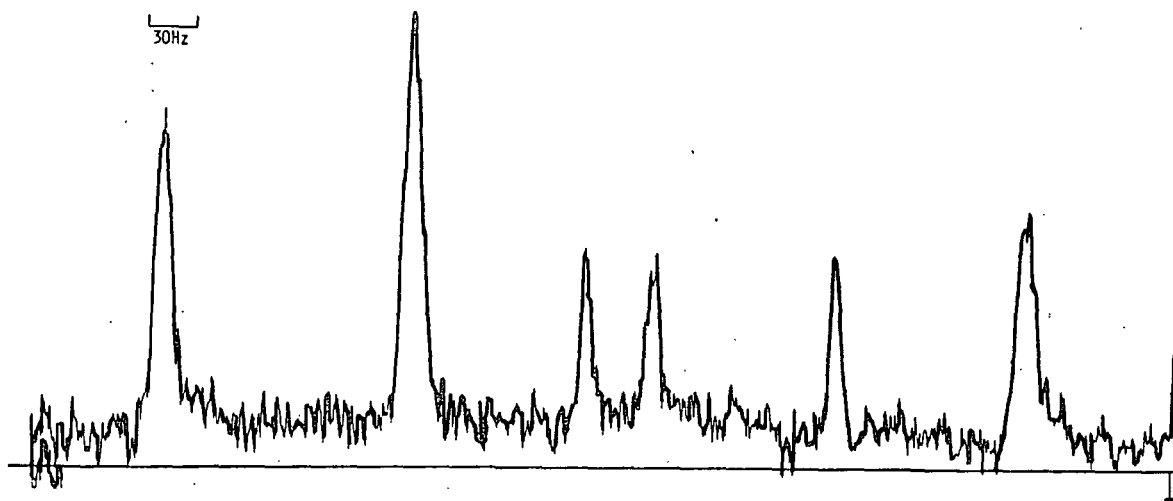
Figure 26. Expansion of downfield portion of Fig. 25. Full scale is 750 Hz.

Metnyl β- Cellobioside
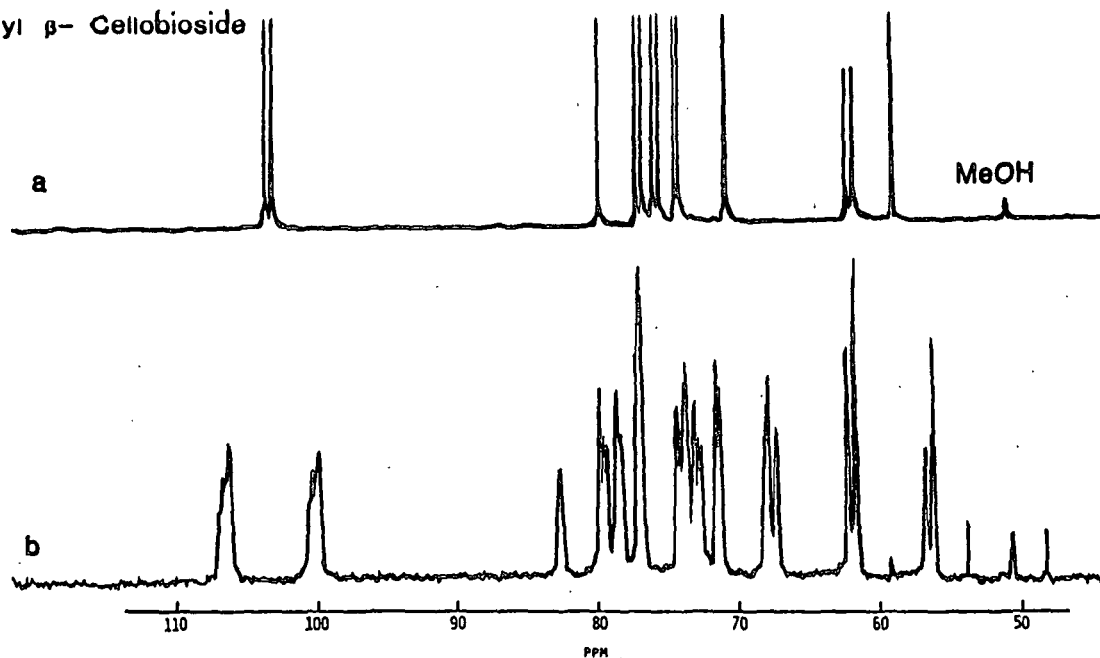
Figure 27. Proton decoupled (a) and proton coupled (b) ^{13}C-NMR spectra of methyl β-cellobioside in D_2O. Assignments are as follows: 103.9 (C_1), 103.4 (C_1'), 79.7 (C_4), 76.8 (C_5'), 76.4 (C_3'), 75.7 (C_5), 75.2 (C_3), 74.0(C_2'), 73.7 (C_2), 70.3 (C_4'),61.5 (C_6'), 61.0 (C_6), and 58.1 (OCH$_3$). These agree with those in the literature ($\underline{1}$). Full scale is 2000 Hz.
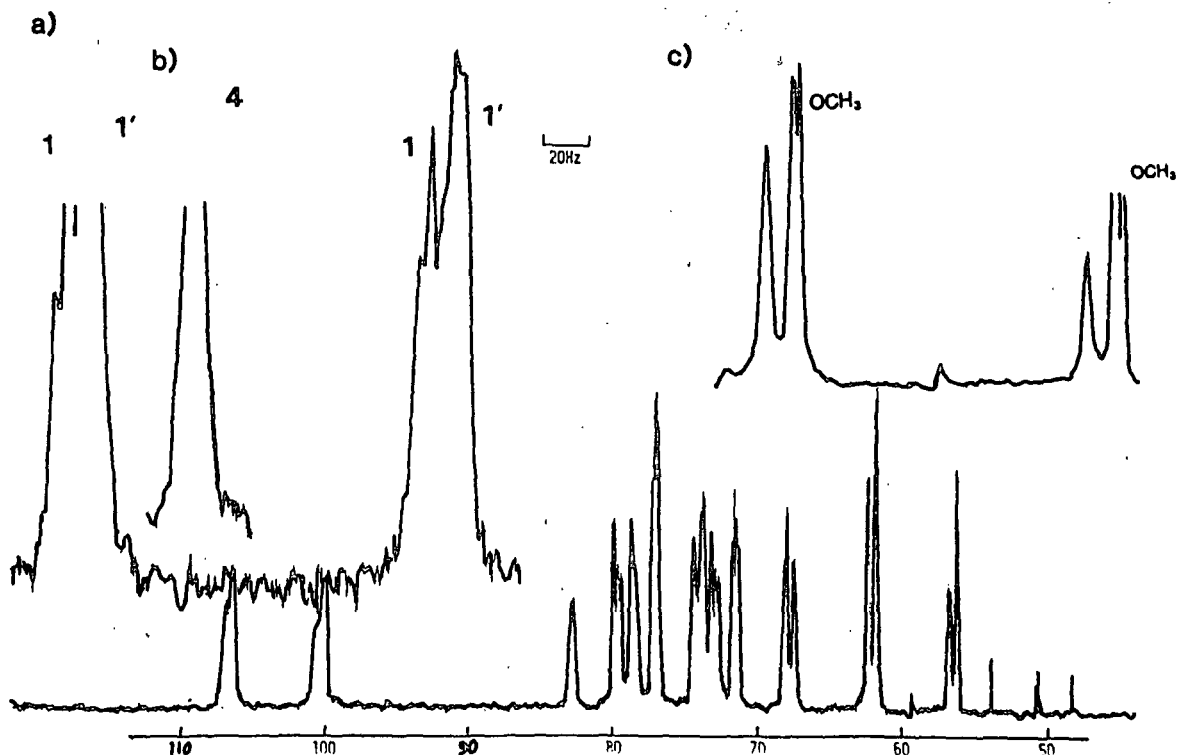
Figure 28. Repeat of Fig. 27b. Insets are the C_1', C_1 region, downfield C_4 signal, and the OCH$_3$ region, as indicated. Full scale is 500 Hz for each.
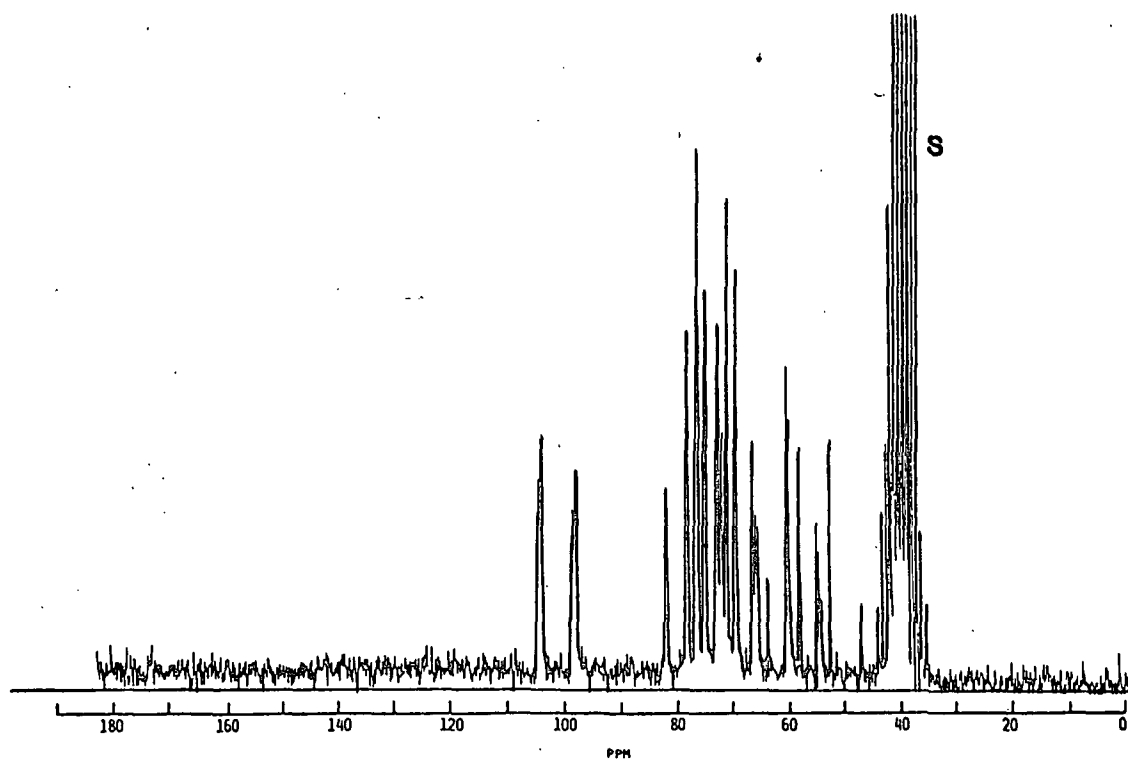
Figure 29. Proton coupled spectrum of methyl β-cellobioside in DMSO-d$_6$. Full scale is 5000 Hz.
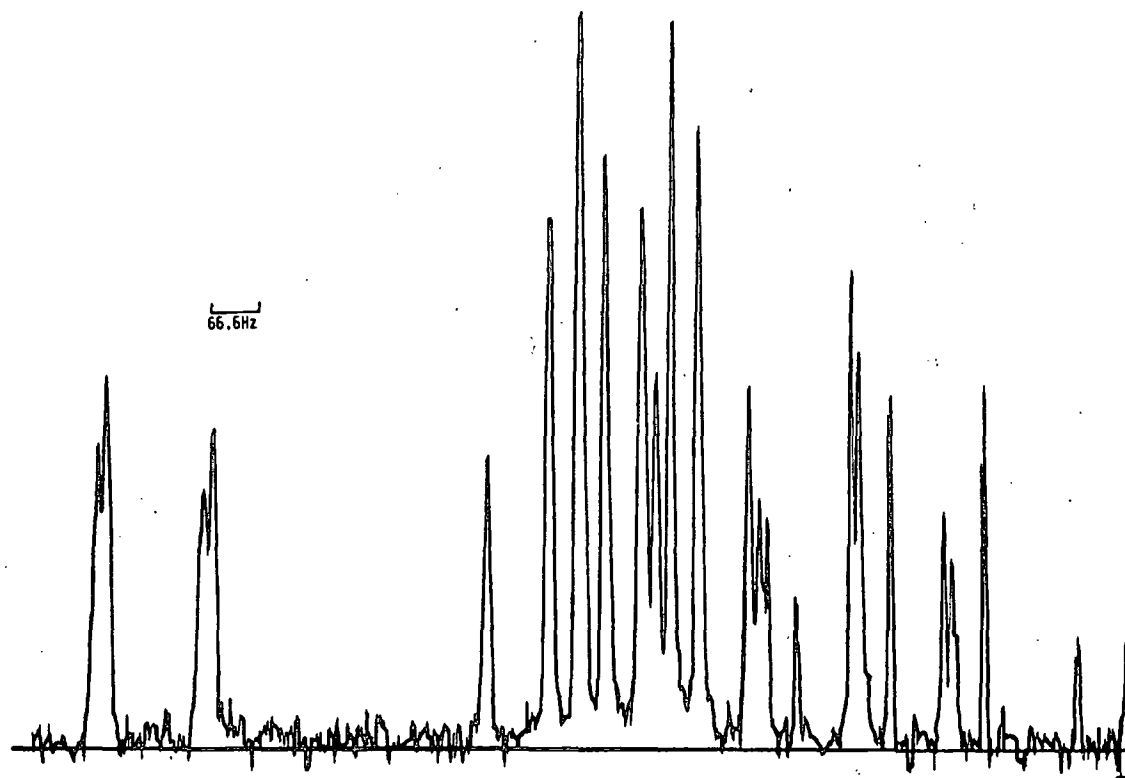
Figure 30. Expansion of Fig. 29 to 1663 Hz full scale.
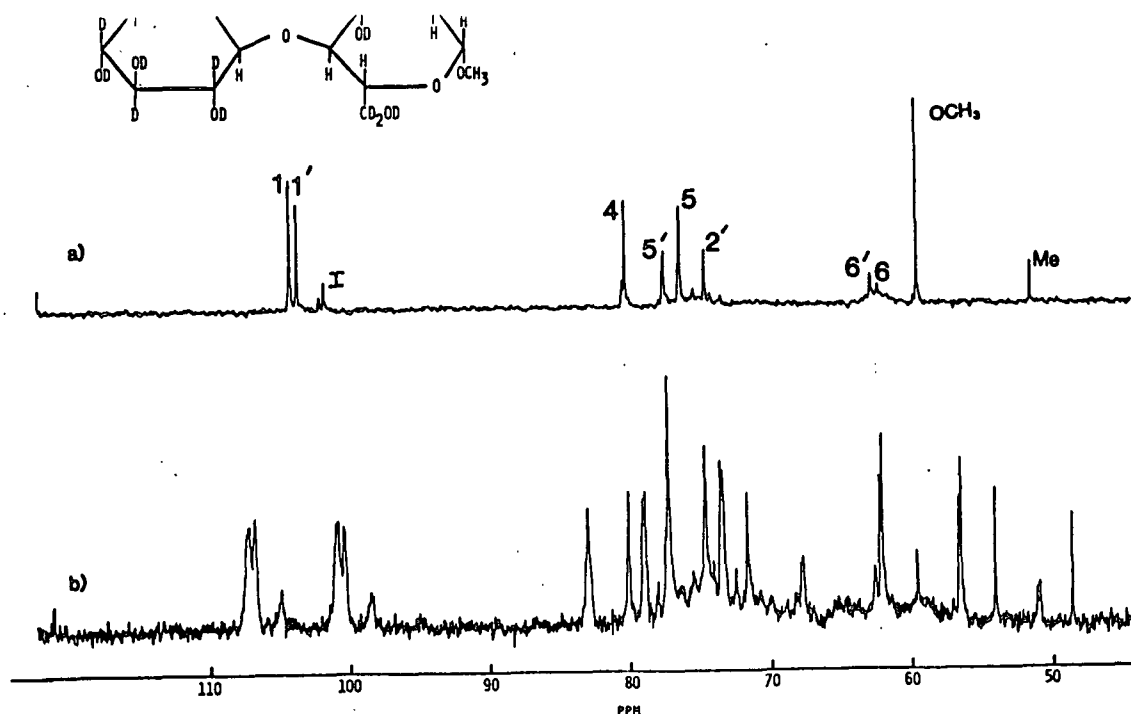
Figure 31. Proton decoupled (a) and coupled (b) ^{13}C-NMR spectra of methyl β-cellobioside-d$_8$. Assignments are shown on the figure. The spectrum is similar to one in the literature (1). Some isomerization is indicated. Full scale is 2000 Hz.
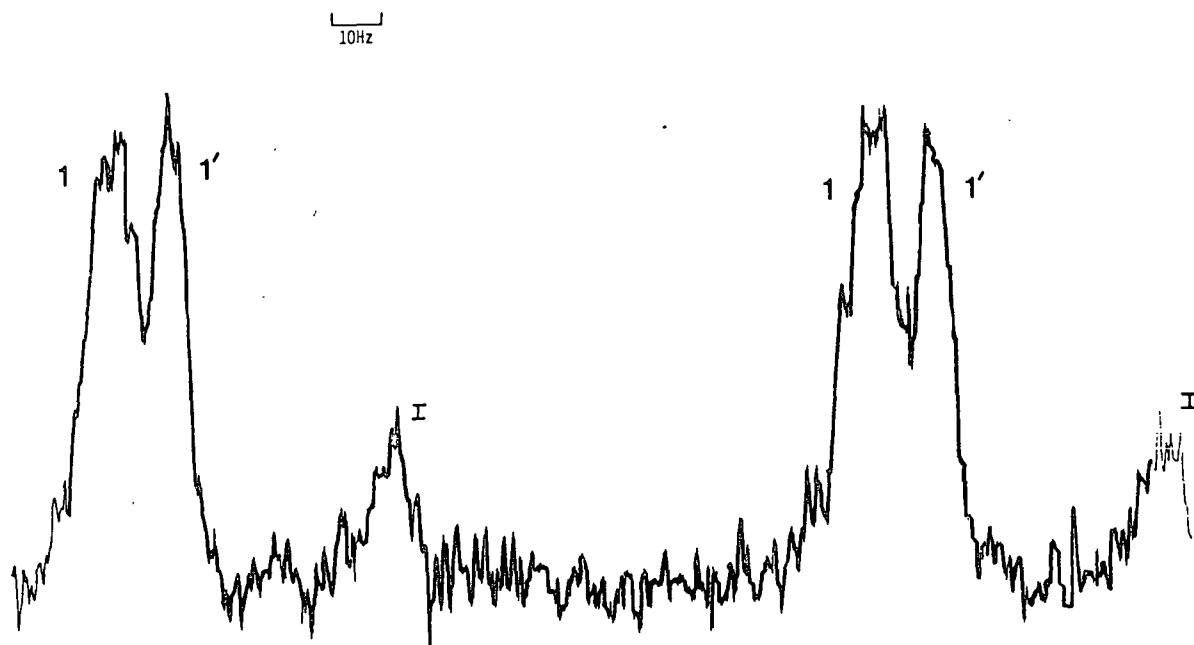
Figure 32. Downfield (C$_1$, C$_1'$) region of Fig. 31. Full scale is 250 Hz.
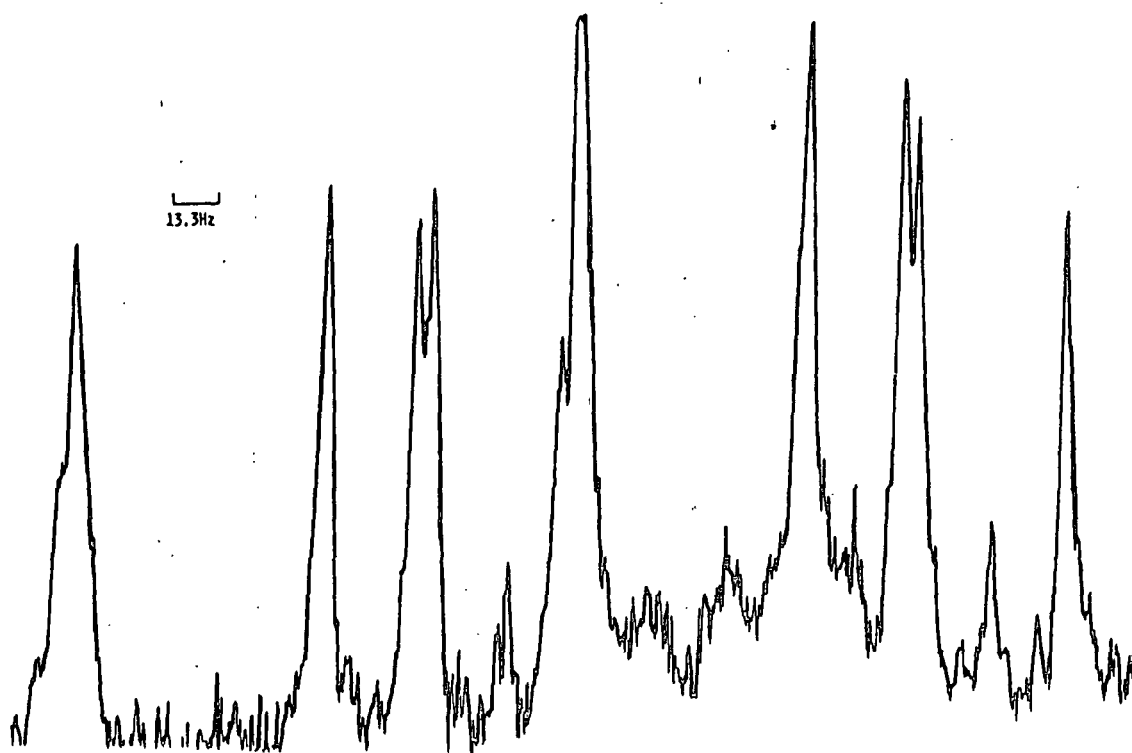
Figure 33. Central region of Fig. 31. Full scale is 333 Hz.
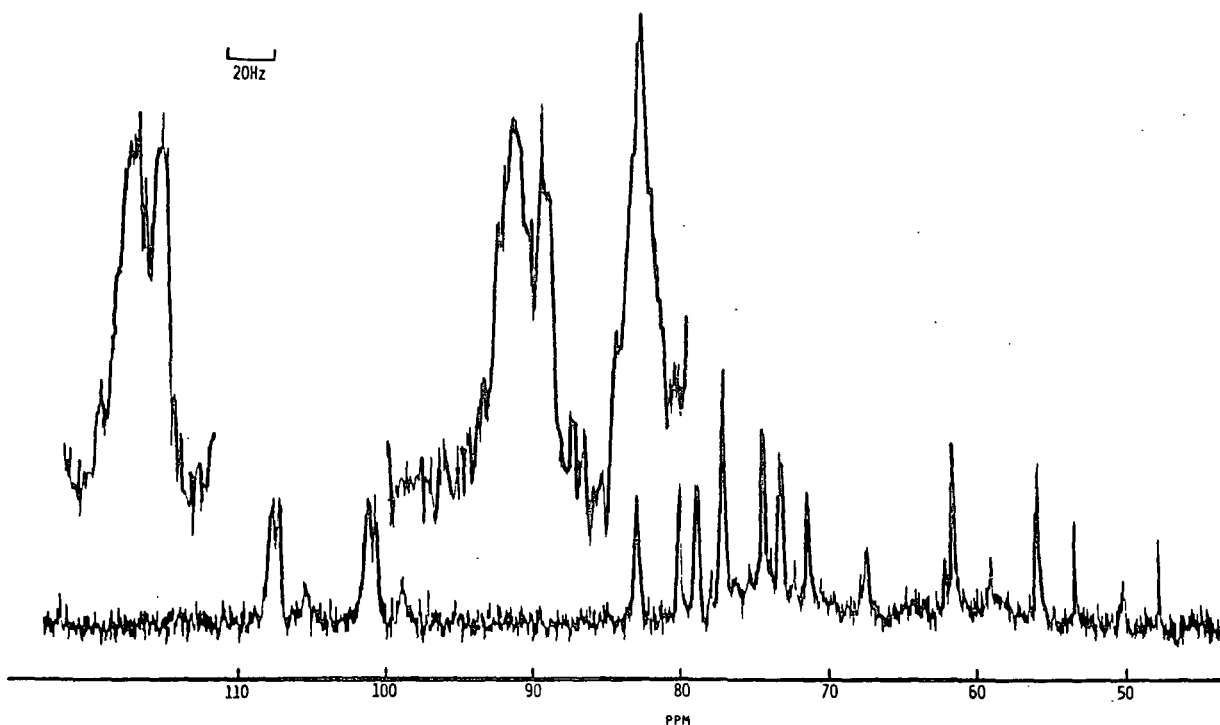
Figure 34. Another proton coupled spectrum of compound 7. Full scale is 2000 Hz. Inset are the downfield C_1, C_1' complex, the upfield C_1, C_1' complex, and the downfield C_4 signal from left to right. Full scale for the insets is 500 Hz.

4-O-(β-D-Glucopyranosyl)-D-Mannopyranose
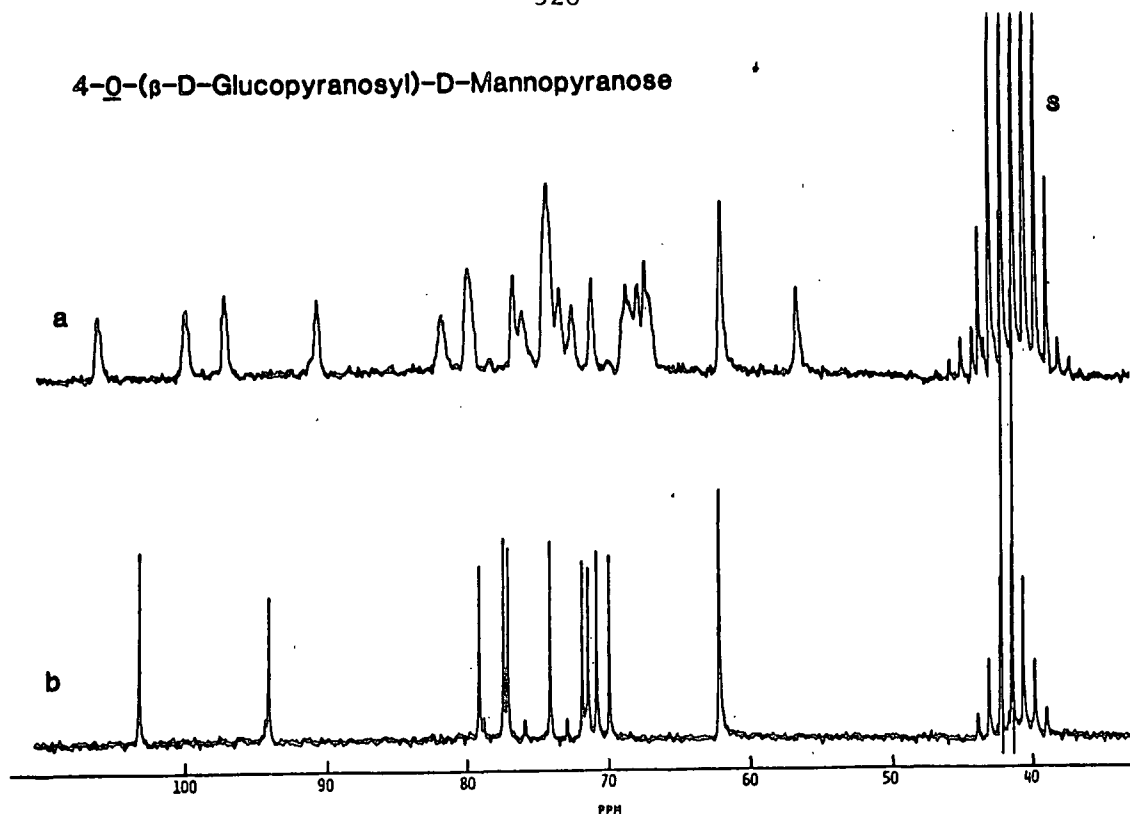
Figure 35. Proton coupled (a) and proton decoupled (b) ^{13}C-NMR spectra of 4-O-(β-D-glucopyranosyl)-D-mannopyranose in DMSO-d$_6$. Note that the α-anomer is dominant. Full scale is 2000 Hz.

Lactose
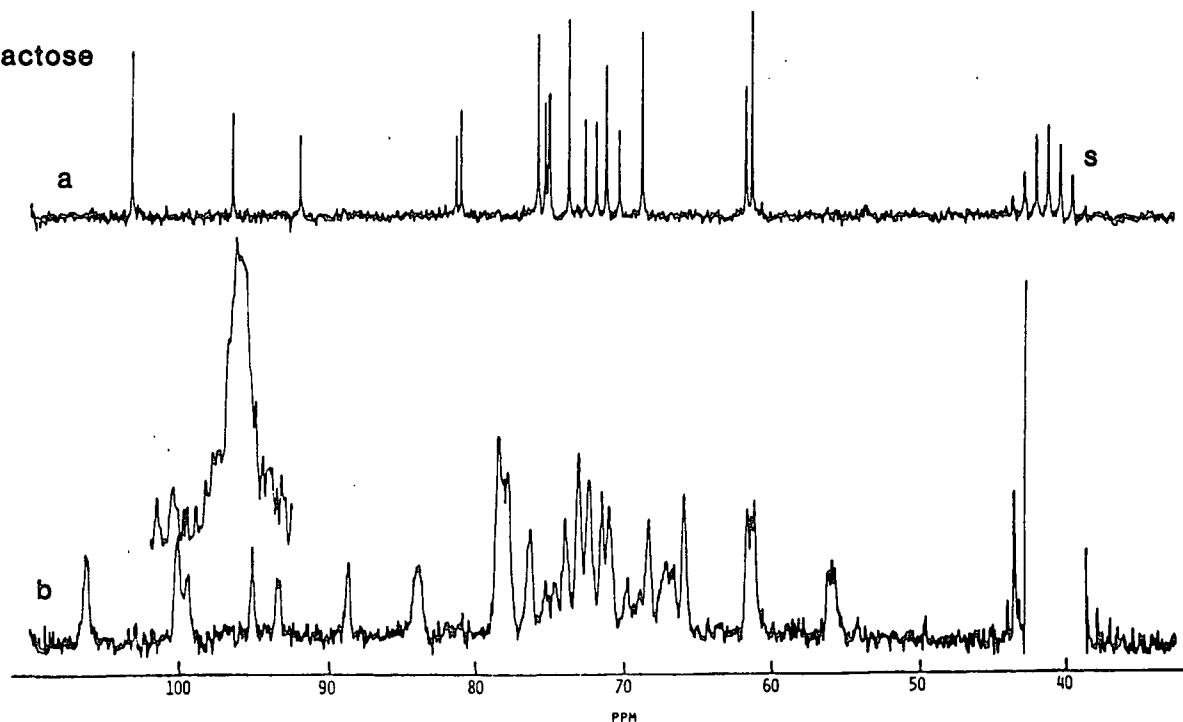
Figure 36. Proton decoupled (a) and coupled (b) spectra of lactose in DMSO-d$_6$. Full scale is 2000 Hz. Inset is the downfield C$_1$' signal at 500 Hz full scale.
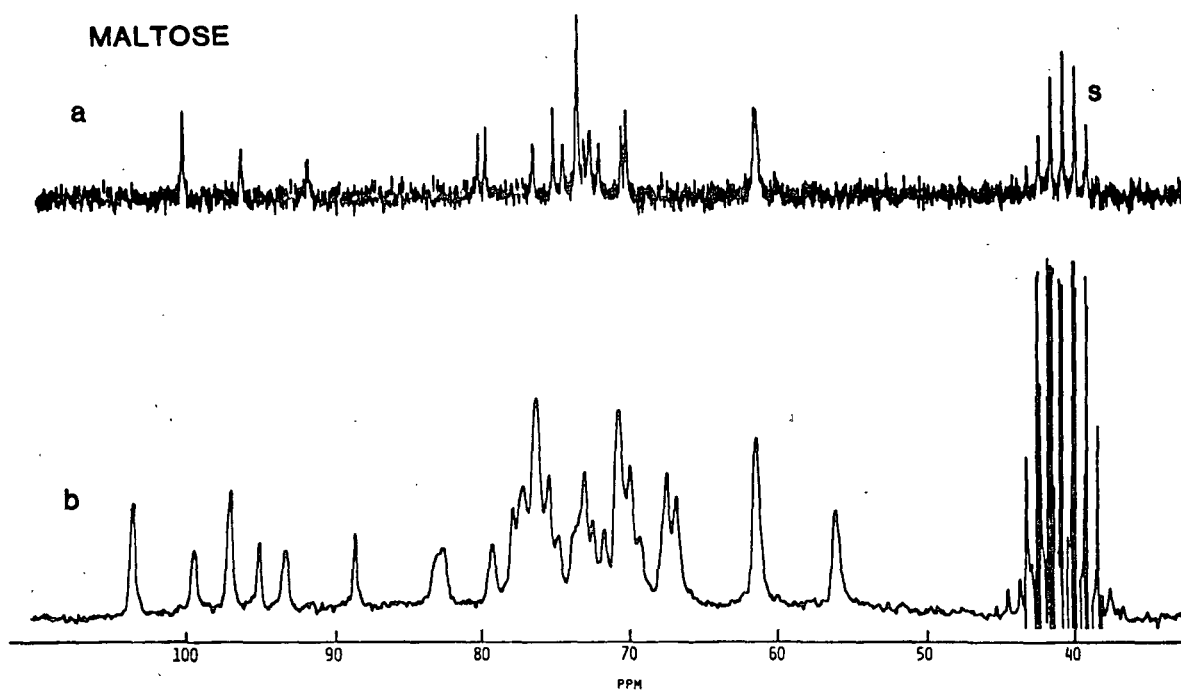
MALTOSE

Figure 37. Proton decoupled (a) and coupled (b) spectra of maltose in DMSO-d_6. Full scale is 2000 Hz.
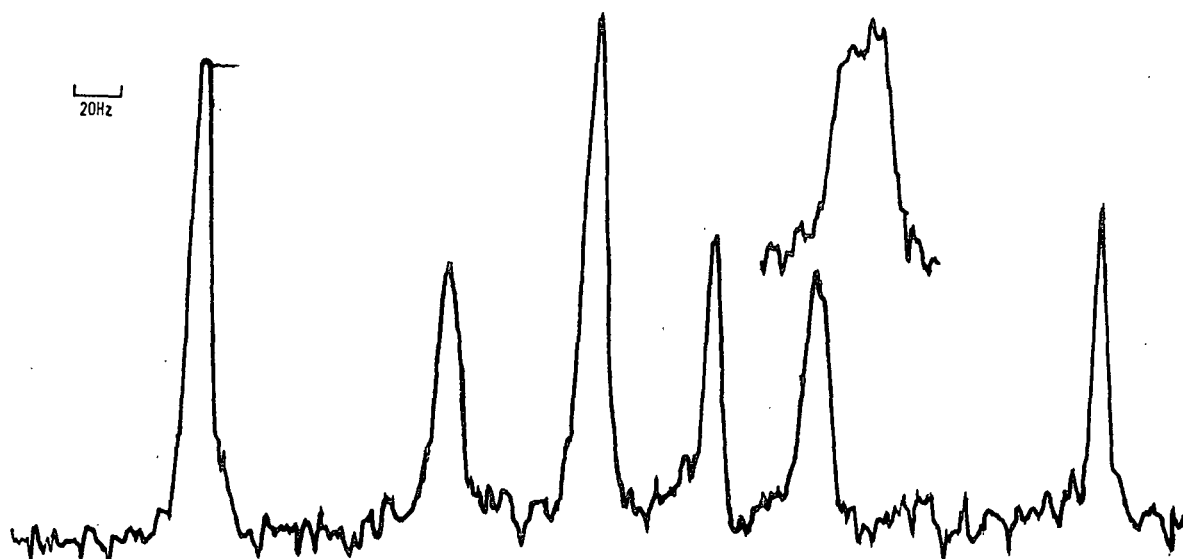
Figure 38. Expansion of the downfield portion of Fig. 37. Full scale is 500 Hz. The downfield C_4 signal is also shown.

LITERATURE CITED

1. Hamer, G. K., Balza, F., Cyr, N., and Perlin, A. S., Can. J. Chem. 56:3109-16 (1978).

2. Parfondry, A., Cyr, N., and Perlin, A. S., Carbohyd. Res. 59:299-309(1977).

3. Kovac, P., Hirsch, J., Shashkov, A. S., Usov, A. I., and Yarotsky, S. V., Carbohyd. Res. 85:177-85(1980).

APPENDIX VI

REPRESENTATIVE ^{1}H-NMR SPECTRA OF SEVERAL β-1,4-LINKED CARBOHYDRATES AND USEFUL MODELS

The following is a collection of representative ^{1}H-NMR spectra of the carbohydrates studied in this thesis. Many additional spectra in DMSO-d_6 were obtained at other temperatures. The results are tabulated in the Appendix VII. The spectra in D_2O are presented for purposes of comparison. The letters designating individual peaks in the DMSO-d_6 spectra are used in the following Appendix in which the chemical shift of each peak, at different temperatures, is tabulated. Table I lists the spectra for easy reference.

TABLE I

| Figure	Compounds	Comments
1	Glucose	
2	Methyl β-glucoside	56°C
3	Xylose	
4	Methyl β-xyloside	
5	Methyl α-xyloside	
6	Methyl β-cellobioside	56°C
7	Methyl β-cellobioside	D_2O
8	Cellobiose	55°C
9	Cellobiose	
10	Cellobiose	64°C
11	Cellobiose	D_2O
12	Cellobiose	Integrated
13	Cellotriose	
14	Cellotetraose	D_2O
15	Lactose	
16	Lactose	66.5°C
17	Glucosyl – Mannose	55.5°C
18	Glucosyl – Mannose	D_2O
19	Mannobiose	D_2O
20	1,5 anhydrocellobiotol	
21	Maltose	
22	Starch	51°C
23	Xylobiose	77.5°C
24	Xylobiose	
25	Xylobiose	D_2O
26	Xylotriose	D_2O
27	Xylotriose	D_2O, expanded
28	Xylotetraose	D_2O
29	Aldotriuronic Acid	
30	Aldotriuronic Acid	D_2O
31	Securidebiose	51°C
32	Securidebiose	67.5°C
33	Methyl β-xylobioside	
34	Benzyl β-xylobioside	
35	Benzyl 2,3 anydro-4-O-(β-D-xylopyranosyl)-D-ribopyranoside	
36	Benzyl 2,3 anydro-4-O-(β-D-glucopyranosyl)-D-ribopyranoside	
37	Benzyl 2,3 anhydro-D-ribopyranoside	
38	Sophorose	
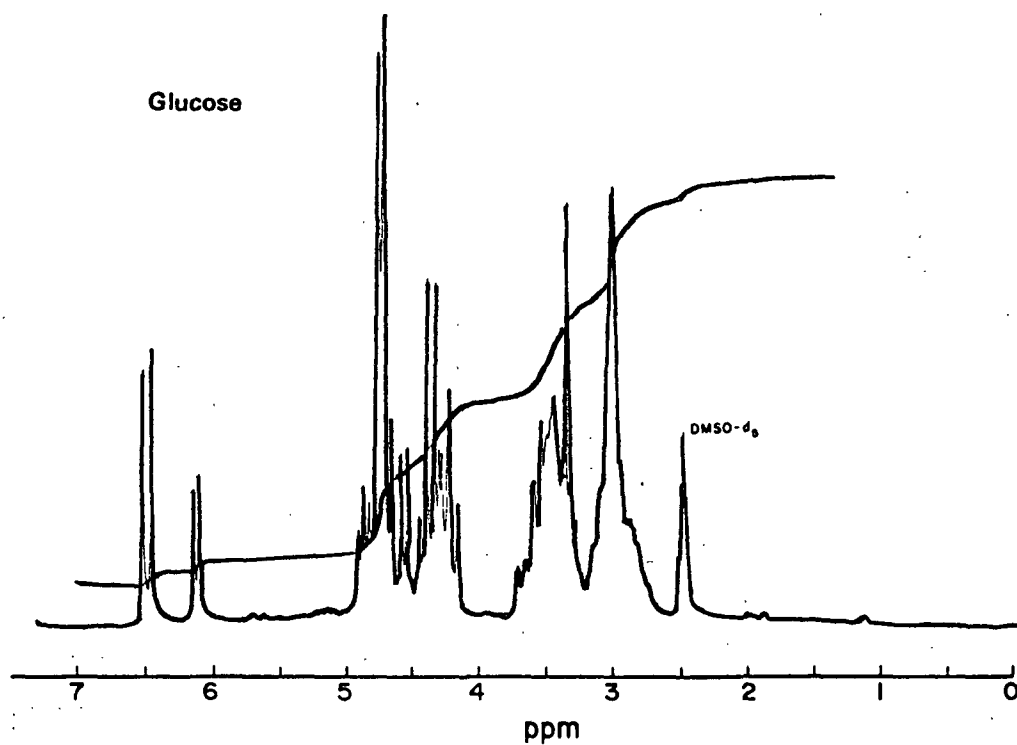
Figure 1. Glucose.
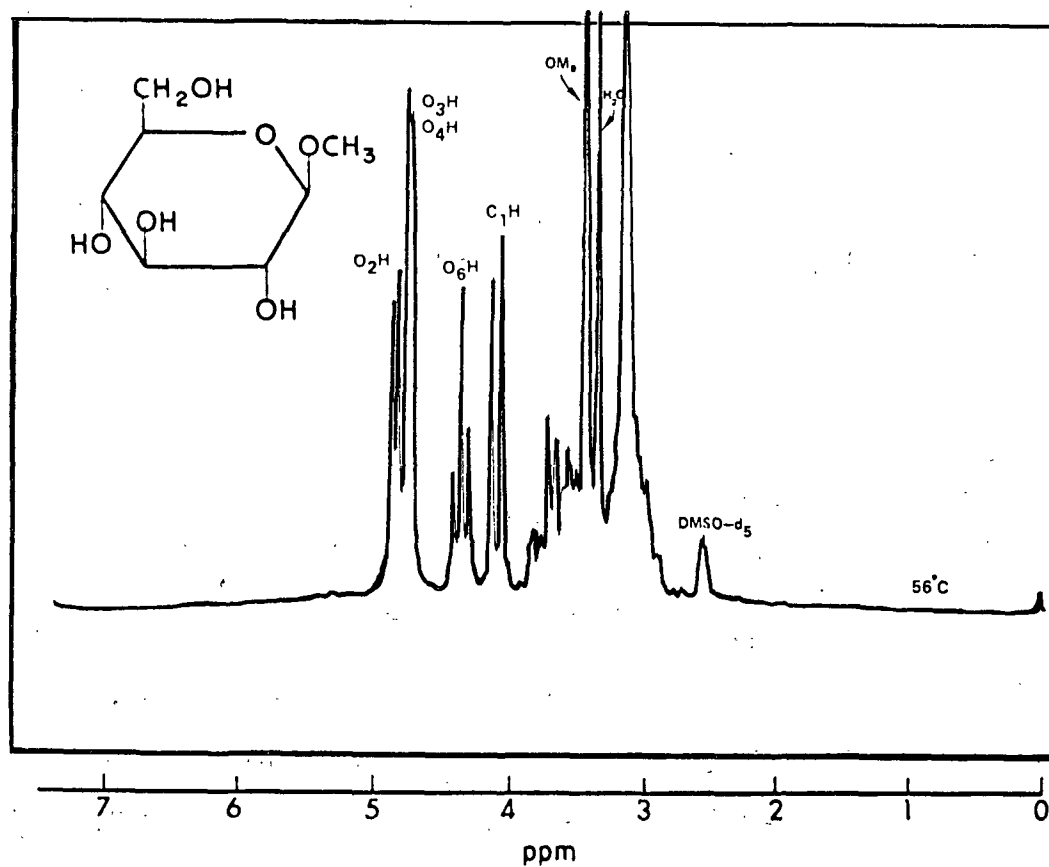
Figure 2. Methyl β-glucoside, 56°C.
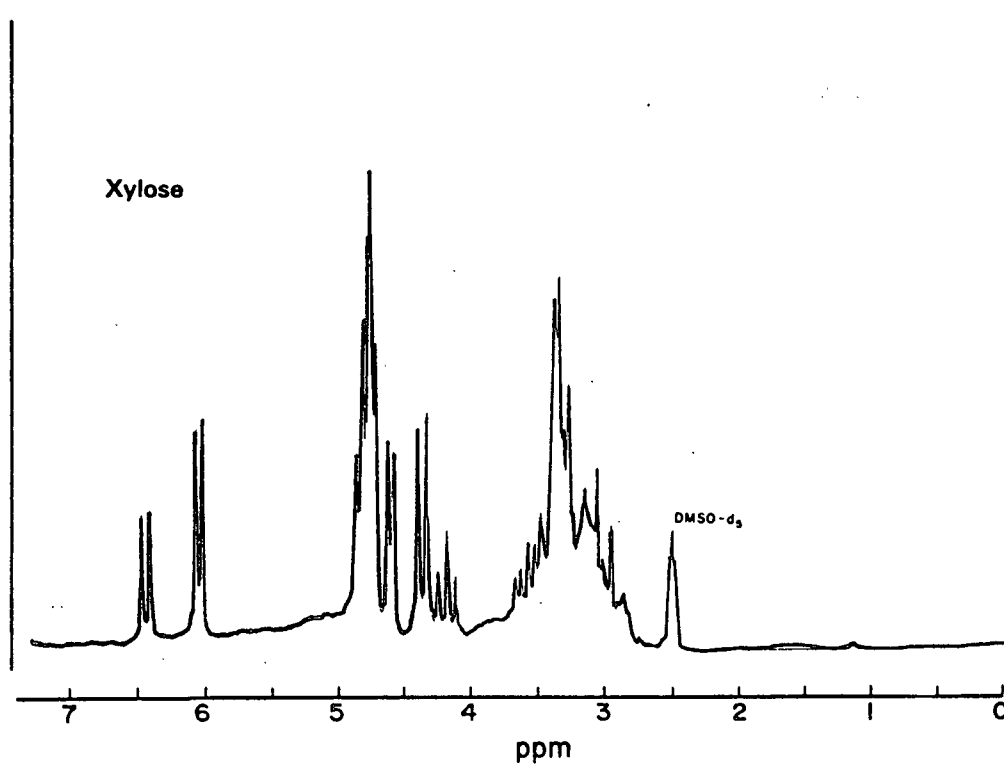
Figure 3. Xylose.

Figure 4. Methyl β-xyloside.
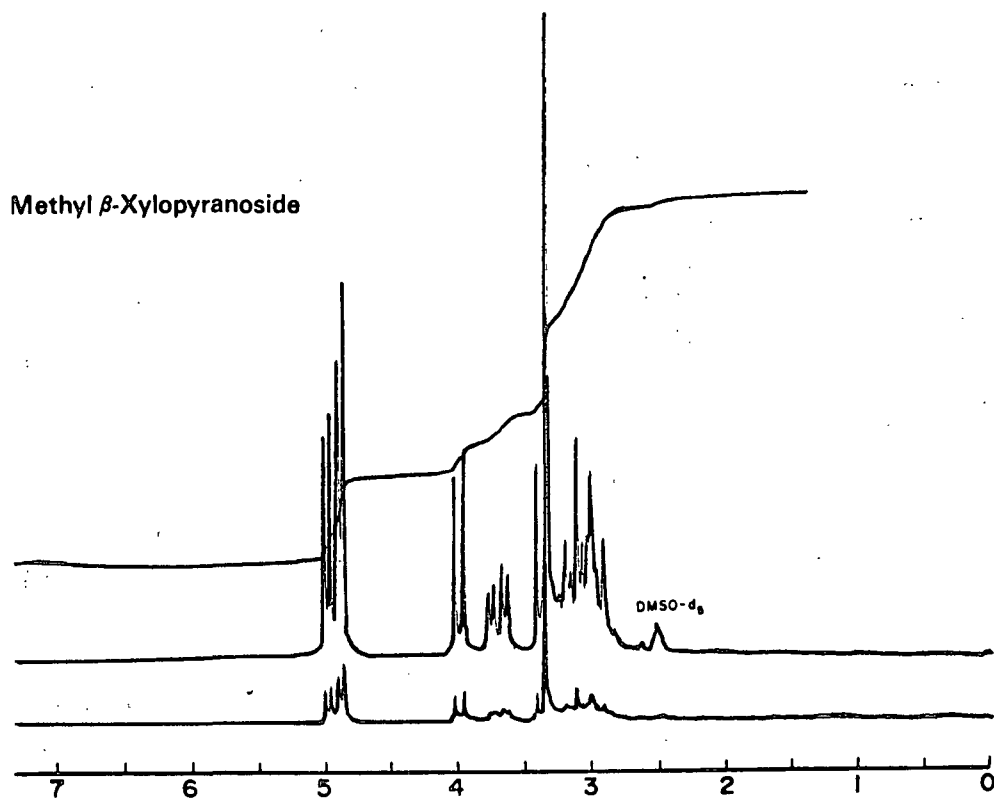
Λethyl α-Xylopyranoside
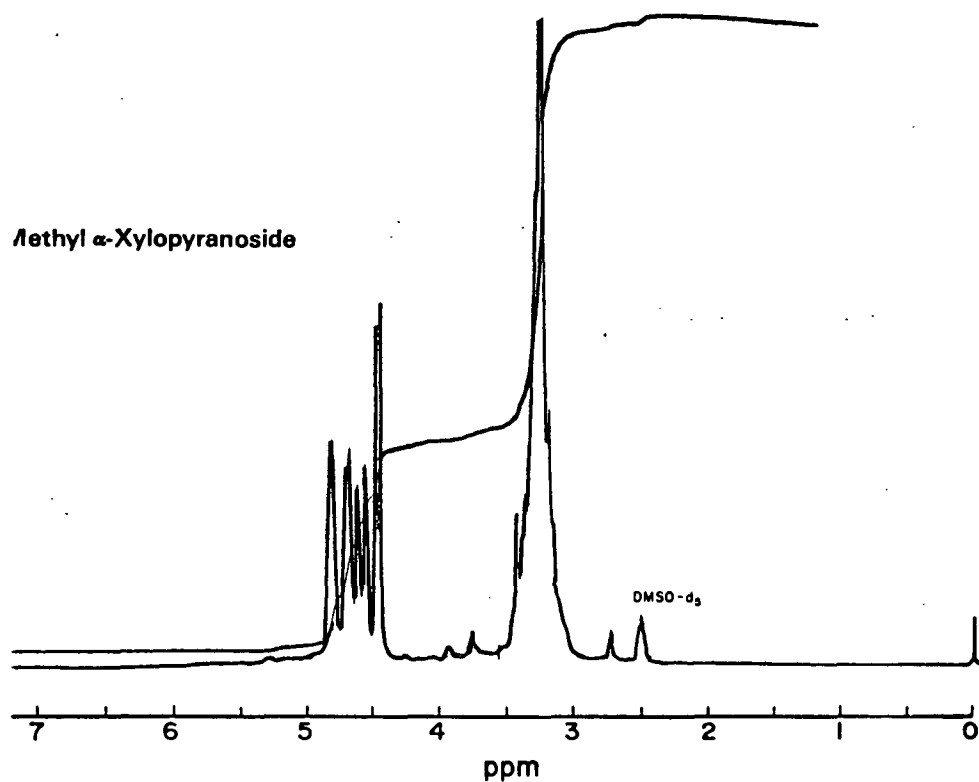
Figure 5. Methyl α-xyloside.

Figure 6. Methyl β-cellobioside, 56°C.

Methyl β-Cellobioside

OMe

HOD

Figure 7. Methyl β-cellobioside, D₂O.

Cellobiose

J-O₃″

55°C

ppm
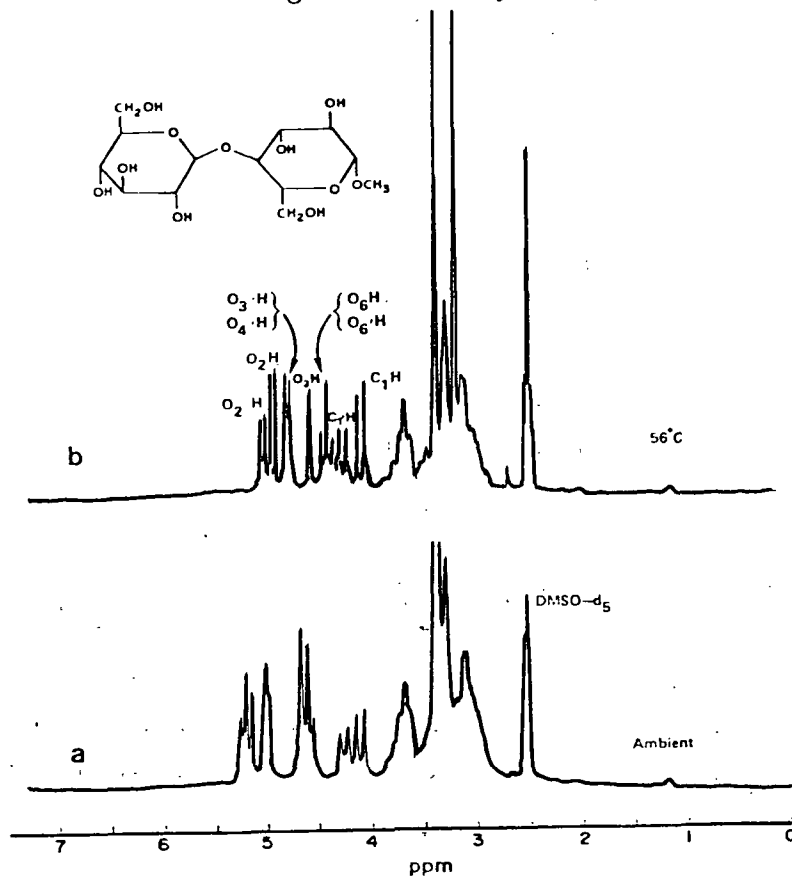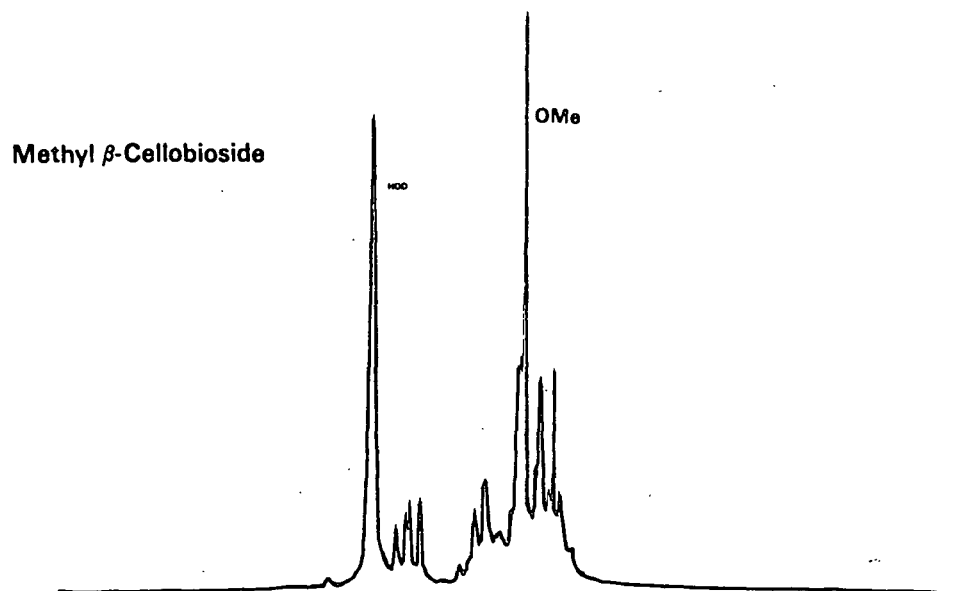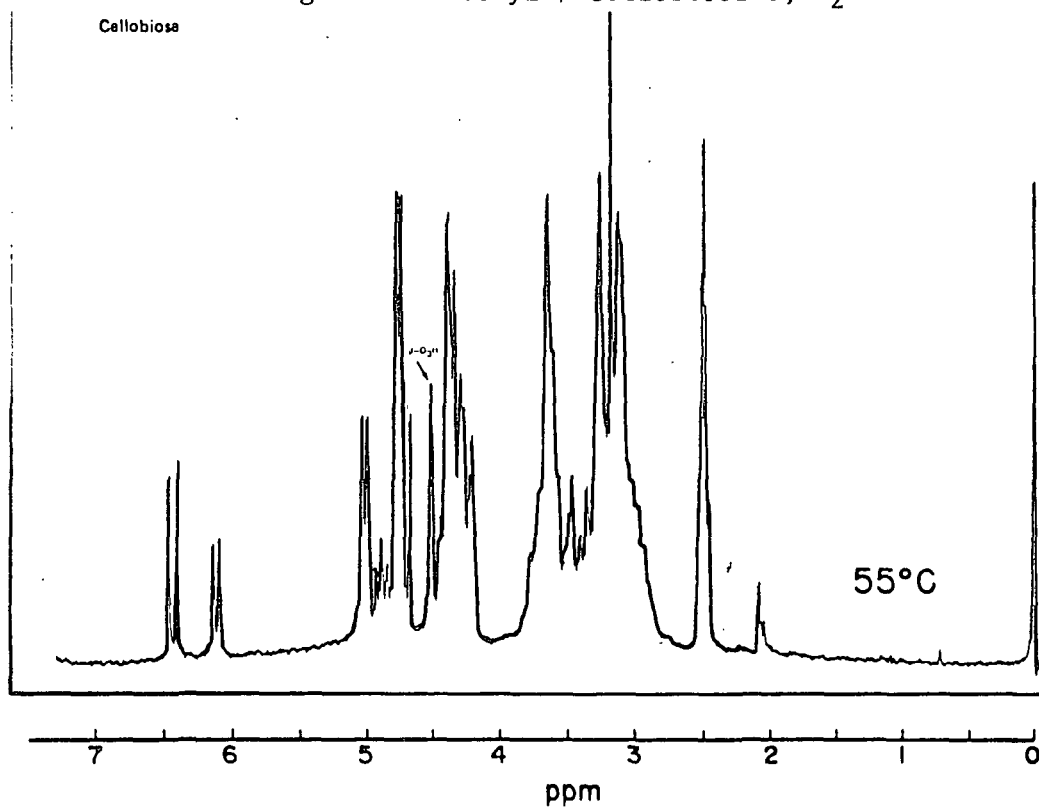
Figure 8. Cellobiose, 55°C.
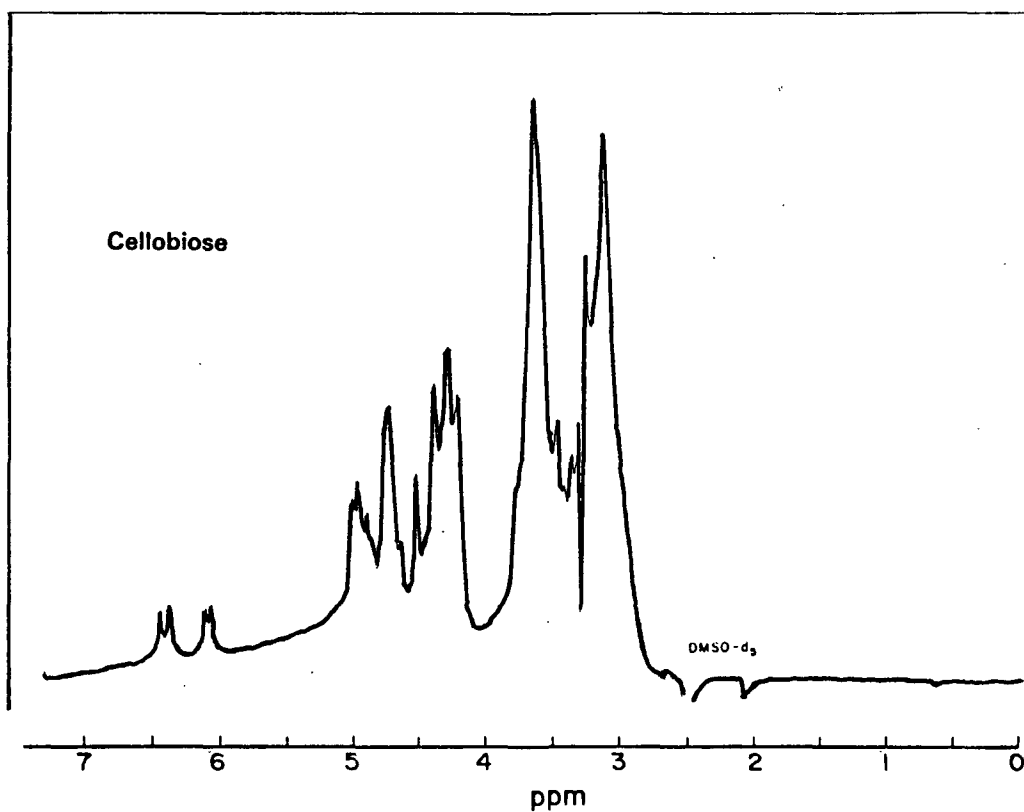
Figure 9. Cellobiose.
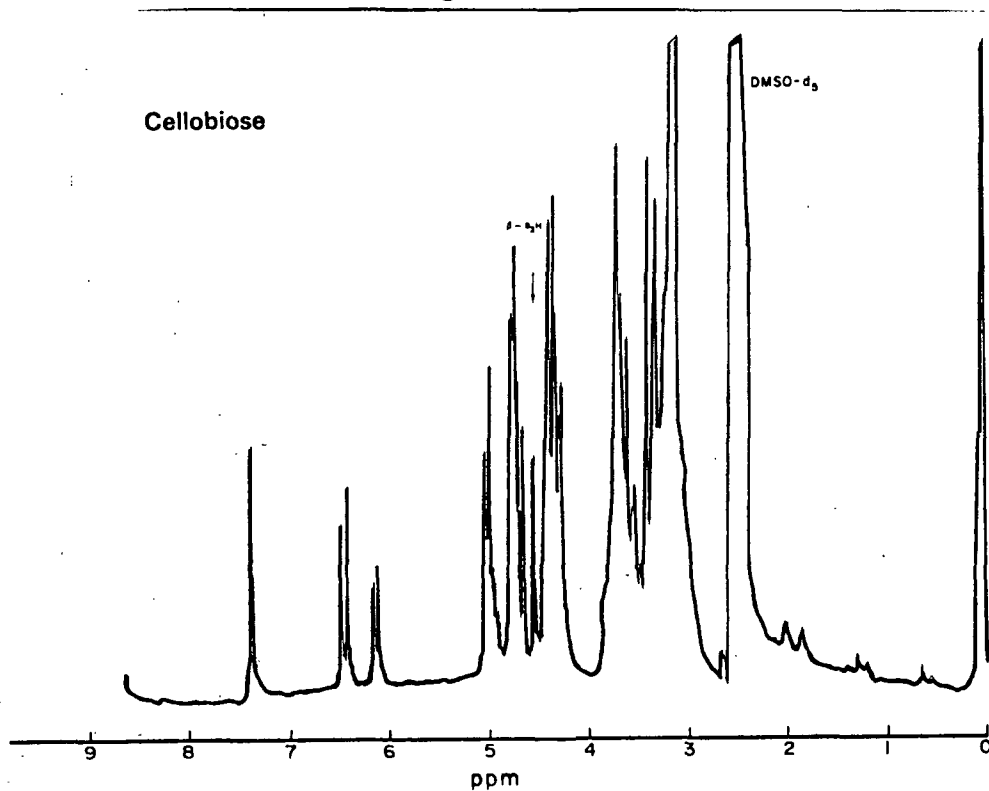
Figure 10. Cellobiose, 64°C.
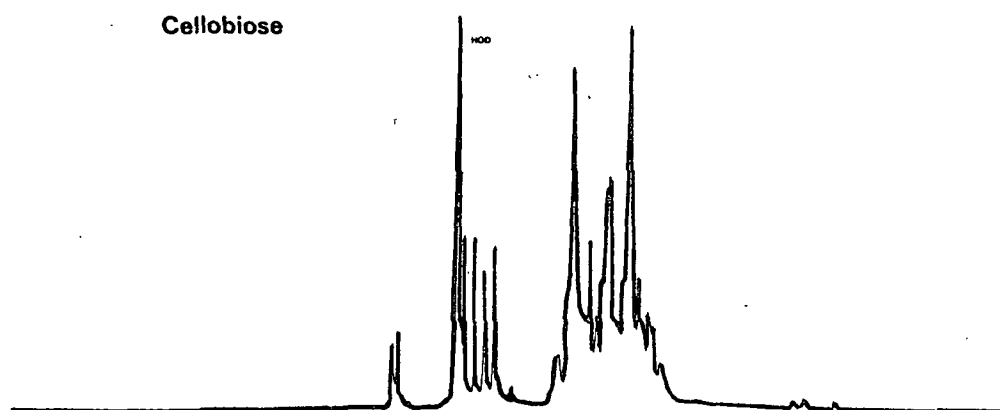
Figure 11. Cellobiose, D$_2$O.

ppm
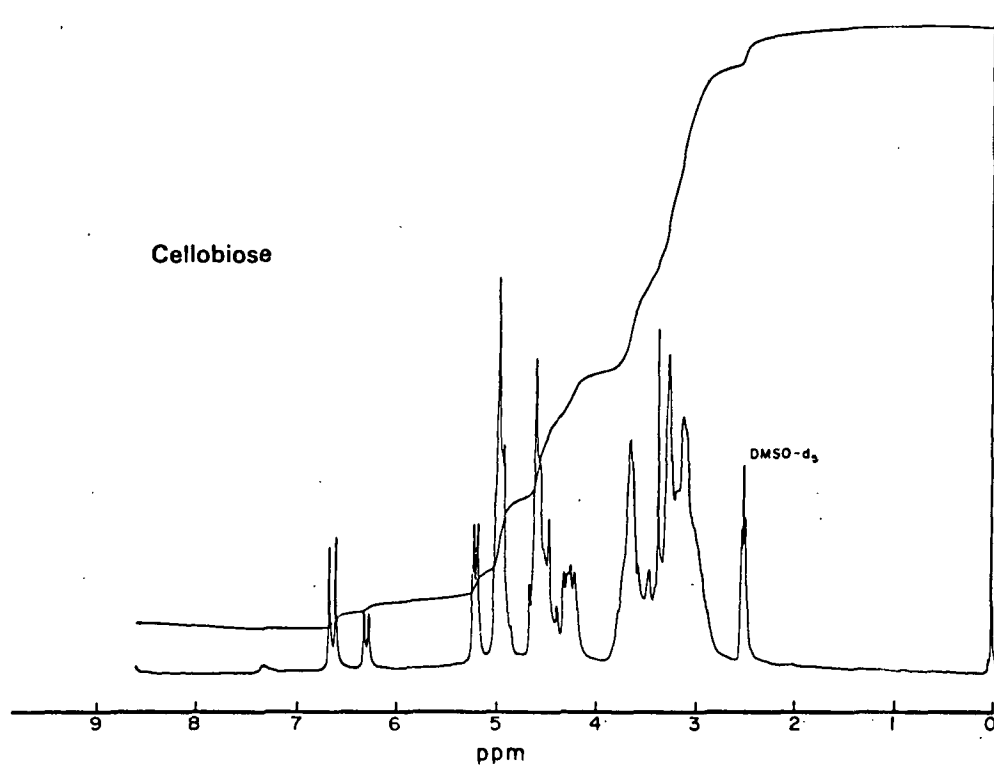
Figure 12. Cellobiose, integrated.
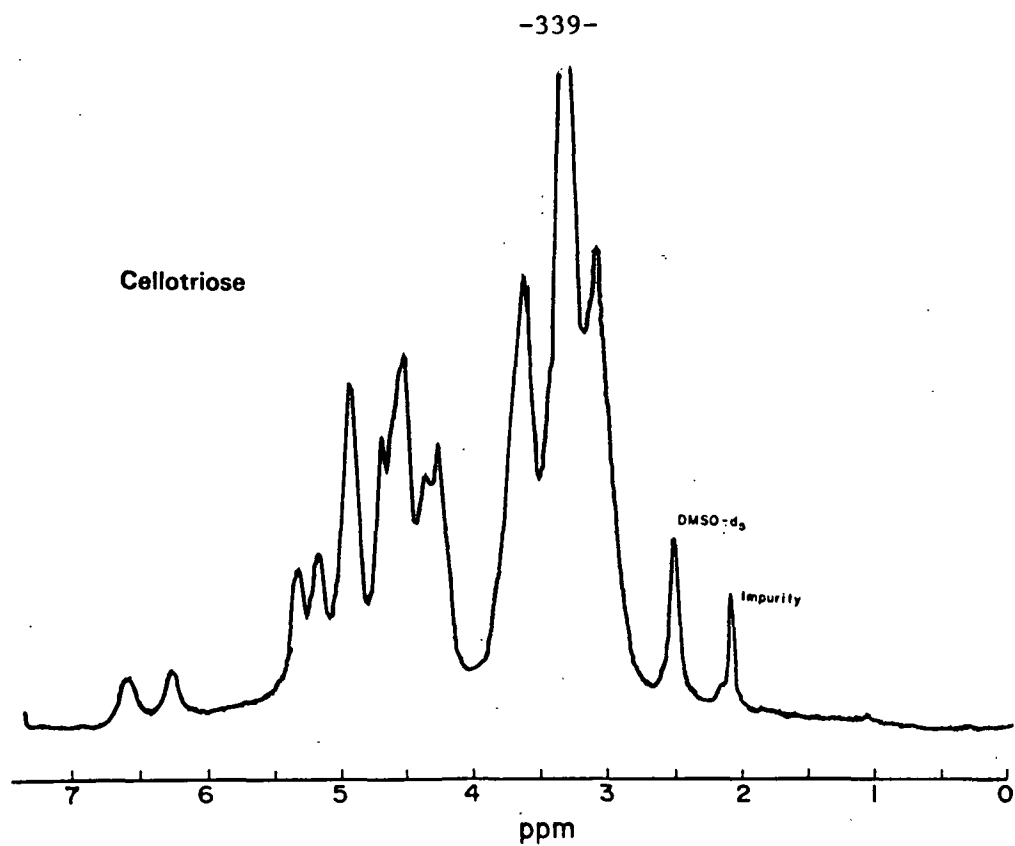
Figure 13. Cellotriose.
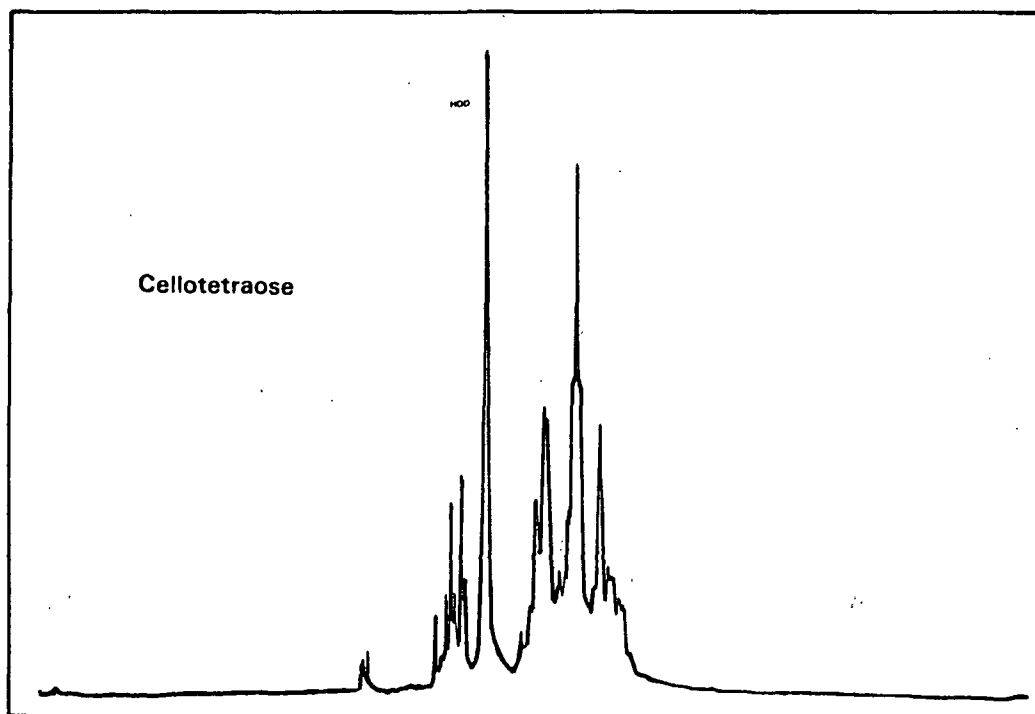
Figure 14. Cellotetraose, D_2O.
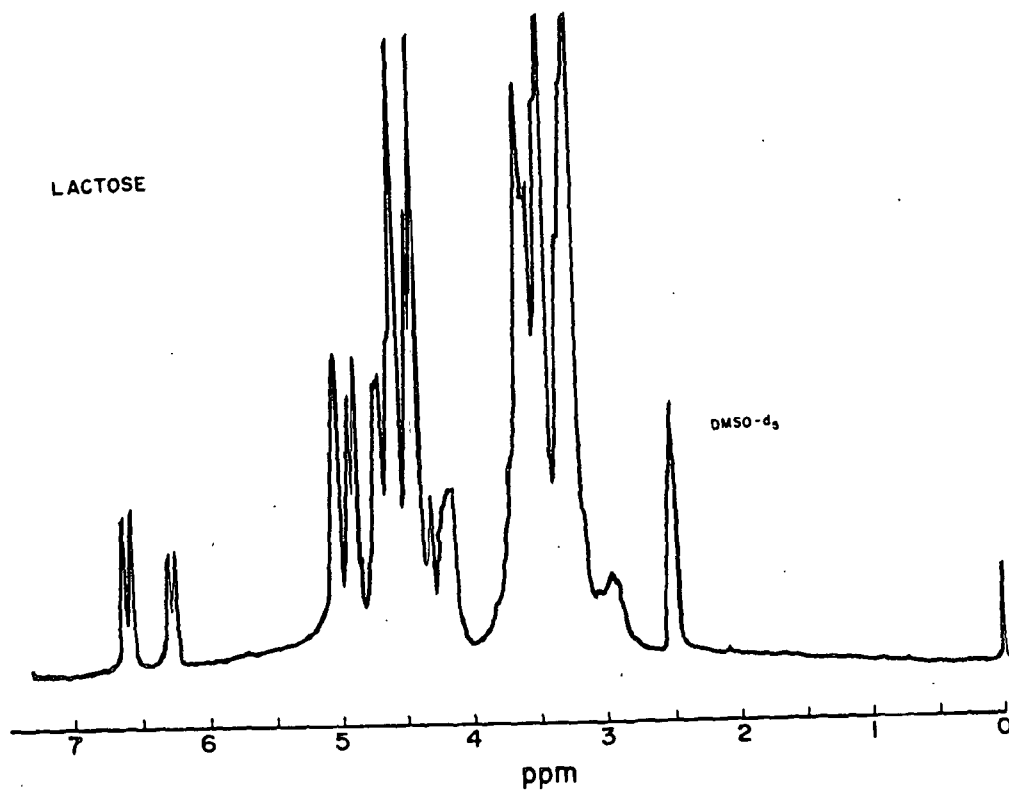
Figure 15. Lactose.
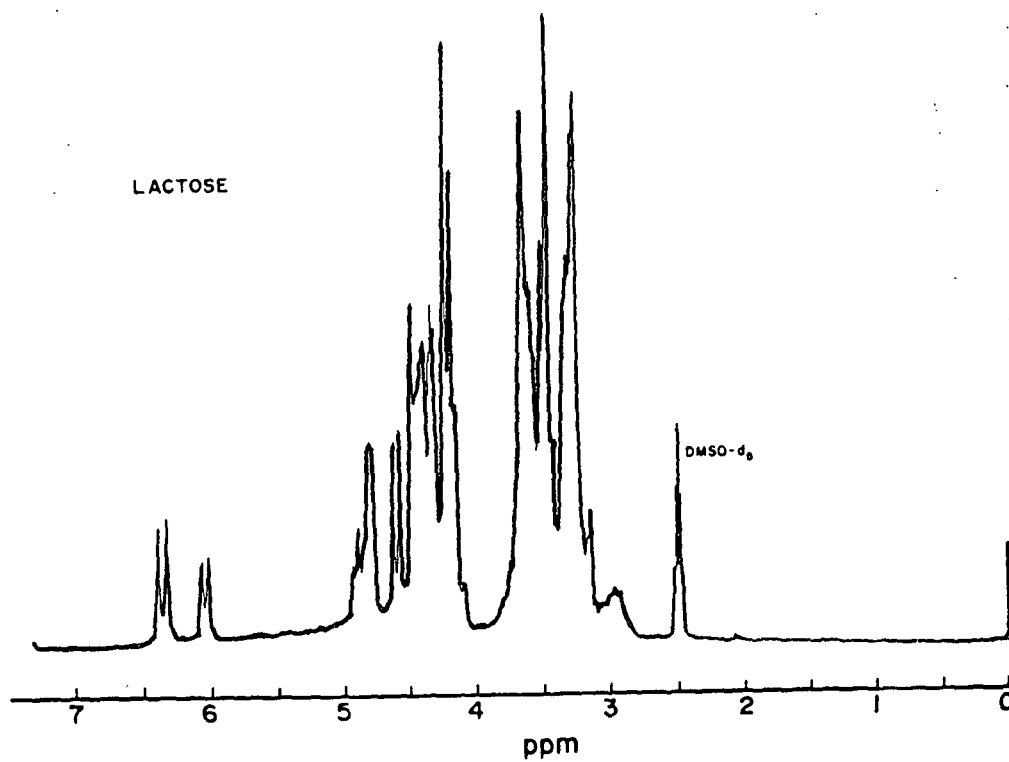
Figure 16. Lactose, 66.5°C.
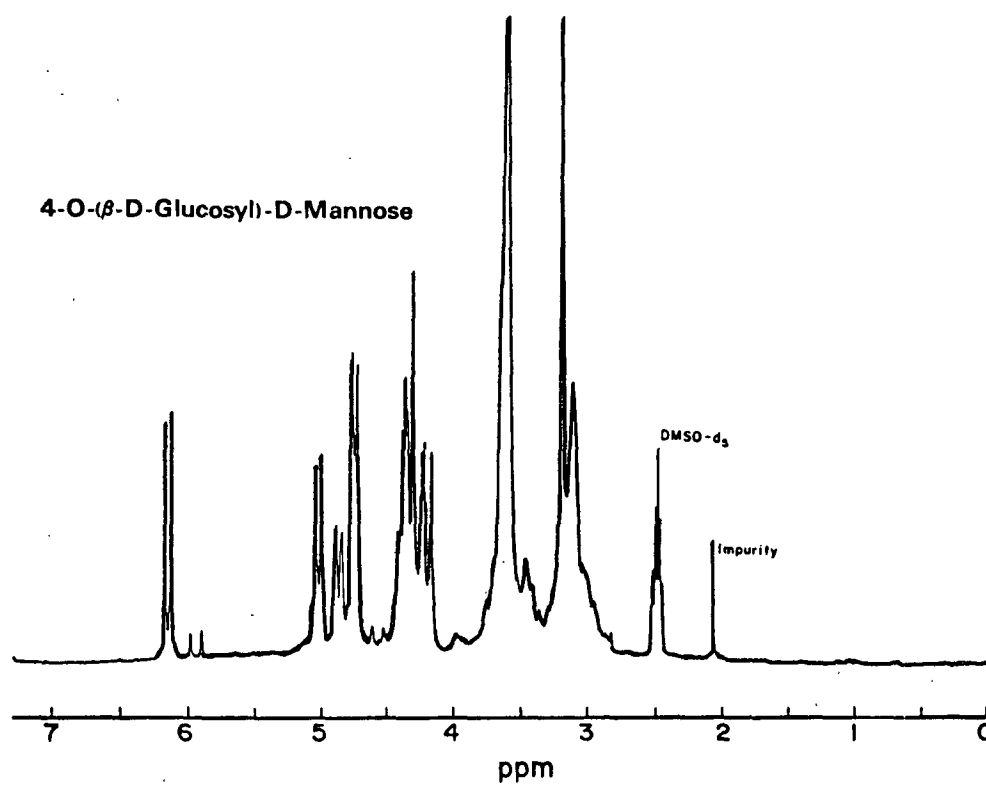
Figure 17. Glucosyl - Mannose, 55.5°C.
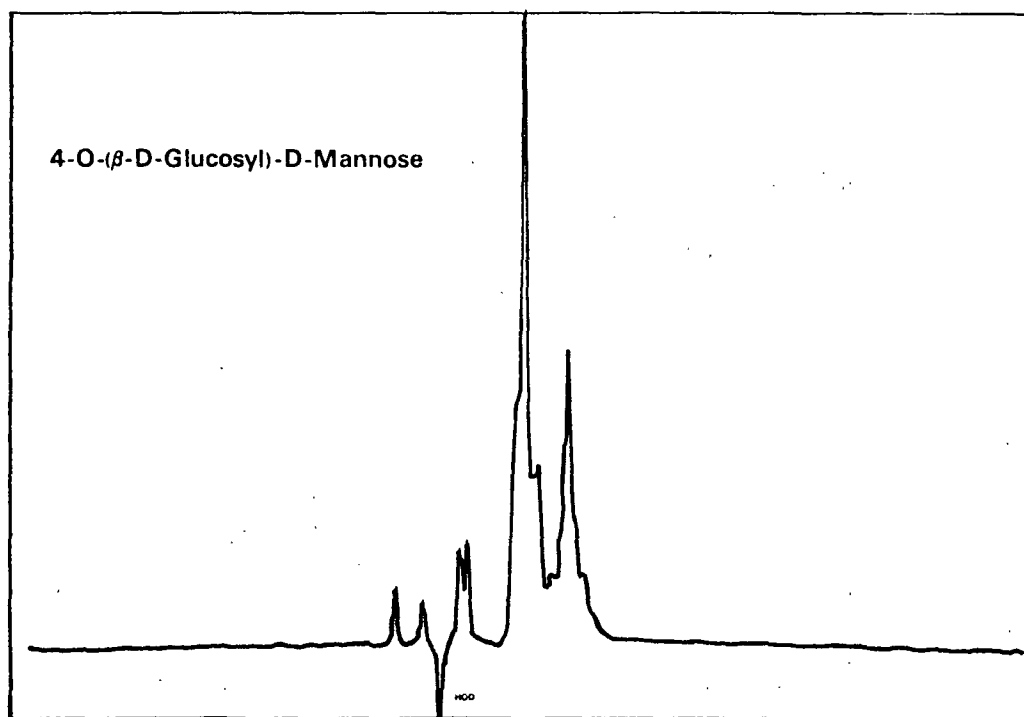
Figure 18. Glucosyl - Mannose, D₂O.
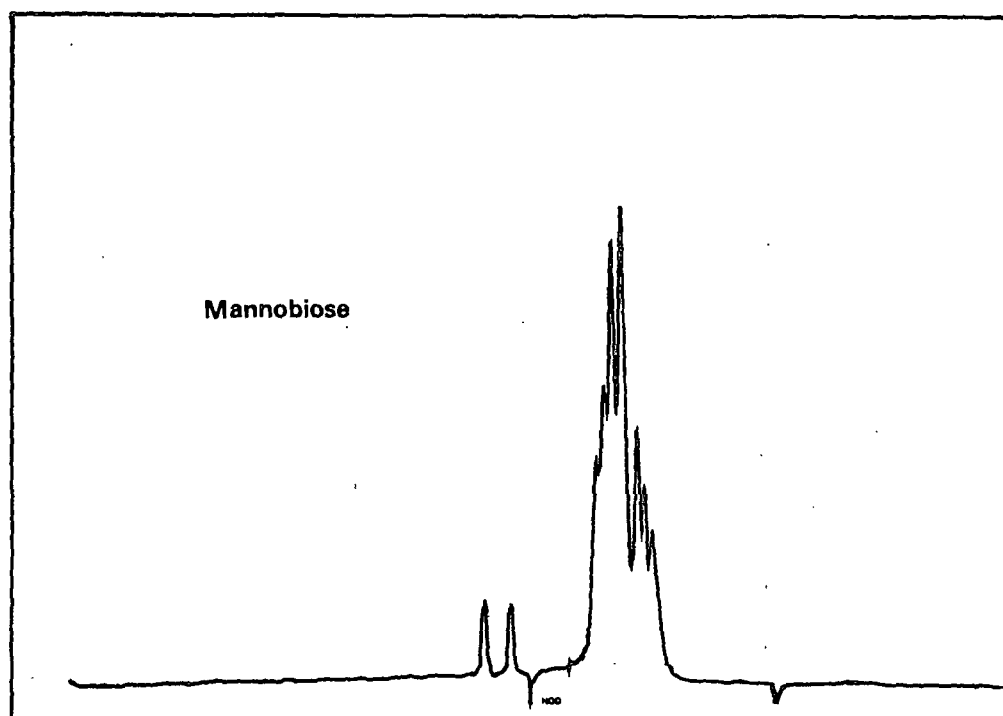
Figure 19. Mannobiose, D_2O.
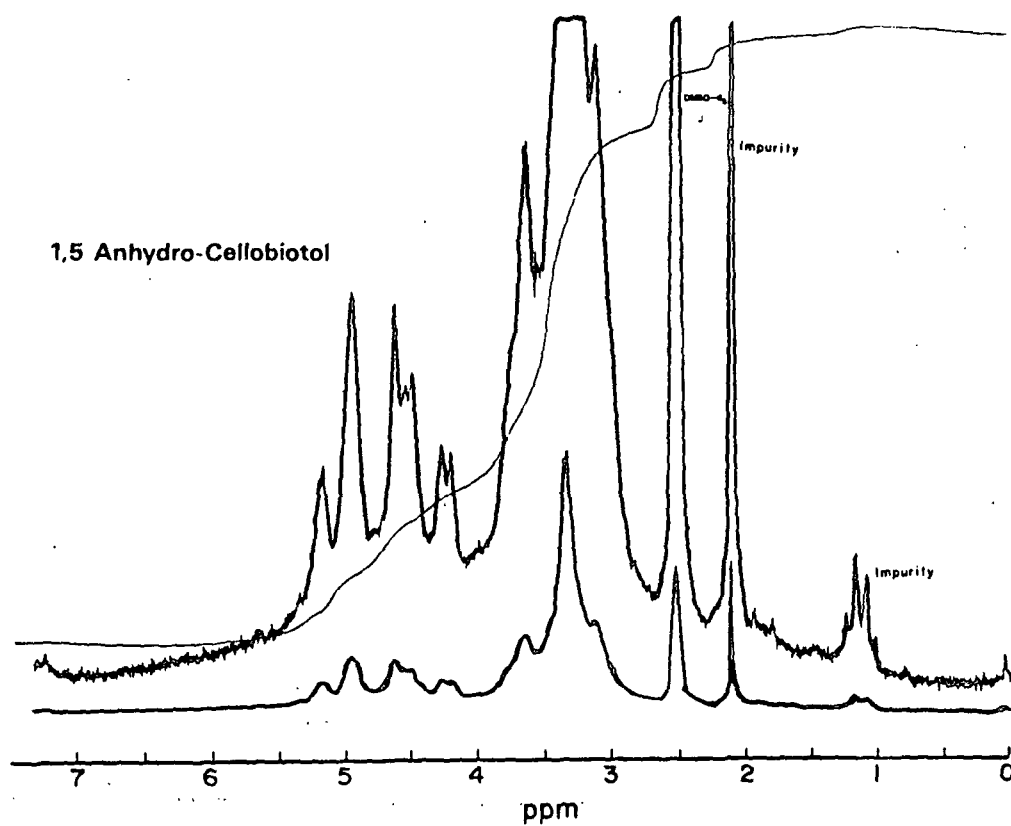
Figure 20. 1,5 anhydrocellobiotol.
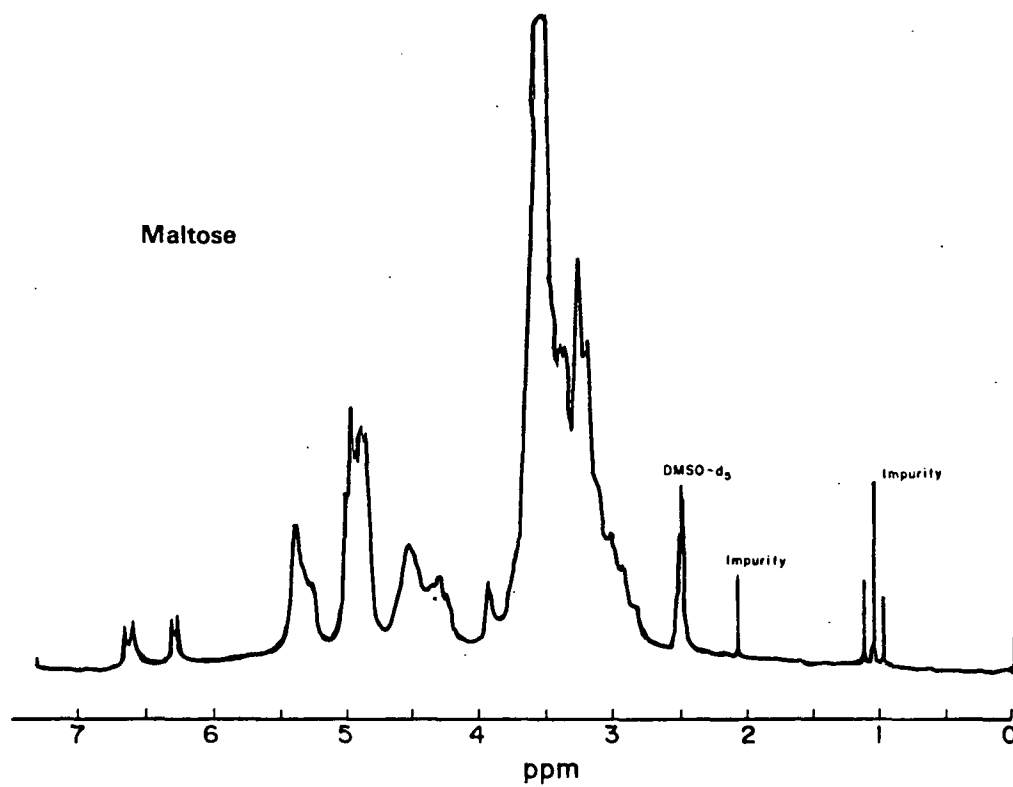
Figure 21. Maltose.

Figure 22. Starch, 51°C.

Xylobiose

DMSO-d₆

Impurity
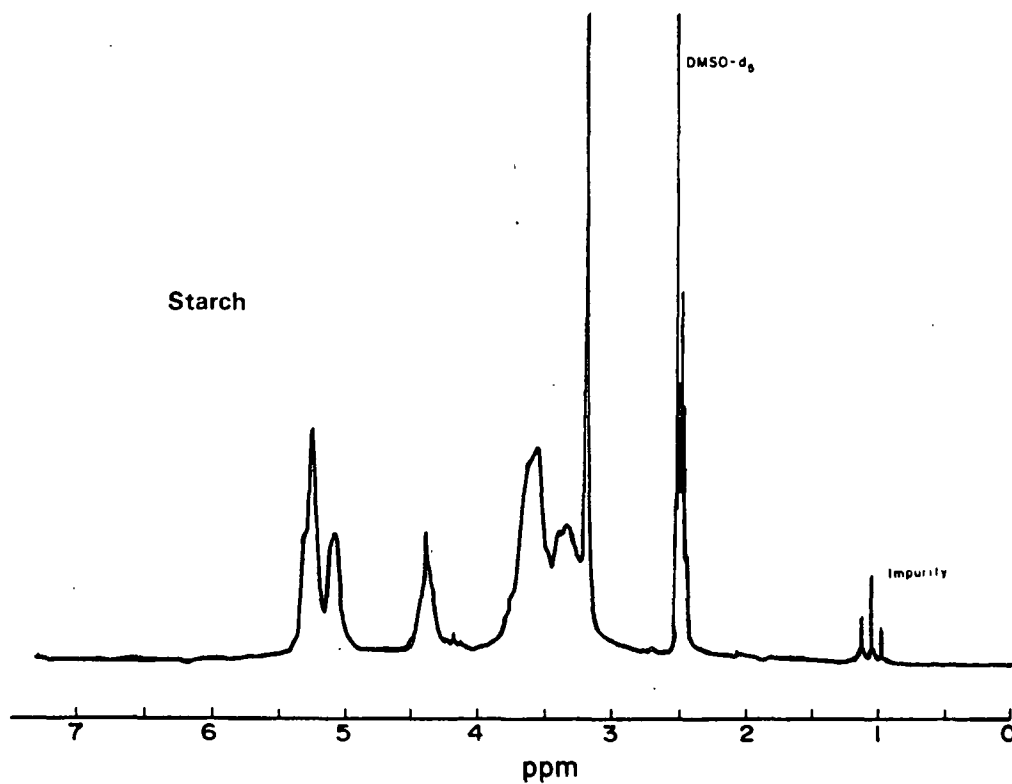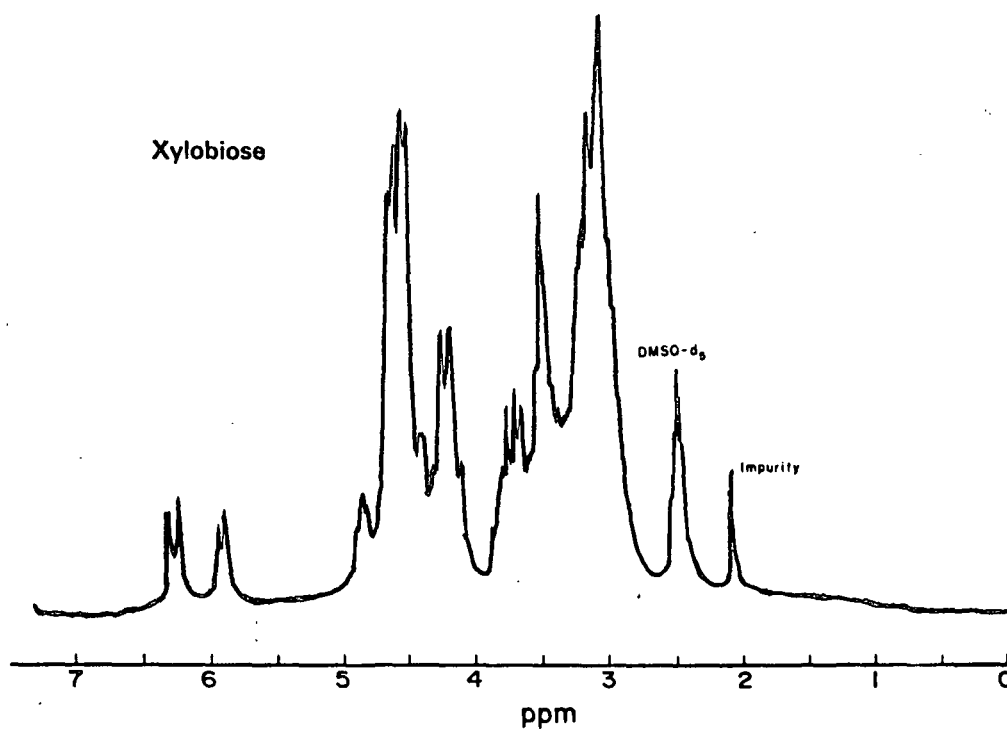
Figure 23. Xylobiose, 77.5°C.

Xylobiose

DMSO-d₅

Impurity
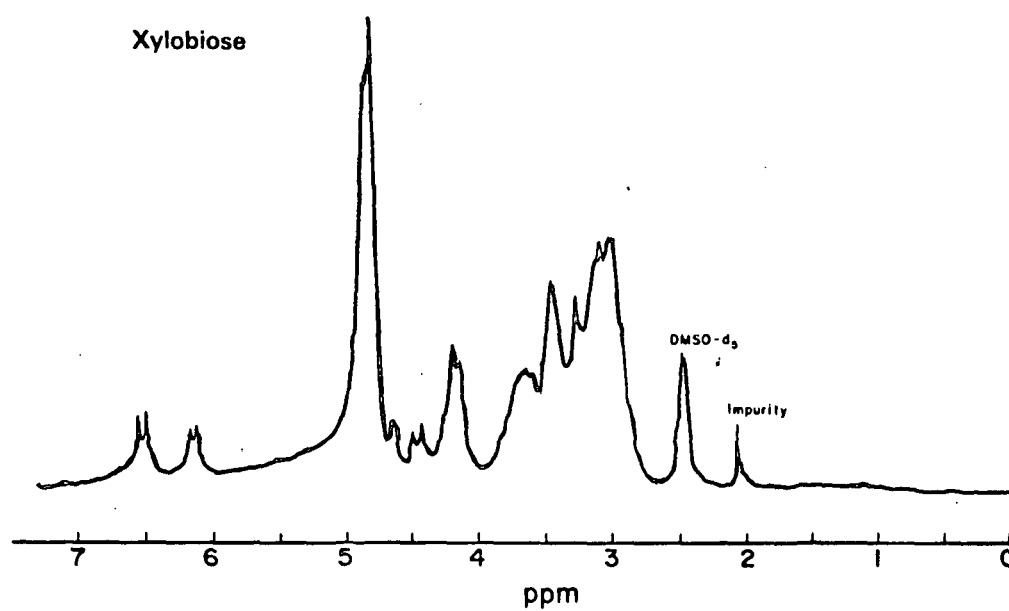
Figure 24. Xylobiose.
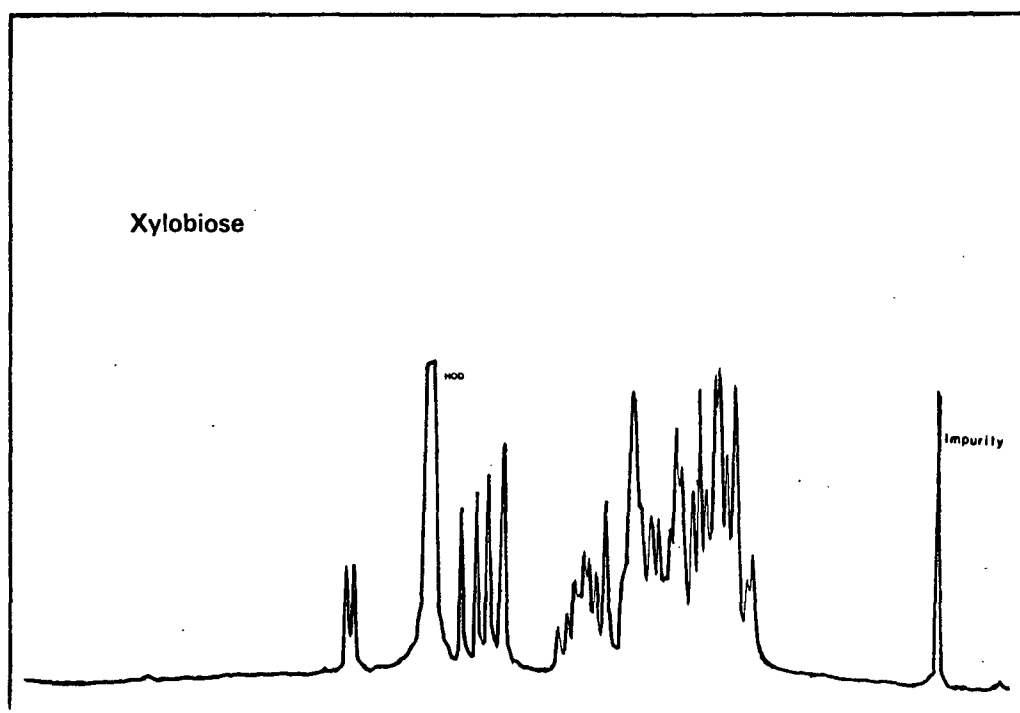
Figure 25. Xylobiose, D_2O.
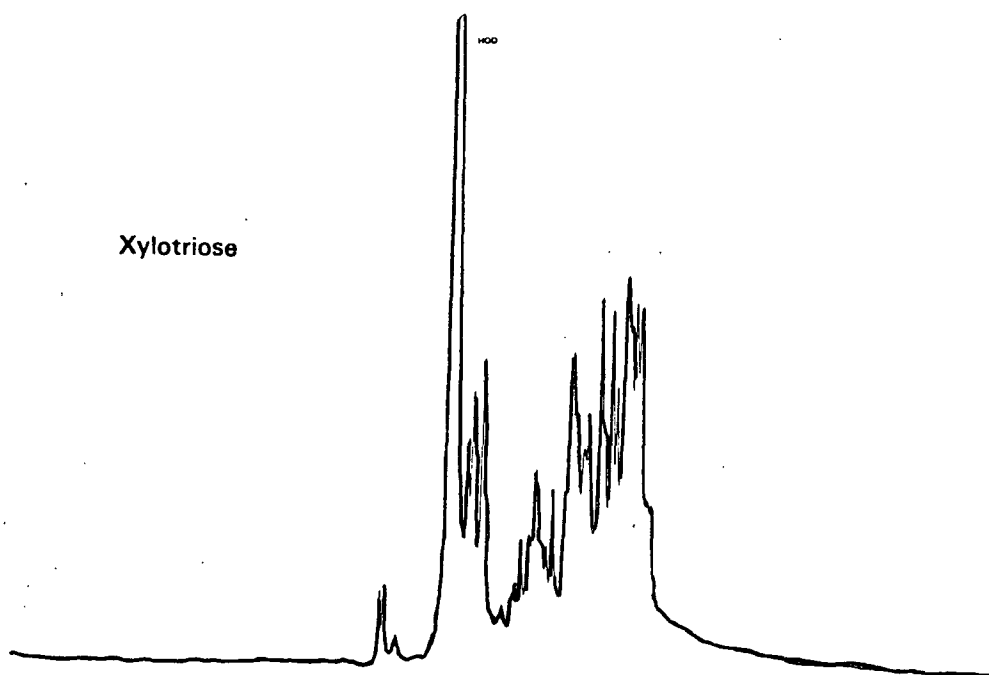
Figure 26. Xylotriose, D_2O.
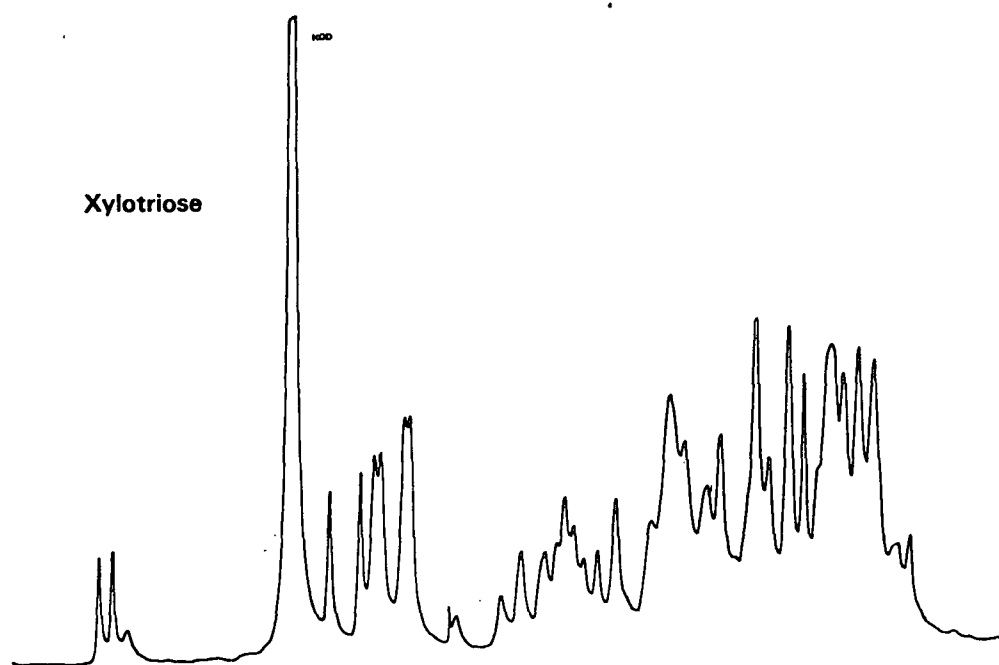
Xylotriose

Figure 27. Xylotriose, D$_2$O, expanded.
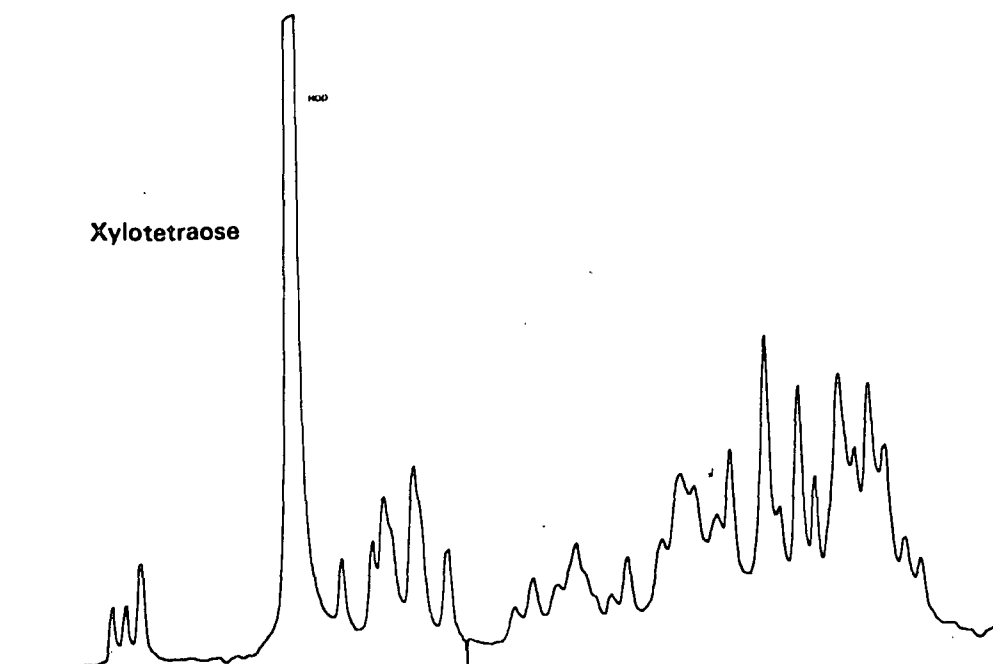
Xylotetraose

Figure 28. Xylotetraose, D$_2$O.

Aldotriuronic Acid

DMSO-d₅

ppm
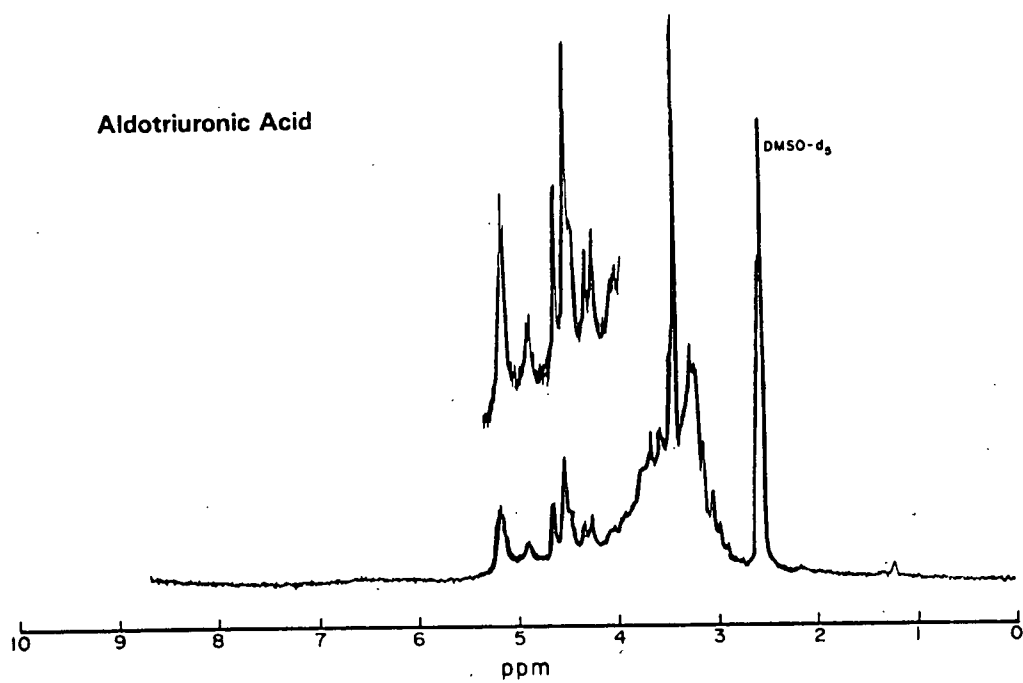
Figure 29. Aldotriuronic Acid.

Aldotriuronic Acid

HOD
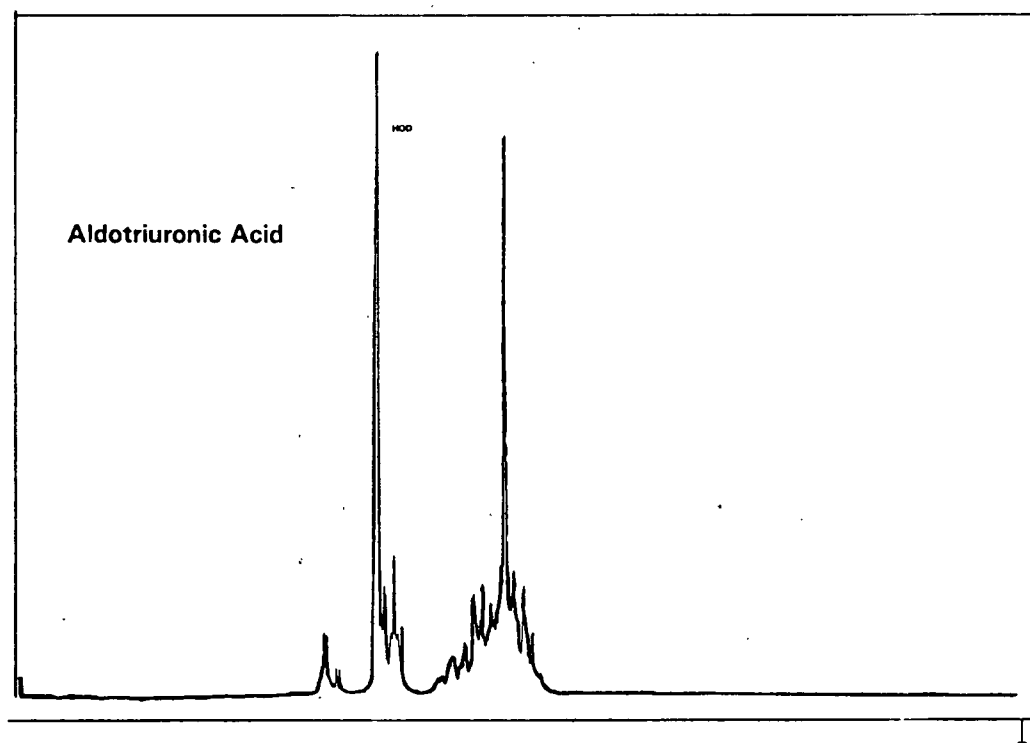
Figure 30. Aldotriuronic Acid, D₂O.
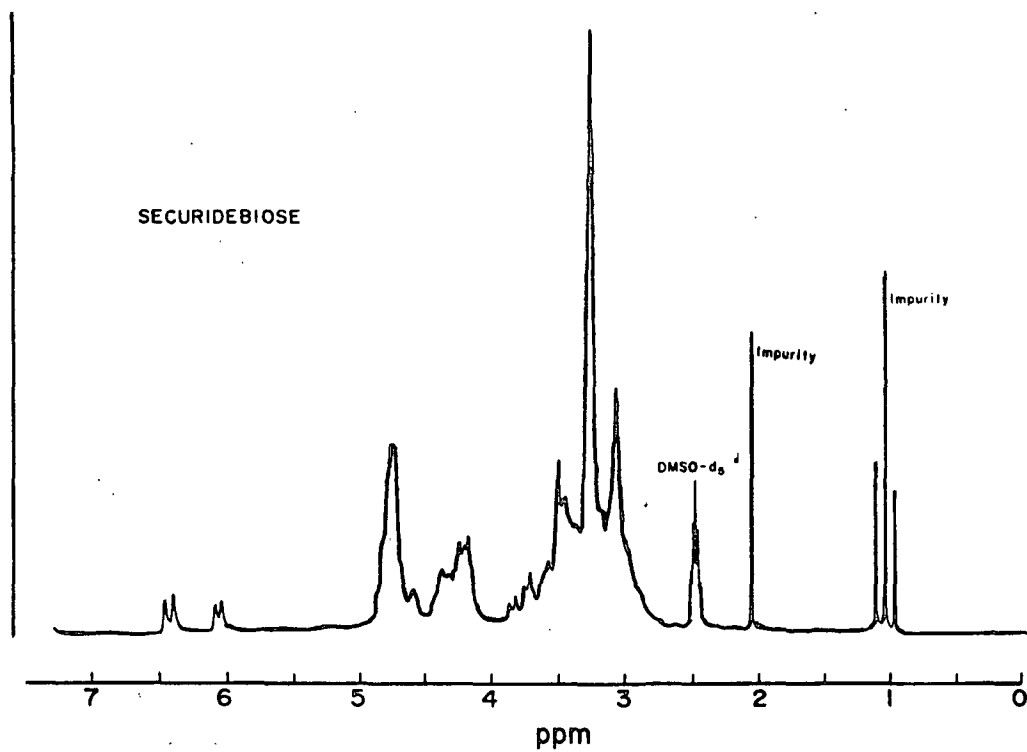
Figure 31.   Securidebiose, 51°C.
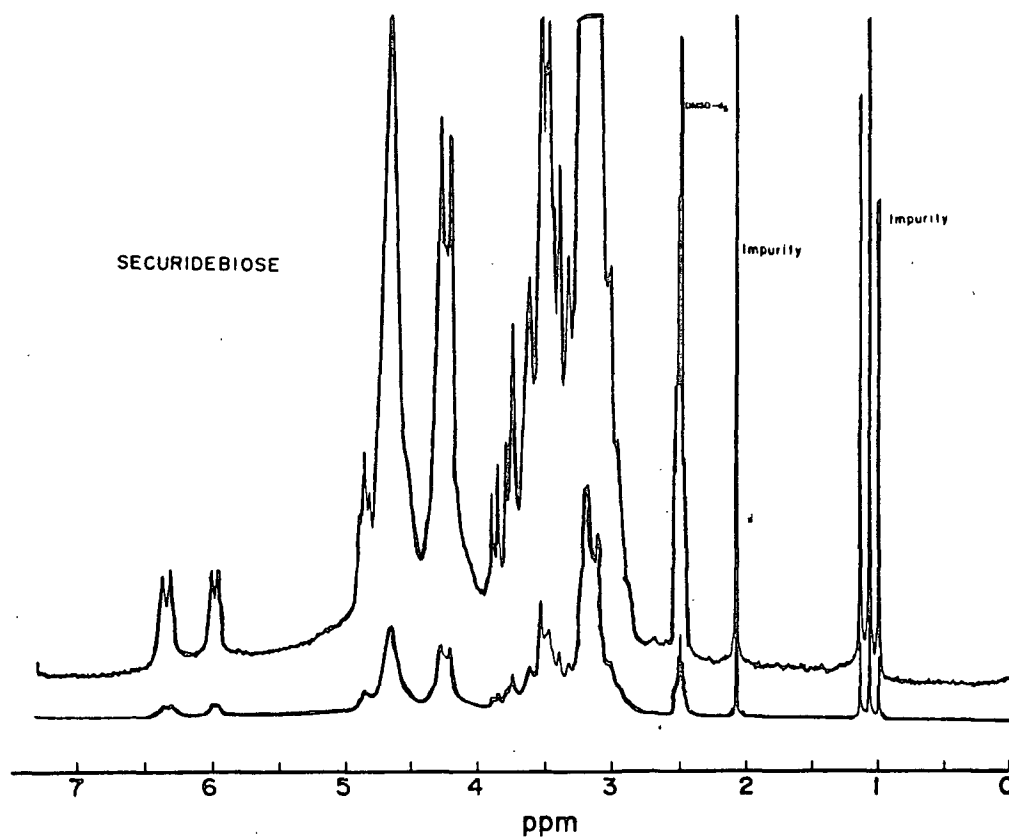
Figure 32.   Securidebiose, 67.5°C.
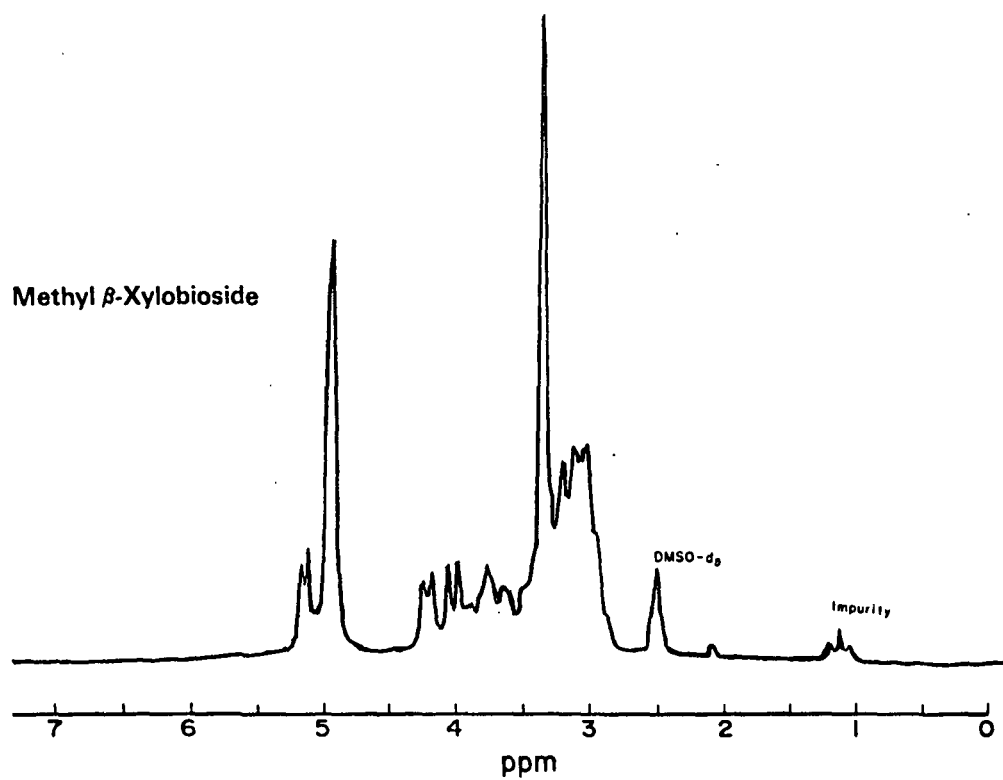
Figure 33.   Methyl β-xylobioside.
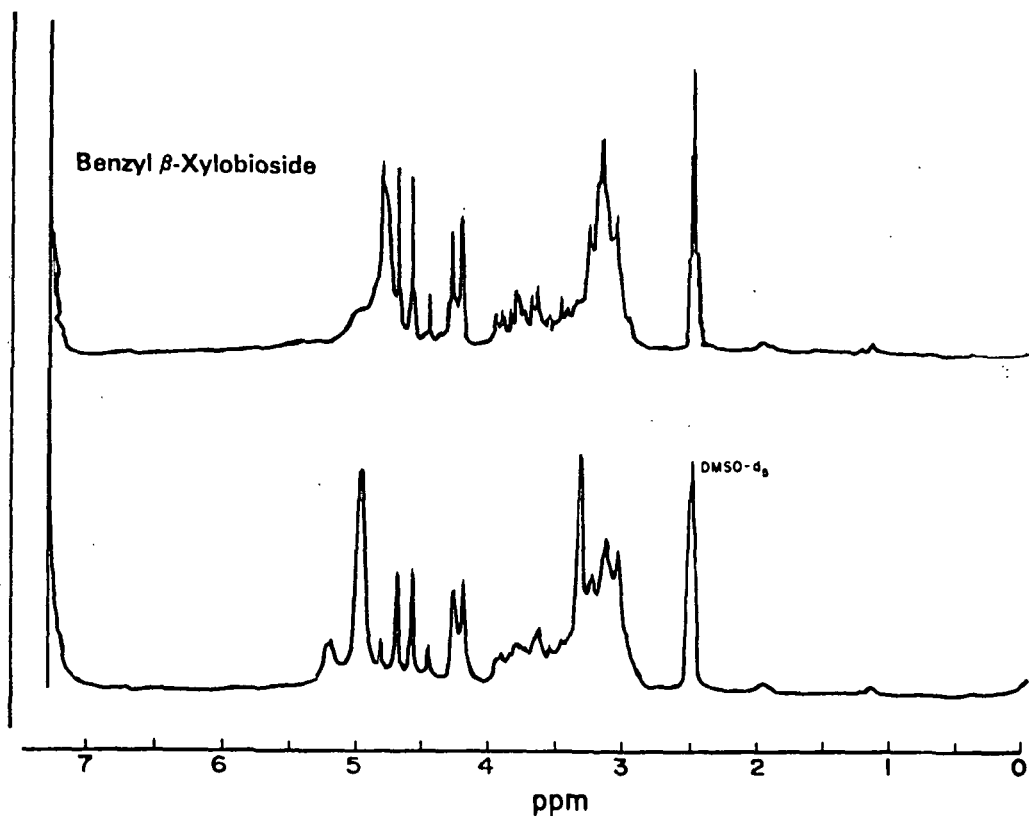
Figure 34.   Benzyl β-xylobioside.
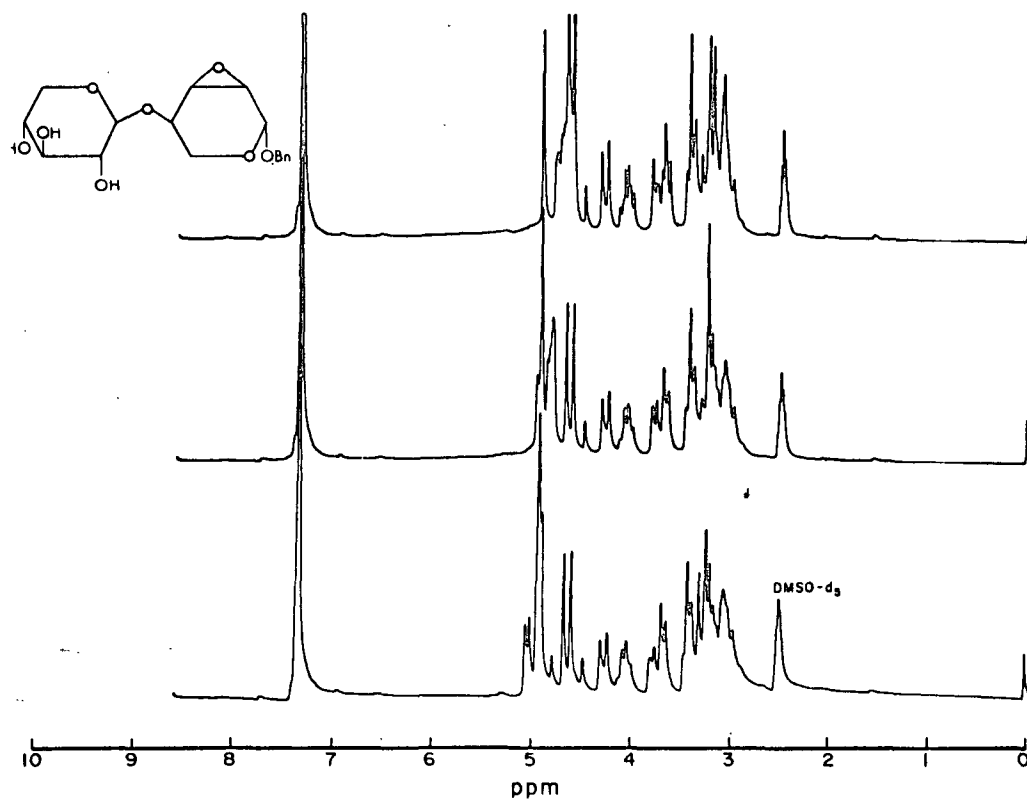
Figure 35. Benzyl 2,3 anhydro-4-O-(β-D-xylopyranosyl)-D-ribopyranoside.
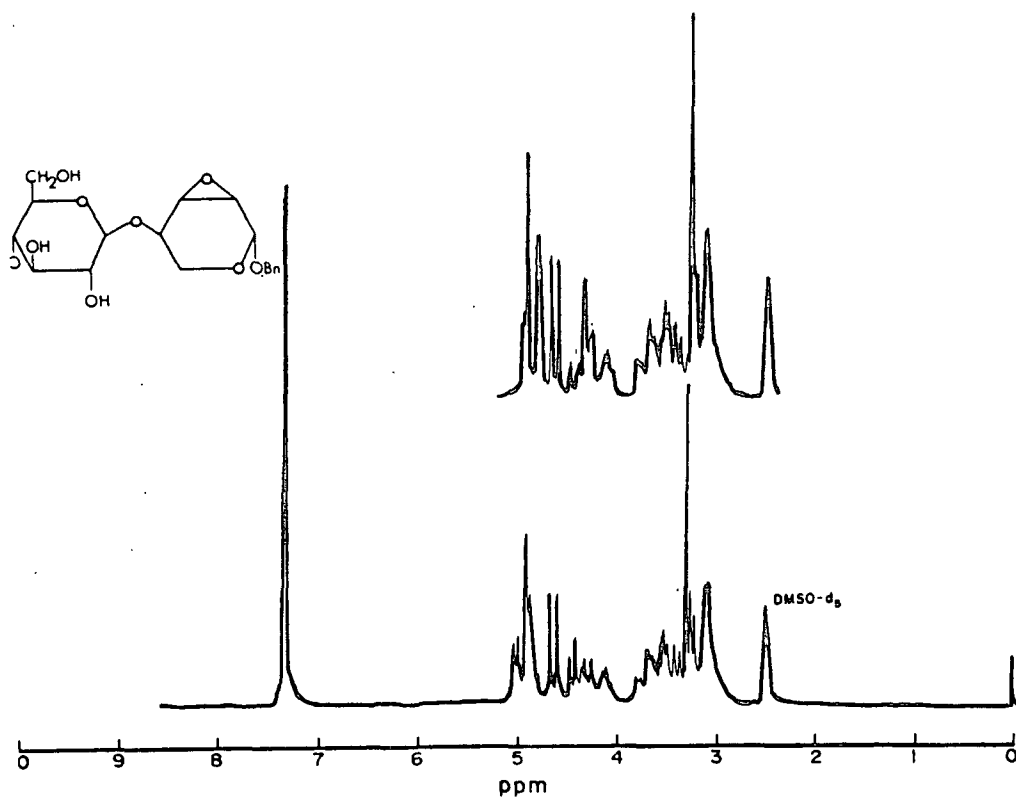
Figure 36. Benzyl 2,3 anhydro-4-O(β-D-glycopyranosyl)-D-ribopyranoside.
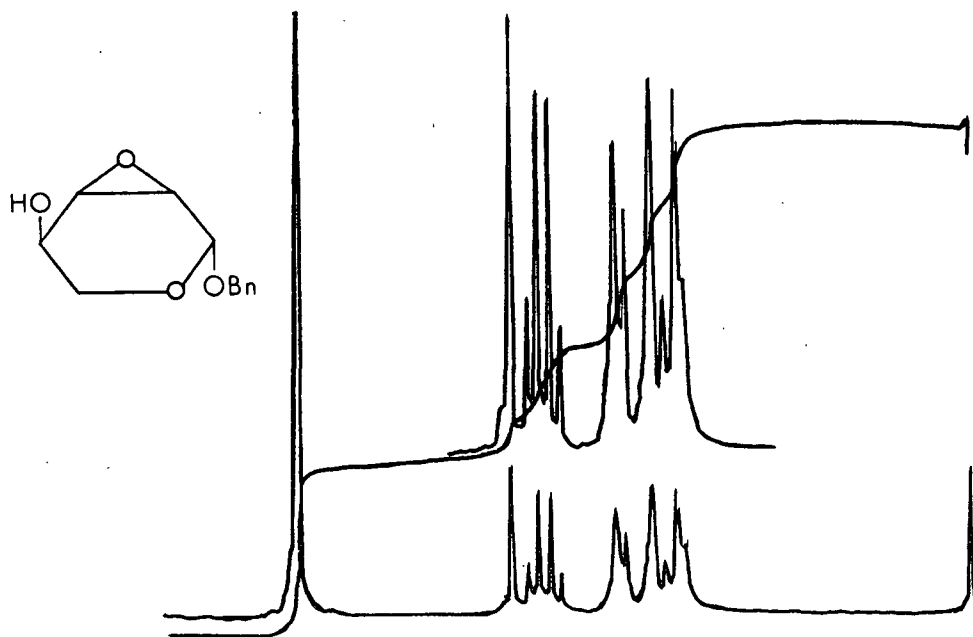
Figure 37. Benzyl 2,3 anhydro-D-ribopyranoside.
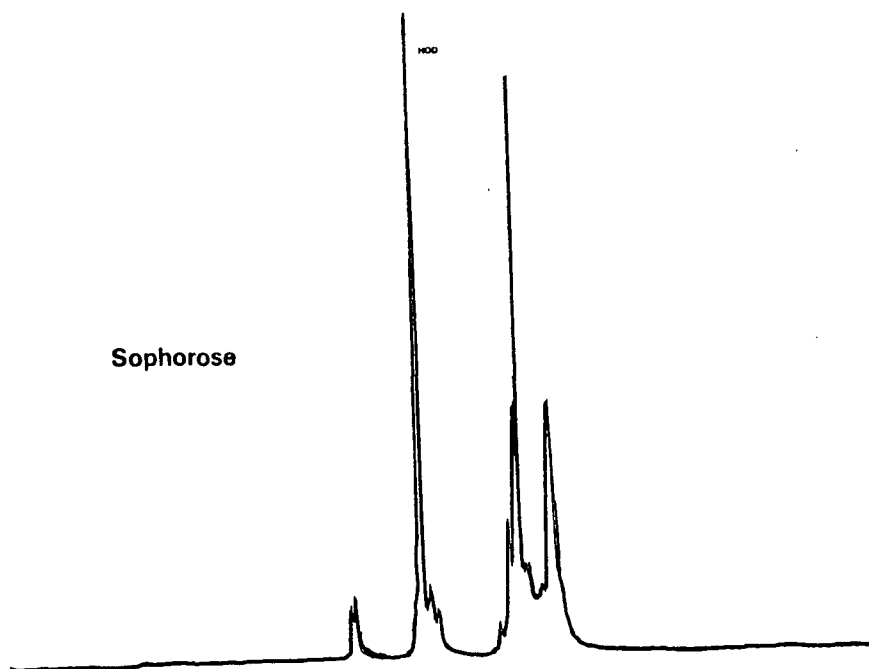
Figure 38. Sophorose.

APPENDIX VII

COMPILATIONS OF THE ^{1}H-NMR CHEMICAL SHIFT, COUPLING-
CONSTANT, AND CHEMICAL SHIFT TEMPERATURE COEFFICIENT
DATA OF THE CARBOHYDRATES STUDIED

The following tables contain the chemical shift, apparent coupling constant,
and temperature coefficient data for those compounds in which the DMSO-d$_6$ spectra
were studied as a function of temperature. The temperature coefficient and extrapo-
lated chemical shift data (to 56°C) were calculated using a least squares linear
regression analysis. In most cases the center of a spin-spin coupled signal set was
used. All shifts are relative to TMS using the DMSO-d$_5$ central peak (2.50 ppm) as
an intermediate reference. The letter designations of the individual signals are
defined in the previous Appendix.

For the most part the values included in the chemical shift tables are taken
directly from the NMR computer listings. Occasionally it was necessary to measure a
signal's location manually. When signals with different temperature coefficients
overlapped it was often difficult to get accurate measurements of the individual
signals. The results in the tables represent the best estimate. Such cases are
marked in the table. The high degree of linearity in the temperature coefficients
suggest that the estimates are reasonable. A key and a list of the compounds con-
tained in the tables is given below.

Compound	Tables
Glucose	1,15
MBG	2,16
Xylose	3,17
MBX	4,18
MαX	5,19
MBC2	6,20
Cellobiose	7,21,22,23,24,25,26
Lactose	8,27
GM	9,28
1,5 ANC2	10,19
Xylobiose	11,30,31,32
GX	12,33
Ben. 2,3 ANXR	13,34
Ben. 2,3 ANGR	14,35

Key:

J = apparent coupling constant (Hz).

* = measured by hand.

P = present as a distinct peak but chemical shift was not measured.

E = estimate, exact position obscured by other peaks.

C = set of coupled signals have coalesced into one broad signal.

TC = chemical shift temperature coefficient (Hz/°C).

R^2 = correlation coefficient from linear regression

Points = number of data points used in the linear regression.

Note: chemical shifts are given in ppm. Temperatures are in degrees centigrade.

TABLE I

GLUCOSE 9.7%[c]

Designation	°C 34	51[a]	56	74	34[b]
A	6.54 (6.5)	6.43 (6.6)	6.40 (6.5)	6.27 (6.5)	6.60
B	6.48	6.37	6.33	6.21	6.53
C	6.16 (4.1)	6.07 (4.1)	P	P	6.20
D	6.12	6.02	P	5.88	6.16
E	-	4.95	P	P	
F	4.90	4.91	P	4.92	
G	4.85	4.86	P	P	
H	4.80 (4.3)	4.66 (3.0)	4.62(C)	4.48(C)	4.85
I	4.76	4.63			4.81
J	-	4.62(E)			
K	4.69	4.58*	4.58	4.43(C)	4.76
L	4.36(E)				P
M	4.31				P
N	4.61 (4.6)	4.49 (4.4)		4.29(E)	4.68
O	4.56	4.44		4.23(E)	4.63
P	4.48		4.35(E)		
Q	4.43	4.29(E)	4.27(E)	4.13(E)	4.50
R	4.36(E)				4.43
S	4.33		4.32(E)	4.36	
T	4.26		4.27(E)	4.29(E)	4.26
U	4.19		4.21	4.23(E)	4.19

Chemical Shift (J)

[a]Recorded several weeks earlier, β-anomer predominates.
[b]4.3% H_2O added.
[c]Three additional samples at 2.0, 5.4, and 9.9% exhibit shifts for A of 6.57 ppm each.

Assignments:

    A,B = β-O_1H
    C,D = α-O_1H
  E,F,G = α-C_1H
    H,I = β-O_3H,α-O_4H   β-O_2H,α-O_4H.
    J,K =   β-O_2H,α-O_4H.
    L,M = α-O_2H
    N,O = α-O_3H
  P,Q,R = O_6H
  S,T,U = β-C_1H

TABLE II

METHYL β-GLUCOPYRANOSIDE
15.1%

Designation	°C 34	Chemical Shift (J) 54.5	56	74
A	5.00 (4.4)	4.84 (4.5)	4.82 (4.4)	4.68 (4.4)
B	4.96	4.78	4.77	4.64
C	4.85(C)	4.72 (3.8)	4.70 (3.0)	4.59 (3.8)
D		4.69	4.67	4.56
E		4.38	4.36	4.25
F	4.47 (5.9)	4.32 (5.9)	4.30 (5.9)	4.19 (5.9)
G	4.41	4.26	4.24	4.13
H	4.06 (7.3)	4.07 (7.2)	4.08 (7.2)	4.09 (7.2)
I	3.99	4.00	4.00	4.02
OMe	3.38	3.38	3.38	3.39

Assignments:
A,B = O_2H
C,D = O_3H, O_4H
E,F,G = O_6H
H,I = C_1H

TABLE III

XYLOSE
8.6%

| | | Chemical Shift (J) | |
Designation	°C 34.2	54	74.5
A	6.52 (6.5)	6.37 (6.5)	6.24
B	6.45	6.31	6.17
C	6.10 (4.8)	5.98 (4.5)	
D	6.06	5.93	5.81
E			
F		4.86	4.87
G		4.81	
H	4.80(C)	4.67(C)	4.49*(C)
I			
J	4.66 (4.1)	4.52 (4.1)	4.40* (3.9)
K	4.62	4.48	4.36
L	4.44 (6.5)	4.28	4.14 (6.6)
M	4.38	4.22(E)	4.08
N	4.27		4.32*
O	4.20	4.22(E)	4.25*
P	4.13	4.16	4.18*

Assignments:
   A,B = β-O_1H
   C,D = α-O_1H
 E,F,G = α-C_1H
   H,I = β-O_2H,β-O_3H,O_4H
   J,K = α-O_3H
   L,M = α-O_2H
 N,O,P = β-C_1H

TABLE IV

METHYL β-XYLOPYRANOSIDE
17.9%

Designation	°C	Chemical Shift (J)		
		34	54.5	74
A		5.00 (4.5)	4.83 (4.7)	4.69 (4.3)
B		4.95	4.78	4.65
C		4.90(C)	4.76*	4.65*
D			4.72(E)	4.60(E)
E		4.85(C)	4.72(E)	4.60(E)
F			4.68*	4.55
G		4.02 (7.0)	4.04 (7.0)	4.06 (7.0)
H		3.95	3.97	3.99
OMe		3.34	3.35	3.35

Assignments:
   A,B = O_2H
C,D,E,F = O_3H, O_4H
   G,H = C_1H

TABLE V

METHYL α-XYLOPYRANOSIDE
15.9%

Designation	°C	Chemical Shift (J)	
		30	56
A		4.83	4.70*
B		4.69	4.55*
C		4.64 (5.9)	4.47*
D		4.58	4.41*
E		4.49	4.51*
F		4.46	4.47*
OMe		3.25	3.26*

Assignments:
   A = O_4H
   B = O_3H
  C,D = O_2H
  E,F = C_1H

TABLE VI

METHYL β-CELLOBIOSIDE
3.6%

		Chemical Shift (J)	
Designation	°C 31	56	63
A	5.22 (4.7)	5.06 (4.5)	5.00 (4.1)
B	5.17	5.01	4.96
C	5.15 (4.8)	4.96 (4.7)	4.88 (4.6)
D	5.10	4.91	4.84
E	4.98(C)	4.81 (4.2)	4.73 (3.4)
F		4.76	4.71
G	4.65(E)	4.58(2.8)[a]	4.56(3.4)
H	4.65(E)	4.47	4.42
I	4.57	4.42	4.36
J	4.52	4.37	P
K	4.29 (7.3)	4.31 (7.5)	4.32 (7.1)
L	4.21	4.24	4.25
M	4.13 (7.7)	4.14 (7.5)	4.15 (7.6)
N	4.06	4.07	4.07
OMe	3.36	3.40	3.40

[a] = whh

Assignments:
$A,B = O_2'H$
$C,D = O_2H$
$E,F = O_3'H, O_4'H$
$G = O_3H$
$H,I,J = O_6H, O_6'H$
$K,L = C_1'H$
$M,N = C_1H$

TABLE VII

CELLOBIOSE[a]
4.1%

				Chemical Shift (J)			
Designation	°C	32	44	55	67	76	90
A		6.65 (6.5)	6.57 (6.6)	6.49 (6.6)	6.41 (6.6)	6.36 (6.4)	6.27 (6.5)
B		6.58	6.51	6.43	6.35	6.29	6.20
C		6.30 (4.5)	6.24 (4.7)	6.16 (4.5)	6.09 (4.3)	6.04 (4.6)	5.95 (4.5)
D		6.26	6.19	6.12	6.05	5.99	5.91
E		5.21 (4.2)	5.13 (3.9)	5.04 (4.1)	4.98 (4.0)	4.93 (3.8)	4.84 (3.3)
F		5.16	5.09	5.01	4.94	4.89	4.80
G			4.94				
H				4.91			4.94
I							4.90
J		4.94(E)	4.89 (4.3)	4.81 (4.1)	4.72 (3.6)	4.63(C)	4.55(C)
K			4.85	4.76	4.69		
L				4.74 (4.7)	4.64 (4.8)	4.57 (4.8)	4.46(E)
M		4.89	4.80	4.69	4.60	4.52	
N		4.60	4.57	4.54 (3.0)[c]	4.52 (3.2)[c]	4.49 (3.2)[c]	4.46(E)
O		4.63		4.46			
P[b]		4.54(E)	4.45(E)	4.38(E)	4.31(E)		
Q		4.32	4.32				
R		4.29	4.30	4.32(E)			
S		4.25	4.25	4.26			
T		4.21	4.23	4.24	4.25		
U		3.66	3.67	3.68	3.68	3.69	3.70
V		3.26	3.27	3.28	3.30	3.31	3.32
W		3.12	3.13	3.15	3.14(E)	3.17	3.18
H_2O		3.32	3.27	3.20	3.14(E)	3.09	3.01

[a]Temperature coefficients are given for samples at other concentrations and with H_2O and D_2O added.

[b]The estimated location of the O_6H, $O_6'H$ peak. Usually the largest peak in this region.

[c]whh.

Assignments:

A,B = β-O_1H
C,D = α-O_1H
E,F = $O_2'H$
G,H,I = α-C_1H
J,K = $O_3'H$,$O_4'H$

L,M = β-O_2H
N = β-O_3H
O,P = O_6H,$O_6'H$ and others

Q,R,S,T = C_1H,$C_1'H$
U,V,W = major back bone signals.

TABLE VIII

LACTOSE 9.6%

Designation	°C 33[a]	40.8	54	66.5	78
		Chemical Shift (J)			
A	6.63 (6.1)	6.58 (6.5)	6.49 (6.5)	6.41 (6.4)	6.34 (6.4)
B	6.57	6.52	6.43	6.34	6.27
C	6.29 (4.6)	6.24 (4.4)	6.16	6.08 (4.6)	6.02 (4.6)
D	6.25	6.20	6.11	6.04	5.97
E				4.95	4.96
F				4.91	4.92
G				4.86	4.88
H	5.04	4.98(2.6)[b]	4.91	4.83	4.75(E)
I	4.93 (4.0)	4.87 (4.8)	4.75 (4.8)	4.65 (4.7)	4.56
J	4.89	4.82	4.70	4.60	4.51
K	4.72(0)	4.68			4.36(E)
L		4.63		4.42	
M	4.59	4.57	4.54	4.51	4.49
N[c]	4.49	4.43	4.34.	4.26	4.20
O[c]	4.44	4.39	4.29	4.22	
P	4.20	4.23			

---

[a]Spectrum has poor resolution.
[b]Actually two peaks resolved in this spectrum at 5.00 at 4.97 ppm.
[c]Largest peaks in the region.

Assignments:
    A,B = β-O_1H
    C,D = α-O_1H
  E,F,G = α-C_1H
    I,J = β-O_2H
      M = β-O_3H
    N,O = O_6H, $O_6'H$
      P = β-C_1H or $C_1'H$

TABLE IX

4-O-(β-D-GLUCOPYRANOSYL)-D-MANNOPYRANOSE
6.1%

Designation	°C 36	Chemical Shift (J) 55.4	72
A	6.31 (4.4)	6.20 (4.5)	6.09 (4.3)
B	6.26	6.15	6.09
C	6.16(E) (8.4)	6.00 (8.6)	5.89 (8.6)
D	6.07(E)	5.91	5.80
E	5.20 (4.2)	5.07 (4.2)	4.96
F	5.16	5.03	4.92
G	4.91(E)	4.92 (4.6)	4.88
H		4.87	
I	4.91(E)	4.80 (4.1)	4.62
J		4.76	
K	4.55		
L	4.39	4.35	4.29
M	4.26(E) (7.4)	4.20	
N	4.21(E)		
P		4.64 (9.0)	4.57
Q		--	

---

[a] Coupling to C_2H is nearly 0 Hz.
[b] Speculative.

Assignments:
    A,B = α-O_1H
    C,D = β-O_1H
    E,F = $O_2'H$
    G,H = α-C_1H[a]
    I,J = $O_3'H$, $O_4'H$
      K = O_1H, $O_6'H$
      L = α-O_3H
    M,N = $C_1'H$
    P,Q = β-C_1H[a,b]

TABLE X

1,5 ANHYDROCELLOBIOTOL

Designation[a]	°C	Chemical Shift (J)		
		36	45	59.5
A		5.23		
B		4.95		
C		4.63	4.61	4.56
D		4.60		
E		4.55		
F		4.28		
G		4.21		

---

[a]Only singlets are observed because of poor resolution.

Assignments:
   A = $O_2'H$
   B = $O_3'H, O_4'H$
   C = O_3H
D,E = $O_6H, O_6'H, O_2H$
F,G = $C_1'H$

TABLE XI

XYLOBIOSE[a] 6.0%

Designation	°C 36	44	Chemical Shift (J) 57	66.5	77.5
A	6.60 (6.5)	6.54 (6.3)	6.45 (6.6)	6.39 (6.6)	6.32 (6.5)
B	6.53	6.48	6.38	6.32	6.25
C	6.20 (4.8)	6.15 (4.2)	6.08 (4.8)	6.01 (4.6)	5.95 (4.7)
D	6.16	6.11	6.03	5.97	5.90
E	P		P	4.91	P
F	--		P	4.88	4.87
G	--		P	4.86	4.84
H	4.93 (4.2)	4.84	4.75(E)	4.67(E)	4.58(E)
I	4.89	4.82	4.70(E)	4.64(E)	4.54(E)
J	P	--	4.79(E)	4.74(E)	4.67(E)
K	4.82(E)	P		4.70(E)	4.64(E)
L	4.69(2.35)[b]	4.63	4.54	4.50	4.44
M	4.54 (6.7)	4.47 (7.0)		P	
N	4.47	4.40	4.33		4.13(E)
O	4.30	4.31			4.35(E)
Q	4.24	4.24	4.26	4.27	4.28
R	4.18	4.19	4.21	4.21	4.23

[a]Temperature coefficient data are also given for less well resolved samples at other concentrations.

[b]Resolved into two peaks at 4.70 and 4.68 ppm.

Assignments:
      A,B = $\beta-O_1H$
      C,D = $\alpha-O_1H$
   E,F,G = $\alpha-C_1H$
H,I,J,K = $O_2{'}, O_3{'}H, O_4{'}H, \beta-O_2H, \beta-O_3H$
          L = $\alpha-O_3H$
      M,N = $\alpha-O_2H$
   O,Q,R = $\beta-C_1H, C_1{'}H$

TABLE XII

SECURIDEBIOSE
7.7%

		Chemical Shift (J)		
Designation	°C	36	51	67.5
A		6.61	6.50	6.41
B		6.55 (6.4)	6.44 (6.6)	6.33
C		6.22	6.12	6.02
D		6.17 (4.6)	6.08 (4.6)	5.98
E			P	4.91
F			P	4.88
G			--	P
H		4.90	4.80	4.68
I		4.73	4.64	
J[a]		4.52(E)	4.42(E)	4.30(E)
K		4.31	P	
L		4.29	4.30	
M		4.24	4.25	
N		4.21	4.23	

[a] Used center of large complex of peaks.

Assignments:
    A,B = β-O_1H
    C,D = α-O_1H
 E,F,G = α-C_1H
        H = O_2´H,O_3´H,O_4´H,β-O_2H,β-O_3H
        I = α-O_3H
        J = O_6´H,αO_2H
K,L,M,N = β-C_1H,C_1´H

TABLE XIII

BENZYL 2,3-ANHYDRO-4-O-(β-D-XYLOPYRANOSYL)-D-RIBOPYRANOSIDE
7.0%

	Chemical Shift (J)		
Designation	°C 34.5	47	70
A	5.06 (4.5)	P	4.79
B	5.02	4.93	4.75
C[b,c]	4.94	4.93	4.93
D	P		4.72(E)
E	4.90	4.83	4.69(E)
F[b]	4.79 (11.7)		
G[b]	4.68	4.68	4.69
H[b]	4.60 (12.0)	4.61 (11.8)	4.63 (11.8)
I[b]	4.48	4.49	4.51
J[b]	4.31 (6.8)	4.32 (9.1)	4.34 (6.8)
K[b]	4.24	4.25	4.28

[a]Speculative.

[b]Remain when D_2O is added.

[c]$^3J_{H_1,H_2} \simeq 0$.

Assignments:
  A,B = O_2′H[a]
    C = C_1H
  D,E = O_3′H,O_4•H
F,G,H,I = O-CH_2-∅
  J,K = C_1′H

TABLE XIV

BENZYL 2,3-ANHYDRO-4-O-(β-D-GLUCOPYRANOSYL)-D-RIBOPYRANOSIDE
5.1%

Designation	Chemical Shift (J)		
	°C	35	70.5
A		5.04 (4.4)	4.78(E) (4.5)
B		5.00	4.74(E)
C a,b		4.93	4.93
D		P	
E		4.88	4.63(E)
F		4.80 (12.1)	4.82(E)
G		4.68	4.70(E)
H		4.61 (12.2)	4.63(E)
I		4.48(E)	4.51
J		4.48(E)	
K		4.42	4.20(E)
L		P	
M		P	4.36 (7.2)
N		4.26	4.29

a Speculative.
b $^3J_{H_1H_2} \simeq 0.$

Assignments:
    A,B = $O_2'H$
      C = C_1H
    D,E = $O_3'H, O_4'H$
F,G,H,I = $O-CH_2-\emptyset$
  J,K,L = $O_6'H$
    M,N = $C_1'H$

TABLE XV-XXXV
TEMPERATURE COEFFICIENT LINEAR REGRESSIONS

Assignment	Designation	TC	Corr.	Shift[b]	Data Points
TABLE XV - GLUCOSE - 9.7%					
β-O_1H	A,B	-0.67	-0.99	6.36	4
α-O_1H	C,D	-0.59	-1	6.01	2
α-C_1H	E,F,G	+0.05	+0.99	4.91	3
β-O_2H,β-O_3H,β-O_4H,α-O_4H	H,I	-0.74	-0.99	4.61	4
α-O_3H	N,O	-0.80	-0.99	4.41	3
O_6H	P,Q,R	-0.74	-0.99	4.26	4
β-C_1H	S,T,U	+0.07	+0.97	4.27	3
TABLE XVI - METHYL β-GLUCOPYRANOSIDE - 15.1%					
O_2H	A,B	-0.80	-0.99	4.80	4
O_3H,O_4H	C,D	-0.67	-0.99	4.70	4
O_6H	E,F,G	-0.70	-0.99	4.31	4
C_1H	H,I	+0.10	+0.99	4.04	4
TABLE XVII - XYLOSE - 8.6%					
β-O_1H	A,B	-0.69	-0.99	6.33	3
α-O_1H	C,D	-0.60	-1	5.95	2
α-C_1H	E,F,G	+0.05	+1	4.86	2
β-O_2H,β-O_3H,O_4H	H,I	-0.77	-0.99	4.64	3
α-O_3H	J,K	-0.64	-0.99	4.50	3
α-O_2H	L,M	-0.74	-0.99	4.24	3
β-C_1H	N,O,P	+0.12	-0.99	4.23	3
TABLE XVIII - METHYL β-XYLOPYRANOSIDE - 17.9%					
O_2H	A,B	-0.77	-0.99	4.80	3
O_4H[a]	C,D	-0.65	-0.99	4.74	3
O_3H[a]	E,F	-0.75	-0.99	4.71	3
C_1H	G,H	+0.10	+0.99	4.00	3

---

[a]Assignments not certain.
[b]56°C by extrapolation.

(Cont'd.)

Assignment	Designation	TC	Corr.	Shift	Data Points
TABLE XIX – METHYL α–XYLOPYRANOSIDE – 15.9%					
O_4H	A	-0.50	-1	4.70	2
O_3H	B	-0.54	-1	4.55	2
O_2H	C,D	-0.65	-1	4.44	2
C_1H	E,F	+0.04	+1	4.49	2
TABLE XX – METHYL β–CELLOBIOSIDE – 3.6%					
$O_2'H$	A,B	-0.67	-0.99	5.03	3
O_2H	C,D	-0.78	-0.99	4.93	3
$O_3'H, O_4'H$	E,F	-0.81	-0.99	4.78	3
O_3H	G	-0.28	-0.99	4.58	3
$O_6H, O_6'H$	H,I,F	-0.64	-0.99	4.41	3
$C_1'H$	K,L	+0.12	+0.99	4.28	3
C_1H	M,N	+0.06	+0.95	4.10	3
TABLE XXI – CELLOBIOSE – 4.1%					
$\beta-O_1H$	A,B	-0.66	-0.99	6.45	6
$\alpha-O_1H$	C,D	-0.62	-0.99	6.13	6
$O_2'H$	E,F	-0.62	-0.99	5.03	6
$\alpha-C_1H$	G,H,I	+0.08	+1	4.91	2
$O_3'H, O_4'H$	J,K	-0.69	-0.99	4.78	5
$\beta-O_2H$	L,M	-0.84	-0.99	4.69	5
$\beta-O_3H$	N	-0.24	-0.99	4.54	6
$\alpha-O_2H, O_6H, O_6'H_1 \alpha-O_3H$	O,P[a]	-0.65	-0.99	4.37	4
$C_1H, C_1'H$	Q,R,S,T[b]	+0.11	-0.98		4
	U	+0.06	+0.98		6
	V	+0.11	+0.99		6
	W	+0.11	+0.99		5
	H_2O	-0.54	-0.99	3.20	6

---

[a]A slower moving signal also is present.
[b]Only peak T.

(Cont'd.)

Assignment	Designation	TC	Corr.	Shift	Data Points
TABLE XXII - CELLOBIOSE - 6.8%					
$\beta\text{-}O_1H$	A,B	-0.62	-0.99	6.45	4
$\alpha\text{-}O_1H$	C,D	-	-	-	-
$O_2'H$	E,F	-0.60	-0.99	5.03	4
$\alpha\text{-}C_1H$	G,H,I	-	-	-	-
$O_3'H,O_4'H$	J,K	-0.68	-0.99	4.78	3
$\beta\text{-}O_2H$	L,M	-0.77	-0.99	4.72	3
$\beta\text{-}O_3H$	N	-0.24	-0.99	4.54	4
$O_6H,O_6'H,\alpha\text{-}O_3H$	P	-0.58	-0.99	4.39	4
	T	-	-	-	-
	H_2O	-0.52	-0.99	3.221	4
TABLE XXIII - CELLOBIOSE - 7.2%					
$\beta\text{-}O_1H$	A,B	-0.63	-0.99	6.45	6
$\alpha\text{-}O_1H$	C,D	-0.58	-0.99	6.13	6
$O_2'H$	E,F	-0.60	-0.99	5.02	6
$\alpha\text{-}C_1H$	G,H,I	+0.09	+0.99	4.90	3
$O_3'H,O_4'H$	J,K	-0.67	-0.99	4.78	4
$\beta\text{-}O_2H$	L,M	-0.80	-0.99	4.69[a]	5
$\beta\text{-}O_3H$	N	-0.25	-0.99	4.53	6
See above	P	-0.65	-0.99	4.38	4
	T	+0.08	+1	4.23	2
	H_2O	-0.55	-0.99	3.21	6

[a]M only.

Assignment	Designation	TC	Corr.	Shift	Data Points
TABLE XXIV - CELLOBIOSE - 7.2%[a], with D_2O added					
$\beta\text{-}O_1H$	A,B	-0.67	-0.99	6.50	5
$\alpha\text{-}O_1H$	C,D	-0.57	-0.99	6.17	3
$O_2'H$	E,F	-0.67	-0.99	5.08[b]	4
$\alpha\text{-}C_1H$	G,H,I	+0.09	+0.99	4.90	3
$O_3'H,O_4'H$	J,K	-0.41	-0.98	4.79[c]	3
$\beta\text{-}O_2H$	L,M	-0.85	-0.99	4.74[d]	4
$\beta\text{-}O_3H$	N	-0.23	-0.97	4.57	4
See above	P	-0.74	-0.99	4.45	5
	T	+0.11	+0.99	4.23	5
	H_2O/HOD	-0.68	-0.99	3.37	5

[a]Solvent contains 4% D_2O added.
[b]E only.
[c]K only.
[d]M only.

(Cont'd.)

Assignment	Designation	TC	Corr.	Shift	Data Points
TABLE XXV – CELLOBIOSE – 8.8%					
$\beta-O_1H$	A,B	-0.61	-0.99	6.47	5
$\alpha-O_1H$	C,D	-0.54	-0.99	6.13	4
$O_2'H$	E,F	-0.60	-0.99	5.02	6
$\alpha-C_1H$	G,H,I	+0.06	+1	4.91	2
$O_3'H,O_4'H$	J,K	-0.65	-0.99	4.71	6
$\beta-O_2H$	L,M	-0.78	-0.99	4.69[a]	5
$\beta-O_3H$	N	-0.22	-0.99	4.54	5
See above	P	-0.64	-0.99	4.37	5
	T	+0.14	+1	4.23	2
	H_2O	-0.52	-0.99	3.23	6

[a]M only.

Assignment	Designation	TC	Corr.	Shift	Data Points
TABLE XXVI – CELLOBIOSE – 8.8%, with H_2O added[a]					
$\beta-O_1H$	A,B	-0.65	-0.99	6.46	
$\alpha-O_1H$	C,D	-0.59	-0.99	6.14	
$O_2'H$	E,F	-0.64	-0.99	5.03	
$\alpha-C_1H$	G,H,I	-0.06	+1	4.95	
$O_3'H,O_4'H$	J,K	-0.70	-0.99	4.79	
$\beta-O_2H$	L,M	-0.82	-0.99	4.71[b]	
$\beta-O_3H$	N	-0.28	-0.99	4.55	
See above	P	-0.56	-0.99	4.40	

[a]2-4% H_2O added; the $\beta-O_3H$ singlet is still observed with up to 6% H_2O. It shifts slightly downfield. (4.56 ppm, 56°C).
[b]M only.

(Cont'd.)

Assignment	Designation	TC	Corr.	Shift	Data Points

TABLE XXVII - LACTOSE - 9.6%

Assignment	Designation	TC	Corr.	Shift	Data Points
β-O_1H	A,B	-0.66	-0.99	6.45	5
α-O_1H	C,D	-0.60	-0.99	6.13	5
α-C_1H	E,F,G	+0.09	+1	4.90	2
	H	-0.63	-0.99	4.89	5
β-O_2H[a]	I,J	-0.82	-0.99	4.71	5
	K,L	-0.81	-0.99	4.54	4
β-O_3H	M	-0.22	-0.99	4.54	5
$O_6H,O_6{'}H$	N[b]	-0.64	-0.99	4.33	5

[a]Assignments made on basis of chemical shift and TC which are analogous to that in cellobiose.
[b]This is not the central O_6H or $O_6{'}H$ signal.

TABLE XXVIII - 4-O-(β-D-GLUCOPYRANOSYL)-D-MANNOPYRANOSE - 6.1%

Assignment	Designation	TC	Corr.	Shift	Data Points
α-O_1H	A,B	-0.55	-0.99	6.17	3
β-O_1H	C,D	-0.78	-0.99	5.96	3
$O_2{'}H$	E,F	-0.66	-0.99	5.05	3
α-C_1H	G,H			4.90[a]	
$O_3{'}H,O_4{'}H$	I,J	-0.74	-0.99	4.77	3
$O_6H,O_6{'}H$	K			4.40[a]	
α-O_3H	L	-0.27	-0.99	4.34	3
$C_1{'}H$	M,N			4.24[a]	
β-C_1H	P,Q			4.60[a]	

[a]Estimates

TABLE XXIX - 1,5 ANHYDROCELLOBIOTOL - 3.0%

Assignment	Designation	TC	Corr.	Shift	Data Points
O_3H	C	-0.28	-0.99	4.57	3

(Cont'd.)

Assignment	Designation	TC	Corr.	Shift	Data Points
TABLE XXX - XYLOBIOSE - 6.0%					
$\beta-O_1H$	A,B	-0.67	-0.99	6.43	5
$\alpha-O_1H$	C,D	-0.62	-0.99	6.06	5
$\alpha-C_1H$	E,F,G			4.88	
$O_3'H, O_4'H$	H,I[a]	-0.82	-0.99	4.74	4
$O_2'H, \beta O_3H$	J[a]	-0.58	-0.99	4.80	3
$\beta-O_2H$	K[a]	-0.42	-0.99	4.74	3
$\alpha-O_3H$	L	-0.60	-0.99	4.54	5
$\alpha-O_2H$	M,N	-0.75	-1	4.35	2
$\beta-C_1H, C_1'H$	Q,R	+0.14	+0.98	4.24	5

[a]Values are approximate because of signal overlap. A slower moving signal is apparent.

TABLE XXXI - XYLOBIOSE - 6.8%[a]					
$\beta-O_1H$	A,B	-0.58	-0.99	6.43	3
$\alpha-O_1H$	C,D	-0.54	-0.98	6.07	3
$\alpha-C_1H$	E,F,G			4.88	2
See above	H,I	-0.62	-0.99	4.77	3
	J,K			4.77[b]	1
$\alpha-O_3H$	L	-0.58	-0.99	4.56	3
$\alpha-O_2H$	M,N	-0.77	-1	4.34	2
$\beta-C_1H, C_1'H$	Q,R	+0.10	-0.99	4.24	5

[a]Resolution poor.
[b]Estimate, only resolved at room temperature.

TABLE XXXII - XYLOBIOSE - 5.1%[a]					
$\beta-O_1H$	A,B	-0.68	-0.99	6.43	4
$\alpha-O_1H$	C,D	-0.61	-0.99	6.06	4
$\alpha-C_1H$	E,F,G			4.88	2
See above	H,I	-0.67	-0.99	4.76	4
	J,K			4.76[b]	1
$\alpha-O_3H$	L	-0.63	-0.99	4.57	3
$\alpha-O_2H$	M,N	-0.84	-1	4.34	2
$\beta-C_1H, C_1'$	Q,R	-0.15	-0.98	4.24	5

[a]Resolution poor.
[b]Estimate, only resolved at room temperature.

(Cont'd).

Assignment	Designation	TC	Corr.	Shift	Data Points
TABLE XXXIII - SECURIDEBIOSE - 7.7%					
$\beta-O_1H$	A,B	-0.66	-0.99	6.44	3
$\alpha-O_1H$	C,D	-0.63	-0.99	6.07	3
$\alpha-C_1H$	E,F,G			4.88	
$O_2{'}H, O_3{'}H, O_4{'}H, \beta-O_2H,\}$ $\beta-O_3H$	H	-0.70	-0.99	4.76	3
$\alpha-O_3H$	I	-0.60	-1	4.61	2
$\alpha-O_2H, O_6{'}H$	J	-0.70	-0.99	4.38	3
$C_1{'}H$	K,L			4.32	
C_1H	M,N	+0.13	+1	4.25	2
TABLE XXXIV - BENZYL 2,3-ANHYDRO-4-O-(β-D-XYLOPYRANOSYL)-D-RIBOPYRANOSIDE - 7.0%					
$O_2{'}H$	A,B	-0.76	-0.99	4.88	3
C_1H	C			4.93	
$O_3{'}H, O_4{'}H$	E	-0.59	-0.99	4.77	3
TABLE XXXV - BENZYL 2,3-ANHYDRO-4-O-(β-D-GLUCOPYRANOSYL)-D-RIBOPYRANOSIDE - 5.1%					
$O_2{'}H$	A,B	-0.73	-1	4.87	2
C_1H	C			4.93	
$O_3{'}H, O_4{'}H$	E	-0.70	-1	4.73	2
$O_6{'}H$	J,K,L	-0.62	-1	4.29	2

APPENDIX VIII

REPRESENTATIVE HOMO- AND HETERONUCLEAR DECOUPLED SPECTRA

DISCUSSION

Assignments for the ^{1}H-NMR spectra presented in the two preceding appendices are based on comparisons to model compounds, intensity measurements, and spin decoupling. The latter technique has the advantage that it is instrumentally based and that in many cases the resulting assignments are unequivocal. This appendix briefly introduces the rationale of the technique followed by a discussion of the decoupled spectra pertinent to the assignments previously made.

Spin decoupling is basically a method by which the apparent spin-spin interaction between coupled nuclei can be modified by applying a second rf field at a specific frequency. For the case of first order spectra ($\delta_{AB} > 7J_{AB}$), if one of a set of coupled nuclei is irradiated with a strong rf field, then, the effects on the spectrum of its interaction with other members of the set are reduced or removed. This is illustrated in the spectrum of ethyl benzene in Fig. 1. In this case, the CH_2 quartet (b) is collapsed to a near singlet by applying a strong rf field to the center of the CH_3 triplet (c).

Spin decoupling is only one of a class of double resonance techniques. The theory for nuclear magnetic double resonance has been reviewed ([1],[2]). Recently several new techniques, homo- and heteronuclear two-dimensional (2D) NMR ([3]), which utilize specific pulse sequences and 2D Fourier transformation, have been developed to identify coupled systems in ^{1}H-NMR. These techniques have recently been used to give a more definitive assignment of the cellobiose skeletal protons in D_2O ([4]).

The spin decoupled spectra in this appendix were all obtained with a Jeol FX-100 FT-NMR utilizing the homonuclear gated decoupling module equipped with
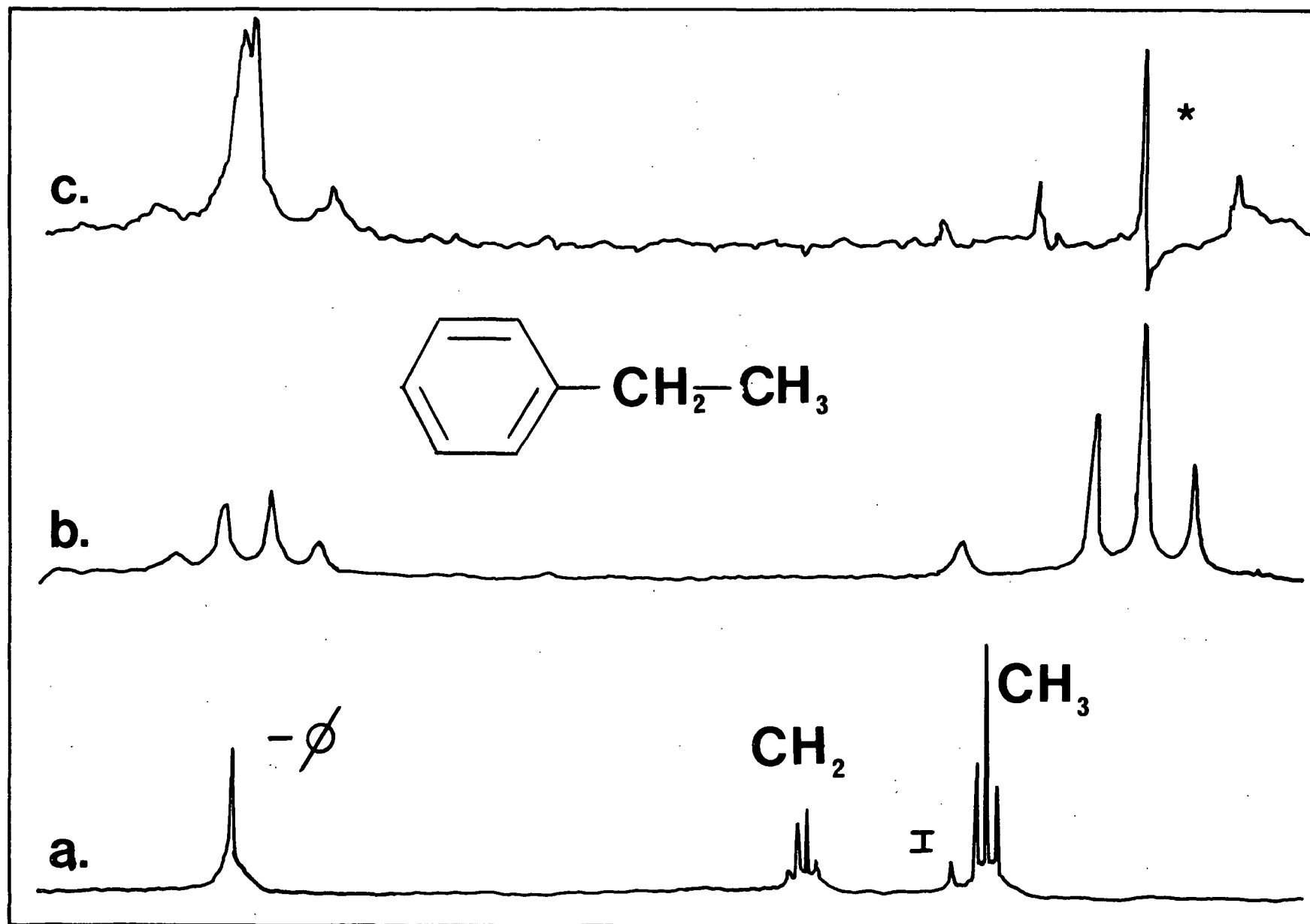
Figure 1. (a) The 1000 Hz ^{1}H-NMR spectrum of 1% ethyl benzene in CDCl$_3$; (b) expansion of (a) in the upfield region (250 Hz full scale); (c) spin decoupled spectrum resulting from irradiation (*) at the central peak of the CH$_3$ triplet.

variable irradiation power. The decoupling frequency can be set to ± 0.2 Hz. The irradiation power was controlled so that complete decoupling was achieved ($\gamma H_2/2\pi >$ 2J) (5) without excessive irradiation of the nearby signals. This necessitates that the coupled systems under study are separated by more than the minimum frequency width of the irradiating signal (approximately 15 Hz) that is necessary to achieve complete decoupling.*

In the spectra that follow emphasis is given to those cases which assist in the assignment of the hydroxy-proton signals observed as singlets (Section III; part III). Prior to this the decoupled spectra of glucose and xylose in DMSO-d_6 are presented to illustrate the power of the technique. The results duplicate those of Perlin (6). This is followed by a series of decoupled spectra for methyl β-cellobioside, which, after one assumption, allow complete assignment of the hydroxy-proton region. This group of spectra contain some examples of selective heteronuclear decoupling, i.e., observation of the ^{13}C-NMR spectrum while irradiating at a specific point in the ^1H-spectrum.

Below is a list of compounds studied by spin-decoupling as well as a key to the symbols used on the spectra.

SPECTRA

Key

* - Location of irradiating signal

I - Impurity

S - Solvent

Δ - Region of spectrum affected by decoupling

---

*For $\Delta\nu = 15$ Hz; $H_2 = \dfrac{2}{\gamma} \Delta\nu$ where $\gamma = \dfrac{\mu}{P} = \dfrac{\mu}{IH}$. $H_2 = 3.5 \times 10^{-3}$ gauss for a conventional spectrometer.

List

Compound	Figure
Glucose	2-4
Xylose	5-6
MBX	7
MBC2	8-23
C2	24-26
Lactose	27
GM	28
X2	29-30
GX	31

Discussion of the Spin-Decoupled Spectra

Starting with the accepted assignments of $\beta-O_1H$ and $\alpha-O_1H$ (7) it is possible, with the assistance of the peak intensities, to assign the rest of the downfield signals in the spectrum, either directly or by deduction. For example, irradiation of the anomeric hydroxyl signals identifies the $\alpha-C_1H$ and $\beta-C_1H$ signals. Simultaneous decoupling of these signals with the O_2H signals verifies the assignments of the latter. Decoupling of the small doublet at 4.52 ppm without a simultaneous decoupling of the anomeric protons indicates that this signal is either $\alpha-O_3H$ or $\alpha-O_4H$. Since the $\alpha-O_4H$ signal is far from the anomeric center it should be nearly coincident with the $\beta-O_4H$ signal; hence the 4.52 ppm signal is $\alpha-O_3H$. The O_6H signal, expected to be a triplet, is anticipated to be in the vicinity of the $\beta-C_1H$ signal on the basis of peak intensities. The complex signal is significantly simplified by irradiation at 3.59 ppm corresponding to the collapse of a triplet. Finally, by the process of elimination, and in accord with the peak intensities the $\beta-O_3H$, $\beta-O_4H$, and $\alpha-O_4H$ signals must be included as part of the large doublet at 4.70 ppm. Indications of the relative order of the strongly coupled skeletal protons are consistent with the spectral assignments obtained at higher field in D_2O (8).
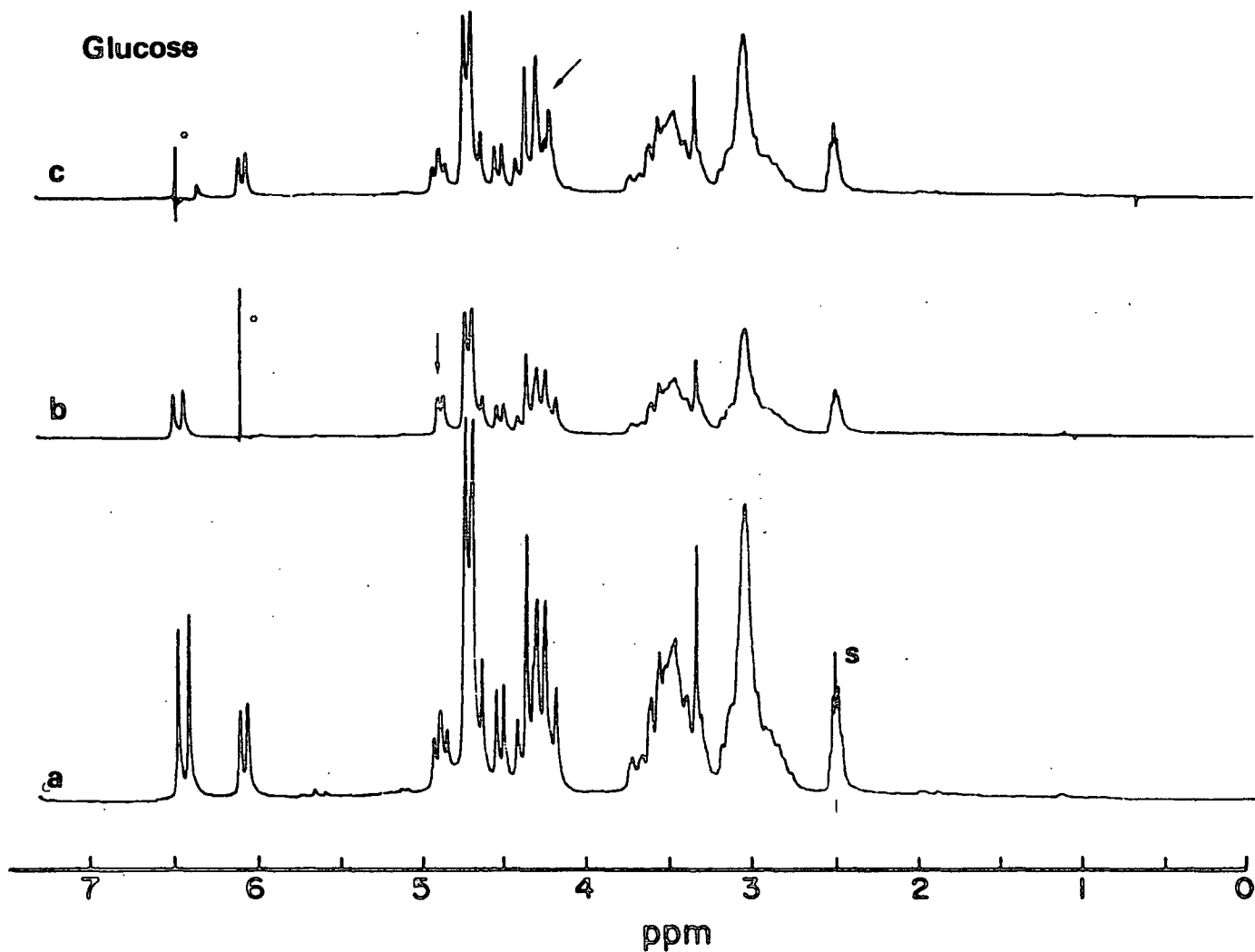
Glucose

Figure 2. (a) ^{1}H-NMR spectrum of glucose at 40.5°C in DMSO-d_6 (9.7%); (b) Irradiation of the α-O_1H signal (6.09 ppm) causes collapse of the α-C_1H signal (4.81 ppm) to a doublet; (c) Irradiation of the β-O_1H signal (6.47 ppm) causes changes near 4.25 ppm (β-C_1H).

Glucose
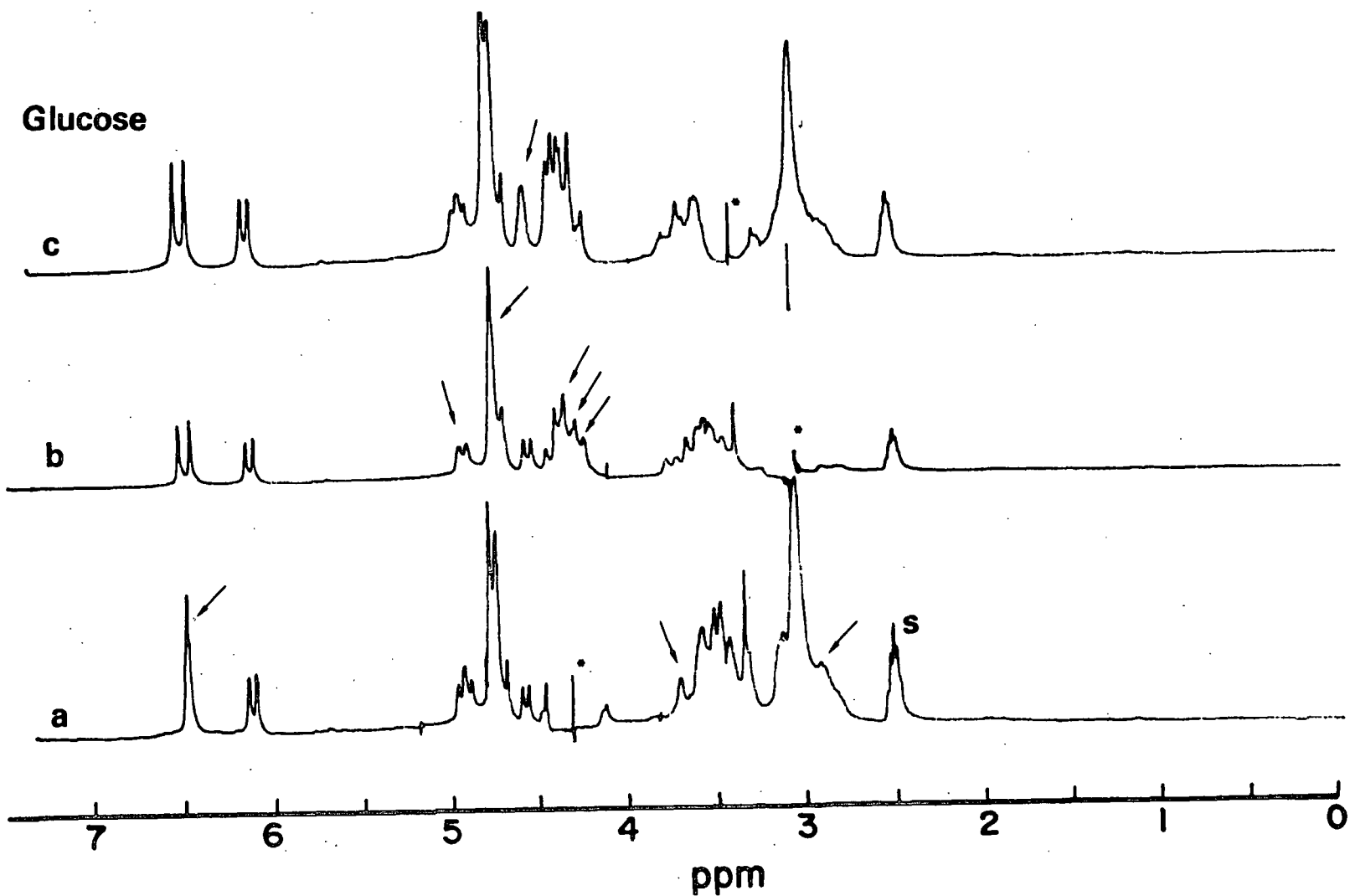
Figure 3. (a) Irradiation at β-C_1H (4.29 ppm) causes collapse of the β-O_1H signal to a singlet plus minor changes in the upfield portion of the spectrum; (b) Irradiation at 3.04 ppm (α-C_2H, β-O_2H) causes collapse of the α-C_1H signal (4.91 ppm) as a doublet, collapse of the large doublet at 4.70 ppm (β-O_2H, β-O_3H, β-O_4H) and changes near 4.30 ppm (β-O_1H, α-O_2H). No change occurs at 4.52 ppm (α-O_3H). Clearly, both C_2 protons are in this region but not α-C_3H; (c) Irradiation at 3.37 ppm (α-C_2H) causes collapse of the α-O_3H signal (4.52 ppm) and no other changes.
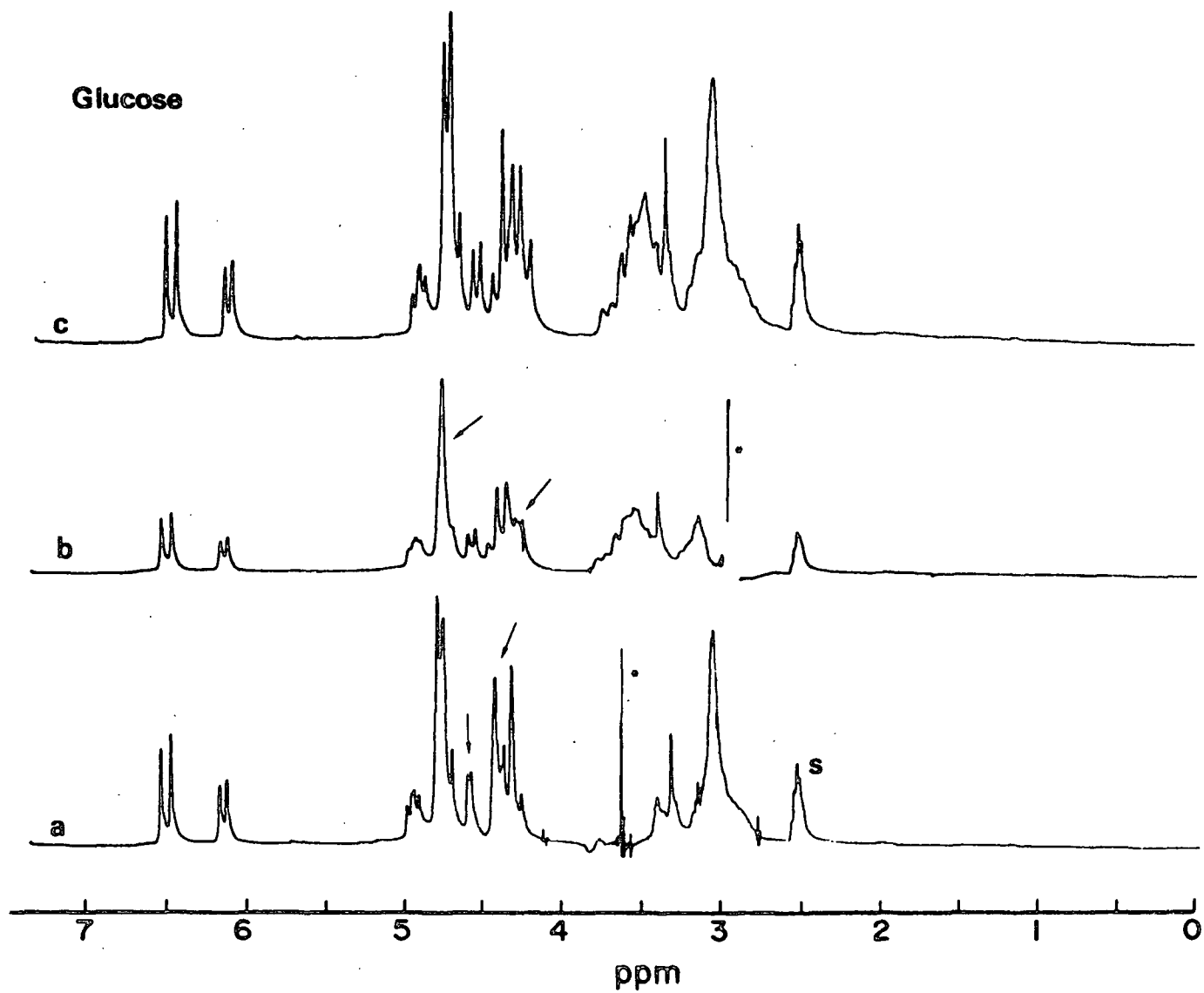
Figure 4. (a) Irradiation at 3.59 ppm (C_6H) causes collapse of the O_6H triplet (4.36 ppm) with some residual effect on the $\alpha-O_3H$ signal (4.52 ppm); (b) Irradiation at 2.93 ppm with similar effects to those observed in Fig. 2b; (c) normal spectrum.
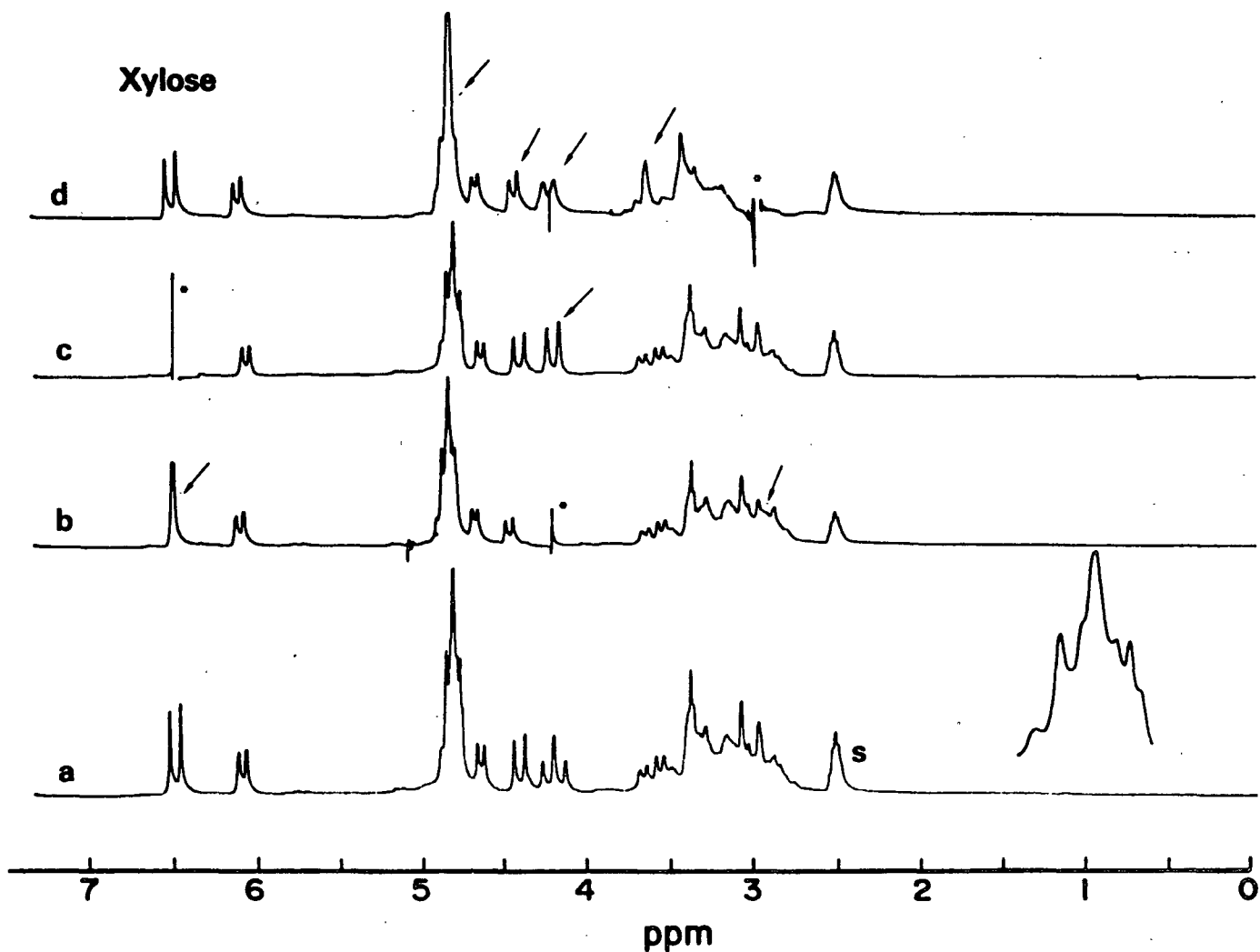
Figure 5. (a) ^{1}H-NMR spectrum of xylose at 34°C in DMSO-d_6; the inset is an expansion of the large signal at 4.81 ppm showing it consists of several signals; (b) Irradiation at β-C_1H (4.20 ppm) causing collapse of the β-O_1H doublet (6.48 ppm) and some changes near 2.97 ppm; (c) Irradiation at β-O_1H (6.49 ppm) causing the β-C_1H apparent triplet to collapse to a doublet; (d) Irradiation at 2.94 ppm (β-C_2H) causing a simultaneous change in the β-C_1H and β-O_2H (large complex at 4.80 ppm) signals. The downfield portion of the $C_{(5)}H_2$ signal (an AB pattern with eight peaks) is also decoupled indicating that C_4H is in this region. The α-O_2H signal (4.41 ppm) is partially collapsed.
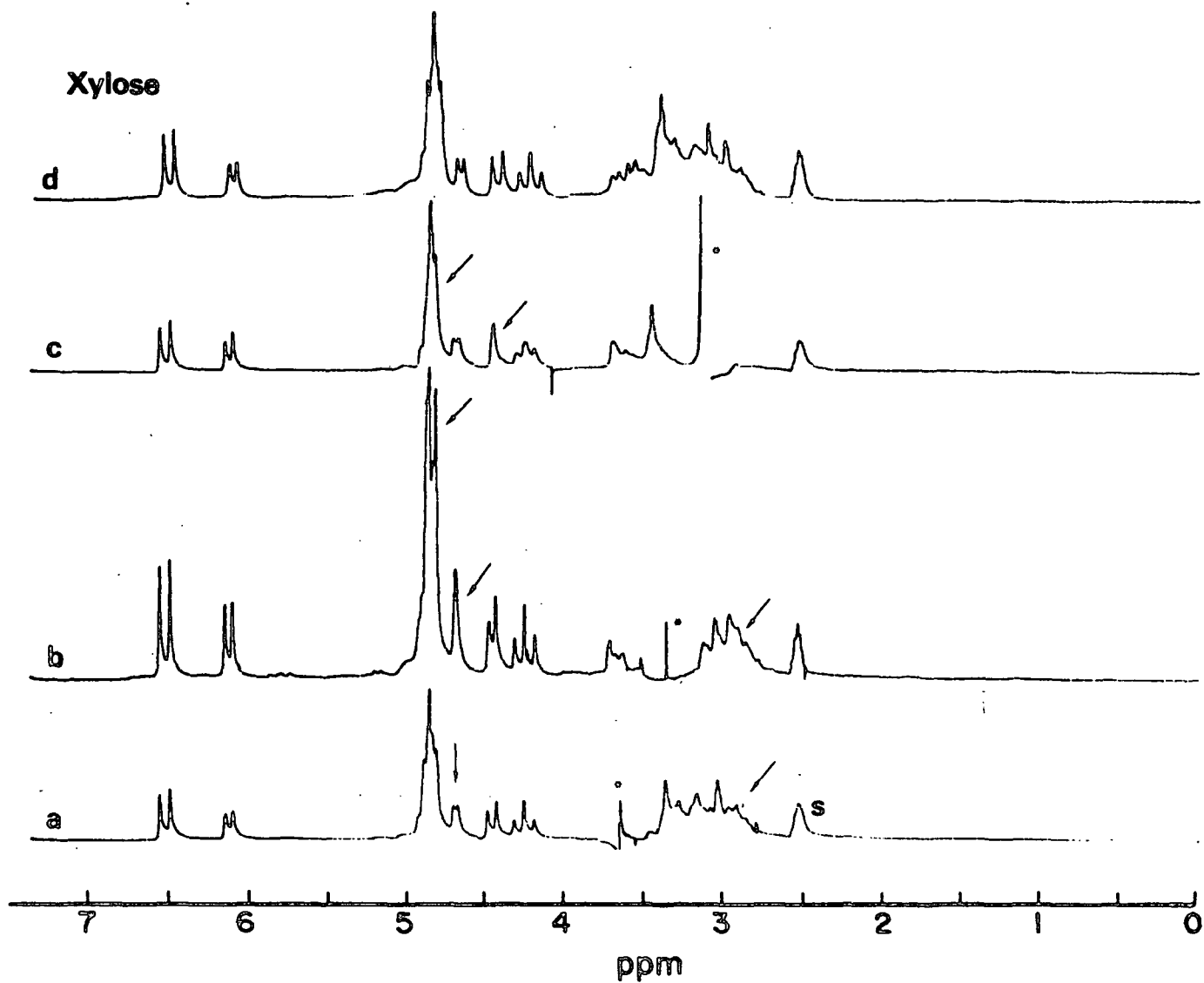
Figure 6. (a) Irradiation of one of the C_5 H signals (3.64 ppm) results in no large effects in the hydroxyl region and a small change near 2.97 ppm; (b) Irradiation at 3.33 ppm decouples the α-O_3H signal (4.64 ppm) and the large complex (4.80 ppm). The β-O_1H signal is not affected; (c) At 3.11 ppm the irradiation decouples the α-O_2H signal (4.41 ppm) and the large complex; (d) The normal spectrum.

Methyl β-Xylopyranoside
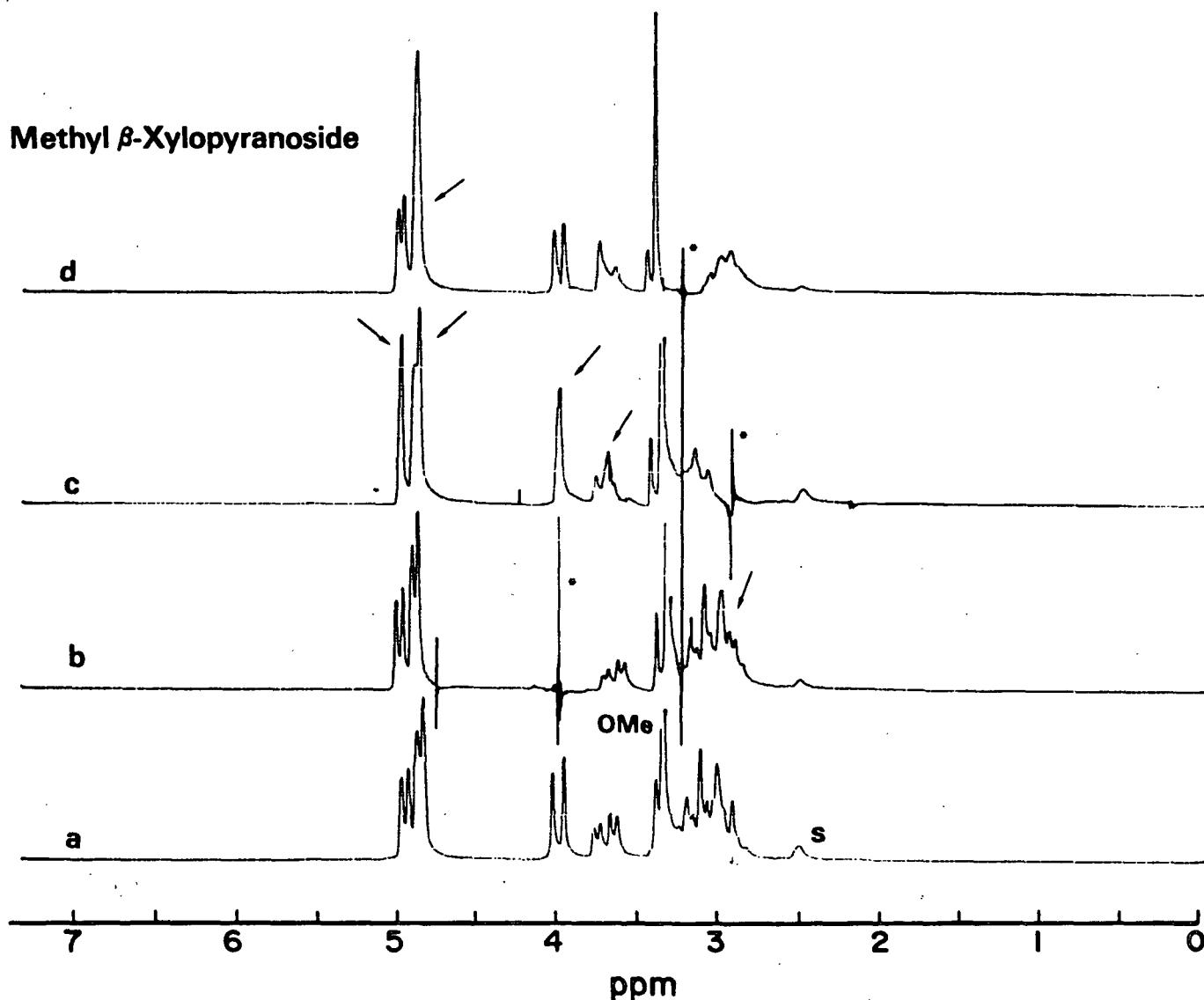
Figure 7. (a) The ^{1}H-NMR spectrum of methyl β-xylopyranoside in DMSO-d_6 (17.9%) at 34.2°C.; (b) Irradiation at C_1H (3.98 ppm) causes a change near 2.92 ppm but none in the hydroxyl region; (c) Irradiation at 2.90 ppm (C_2H) results in a simultaneous decoupling at 3.98 and 4.98 ppm indicating that these signals represent protons coupled to the same proton. The large doublet at 4.90 ppm is partially affected; (d) Irradiation at 3.21 ppm decouples the large signal at 4.90 ppm. Neither the C_1H signal or the 4.98 ppm signal are affected proving that the latter results from O_2H.
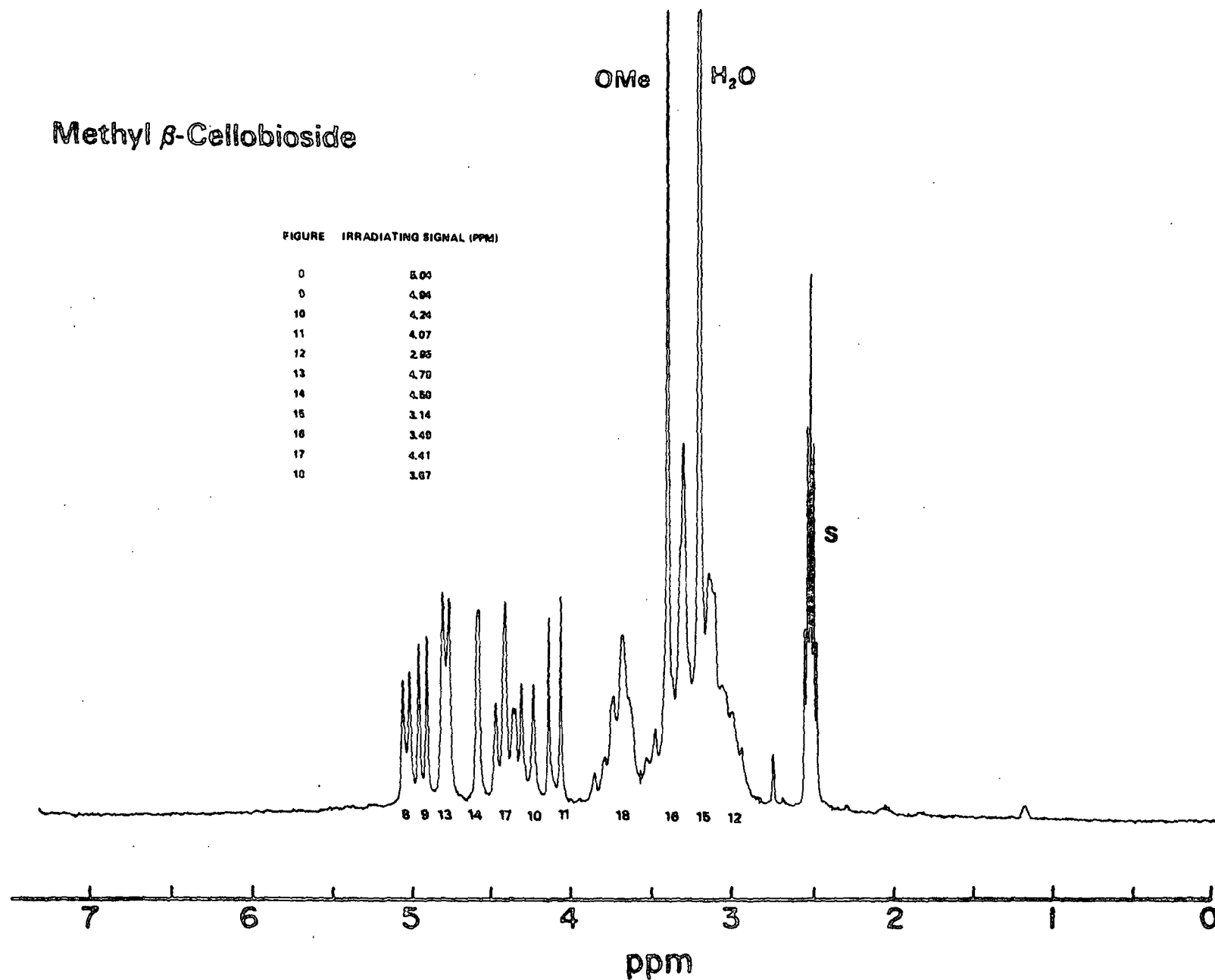
Figure 8: The ¹H-NMR spectrum of methyl β-cellobioside at 56°C in DMSO-d$_6$ (3.6%). Points of irradiation in the subsequent spectra are indicated by numbers.

Methyl β-Cellobioside
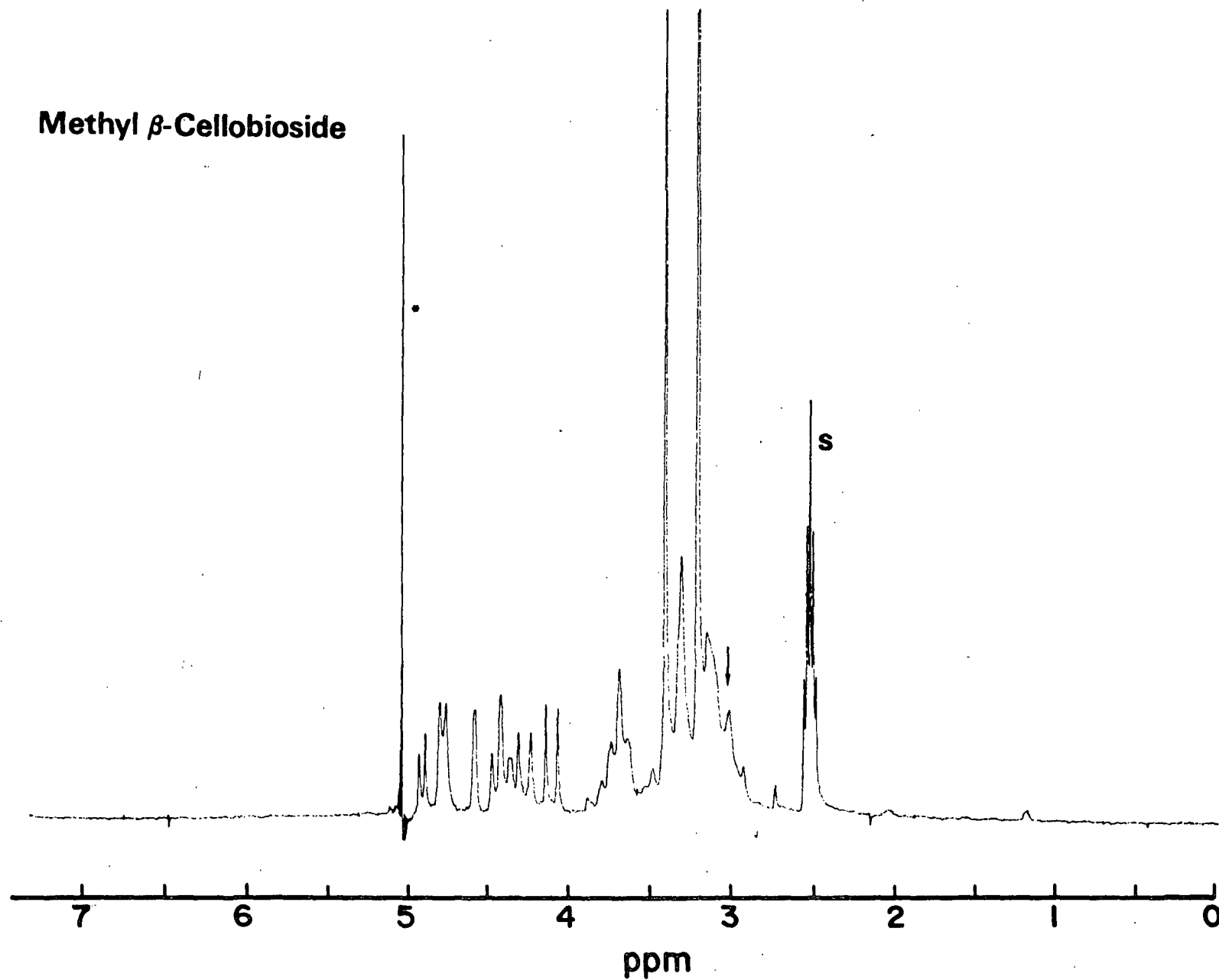
Figure 9. Irradiation at 5.04 ppm ($O_{2'}H$) causes a change near 2.95 ppm ($C_{2'}H$).

Methyl β-Cellobioside
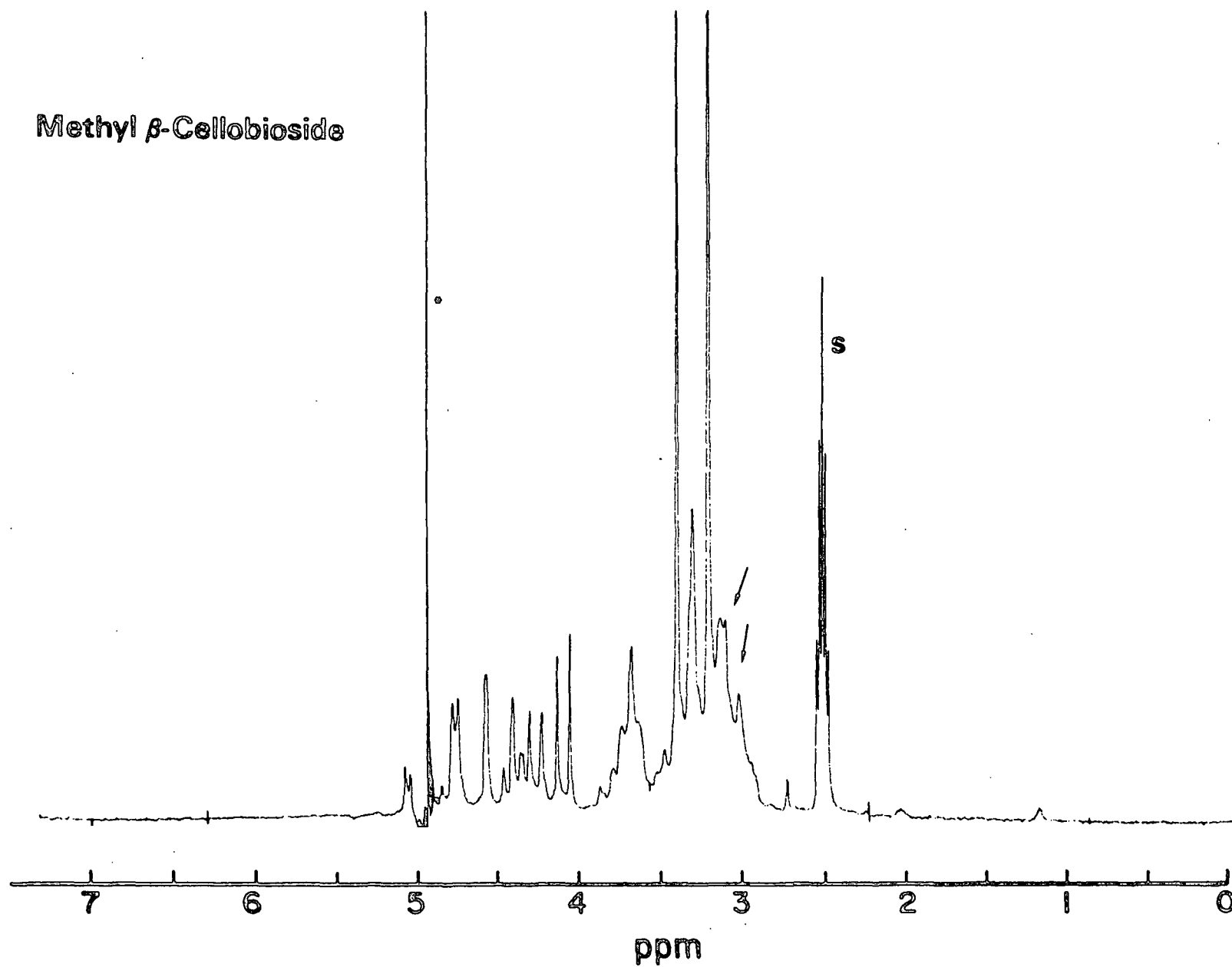
Figure 10. Irradiation at 4.94 ppm (O_2H) causes a change near 2.95 ppm (C_2H).

Methyl β-Cellobioside
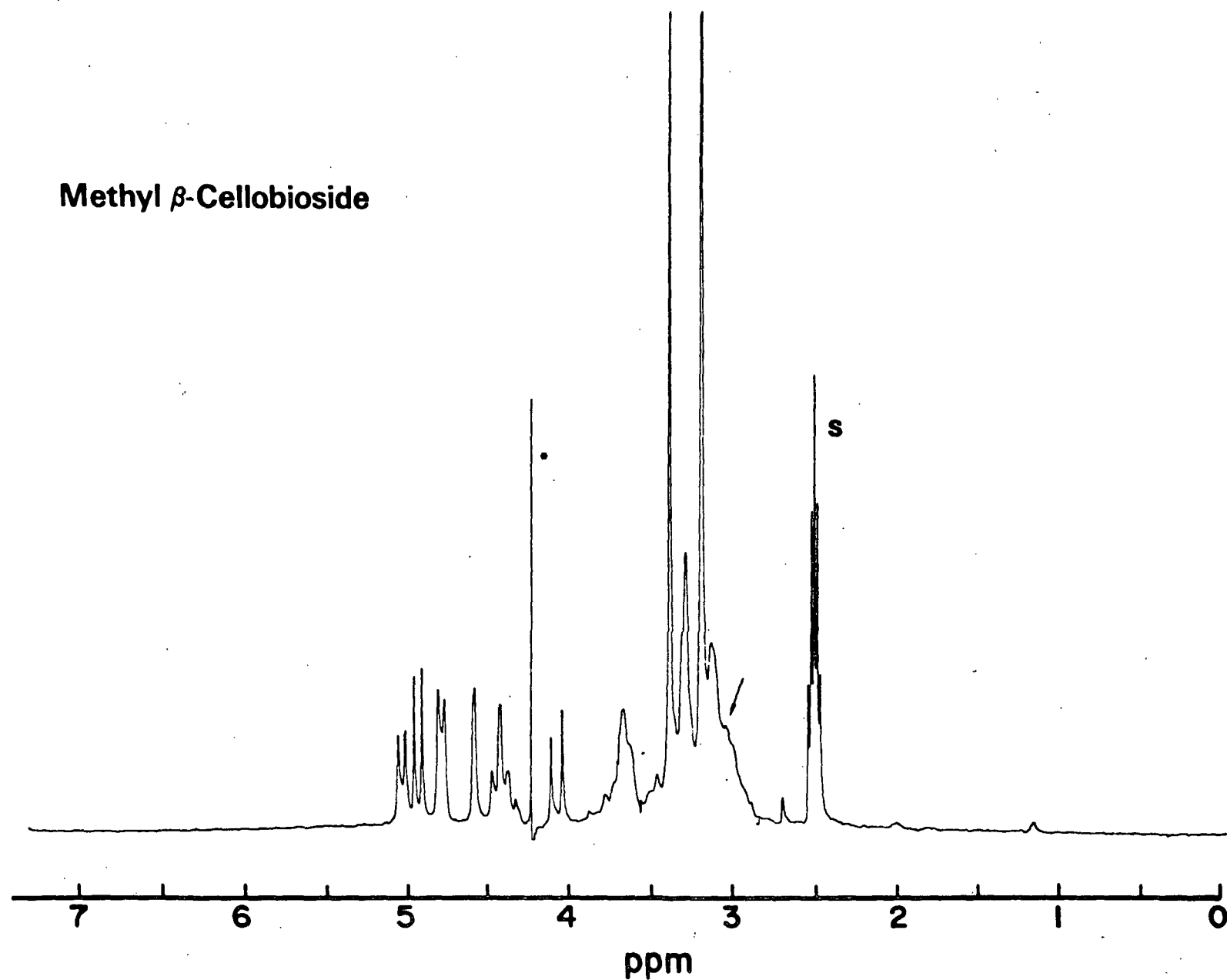
Figure 11. Irradiation near 4.24 ppm (C_1'H) causes a change near 2.95 ppm (C_2'H). No other changes occur in the hydroxyl region.

Methyl β-Cellobioside
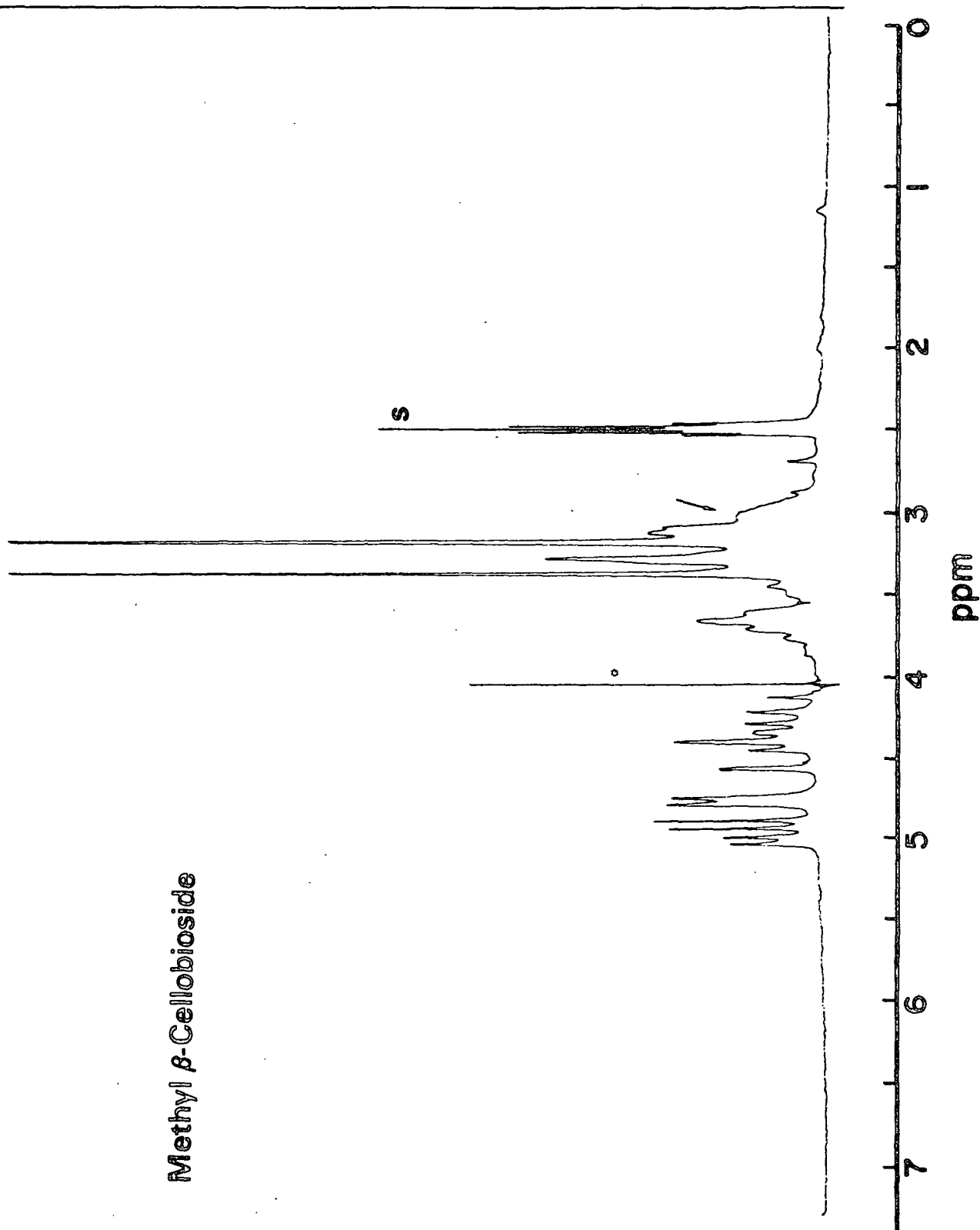
Figure 12. Irradiation near 4.08 ppm (C_1H) causes a change near 2.95 ppm (C_2H).

Methyl β-Cellobioside
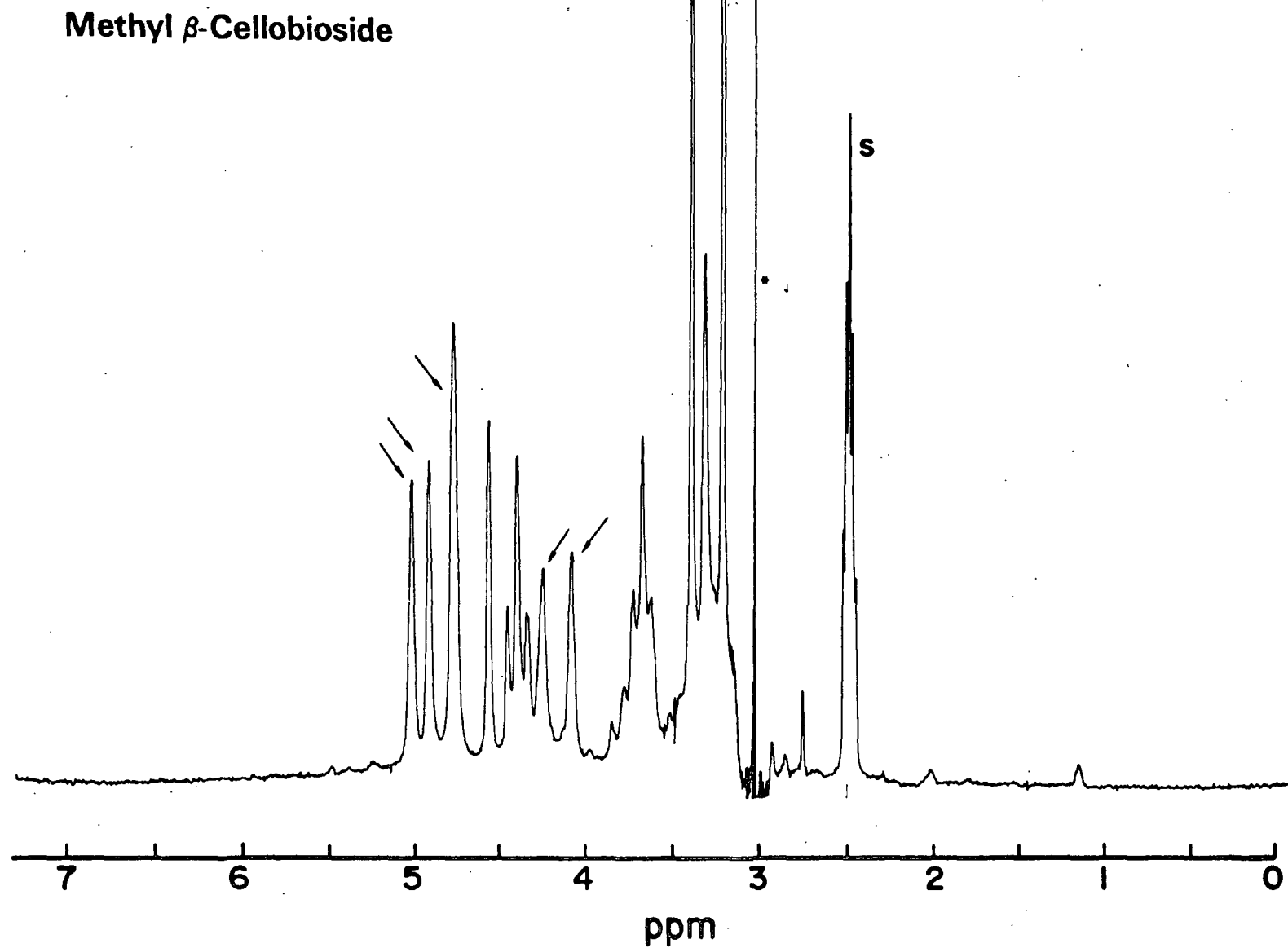
Figure 13. Irradiation near 2.95 ppm (C_2H, $C_2'H$) causes a collapse of all the doublets in the hydroxyl region.

Methyl β-Cellobioside
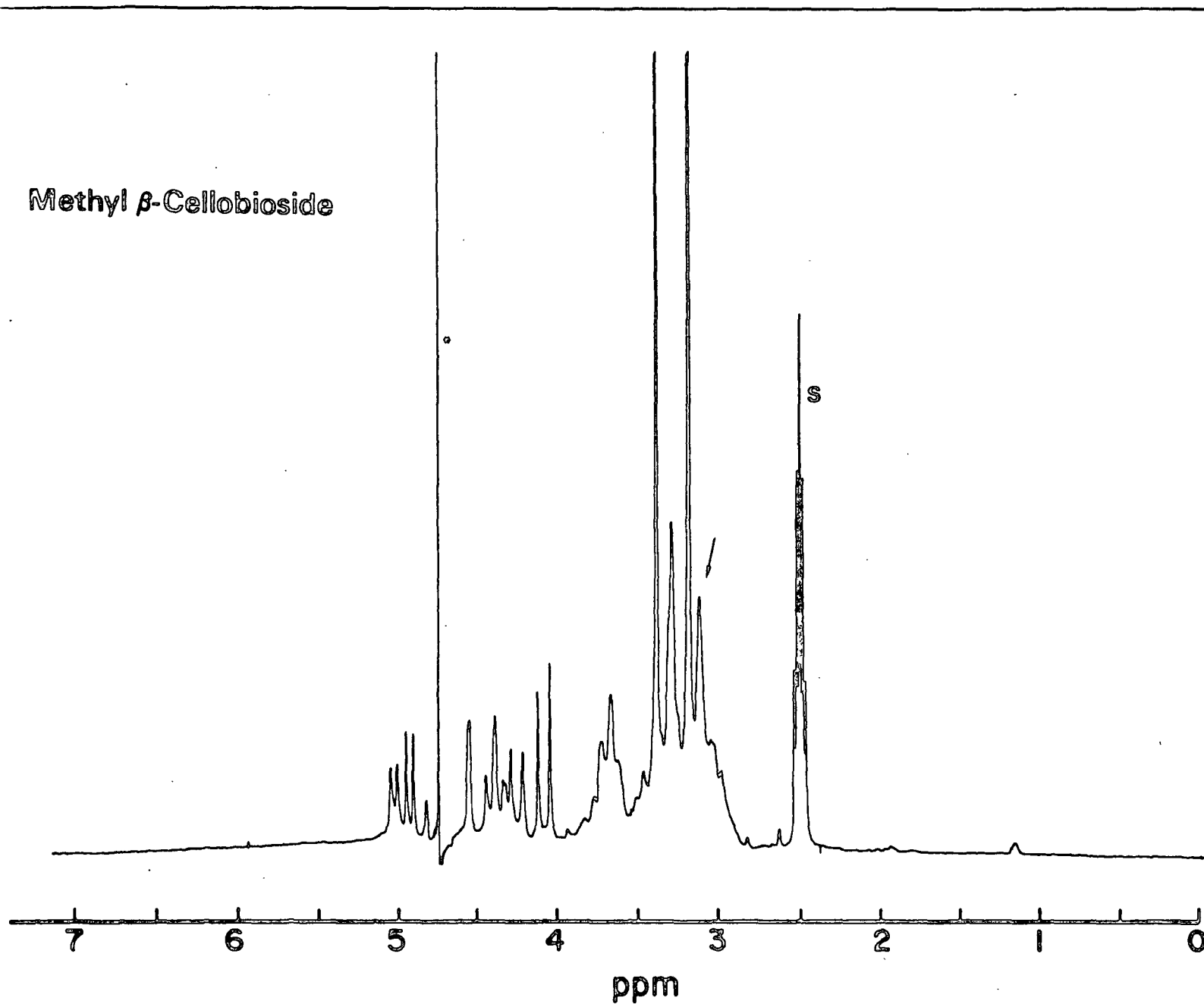
Figure 14. Irradiation at 4.78 ppm (O_3'H, O_4'H) produces no change in the hydroxyl
region and a small sharpening of the signals near 3.05 ppm.

Methyl β-Cellobioside
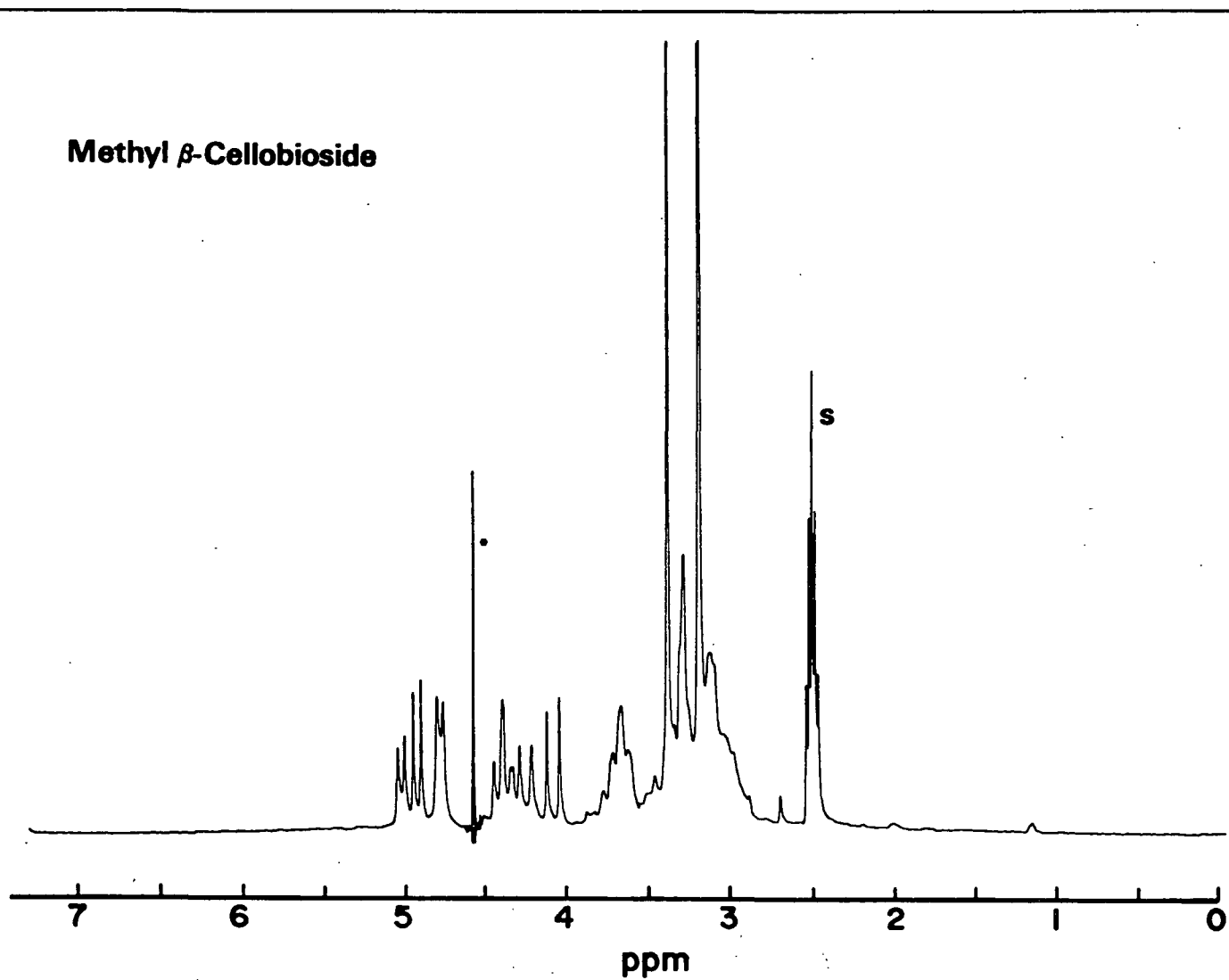
Figure 15. Irradiation of the singlet at 4.58 ppm causes no significant change in the spectrum. This is expected since by definition this peak is only weakly coupled to another proton.

Methyl β-Cellobioside
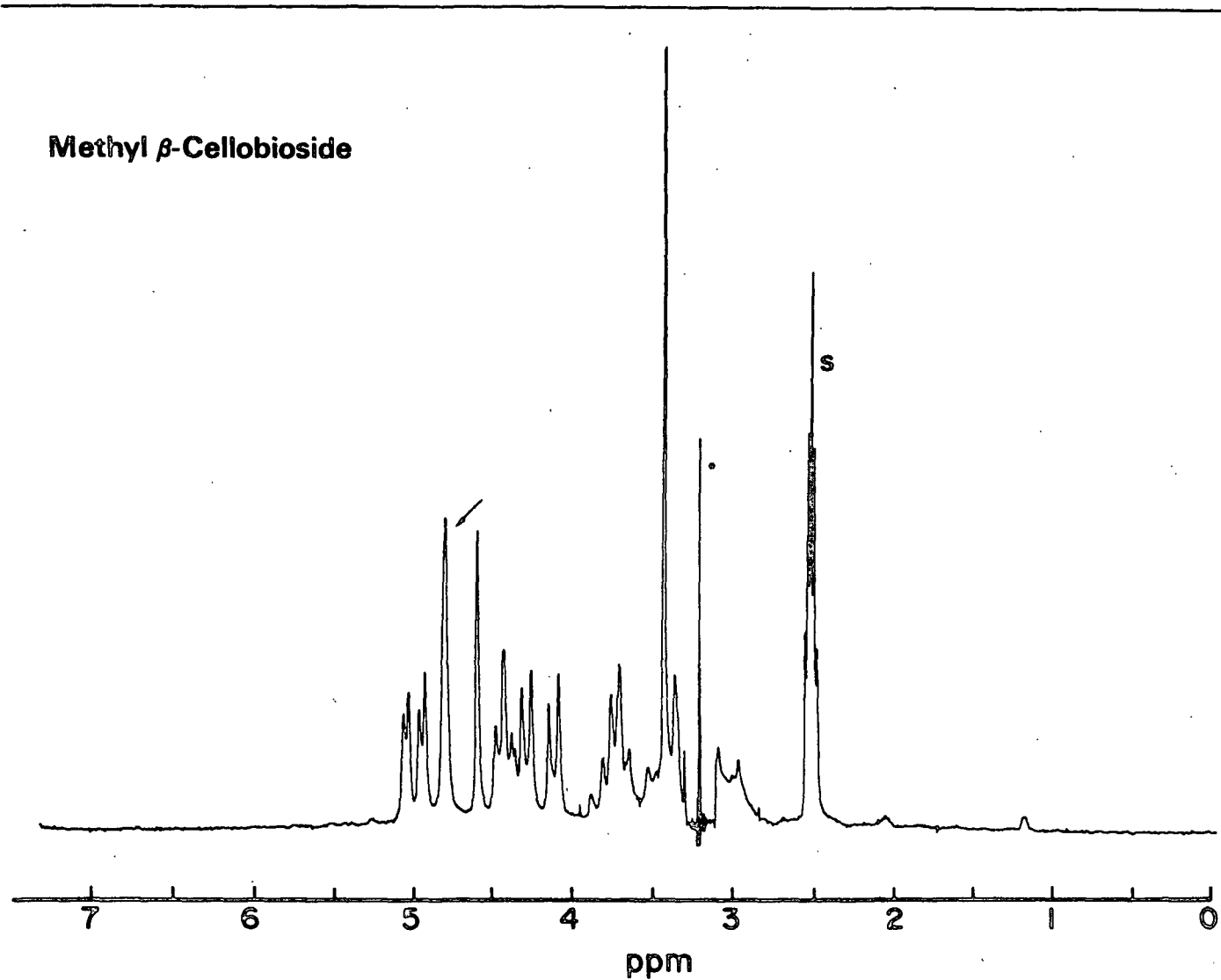
Figure 16. Irradiation at 3.14 ppm causes a collapse of the large doublet at 4.78 ppm with only a slight change of the anomeric proton doublets. This proves that the large doublet does not result from either $O_2'H$ or O_2H.

Methyl β-Cellobioside
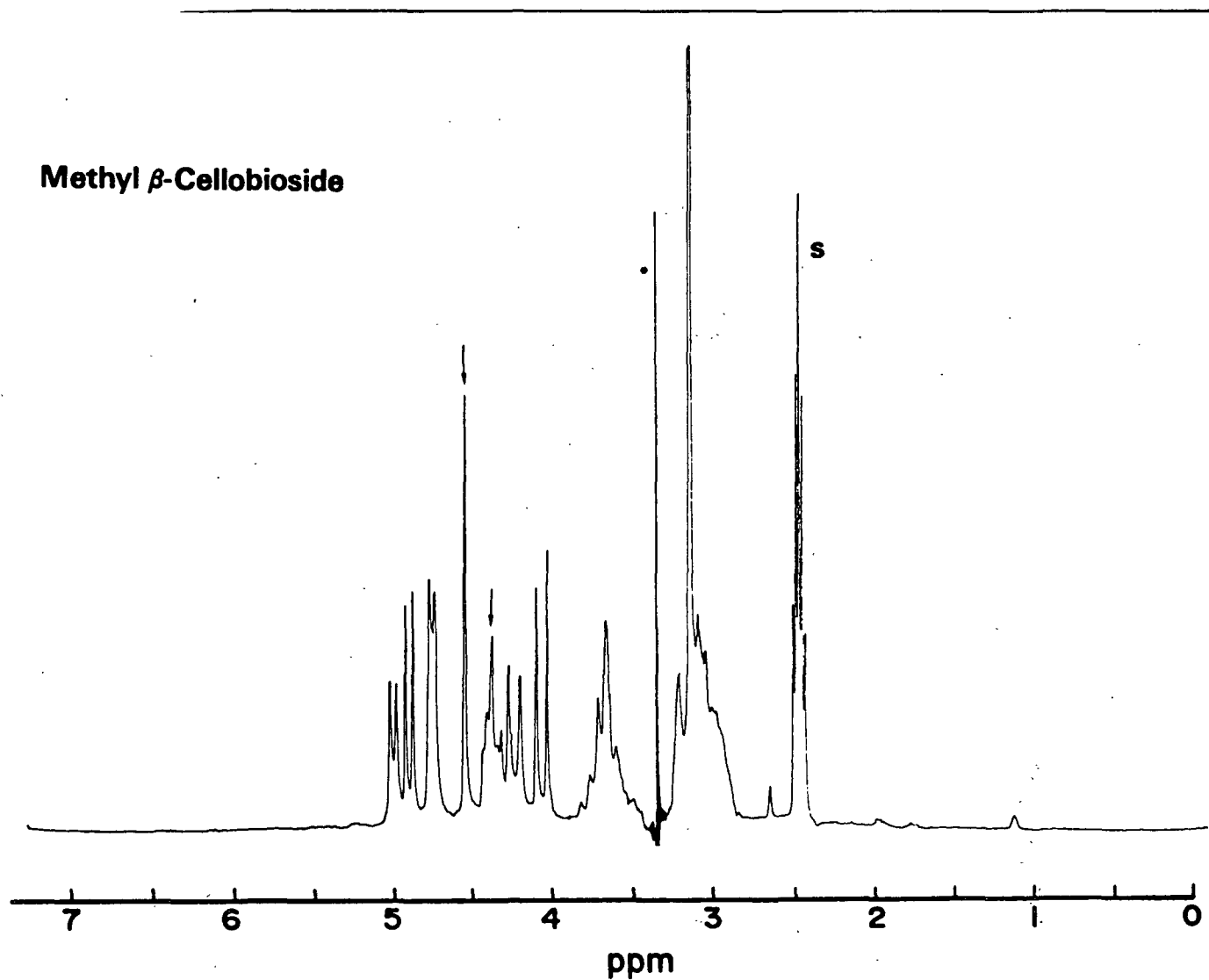
Figure 17. Irradiation at 3.40 causes a sharpening of the singlet at 4.58 ppm. No other hydroxyl signals are affected. On the basis of the logic previously developed the singlet can be assigned to O_3H at this point.

Methyl β-Cellobioside

ppm
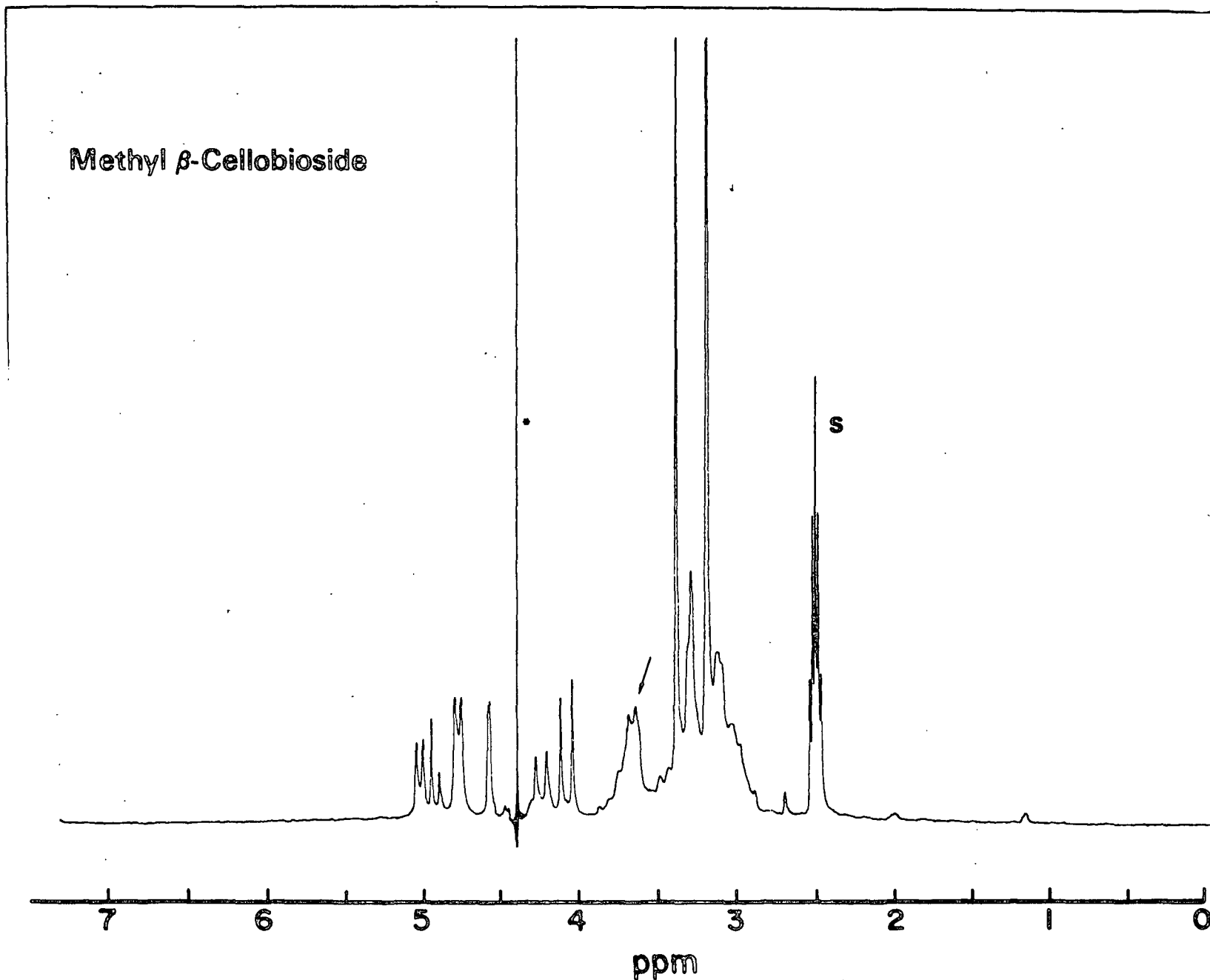
Figure 18. Irradiation at 4.41 ppm (O_6H, $O_6'H$) produces a change around 3.69 ppm. The O_2H intensity is also affected.

Methyl β-Cellobioside

H₂O

S
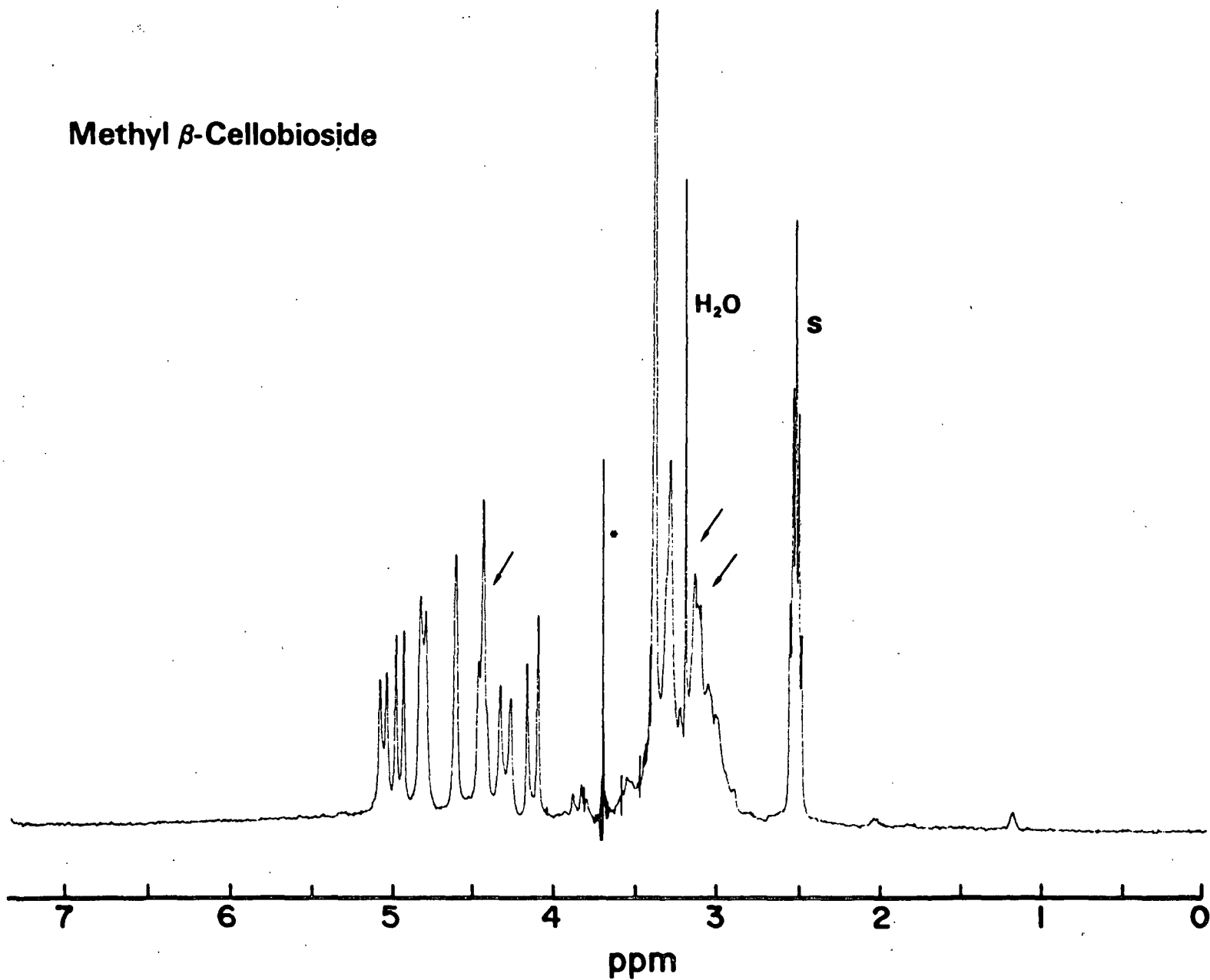
Figure 19. Irradiation near 3.67 ppm causes collapse of the triplet at 4.42 ppm. The H$_2$O signal as well as the upfield skeletal proton region are also affected.

Methyl β-Cellobioside

1 = 103.0 PPM	3 = 75.2 PPM
1' = 103.4 PPM	2' = 74.0 PPM
4 = 78.6 PPM	2 = 73.7 PPM
5' = 76.8 PPM	4' = 70.3 PPM
5' = 76.4 PPM	6' = 61.5 PPM
5 = 75.6 PPM	6 = 61.0 PPM
	OCH3 = 56.0 PPM
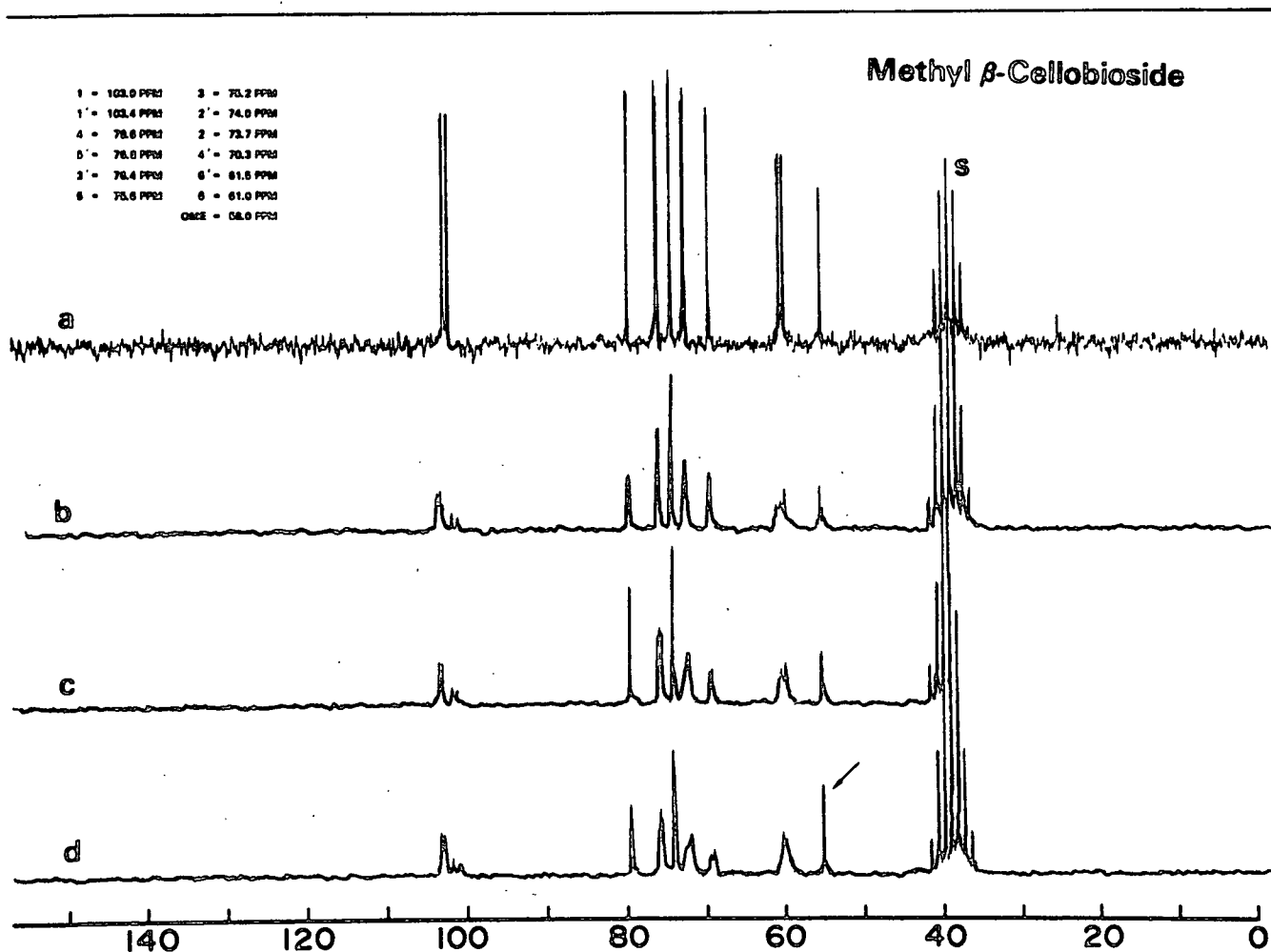
Figure 20. (a) The completely proton decoupled ^{13}C-NMR spectrum of methyl β-cellobioside in DMSO-d_6 (3.6%) at 56°C; (b,c,d) Selective heteronuclear decoupled spectra* with the irradiating frequency placed in the ^{1}H-NMR spectrum at approximately 3.14, 3.30, and 3.40 ppm; respectively. In spectra (b) and (c) only the C_1, C_1', C_6, C_6' and OCH3 signals appear coupled. In spectrum (d) the OCH3 peak is decoupled which is expected since the methyl protons resonate at 3.40 ppm. It can be noted that the C_2 and C_2' signals show increased ^{13}C-^{1}H coupling as the irradiating frequency moved further from 3.00 ppm.

*In ^{13}C-NMR specific heteronuclear decoupling, a carbon coupled to the irradiated proton should appear as a sharp singlet, in contrast to the other carbons which exhibit ^{13}C-^{1}H couplings.

Methyl β-Cellobioside
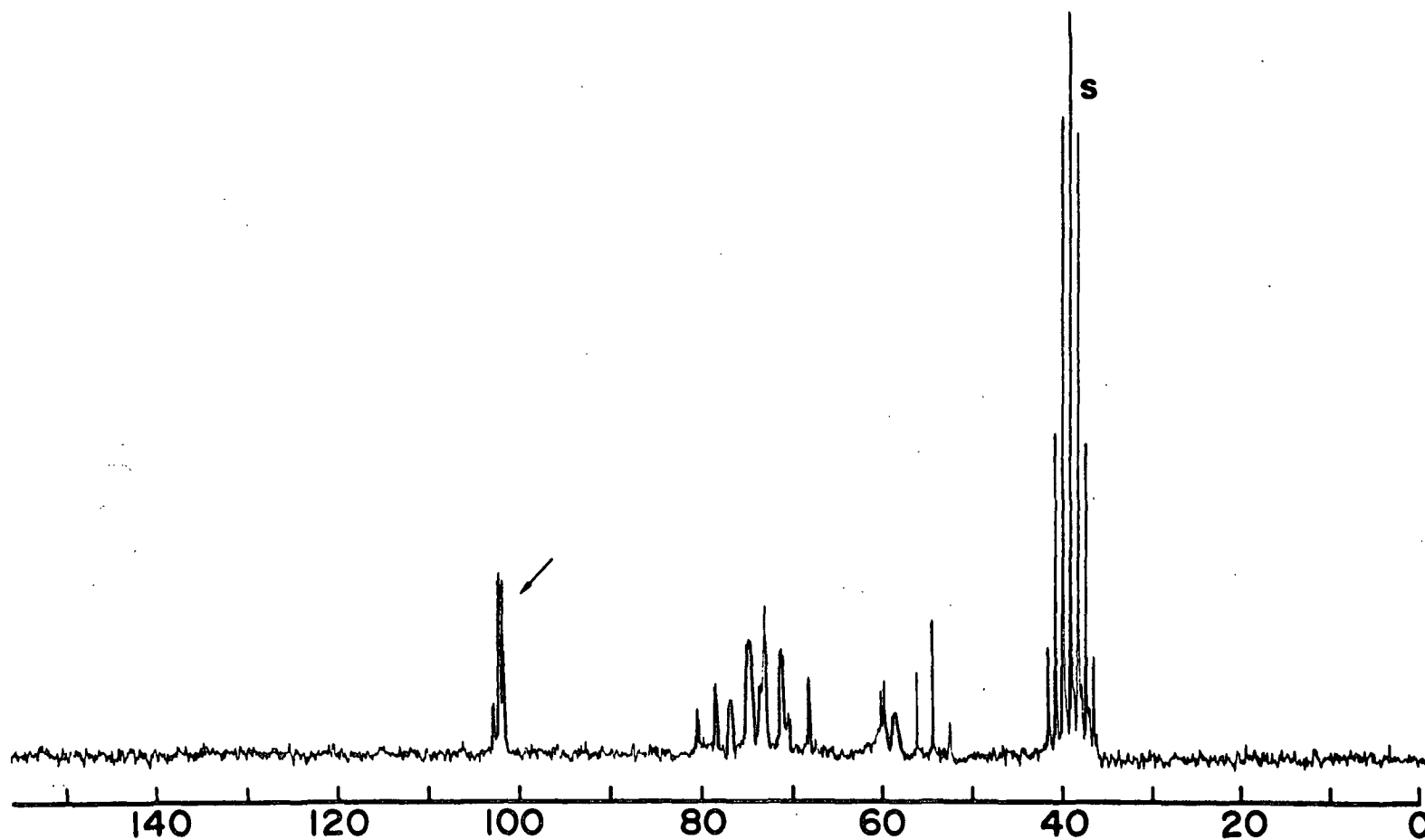
Figure 21. Selective heteronuclear decoupled spectrum with the decoupler set near
4.36 ppm (downfield of C_1'H) in the ^{1}H-spectrum. The carbon signal at
103.4 ppm (C_1') is most intense.
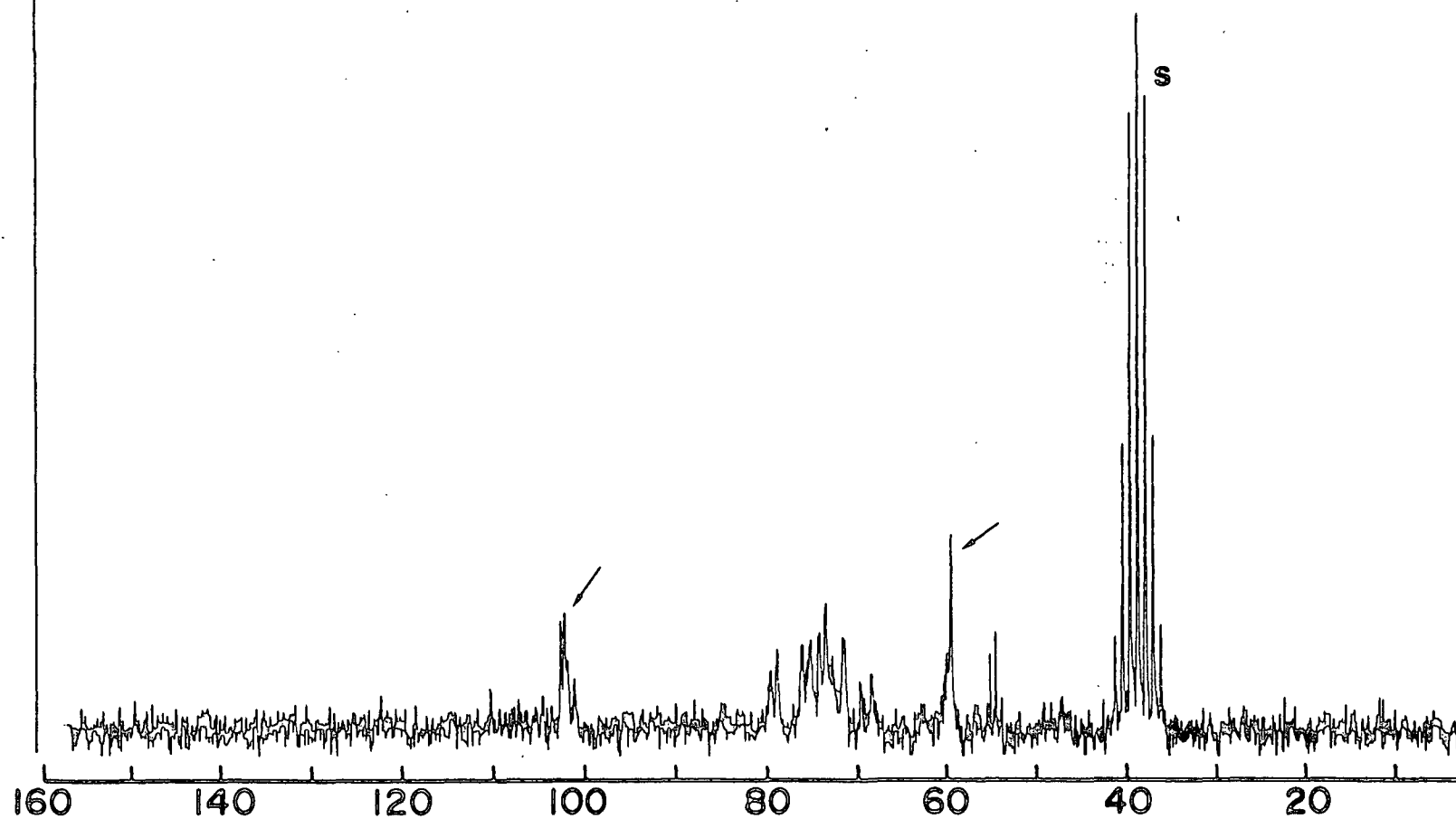
Figure 22. Selective heteronuclear decoupled spectrum with the decoupler set near 3.70 ppm (C_6H_a, C_6H_b) in the ^{1}H-spectrum. The most intense signal is the C_6 region. Additionally, the C_1 signal is sharpened indicating the C_1H is upfield of $C_1'H$.
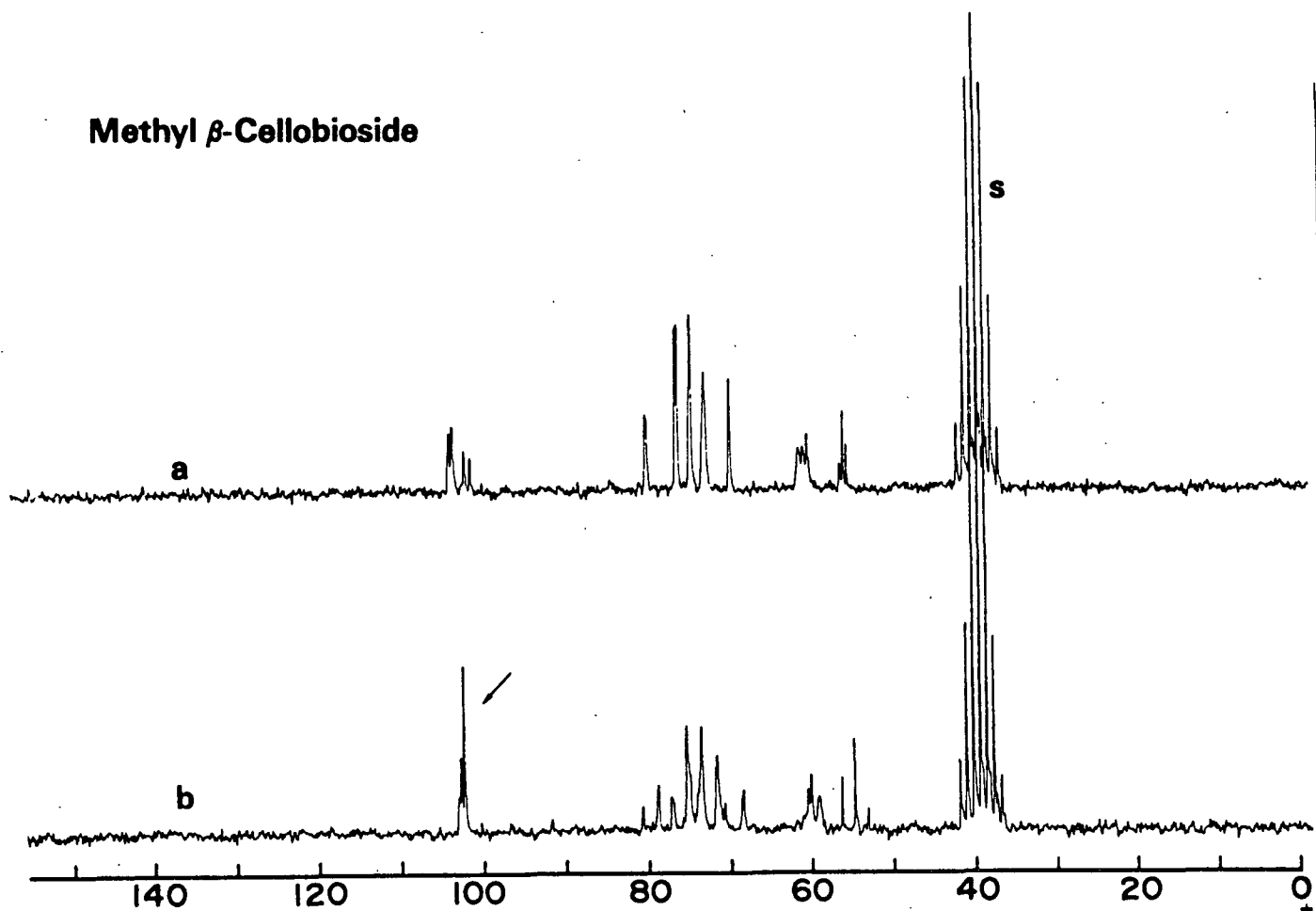
Figure 23. Selective heteronuclear decoupled spectra with the decoupler set near
(a) 3.18 ppm and (b) 4.28 ppm (C_1'H) in the [1]H-spectrum. Spectrum (a)
is similar to that in Fig. 20b. Spectrum (b) verifies that the proton
resonating at 4.28 ppm is coupled to the 103.4 ppm peak in the carbon
spectrum. The proton doublet centered at 4.10 ppm can be assigned, by
analogy to methyl-β-glucopyranoside, to C_1H. Therefore, all the assign-
ments can be made. The ^{13}C-NMR assignments agree with those in the
literature (10).
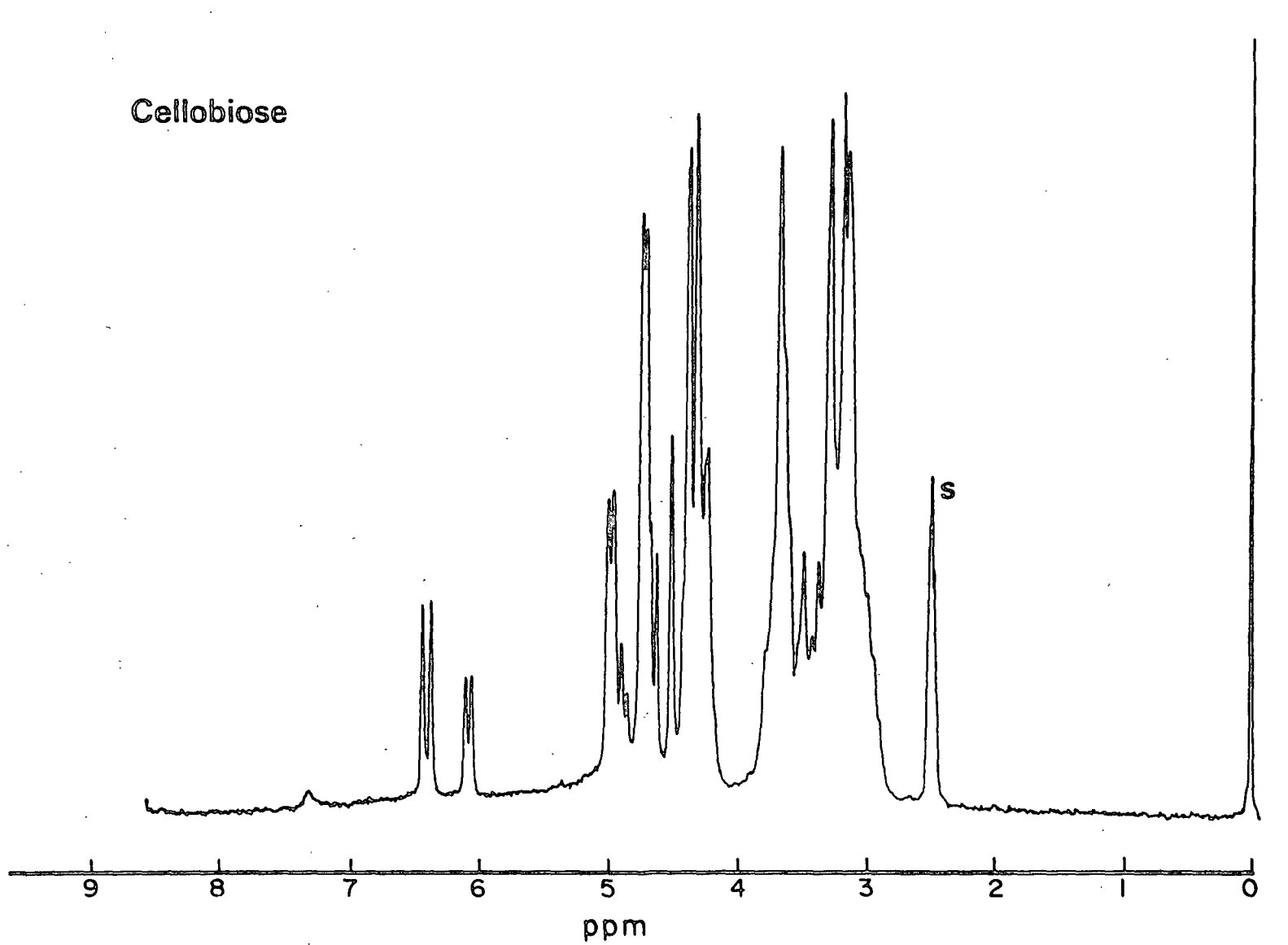
Cellobiose

Figure 24. The ^{1}H–NMR spectrum of cellobiose in DMSO-d$_6$ (6.8%) at 63°C (1000 H$_z$ sweep width).

Cellobiose
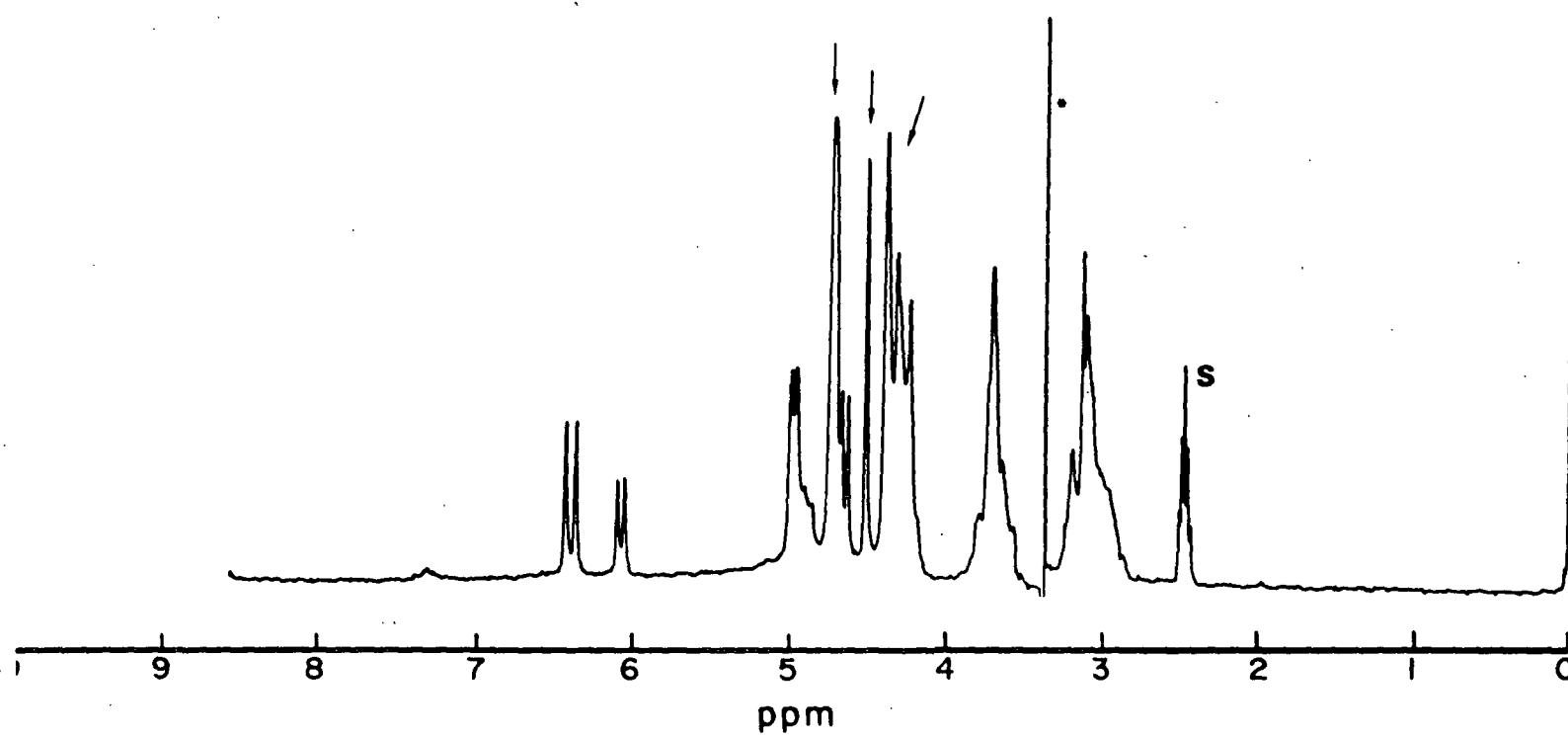
Figure 25. Irradiation near 3.37 ppm resulting in the enhancement of the singlet at 4.53 ppm ($\beta-O_3H$). No other hydroxyl signals are significantly affected.

Cellobiose
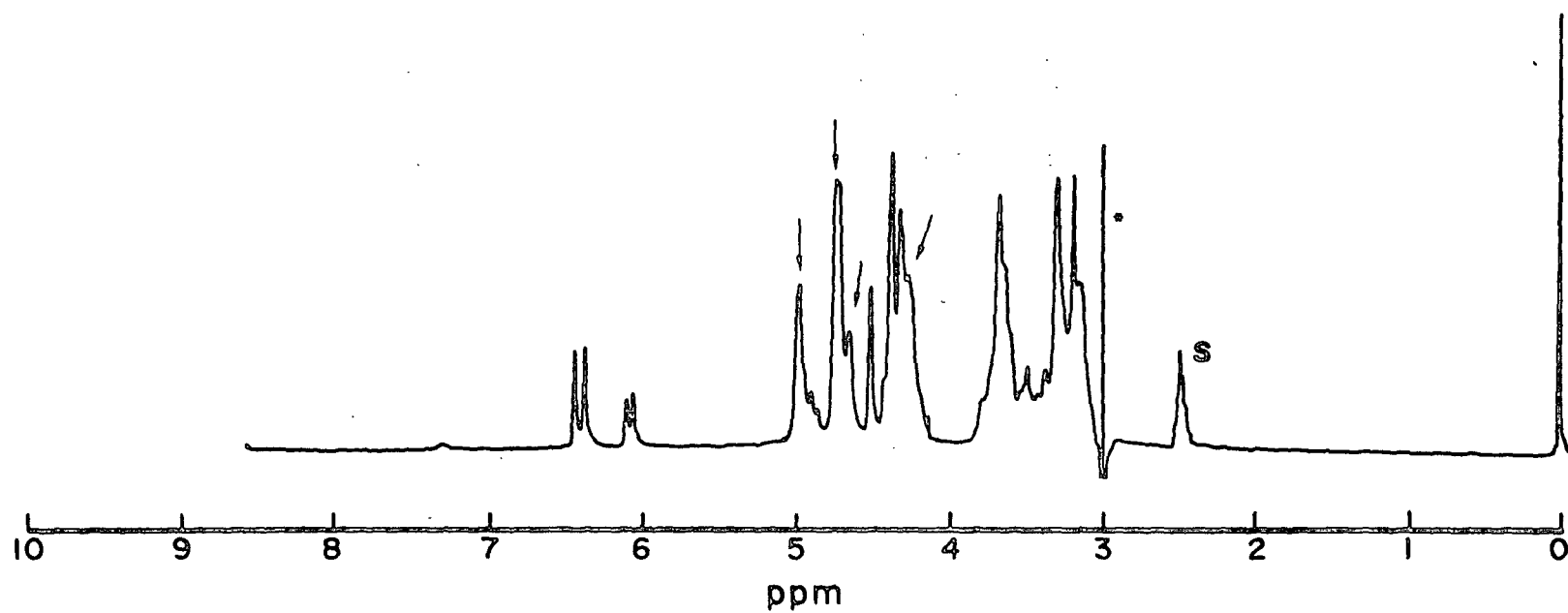
Figure 26. Irradiation near 3.00 ppm resulting in the collapse of doublets at 4.98 (O_2'H) 4.74 (O_3'H, O_4'H), and 4.67 ppm (β-O_2H). The C_1H, C_I'H region is also affected.
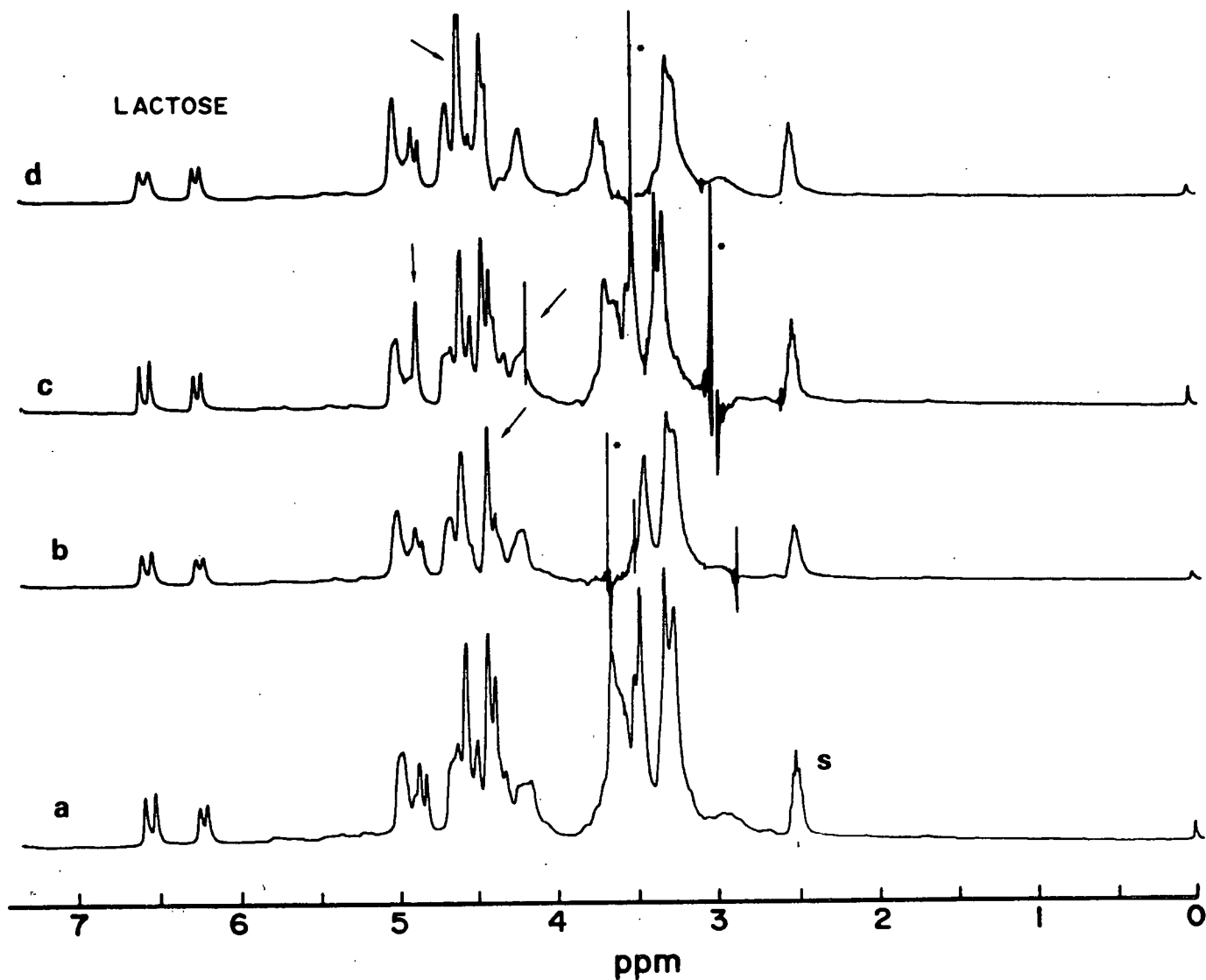
Figure 27. (a) The ^{1}H-NMR spectrum of lactose in DMSO-d_6 (4.6%) at 42.5°C, (b) Irradiation at 3.66 ppm causing a change near 4.41 ppm (O_6H), (c) Irradiation at 2.98 ppm causing changes at 4.84 ppm (β-O_2H), changes near the $C_1'H$, C_1H region are obscured by a spurious signal symmetrical about the midpoint with the irradiating frequency, (d) Irradiation at 3.50 ppm causes an enhancement of the singlet at 4.57 ppm. These results are consistent with the assignment of the singlet to β-O_3H.

4-O-(β-D-Glucosyl)-D-Mannose
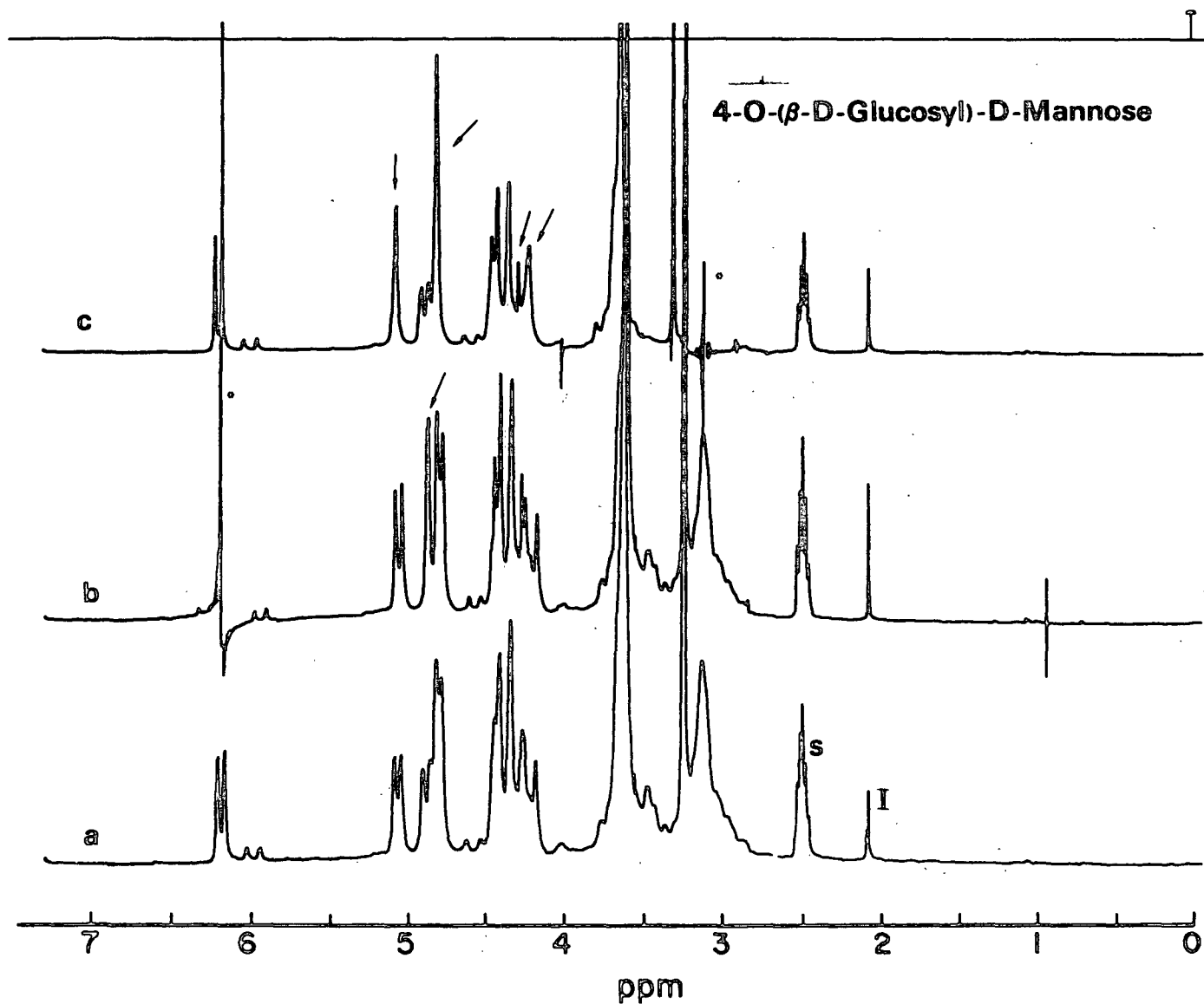
Figure 28. (a) The ^{1}H-NMR spectrum of 4-O-(β-D-glucopyranosyl)-D mannopyranose in DMSO-d$_6$ (6.1%) at 49°C, (b) Irradiation at 6.20 ppm (α-O$_1$H) causes decoupling of the doublet at 4.90 ppm (α-C$_1$H) (C) Irradiation at 3.11 ppm causing collapse of the doublets at 5.07 (O$_2$'H) and 4.80 ppm (O$_3$'H, O$_4$'H) as well as near the C$_1$H region. The singlet assigned to α-O$_3$H is not affected. These results indicate that the α-anomer predominates in this compound and are consistent with the assignment of α-O$_3$H.
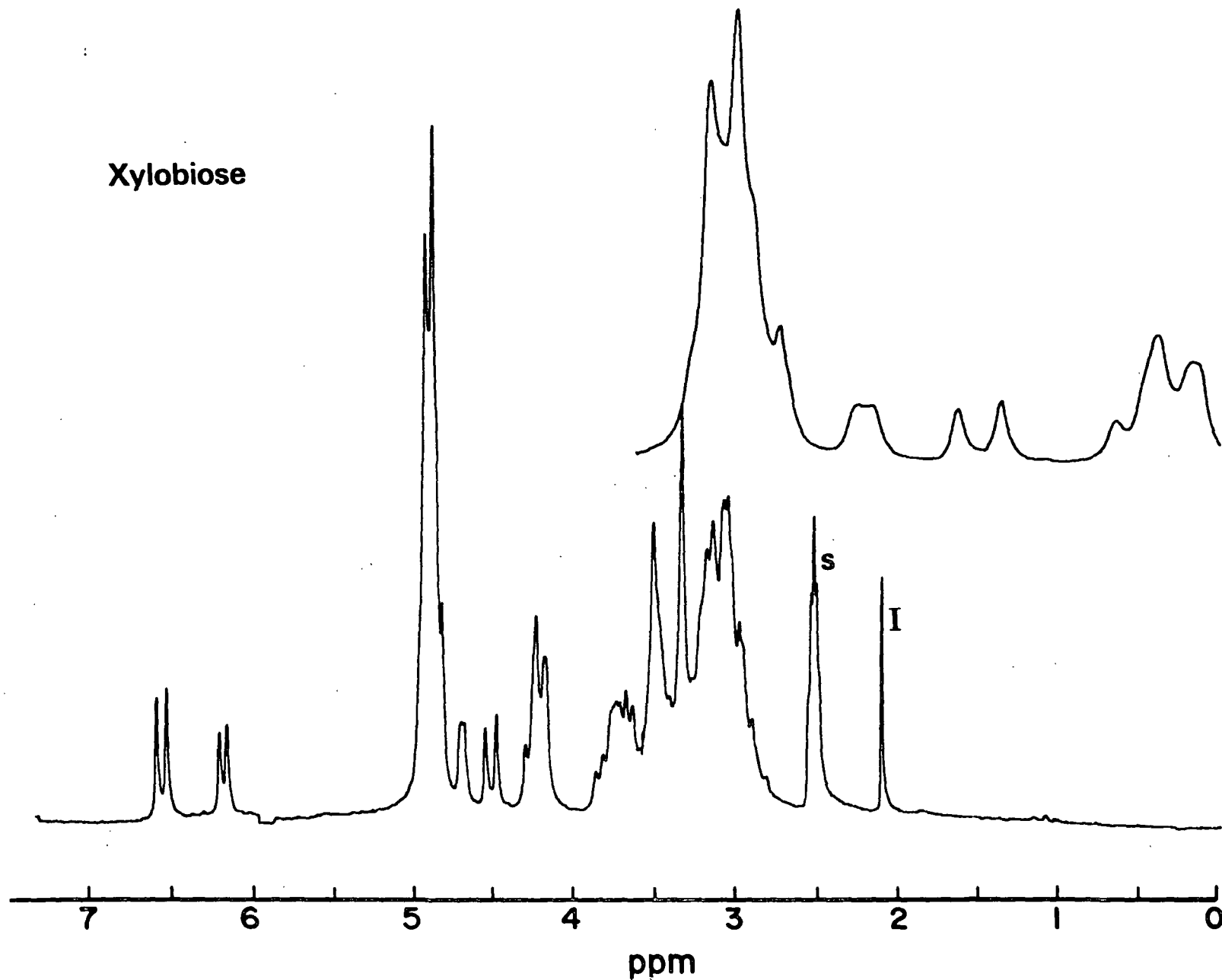
Xylobiose

Figure 29. The ^{1}H-NMR spectrum of xylobiose in DMSO-d_6 (6.0%) at 35.5°C. The inset is an expansion of the nonanomeric hydroxyl region. Note that the singlet at 4.69 ppm is actually a weak doublet.
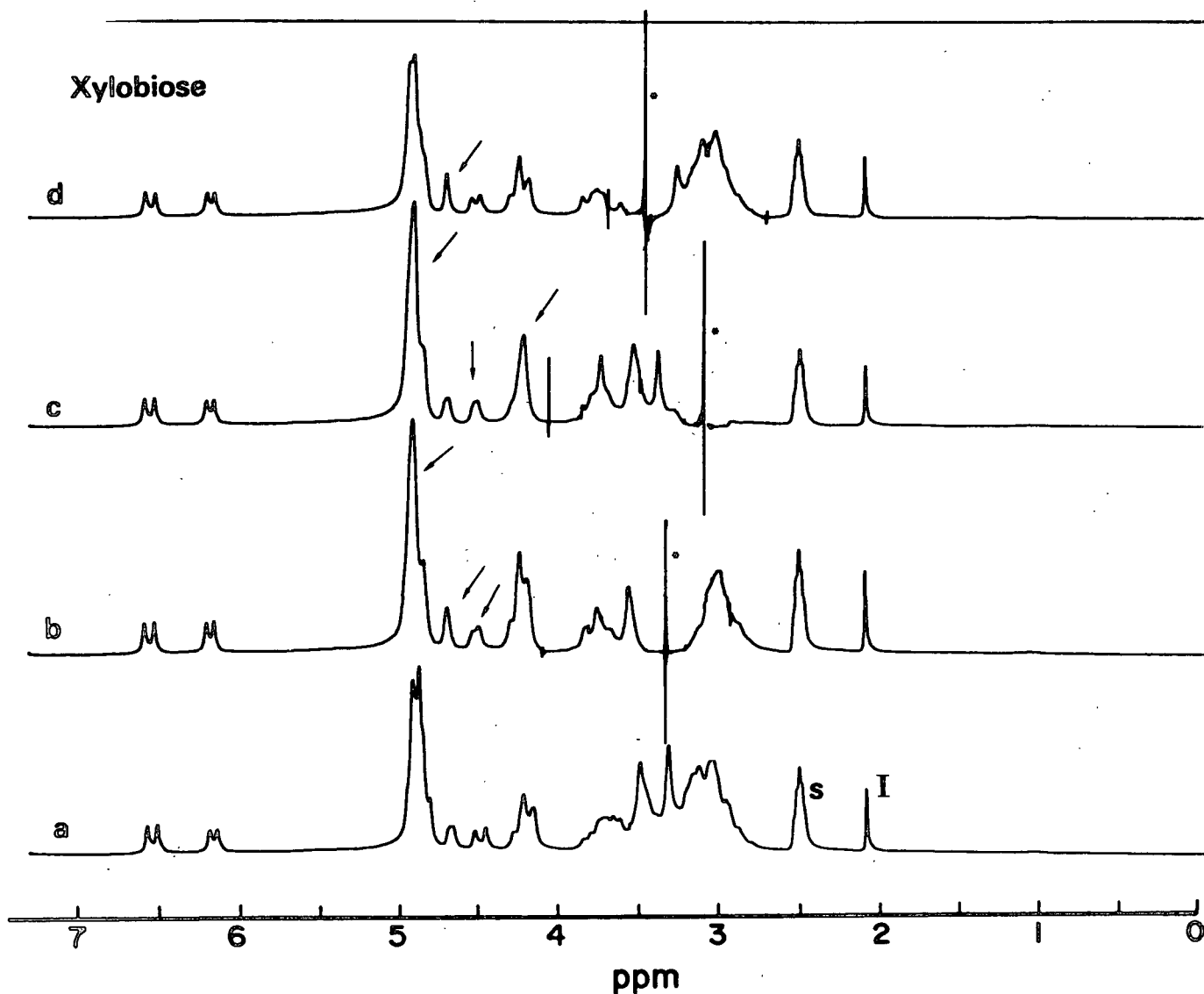
Figure 30: (a) Same as Fig. 29, (b) Irradiation at 3.32 ppm causes an enhancement of the singlet at 4.69 ppm (α-O_3H), and a partial collapse of the doublet at 4.50 ppm (α-O_2H), (c) Irradiation at 3.09 ppm affects the C_1H and C_1'H signals at 4.24 ppm as well as the large doublet at 4.91 ppm (O_2'H, O_3'H, O_4'H). The doublet at 4.50 ppm is partially collapsed. Irradiation near 3.20 ppm completely collapses it, (d) Irradiation at 3.46 ppm results in a sharpening of the singlet at 4.69 ppm with no change in the C_1H_1, C_1'H region.
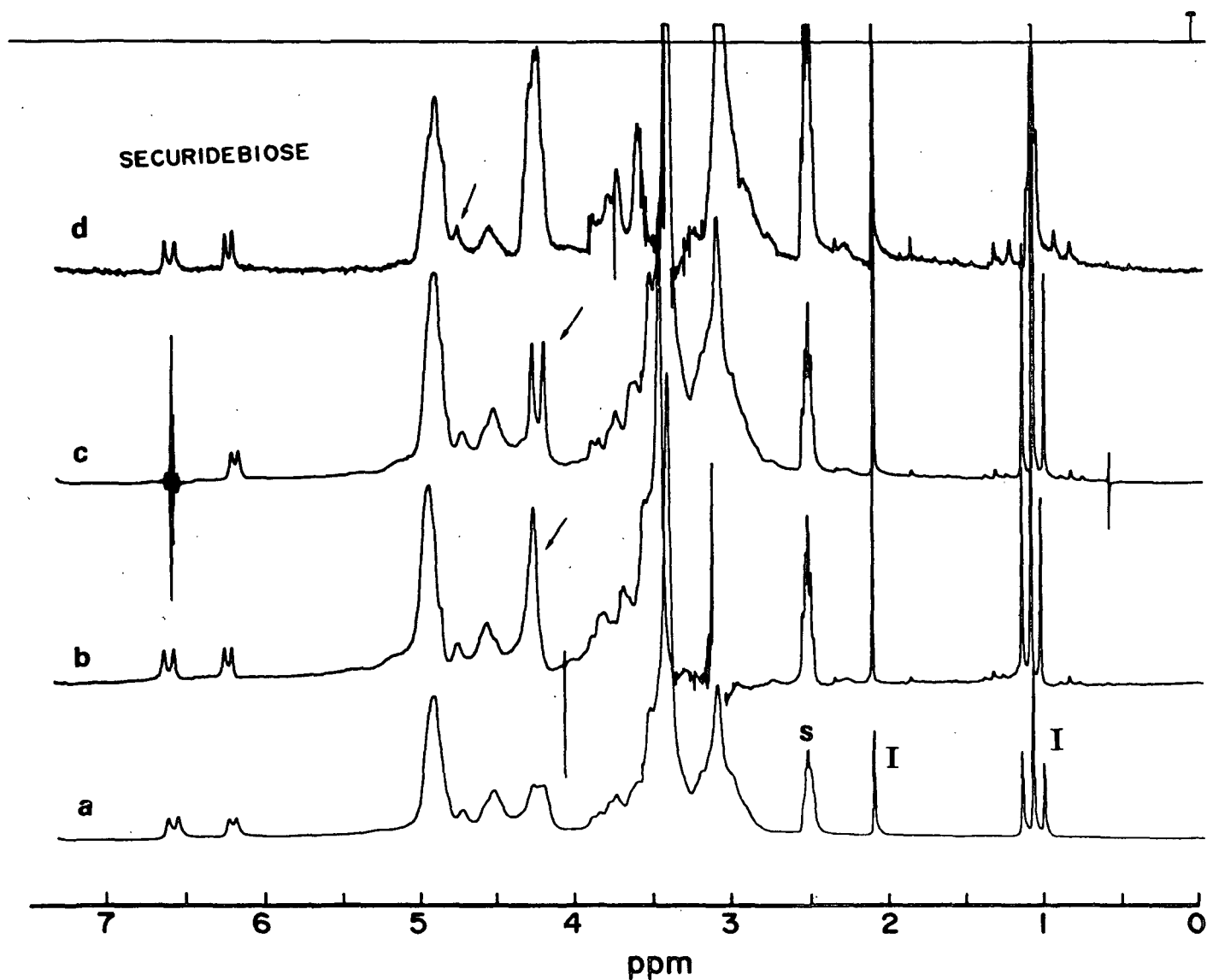
Figure 31. (a) A poorly resolved ^{1}H-NMR spectrum of securidebiose* in DMSO-d$_6$ (7.7%) at 34.5°C., (b) Irradiation at 3.08 ppm sharpens the C$_1$'H, C$_1$H signals at 4.21-4.31 ppm, (c) Irradiation at 6.60 ppm collapses the C$_1$H, C$_1$'H signals to a doublet, (d) Irradiation at 3.40 ppm partially sharpens the broadened singlet at 4.74 ppm. This is consistent with the results for xylobiose.

Again, the simultaneous use of peak intensities and spin decoupling allows complete assignment of the spectrum. Using the anomeric hydroxyl signals as a starting point (7), the β-C_1H signal can be assigned. The intensities of the signals at 4.41 and 4.64 ppm indicate that these result from the α-anomer. By the process of elimination the large complex must consist of the β-O_2H, β-O_3H, β-O_4H, α-C_1H, and α-O_4H signals. This exactly parallels the glucose assignments. A preliminary assignment of the 4.41 ppm signal to α-O_2H is based on the location of the α-C_2H signal (3.11 ppm) which decouples it. This is near the α-C_2H signal in glucose. An unequivocal assignment could be made at a higher temperature where the α-C_1H and α-O_2H signals would decouple simultaneously (7). The relative order of the skeletal protons agrees with that observed at higher fields for xylose in D_2O (6,9).

It should be pointed out that the singlet at 4.58 ppm is not affected in any of the spectra in Fig. 9-14. The doublets centered at 4.10 and 4.28 ppm are the anomeric protons on the basis of their resistance to D_2O and their temperature independence. The doublets at 5.04 and 4.94 ppm are simultaneously decoupled with the anomeric protons. By analogy with glucose, xylose, and methyl β-xylopyranoside it can be assumed that the large doublet centered at 4.78 ppm results from $O_3'H$ and $O_4'H$. Therefore, if it can be shown that the singlet at 4.58 ppm can be sharpened by irradiation at a location that does not cause simultaneous decoupling of one of the anomeric protons, then, by the process of elimination, the downfield doublets must be assigned to $O_2'H$ and O_2H and the singlet to O_3H.

The O_6H and $O_6'H$ signals are expected to be nearly coincident triplets. The decoupling results in Fig. 18 and 19 support their assignment to the 4.42 ppm signal but do not prove it. Specific heteronuclear decoupling unequivocally proves the assignments.

The above discussion verifies the assignment of the 4.58 ppm singlet to O_3H in methyl β-cellobioside (56°C.). Only one assumption is required; i.e., the large doublet at 4.78 ppm contains contributions from $O_3'H$ and $O_4'H$ but not O_3H. This is reasonable based on the monosaccharide spectra and the expectation that the β-1,4-glycosidic linkage will have a larger impact on O_3H than either $O_3'H$ or $O_4'H$. Differentiation of the downfield doublets, between O_2H and $O_2'H$ is not possible through decoupling experiments at low magnetic field strengths. However, the spectra of cellobiose and the methyl β-glycosides support the assignments given for O_2H and O_2^1H.

The results depicted in Fig. 24-26 are completely analogous to those found for methyl-β-cellobioside.

The results presented in Fig. 29-30 are consistent with the assignment of the singlet at 4.69 ppm to an O_3H proton. Assignment to the α-anomer is based on the intensity and a comparison to the methyl β-xylobioside spectrum.

LITERATURE CITED

1. Baldeschwieler, J. D. and Randall, E. W., Chem. Rev. 63:81-110(1963).

2. McFarlane, W., In An Annual Review of NMR Spectroscopy 5A, 1972. p. 353-93.
    E. F. Mooney, ed.

3. Ave, W. P., Karhan, J., and Ernst, R. R., J. Chem. Phys. 64:4226-7(1976).

4. Hall, L. D., Morris, G. A., and Sukumar, S., J. Amer. Chem. Soc. 102:1745-7
    (1980).

5. Becker, E. D., High Resolution NMR - Theory and Chemical Applications.
    Academic Press, Inc., 1969.

6. Perlin, A. S., Can. J. Chem. 44:539-50(1966).

7. Perlin, A. S. and Mackie, W., Can. J. Chem. 44:2039-49(1966).

8. Koch, H. J. and Perlin, A. S., Carbohyd. Res. 15:403-10(1970).

9. Lemieux, R. L. and Stevens, J. D., Can. J. Chem. 44:249-62(1966).

10. Hamer, G. K., Balza, F., Cyr, N., and Perlin, A. S., Can. J. Chem. 56:3109-16
    (1978).

APPENDIX IX

LOCAL CONFORMATION AT $O_{2'}H$

Earlier, it was shown that the downfield doublet at 5.03 ppm (56°C) in $\underset{\sim}{1}$ (cellobiose) can be assigned to $O_{2'}H$. For the methyl β-glycosides another doublet assigned to O_2H is found at 4.94 ppm (56°C, $\underset{\sim}{2}$). In both cases, the doublet is shifted downfield from its location in the monosaccharide. Contrasted to this are the disaccharides $\underset{\sim}{5}$ and $\underset{\sim}{6}$ in which the $O_{2'}H$ signal is not shifted from its location in β-xylose. The reason for this difference must be related to the presence of the glycosidic group. Since xylose and glucose differ only at C_5, six bonds removed from $O_{2'}H$, this effect must be related to the steric environment created by the aglycon around $O_{2'}H$.

Figure 1 compares the steric environment around $O_{2'}H$ for the three situations discussed above. With a xylopyranosyl group as the aglycon, a steric environment relatively free of steric hindrance is present. When a methyl or glucopyranosyl group is the aglycon, a sterically hindered environment exists. In the latter case, it is the presence of the hydroxymethyl group attached to C_5 that creates the hindrance.

Radar has previously discussed the probable orientations of the hydroxyl group in cyclohexanols and simple alcohols (3,4). Three possible conformations, related by 120° rotations of χ, are depicted in Fig. 2 for a hydroxyl proton. For secondary alcohols, a preference for the rotamers with χ = 60° was found, though all three noneclipsed rotamers are populated. As larger substituents are added, the proportion of conformation II (χ = 180°) is decreased but with a compensating constriction of the dihedral angles observed in conformations I and III. This results in an increase in the coupling constant. It was also shown that the hydroxyl proton chemical shift was both a function of H-bond strength and rotamer conformation.
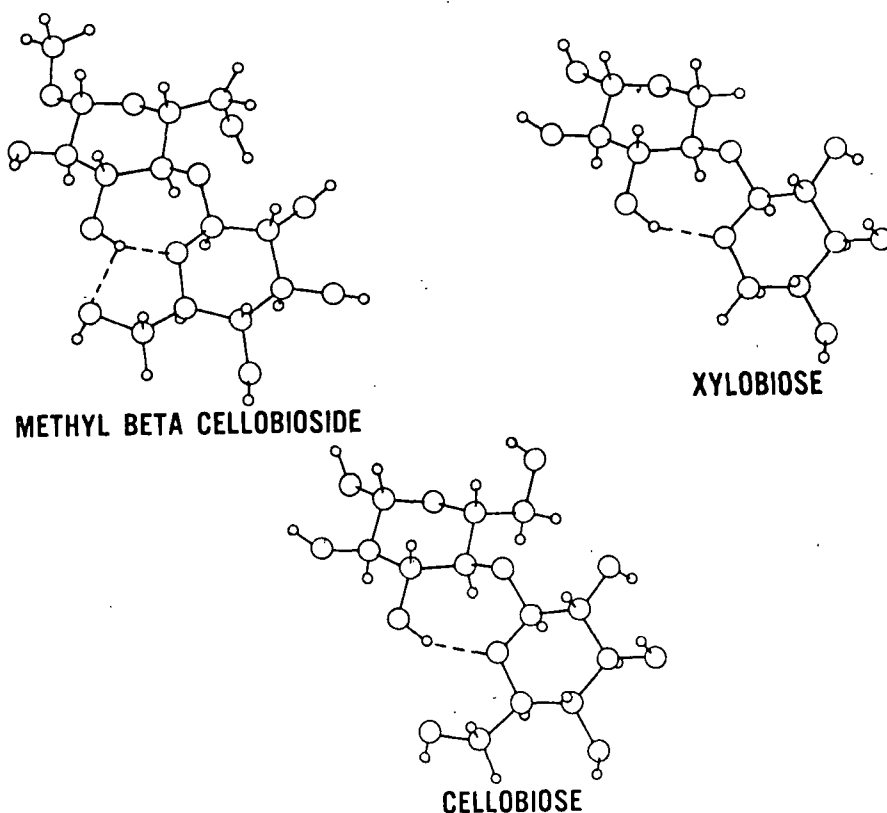
METHYL BETA CELLOBIOSIDE

XYLOBIOSE

CELLOBIOSE

Figure 1. Computer drawings depicting the role of the hydroxymethyl group at C_5 and the O-methyl group in effecting the conformation of O_2,H and O_2H respectively. The drawings were generated using the crystal structure data in Ref. (1) and (2). The conformations depicted here are not necessarily observed in solution.
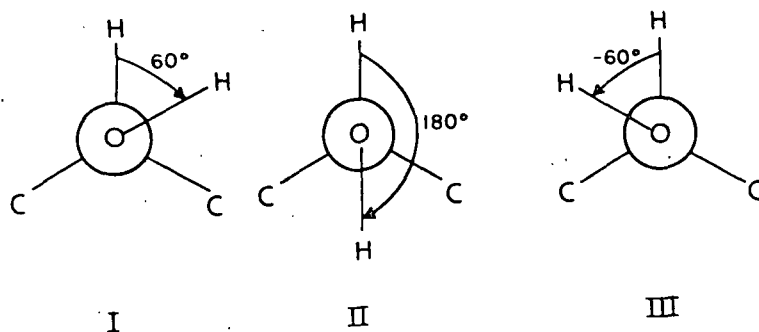

I   II   III

Figure 2. The noneclipsed rotamers populated by the hydroxyl protons in simple secondary alcohols (4).

The effect of 1,3-trans-diequitorial interactions between adjacent hydroxyls was previously used to predict that in amylose the preferred rotamer has a value of χ = 110° (5). For this dihedral angle, it was shown that nearly a linear intramolecular H-bond with $O_{2'}$ occurs. It was argued that the alternate choice of χ = 60° is destablized by a 1,3-trans-diequitorial interaction with the bridge oxygen. Furthermore, on the basis of the independence of the coupling constant on temperature, it was argued that no other rotamers are significantly populated. It can be pointed out that a value for χ of 110° represents a nearly eclipsed conformation and does not correspond to any of the rotamers, I-III, in Fig. 2.[*]

Table I gives the $^3J_{HCOH}$ values for the isolated hydroxyl signals observed in this study. Over the temperature range studied, these values are constant, with the exception of $O_{2'}H$, indicating that one rotamer is predominant. A value of 5.18 Hz has been observed for neat methanol in which nearly free rotation between conformers I-III is known (4). Most of the values in Table I depart from this significantly; further indicating that rotation of the hydroxyl is restricted for carbohydrates dissolved in DMSO-d_6. This should be expected for a hydroxyl participating in a strong donor H-bond to DMSO since, in general, a movement between rotamers would involve moving two large groups (DMSO, the sugar) past one another.[**]

The steric interactions present for $O_{2'}H$ or O_2H are illustrated in Fig. 3 for disaccharides 1, 2, and 5. For 1, the value of $^3J_{HCOH}$ for β-O_2H is 4.8 Hz but for

---

[*]A value of χ = 110° is favored for the $O_3H\ldots O_{2'}$ intramolecular H-bond in α-1,4-linked glucans on the basis of the formation of a nearly linear H-bond (5). Since the temperature dependence of O_3H is intermediate, between that found in 1 and the hydroxyls that freely associate with the solvent, it appears likely that in this case, the solvent partially H-bonds to O_3H. From this, it follows that the intramolecular H-bond is not necessarily linear and that the value of χ = 110° must remain speculative.

[**]The lifetime of the H-bond should be longer than a single rotamer lifetime since the energy of H-bond formation (3-10 Kcal/mole) is greater than that of rotation (1 Kcal/mole) (4,6).

$O_{2'}H$, the value is 4.1 Hz. Clearly, the presence of the aglycon affects the rotamer distribution of the $O_{2'}H$ group relative to $\beta-O_2H$. For the methyl β-glycosides $^3J_{HCOH}$ is 4.4-4.6* for O_2H indicating that the distribution of rotamers is also perturbed by the methyl group.

TABLE I

$^3J_{HCOH}$ VALUES FOR ISOLATED HYDROXYL SIGNALS IN SEVERAL
GLUCOSE OR XYLOSE CONTAINING CARBOHYDRATES[a]

	$\beta-O_1H$	$\alpha-O_1H$	$\beta-O_2H$	$\alpha-O_2H$	$\alpha-O_3H$	$O_{2'}H$
1[b,c,d]	6.5(0.1)	4.5(0.2)	4.8(0.1)			4.1(0.1)
2			4.7(0.1)			4.3(0.3)
3	6.5	4.7(0.3)[e]		6.6	4.1	
3c			4.6			
3d				5.9		
4[f]	6.5	4.1[e]			4.5	
4c			4.4			
5	6.5(0.1)	4.6(0.3)		6.8(0.2)		
6	6.5(0.1)	4.7(0.2)				
7A[g]			5.1(0.1)			
9	6.1					
10	6.4(0.2)	4.5(0.1)	4.8(0.1)			
11	8.5	4.4(0.1)				5.2

[a]Standard deviations (σ) are given is parentheses. Results are an average over all available samples and temperatures in which the hydroxyl is isolated. If no σ is given, it is less than 0.1 Hz.
[b]An average over four samples.
[c]In some samples the $O_{2'}H$ signal shows a steady decrease of $^3J_{HCOH}$ with increasing temperature. These values are not included.
[d]The coincident signals $O_{3'}H$, $O_{4'}H$ show a sharp coupling of 4.1 Hz (56°C).
[e]In mixtures of acetone-d_6 and DMSO-d_6 a small long range coupling to C_2H has been reported (7).
[f]The large peak comprising $\beta-O_2H$, $\beta-O_3H$, and $\beta-O_4H$ shows a sharp splitting of 4.3 Hz (34°C).
[g]Averaged over two concentrations.

Radar has shown that the chemical shift of a H-bonded hydroxyl is affected by both the H-bond strength and the distribution of rotameric conformations (3). Apparently, both of these factors are operative in determining the relative chemical

---

*For 2 , the value is 4.7 Hz.

shift of O_2,H in $\underset{\sim}{1}$ compared to $\underset{\sim}{5}$. In the latter case, the shift is no different from that in xylose or glucose. In $\underset{\sim}{1}$ and $\underset{\sim}{2}$, it is shifted downfield partly as a result of a different distribution of hydroxyl rotamers. Since the only structural difference between $\underset{\sim}{1}$ and $\underset{\sim}{5}$ is the presence of the hydroxymethyl group, it is probable that this group either sterically hinders or promotes specific rotameric conformations of O_2,H.

front view   side view

Non-Bonded Interactions for O_2,H

X(DEGREES)	INTERACTION
0	1,2 eclipsed ($C_2 \cdot$ H)
60	1,3 trans di-equitorial (O_{link})
120	1,2 eclipsed ($C_1 \cdot$)
180	1,3 di-axial ($C_1 \cdot$ H, $C_3 \cdot$ H)
-120	1,2 eclipsed (C_3)
-60	1,3 trans di-equitorial ($O_3 \cdot$)
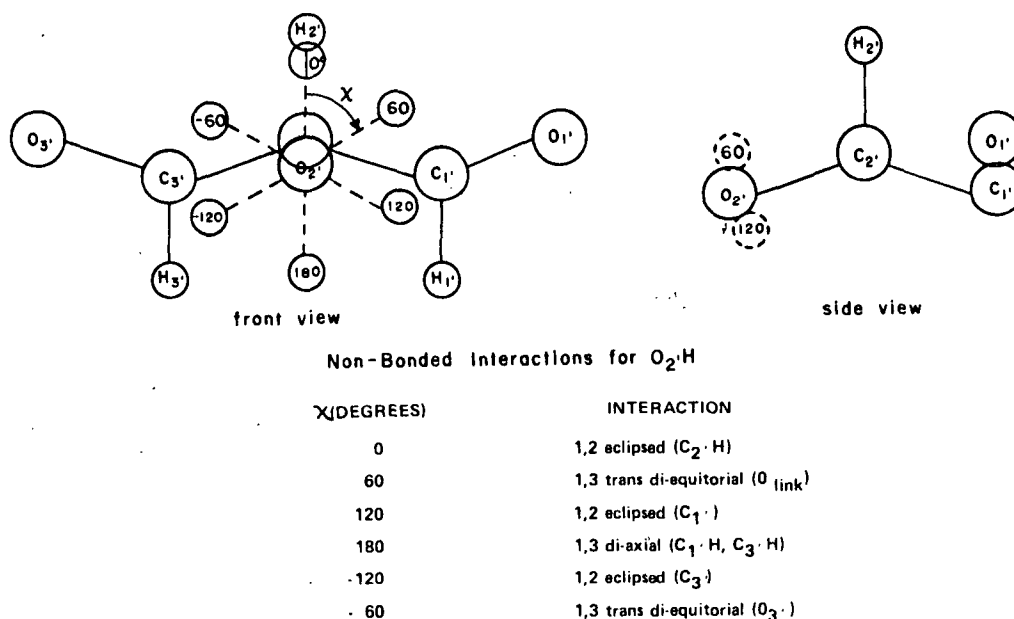
Figure 3. Illustration of the nonbonded interactions present for six O_2,H rotamers related by 60° rotations. The front view represents a projection unto the plane containing C_1,, C_2,, H_1,, and H_3,. The side view represents a projection unto the perpendicular plane containing C_2, and H_2,. The latter view illustrates that the distances O_2,H - C_1, (X = 120°) and O_2,H - O_1, (X = 60°) are nearly equivalent. The drawings are not to scale.

Several facts indicate that the action of the hydroxymethyl group is to promote a specific interaction with O_2,H leading to an increase in the rotamer corresponding to approximately χ = 120°. Models show that this would allow the formation of a weak intramolecular H-bond with O_6(O_2,H....O_6). This rotamer represents a nearly eclipsed conformation with C_1,, not unlike that proposed for O_3H in maltose ($\underline{5}$). The O_2,H....O_6 bond has been previously proposed ($\underline{8}$).

One of the facts supporting this is the slightly reduced temperature dependence of the $O_{2'}H$ chemical shift relative to the O_2H shift. The O_2H temperature coefficient is slightly higher than that of the other hydroxyl signals (Tables VI and VII in Section 3, Part 3), in both reducing sugars and methyl β-glycosides. The $O_{2'}H$ temperature coefficient in $\underset{\sim}{1}$ and $\underset{\sim}{2}$ is slightly reduced, indicating that it is slightly less available to H-bond to the solvent. The second fact is that the value for $^3J_{HCOH}$ of the $O_{2'}H$ signal is observed to decrease with temperature while for the other hydroxyl signals it does not.[*] This indicates that a shift in rotamer distribution occurs, probably with the result that the weak intramolecular H-bond is disrupted.

While it is tempting to further speculate on the existence of specific rotamers, it should be remembered that; values for χ from Eq. (1) (Section 3, Part 3) are only approximate (9), and that the effect of 1,3 trans-diequitorial interactions involving adjacent hydroxyl groups has not been thoroughly studied (5). A possible approach to this could involve the study of hydroxyl coupling-constants and their variation with temperature using the inositols as models.

---

[*]This is partially related to sample purity. The reduction of $^3J_{HCOH}$ for $O_{2'}H$ does not occur in all samples but when it does occur, this hydroxyl is affected first. If slightly acidic conditions prevail, then all hydroxyl signals eventually broaden and J decreases.

LITERATURE CITED

1. Chu, S. S. C. and Jeffry, G. A., Acta Crystallogr. B24:830-8(1968).

2. Ham, J. T. and Williams, D. G., Acta Crystallogr. B26:1373-83(1970).

3. Radar, C. P., J. Amer. Chem. Soc. 88:1713-18(1966).

4. Radar, C. P., J. Amer. Chem. Soc. 91:3248-56(1969).

5. St.-Jacques, M., Sundararajan, P. R., Taylor, K. J., and Marchessault, R. H., JACS 98:4386-91(1976).

6. Pimental, G. C. and McClellan, A. L. The Hydrogen Bond. W. H. Freeman and Co., 1960.

7. Jochims, J. C., Taigel, G., Seelinger, A., Lutz, P., and Driesen, H. E., Tetrahedron Letters 44:4363-9(1967).

8. Sarko, A., Appl. Polym. Symp. 28:729-42(1976).

9. Fraser, R. R., Kaufman, M., Morand, P., and Gouil, G., Can. J. Chem. 47:403-9 (1969).

APPENDIX X

PROCEDURES

GENERAL PROCEDURES

NMR spectra were obtained on a Jeol FX-100 spectrometer operating at 25.05 MHz (^{13}C) or 99.60 MHz (^1H). Magnetic field stabilization was achieved using the internal deuterium lock feature. Ambient probe temperatures (micro, 5MM, 10MM) were used unless otherwise noted. In most cases, $(CH_3)_4Si$ was used as an internal standard in organic solvents and p-dioxane (67.4 ppm) in D_2O.

Melting points were determined on a calibrated Thomas-Hoover capillary apparatus. Thin layer chromatography (TLC) used silica gel G coated onto microscope slides. Methanolic sulfuric acid (5:1, v/v) spray with charring was used for detection. Paper chromatography used Whatman No. 1 filter paper. Detection was with silver nitrate in acetone followed by caustic and sodium thiosulfate washing.

Solvents were purified using conventional distillation methods when necessary. Chloroform was extracted twice with water in a separatory funnel to remove ethanol. It was dried with calcium chloride, filtered, and refluxed over calcium sulfate using a Vigreux column. The fraction boiling from 59-60°C was collected and stored in the dark. Dry acetone was prepared by storing over Drierite. Dry benzene was prepared by refluxing over phosphorus pentoxide and then collecting the 75-79°C fraction using a Vigreux column. Solvent stripping was done under vacuum using a common laboratory rotary evaporator.

MONOSACCHARIDE DERIVATIVES

Benzyl β-D-arabinopyranoside (16)

Arabinose (75.0 g, Matheson-Coleman-Bell) and benzyl alcohol (375 mL) were placed in a flask and stirred (30 minutes) in an ice-salt bath. Acetyl chloride (37.5 mL) was then added dropwise over a 1 hour (h) period, taking care not to let the temperature go over 60°F. The mixture was stirred for 12 h until it formed a gel. It was monitored by TLC using chloroform-methanol (3:1, vol.). Ethyl ether (750 mL) was added and the mixture was allowed to stand, with occasional stirring, 4 hours in an ice-salt bath to promote crystallization. The mixture was filtered and the residue was dried overnight in vacuo (50°C) to yield crystalline 16 (80.5 g, 67%); m.p. 169.5-172°C. Literature (1); m.p. 169-171°C.

Benzyl 3,4-isopropylidene β-D-arabinopyranoside (17)

Dry acetone (18 mL), 2,2-dimethoxypropane (18 mL), and compound 16 (5.2 g) were mixed in a flask with p-toluene sulfonic acid (180 mg). The mixture was gently heated (70°C) with continuous stirring until all solids were dissolved. A drying tube was used to exclude moisture. The mixture was allowed to stand for 1 h at room temperature and then neutralized with excess potassium carbonate. TLC with chloroform-ethylacetate (4:1, vol.) was used to monitor the reaction. The slurry was filtered and evaporated in vacuo to a pale yellow syrup. The syrup was dissolved in ethyl ether (15 mL), filtered to remove unreacted 16, and reduced to a syrup in vacuo. Seeding affected crystallization as large rectangular crystals. Recrystallization from a minimum of ethyl ether, to which low boiling petroleum ether was added until cloudy, afforded crystalline 17 (5.0 g 82%); m.p. 57-58°C. Literature (1) m.p. 55-58°C.

Benzyl 2-O-tosyl-3,4-O-isopropylidene-β-D-arabinopyranoside (18)

Compound 17 (23.0 g) was crushed and added in a flask to pyridine (96 mL) con-
taining p-toluene sulfonyl chloride (27.5 g). The mixture was held at 50° (ca. 6
h) until TLC indicated it was complete. TLC monitoring was with chloroform-
ethyl acetate (4:1, vol.). The cooled solution was extracted with chloroform (240
mL). The chloroform layer was then washed with successive portions of aqueous
sulfuric acid (2N, 120 mL) until the top layer remained acidic after vigorous shaking
and then with water (120 mL) until the top layer was neutral. The chloroform solu-
tion was then dried over calcium sulfate, filtered, and evaporated in vacuo to a
thick brown syrup. Crystallization from ethanol water (90% vol.) produced 18 (28.9
gm, 81%); m.p. 91.5-93.5°C. Literature (1), m.p. 96°C.

Benzyl 2-O-tosyl-β-D-arabinopyranoside (19)

Compound 18 (16.0 g) was added to aqueous ethanol (80% vol.; 112 mL) containing
Amberlite IR-120 ion exchange resin (H$^+$, 7.7 g) and refluxed (ca. 8 h). The reac-
tion was monitored by TLC using ethanol-ethyl acetate (4:1, vol.) with additional
IR-120 being added when needed. The solution was filtered while hot and evaporated
in vacuo until near dryness. A granular white precipitate formed. The precipitate
was filtered, washed with water, and dried in a vacuum oven. Recrystallization from
isopropyl ether-ethyl acetate (20:1, vol.) gave crystalline 19 (14.0 g. 96%); m.p.
123-125°C. Literature (1); m.p. 123.5-124.5°C.

Benzyl 2,3-anhydro-β-D-ribopyranoside (15)

Compound 19 (8.5 g) was dissolved in methanolic sodium methoxide (0.5N, 67 mL)
and held at 50°C (ca. 6 h) with continuous stirring. The cool solution was allowed
to stand for 4 h and was then evaporated in vacuo to about 20 mL volume. The solu-
tion was neutralized by adding sulfuric acid dropwise. After standing for several
days a few drops of water were added to promote crystallization. The resulting

crystalline material was filtered, washed with water, and dried in vacuo (4.5 gm. 90%); m.p. 66-74°C. Literature (1); m.p. 76-77°C.

2,3,4-tri-O-acetyl-α-β-xylopyranosyl Bromide (13)

β-D-xylopyranose tetraacetate (70 g, student preparation) was mixed with 1,2-dichloroethane (130 mL) in a stirred Erlenmeyer flask. Hydrogen bromide in acetic acid (41%, vol., 77 mL) was added slowly. The mixture was stoppered and allowed to stand quiessently for several hours. The reaction was monitored by t.l.c. with chloroform-ethyl acetate (2:1, vol.). After 4 h additional hydrogen bromide was added. After 7 h additional chloroform (350 mL) was added. The mixture was slowly poured into ice-water (3L) with vigorous stirring, and the chloroform layer separated. The water layer was washed several times with additional chloroform. The combined chloroform fractions were dried over calcium chloride, filtered, and reduced in vacuo just until crystals began to form. The syrup was allowed to crystallize overnight in the refrigerator. The product was recrystallized twice from isopropyl ether (51.3 gm. 64%); m.p. 85-100°C. The product was dissolved in dry chloroform and stored in the refrigerator until completely used in subsequent reactions. In earlier reactions the product was taken up in dry benzene. No further characterization was attempted.

2,3,4,6-tetra-O-acetyl-α-D-glucopyranosyl Bromide (14)

α,β-D-Glucose pentaacetate (37.7 g, Pfanstiel) was mixed with 1,2-dichloroethane (105 mL) and hydrogen bromide in acetic acid (32%, vol., 120 mL). Workup was identical to that of 13 except that sodium bicarbonate in water was used to wash the combined chloroform layer. After two recrystallizations the final product was obtained (29.5 g, 69%); m.p. 88-90°C. Literature (2); m.p. 88-89°C. Without further characterization, the product was dissolved in dry chloroform for subsequent reaction.

DISACCHARIDE DERIVATIVES

Benzyl 2,3-anhydro-O-(2',3',4'tri-O-acetyl-xylopyranosyl)-β-D-ribopyranoside (6)

Benzyl 2,3-anhydro-β-D-ribopyranoside (10 g) was stirred at room temperature (ca. 24 h) with silver oxide (33.7 g), 10-20 mesh drierite (62.5 g), and dry chloroform (162 mL) to ensure removal of all water from the system.

In earlier reactions dry benzene had been used. Molecular sieves (20 g, Linde A-4) were then added to ensure complete removal of water. The flask was fitted with a drying tube to exclude moisture and covered to exclude light. Iodine (3.75 g) and the bromide (13), in dry chloroform (38 g in 250 mL), were then added; the bromide was added dropwise over several hours. The reaction was continued (ca. 6 days) until the bromide concentration was no longer decreasing as indicated by TLC. The TLC solvent was chloroform-ethylacetate (4:1, vol.). The reaction was terminated by filtering through a bed of celite, washing the celite with chloroform and washing the liquor with aqueous sodium thiosulfate (0.5 m, 100 mL). The filtrate was dried in vacuo to a pale yellow syrup. TLC indicated at least 3 components. Crystals would not form even when seeded.

Benzyl 2,3-anhydro-4-O-(β-D-xylopyranosyl-D-xylopyranoside (5)

Pale yellow syrup 6 (40 g) was mixed with methanol (100 mL) and methanolic sodium methoxide (0.5N, 8 mL). The mixture was heated on a steam bath for approximately 5 minutes. The reaction was monitored by TLC with chloroform-ethylacetate (4:1, vol.). Additional cycles of methoxide addition followed by heating were used until TLC indicated the reaction was complete. The mixture was refrigerated until crystallization was complete. The crystalline mass was filtered, washed with cold methanol, and dried in vacuo (5.0 g, 31% based on 15); m.p. 198-201°C. Recrystallization of a portion from methanol gave white needle like crystals; m.p. 200-203°C. Literature (1) m.p. 202.5-203°C.

Benzyl β-D-xylobioside (3)

Compound 5 (1.5 g) was dissolved in aqueous sodium hydroxide (2N, 150 mL) and heated to near reflux temperature. The flask was fitted with a reflux condenser, magnetic-stirrer, and facilities to continuously bubble nitrogen into the solution. The reaction was stopped after 7 h, cooled, and poured slowly, with vigorous stirring, into a slurry of Amberlite IR-120 ion exchange resin (180 mL, acid form). The mixture was filtered, washed with hot water, and evaporated in vacuo to a hard syrup (1.5 g, 95%) which did not crystallize. ^{13}C-NMR spectroscopy in D_2O confirmed in to be 3.

Xylobiose (1)

Benzyl β-xylobiose syrup (2.7 g) was dissolved in an ethanol-water (50:50, 250 mL) mixture and mixed with 10% palladium on carbon catalyst (1.7 g). The mixture was attached to a hydrogenation device for atmospheric hydrogenation. The system was evacuated and then filled with hydrogen. As the hydrogen was used up the mercury level in the attached buret changed. Hydrogen was then reintroduced as needed. THe slurry was stirred in this device until no additional hydrogen was taken up (7 days). The reaction was monitored by TLC with chloroform-methanol (4:1 vol.). The slurry was filtered through celite, washed with hot water (50 mL) and hot ethanol (50 mL), and evaporated in vacuo to a syrup. The syrup was redissolved twice in ethanol followed by evaporation to a gummy precipitate. Acetone was added to this followed by mechanical working with a stirring rod to produce a white granular powder which was vacuum dried (1.8 g, 88%). Paper chromatography with ethylacetate-pyridine-water (8:2:1, vol.) showed the material to be xylobiose with a slight impurity presumed to be the arabino analog (1). A sharp melting point was not obtained. A portion of 1 was dissolved in H_2O and treated with Amberlite IR-120 ion exchange resin (acid form) to remove any transition metal ions. The solution was

filtered, evaporated in vacuo, and recovered as the acetone powder in the same manner as above.

Benzyl 2,3-anhydro-4-O-(2',3',4',6'-tetra-O-acetyl-β-D-glucopyranosyl)-β-D-ribo-pyranoside (12)

Compound 15 (5.0 g) was combined with dry chloroform (81 mL), 10-20 mesh Drierite (31 g), A-4 molecular sieves (10 g), and freshly prepared silver oxide (16.7 g). Iodine (1.8 g) was added after 24 hours of stirring in the dark. The glucosyl bromide 14 (30 g) in dry chloroform (160 mL) was then added slowly. Reaction procedures and work-up were the same as for compound 6. A light yellow syrup showing 4 spots by TLC was obtained (30 g).

Benzyl 2,3-anhydro-4-O-(β-D-glucopyranosyl)-B-D-ribopyranoside (11)

The syrup (12) from the Koenigs-Knorr condensation was deacetylated with metha-nolic sodium methoxide in a manner similar to 5. The resulting syrup was frac-tionated on a silica-gel column with chloroform/methanol (4:1). Four fractions resulted which were characterized by ^{13}C-NMR. The fractions corresponding to 11 were evaporated in vacuo to a syrup which rapidly crystallized. Recrystallization was from water; mp. 139-141°C. The crystals were needle-like in appearance [1.5 g, 17% (based on 15)].

Benzyl 4-O-(β-D-glucopyranosyl)-β-D-xylopyranose (9)

Compound 11 (970 mg) was reacted in aqueous sodium hydroxide (2N, 100 mL) at near boiling (77°C, 6 hours) under a nitrogen atmosphere with stirring. The solu-tion was cooled, deionized with Amberlite IR-120 resin, filtered, with subsequent washing of the resin with hot water, and evaporated to a hard brown syrup (approximately 1 g, ca. 100%).

4-O-β-D-glucosyl-D-xylose (Securidebiose) (7)

Syrupy compound 9 (1 g) was mixed with 10% palladium-on-carbon catalyst (500 mg) in a water/methanol (50:50 v/v, 80 mL) solvent and hydrogenated at atmospheric pressure for 4 days. The resulting slurry was filtered through celite, the celite washed with hot methanol and hot water, deionized with IR-120 resin, and evaporated to a syrup. Powdered 7 was obtained by macerating under acetone. Compound 7 was first precipitated by successively adding and evaporating ethanol from the syrup. Powdered 7 (600 mg, 77%) did not give a sharp melting point.

METHYL-β-CELLOBIOSIDE SYNTHESIS

Cellobiose Octaacetate (27)

Compound 27 was prepared by reacting cellobiose (2 g, Matheson-Coleman-Bell) with sodium acetate (2.4 g) and acetic anhydride (37 mL) at reflux with stirring (3.5 h). The mixture was cooled and poured into ice-water (350 mL) with vigorous stirring. Crystals formed overnight, were filtered, washed with water, and evaporated in vacuo (3.3 g, yield 83%). The product was recrystallized from ethanol; m.p. 190-193. Literature (3) m.p. 192°C.

Hepta-O-acetyl-α-cellobiosyl Bromide (25)

The bromide was prepared by reacting 27 (3.1 g) with HBr (32% in acetic acid, 18 mL) in a stoppered flask on a shaker for 1.5 hours. The mixture was immediately poured into ice-water (160 mL) with vigorous stirring. Chloroform (30 mL) was immediately added, the chloroform layer separated, and the residual water washed with chloroform. The combined chloroform layers were washed successively with cold water and aqueous sodium bicarbonate (100 mL, saturated). The chloroform layer was dried over calcium chloride, evaporated in vacuo to a syrup, and was treated with petroleum ether (low boiling) until turbid. A crystalline material formed which was filtered, washed with petroleum ether, and dried in vacuo (2.5 g, 78%); m.p. 195-198°C.

Methyl β-cellobioside Heptaacetate (23)

Compound 25 (2.1 g) was mixed with dry chloroform (20 mL) and dropped over a 1 hour period into a 3-necked flask containing 10-20 mesh Drierite (4 g), mercuric oxide (700 mg, yellow), mercuric bromide (40 g), dry chloroform (10 mL), and methanol (0.6 mL). The contents had been equilibrated for 1 hour prior to addition of the 25. The mixture was stirred for 15 hours at room temperature, filtered through celite, and washed with additional chloroform. The filtrate was evaporated in vacuo to a syrup. The syrup was dissolved in methanol from which crystals formed upon refrigeration. These were filtered, washed with cold methanol, and dried in vacuo (750 mg, 38%); m.p. 181-185°C. ^{13}C-NMR confirmed the assignment of this compound.

Methyl-β-cellobioside (21)

Methyl-β-cellobioside was formed from 23 (350 mg) by treating a methanol solution of 23 with methanolic sodium methoxide (0.5N, 5 mL) over a steam bath. The reaction was monitored by TLC using chloroform-methanol (4:1, vol.). The mixture was refrigerated with crystals forming after several days. The crystals were filtered, washed with cold methanol, and dried in vacuo (225 mg, 100%); m.p. 175-178. Literature (3) m.p. 170.5-174.

METHYL β-XYLOBIOSIDE SYNTHESIS

The synthesis of methyl β-xylobioside from xylobiose was essentially the same as the synthesis of methyl β-cellobioside (21) from cellobiose. Refer to the description of the synthetic sequence for 21 for details.

Xylobiose Hexaacetate (2)

The procedure used was essentially that of Whistler (4). Synthetically prepared xylobiose (1.8 g) was combined with acetic acid (1.8 mL), acetic anhydride (10 mL), and sodium acetate (1.8 g) and heated on a steam bath for about 1 hour.

TLC with chloroform-ethylacetate (4:1, vol.) was used to monitor the reaction. After cooling, the reaction mixture was poured into ice water (75 mL) with vigorous stirring. This resulted in a syrup which formed on standing. The syrup was taken up in chloroform. The chloroform solution was washed with saturated sodium bicarbonate solution followed by water until the wash was neutral. The chloroform solution was dried over calcium chloride, filtered, and reduced to a syrup (3.7 g). The syrup was crystallized from ethanol (1.5 g, 44%); m.p. 144-149. Literature (4) m.p. 155.5-156°C. ^{13}C-NMR indicated a minor impurity.

Penta-O-acetyl-α-xylobiosyl Bromide (24)

Compound 2 (1.4 g) was dissolved in dry chloroform (14 mL) to which hydrogen bromide in acetic acid (5 mL, 42%) was slowly added. The mixture was kept at 0°C. for 2 hours. The mixture was poured into ice water and worked up in the same manner as 25. The resulting syrup (1.2 g) did not crystallize.

Methyl β-xylobioside Pentaacetate (22)

Compound 24 (1.2 g) in chloroform (20 mL) was slowly added to a stirred slurry containing chloroform (20 mL), 10-20 mesh Drierite, mercuric oxide (1.1 g, yellow), and mercuric bromide (100 mg). The mixture was allowed to react overnight and then worked up in the same manner as for 23. The resulting syrupy product (1.3 g) was deacetylated immediately.

Methyl β-xylobioside (20)

The syrup (1.3 g) obtained in the synthesis of 22 was dissolved in methanol (10 mL) and deacetylated on a steam bath with methanolic sodium methoxide (5 mL, 0.5N). The clear solution was refrigerated several days without producing crystals, filtered, and evaporated in vacuo to a syrup. The syrup would not crystallize. It was redissolved in water and treated with Amberlite IR-120 ion-exchange resin until

neutral. The solution was filtered and reduced again to a syrup <u>in vacuo</u>. ^{13}C-NMR
was consistent with $\underset{\sim}{20}$ but with several impurities. TLC using chloroform-
methanol (3:1, vol.) indicated at least 3 components. The syrup (0.5 g) was
treated at 0°C. with acetic anhydride-pyridine (50:50) to reform the acetate ($\underset{\sim}{22}$).
The mixture was dissolved in ice water, taken up in chloroform, and washed with
dilute sulfuric acid and water to remove excess pyridine. The chloroform was dried
and reduced to a syrup (1.8 g). TLC in chloroform-ethyl acetate (4:1, vol.)
showed two components. The syrup was fractionated by passing over a silica-gel
column using chloroform-ethylacetate (4:1) as the solvent. A middle fraction was
collected, reduced to a syrup, and shown to be the acetate $\underset{\sim}{22}$ by ^{13}C-NMR. Some
crystals formed in the syrup. The major impurity was determined to be methyl β-
xyloside triacetate by ^{13}C-NMR.

The acetate syrup was deacetylated in the same manner as before. The resulting
syrup crystallized. Successive recrystallization from ethanol gave an NMR pure pro-
duct (26.4 mg) m.p. 174-177.5. Literature ($\underset{\sim}{4,5}$) m.p. 103-104°C. and 148.5-149°C.,
suggesting several polymorphs may exist.

PREPARATION OF C-DEUTERATED COMPOUNDS

Backbone deuteration of the hydroxylated carbons were affected using the Raney
nickel procedures described by Koch and Stuart ($\underset{\sim}{5}$). Pure compounds are not obtained
because of a tendency to invert configuration; particularly at C_4. Also, only par-
tial exchange occurs at some carbons, notably C_2, because of steric hindrance. The
reactions are conveniently monitored by ^{13}C-NMR. The major products are described
below.

Methyl β-xyloside-3,4-d$_2$ ($\underset{\sim}{29}$)

Methyl β-xylopyranoside ($\underset{\sim}{28}$) (1.0 g, Pfanstiehl) was dissolved in D$_2$O (20 mL)
and allowed to stand in a vacuum oven (40°C.) overnight until a dried film was

obtained. This material was mixed with D_2O (60 mL) and deuterated Raney-nickel (20 mL settled volume) and refluxed for 12 hours. Samples were periodically taken for TLC and NMR analysis. The cooled mixture was filtered through celite, washed with water, and evaporated in vacuo to a syrup. ^{13}C-NMR confirms that the major product is methyl-β-xylopyranoside-2,4-d_2.

Methyl β-glucoside-3,4,6,6',-d_4 (31)

Methyl β-glucoside (30) (1.5 g) was treated in an identical manner as for 28 for 20 hours. The filtrate was treated with Amberlite IR-120 ion-exchange to remove any transition metal ion impurities. A clear white syrup resulted. The assignment was confirmed by ^{13}C-NMR.

Methyl-β-cellobioside-3,6$_a$,6$_b$,2',3',4',6'$_a$, 6'$_b$-d_8 (32)

MBC2-d_8 was prepared by refluxing 21 (200 mg) in D_2O (50 mL) with deuterated Raney-nickel. Progress of the reaction was followed by ^{13}C-NMR. When the reaction was complete (11 hours) the mixture was filtered through celite, the celite was washed with water, the combined filtrates deionized with Amberlite IR-120, and the filtrate evaporated to a syrup in vacuo. The syrup would not crystallize from methanol. It was used directly for NMR experiments. The NMR spectrum was nearly identical to that in the literature (7).

MISCELLANEOUS COMPOUNDS

A number of compounds were obtained in small quantities from other investigators. The compounds and their source are indicated below. In each case the ^{13}C-NMR spectrum was consistent with the proposed structure.

The xylo-oligosaccharides were obtained from Dr. K. P. Carlson (IPC) as were samples of cellotetraose. The former had come from the laboratory of Professor T.

E. Timell (SUNY-Syracuse). The latter was obtained by Carlson from cellulose acid hydrolysis and carbon-celite column chromatography (8). Cellotriose was obtained from Professors A. J. Michell (Division of Forest Products, C.S.I.R.O., South Melbourne, Australia) and R. Brown, Jr. (Virginia Polytechnic Institute). The cello-oligosaccharide peracetates were obtained from Dr. L. Schroeder (IPC). Mannobiose and 4-O-β-D-glucosyl-D-mannopyranose were obtained from Dr. N. S. Thompson (IPC). A sample of 1,5 anhydrocellobiotol was obtained with the aid of Dr. T. Wylie (9).

CATALYSTS AND REAGENTS

Hydrogen Bromide in Acetic Acid

Prepared by bubbling HBr gas through a series of vessels containing neat acetic acid. Composition was monitored by observing changing sample weight.

Methanolic Sodium Methoxide (0.5N)

Sodium metal (11 g) was slowly added to methanol (1L). Care was taken to avoid excessive generation of heat.

Silver Oxide

A hot caustic solution (46 g sodium hydroxide in 14.75 mL water) was slowly poured into a hot solution of silver nitrate (200 g in 1920 mL water) with vigorous stirring in minimal light. The slurry was filtered, washed 5 times with water (1L), once with acetone (500 mL), and once with low boiling petroleum ether (500 mL). The product was placed in a covered dish to exclude light and dried in vacuo. The product was stored in the dark.

Palladium on Carbon Catalyst (10%)

Sufficient catalyst was obtained from Dr. R. Niebauer (IPC) (10).

Deuterated Raney Nickel

Nickel-aluminum alloy (75 g; 50:50) was slowly added to an aqueous caustic solution (95 g sodium hydroxide in 25 mL H_2O) with occasional stirring. A 2-liter flask was used to allow for some foaming. Care was taken to avoid boiling of the mixture though the slurry was allowed to get hot to the touch. The slurry was allowed to stand overnight. After standing the slurry was heated on a steam bath for 2 hours. The aqueous phase was decanted and replaced with 1-2L of water. This was repeated about 20 times until the wash water was neutral. Care must be taken not to allow the solid material to dry because of its pyrophoric nature. The slurry was stirred under water in a tightly capped bottle in the refrigerator.

Prior to deuteration, the necessary amount of catalyst was placed in a sintered glass filter. The excess water was drawn off the top and then replaced with deuterium oxide (98%). The process was repeated 5-6 times so that replacement of the water with D_2O is about complete.

LITERATURE CITED

1. Kidd, J. R. Synthesis and alkaline degradation of xylobiose and 2',3',4'-tri-0-methyl xylobiose. Doctoral Dissertation. The Institute of Paper Chemistry, Appleton, WI. 1980.

2. Bates, F. J. Polarimetry, saccharimetry, and the sugars, 500 p. U.S. Government Printing Office, Washington, D.C. 1942.

3. Best, E. V. Kinetics of hot alkaline cleavage of the glycoside bonds of methyl β-0-glucoside and methyl β-cellobioside. Doctoral Dissertation. The Institute of Paper Chemistry, Appleton, WI. 1968.

4. Whistler, R. L., Bachrach, J., and Tu, C. C., J. Chem. Soc. 74:3059-60(1952).

5. Kovac, P., Hirsch, J., and Kovacik, V., Chem. Zvesti 32:514-18(1978).

6. Koch, H. J. and Stuart, R. S., Carbohyd. Res. 59:C1-6(1977).

7. Hamer, G. K., Balza, F., Cyr, N., and Perlin, A. S., Can. J. Chem. 56:3109-16 (1978).

8. Carlson, K. P. An investigation of the vibrational spectra of the cellodextrins. Doctoral Dissertation. The Institute of Paper Chemistry, Appleton, WI. 1979.

9. Wylie, T. R. The alkaline degradation of 1,5 anhydro-2,3,6-tri-0-methyl-cellobiotol. Doctoral Dissertation. The Institute of Paper Chemistry, Appleton, WI. 1979.

10. Neibauer, R. The degradation of ethyl 3,4,6-tri-0-methyl-β-D-arabino-hexopyrano-sidulose in aqueous alkaline hydrogen peroxide solution. Doctoral Dissertation. The Institute of Paper Chemistry, Appleton, WI. 1979.

APPENDIX XI

^{13}C-NMR SPECTRA OF DERIVATIVES PREPARED IN ROUTE TO XYLOBIOSE (1), SECURIDEBIOSE (7), METHYL β-XYLOBIOSIDE (20), AND METHYL β-CELLOBIOSIDE (21)

This appendix contains the decoupled ^{13}C-NMR spectra (25.05 MHZ) of the derivatives obtained in route to compounds 1, 7, 20, and 21. Refer to Section 4, Part I for the general synthetic scheme and Section 4, Part II for detailed assignments.

Key

I = impurity

S = solvent
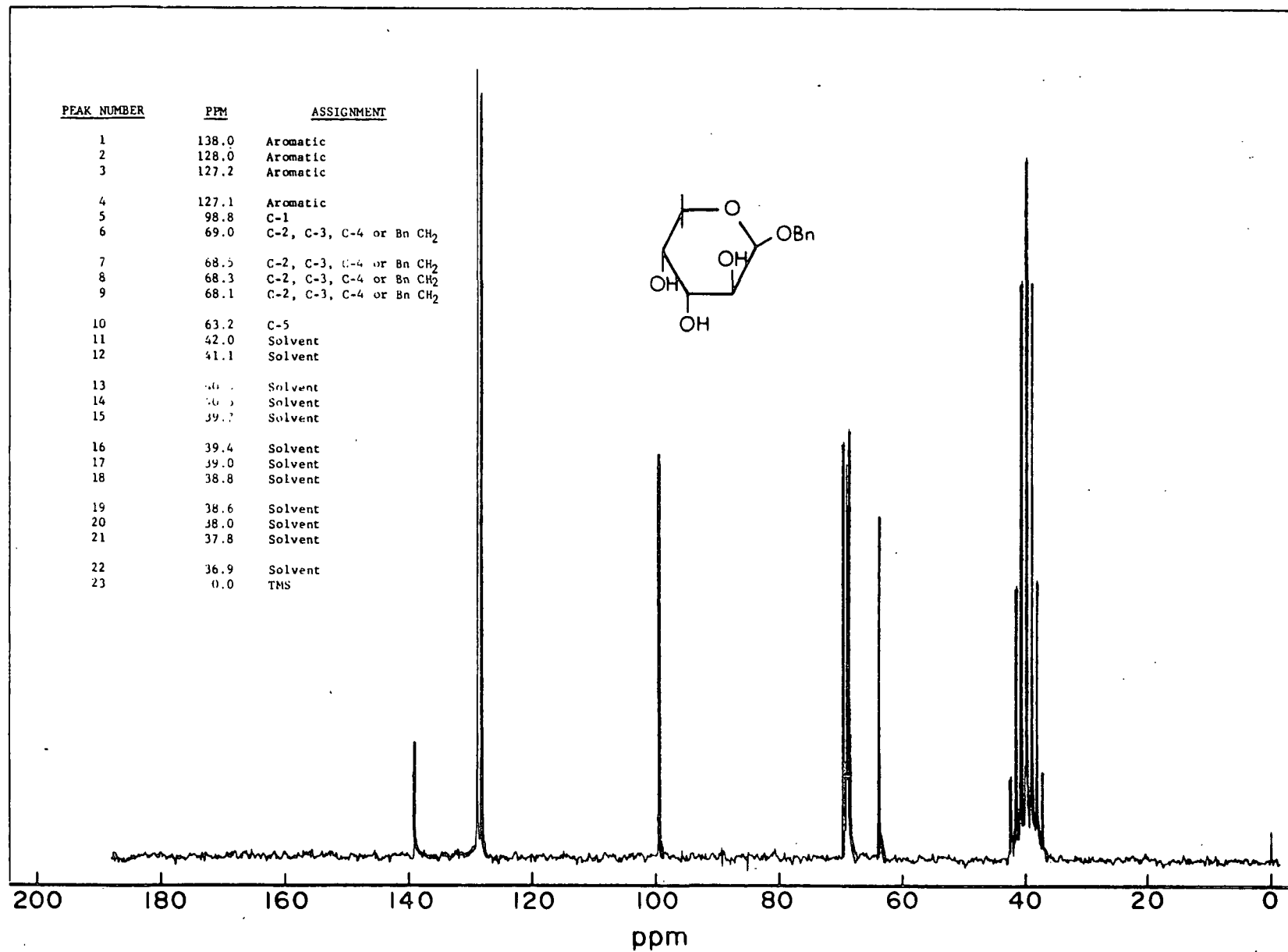
Figure 1. Benzyl β-D-arabinopyranoside (16) in DMSO -d₆.

PEAK NUMBER	PPM	ASSIGNMENT
1	137.1	Aromatic
2	128.5	Aromatic
3	127.9	Aromatic
4	109.2	Acetal Carbon
5	96.9	C-1
6	78.3	Solvent
7	77.0	Solvent
8	75.9	C-3 or C-4
9	75.8	Solvent
10	72.9	C-3 or C-4
11	69.9	C-2 or Bn CH_2
12	69.8	C-2 or Bn CH_2
13	60.0	C-5
14	27.8	Methyl
15	25.9	Methyl
16	0.0	TMS

where R is methyl
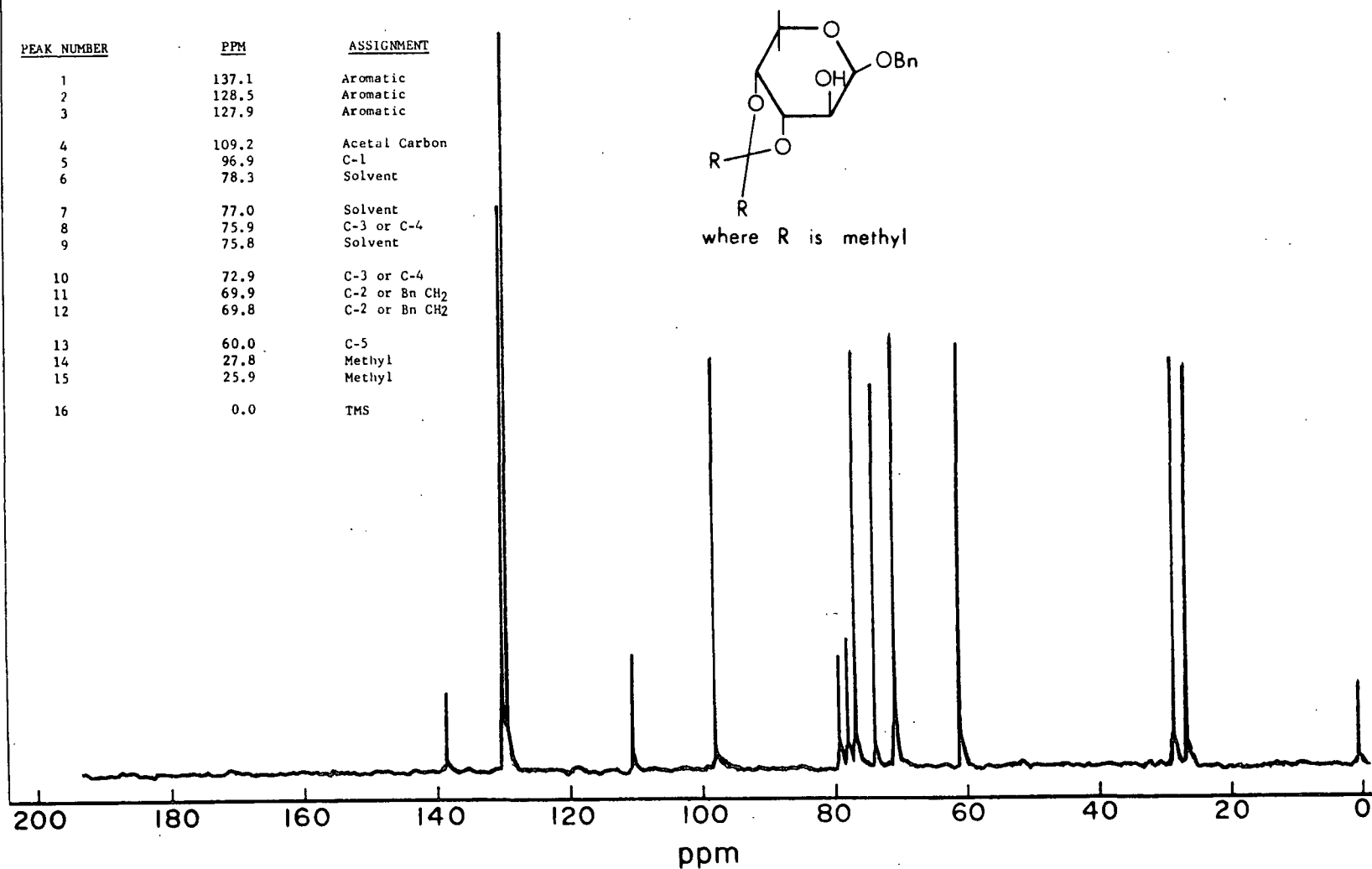
Figure 2. Benzyl 3,4-$\underline{O}$ – isopropylidene – β–D–arabinopyranoside (<u>17</u>) in $CDCl_3$.

PEAK NUMBER	PPM	ASSIGNMENT
1	145.5	Aromatic
2	137.6	Aromatic
3	134.1	Aromatic
4	130.3	Aromatic
5	128.7	Aromatic
6	128.5	Aromatic
7	128.1	Aromatic
8	109.3	Acetal
9	96.4	C-1
10	80.1	C-2, C-3, or C-4
11	74.5	C-2, C-3, or C-4
12	73.1	C-2, C-3, or C-4
13	70.2	Bn CH_2
14	59.1	C-5
15	31.3	Solvent
16	30.3	Solvent
17	29.7	Solvent
18	28.9	Solvent
19	28.2	Solvent
20	27.8	Methyl
21	26.2	Methyl
22	21.4	Methyl
23	6.5	Carbonyl foldback

where R is p-toluenesulphonate

where R' is methyl

ppm

-436-

Figure 3. Benzyl 2-O-p-tosylsulfonsyl - 3,4-O-isopropylidene - β-O-arabinopyranoside (18) in acetone -d_6.

PEAK NUMBER	PPM	ASSIGNMENT
1	145.2	Aromatic
2	129.8	Aromatic
3	129.6	Aromatic
4	128.4	Aromatic
5	128.3	Aromatic
6	127.9	Aromatic
7	127.8	Aromatic
8	95.8	C-1
9	78.2	C-2
10	78.1	Solvent
11	77.0	Solvent
12	75.7	Solvent
13	69.6	C-3, C-4 or Bn CH_2
14	69.4	C-3, C-4 or Bn CH_2
15	67.2	C-3, C-4 or Bn CH_2
16	62.0	C-5
17	21.6	Methyl
18	0.0	TMS

where R is p-toluenesulphonate
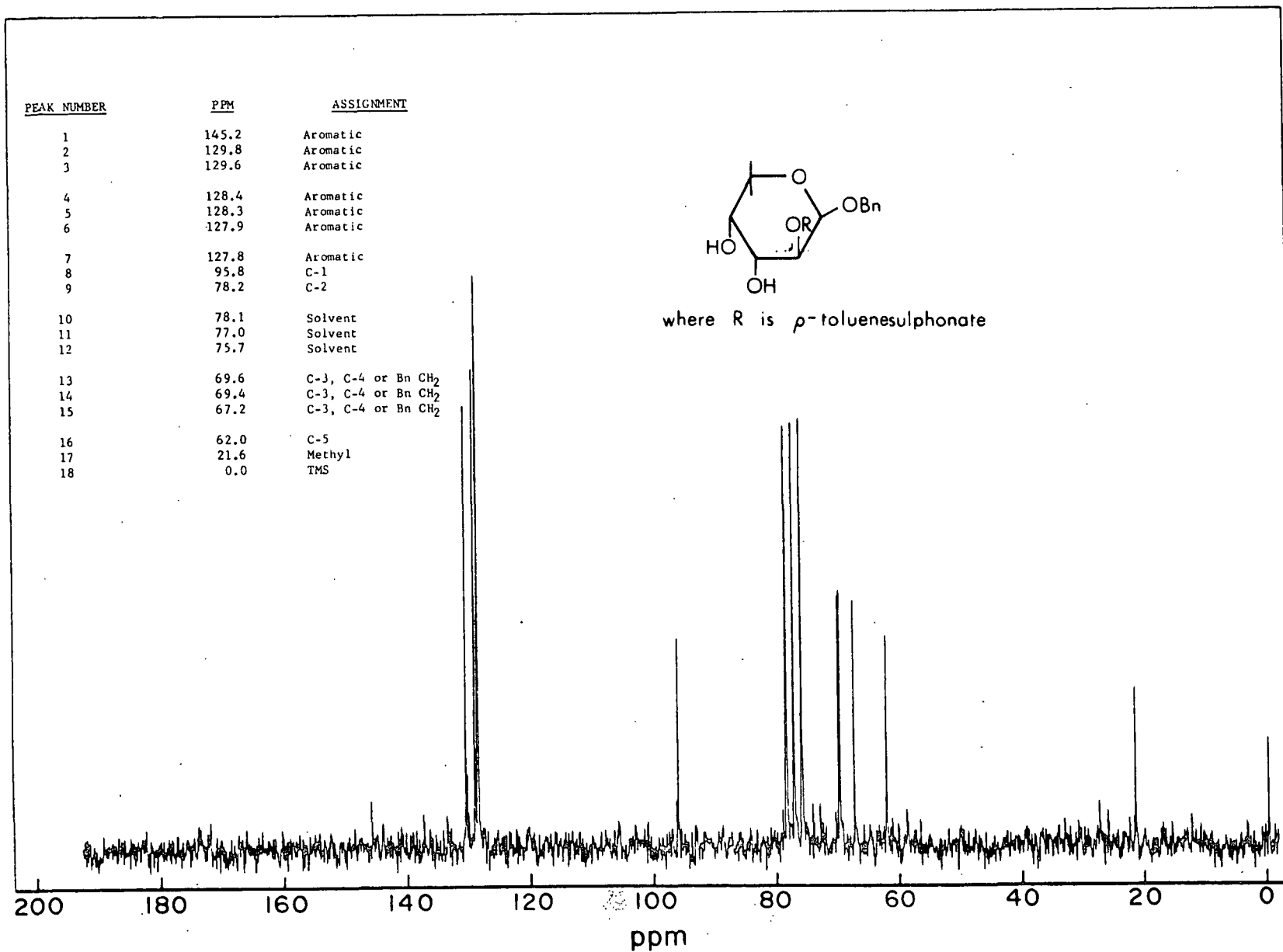
Figure 4. Benzyl 2-O – p-tosylsulfonsyl – β-D-arabinopyranoside (19) in $CDCl_3$.

PEAK NUMBER	PPM	ASSIGNMENT
1	137.0	Aromatic
2	128.4	Aromatic
3	128.0	Aromatic
4	127.9	Aromatic
5	93.6	C-1
6	78.4	Solvent
7	77.1	Solvent
8	75.8	Solvent
9	70.0	Bn CH$_2$
10	62.1	C-5
11	61.7	C-4
12	51.9	C-2 and C-3
13	0.0	TMS
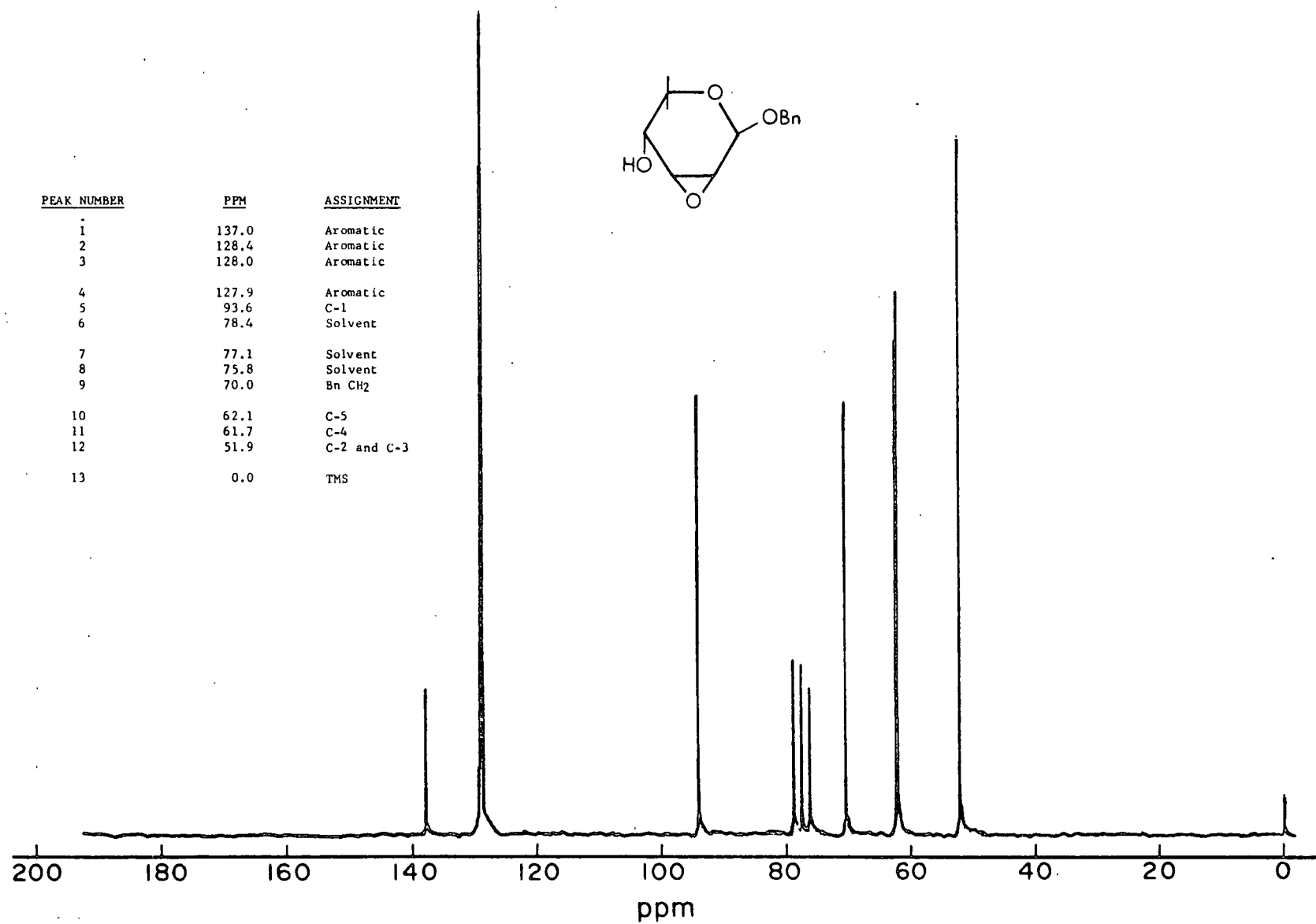
Figure 5.   Benzyl 2,3-anhydro – β-D-ribopyranoside (15) in CDCl$_3$.

PEAK NUMBER	PPM	ASSIGNMENT
1	169.8	Carbonyl
2	169.2	Carbonyl
3	138.4	Aromatic
4	128.8	Aromatic
5	128.4	Aromatic
6	128.2	Aromatic
7	101.2	C-1'
8	95.5	C-1
9	72.2	C-2', C-3' or C-4
10	71.8	C-2', C-3' or C-4
11	71.5	C-2', C-3' or C-4
12	70.6	C-4' or Bn CH_2
13	69.6	C-4' or Bn CH_2
14	62.7	C-5'
15	59.6	C-5
16	53.4	C-3
17	51.9	C-2
18	32.0	Solvent
19	31.3	Solvent
20	30.5	Solvent
21	29.8	Solvent
22	29.0	Solvent
23	28.2	Solvent
24	27.4	Solvent
25	20.6	Methyl
26	6.4	Carbonyl foldback
27	0.0	TMS

where R is acetate

-439-

Figure 6. Benzyl 2,3-anhydro-4-O-(2',3',4' tri-O-acetyl-β-xylopyranosyl) - β-D-ribopyranoside (6) in acetone -d_6.

PEAK NUMBER	PPM	ASSIGNMENT
1	137.4	Aromatic
2	128.1	Aromatic
3	127.6	Aromatic
4	127.5	Aromatic
5	103.5	C-1'
6	94.2	C-1
7	76.5	C-3'
8	72.9	C-2'
9	69.8	C-4' or C-4
10	69.3	Bn CH$_2$ and C-4' or C-4
11	65.6	C-5'
12	58.8	C-5
13	52.0	C-3 or C-2
14	51.1	C-2 or C-3
15	41.9	Solvent
16	41.1	Solvent
17	40.3	Solvent
18	39.4	Solvent
19	38.5	Solvent
20	37.7	Solvent
21	36.9	Solvent
22	0.0	TMS

-440-
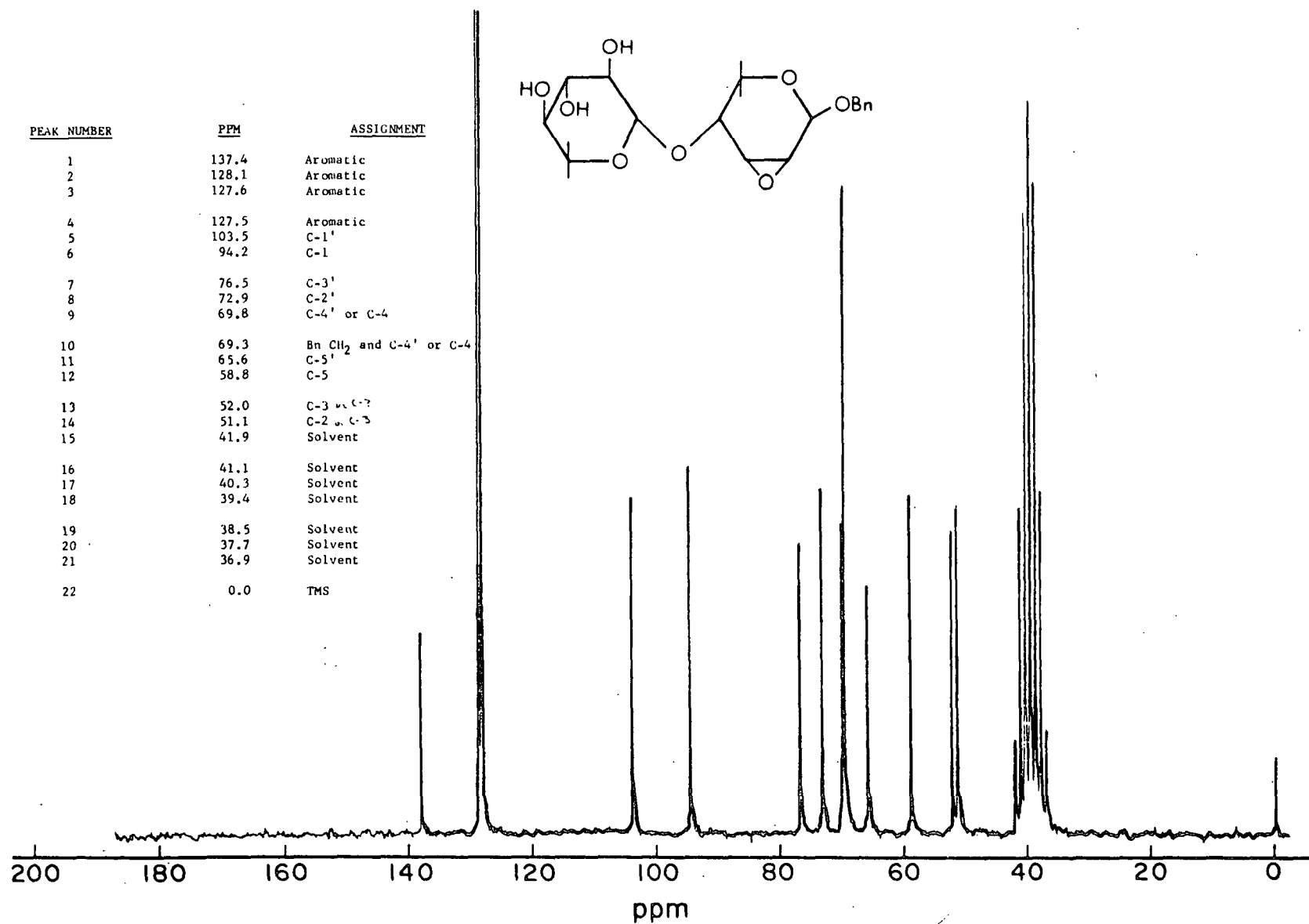
Figure 7. Benzyl 2,3-anhydro-4-O -(β-D-xylopyranosyl)-β-D-ribopyranoside (5) in DMSO -d$_6$.
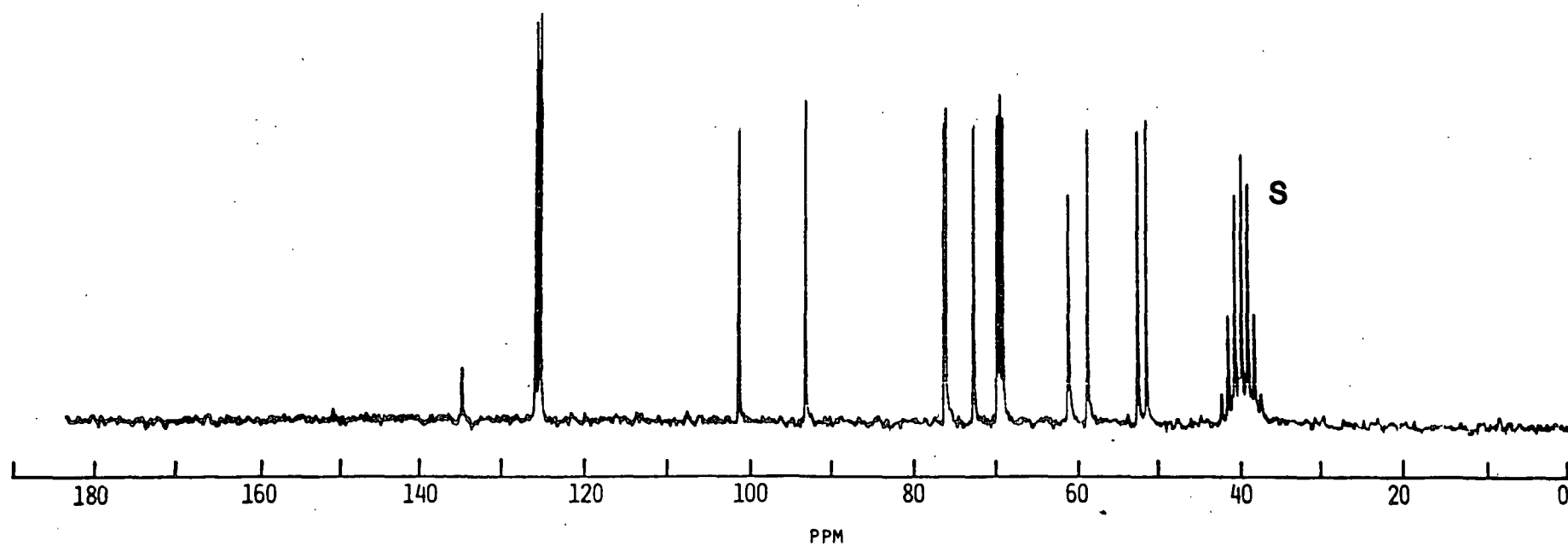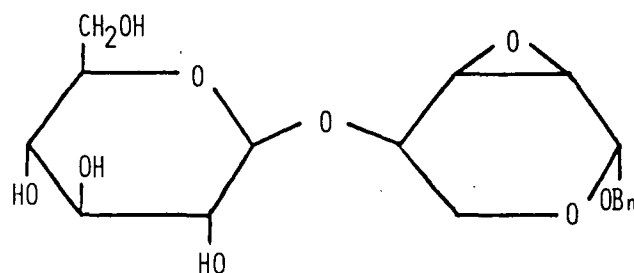
Figure 8. Benzyl 2,3-anhydro-4-O-(β-D-glucopyranosyl)-β-D-ribopyranoside (11) in DMSO-d6.
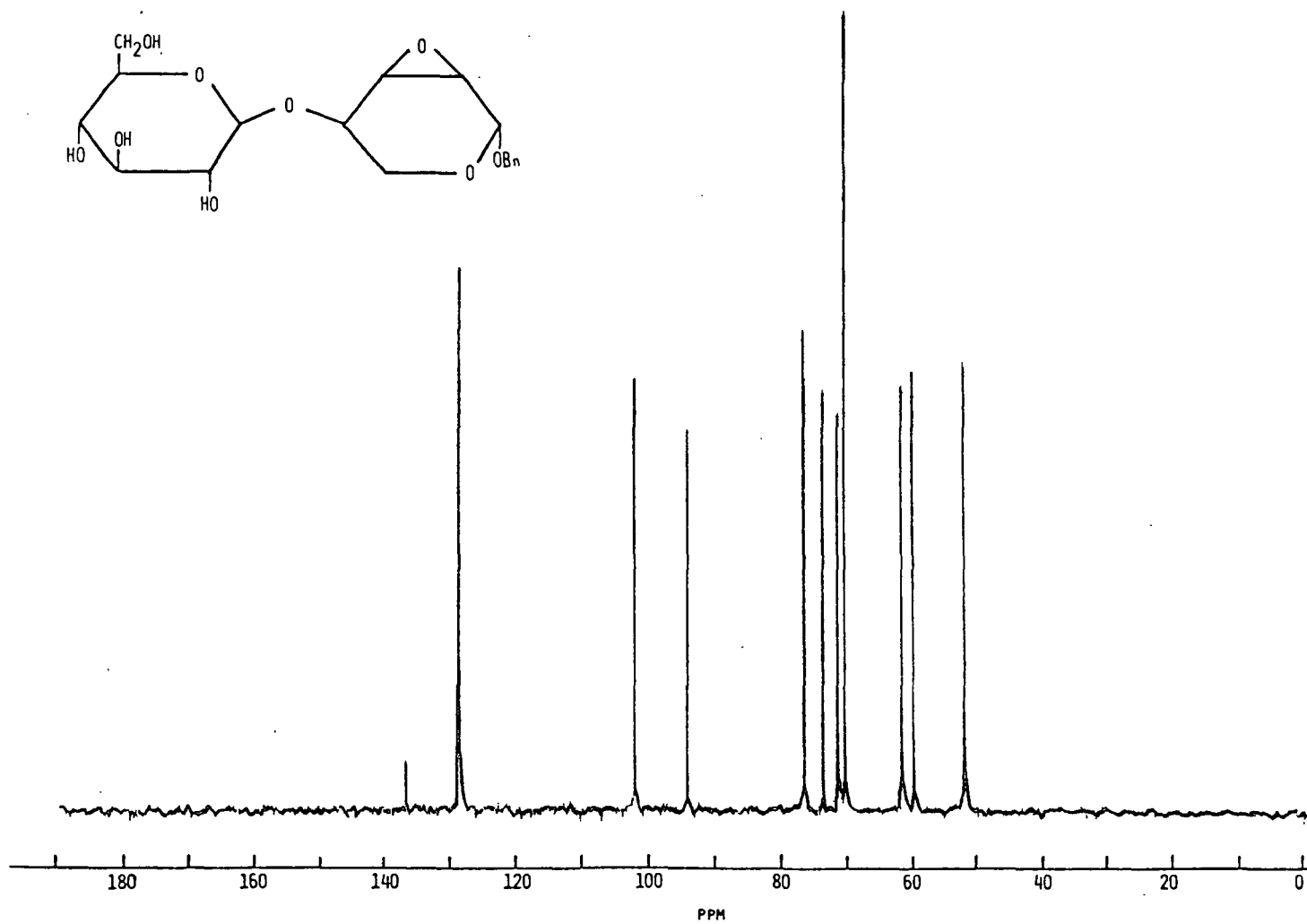
Figure 9. Benzyl 2,3-anhydro-4-O-(β-D-glucopyranosyl)-β-D-ribopyranoside (11) in D₂O.

PEAK NUMBER	PPM	ASSIGNMENT
1	137.8	Aromatic
2	128.0	Aromatic
3	127.4	Aromatic
4	102.7	C-1'
5	101.8	C-1
6	76.1	C-3' or C-4
7	75.3	C-3' or C-4
8	74.1	C-2, C-2' or C-3
9	73.1	C-2, C-2' or C-3
10	72.4	C-2, C-2' or C-3
11	69.6	Bn CH₂
12	69.4	C-4'
13	65.7	C-5'
14	63.1	C-5
15	56.0	
16	41.8	Solvent
17	41.0	Solvent
18	40.2	Solvent
19	39.3	Solvent
20	38.4	Solvent
21	37.6	Solvent
22	36.8	Solvent
23	18.4	
24	0.0	TMS
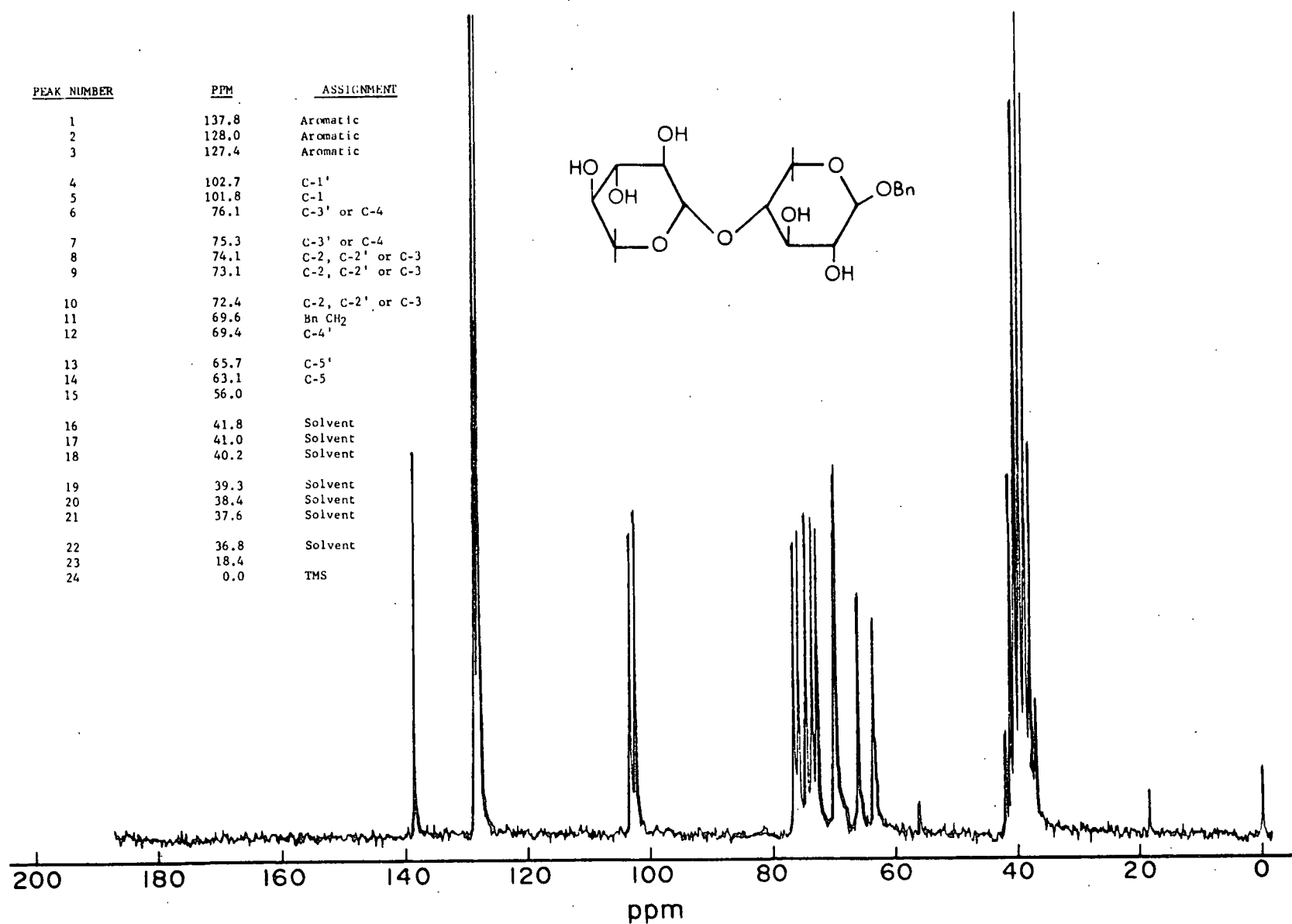
Figure 10. Benzyl xylobioside (3) in DMSO-d₆.
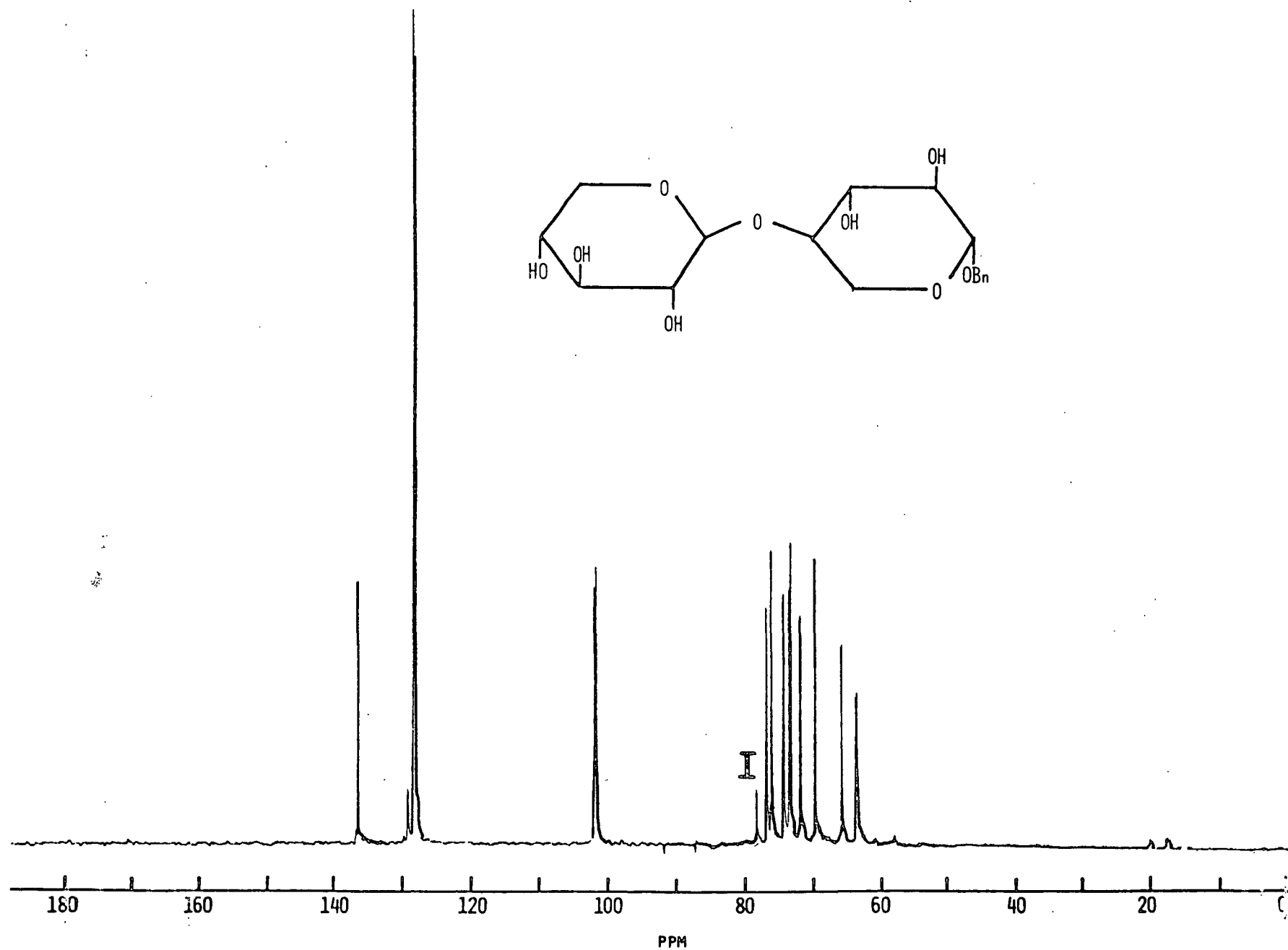
Figure 11. Benzyl xylobioside (3) in D$_2$O.
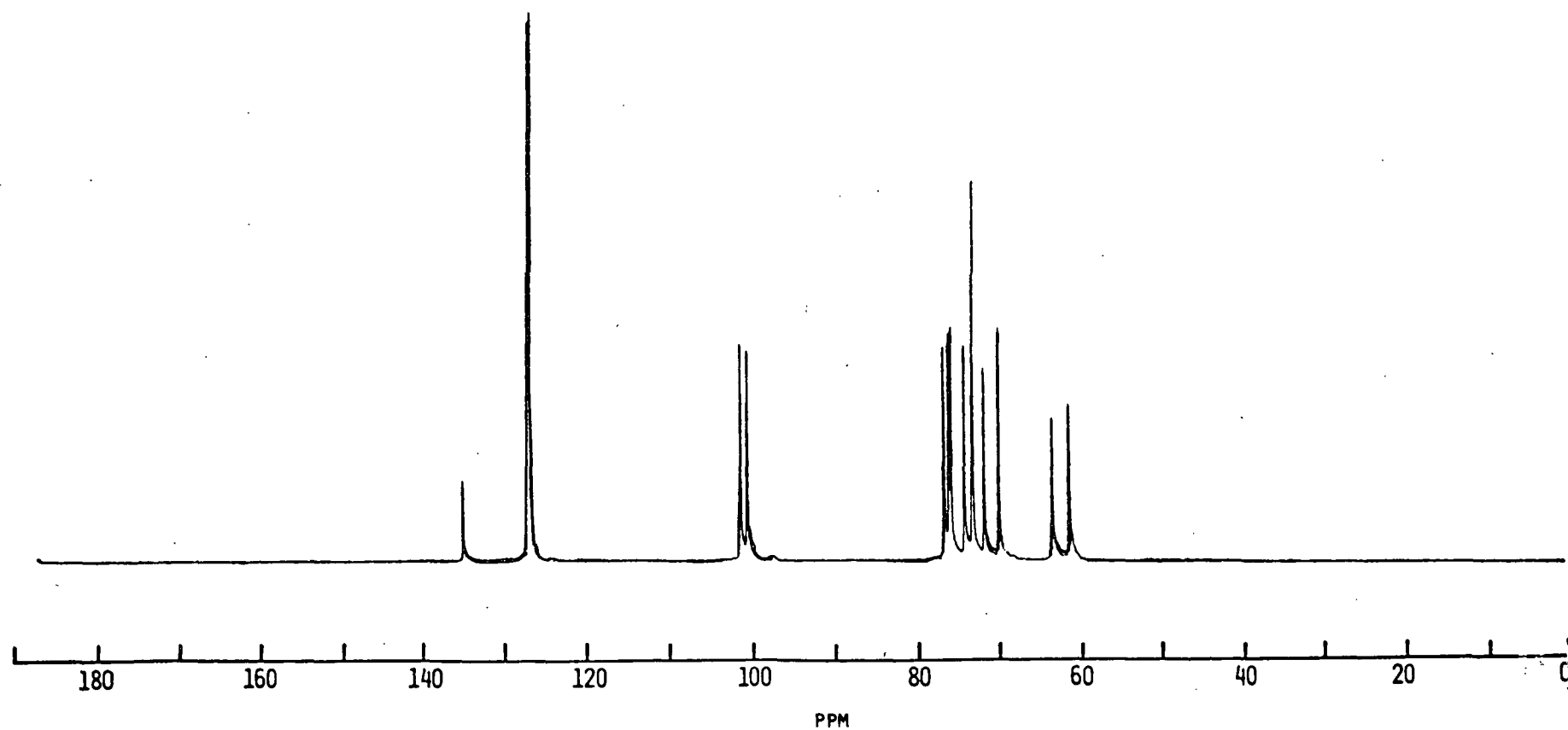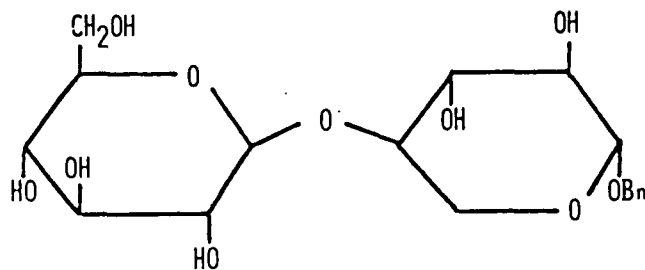
Figure 12. Benzyl 4-O-(β-D-glucopyranosyl)-D-xylopyranose (9) in D₂O.

PEAK NUMBER	PPM	ASSIGNMENT
1	169.8	Carbonyl
2	169.4	Carbonyl
3	169.2	Carbonyl
4	100.6	C-1'
5	92.7	C-1
6	75.4	C-4
7	72.6	C-2, C-2', C-3 or C-3'
8	71.9	C-2, C-2', C-3 or C-3'
9	71.3	C-2, C-2', C-3 or C-3'
10	70.6	C-2, C-2', C-3 or C-3'
11	69.4	C-4'
12	63.9	C-5 or C-5'
13	62.5	C-5 or C-5'
14	32.0	Solvent
15	31.3	Solvent
16	30.5	Solvent
17	29.8	Solvent
18	29.0	Solvent
19	28.2	Solvent
20	27.4	Solvent
21	20.8	Methyl
22	20.6	Methyl
23	6.4	Carbonyl foldback
24	0.0	TMS

where R is acetate

Figure 13. β-xylobiose hexaacetate (2b) in acetone-d_6.
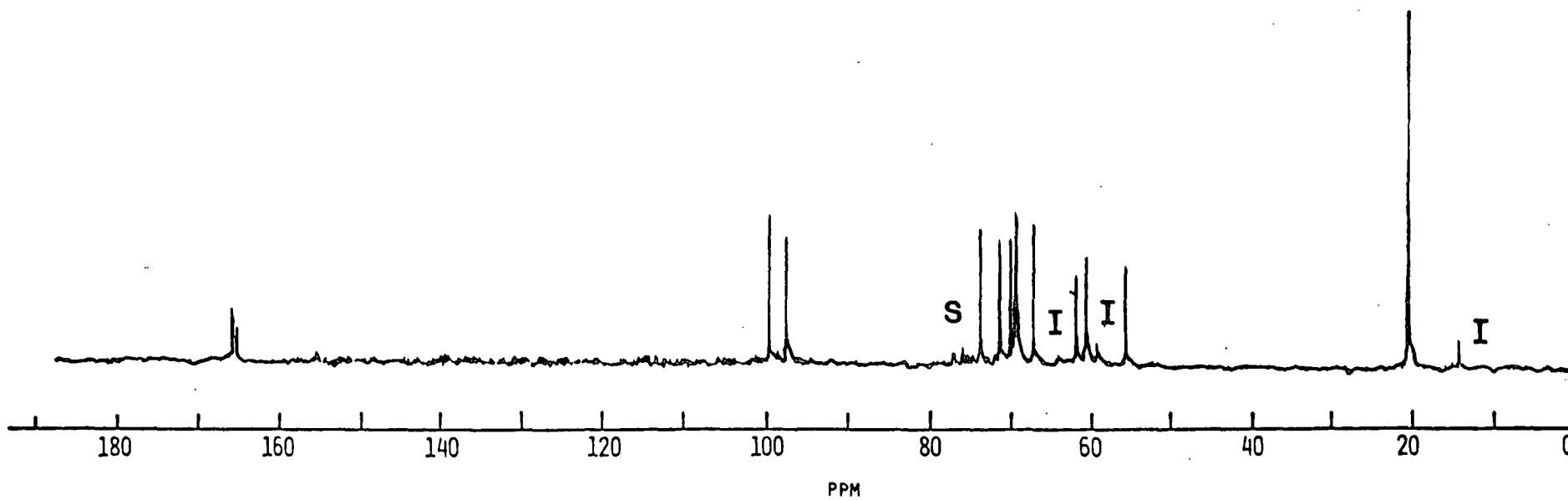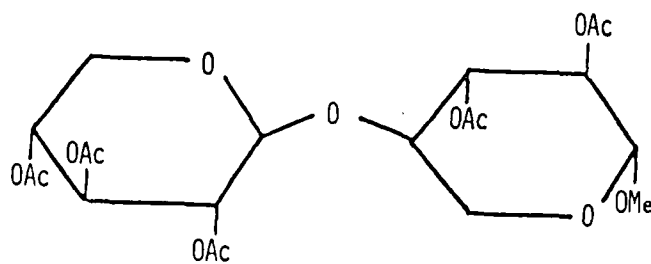
Figure 14. Methyl β-xylobioside pentaacetate (22) in CDCl₃.
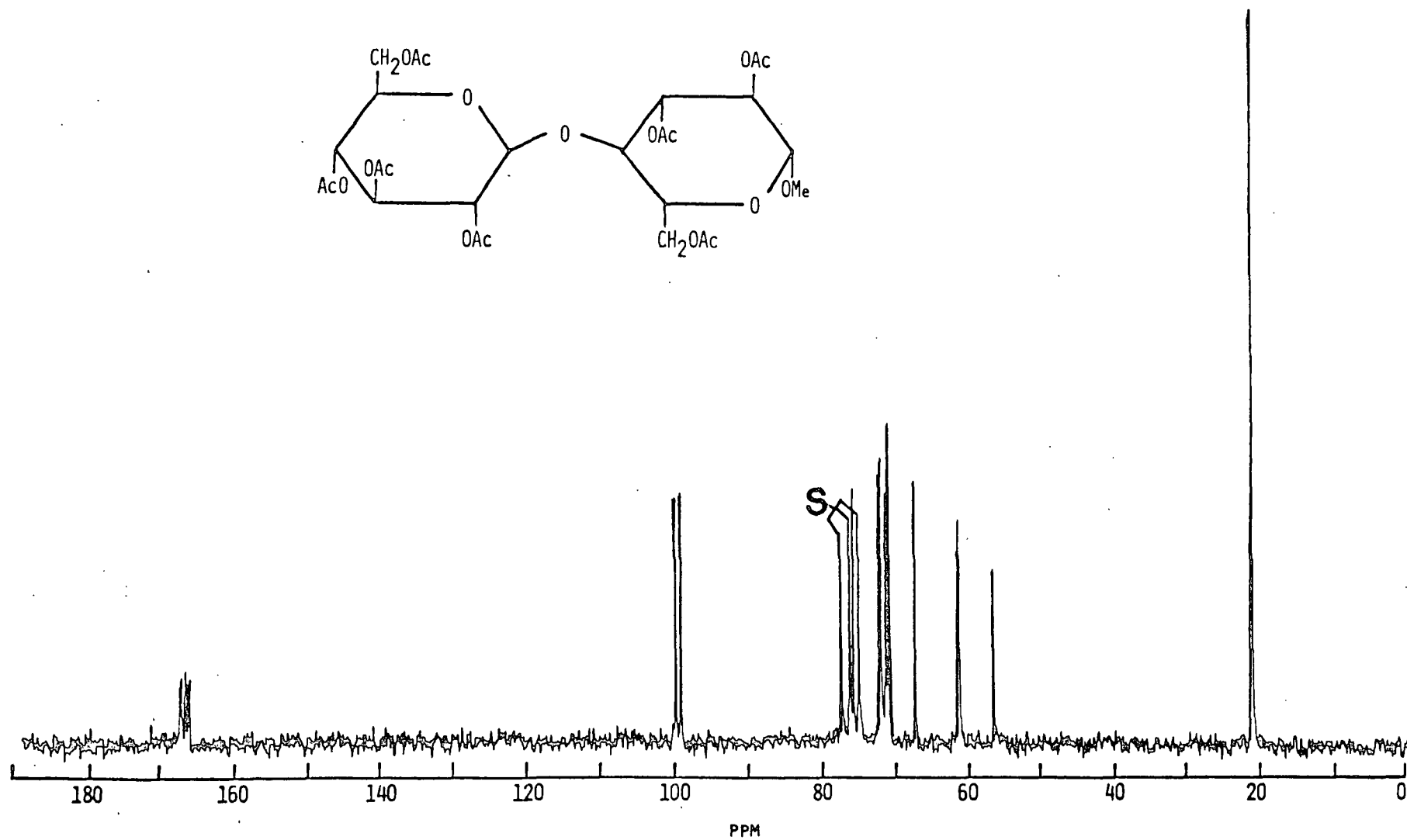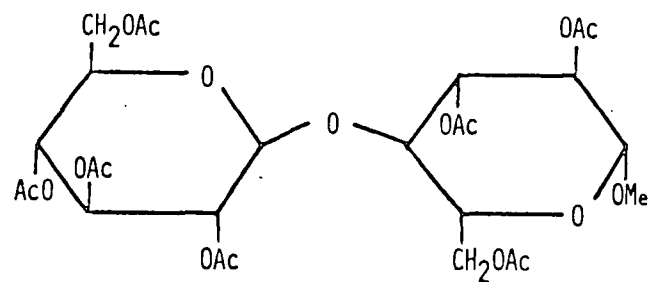
Figure 15. Methyl β-cellobioside heptaacetate (23) in CDCl₃.

APPENDIX XII

^{13}C-NMR SPECTRA AND ASSIGNMENTS OF THE CELLO-OLIGOSACCHARIDE
PERACETATES AND RELATED COMPOUNDS

During the course of this work the decoupled ^{13}C-NMR spectra of the cello-oligosaccharide peracetates, up to the hexamer, were recorded in acetone-d_6. The spectra are shown in Fig. 1 to 5. It was hoped that variations in signal intensity from the dimer to the hexamer would be beneficial in assigning signals to the terminal and internal anhydroglucose residues, as well as to the individual carbon atoms of the disaccharide. If specific assignments could be made, then the spectrum of β-xylobiose hexaacetate might also be assigned with confidence, using the acetyl substitute effects derived from the data.

Assignments for the mono- and disaccharides are listed in Table I and assignments for the oligosaccharides in Table II. Several assignments are also given from the literature for Ref. (1,2,3). The assignments given here are consistent, in relative order, with recent literature assignments.

One problem with comparing this work to the literature is that different solvents [acetone-d_6 here, CDCl$_3$ in the literature (1,2,3)] were used, with the consequence that the appearance of the spectra are slightly different. For example, the oligosaccharide signals at about 69.8 and 70.3 ppm in acetone-d_6 appear as one signal in CDCl$_3$ at 69.4 ppm.

Assignment of the oligosaccharide signals to the internal and terminal units is straightforward on the basis of peak intensities for the spectra shown. Signals that steadily increase in intensity with increasing chain length are indicated in Table II and are assigned to the internal units. Unfortunately, assignment of signals to the individual C_2, C_3, and C_5 carbons is still not feasible. This is

because of the close proximity of signals in the region from 69.8 to 73.5 ppm. If these assignments could be made with confidence, by spin decoupling or other methods, then it might be possible to determine the specific acetyl substituent effects in the cello-oligosaccharides.

Key

S = solvent

R = reference
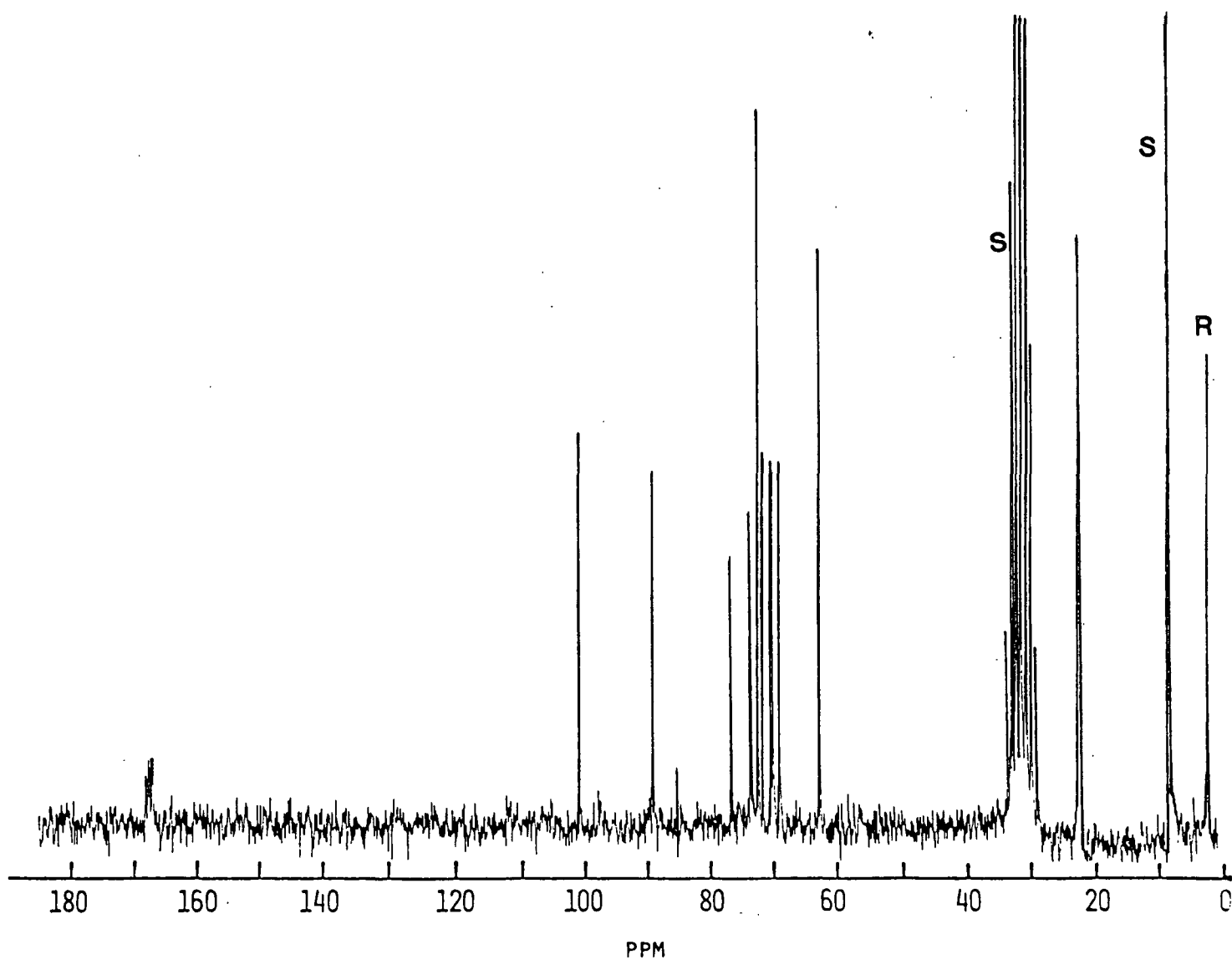
Figure 1. ^{13}C-NMR spectrum of α-cellobiose octaacetate in acetone-d_6.
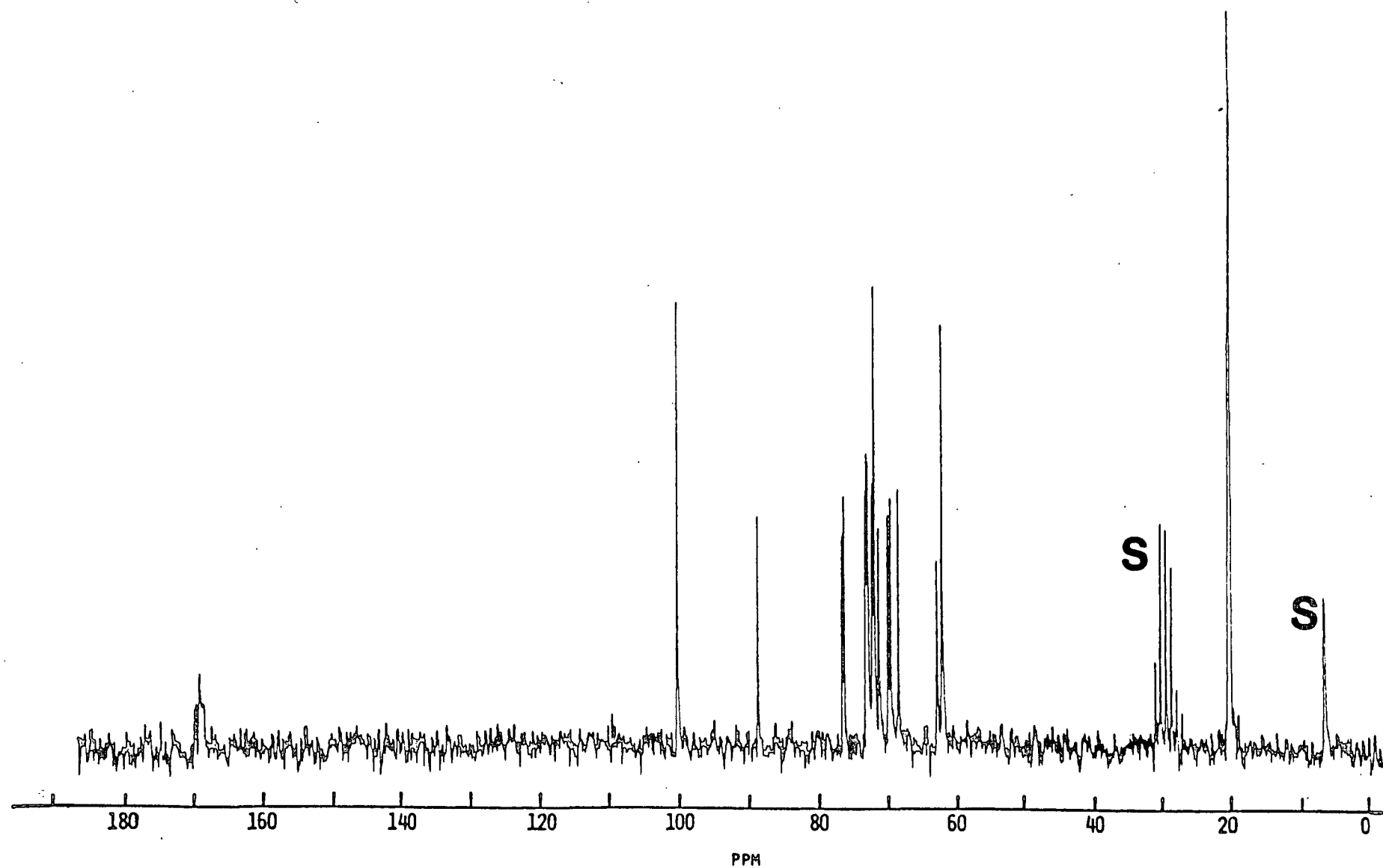
Figure 2. ^{13}C-NMR spectrum of α-cellotriose peracetate in acetone-d_6.
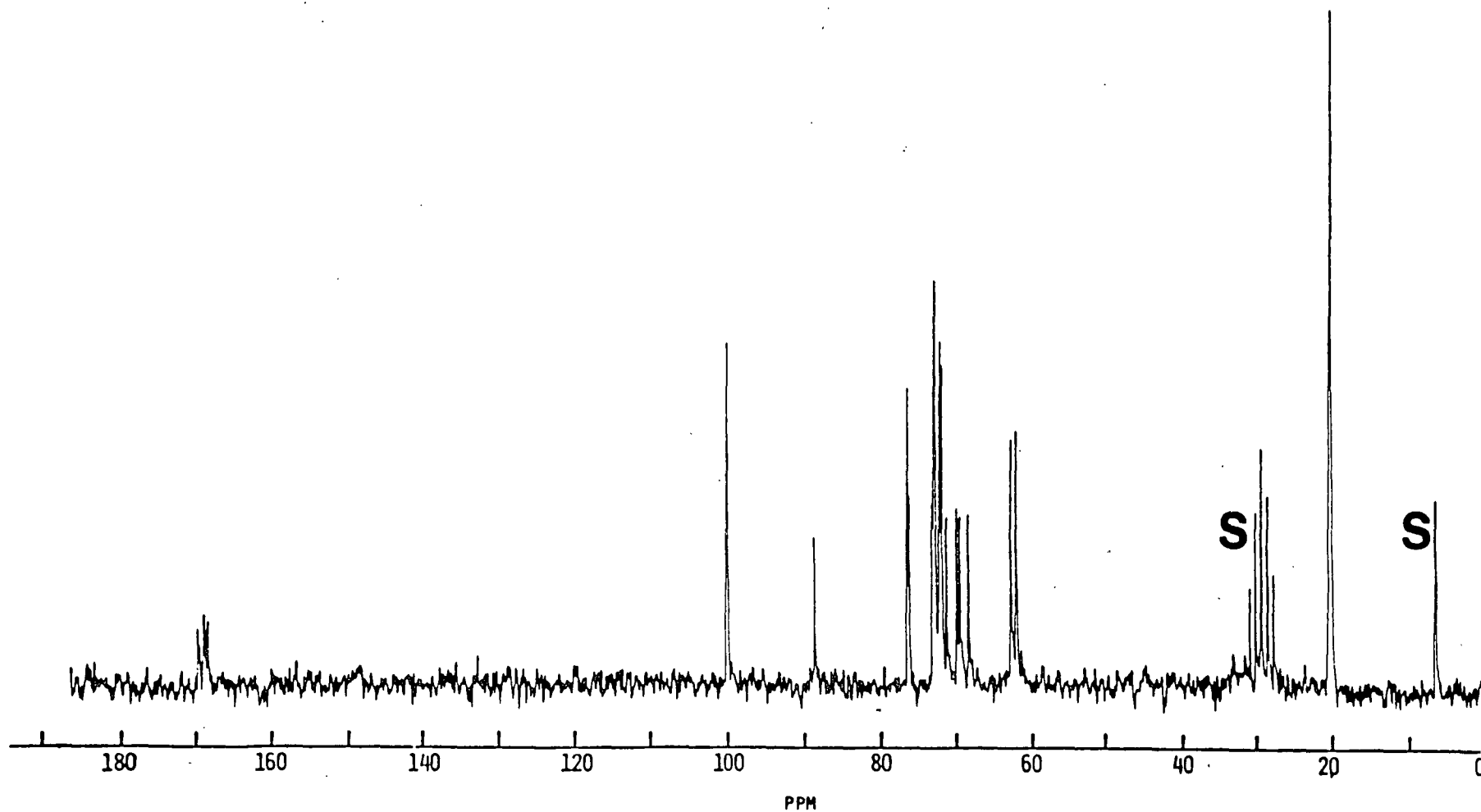
Figure 3. ^{13}C-NMR spectrum of α-cellotetraose peracetate in acetone-d$_6$.
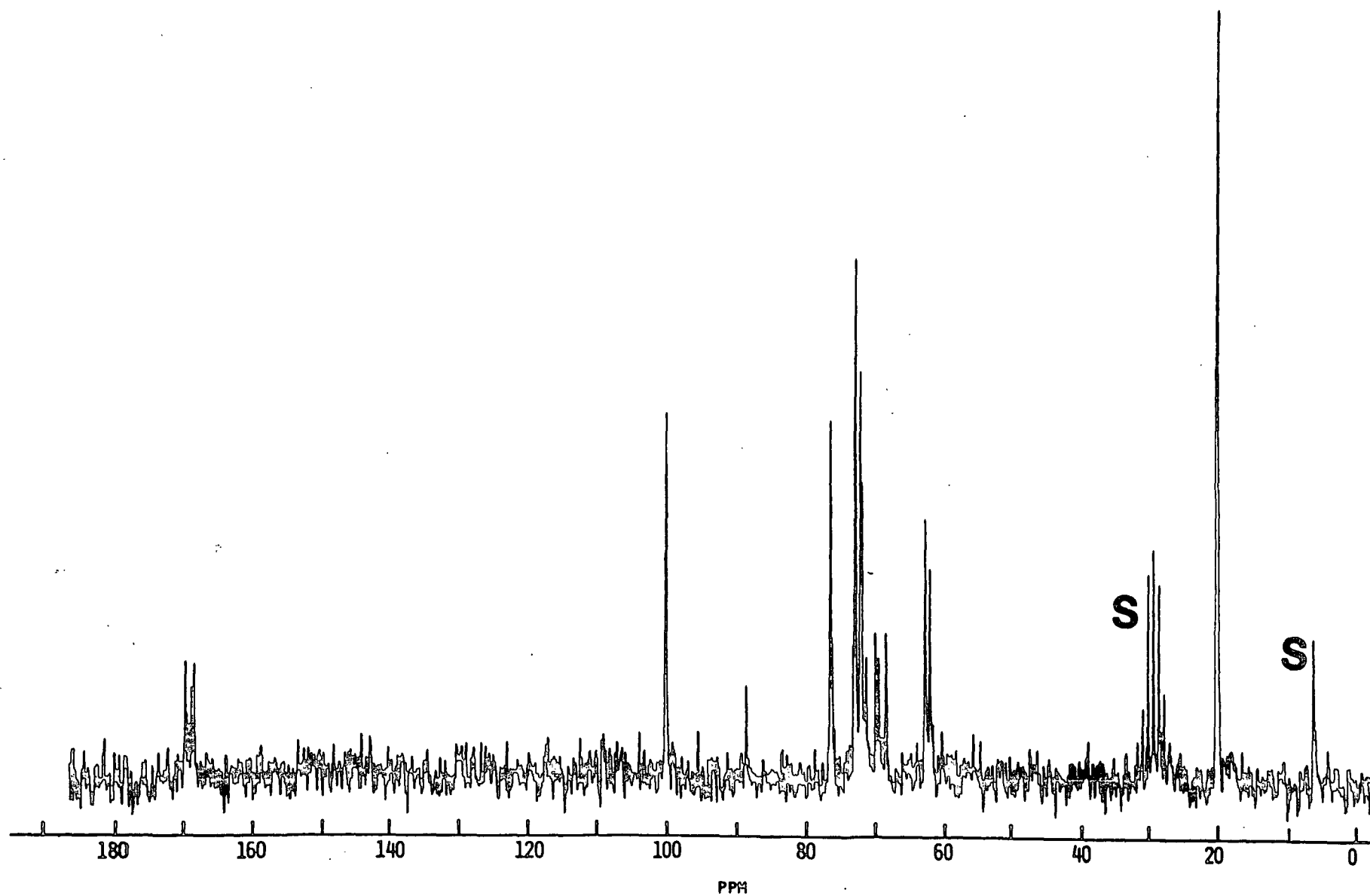
Figure 4. ^{13}C-NMR spectrum of α-cellopentaose peracetate in acetone-d_6.
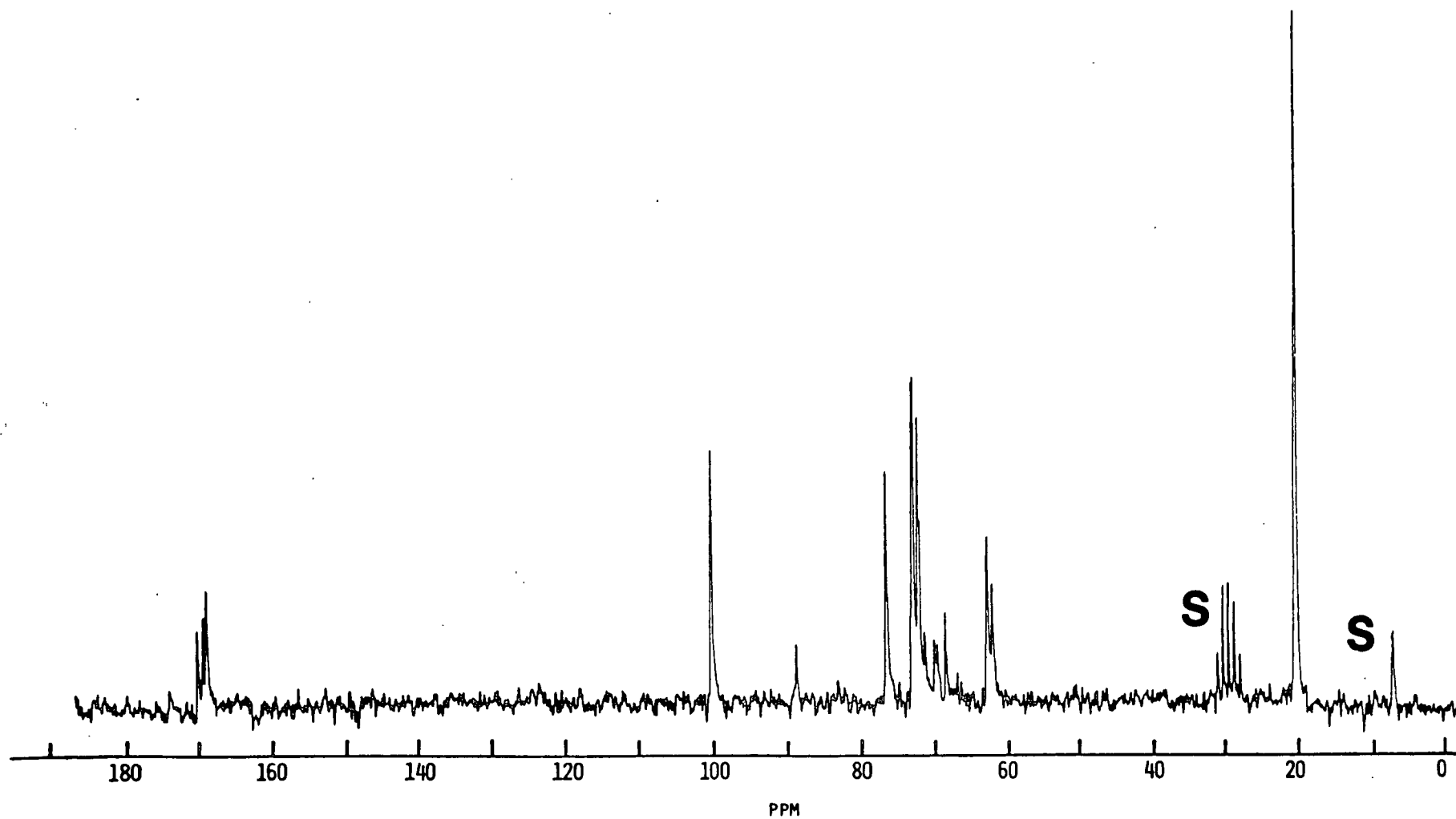
Figure 5. ^{13}C-NMR spectrum of α-cellohexaose peracetate in acetone-d$_6$.

TABLE I

^{13}C-NMR ASSIGNMENTS[a] FOR THE ACETYLATED β-ANOMERS OF XYLOSE, GLUCOSE, XYLOBIOSE, AND CELLOBIOSE

Compound	Solvent	1	2	3	4	5	6	1'	2'	3'	4'	5'	6'	Ref.
β-X1Ac[d]	Acetone-d_6	92.2	69.6[b]	71.1[b]	68.5	62.9								Utille
β-X2AC	Acetone-d_6	92.7	70.6[b]	72.6[b]	75.4	63.9		100.6	71.3[b]	71.6	69.4	62.5		
β-G1AC	Acetone-d_6	92.1	71.1[b]	73.0[b]	68.7	73.0[b]	62.3							Capon Gagnaire
β-G2AC	CDCl$_3$	91.6	70.4[b,d]	72.4[b,d]	75.9	73.6[b]	61.7	100.7	71.6[b]	72.9[b]	67.9	72.0[b]	61.7	"[c]

[a]Relative to internal $(CH_3)_4$ Si.
[b]Assignment tentative, can be exchanged with nearby signal.
[c]Spectrum taken from the literature.
[d]Nomenclature: X1AC = xylose tetraacetate, X2AC = xylobiose hexaacetate, G1AC = glucose pentaacetate and
C2AC = cellobiose octaacetate.

TABLE II

^{13}C-NMR ASSIGNMENTS[a] OF THE CELLO-OLIGOSACCHARIDE PERACETATES IN ACETONE-d_6

Compound	Unit	Solvent	1	2	3	4	5	6
αG1AC[c,d]		CDCl$_3$	89.1	69.3^b	69.9^b	68.0	69.9^b	61.5
αC2AC	Reducing	Acetone-d_6	89.3	70.2^b	69.8^b	76.6	71.5^b	62.3
	terminal		101.2	72.3^b	73.5^b	68.8	72.3^b	62.3
αC2AC	Reducing	"	89.4	70.3^b	69.9^b	76.7	71.6^b	62.3
	Internal		101.2	72.5^b	73.2^b	76.9	73.4^b	63.1
	terminal		101.2	72.3^b	73.5^b	68.7	72.3^b	62.3
αC4AC	Reducing	"	89.4	70.3^b	69.9^b	76.7	71.6^b	62.3
	Internal		101.2	72.5^{b}X	77.3^{b}X	76.9X	73.3^{b}X	63.0X^f
	terminal		101.2	72.3^b	73.5^b	68.7	72.3^b	62.3
αC5AC	Reducing	"	89.4	70.3^b	69.7^b	76.7	71.6^b	62.3
	Internal		101.0	72.5^{b}X	73.3^{b}X	77.0X	73.3^{b}X	63.0
	terminal		101.0	73.5^b	68.8	72.3^b	62.3	
αC6AC	Reducing	"	89.3	70.2^b	69.8^b	76.7	71.5^b	62.3
	Internal		101.0	72.5^b	73.1^b	76.9	73.3^b	63.0
	terminal		101.0	72.4^{b,c}	73.3	68.7	72.4^{b,c}	62.3

[a]Relative to internal $(CH_3)_4Si$. In some cases acetone-d_6 at 29.7 ppm was used as a secondary reference to avoid contamination of the sample.
[b]Assignment tentative; can be exchanged with nearby signal of similar intensity.
[c]See Ref. 1.
[d]Nomenclature: Gl-glucose, C2-cellobiose, C3-cellotriose, etc.
[e]Observed as shoulder on a larger signal.
[f]X refers to signal that is relatively more intense in this spectrum than in the one above.

LITERATURE CITED

1. Capon, B., Rycroft, D. S., and Thomson, J. W., Carbohyd. Res. 70:145-9(1979).

2. Gagnaire, P. V., Taravel, F. R., and Vignon, M. R., Carbohyd. Res. 51:157-68 (1976).

3. Utille, J. P. and Vottero, P. J. A., Carbohyd. Res. 85:289-97(1980).

APPENDIX XIII

^{13}C-NMR SPECTRA OF THE XYLO- AND CELLO-OLIGOSACHARIDES
AND RELATED CARBOHYDRATES

This appendix contains the decoupled ^{13}C-NMR spectra (25.05 MHZ) of the xylo-
and cello-oligosaccharides, and related compounds. Refer to Section 4, Part III for
detailed assignments. Spectra of esparto-xylan and maltose are also included. All
spectra are at ambient temperature unless otherwise noted.

<u>Key</u>

I = impurity

S = solvent

D = dioxane
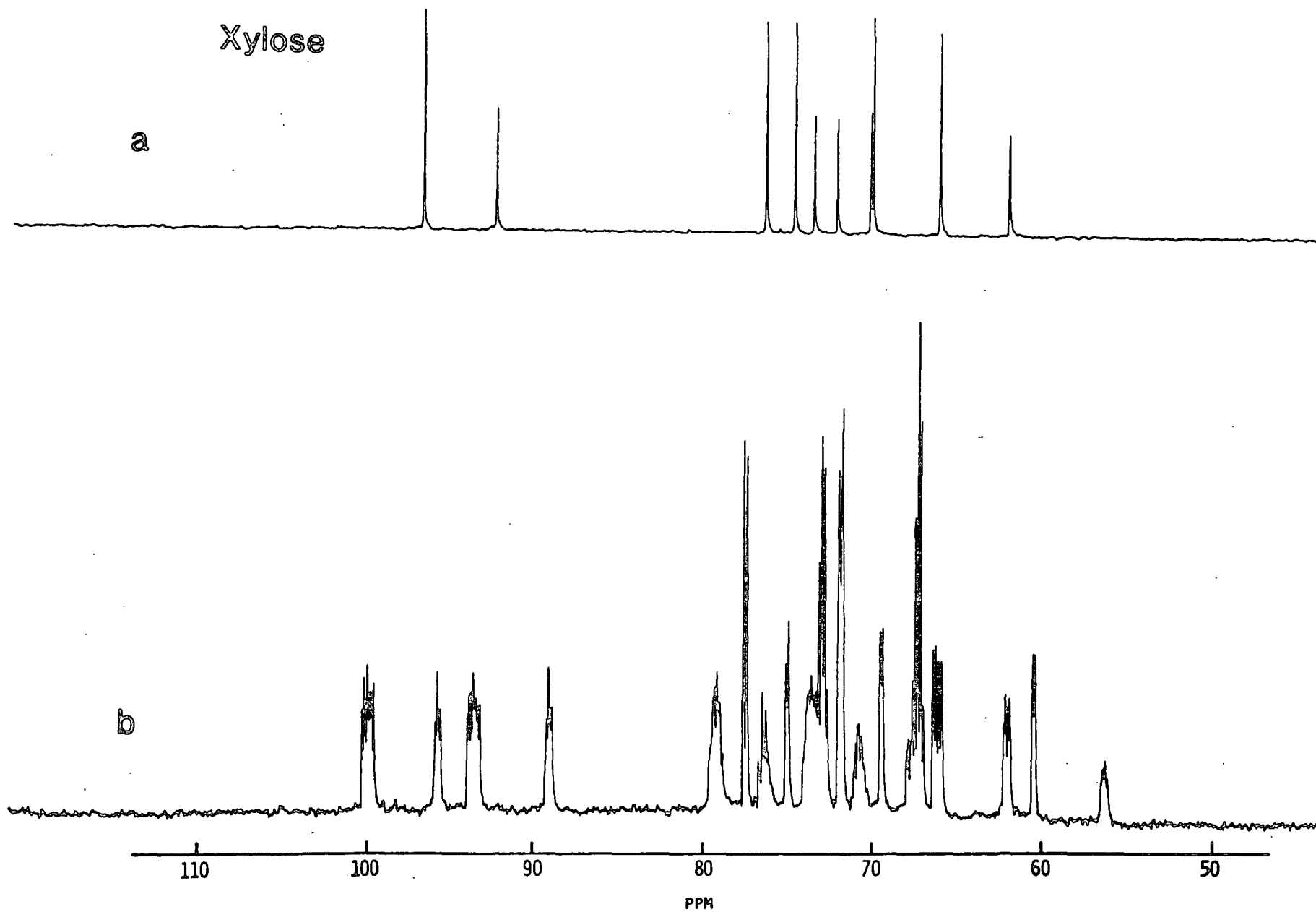
Figure 1.   Xylose in D_2O.
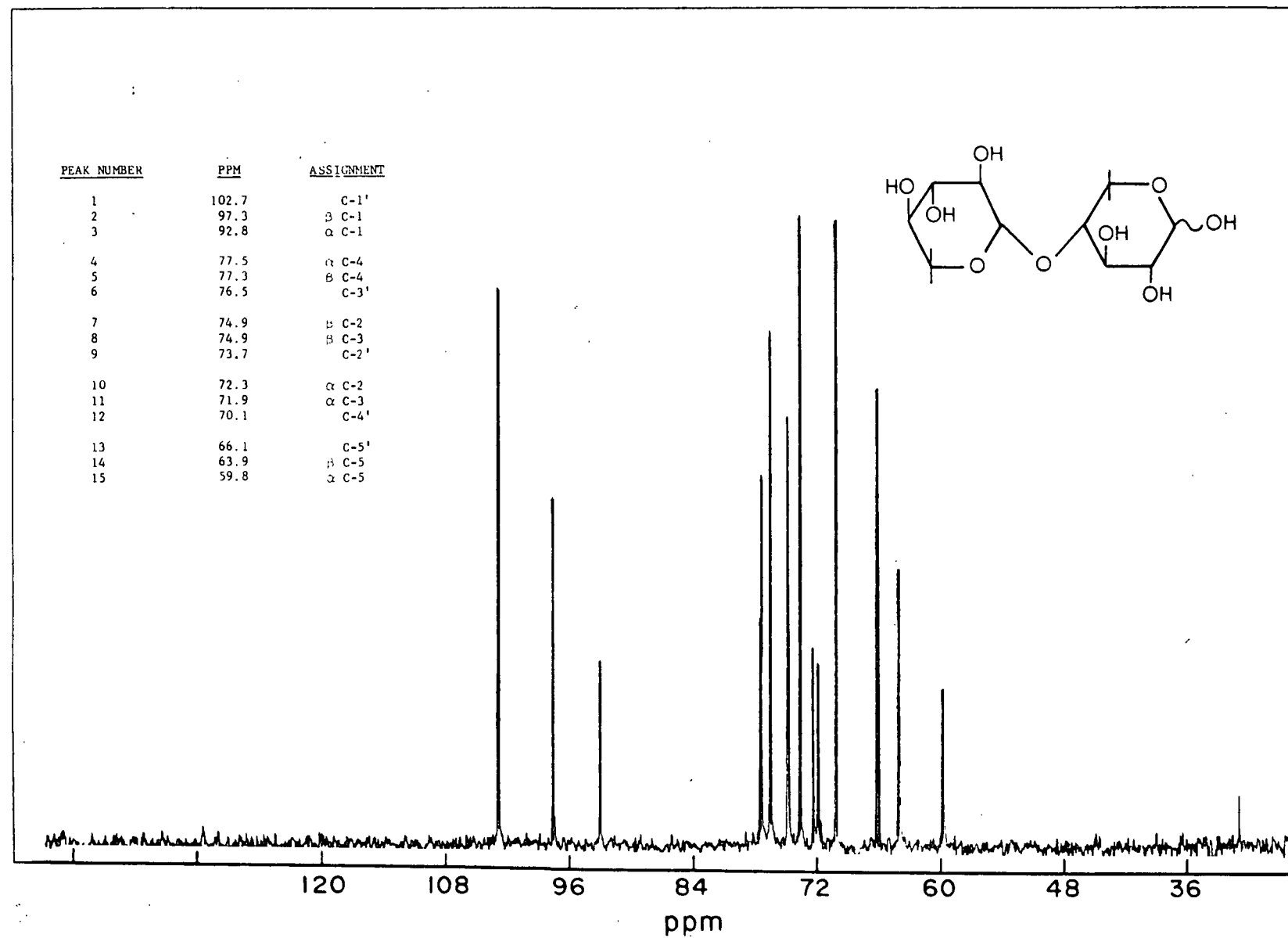
Figure 2. Xylobiose in D₂O.
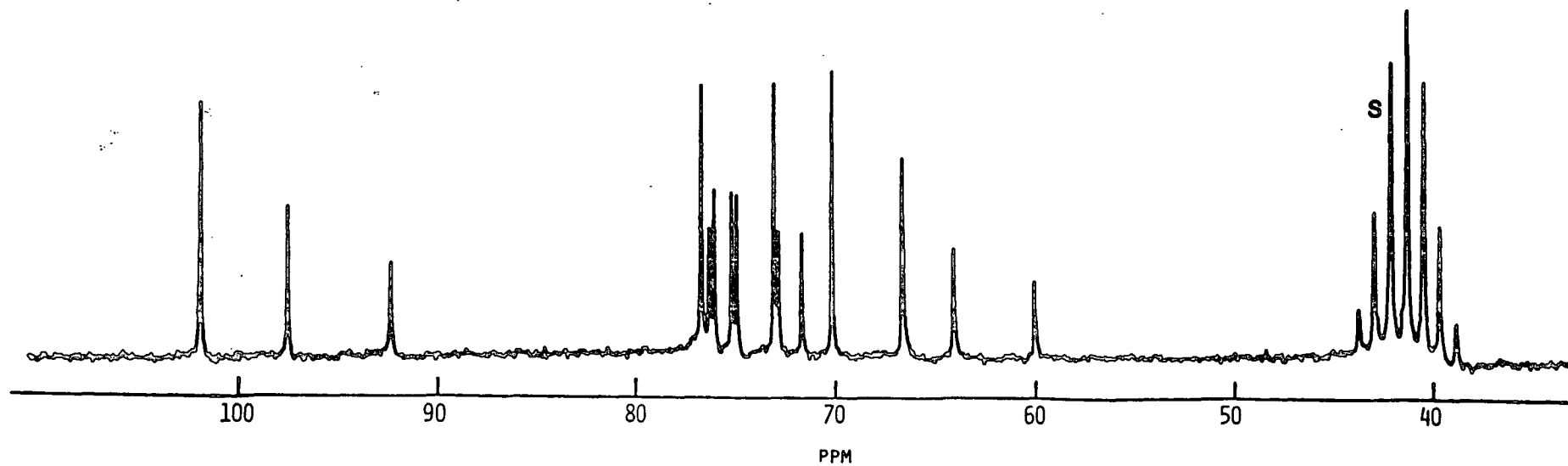
Figure 3. Xylobiose in DMSO-d$_6$.

XYLOTRIOSE
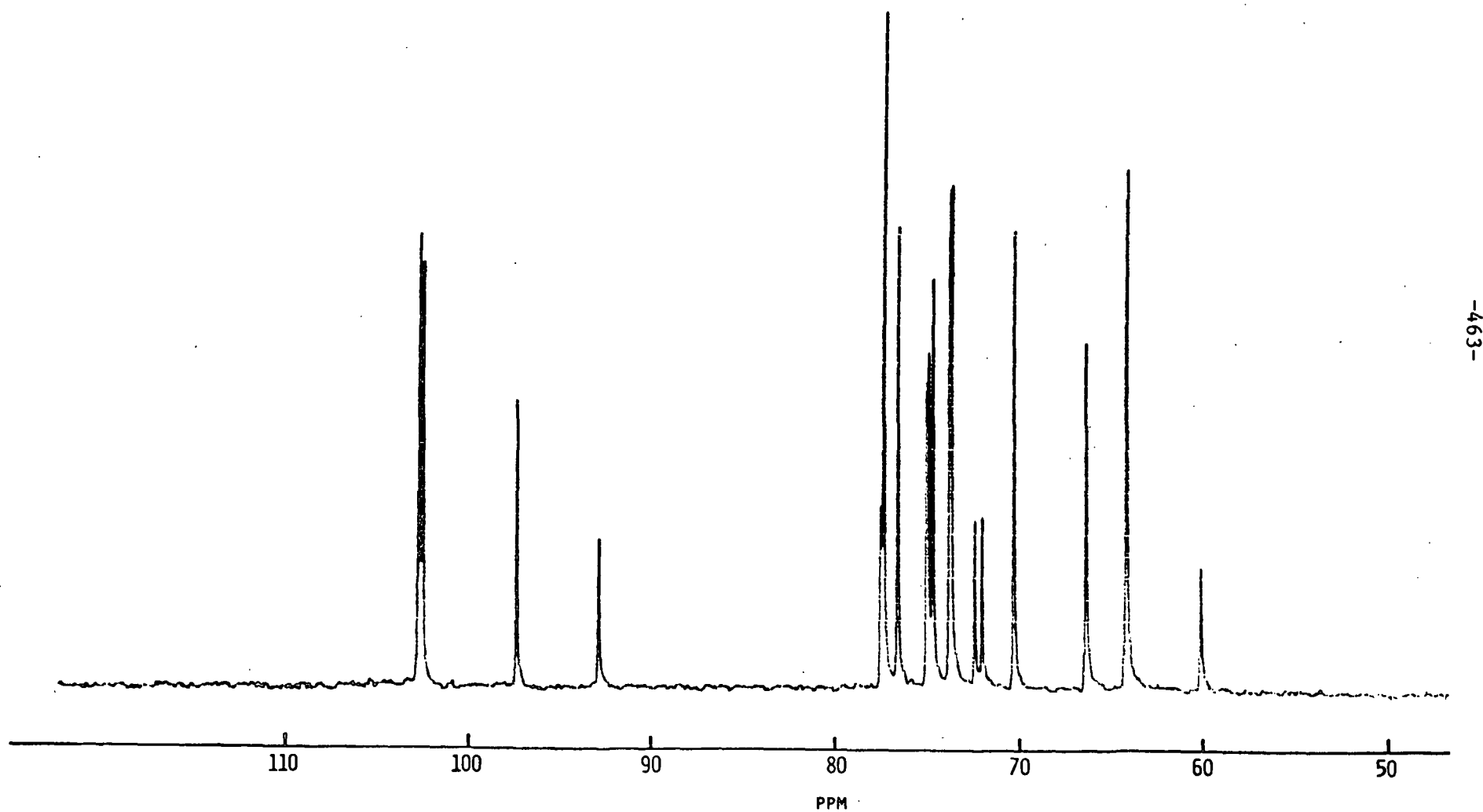
Figure 4.   Xylotriose in D_2O.

XYLOTETRAOSE
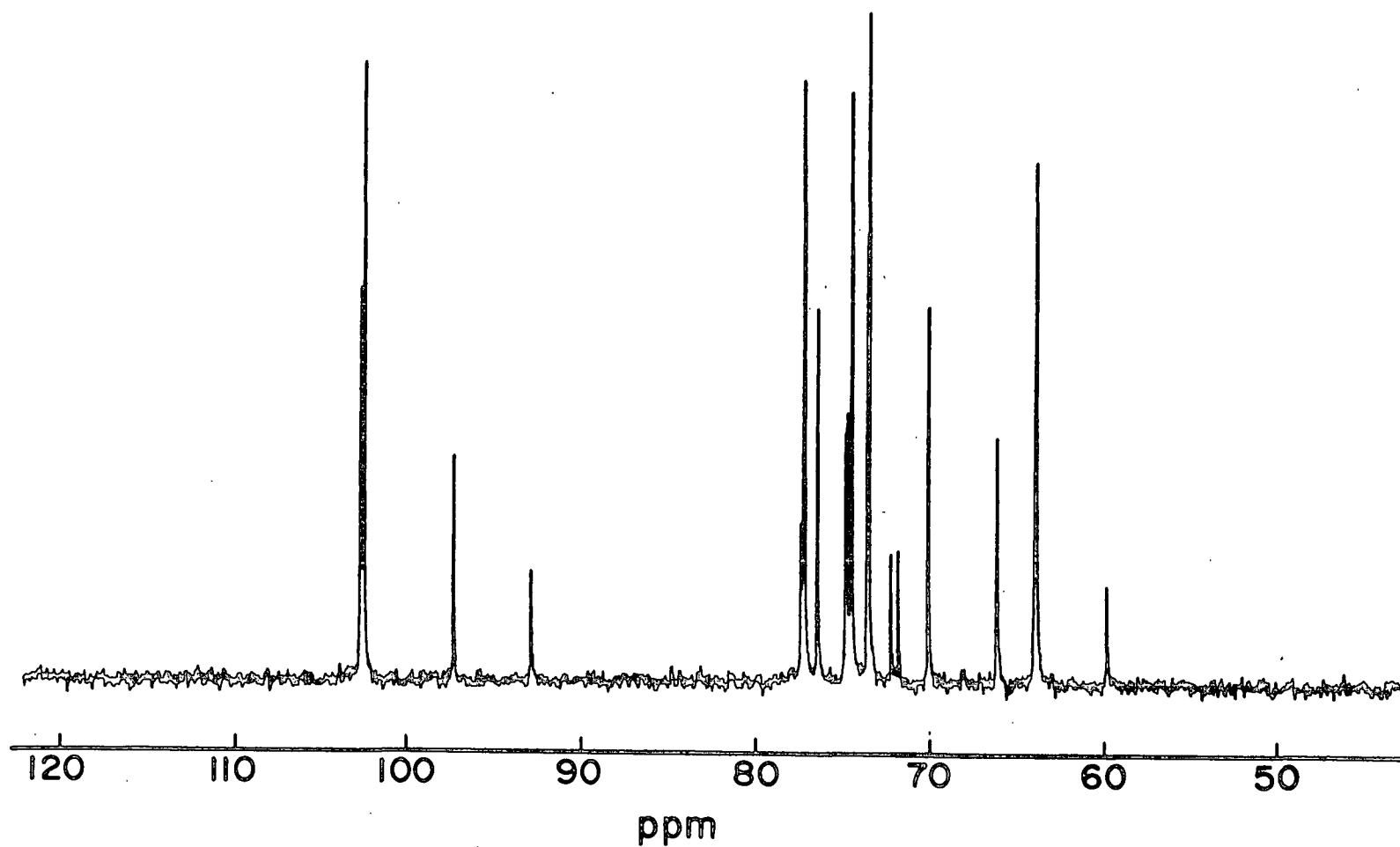
Figure 5. Xylotetraose in D_2O.

XYLOPENTAOSE
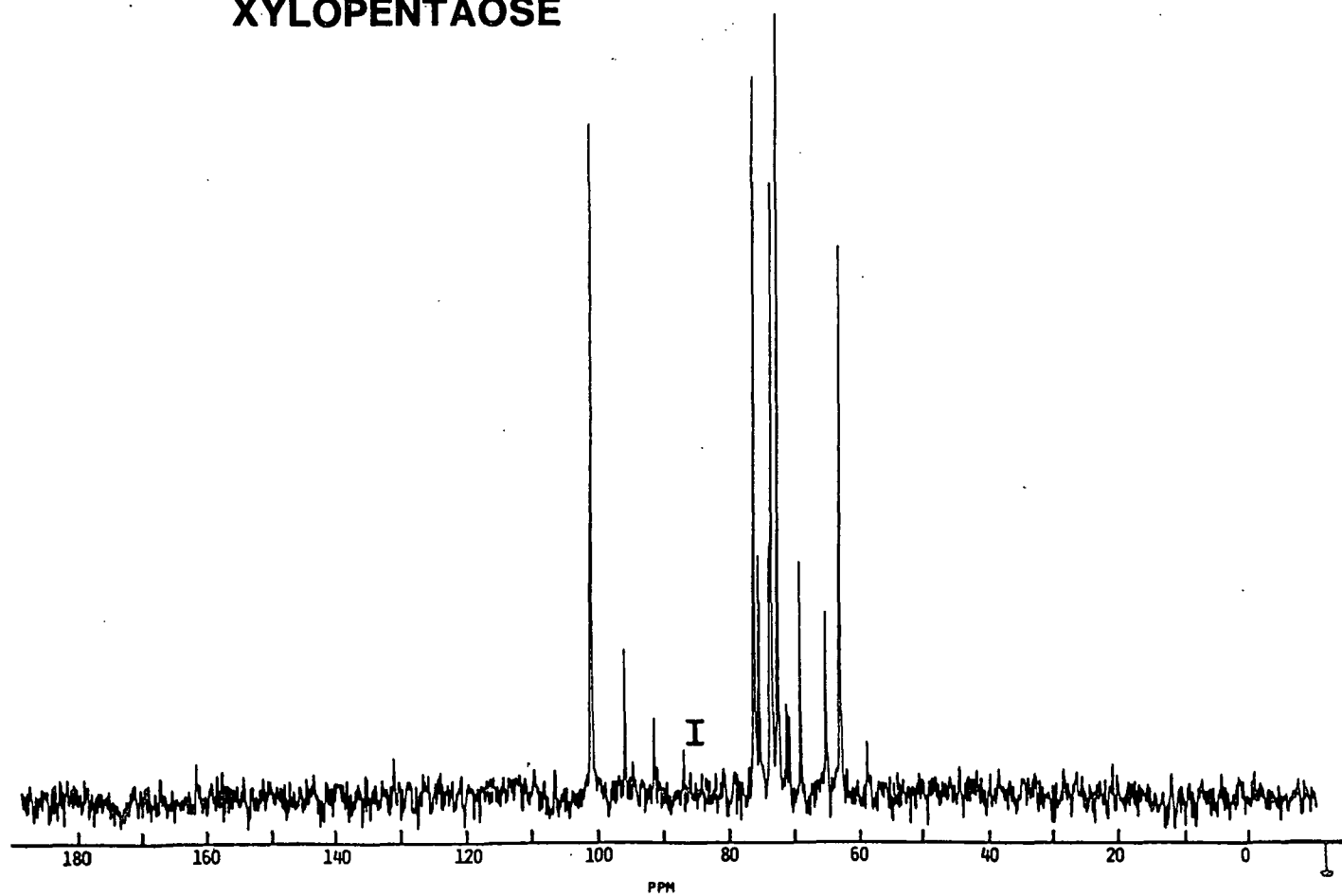
Figure 6. Xylopentaose in D_2O.
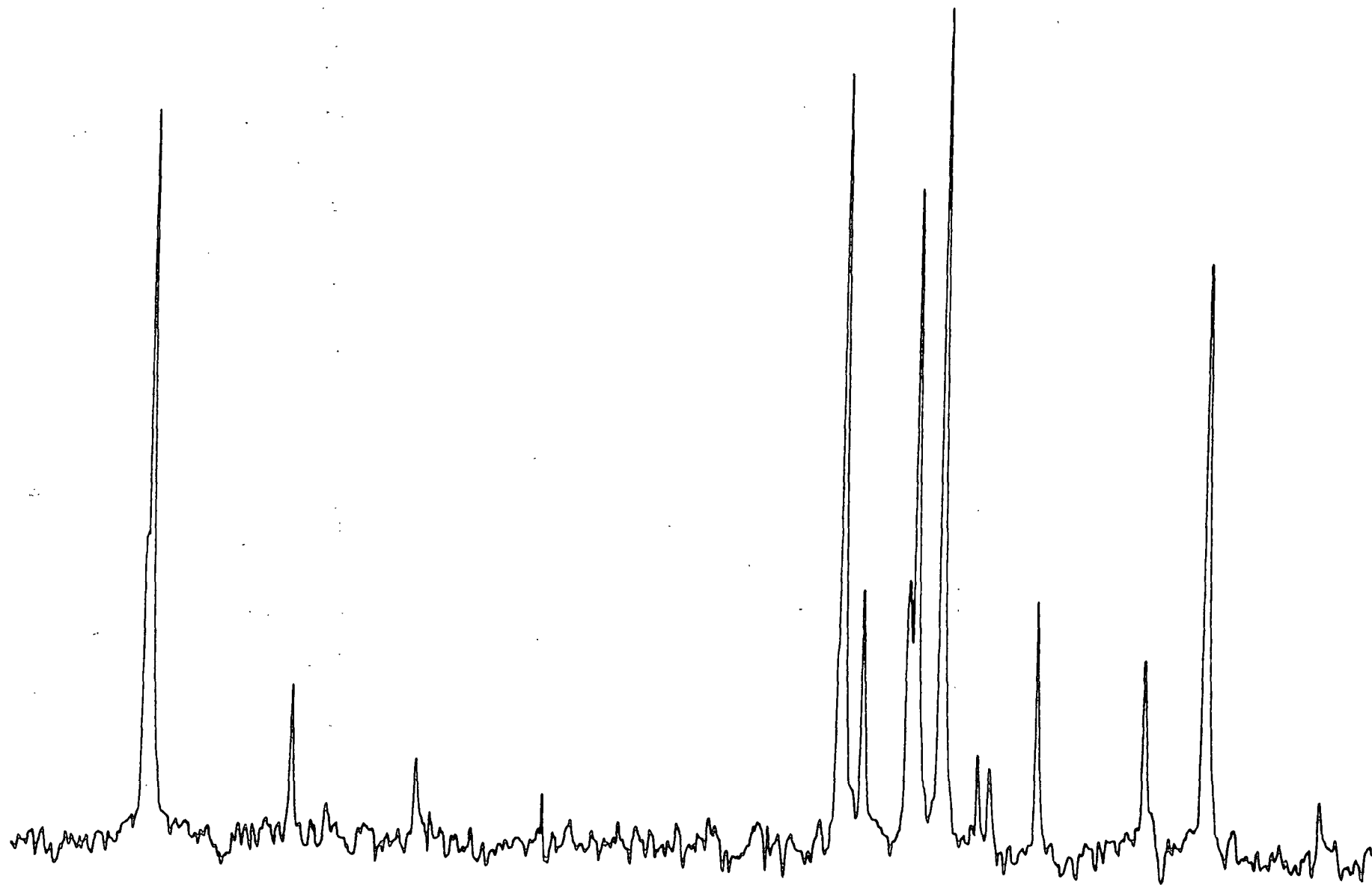
Figure 7. Expansion of Fig. 6.

C_1 102.5

C_4 77.3

C_3 74.6

C_2 73.6

C_5 63.9
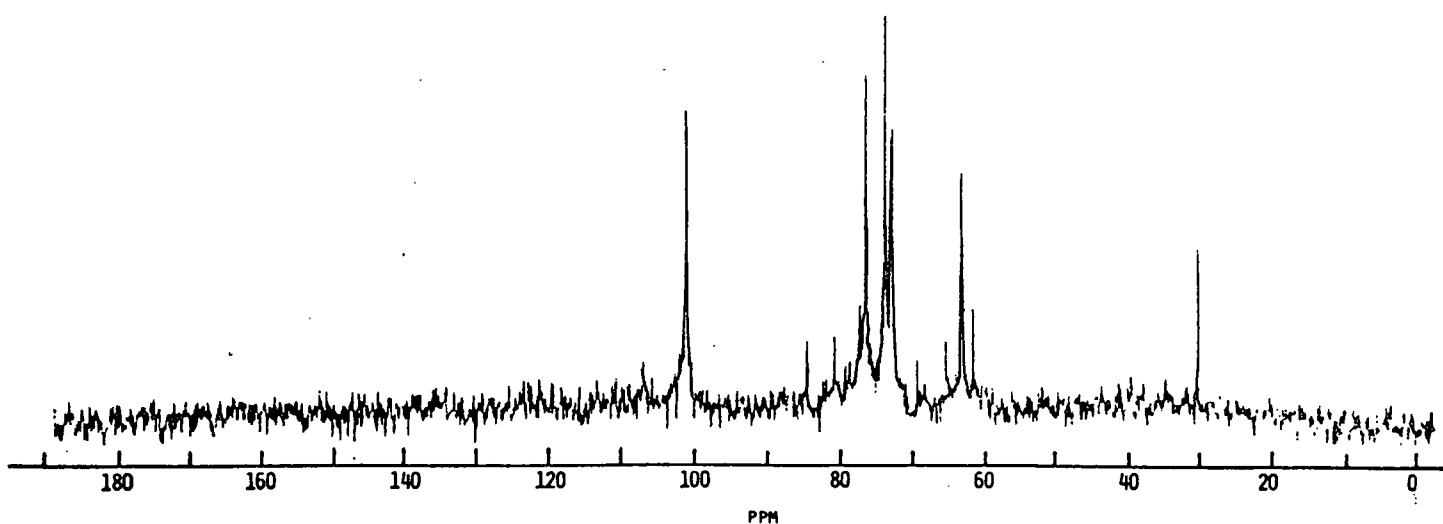
Figure 8. Esparto xylan in D_2O at 58°C. Refer to the literature for more in-depth assignments (1,2). The spectrum is consistent with primarily a β-1,4-linked xylan containing some β-1,3-linked side chains.
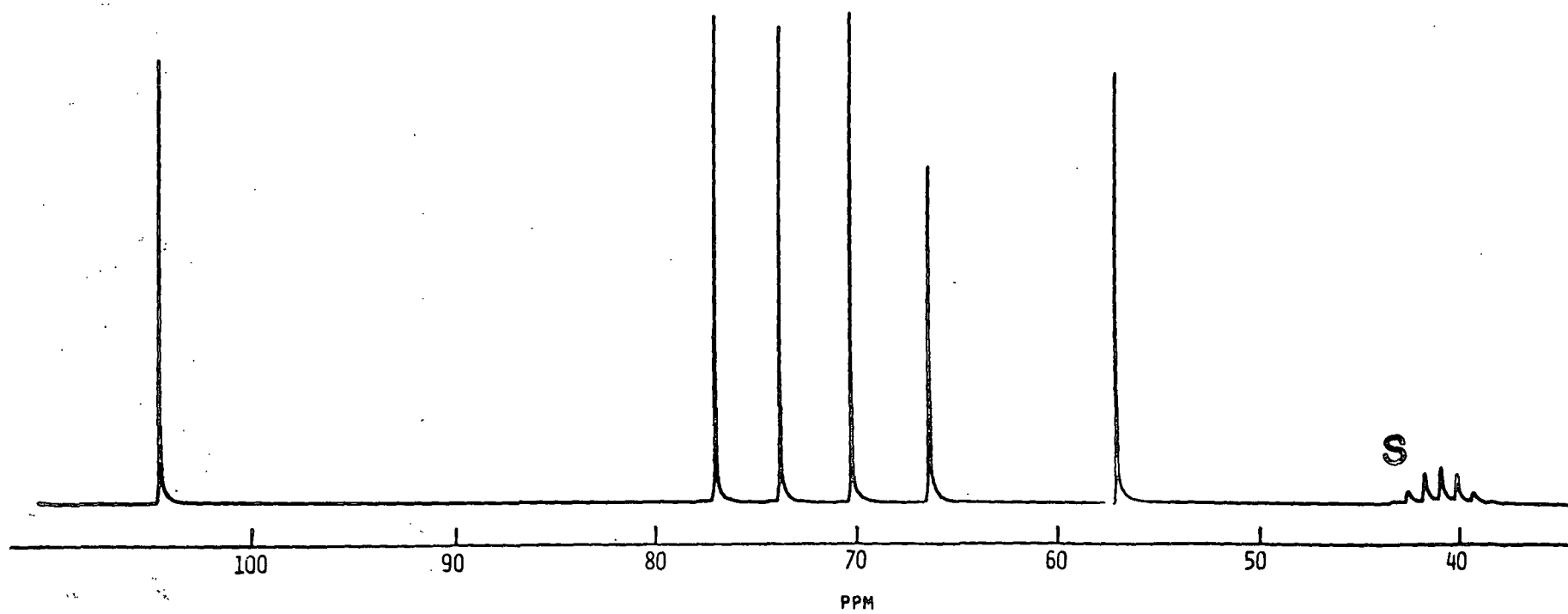
Figure 9.   Methyl β-xyloside in DMSO-d$_6$.

METHYL β-XYLOBIOSIDE
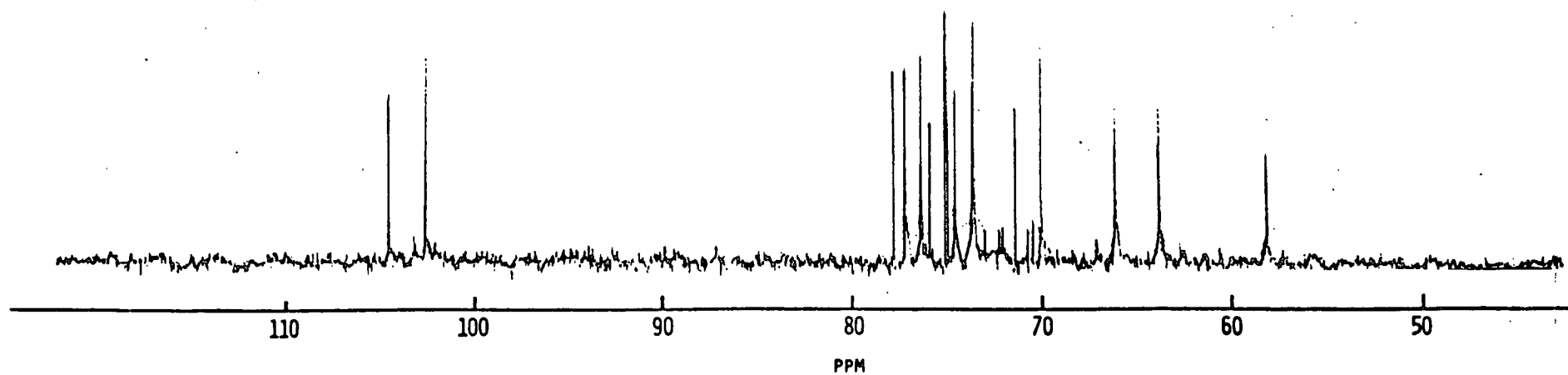
Figure 10. Methyl β-xylobioside in D$_2$O.

ALDOTRIURONIC ACID
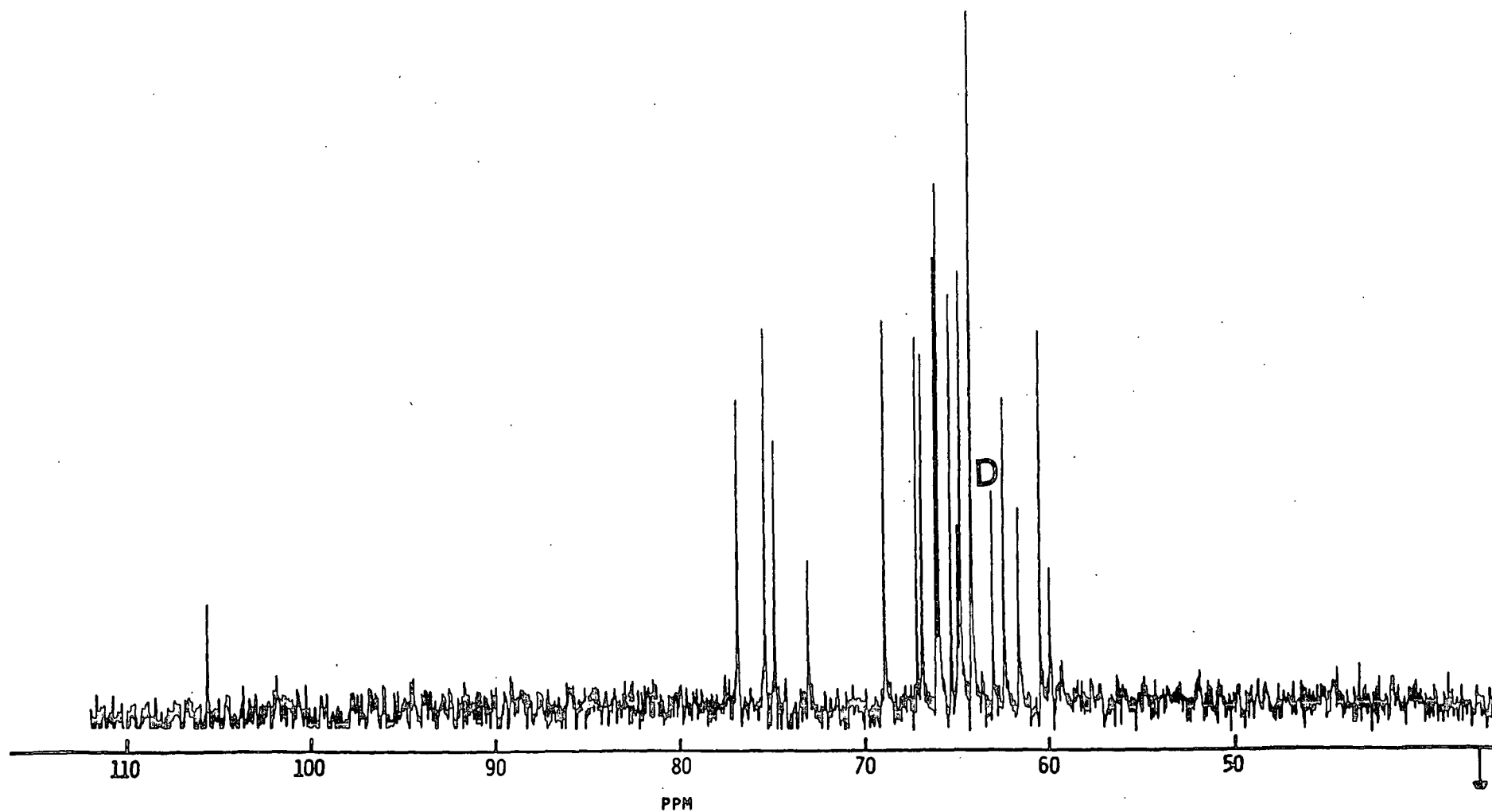
Figure 11. Aldotriuronic acid in D_2O.

SECURIDEBIOSE
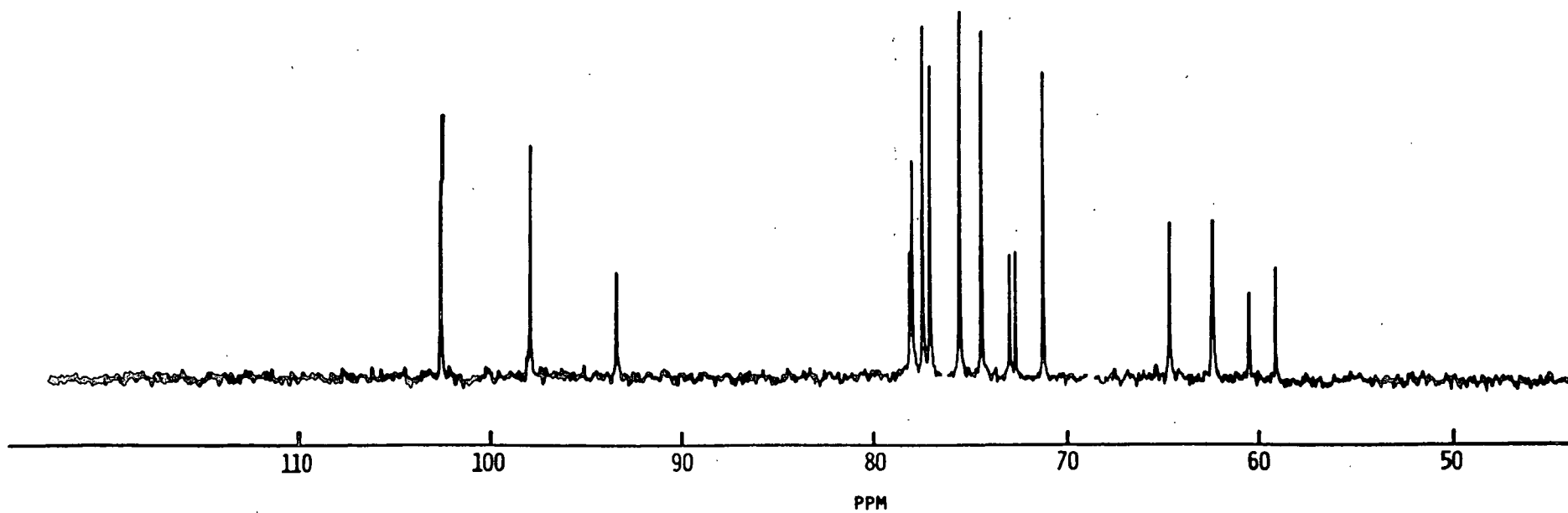
Figure 12.   Securidebiose in D_2O.

GLUCOSE
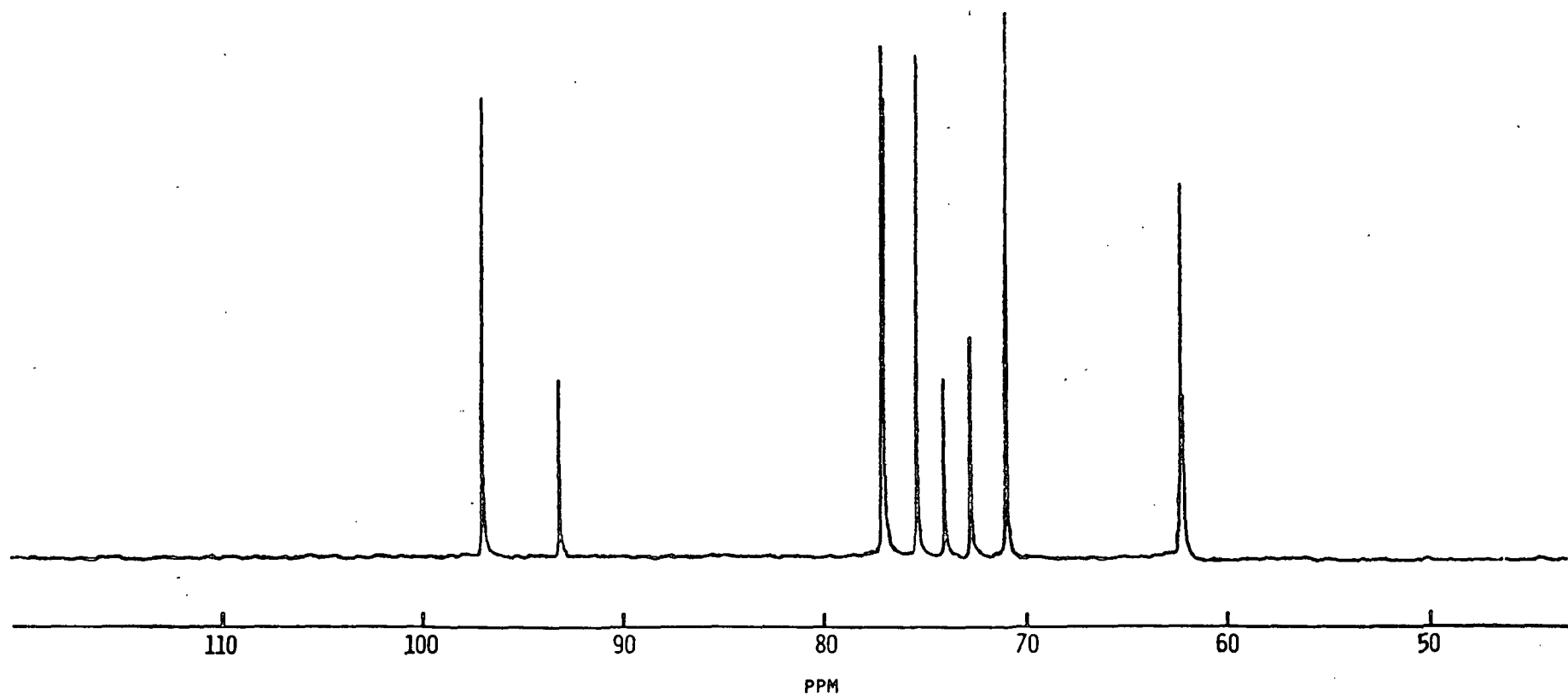
Figure 13. Glucose in D_2O.
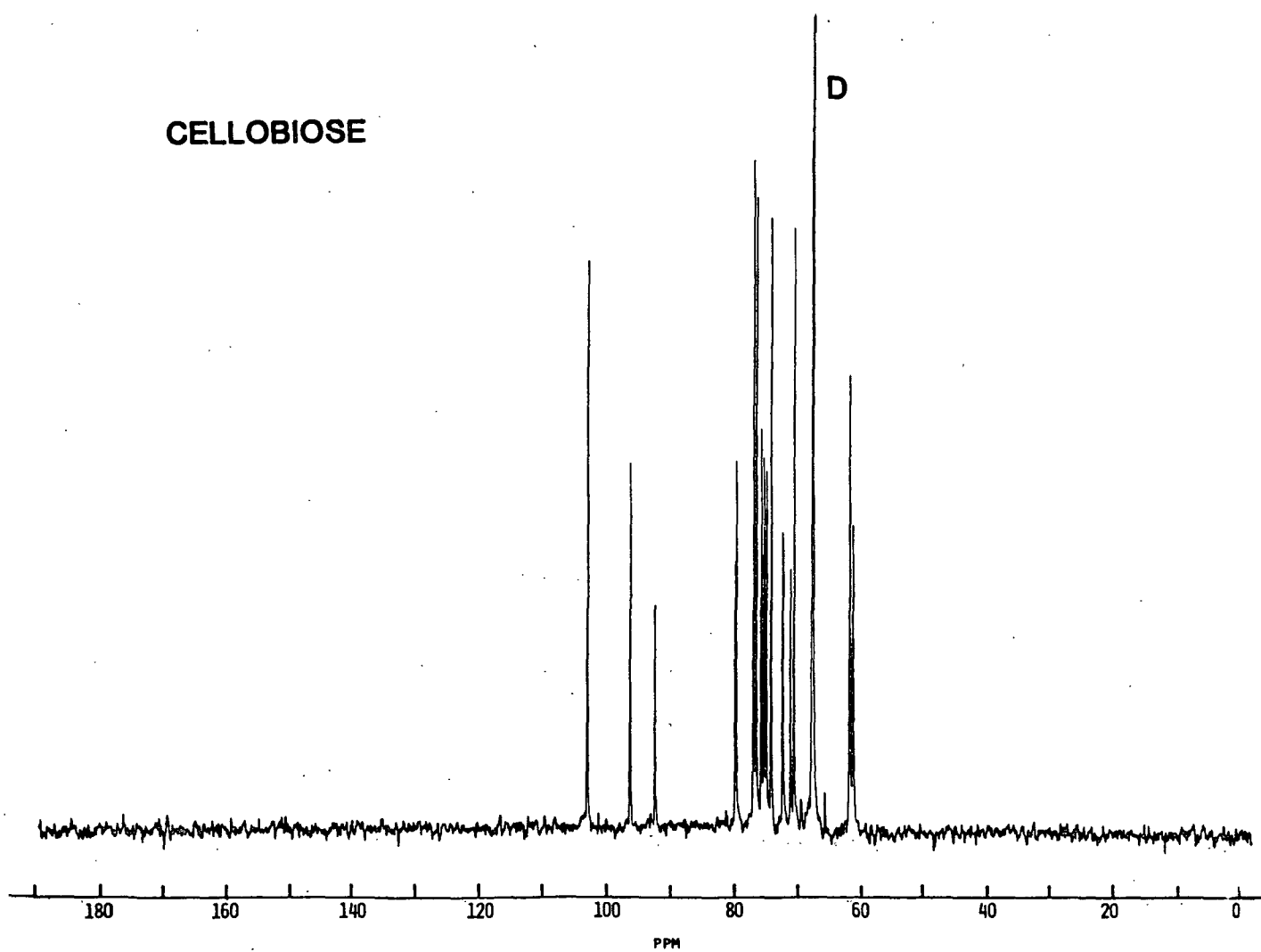
Figure 14. Cellobiose in D_2O.
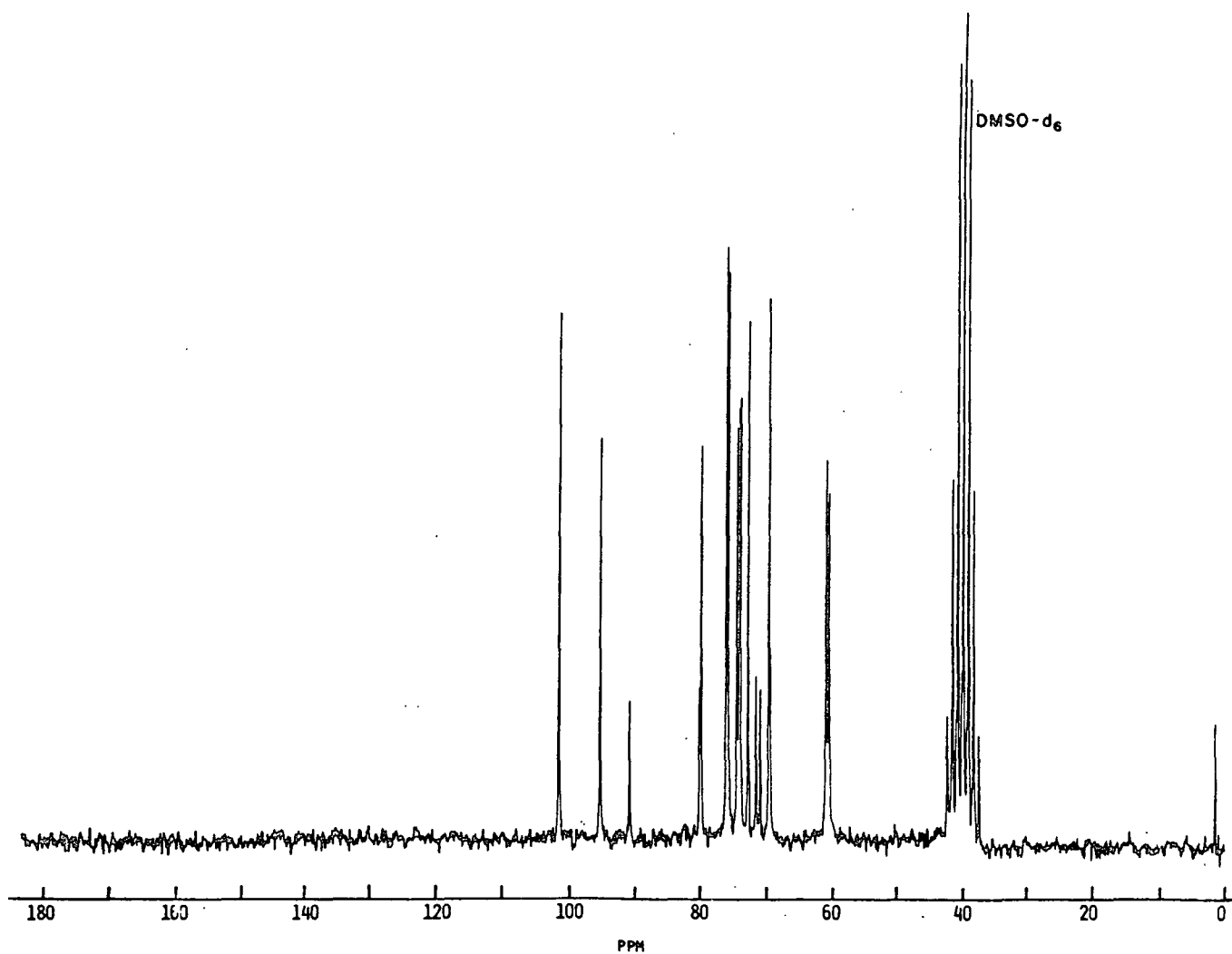
Figure 15. Cellobiose in DMSO-d_6.
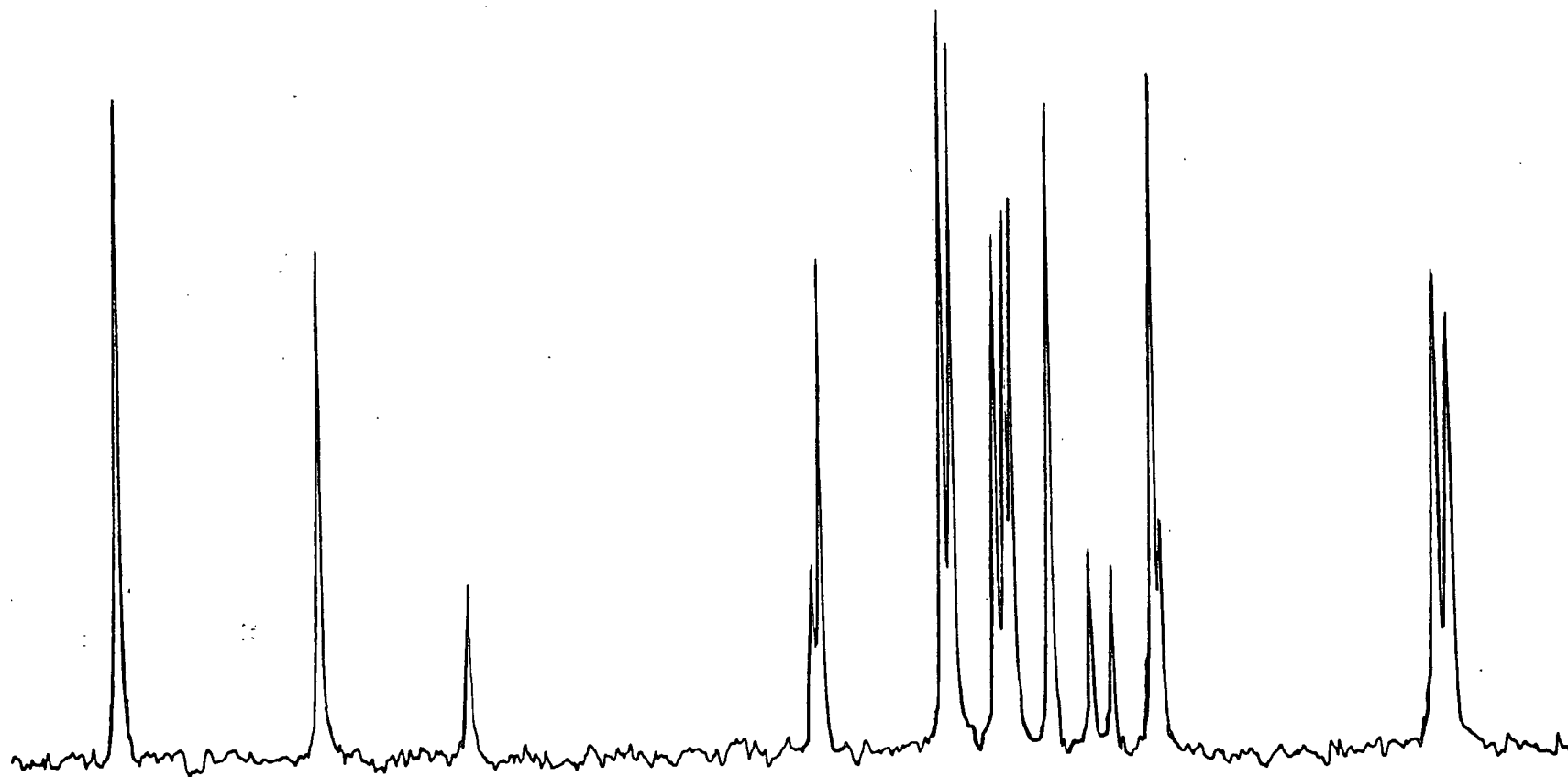
Figure 16.   Expansion of Fig. 15.

CELLOTRIOSE
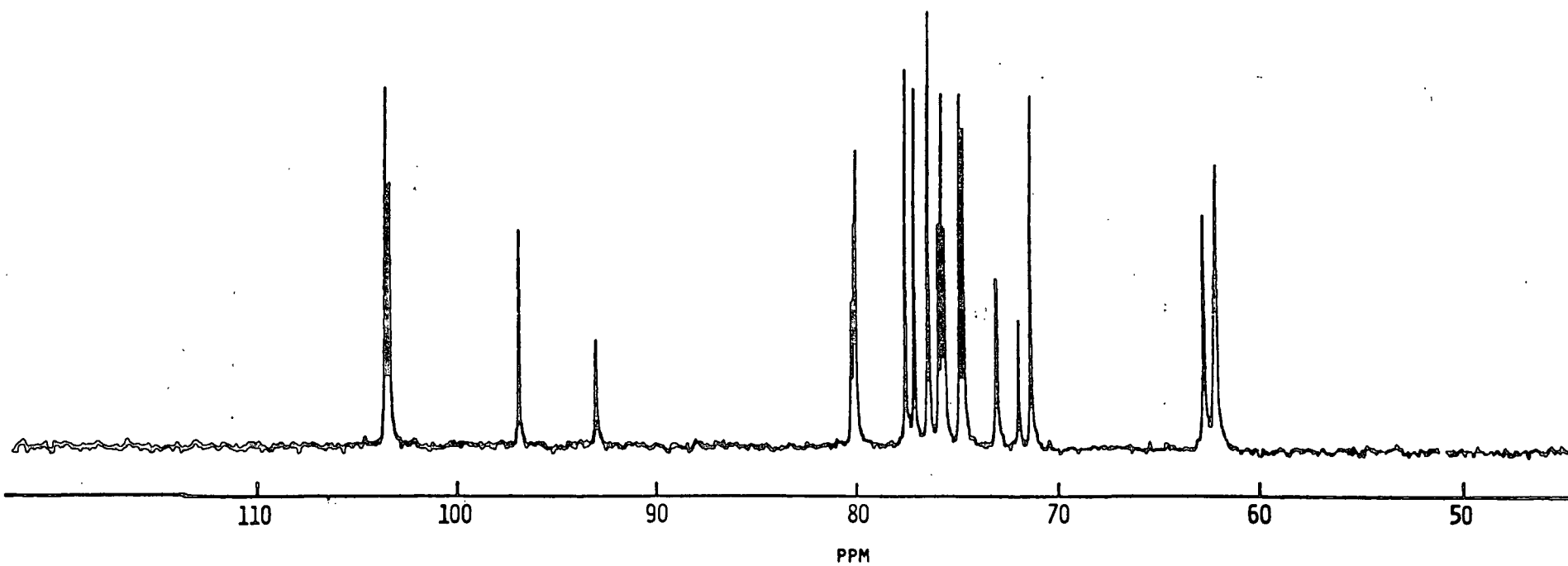
Figure 17.   Cellotriose in D_2O.

CELLOTETRAOSE

PPM
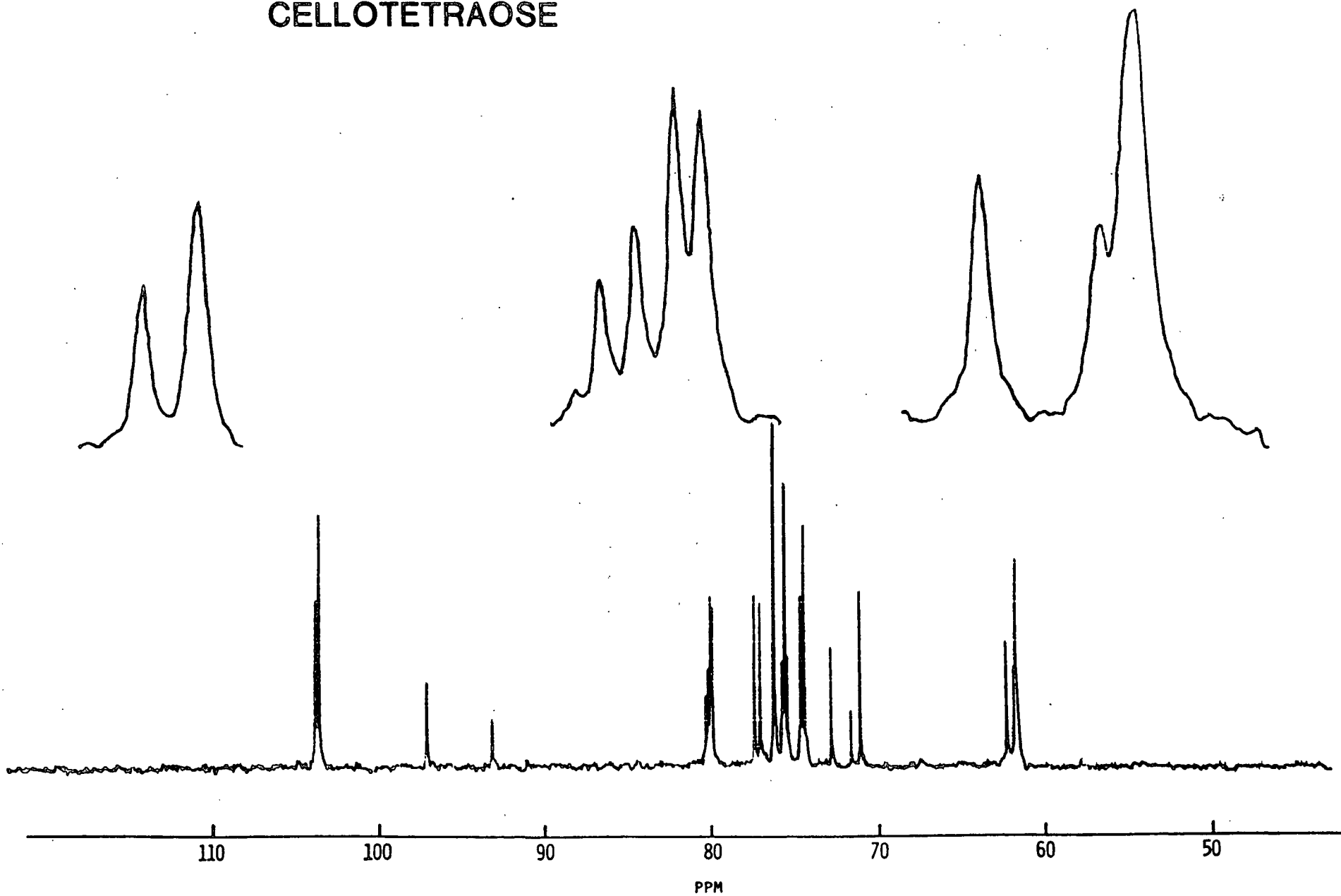
Figure 18. Cellotetraose in D_2O at 54°C with expanded C_1, C_4, and C_6 regions.
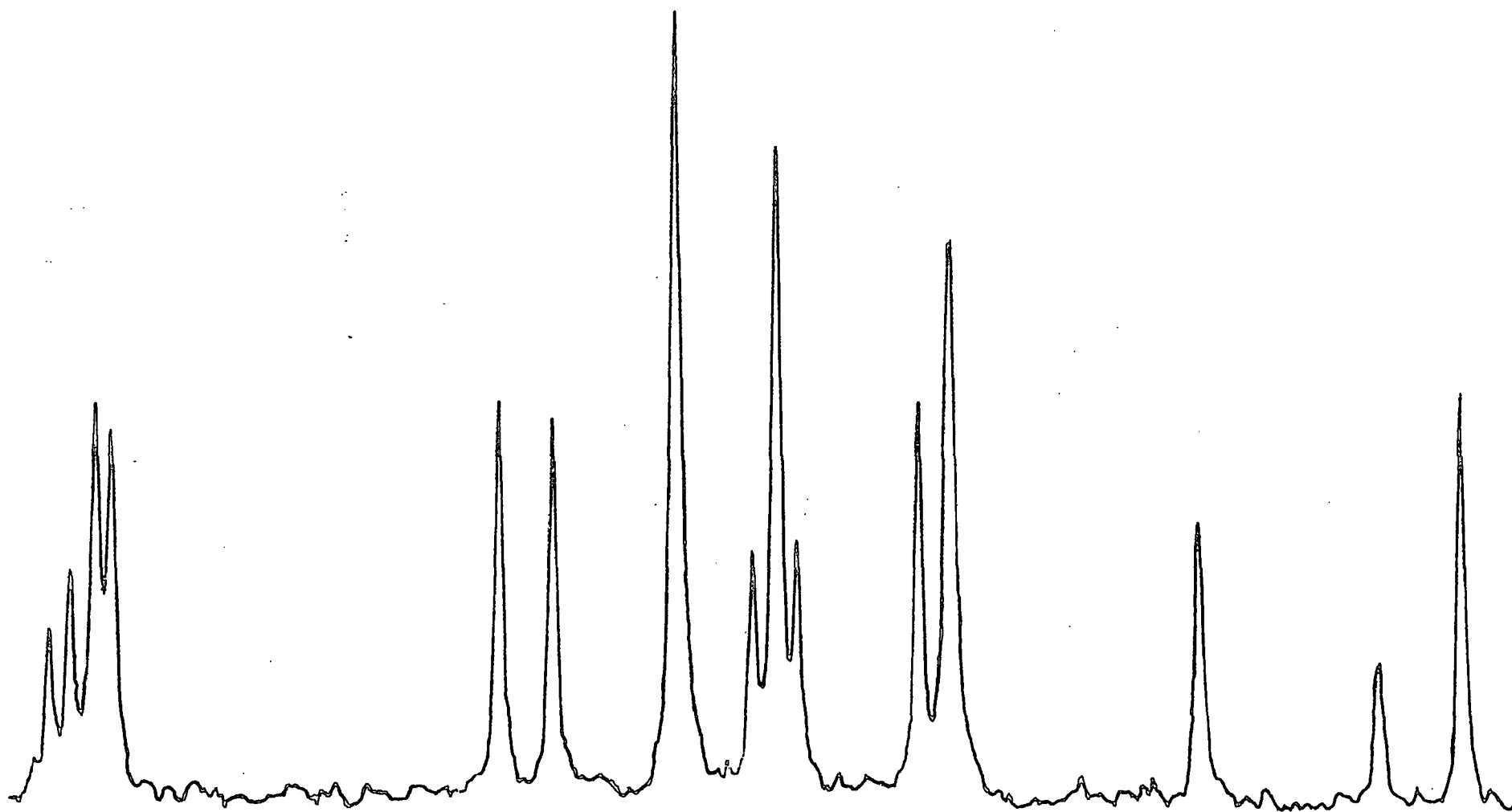
Figure 19.   Expansion of Fig. 18 from 69-81 ppm.

Methyl β-Glucoside
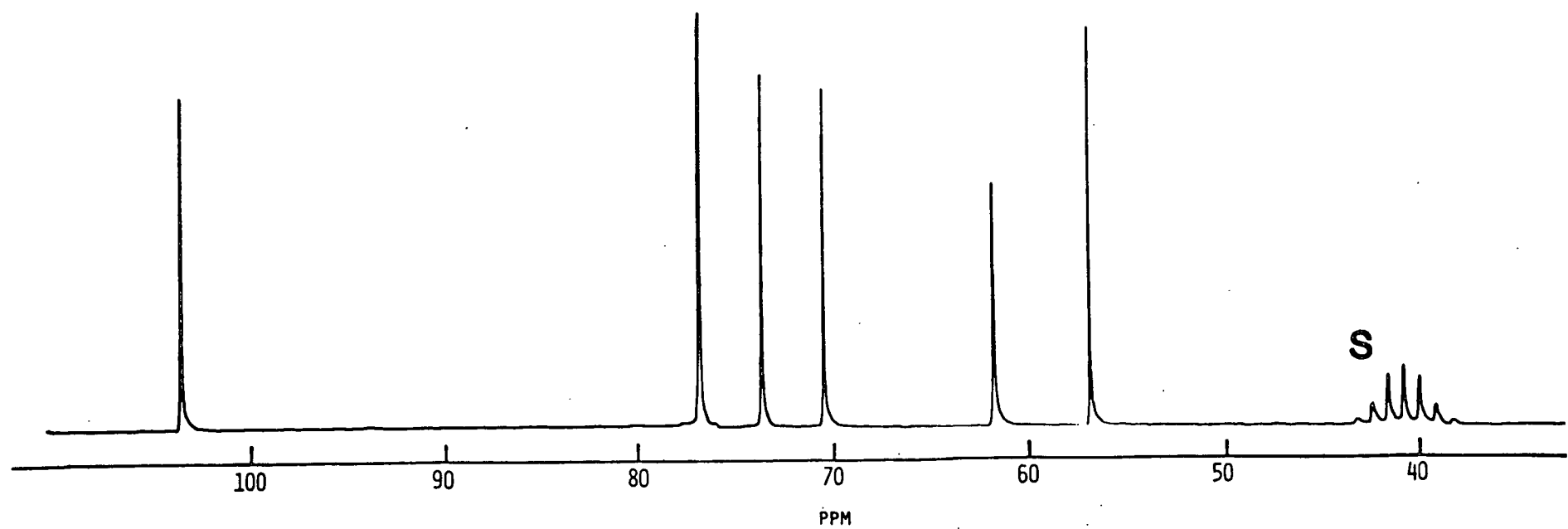
Figure 20. Methyl β-glucoside in DMSO-d$_6$.
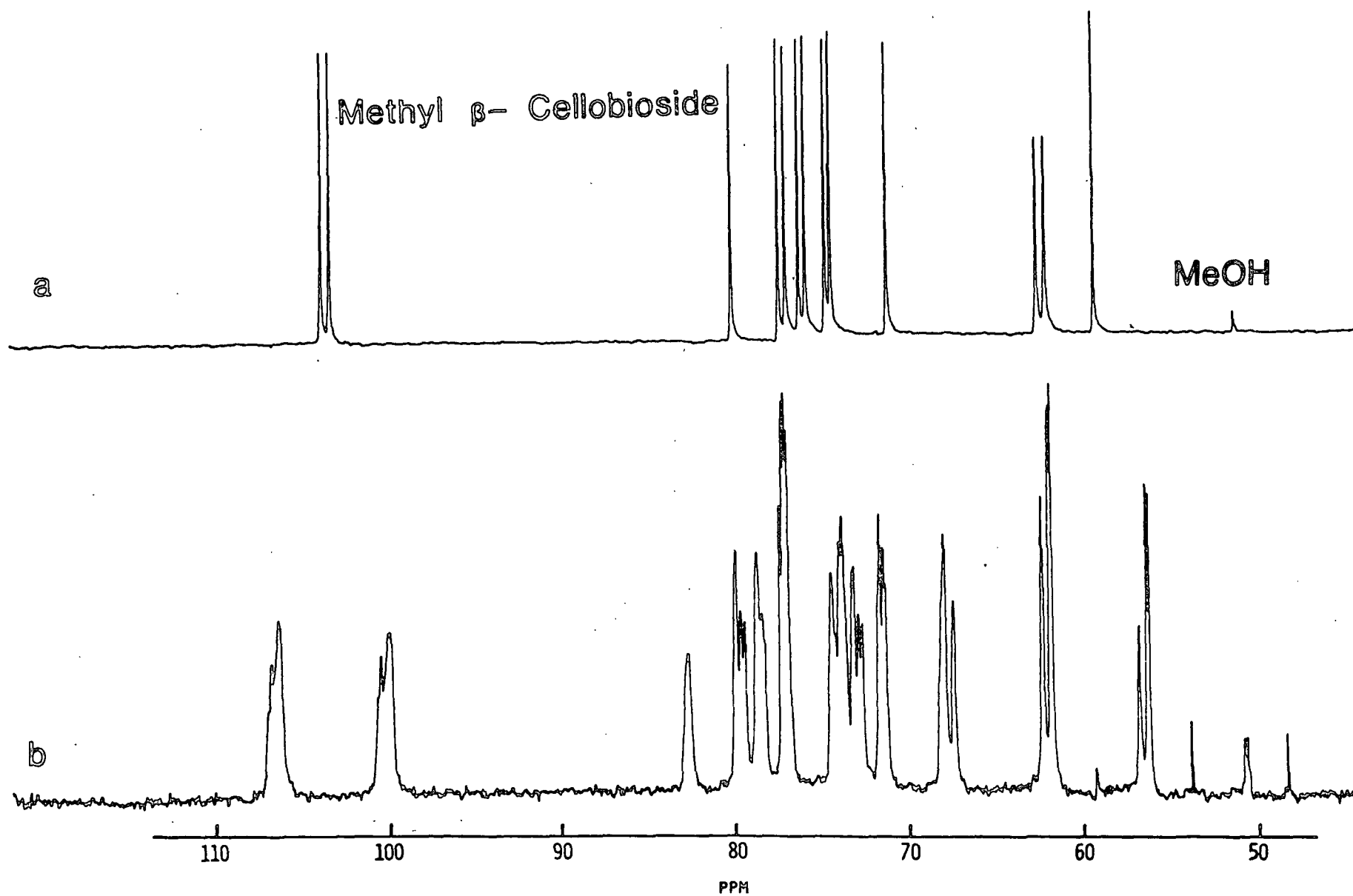
Figure 21. Methyl β-cellobioside in D_2O.

1,5 ANHYDROCELLOBIOTOL
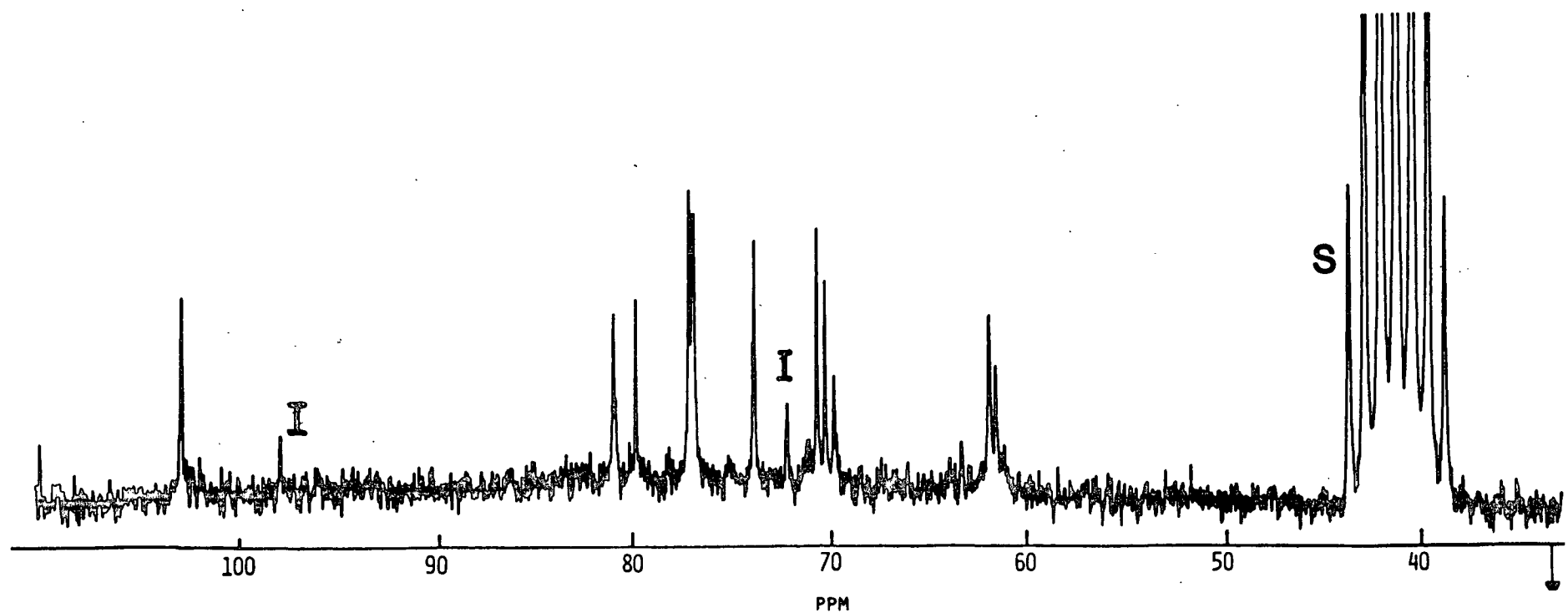
Figure 22. 1,5 Anhydrocellobiotol in DMSO-d$_6$.

Lactose
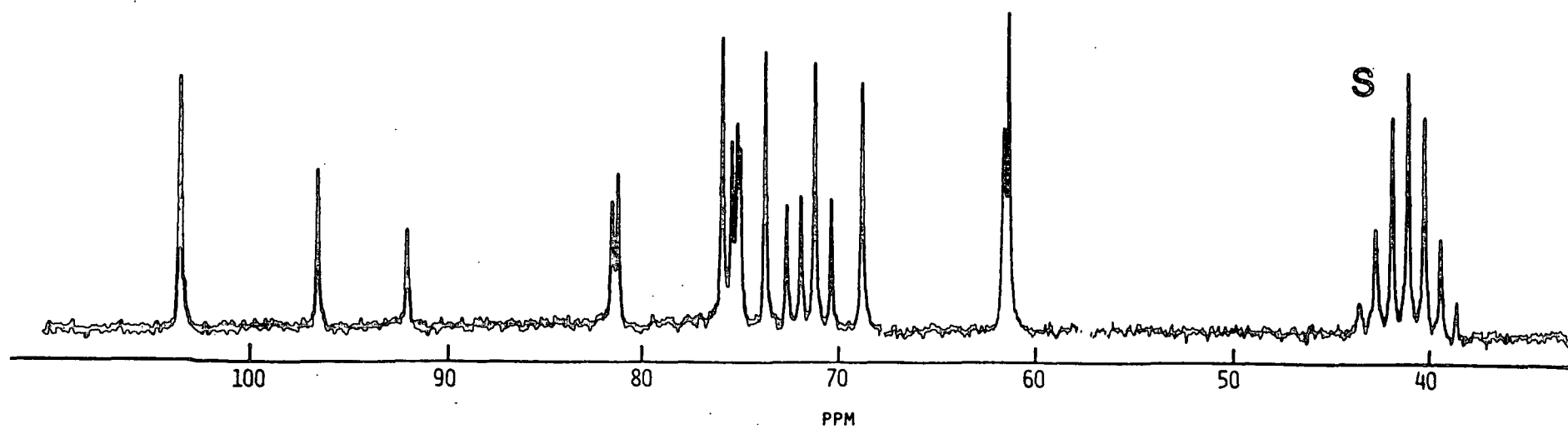
Figure 23. Lactose in DMSO-d$_6$.

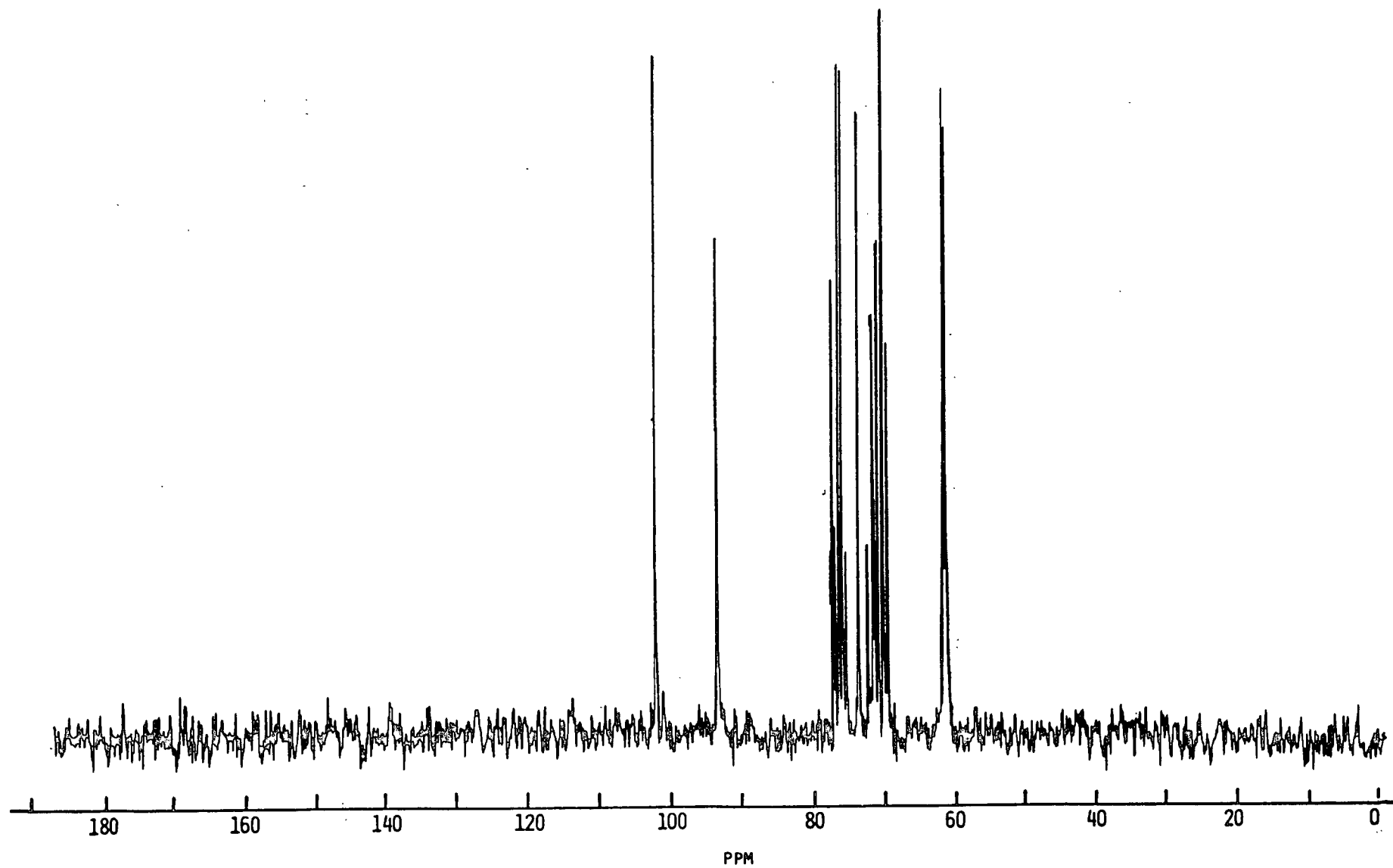Figure 24. 4-O-(β-D-glucopyranosyl)-D-mannopyranose in D_2O.

Mannobiose

PPM

Figure 25.   Mannobiose in D_2O.
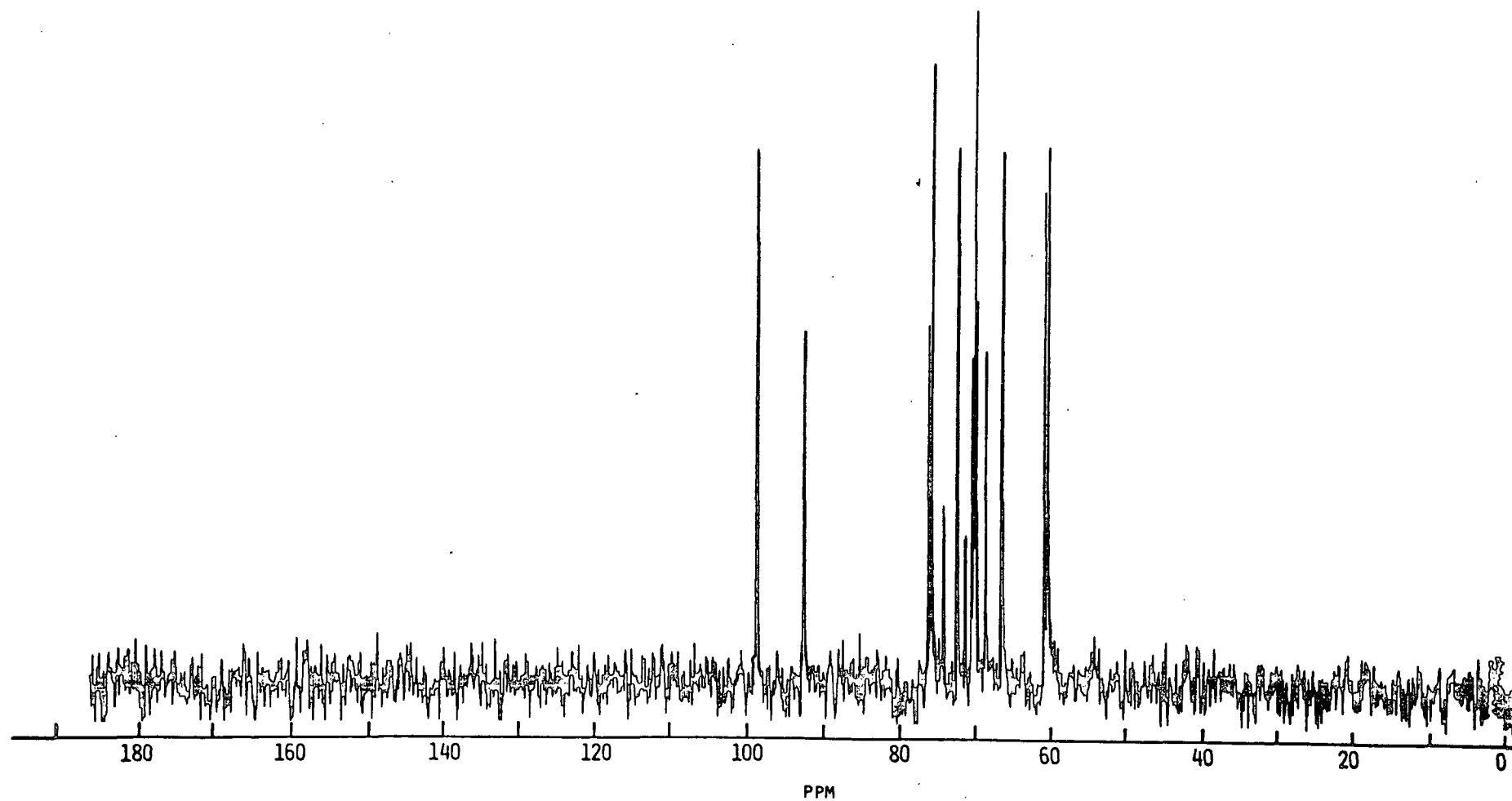
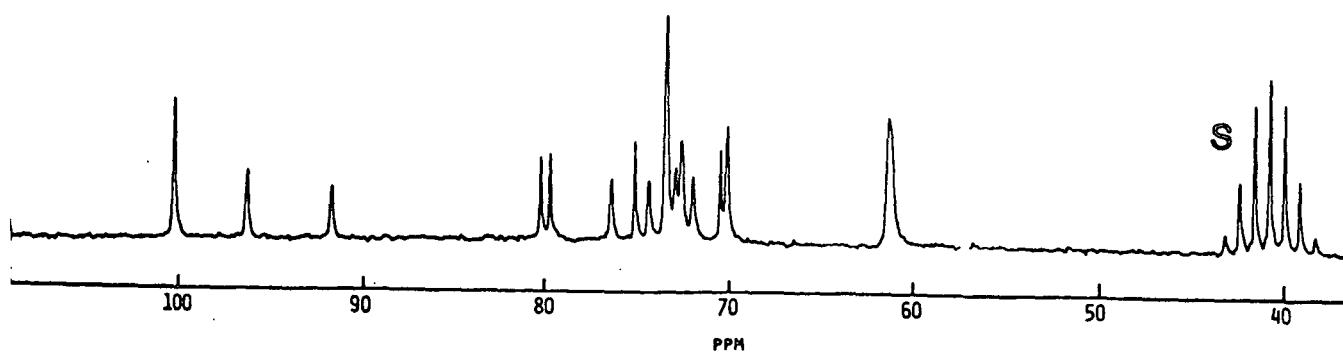| PPM	CARBON	PPM	CARBON
100.4	$C_{1'}$	72.4	$\{C_{2'}$
96.6	$\beta-C_1$	72.3	
91.9	$\alpha-C_1$	71.8	$\alpha-C_2$
80.0	$\alpha-C_4$	70.2	$\alpha-C_5$
79.5	$\beta-C_4$	70.0	$C_{4'}$
76.3	$\beta-C_3$	60.9	$C_{6'}$
75.0	$\beta-C_5$	60.6	$\beta-C_6$ OR $\alpha-C_6$
74.3	$\beta-C_2$	60.6	$\beta-C_6$ OR $\alpha-C_6$
73.1	$C_{3'}, C_{5'}$		
72.7	$\alpha-C_3$		

MALTOSE

Figure 26. Maltose in DMSO-d$_6$ at 63°C. The assignments given are from the literature (3).

LITERATURE CITED

1. Kovac, P., Hirsch, J., Shashkov, A. S., Usov, A. I., and Yarotsky, S. V.,
   Carbohyd. Res. 85:177-85(1980).

2. Lee, J. Y., Ishizu, A., Hosoya, S., and Nakano, J., Cellulose Chem. Tech.
   13:739-45(1979).

3. Heyraud, A., Rinaudo, M., Vignon, M., and Vincendone, M., Biopolymers 18:167-85
   (1979).